UNIWERSYTET MARII CURIE-SKŁODOWSKIEJ
W LUBLINIE
Szkoła Doktorska Nauk Ścisłych i Przyrodniczych

Dziedzina: **Nauki ścisłe i przyrodnicze**
Dyscyplina: **Nauki chemiczne**

mgr Katarzyna Burdzy
nr albumu: 261711

Zastosowanie biodegradowalnych czynników kompleksujących w procesie odzysku pierwiastków ziem rzadkich metodą wymiany jonowej na jonitach różnego typu

(Application of biodegradable complexing agents in the recovery of rare earth elements by the ion exchange on the various types of ion exchangers)

Rozprawa doktorska przygotowywana pod kierunkiem naukowym
prof. dr hab. Doroty Kołodyńskiej

w Instytucie Nauk Chemicznych

LUBLIN, 2023

Pragnę podziękować Pani promotor

Prof. dr hab. Dorocie Kołodyńskiej

za poświęcony mi czas, cenne rady, zaangażowanie

i wsparcie w realizacji pracy doktorskiej.

Serdecznie dziękuję Koleżankom, Kolegom

oraz Pracownikom Katedry Chemii Nieorganicznej

za wspaniałą atmosferę i *okazaną pomoc.*

Szczególne podziękowania składam Moim Bliskim

za ogromne wsparcie, motywację i wiarę w moje możliwości.

Spis treści

1. Wykaz skrótów

REE (ang. *rare earth elements*) - pierwiastki ziem rzadkich

SEM (ang. *scanning electron microscopy*) - skaningowa mikroskopia elektronowa

pH_{pzc} (ang. *point of zero charge*) - punkt ładunku zerowego

ATR-FTIR (ang. *attenuated total reflectance Fourier transform infrared spectroscopy*) - spektroskopia w podczerwieni z transformatą Fouriera z techniką osłabionego całkowitego odbicia

XPS (ang. *X-ray photoelectron spectroscopy*) - spektroskopia fotoelektronów w zakresie promieniowania rentgenowskiego

ICP-OES (ang. *inductively coupled plasma optical emission spectrometry*) - optyczna spektrometria emisyjna ze wzbudzeniem w plazmie indukcyjnie sprzężonej

PFO (ang. *pseudo-first order*) - model pseudo-pierwszego rzędu

PSO (ang. *pseudo-second order*) - model pseudo-drugiego rzędu

Ln(III) - lantanowiec

L - czynnik kompleksujący

CA - kwas cytrynowy

IDHA - kwas iminodibursztynowy

GLDA - kwas glutaminodioctowy

S957 - jonit chelatujący Purolite S957

S950 - jonit chelatujący Purolite S950

SP112 - kationit Lewatit MonoPlus SP112

M500 - anionit silnie zasadowy Lewatit MonoPlus M500

M600 - anionit silnie zasadowy Lewatit MonoPlus M600

MP500 - anionit silnie zasadowy Lewatit MonoPlus MP500

4200 - anionit silnie zasadowy Amberjet 4200

4400 - anionit silnie zasadowy Amberjet 4400

4600 - anionit silnie zasadowy Amberjet 4600

IRA 458 - anionit silnie zasadowy Amberlite IRA 458

IRA 958 - anionit silnie zasadowy Amberlite IRA 958

IRA 67 - anionit słabo zasadowy Amberlite IRA 67

PS-DVB - polistyren usieciowany diwinylobenzenem

SD - odchylenie standardowe

2. Wykaz prac naukowych wchodzących w skład rozprawy doktorskiej

Rozprawę doktorską stanowi cykl powiązanych tematycznie artykułów naukowych opublikowanych w czasopismach z aktualnego wykazu wydanego przez Ministerstwo Edukacji i Nauki. Prace naukowe oznaczono symbolami **D1**, **D2**, **D3** i **D4**, natomiast materiały uzupełniające do artykułów odpowiednio **SD2**, **SD3** i **SD4**.

D1 **K. Araucz**, A. Aurich, D. Kołodyńska, *Novel multifunctional ion exchangers for metal ions removal in the presence of citric acid*, Chemosphere, 251 (2020) 126331.

IF_{2020}: 7,086 **Punkty MEiN**: 100

D2 **K. Burdzy**, A. Aurich, S. Hunger, R. Jastrząb, M. Zabiszak, D. Kołodyńska, *Green citric acid in the sorption process of rare earth elements*, Chemical Engineering Journal, 437 (2022) 135366.

IF_{2022}: 16,744 **Punkty MEiN**: 200

D3 **K. Burdzy**, Y. Ju, D. Kołodyńska, *Iminodisuccinic acid (IDHA) as an effective biodegradable complexing agent in the adsorption process of La(III), Nd(III) and Ho(III) ions*, Chemical Engineering Journal, 461 (2023) 142059.

IF_{2022}: 16,744 **Punkty MEiN**: 200

D4 **K. Burdzy**, R. Jastrząb, D. Kołodyńska, *GLDA and ion exchangers: unlocking sustainable solutions for recovery of rare earth elements*, Sustainable Materials and Technologies (2023) – w recenzji.

IF_{2022}: 10,681 **Punkty MEiN**: 200

Sumaryczny IF: 51,255

Sumaryczna liczba punktów MEiN: 700

3. Wprowadzenie

Pierwiastki ziem rzadkich (REE), obejmujące skand (Sc), itr (Y) oraz lantanowce (La-Lu) ze względu na wyjątkowe właściwości magnetyczne, optyczne i fluorescencyjne zyskały w ostatnich latach miano pierwiastków strategicznych dla rozwoju nowoczesnych technologii [1]. Ich wykorzystanie w szerokiej gamie produktów high-tech wraz z szybkim rozwojem technologicznym sprawia, że popyt na te metale stale rośnie [2]. Jednocześnie, bardzo duże rozproszenie złóż tych pierwiastków w skorupie ziemskiej oraz ich problematyczne pozyskiwanie i rozdzielanie stało się przyczyną dominacji na światowym rynku jednego państwa – Chin, doprowadzając do wzrostu cen i ograniczenia dostaw tych niezwykle cennych surowców.

Dlatego też coraz więcej uwagi poświęca się opracowaniu efektywnych metod odzysku REE ze źródeł wtórnych, m.in. ze zużytego sprzętu elektronicznego [3–6]. Wśród metod służących do odzysku i rozdzielania jonów metali można wyróżnić metody strąceniowe, procesy utleniania i redukcji, ekstrakcję rozpuszczalnikową, frakcjonowaną krystalizację oraz adsorpcję. Jedną z najczęściej wykorzystywanych metod rozdziału jest adsorpcja, która charakteryzuje się wysoką wydajnością oraz możliwością uzyskania pierwiastków o wysokim stopniu czystości, przy jednoczesnej prostocie i niskich kosztach procesu [7]. Pierwszym, bardzo istotnym etapem projektowania układu adsorpcyjnego, który pozwoliłby na zadowalający odzysk jonów metali jest dobór odpowiedniego adsorbentu. W handlu dostępna jest szeroka gama adsorbentów, wśród których popularną grupą są wymieniacze jonowe. Ponadto, należy rozważyć możliwość wprowadzenia do układu związków zwiększających efektywność tego procesu, np. czynników kompleksujących.

Czynniki kompleksujące to związki posiadające zdolność tworzenia stabilnych, rozpuszczalnych w wodzie kompleksów z licznymi jonami metali. Doskonałe właściwości kompleksujące stały się przyczyną ich szerokiego zastosowania m.in. w przemyśle spożywczym, kosmetycznym, tekstylnym, ale także w rolnictwie i medycynie. Związki te stosowane są także w procesach usuwania i odzysku jonów metali [8–10]. Powszechnie znanymi i wykorzystywanymi przedstawicielami tej grupy są kwas etylenodiaminotetraoctowy (EDTA) oraz kwas dietylenotriaminopentaoctowy (DTPA). Jednak istotną wadą wymienionych związków jest ich słaba biodegradowalność, która w połączeniu z trwałością tworzonych przez nich kompleksów powoduje zaburzenie naturalnej specjacji pierwiastków w środowisku. Konsekwencją tego jest uwalnianie toksycznych jonów metali z osadów, zwiększenie ich mobilności oraz zagrożenie zanieczyszczeniem wód [11]. Rosnąca

świadomość społeczna na temat zagrożeń środowiska sprawia, że prowadzonych jest coraz więcej badań nad zastąpieniem w/w związków tymi o korzystniejszym profilu ekologicznym. Dlatego też w ostatnich latach zwiększonym zainteresowaniem cieszą się czynniki kompleksujące takie jak kwas iminodibursztynowy (IDHA) oraz kwas glutaminodioctowy (GLDA), ale także kwas cytrynowy (CA). W odróżnieniu od tradycyjnych kompleksonów charakteryzują się one wysoką zdolnością do biodegradacji oraz bezpieczeństwem użytkowania [12–14]. Przeprowadzone badania porównawcze dotyczące kompleksowania jonów metali takich jak Fe, Mn, Zn, Cu, Cd oraz Pb dowodzą, że mogą stać się one skuteczną alternatywą dla konwencjonalnych czynników kompleksujących [8,15–18]. Pomimo wielu doniesień literaturowych na temat kompleksów kwasu cytrynowego, IDHA oraz GLDA z jonami metali ciężkich, czy Ca, Mg i Ba, niewiele wiadomo o tego typu połączeniach z jonami pierwiastków ziem rzadkich, a także możliwości zastosowania biodegradowalnych kompleksonów w procesie odzysku tych cennych jonów metali.

4. Cel rozprawy doktorskiej

Celem rozprawy doktorskiej było określenie możliwości zastosowania czynników kompleksujących charakteryzujących się wysoką biodegradowalnością, tj. kwasu 2-hydroksy-1,2,3-propanotrikarboksylowego (CA, kwas cytrynowy), kwasu N-(1,2-dikarboksyetylo)-D,L-asparaginowego (IDHA, kwas iminodibursztynowy) oraz kwasu N,N-bis(karboksymetylo)-L-glutaminowego (GLDA, kwas glutaminodioctowy) w procesie efektywnego odzysku wybranych pierwiastków ziem rzadkich (La(III), Nd(III) i Ho(III)) metodą adsorpcji z zastosowaniem wymieniaczy jonowych różniących się matrycą (polistyrenowe i poliakrylowe), grupami funkcyjnymi (fosfonowe, sulfonowe, aminofosfonowe, IV-rzędowe amoniowe typu I, IV-rzędowe amoniowe typu II, III-rzędowe aminowe), wielkością ziarna oraz strukturą (makroporowate lub żelowe).

Główne etapy badawcze zrealizowane w ramach przedstawionego zagadnienia obejmowały:

- badania potencjometryczne czynników kompleksujących oraz ich kompleksów z wybranymi jonami pierwiastków ziem rzadkich tj. La(III), Ce(III), Pr(III), Nd(III), Sm(III) i Ho(III),
- charakterystykę fizykochemiczną zastosowanych wymieniaczy jonowych (Purolite S957, Purolite S950, Lewatit MonoPlus SP112, Lewatit MonoPlus M500, Lewatit MonoPlus M600, Lewatit MonoPlus MP500, Amberjet 4200, Amberjet 4400, Amberjet 4600, Amberlite IRA 458, Amberlite IRA 958 i Amberlite IRA 67) metodami skaningowej mikroskopii elektronowej (SEM), spektroskopii w podczerwieni z transformatą Fouriera z techniką osłabionego całkowitego odbicia (ATR-FTIR), spektroskopii fotoelektronów w zakresie promieniowania rentgenowskiego (XPS), miareczkowania potencjometrycznego (MPT) oraz dryftu (MD), a także analizy sitowej,
- badania adsorpcji kompleksów La(III), Nd(III) i Ho(III) z biodegradowalnymi czynnikami kompleksującymi metodą statyczną, z uwzględnieniem parametrów procesu takich jak masa jonitu, stosunek molowy metal:ligand, pH roztworu, czas kontaktu faz, stężenie początkowe roztworu i temperatura, oraz regenerację zastosowanych jonitów,
- badania adsorpcji kompleksów La(III) z biodegradowalnymi czynnikami kompleksującymi metodą dynamiczną.

Wstępem do głównej części prac badawczych było zweryfikowanie, czy proces adsorpcji jonów La(III) (oraz dodatkowo jonów Ni(II)) może zachodzić z dobrą wydajnością z zastosowaniem biodegradowalnego czynnika kompleksującego, na przykładzie handlowo dostępnego kwasu cytrynowego [**D1**]. Kolejnym etapem było rozszerzenie badań o innych przedstawicieli REE (Nd(III) i Ho(III)). Do badań wytypowano szereg jonitów o różnych parametrach fizykochemicznych. Dla tak zaprojektowanych układów prowadzono proces adsorpcji z wykorzystaniem biodegradowalnych czynników kompleksujących:

- CA otrzymany we współpracy z Helmholtz-Centre for Environmental Research-UFZ (Niemcy) w procesie fermentacji przy udziale drożdży z gatunku *Yarrowia lipolytica* H181 [**D2**],
- IDHA (Baypure CX 100, Lanxess, Bayer AG Leverkusen, Niemcy) [**D3]**,
- GLDA (Dissolvine GL, Akzo-Nobel, Holandia) [**D4**].

Dodatkowo zbadano układy Ln(III) (La(III), Ce(III), Pr(III), Nd(III), Sm(III) i Ho(III)) z czynnikami kompleksującymi CA [**D2**], IDHA [**D3**] oraz GLDA [**D4**] z zastosowaniem miareczkowania potencjometrycznego.

5. Materiały i metody badawcze

5.1. Badania potencjometryczne czynników kompleksujących oraz ich kompleksów z jonami pierwiastków ziem rzadkich

Pomiary potencjometryczne prowadzono w układach dwuskładnikowych (jon metalu-czynnik kompleksujący) za pomocą titratora 907 Titrando wyposażonego w system dozujący 800 Dosino z zespoloną elektrodą pH Metrohm 6.0259.100, mieszadłem magnetycznym typu 801 i czujnikiem temperatury Pt 1000 (Metrohm, Szwajcaria). Do termostatowanego naczynka wprowadzano odpowiednie ilości: uwodnionych azotanów(V) pierwiastków ziem rzadkich ($La(NO_3)_3 \cdot 6H_2O$, $Ce(NO_3)_3 \cdot 6H_2O$, $Pr(NO_3)_3 \cdot 6H_2O$, $Nd(NO_3)_3 \cdot 6H_2O$, $Sm(NO_3)_3 \cdot 6H_2O$ lub $Ho(NO_3)_3 \cdot 5H_2O$, Sigma-Aldrich, Niemcy), czynnika kompleksującego (CA, IDHA lub GLDA), mianowanego 0,1 M HCl (Chempur, Polska), 1 M KNO_3 (Chempur, Polska) oraz wody demineralizowanej. Stężenie jonów Ln(III) w próbce wynosiło $1{,}0 \times 10^{-3}$ M. Badania prowadzono przy stałej sile jonowej wynoszącej 0,1 M dla stosunków molowych metalu do czynnika kompleksującego równych 1:1, 1:2 oraz 2:1. Próbkę termostatowano w temperaturze 293 ± 1 K przez 15 minut, a następnie miareczkowano w zakresie pH od 2,5 do 11,0 mianowanym roztworem wodorotlenku sodu NaOH wolnym od CO_2 (Chempur, Polska) w środowisku gazu obojętnego (hel 5.0). Do wyznaczenia wartości stałych protonacji czynników kompleksujących oraz stałych trwałości ich kompleksów z jonami Ln(III) zastosowano program HYPERQUAD2008, uwzględniając w analizie od 150 do 350 punktów dla każdego pomiaru.

5.2. Charakterystyka fizykochemiczna zastosowanych wymieniaczy jonowych

Do badań adsorpcji wybrano 12 handlowych wymieniaczy jonowych różnego typu:

- Purolite S957 - jonit chelatujący z fosfonowymi i sulfonowymi grupami funkcyjnymi, makroporowaty o matrycy PS-DVB (Purolite International Ltd., USA),
- Purolite S950 - jonit chelatujący z aminofosfonowymi grupami funkcyjnymi, makroporowaty o matrycy PS-DVB (Purolite International Ltd., USA),
- Lewatit MonoPlus SP112 - kationit z sulfonowymi grupami funkcyjnymi, makroporowaty o matrycy PS-DVB (Lanxess, Niemcy),
- Lewatit MonoPlus M500 - anionit silnie zasadowy z IV-rzędowymi amoniowymi grupami funkcyjnymi typu I, żelowy o matrycy PS-DVB (Lanxess, Niemcy),
- Lewatit MonoPlus M600 - anionit silnie zasadowy z IV-rzędowymi amoniowymi grupami funkcyjnymi typu II, żelowy o matrycy PS-DVB (Lanxess, Niemcy),

- Lewatit MonoPlus MP500 - anionit silnie zasadowy z IV-rzędowymi amoniowymi grupami funkcyjnymi typu I, makroporowaty o matrycy PS-DVB (Lanxess, Niemcy),
- Amberjet 4200 - anionit silnie zasadowy z IV-rzędowymi amoniowymi grupami funkcyjnymi typu I, żelowy o matrycy PS-DVB (Rohm and Haas, Francja),
- Amberjet 4400 - anionit silnie zasadowy z IV-rzędowymi amoniowymi grupami funkcyjnymi typu I, żelowy o matrycy PS-DVB (Rohm and Haas, Francja),
- Amberjet 4600 - anionit silnie zasadowy z IV-rzędowymi amoniowymi grupami funkcyjnymi typu II, żelowy o matrycy PS-DVB (Rohm and Haas, Francja),
- Amberlite IRA 458 - anionit silnie zasadowy z IV-rzędowymi amoniowymi grupami funkcyjnymi typu I, żelowy o matrycy poliakrylowej (Rohm and Haas, Francja),
- Amberlite IRA 958 - anionit silnie zasadowy z IV-rzędowymi amoniowymi grupami funkcyjnymi typu I, makroporowaty o matrycy poliakrylowej (Rohm and Haas, Francja),
- Amberlite IRA 67 - anionit słabo zasadowy z III-rzędowymi aminowymi grupami funkcyjnymi, żelowy o matrycy poliakrylowej (Rohm and Haas, Francja).

Wymieniacze jonowe przemywano wodą destylowaną w celu usunięcia zanieczyszczeń, dekantowano i suszono w temperaturze pokojowej.

Skaningową mikroskopię elektronową (SEM) wykorzystano w celu poznania morfologii i struktury powierzchni jonitów. Zdjęcia SEM wymieniaczy jonowych przed i po adsorpcji badanych kompleksów rejestrowano przy użyciu wysokorozdzielczego skaningowego mikroskopu elektronowego Quanta 3D FEG (FEI, USA).

Punkt ładunku zerowego (pH_{pzc}) badanych jonitów wyznaczono metodą miareczkowania potencjometrycznego oraz metodą dryftu. W metodzie miareczkowania potencjometrycznego zastosowano zestaw analityczny 907 Titrando (Metrohm, Szwajcaria). W tym celu 0,5 g jonitu wprowadzano do 50 mL roztworu NaCl, a następnie miareczkowano mianowanymi roztworami 1 M HCl i 1 M NaOH. Badania prowadzono przy trzech siłach jonowych 0,1 M, 0,01 M oraz 0,001 M. W celu wyznaczenia pH_{pzc} wymieniaczy jonowych metodą dryftu do kolb stożkowych o pojemności 100 mL dodawano 0,2 g odpowiedniego jonitu oraz 20 mL 0,1 M roztworu NaCl o pH w zakresie od 2,0 do 12,0 (pH_0) i wytrząsano z szybkością 180 obr./min przez 24 godziny. Po tym czasie zmierzono pH roztworów (pH_1). Punkt przecięcia z osią x krzywej na wykresie pH_1-pH_0 vs. pH_0 był równy wartości pH_{pzc}.

Identyfikacja grup funkcyjnych na powierzchni jonitów była możliwa poprzez rejestrację widm FTIR metodą spektroskopii w podczerwieni z transformatą Fouriera z techniką

osłabionego całkowitego odbicia (ATR-FTIR) z zastosowaniem spektrometru Agilent Cary 630 FT-IR (Agilent Technologies, USA).

Analizę składu pierwiastkowego powierzchni wymieniaczy jonowych dokonano za pomocą spektroskopii fotoelektronów w zakresie promieniowania rentgenowskiego (XPS) stosując wielokomorowy system analityczny UHV (Prevac, Polska).

Rozkład wielkości ziaren badanych jonitów określono za pomocą analizy sitowej, wykonanej z zastosowaniem sit laboratoryjnych o średnicy 200 × 50 mm i wielkości oczek od 100 do 900 μm (Retsch, Polska).

5.3. Badania adsorpcyjne metodą statyczną

Roztwory podstawowe jonów Ln(III) o stężeniu $1{,}0\times10^{-2}$ M przygotowywano poprzez rozpuszczenie odpowiednich ilości uwodnionych azotanów(V) pierwiastków ziem rzadkich $La(NO_3)_3\cdot6H_2O$, $Nd(NO_3)_3\cdot6H_2O$ lub $Ho(NO_3)_3\cdot5H_2O$ w wodzie destylowanej. W celu sporządzenia roztworów roboczych kompleksów do roztworu czynnika kompleksującego (L) wprowadzano odpowiednie ilości roztworu podstawowego jonów Ln(III). Badania adsorpcji kompleksów Ln(III) z biodegradowalnymi czynnikami kompleksującymi metodą statyczną prowadzono w kolbach stożkowych o pojemności 100 mL. Do 0,1 g odpowiedniego jonitu dodawano 10 mL roztworu kompleksów Ln(III)-L, a następnie wytrząsano przy użyciu wytrząsarek laboratoryjnych Elpin+ typ 357 oraz Elpin+ typ 358A (Elpin Plus, Polska) z prędkością 180 obr./min i amplitudą 8. Po upływie określonego czasu jonit oddzielano od roztworu metodą filtracji. Stężenie jonów Ln(III) w przesączu analizowano metodą optycznej spektrometrii emisyjnej ze wzbudzeniem w plazmie indukcyjnie sprzężonej z zastosowaniem spektrometru ICP-OES Varian 720-ES (Varian Inc., USA) przy długościach fali 333,749 nm dla La(III), 401,224 nm dla Nd(III) i 345,600 nm dla Ho(III). Przebadano wpływ różnych czynników na adsorpcję kompleksów Ln(III)-L:

- masy jonitu (0,1-0,2 g),
- stosunku molowego metal:ligand (Ln(III)-L=1:1, 1:2, 1:4),
- pH roztworu (2,0-12,0),
- czasu kontaktu faz (1-240 minut),
- stężenia początkowego roztworu ($0{,}5\times10^{-3}$-$1{,}4\times10^{-2}$ M),
- temperatury (293-333 K).

Ze względu na wysoką efektywność adsorpcji, podczas badań wpływu pH stosowano 0,05 g jonitu oraz 20 mL roztworu kompleksów Ln(III)-L. Początkowe pH roztworów

doprowadzano do wartości pożądanej za pomocą 1 M HNO_3 oraz 1 M NaOH (Chempur, Polska).

Na podstawie przeprowadzonych badań wyznaczono pojemności adsorpcyjne w stanie równowagi q_e [mg/g], pojemności adsorpcyjne po określonym czasie q_t [mg/g] oraz procent adsorpcji $\%S$ stosując następujące wzory:

$$q_e=(C_0-C_e)\times\frac{V}{m} \tag{1}$$

$$q_t=(C_0-C_t)\times\frac{V}{m} \tag{2}$$

$$\%S=\frac{(C_0-C_t)}{C_0}\times 100\% \tag{3}$$

gdzie: C_0 to stężenie początkowe jonów Ln(III) [mg/L], C_e to stężenie równowagowe jonów Ln(III) [mg/L], C_t to stężenie jonów Ln(III) po czasie t [mg/L], V to objętość roztworu [L], m to masa jonitu [g].

Badania kinetyczne przeprowadzono dla stężeń początkowych w przedziale od $0{,}5\times10^{-3}$ M do $2{,}5\times10^{-3}$ M. Uzyskane wyniki analizowano za pomocą następujących modeli kinetycznych [19–23]:

- model pseudo-pierwszego rzędu (PFO)

$$q_t=q_e(1-exp(-k_1t)) \tag{4}$$

- model pseudo-drugiego rzędu (PSO)

$$q_t=\frac{k_2q_e^2t}{1+k_2q_et} \tag{5}$$

- model dyfuzji wewnątrzziarnowej Webera-Morrisa

$$q_t=k_it^{0,5}+C \tag{6}$$

- model Boyda

$$B_t=(\sqrt{\pi}-\sqrt{\pi-\frac{\pi^2F}{3}})^2\text{, dla wartości F < 0,85} \tag{7}$$

$$B_t=-0{,}4977-ln(1-F)\text{, dla wartości F > 0,85} \tag{8}$$

- model Dumwalda-Wagnera

$$log(1-F^2)=-\frac{k}{2{,}303t} \tag{9}$$

gdzie: k_1 to stała szybkości reakcji dla modelu PFO [1/min], k_2 to stała szybkości reakcji dla modelu PSO [g/mg min], k_i to stała szybkości dyfuzji dla modelu dyfuzji wewnątrzziarnowej

Webera-Morrisa [mg/g $min^{1/2}$], C to stała określająca grubość warstwy granicznej, F to stosunek pojemności adsorpcyjnej po czasie t do pojemności równowagowej ($F=q_t/q_e$), B_t to funkcja matematyczna parametru F, k to stała szybkości w modelu Dumwalda-Wagnera [1/min].

Do opisu wyników badań równowagowych zastosowano modele izoterm adsorpcji [24–26]:

- Langmuira

$$q_e=\frac{q_0 K_L C_e}{1+K_L C_e} \tag{10}$$

- Freundlicha

$$q_e=K_F C_e^{1/n} \tag{11}$$

- Temkina

$$q_e=B\ln A+B\ln C_e \tag{12}$$

gdzie: q_0 to maksymalna pojemność adsorpcyjna [mg/g], K_L to stała Langmuira [L/mg], K_F to stała Freundlicha [mg/g], n to parametr związany z intensywnością adsorpcji, A to stała Temkina odpowiadająca maksymalnej energii wiązania [L/g], B to stała Temkina odpowiadająca ciepłu adsorpcji [J/mol]. Stała Temkina B może być wyrażona jako $B=RT/b_T$ (R to stała gazowa (8,314 J/mol K), T to temperatura bezwzględna [K], b_T to stała izotermy Temkina).

Dopasowanie modeli kinetycznych i równowagowych do danych eksperymentalnych oceniano na podstawie analizy współczynników korelacji R^2 oraz testu niezależności Chi kwadrat χ^2.

Przeprowadzone badania wpływu temperatury na adsorpcję kompleksów Ln(III)-L pozwoliły na wyznaczenie podstawowych parametrów termodynamicznych, takich jak zmiana energii swobodnej Gibbsa $\Delta G°$ [kJ/mol], zmiana entalpii $\Delta H°$ [kJ/mol] i entropii $\Delta S°$ [J/mol K], z zastosowaniem następujących zależności:

$$\Delta G^o=-RT\ln K_c \tag{13}$$

$$\ln K_c=\frac{\Delta S^o}{R}-\frac{\Delta H^o}{RT} \tag{14}$$

gdzie: K_c to bezwymiarowa stała równowagi podziału [27].

$$K_d=\frac{q_e}{C_e} \tag{15}$$

Oceny zdolności regeneracyjnych wymieniaczy jonowych dokonano na podstawie badań desorpcji. Jako czynniki desorbujące wybrano kwas chlorowodorowy oraz kwas azotowy(V) o stężeniach 0,5, 1 i 2 M. Do kolb stożkowych o pojemności 100 mL wprowadzano 0,1 g wysuszonego jonitu po adsorpcji kompleksów Ln(III)-L, zalewano 10 mL czynnika desorbującego i wytrząsano z szybkością 180 obr./min w temperaturze 293 K przez 240 minut. Próbki przesączono, a zawartość jonów Ln(III) analizowano metodą ICP-OES. Efektywność desorpcji oceniono na podstawie wartości procentu desorpcji %*D*, wyznaczonego na podstawie wzoru:

$$\%D = \frac{C_{des}}{C_0} \times 100\% \tag{16}$$

gdzie: C_{des} to stężenie jonów Ln(III) po procesie desorpcji [mg/L].

Możliwość ponownego zastosowania wymieniaczy jonowych przedstawiono w pracach **D2** i **D3**. W tym celu przeprowadzono pięć cykli adsorpcji/desorpcji kompleksów La(III)-CA oraz La(III)-IDHA z wykorzystaniem eluentu, dla którego uzyskano najwyższe wydajności desorpcji.

5.4. Badania adsorpcyjne metodą dynamiczną

Badania z zastosowaniem metody dynamicznej przeprowadzono dla kompleksów La(III)-L [**D2**, **D3**, **D4**] stosując w tym celu parametry procesu, dla których podczas badań metodą statyczną uzyskano najwyższe pojemności adsorpcyjne. Kolumny szklane o średnicy 1,5 cm i wysokości 25 cm wypełniano 10 mL spęczniałego jonitu. Przez złoże przepuszczano roztwór kompleksów La(III)-L o stężeniu $1{,}0\times10^{-3}$ M ze stałą prędkością 0,6 mL/min. Badania prowadzono w temperaturze 293 K. Eluat zbierano frakcjami o określonej objętości i analizowano za pomocą metody ICP-OES. Proces prowadzono do momentu, gdy stężenie jonów La(III) w wycieku było równe stężeniu roztworu wprowadzanego na kolumnę. Na podstawie uzyskanych wyników sporządzono krzywe przebicia C/C_0=f(V) oraz wyznaczono podstawowe parametry dynamiczne, takie jak pojemność adsorpcyjna jonitu w stanie równowagi q_e [mg/g], robocza zdolność wymienna C_w [mg/mL], całkowita zdolność wymienna C_t [mg/mL], masowy współczynnik podziału D_g i objętościowy współczynnik podziału D_v, opisane przez następujące zależności:

$$q_e = \frac{1}{m_j} \int_0^{V_k} (C_0 - C)dV \tag{17}$$

$$C_w = \frac{U \times C_0}{V_j} \tag{18}$$

$$C_t = \frac{\bar{U} \times C_0}{V_j} \tag{19}$$

$$D_g = \frac{\bar{U} - U_0 - V}{m_j} \tag{20}$$

$$D_v = \frac{\bar{U} - U_0 - V}{V_j} \tag{21}$$

gdzie: C_0 to stężenie jonów La(III) w roztworze wprowadzanym na kolumnę [mg/mL], C to stężenie jonów La(III) w wycieku [mg/mL], V_k to objętość roztworu wprowadzona na kolumnę do momentu wyczerpania złoża [mL], m_j to masa suchego złoża jonitu [g], U to objętość zebranego wycieku do osiągnięcia przebicia złoża [mL], V_j to objętość jonitu umieszczonego w kolumnie [mL], $\bar{U}$ to objętość wycieku do momentu, gdy C/C_0=0,5 [mL], U_0 to objętość martwa kolumny [mL], V to objętość pustej przestrzeni pomiędzy ziarnami jonitu (0,4 mL).

Dynamikę adsorpcji kompleksów La(III)-L w układach kolumnowych opisano z zastosowaniem następujących modeli matematycznych [28–31]:

- model Thomasa

$$ln\left(\frac{C_0}{C} - 1\right) = \frac{k_{Th} q_0 m}{Q} - \frac{k_{Th} C_0}{Q} V \tag{22}$$

- model Adamsa-Boharta

$$ln\left(\frac{C}{C_0}\right) = k_{AB} C_0 t - k_{AB} q \frac{H}{v} \tag{23}$$

- model Yoona-Nelsona

$$ln\left(\frac{C}{C_0 - C}\right) = k_{YN} t - k_{YN} \tau \tag{24}$$

- model Wolborskiej

$$ln\left(\frac{C}{C_0}\right) = \frac{\beta C_0}{q} t - \frac{\beta H}{v} \tag{25}$$

$$\beta = \frac{v^2}{2D}\left(\sqrt{1 + \frac{4\beta_0 D}{v^2}} - 1\right) \tag{26}$$

gdzie: k_{Th} to stała szybkości w modelu Thomasa [mL/mg min], q_0 to pojemność adsorpcyjna jonitu [mg/g], m to masa suchego złoża jonitu [g], Q to prędkość przepływu [mL/min], V to objętość wycieku [L], k_{AB} to stała szybkości w modelu Adamsa-Boharta [L/mg min], t to czas

[min], q to pojemność adsorpcyjna jonitu na jednostkę objętości złoża [mg/L], v to prędkość liniowa [cm/min], H to wysokość złoża kolumny [cm], k_{YN} to stała szybkości w modelu Yoona-Nelsona [1/min], τ to czas potrzebny do osiągnięcia 50% wyczerpania złoża [min], β to współczynnik kinetyczny zewnętrznego przenoszenia masy [1/min], D to współczynnik dyfuzji osiowej [cm^2/min], β_0 to współczynnik zewnętrznego przenoszenia masy przy pomijalnym współczynniku dyspersji osiowej D.

6. Omówienie wyników

6.1. Badania potencjometryczne biodegradowalnych czynników kompleksujących i ich kompleksów

Pomiary potencjometryczne rozpoczęto od wyznaczenia stałych protonacji czynników kompleksujących CA, IDHA oraz GLDA. Stwierdzono, że w cząsteczkach IDHA i GLDA, zawierających grupę aminową, w środowisku silnie zasadowym pierwszym etapem protonacji jest przyłączenie protonu do atomu azotu. W przypadku CA protonacja w grupie hydroksylowej następuje przy bardzo wysokim pH (pK_a=11,6), przez co jest często pomijana, a CA jest traktowany jako cząsteczka o trzech grupach zdolnych do dysocjacji [32]. Wraz ze spadkiem pH roztworu następuje przyłączanie kolejnych protonów do grup karboksylowych, czemu odpowiadają kolejne wartości log$K$ (Tabela 1).

Tabela 1. Ogólne (logβ) i stopniowe (log$K$) stałe protonacji czynników kompleksujących.

Równanie ogólne protonacji	**CA [D2]**			**IDHA [D3]**			**GLDA [D4]**		
	logβ	SD	log$K$	logβ	SD	log$K$	logβ	SD	log$K$
$L + H^+ \rightleftarrows HL$	5,36	0,04	5,36	10,12	0,01	10,12	9,69	0,01	9,69
$HL + H^+ \rightleftarrows H_2L$	9,48	0,04	4,12	14,67	0,01	4,56	14,66	0,01	4,97
$H_2L + H^+ \rightleftarrows H_3L$	12,64	0,04	3,16	18,32	0,01	3,65	18,27	0,01	3,61
$H_3L + H^+ \rightleftarrows H_4L$	-	-	-	21,63	0,01	3,30	20,88	0,02	2,61

W kolejnym kroku analizie poddano układy dwuskładnikowe jonów Ln(III) z czynnikami kompleksującymi, dla których stosunek molowy metal:ligand wynosił 1:1, 1:2 lub 2:1. Zaobserwowano występowanie trzech głównych form kompleksów (kompleksy typu LnL, kompleksy protonowane LnH_xL oraz hydroksokompleksy $LnL(OH)_x$), a także, w zależności od badanego układu, jednak w mniejszych ilościach, formy $LnHL_2$, LnL_2, Ln_2L, $Ln_2L(OH)_2$. Porównanie wyznaczonych stałych trwałości kompleksów, na przykładzie układów zawierających jony La(III), zaprezentowano w Tabeli 2 (dla stosunku molowego Ln(III)-L=1:1).

Tabela 2. Stałe trwałości kompleksów La(III)-L przy stosunku molowym metal:ligand równym 1:1.

Forma kompleksu	**CA [D2]**			**IDHA [D3]**			**GLDA [D4]**		
	logβ	SD	log$K$	logβ	SD	log$K$	logβ	SD	log$K$
LaH_2L	-	-	-	18,19	0,02	3,51	18,70	0,02	4,04
LaHL	9,52	0,03	4,16	14,41	0,01	4,30	15,01	0,01	5,33
LaL	6,15	0,01	6,15	9,75	0,01	9,75	9,95	0,02	9,95
LaL(OH)	-1,01	0,04	6,60	0,31	0,02	4,33	0,20	0,02	4,02
$LaL(OH)_2$	-7,59	0,05	7,19	-	-	-	-	-	-
$LaHL_2$	-	-	-	23,85	0,03	3,98	24,21	0,04	4,57

Na podstawie uzyskanych stałych trwałości analogicznych form kompleksów Ln(III)-L można stwierdzić, że najwyższą stabilnością charakteryzują się kompleksy z GLDA. Nieco niższe wartości otrzymano dla IDHA, a najniższe dla CA.

6.2. Charakterystyka fizykochemiczna zastosowanych wymieniaczy jonowych

Analiza zdjęć SEM wykazała, że badane wymieniacze jonowe mają postać ziaren o kulistym kształcie. Na powierzchni jonitów makroporowatych można zaobserwować obecność porów i szczelin, które są typowe dla tego typu materiałów, podczas gdy jonity o strukturze żelowej charakteryzują się bardziej jednorodną i zwartą budową [D2]. Porównując obrazy SEM przed i po adsorpcji kompleksów La(III)-L stwierdzono, że powierzchnia żelowych wymieniaczy jonowych stała się nieco bardziej zwarta i upakowana. Największe zmiany zarejestrowano dla jonitu IRA 67, gdzie po adsorpcji powierzchnia była jeszcze bardziej chropowata i niejednorodna [D2-D4].

Przegląd literatury pozwolił na porównanie powierzchni właściwej (S_{BET}) oraz średniego rozmiaru porów (D) badanych jonitów, których wartości mieściły się odpowiednio w zakresie 0,45-14,98 m^2/g i 2,84-34,10 nm, co świadczy o tym, że są to materiały adsorpcyjne o niezbyt rozwiniętej powierzchni, charakteryzujące się obecnością mezoporów [D2].

Punkt ładunku zerowego pH_{pzc} jest ważnym parametrem pozwalającym określić ładunek powierzchni adsorbentu w zależności od pH roztworu. Na podstawie jego wartości można przewidzieć występujące oddziaływania elektrostatyczne pomiędzy powierzchnią, a obecnymi w roztworze jonami [33]. Wartości pH_{pzc} badanych jonitów wyznaczono z zastosowaniem metody potencjometrycznej oraz metody dryftu [D2]. Wyniki uzyskane w/w metodami były zbliżone. Rozważając ładunek powierzchni jonitów w odniesieniu do uzyskanych wartości pH_{pzc} można stwierdzić, że ujemnie naładowane kompleksy Ln(III)-L będą adsorbować się z największą efektywnością, gdy pH roztworu będzie niższe od pH_{pzc}, a powierzchnia przyjmie ładunek dodatni. Głównym mechanizmem adsorpcji w takim przypadku są oddziaływania elektrostatyczne. Jednak w znacznej większości analizowanych układów adsorpcja była bardziej uprzywilejowana przy pH wyższym niż pH_{pzc}, co sugeruje udział innych mechanizmów w proces adsorpcji kompleksów Ln(III)-L.

Zestawienie uzyskanych zdjęć SEM jonitów oraz ich powierzchni właściwej (S_{BET}), średniego rozmiaru porów (D) i wartości punktu ładunku zerowego pH_{pzc} zaprezentowano w Tabeli 3.

Tabela 3. Charakterystyka fizykochemiczna badanych wymieniaczy jonowych.

	Zdjęcie SEM (×10000)	S_{BET} [m^2/g]	D [nm]	pH_{pzc}		Rozkład wielkości ziarna vs. % frakcji
				MPT	MD	
S957	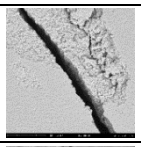	14,90	34,10	1,96	1,60	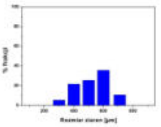
S950	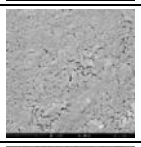	14,90	30,90	9,81	9,82	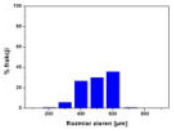
SP112	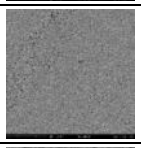	14,98	32,72	6,06	6,43	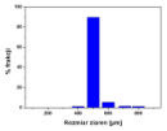
M500	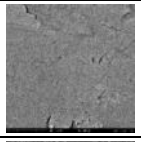	2,38	2,84	5,06	4,25	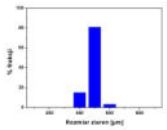
M600	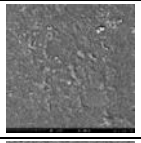	0,45	19,22	6,31	6,26	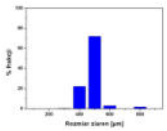
MP500	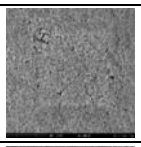	1,87	9,60	7,35	7,08	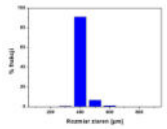
4200	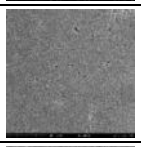	5,27	9,03	6,42	6,72	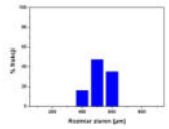
4400	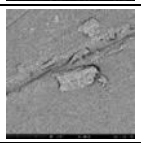	1,96	6,14	6,41	6,25	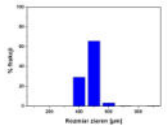
4600	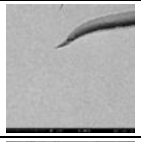	1,47	17,53	6,78	6,60	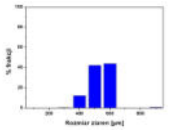
IRA 458	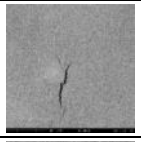	2,03	3,60	6,33	6,55	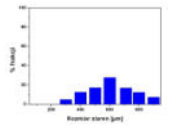
IRA 958	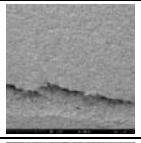	2,03	6,46	5,99	6,41	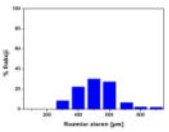
IRA 67	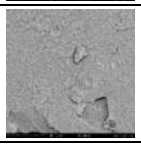	4,05	7,10	9,50	9,67	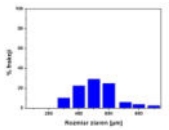

Identyfikacji grup funkcyjnych obecnych na powierzchni wymieniaczy jonowych oraz ich potencjalnych oddziaływań z kompleksami Ln(III)-L w procesie adsorpcji dokonano wykorzystując metodę spektroskopii w podczerwieni z transformatą Fouriera z techniką osłabionego całkowitego odbicia (ATR-FTIR). W tym celu zarejestrowano widma jonitów przed i po adsorpcji kompleksów La(III), Nd(III) i Ho(III) z badanymi czynnikami kompleksującymi [D2-D4]. Dla wszystkich widm zaobserwowano obecność szerokiego pasma w zakresie 3500-3300 cm^{-1}, które przypisywane jest drganiom rozciągającym grup O-H, pochodzącym od cząsteczek wody zawartej w fazie jonitu oraz grup N-H, które, z wyjątkiem jonitów S957 i SP112, można przypisać obecnym w strukturze IV-rzędowym grupom amoniowym, III-rzędowym grupom aminowym lub grupom aminofosfonowym. Kolejne pasma, pochodzące od matrycy jonitów, obecne są w zakresie 3050-3015 cm^{-1} (drgania rozciągające C-H w pierścieniu benzenowym), 2940-2920 cm^{-1} oraz 2850-2840 cm^{-1} (asymetryczne i symetryczne drgania rozciągające C-H w grupach $-CH_2$), a także 1480-1470, 1420-1410 i 1380-1370 cm^{-1} (asymetryczne drgania rozciągające C=C w pierścieniu oraz asymetryczne drgania nożycowe w grupach metylenowych). Potwierdzono również obecność grup funkcyjnych:

- fosfonowych i sulfonowych w przypadku jonitu S957 (pasma przy 2283 i 2112 cm^{-1} oraz przy 1123 i 988 cm^{-1} - drgania rozciągające grup P-OH i S-OH oraz grup P=O, P-O, S=O i S-O),
- fosfonowych w przypadku jonitu S950 (pasma przy 2312 cm^{-1} oraz 1083 i 973 cm^{-1} - drgania rozciągające grup P-OH, P=O i P-O),
- sulfonowych w przypadku jonitu SP112 (pasma przy 1177, 1123, 1037 i 1008 cm^{-1} - drgania rozciągające grup S=O i S-O),
- IV-rzędowe amoniowe w przypadku anionowych wymieniaczy jonowych (pasmo przy 975 cm^{-1}).

Widma jonitów po adsorpcji kompleksów Ln(III) z CA, IDHA lub GLDA wskazywały na podobny mechanizm ich adsorpcji, niezależnie od zastosowanego czynnika kompleksującego. Analiza widm jonitów S957, S950 i SP112 wykazała zmiany w intensywności oraz niewielkie przesunięcia pasm pochodzących od grup fosfonowych i sulfonowych. Świadczy to o udziale tych grup w procesie adsorpcji. Można zatem wnioskować, że w tym przypadku dochodzi do rozpadu kompleksów w fazie jonitu, a następnie tworzenia wiązań pomiędzy wolnymi jonami metali a zdysocjowanymi grupami fosfonowymi lub sulfonowymi. Widma uzyskane dla anionowych wymieniaczy jonowych sugerują

natomiast obecność kompleksów w fazie jonitu, co wynika z pojawienia się nowych pasm w zakresie 1600-1565 cm^{-1} i 1380-1330 cm^{-1}, reprezentujących odpowiednio asymetryczne i symetryczne drgania rozciągające grup karboksylowych.

Analizę składu pierwiastkowego powierzchni wymieniaczy jonowych zarówno przed, jak i po adsorpcji kompleksów La(III)-L dokonano z zastosowaniem spektroskopii fotoelektronów w zakresie promieniowania rentgenowskiego XPS [D3, D4]. Uzyskane widma ujawniły obecność pasm C 1s oraz O 1s, pochodzących od C i O, stanowiących matrycę jonitów, a także pasm potwierdzających obecność fosfonowych (pasma P 2p), sulfonowych (pasma S 2p) oraz aminowych i amoniowych (pasma N 1s) grup funkcyjnych. Na widmach jonitów po adsorpcji kompleksów La(III)-L pojawiły się pasma w zakresie 833,0-836,7 eV, które przypisano poziomowi La 3d [34]. Jest to potwierdzeniem obecności La na powierzchni wymieniaczy jonowych, a zarazem skutecznej adsorpcji. Zawartość La, według składu pierwiastkowego, mieściła się w zakresie od 0,1 do 0,9 %. Zarejestrowane pasma Na 1s (widma jonitów S950 i SP112) oraz Cl 1s (widma anionitów), pochodzące od formy sodowej lub chlorkowej jonitów, uległy zmniejszeniu lub całkowitemu zanikowi, co wskazuje na wymianę jonową.

W pracy [D4] zaprezentowano wyniki analizy sitowej badanych wymieniaczy jonowych, której celem było określenie wielkości ziaren oraz procentowego rozkładu ich frakcji (Tabela 3). Potwierdzono monodyspersyjność jonitów SP112, M500, MP500 i M600. Badania wykazały, że 90% ziaren kationitu SP112 posiadało rozmiar 500 µm, natomiast 91% anionitu MP500 charakteryzowało się wielkością 400 µm. Anionity M500 i M600 cechowała nieco większa różnorodność w wielkości ziaren, odpowiednio 81% i 72% frakcji o wielkości 500 µm. Pozostałe wymieniacze jonowe sklasyfikowano jako polidyspersyjne.

6.3. Badania adsorpcyjne metodą statyczną

6.3.1. Wpływ masy jonitu

Badania nad wpływem masy jonitu na adsorpcję kompleksów przeprowadzono dla wybranych wymieniaczy jonowych (S957 i S950), a uzyskane wyniki opisano w pracach [D1, D3]. Niezależnie od badanego czynnika kompleksującego, a także jonitu stwierdzono, że wzrost masy wymieniacza jonowego zastosowanego w procesie powoduje znaczny (nawet dwukrotny) spadek uzyskiwanych pojemności adsorpcyjnych. Jest to spowodowane niewysyceniem wszystkich dostępnych miejsc adsorpcji [35]. Dlatego też, zgodnie

z uzyskanymi wynikami, badania adsorpcji metodą statyczną przeprowadzono stosując 0,1 g jonitu (dawka 10 g/L, wyjątek badania wpływu pH roztworu).

6.3.2. Wpływ stosunku molowego metal:ligand

Stosunek molowy jonu metalu do ligandu obecnego w roztworze determinuje stopień skompleksowania metalu, a także rodzaj oraz ilość powstających kompleksów. W związku z tym dobór odpowiednich proporcji pomiędzy stężeniem jonu metalu i czynnika kompleksującego jest istotny w procesie optymalizacji procesu adsorpcji. Badania przeprowadzono dla trzech stosunków molowych metal:ligand, wynoszących 1:1, 1:2 i 1:4 tj. w zakresie zmiany stężenia ligandu od $1{,}0\times10^{-3}$ do $4{,}0\times10^{-3}$ M. Stężenie jonów Ln(III) było stałe i wynosiło $1{,}0\times10^{-3}$ M. Jonity chelatujące S957 i S950 wykazywały wysokie zdolności adsorpcyjne niezależnie od zastosowanego stosunku molowego. Podczas zastosowania GLDA jako czynnika kompleksującego uzyskane wartości pojemności adsorpcyjnych dla tych jonitów mieściły się w zakresie 13,88-14,30 mg/g dla układu La(III)-S957, 13,81-14,23 mg/g dla układu La(III)-S950, 13,56-13,71 mg/g dla układu Nd(III)-S957, 13,33-13,65 mg/g dla układu Nd(III)-S950, 15,79-16,01 mg/g dla układu Ho(III)-S957 oraz 9,54-12,94 mg/g dla układu Ho(III)-S950. W przypadku kationitu SP112 wzrost stężenia czynnika kompleksującego powodował znaczny spadek pojemności adsorpcyjnej. Podczas adsorpcji kompleksów La(III)-GLDA na SP112 wartości q_e zmniejszyły się z 7,67 do 0,23 mg/g, natomiast dla kompleksów Nd(III) i Ho(III) odpowiednio z 6,99 do 1,69 mg/g i 4,77 do 0,24 mg/g. Dla silnie zasadowych anionitów zaobserwowano wzrost efektywności adsorpcji podczas zmiany stosunku molowego z 1:1 do 1:2, natomiast dalsze zwiększanie stężenia ligandu nie wpływało już znacząco na efektywność tego procesu. W przypadku, gdy jako adsorbent wykorzystano IRA 67, duży nadmiar czynnika kompleksującego (stosunek molowy 1:4) powodował pogorszenie adsorpcji. Analogiczne wyniki uzyskano dla wszystkich badanych czynników kompleksujących [D2, D3, D4].

6.3.3. Wpływ pH roztworu

Wpływ pH na efektywność adsorpcji kompleksów Ln(III)-L był uzależniony od typu zastosowanego jonitu oraz od rodzaju czynnika kompleksującego obecnego w układzie. W przypadku, gdy do kompleksowania jonów Ln(III) zastosowano CA, jonity chelatujące S957 i S950 oraz kationit SP112 wykazywały wysoką wydajność adsorpcji w szerokim zakresie pH, a ich pojemności adsorpcyjne zmniejszały się jedynie przy pH 12,0. Wyjątek stanowiły tu układy Nd(III)-CA-S950, Nd(III)-CA-SP112, Ho(III)-CA-SP112, gdzie następował spadek

efektywności adsorpcji wraz ze wzrostem pH. Adsorpcja kompleksów z CA na anionitach silnie zasadowych była największa przy pH 8,0, natomiast na anionicie słabo zasadowym IRA 67 przy pH 4,0 [D2]. W przypadku, gdy jako czynnik kompleksujący zastosowano IDHA lub GLDA, jonity chelatujące wykazywały podobną zależność jak w przypadku CA (wysokie pojemności adsorpcyjne w zakresie pH 2,0-10,0). Podczas adsorpcji kompleksów La(III)-GLDA uzyskane wartości q_e wynosiły od 55,03 do 56,98 mg/g dla jonitu S957 oraz od 42,98 do 47,31 mg/g dla jonitu S950. Dla kompleksów Nd(III)-GLDA pojemności adsorpcyjne wahały się od 56,17 do 57,13 mg/g dla S957 i od 35,75 do 40,94 mg/g dla S950. Wartości q_e podczas adsorpcji kompleksów Ho(III)-GLDA na jonicie S957 również wykazywały stabilność wraz ze zmianami pH (od 63,85 do 65,34 mg/g), jednak wyjątek stanowił układ Ho(III)-GLDA-S950, gdzie wzrost pH powodował zmniejszenie pojemności adsorpcyjnej z 44,88 do 24,63 mg/g. Dla jonitu SP112 zadowalającą wydajność adsorpcji zaobserwowano jedynie w środowisku kwaśnym, natomiast dla anionitów silnie zasadowych przy pH 10,0 [D3, D4]. W układach zawierających czynnik kompleksujący GLDA i kationit SP112 maksymalne pojemności adsorpcyjne uzyskane przy pH 2,0 wynosiły 56,56 mg/g dla kompleksów La(III), 55,86 mg/g dla kompleksów Nd(III) oraz 64,30 mg/g dla kompleksów Ho(III), podczas gdy wzrost pH do 12,0 spowodował ich spadek odpowiednio do 20,24; 10,46 i 13,19 mg/g. Badania przeprowadzone z zastosowaniem anionitów silnie zasadowych i GLDA przy pH 10,0 pozwoliły na uzyskanie następujących maksymalnych wartości q_e:

- dla kompleksów La(III): 54,58 mg/g dla M500, 54,25 mg/g dla M600, 53,76 mg/g dla MP500, 54,67 mg/g dla 4200, 53,24 mg/g dla 4400, 54,64 mg/g dla 4600, 54,14 mg/g dla IRA 458 i 53,55 mg/g dla IRA 958,
- dla kompleksów Nd(III): 58,20 mg/g dla M500, 58,24 mg/g dla M600, 58,18 mg/g dla MP500, 58,31 mg/g dla 4200, 57,91 mg/g dla 4400, 58,22 mg/g dla 4600, 58,06 mg/g dla IRA 458 i 57,97 mg/g dla IRA 958,
- dla kompleksów Ho(III): 66,35 mg/g dla M500, 66,33 mg/g dla M600, 66,32 mg/g dla MP500, 66,34 mg/g dla 4200, 66,26 mg/g dla 4400, 66,33 mg/g dla 4600, 66,32 mg/g dla IRA 458 i 66,31 mg/g dla IRA 958.

Wyniki uzyskane dla anionitu słabo zasadowego IRA 67 były analogiczne dla wszystkich badanych czynników kompleksujących, najwyższe wartości q_e uzyskano przy pH 4,0, a w przypadku układów z GLDA wynosiły one 50,97 mg/g dla kompleksów La(III), 51,96 mg/g dla Nd(III) i 62,97 mg/g dla Ho(III).

Znacznie korzystniejsze warunki adsorpcji w środowisku kwaśnym w przypadku kationitu SP112 wynikają prawdopodobnie z obecności wolnych kationów Ln^{3+}, które są kompleksowane tylko w niewielkim stopniu. Zależność uzyskana dla anionitów silnie zasadowych, gdzie wzrost pH powodował zwiększenie pojemności adsorpcyjnych (najwyższe wartości przy pH 8,0 dla CA oraz 10,0 dla IDHA i GLDA), jest związana z obecnością w tych warunkach ujemnie naładowanych kompleksów Ln(III)-L, które mogą być adsorbowane przez IV-rzędowe amoniowe grupy funkcyjne:

$$R\text{-}^{+}N(CH_3)_3Cl^{-} + [LnL]^{-} \rightleftarrows [R\text{-}^{+}N(CH_3)_3][LnL]^{-} + Cl^{-} \quad (27)$$

$$R\text{-}^{+}N(CH_3)_2CH_2CH_2OHCl^{-} + [LnL]^{-} \rightleftarrows [R\text{-}^{+}N(CH_3)_2CH_2CH_2OH][LnL]^{-} + Cl^{-} \quad (28)$$

Najwyższe pojemności adsorpcyjne uzyskane przy pH 4,0 w przypadku anionitu słabo zasadowego IRA 67 można natomiast wytłumaczyć obecnością III-rzędowych grup aminowych na jego powierzchni. Grupy te w środowisku obojętnym i zasadowym dysocjują w niewielkim stopniu zgodnie z równaniem:

$$R\text{-}N(CH_3)_2 \cdot H_2O \rightleftarrows R\text{-}^{+}NH(CH_3)_2OH^{-} \quad (29)$$

Jest to przyczyną słabej adsorpcji w tych warunkach. Dla wystarczająco wysokiego stężenia jonów wodorowych (niskie wartości pH) zachodzi protonacja grup funkcyjnych i adsorpcja wzrasta [36]. Jednak przy zbyt niskim pH, w roztworze obecne są głównie całkowicie sprotonowane cząsteczki czynnika kompleksującego oraz wolne jony Ln^{3+}, które nie są adsorbowane przez jonit.

6.3.4. Kinetyka adsorpcji

Badania kinetyczne adsorpcji są niezbędnym etapem pozwalającym na wyznaczenie czasu, w którym układ osiąga stan równowagi. Czas ten jest jednym z ważniejszych parametrów, jakie należy rozważyć podczas projektowania układów adsorpcyjnych. W związku z tym przeanalizowano w jaki sposób czas kontaktu faz jonit-roztwór kompleksów Ln(III)-L wpłynie na adsorpcję. Badania przeprowadzono dla różnych stężeń początkowych w zakresie $0{,}5\times10^{-3}$-$2{,}5\times10^{-3}$ M. Wykazano, że adsorpcja kompleksów Ln(III) z CA, IDHA oraz GLDA w niemal wszystkich przypadkach przebiega bardzo szybko, a równowaga zostaje osiągnięta w ciągu 30-60 minut. Dla jonitów S950 oraz IRA 67 czas ten nie był dłuższy niż 240 minut. Jonit chelatujący S957 adsorbował wszystkie badane kompleksy z wydajnością równą 100%. Najniższą efektywność procesu odnotowano dla układu La(III)-CA-SP112, gdzie przy stężeniu $2{,}5\times10^{-3}$ M wartość *%S* wynosiła 60% [D2]. W przypadku pozostałych wymieniaczy jonowych efektywność adsorpcji przewyższała 93%. Podczas badań wpływu czasu kontaktu faz na adsorpcję La(III) i Nd(III) prowadzonych w obecności czynnika

kompleksującego IDHA na jonicie IRA 67 ilość zaadsorbowanych kompleksów wzrastała w ciągu pierwszych 120 minut, po czym po czasie 240 minut malała na skutek procesu desorpcji [D3].

Do opisu kinetyki adsorpcji zastosowano modele pseudo-pierwszego rzędu, pseudo-drugiego rzędu, dyfuzji wewnątrzziarnowej, Boyda oraz Dumwalda-Wagnera. Badania przeprowadzone z wykorzystaniem CA wykazały, że za pomocą modelu PSO można uzyskać najlepsze dopasowanie do danych eksperymentalnych [D2]. W przypadku, gdy adsorpcji poddano kompleksy Ln(III) z IDHA oraz GLDA wybór odpowiedniego modelu kinetycznego był zależny od zastosowanego w układzie jonitu. Proces przeprowadzony z jonitem chelatującym S957, kationitem SP112 lub anionitami silnie zasadowymi był najlepiej opisywany przez model PFO, podczas gdy model PSO znalazł zastosowanie do opisu kinetyki adsorpcji na jonicie chelatującym S950 i anionicie słabo zasadowym IRA 67 [D3, D4]. Jedynie dla układów La(III)-IDHA na anionitach silnie zasadowych proces adsorpcji przebiegał zgodnie z modelem PSO [D3].

Analiza uzyskanych danych eksperymentalnych z zastosowaniem modeli dyfuzji wewnątrzziarnowej, Boyda oraz Dumwalda-Wagnera wskazała, że adsorpcja kompleksów Ln(III) z CA, IDHA oraz GLDA na wybranych wymieniaczach jonowych jest procesem złożonym, na szybkość którego mają wpływ dyfuzja w warstwie granicznej oraz dyfuzja wewnątrzziarnowa [D2, D3, D4].

6.3.5. Badania równowagowe

Opisu badań równowagowych dokonano stosując modele izoterm Langmuira, Freundlicha oraz Temkina. Wyznaczenie izoterm adsorpcji jest ważnym elementem badań w układach ciało stałe-ciecz, ponieważ umożliwiają one określenie interakcji pomiędzy adsorbatem a adsorbentem, dostarczając informacji na temat mechanizmu procesu.

W przypadku adsorpcji kompleksów Ln(III)-CA w niemal wszystkich badanych układach modelem, najlepiej opisującym proces był model Langmuira, co sugeruje adsorpcję monowarstwową na energetycznie jednorodnej powierzchni adsorbentu. Jednak dla układów Nd(III)-CA-SP112, La(III)-CA-IRA 67 oraz Ho(III)-CA-IRA 67 odnotowano lepsze dopasowanie do modelu Freundlicha, wskazujące na adsorpcję na powierzchni heterogenicznej [D2]. Wyniki badań równowagowych adsorpcji jonów Ln(III) z zastosowaniem IDHA oraz GLDA jako czynników kompleksujących wykazały, że proces zachodzący na jonitach chelatujących S957, S950 i kationicie SP112 jest zgodny z modelem Temkina (adsorpcja wielowarstwowa, z uwzględnieniem oddziaływań adsorbent-adsorbat). Wprowadzenie do

układu silnie zasadowych anionitów powodowało, że adsorpcję najlepiej opisywał model Langmuira, podczas gdy adsorpcja kompleksów Ln(III)-IDHA oraz Ln(III)-GLDA na anionicie słabo zasadowym IRA 67 przebiegała według modelu Freundlicha. Odstępstwem od opisanych zależności były układy La(III)-IDHA-S957 oraz Nd(III)-IDHA-IRA 458, które wykazały większą zgodność odpowiednio z modelami Langmuira oraz Temkina [D3, D4].

Na podstawie przeprowadzonych badań ustalono szeregi powinowactwa wybranych wymieniaczy jonowych w stosunku do kompleksów Ln(III) z CA, IDHA oraz GLDA, i zaprezentowano je w pracach [D2, D3, D4]. W przypadku układów zawierających czynnik kompleksujący GLDA szeregi powinowactwa prezentowały się następująco:

- dla kompleksów La(III): IRA 67 < 4400 < 4600 < M600 < IRA 958 < 4200 < M500 < MP500 < IRA 458 < S950 < S957 < SP112,
- dla kompleksów Nd(III): IRA 67 < 4400 < M600 < MP500 < M500 < 4600 < IRA 958 < 4200 < S950 < IRA 458 < SP112 < S957,
- dla kompleksów Ho(III): S950 < IRA 67 < 4400 < MP500 < M600 < IRA 958 < M500 < 4200 < 4600 < IRA 458 < SP112 < S957.

Uzyskane maksymalne pojemności adsorpcyjne jonitów wskazują na bardzo dobrą efektywność adsorpcji badanych kompleksów. Zdolności adsorpcyjne niektórych wymieniaczy jonowych różniły się w zależności od zastosowanego czynnika kompleksującego lub jonu Ln(III). Jonit chelatujący S950 charakteryzował się wysokimi wartościami pojemności adsorpcyjnych (do 139,15 mg/g dla kompleksów La(III)-CA), jednak w układzie z kompleksami Ho(III)-GLDA uzyskano wartość q_e równą 55,66 mg/g, najniższą wśród badanych wymieniaczy jonowych. Analogicznie w przypadku kationitu SP112 i kompleksów Ho(III)-IDHA zdolność adsorpcji wynosiła 201,74 mg/g, a dla kompleksów La(III)-CA była równa 40,40 mg/g. Spośród 12 wybranych do badań wymieniaczy jonowych jako ten o najwyższej zdolności adsorpcji jonów Ln(III) z czynnikami kompleksującymi CA, IDHA oraz GLDA wybrano jonit chelatujący S957, dla którego uzyskane pojemności adsorpcyjne zestawiono w Tabeli 4.

Tabela 4. Maksymalne pojemności adsorpcyjne jonitu chelatującego S957 względem kompleksów Ln(III)-L.

Maksymalna pojemność adsorpcyjna q_e [mg/g]	**CA**	**IDHA**	**GLDA**
La(III)	162,04	142,29	138,66
Nd(III)	142,65	149,15	152,72
Ho(III)	180,26	166,01	151,29

6.3.6. Badania termodynamiczne

Badania adsorpcji kompleksów Ln(III)-L przeprowadzono w trzech temperaturach 293, 313 i 333 K. Na podstawie uzyskanych wyników określono wpływ temperatury na badany proces, a także wyznaczono parametry termodynamiczne. Większość wymieniaczy jonowych charakteryzowała się zależnością często opisywaną w literaturze, gdzie wzrost temperatury sprzyjał poprawie efektywności adsorpcji (proces endotermiczny) [37–39]. Przyczyną tego jest wzrost energii kinetycznej cząsteczek adsorbatu, co zwiększa ich mobilność do miejsc aktywnych [40,41]. W przypadku adsorpcji kompleksów z CA, IDHA oraz GLDA na anionicie słabo zasadowym IRA 67 zmiana temperatury z 293 K do 333 K powodowała znaczny spadek wydajności procesu, co świadczy o jego egzotermicznej naturze [D2-D4]. Przykładowo w układzie La(III)-GLDA-IRA 67 wraz ze wzrostem temperatury odnotowano spadek pojemności adsorpcyjnej z 52,83 do 39,38 mg/g. Analogiczne wyniki uzyskano podczas adsorpcji kompleksów La(III) z CA na SP112 [D2], Nd(III) i Ho(III) z IDHA na IRA 459 i IRA 958 [D3] oraz La(III), Nd(III) i Ho(III) z GLDA na IRA 459 i IRA 958 [D4]. W większości w/w jonity posiadały matrycę poliakrylową. Dla tego typu układów proces należy zatem prowadzić w temperaturze 293 K. Można wnioskować, że dla opisanych układów wzrost temperatury sprzyjał desorpcji poprzez osłabienie sił adsorpcyjnych pomiędzy miejscami aktywnymi a kompleksami [42].

Wyznaczone parametry termodynamiczne wskazują, że proces adsorpcji był korzystny termodynamicznie i spontaniczny. Wartości $\Delta G°$ mieszczące się w zakresie od -20 do 0 kJ/mol oraz wartości $\Delta H°$ poniżej 40 kJ/mol sugerują znaczny udział oddziaływań fizycznych w procesie adsorpcji kompleksów Ln(III)-L (oddziaływania elektrostatyczne) [43,44]. Ponadto, uzyskane wartości $\Delta H°$ potwierdziły w/w efekt energetyczny adsorpcji.

6.3.7. Badania desorpcji

Istotnym aspektem podczas doboru odpowiedniego wymieniacza jonowego, ze względu na kwestie ekonomiczne oraz środowiskowe, jest możliwość jego ponownego zastosowania. Regeneracja materiałów adsorpcyjnych, która jednocześnie pozwala na odzysk jonów metali, jest bardzo często prowadzona z zastosowaniem kwasów nieorganicznych [45,46]. W związku z tym przeprowadzono badania desorpcji, określając wpływ rodzaju czynnika desorbującego (HCl, HNO_3) oraz jego stężenia (0,5, 1, 2 M). Czynnik kompleksujący stosowany w etapie adsorpcji nie miał znaczącego wpływu na proces desorpcji. Wykazano, że desorpcja z zastosowaniem jonitów chelatujących S957 i S950 oraz kationitu SP112 była zależna

w głównej mierze od stężenia czynnika desorbującego, a wydajność procesu rosła wraz ze wzrostem jego stężenia. Maksymalna uzyskana wydajność desorpcji wynosiła 69% dla S957 przy zastosowaniu 2 M HNO_3 jako eluentu, jednak w pozostałych układach była znacznie niższa [D2]. Wskazuje to na duże powinowactwo badanych kompleksów do jonitów S957, S950 oraz SP112, a zarazem konieczność dalszych badań nad poszukiwaniem odpowiednich czynników desorbujących lub warunków procesu. Najlepsze właściwości regeneracyjne uzyskano dla anionowych wymieniaczy jonowych, gdzie niezależnie od czynnika desorbującego oraz jego stężenia efektywność desorpcji była wysoka i sięgała nawet 100%.

Na przykładzie kompleksów La(III)-CA oraz La(III)-IDHA przeprowadzono dodatkowo pięć cykli adsorpcji i desorpcji w celu oceny możliwości wielokrotnego zastosowania badanych wymieniaczy jonowych [D2, D3]. Jako czynniki desorbujące na tym etapie badań wybrano eluenty, dla których uzyskano najwyższe wartości *%D*. Wyniki pozwoliły stwierdzić, że jonity S957, S950 oraz SP112 z powodzeniem mogą być wielokrotnie stosowane bez spadku ich pojemności adsorpcyjnej. Po pięciu cyklach adsorpcji/desorpcji efektywność adsorpcji wciąż wynosiła niemal 100%. Spadek efektywności procesu, ale nie więcej niż o 15% zaobserwowano w przypadku polistyrenowych anionowych wymieniaczy jonowych, a dla anionitów poliakrylowych IRA 458, IRA 958 oraz IRA 67 nawet do 30%. Prowadzi to do stwierdzenia, że jonity polistyrenowe posiadają lepszą zdolność do regeneracji w porównaniu z poliakrylowymi.

6.4. Badania adsorpcyjne metodą dynamiczną

W celu weryfikacji wyników uzyskanych metodą statyczną badania adsorpcji, na przykładzie kompleksów La(III) z CA, IDHA oraz GLDA, przeprowadzono stosując układy kolumnowe, powszechnie wykorzystywane w procesach przemysłowych [47]. Badania wykazały, że anionit słabo zasadowy IRA 67 nie jest odpowiedni do tego celu i już pierwsze 100 mL roztworu kompleksów La(III)-L powodowało przebicie złoża i pojawienie się La(III) w wycieku. Lepsze właściwości adsorpcyjne posiadały silnie zasadowe anionity. W grupie anionitów większe powinowactwo do kompleksów La(III)-L posiadały jonity polistyrenowe. Z kolei dla anionitów poliakrylowych (IRA 458 i IRA 958) zaobserwowano nieco niższą efektywność adsorpcji. Zastosowanie w układzie kolumnowym jonitów S950 oraz SP112 pozwoliło na uzyskanie wyższych pojemności adsorpcyjnych w porównaniu z anionitami. Wyznaczone parametry dynamiczne potwierdziły, że najlepsze zdolności adsorpcyjne względem badanych kompleksów posiada jonit chelatujący S957, dla którego robocza zdolność wymienna C_w wyniosła 102,96 mg/mL, 93,82 mg/mL oraz 77,72 mg/mL odpowiednio dla

kompleksów La(III) z CA, IDHA oraz GLDA. Porównanie krzywych przebicia złoża wyznaczonych dla jonitu S957 podczas adsorpcji kompleksów La(III)-L oraz krzywe przebicia złoża wszystkich badanych wymieniaczy jonowych na przykładzie adsorpcji kompleksów La(III)-GLDA przedstawiono na Rysunku 1.

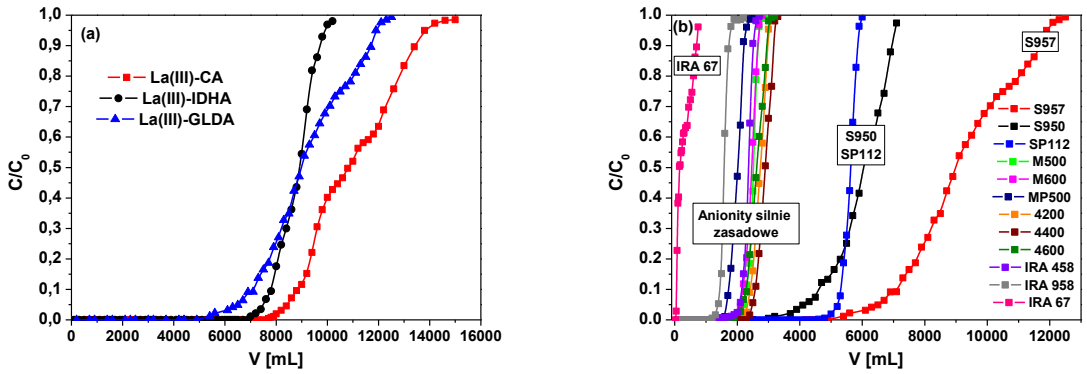

Rys. 1. Porównanie krzywych przebicia złoża (a) jonitu S957 podczas adsorpcji kompleksów La(III) z CA, IDHA oraz GLDA, (b) jonitów S957, S950, SP112, M500, M600, MP500, 4200, 4400, 4600, IRA 458, IRA 958 i IRA 67 podczas adsorpcji kompleksów La(III)-GLDA (C_0=1,0×10^{-3} M).

Dane eksperymentalne adsorpcji kompleksów La(III) z czynnikami kompleksującymi CA, IDHA oraz GLDA metodą dynamiczną przeanalizowano z zastosowaniem modeli matematycznych Thomasa, Adamsa-Boharta, Yoona-Nelsona i Wolborskiej. Modele te są jednymi z najczęściej wykorzystywanych w celu interpretacji danych dotyczących adsorpcji w kolumnach ze złożem stałym [48,49]. Należy jednak podkreślić, że stosując modele Thomasa oraz Yoona-Nelsona możliwy jest opis krzywych przebicia w całym ich zakresie, podczas gdy modele Adamsa-Boharta i Wolborskiej służą jedynie do opisu ich początkowej części (C/C_0<<1) [48]. Zastosowanie powyższych modeli pozwoliło na wyznaczenie istotnych parametrów, takich jak stałe szybkości, czas potrzebny do osiągnięcia 50% wyczerpania złoża, czy pojemności adsorpcyjne, które zostały przedstawione w [SD2], [SD3] i [SD4]. Analiza uzyskanych wyników pozwoliła stwierdzić, że jonit chelatujący S957 posiadał największą zdolność adsorpcji badanych kompleksów, co jest potwierdzeniem badań prowadzonych metodą statyczną. Zestawienie parametrów uzyskanych za pomocą modeli dla S957 podczas adsorpcji La(III) z biodegradowalnymi czynnikami kompleksującymi zaprezentowano w Tabeli 5.

Tabela 5. Parametry adsorpcji kompleksów La(III)-L wyznaczone na podstawie modeli Thomasa, Adamsa-Boharta, Yoona-Nelsona i Wolborskiej dla jonitu chelatującego S957.

Parametr	La(III)-CA	La(III)-IDHA	La(III)-GLDA
Model Thomasa			
$k_{Th} \times 10^3$ [mL/mg min]	5,06	11,01	4,52
q_0 [mg/g]	347,71	274,89	308,95
R^2	0,944	0,990	0,966
Model Adamsa-Boharta			
$k_{AB} \times 10^6$ [L/mg min]	6,46	9,20	2,32
q [mg/L]	116211,44	97678,56	130779,92
R^2	0,903	0,961	0,866
Model Yoona-Nelsona			
k_{YN} [1/min]	0,0007	0,0015	0,0007
τ [min]	18506,58	14595,54	15275,70
R^2	0,944	0,990	0,966
Model Wolborskiej			
β [1/min]	0,751	0,899	0,304
q [mg/L]	116211,44	97678,56	130779,92
R^2	0,903	0,961	0,866

Na podstawie wartości współczynników korelacji R^2 wykazano, że dla jonitu S957, modele Thomasa i Yoona-Nelsona nieco lepiej opisują uzyskane dane eksperymentalne. Porównanie parametrów wyznaczonych dla układów z poszczególnymi czynnikami kompleksującymi pokazuje, że w przypadku analizowanych jonów La(III) najwyższe wartości uzyskano dla adsorpcji w obecności CA.

7. Podsumowanie i wnioski

Badania zrealizowane w ramach przedstawionej rozprawy doktorskiej miały na celu określenie możliwości wykorzystania biodegradowalnych czynników kompleksujących (CA, IDHA, GLDA) w procesie adsorpcji wybranych pierwiastków ziem rzadkich (La(III), Nd(III) i Ho(III)) z zastosowaniem wymieniaczy jonowych różnego typu.

Pierwszym etapem badań była analiza w/w czynników kompleksujących, a także ich kompleksów z jonami Ln(III) przeprowadzona za pomocą miareczkowania potencjometrycznego. Pozwoliło to na szczegółowe opisanie procesu protonacji ligandów (wyznaczenie stałych protonacji) oraz tworzenia kompleksów Ln(III)-L (wyznaczenie stałych trwałości). Jako główne formy kompleksów zidentyfikowano typ LnL, kompleksy protonowane LnH_xL oraz hydroksokompleksy $LnL(OH)_x$. Na podstawie stałych trwałości stwierdzono, że najwyższą stabilnością charakteryzowały się kompleksy utworzone z czynnikiem kompleksującym GLDA. Kompleksy Ln(III)-CA były najmniej trwałe.

Do badań adsorpcyjnych wytypowano 12 jonitów, które poddano charakterystyce fizykochemicznej. Posiadały one ziarna o kulistym kształcie i w zależności od typu struktury (makroporowate lub żelowe) różną morfologię powierzchni. Wybrane charakteryzowały się niezbyt rozwiniętą powierzchnią właściwą i obecnością mezoporów w strukturze. Po adsorpcji kompleksów Ln(III)-L różnice zaobserwowano w przypadku jonitów żelowych, gdzie powierzchnia ta stała się bardziej zwarta i upakowana. Wyznaczono wartości punktu ładunku zerowego pH_{pzc} jonitów, które mieściły się w zakresie od 1,60 do 9,82. Analiza FTIR wykazała obecność typowych dla badanych jonitów grup funkcyjnych i potwierdziła skuteczną adsorpcję kompleksów Ln(III)-L na anionitach oraz na wymieniaczach jonowych S957, S950 i SP112, gdzie proces zachodzi poprzez wiązanie przez grupy funkcyjne jonów Ln(III), uwolnionych podczas rozpadu kompleksów w fazie jonitu. Na podstawie widm uzyskanych metodą XPS można wnioskować, że główny mechanizm adsorpcji oparty jest na wymianie jonowej.

Adsorpcję jonów Ln(III) w obecności czynników kompleksujących CA, IHDA oraz GLDA przeprowadzono metodą statyczną analizując wpływ masy jonitu, stosunku molowego Ln(III):L, pH roztworu, czasu prowadzenia procesu, stężenia początkowego roztworu oraz temperatury, co pozwoliło na wybór najbardziej korzystnych parametrów pozwalających uzyskać najwyższe pojemności adsorpcyjne. Stwierdzono, że rodzaj wymieniacza jonowego ma kluczowy wpływ na optymalizację warunków procesu.

Adsorpcja kompleksów Ln(III) z CA, IDHA oraz GLDA na badanych jonitach była procesem szybkim. W większości układów możliwe było usunięcie ponad 93% kompleksów

w czasie do 60 minut. Badania kinetyczne wykazały, że zarówno model PFO, jak i PSO znajdują zastosowanie do opisu danych eksperymentalnych, przy czym jest to zależne od czynnika kompleksującego, typu wymieniacza jonowego, a w pewnych przypadkach także od jonu Ln(III) obecnego w układzie. Modele dyfuzyjne potwierdziły, że adsorpcja kompleksów Ln(III)-L jest procesem złożonym, którego szybkość warunkowana jest przez dyfuzję w warstwie granicznej oraz dyfuzję wewnątrzziarnową.

Na podstawie badań równowagowych stwierdzono, że jonitem charakteryzującym się największym powinowactwem do kompleksów Ln(III) zarówno z CA, IDHA oraz GLDA był jonit chelatujący S957, a najwyższą pojemność adsorpcyjną uzyskano w stosunku do kompleksów Ho(III)-CA wynoszącą 180,26 mg/g.

Wykazano, że adsorpcja jonów Ln(III) w obecności CA, IDHA oraz GLDA na badanych jonitach to proces spontaniczny o znacznym udziale oddziaływań fizycznych. Podwyższenie temperatury zwiększało zdolności adsorpcyjne jonitów polistyrenowych (proces endotermiczny), podczas gdy dla jonitów poliakrylowych zaobserwowano obniżenie efektywności (proces egzotermiczny).

Anionity wykazywały bardzo dobrą podatność na regenerację (do 100%) z zastosowaniem kwasów HCl oraz HNO_3. Odzysk jonów Ln(III) z jonitów chelatujących S957, S950 oraz kationitu SP112 był utrudniony (poniżej 69%), co wskazuje na konieczność dalszych badań nad wyborem bardziej efektywnych czynników desorbujących. Na podstawie cykli adsorpcji/desorpcji potwierdzono, że jonity polistyrenowe wykazują lepszą zdolność do regeneracji w porównaniu z poliakrylowymi.

Badania przeprowadzone w układach kolumnowych nie tylko potwierdziły wysoką skuteczność S957 w porównaniu do innych jonitów, ale i wykluczyły anionit słabo zasadowy IRA 67 jako nieodpowiedni do zastosowania w procesie adsorpcji kompleksów Ln(III) z CA, IDHA lub GLDA.

Zaprezentowane w niniejszej rozprawie doktorskiej wyniki badań dowodzą, że biodegradowalne i bezpieczne dla środowiska czynniki kompleksujące takie jak kwas cytrynowy, kwas iminodibursztynowy oraz kwas glutaminodioctowy charakteryzują się bardzo dobrymi właściwościami kompleksującymi w stosunku do jonów pierwiastków ziem rzadkich. Poprzez dobór odpowiednich parametrów związki te mogą zostać z powodzeniem wykorzystane w procesie odzysku REE metodą adsorpcji. Ponadto mogą być alternatywą dla konwencjonalnych ligandów tego typu.

8. Literatura

[1] V. Balaram, Rare earth elements: A review of applications, occurrence, exploration, analysis, recycling, and environmental impact, Geosci. Front. 10 (2019) 1285–1303.

[2] T. Dutta, K.H. Kim, M. Uchimiya, E.E. Kwon, B.H. Jeon, A. Deep, S.T. Yun, Global demand for rare earth resources and strategies for green mining, Environ. Res. 150 (2016) 182–190.

[3] H. Liu, S. Li, B. Wang, K. Wang, R. Wu, C. Ekberg, A.A. Volinsky, Multiscale recycling rare earth elements from real waste trichromatic phosphors containing glass, J. Clean. Prod. 238 (2019) 117998.

[4] M. Petranikova, I. Herdzik-Koniecko, B.M. Steenari, C. Ekberg, Hydrometallurgical processes for recovery of valuable and critical metals from spent car NiMH batteries optimized in a pilot plant scale, Hydrometallurgy. 171 (2017) 128–141.

[5] N. Schaeffer, H. Passos, I. Billard, N. Papaiconomou, J.A.P. Coutinho, Recovery of metals from waste electrical and electronic equipment (WEEE) using unconventional solvents based on ionic liquids, Crit. Rev. Environ. Sci. Technol. 48 (2018) 859–922.

[6] N. Um, Hydrometallurgical recovery process of rare earth elements from waste: Main application of acid leaching with devised τ-T diagram, in: J.E.A. Orjuela (Ed.), Rare Earth Elem., IntechOpen, 2017: pp. 41–60.

[7] T.B. da Costa, M.G.C. da Silva, M.G.A. Vieira, Recovery of rare-earth metals from aqueous solutions by bio/adsorption using non-conventional materials: a review with recent studies and promising approaches in column applications, J. Rare Earths. 38 (2020) 339–355.

[8] N. Kržišnik, A. Mladenovič, A.S. Škapin, L. Škrlep, J. Ščančar, R. Milačič, Nanoscale zero-valent iron for the removal of Zn^{2+}, Zn(II)-EDTA and Zn(II)-citrate from aqueous solutions, Sci. Total Environ. 476–477 (2014) 20–28.

[9] G.P. Nayaka, J. Manjanna, K. V. Pai, R. Vadavi, S.J. Keny, V.S. Tripathi, Recovery of valuable metal ions from the spent lithium-ion battery using aqueous mixture of mild organic acids as alternative to mineral acids, Hydrometallurgy. 151 (2015) 73–77.

[10] S.M. Grimes, N.G. Yasri, A.J. Chaudhary, Recovery of critical metals from dilute leach solutions – Separation of indium from tin and lead, Inorganica Chim. Acta. 461 (2017) 161–166.

[11] I.S.S. Pinto, I.F.F. Neto, H.M.V.M. Soares, Biodegradable chelating agents for industrial, domestic, and agricultural applications-a review, Environ. Sci. Pollut. Res. 21 (2014) 11893–11906.

[12] J. Wen, S.P. Stacey, M.J. McLaughlin, J.K. Kirby, Biodegradation of rhamnolipid, EDTA

and citric acid in cadmium and zinc contaminated soils, Soil Biol. Biochem. 41 (2009) 2214–2221.

[13] Z. Cokesa, H.J. Knackmuss, P.G. Rieger, Biodegradation of all stereoisomers of the EDTA substitute iminodisuccinate by *Agrobacterium tumefaciens* BY6 requires an epimerase and a stereoselective C-N lyase, Appl. Environ. Microbiol. 70 (2004) 3941–3947.

[14] C.G. van Ginkel, R. Geerts, Biodegradation of N,N-bis(carboxymethyl)-L-glutamate and its utilization as sole source of carbon, nitrogen, and energy by a *Rhizobium radiobacter* strain in seawater, Toxicol. Environ. Chem. 98 (2016) 26–35.

[15] J.J. Lucena, J.A. Sentís, M. Villén, T. Lao, M. Pérez-Sáez, IDHA chelates as a micronutrient source for green bean and tomato in fertigation and hydroponics, Agron. J. 100 (2008) 813–818.

[16] G. Wang, X. Pan, S. Zhang, Q. Zhong, W. Zhou, X. Zhang, J. Wu, M.G. Vijver, W.J.G.M. Peijnenburg, Remediation of heavy metal contaminated soil by biodegradable chelator–induced washing: Efficiencies and mechanisms, Environ. Res. 186 (2020) 109554.

[17] F. Masoudi, M. Shirvani, H. Shariatmadari, M.R. Sabzalian, Performance of new biodegradable chelants in enhancing phytoextraction of heavy metals from a contaminated calcareous soil, J. Environ. Heal. Sci. Eng. 18 (2020) 655–664.

[18] H. Guan, L. Dong, Y. Zhang, S. Bai, L. Yan, GLDA and EDTA assisted phytoremediation potential of *Sedum hybridum* 'Immergrunchen' for Cd and Pb contaminated soil, Int. J. Phytoremediation. 24 (2022) 1395–1404.

[19] S. Lagergren, About the theory of so-called adsorption of soluble substances, K. Sven. Vetenskapsakademiens Handl. 24 (1898) 1–39.

[20] G. Blanchard, M. Maunaye, G. Martin, Removal of heavy metals from waters by means of natural zeolites, Water Res. 18 (1984) 1501–1507.

[21] W.J. Weber, J.C. Morris, Kinetics of adsorption on carbon from solution, J. Sanit. Eng. Div. 89 (1963) 31–60.

[22] G.E. Boyd, A.W. Adamson, L.S. Myers, The exchange adsorption of ions from aqueous solutions by organic zeolites II. Kinetics, J. Am. Chem. Soc. 69 (1947) 2836–2848.

[23] H.X. Zhu, X.J. Cao, Y.C. He, Q.P. Kong, H. He, J. Wang, Removal of Cu^{2+} from aqueous solutions by the novel modified bagasse pulp cellulose: Kinetics, isotherm and mechanism, Carbohydr. Polym. 129 (2015) 115–126.

[24] I. Langmuir, The adsorption of gases on plane surfaces of glass, mica and platinum, J. Am. Chem. Soc. 40 (1918) 1361–1403.

[25] H.M.F. Freundlich, Over the adsorption in solution, J. Phys. Chem. 57 (1906) 385–471.

[26] M.I. Temkin, V. Pyzhev, Kinetics of ammonia synthesis on promoted iron catalysts, Acta

Physicochim. URSS. 12 (1940) 327–356.

[27] S.K. Milonjić, A consideration of the correct calculation of thermodynamic parameters of adsorption, J. Serbian Chem. Soc. 72 (2007) 1363–1367.

[28] H.C. Thomas, Heterogeneous ion exchange in a flowing system, J. Am. Chem. Soc. 66 (1944) 1664–1666.

[29] G.S. Bohart, E.Q. Adams, Some aspects of the behavior of charcoal with respect to chlorine, J. Am. Chem. Soc. 42 (1920) 523–544.

[30] Y.H. Yoon, J.H. Nelson, Application of gas adsorption kinetics I. A theoretical model for respirator cartridge service life, Am. Ind. Hyg. Assoc. J. 45 (1984) 509–516.

[31] A. Wolborska, Adsorption on activated carbon of p-nitrophenol from aqueous solution, Water Res. 23 (1989) 85–91.

[32] A.M.N. Silva, X. Kong, R.C. Hider, Determination of the pKa value of the hydroxyl group in the α-hydroxycarboxylates citrate, malate and lactate by $_{13}$C NMR: implications for metal coordination in biological systems, Biometals. 22 (2009) 771–778.

[33] A.M. Cardenas-Peña, J.G. Ibanez, R. Vasquez-Medrano, Determination of the point of zero charge for electrocoagulation precipitates from an iron anode, Int. J. Electrochem. Sci. 7 (2012) 6142–6153.

[34] R.C. Oliveira, P. Hammer, E. Guibal, J.M. Taulemesse, O. Garcia, Characterization of metal-biomass interactions in the lanthanum(III) biosorption on *Sargassum* sp. using SEM/EDX, FTIR, and XPS: Preliminary studies, Chem. Eng. J. 239 (2014) 381–391.

[35] A. Shukla, Y.-H. Zhang, P. Dubey, J.L. Margrave, S.S. Shukla, The role of sawdust in the removal of unwanted materials from water, J. Hazard. Mater. B95 (2002) 137–152.

[36] C. Stöhr, J. Horst, W.H. Höll, Application of the surface complex formation model to ion exchange equilibria - Part V. Adsorption of heavy metal salts onto weakly basic anion exchangers, React. Funct. Polym. 49 (2001) 117–132.

[37] C. Xiong, J. Zhu, C. Shen, Q. Chen, Adsorption and desorption of praseodymium(III) from aqueous solution using D72 resin, Chinese J. Chem. Eng. 20 (2012) 823–830.

[38] F. Zhou, J. Feng, X. Xie, B. Wu, Q. Liu, X. Wu, R. Chi, Adsorption of lanthanum(III) and yttrium(III) on kaolinite: Kinetics and adsorption isotherms, Physicochem. Probl. Miner. Process. 55 (2019) 928–939.

[39] K. Burdzy, Y.-G. Chen, G.-Y. Lv, S.-H. Chen, D. Kołodyńska, Application of ion exchangers with the N-methyl-D-glucamine groups in the V(V) ions adsorption process, Materials. 15 (2022) 1026.

[40] Z. Aksu, A.I. Tatli, Ö. Tunç, A comparative adsorption/biosorption study of Acid Blue 161: Effect of temperature on equilibrium and kinetic parameters, Chem. Eng. J. 142

(2008) 23–39.

[41] M. Al-Ghouti, M.A.M. Khraisheh, M.N.M. Ahmad, S. Allen, Thermodynamic behaviour and the effect of temperature on the removal of dyes from aqueous solution using modified diatomite: A kinetic study, J. Colloid Interface Sci. 287 (2005) 6–13.

[42] A.E. Ofomaja, Y.S. Ho, Equilibrium sorption of anionic dye from aqueous solution by palm kernel fibre as sorbent, Dye. Pigment. 74 (2007) 60–66.

[43] W. Konicki, M. Aleksandrzak, E. Mijowska, Equilibrium, kinetic and thermodynamic studies on adsorption of cationic dyes from aqueous solutions using graphene oxide, Chem. Eng. Res. Des. 123 (2017) 35–49.

[44] V.S. Munagapati, D.S. Kim, Equilibrium isotherms, kinetics, and thermodynamics studies for congo red adsorption using calcium alginate beads impregnated with nano-goethite, Ecotoxicol. Environ. Saf. 141 (2017) 226–234.

[45] I. Anastopoulos, A. Bhatnagar, E.C. Lima, Adsorption of rare earth metals: A review of recent literature, J. Mol. Liq. 221 (2016) 954–962.

[46] R.M. Ashour, A.F. Abdel-Magied, A.A. Abdel-khalek, O.S. Helaly, M.M. Ali, Preparation and characterization of magnetic iron oxide nanoparticles functionalized by L-cysteine: Adsorption and desorption behavior for rare earth metal ions, J. Environ. Chem. Eng. 4 (2016) 3114–3121.

[47] H. Patel, Fixed-bed column adsorption study: a comprehensive review, Appl. Water Sci. 9 (2019) 1–17.

[48] M.S. Podder, C.B. Majumder, Biological detoxification of As(III) and As(V) using immobilized bacterial cells in fixed-bed bio-column reactor: Prediction of kinetic parameters, Groundw. Sustain. Dev. 6 (2018) 14–42.

[49] A. Katsigiannis, C. Noutsopoulos, J. Mantziaras, M. Gioldasi, Removal of emerging pollutants through Granular Activated Carbon, Chem. Eng. J. 280 (2015) 49–57.

9. Streszczenie w języku polskim

Rozwój nowoczesnych technologii corocznie zwiększa zapotrzebowanie przemysłu na metale takie jak pierwiastki ziem rzadkich (REE), które zostały uznane za surowce krytyczne pod względem dostępności. Duże rozproszenie złóż w skorupie ziemskiej, problematyczne pozyskiwanie oraz ich rozdzielanie doprowadziły do dominacji Chin na światowym rynku REE, co powoduje wiele obaw o zapewnienie ciągłości dostaw oraz utrzymanie cen na poziomie opłacalności produkcyjnej. Dlatego też tematem wielu badań jest możliwość recyklingu REE ze źródeł wtórnych, np. sprzętów elektronicznych, co pozwoliłoby na zabezpieczenie zasobów tych wartościowych pierwiastków. W procesach odzysku jonów metali szeroko stosowaną metodą jest adsorpcja, dysponująca szeroką gamą adsorbentów różnego rodzaju, w tym grupą wymieniaczy jonowych.

W zaprezentowanej rozprawie doktorskiej opisane zostały zagadnienia dotyczące zastosowania czynników kompleksujących, należących do grupy związków biodegradowalnych (kwas cytrynowy, kwas iminodibursztynowy, kwas glutaminodioctowy), w procesie adsorpcji jonów pierwiastków ziem rzadkich z wykorzystaniem wymieniaczy jonowych różniących się matrycą, grupami funkcyjnymi, wielkością ziarna oraz strukturą.

Analizie poddano kompleksy biodegradowalnych czynników kompleksujących tworzone z jonami REE i wyznaczono ich stałe trwałości. Opisu właściwości fizykochemicznych 12 wytypowanych do badań wymieniaczy jonowych, zarówno przed jak i po procesie adsorpcji kompleksów, dokonano stosując metody skaningowej mikroskopii elektronowej, spektroskopii w podczerwieni z transformatą Fouriera, spektroskopii fotoelektronów w zakresie promieniowania rentgenowskiego, miareczkowania potencjometrycznego oraz dryftu, a także analizy sitowej. Proces adsorpcji z zastosowaniem metody statycznej przeprowadzono dla wybranych REE (La(III), Nd(III) i Ho(III)) rozpatrując wpływ takich warunków procesu jak masa jonitu, stosunek molowy Ln(III):L, pH roztworu, czas kontaktu faz, stężenie początkowe roztworu oraz temperatura. Wykazano wysoką zależność efektywności adsorpcji od w/w parametrów. Istotnym etapem była ocena możliwości ponownego zastosowania wymieniaczy jonowych. Uzyskane wyniki zweryfikowano przeprowadzając adsorpcję kompleksów Ln(III)-L metodą dynamiczną, powszechnie stosowaną w procesach przemysłowych. Dane eksperymentalne zostały opisane za pomocą modeli kinetycznych pseudo-pierwszego rzędu, pseudo-drugiego rzędu, dyfuzji wewnątrzziarnowej, Boyda oraz Dumwalda-Wagnera, modeli izoterm Langmuira, Freundlicha oraz Temkina, a także modeli wyjaśniających dynamikę adsorpcji w układach kolumnowych

Thomasa, Adamsa-Boharta, Yoona-Nelsona oraz Wolborskiej. Wyznaczono ponadto parametry termodynamiczne adsorpcji kompleksów. Ta szczegółowa analiza umożliwiła określenie szybkości adsorpcji, wskazanie mechanizmu oraz natury procesu.

Przedstawione wyniki badań adsorpcji kompleksów pierwiastków ziem rzadkich z kwasem cytrynowym, kwasem iminodibursztynowym oraz kwasem glutaminodioctowym dowodzą, że biodegradowalne czynniki kompleksujące wykazują bardzo dobre właściwości kompleksujące i po odpowiedniej optymalizacji procesu mogą zostać z powodzeniem wykorzystane w recyklingu REE, jednocześnie eliminując negatywny wpływ na środowisko tradycyjnych słabo biodegradowalnych ligandów.

10. Streszczenie w języku angielskim

The development of modern technologies results in the annual increase in the demand for metals such as rare earth elements (REEs), which were identified as critical raw materials with risk availability. The large dispersion of deposits in the earth crust, problematic sourcing and separation led to the dominance of China on the global REE market, which raises a lot of concern about ensuring constant supply and maintaining prices at a viable production level. Therefore, the topic of many studies is the possibility of REEs recycling from secondary sources, such as electronic equipment, which would help safeguard the resources of these valuable elements. The recommended method in the metal ion recovery processes is adsorption, which employs a wide range of adsorbents of various types, including a group of ion exchangers.

The presented doctoral dissertation describes the issues concerning the application of complexing agents belonging to the group of biodegradable compounds (citric acid, iminodisuccinic acid, and glutamic acid) in the adsorption process of rare earth element ions using ion exchangers differing in matrix, functional groups, bead size, and structure.

The complexes of biodegradable complexing agents formed with REE ions were analyzed, and their stability constants were determined. The physicochemical properties of the 12 ion exchangers selected for the study, both before and after the complexes adsorption, were described using scanning electron microscopy, Fourier transform infrared spectroscopy, X-ray photoelectron spectroscopy, potentiometric titration and drift method, as well as sieve analysis. Using the static method the adsorption process was carried out for selected REE (La(III), Nd(III) and Ho(III)) considering the influence of such process conditions as ion exchanger mass, Ln(III):L molar ratio, solution pH, phase contact time, initial solution concentration, and temperature. The adsorption efficiency proved to be largely dependent on the studied factors. An important step was to evaluate the feasibility of the ion exchangers reuse. The obtained results were verified conducting the adsorption of Ln(III)-L complexes by means of the dynamic method commonly used in industrial processes. The experimental data were described using the pseudo-first order, pseudo-second order, intraparticle diffusion, Boyd and Dumwald-Wagner kinetic models, Langmuir, Freundlich, and Temkin isotherm models as well as the models explaining adsorption dynamics in the column systems by Thomas, Adams-Bohart, Yoon-Nelson, and Wolborska. In addition, the thermodynamic parameters of the complexes adsorption were determined. This detailed analysis made it possible to determine the adsorption rate and to identify the mechanism and nature of the process.

The presented results of the adsorption studies of rare earth element complexes with citric acid, iminodisuccinic acid, and glutamic acid prove very good complexing properties of the biodegradable complexing agents and that, after the appropriate process optimization, they can be successfully used in the REE recycling while eliminating the negative environmental impact of the traditional poorly biodegradable ligands.

11. Dorobek naukowy

Wykaz publikacji naukowych w czasopismach indeksowanych w bazie JCR będących podstawą rozprawy doktorskiej:

1. **K. Araucz**, A. Aurich, D. Kołodyńska, *Novel multifunctional ion exchangers for metal ions removal in the presence of citric acid*, Chemosphere, 251 (2020) 126331, doi:10.1016/j.chemosphere.2020.126331, IF_{2020} 7,086, 100 pkt MEiN.
2. **K. Burdzy**, A. Aurich, S. Hunger, R. Jastrząb, M. Zabiszak, D. Kołodyńska, *Green citric acid in the sorption process of rare earth elements*, Chemical Engineering Journal, 437 (2022) 135366, doi:10.1016/j.cej.2022.135366, IF_{2022} 16,744, 200 pkt MEiN.
3. **K. Burdzy**, Y. Ju, D. Kołodyńska, *Iminodisuccinic acid (IDHA) as an effective biodegradable complexing agent in the adsorption process of La(III), Nd(III) and Ho(III) ions*, Chemical Engineering Journal, 461 (2023) 142059, doi:10.1016/j.cej.2023.142059, IF_{2022} 16,744, 200 pkt MEiN.
4. **K. Burdzy**, R. Jastrząb, D. Kołodyńska, *GLDA and ion exchangers: unlocking sustainable solutions for recovery of rare earth elements*, Sustainable Materials and Technologies (2023) – w recenzji.

Rozdziały w monografiach:

1. **K. Araucz**, D. Fila, D. Kołodyńska, *Ocena efektywności sorpcji jonów lantanu(III) i niklu(II) na jonitach Purolite S957 i Diphonix*, w: Nauka i przemysł – lubelskie spotkania studenckie (red. D. Kołodyńska), Wydawnictwo UMCS, Lublin 2019, ISBN 978-83-227-9220-9, str. 13-16.
2. **K. Araucz**, D. Kołodyńska, *IDHA, EDDS i GLDA jako czynniki kompleksujące w procesie sorpcji lantanu(III)*, w: Nauka i przemysł – metody spektroskopowe w praktyce, nowe wyzwania i możliwości (red. Z. Hubicki), Wydawnictwo UMCS, Lublin 2020, ISBN 978-83-227-9369-5, str. 461-469.
3. **K. Araucz**, D. Kołodyńska, *Usuwanie pierwiastków ziem rzadkich w obecności biodegradowalnych czynników kompleksujących na jonicie Purolite S957*, w: Nauka i przemysł – lubelskie spotkania studenckie (red. D. Kołodyńska), Wydawnictwo UMCS, Lublin 2020, ISBN 978-83-227-9370-1, str. 15-18.

4. **K. Araucz,** A. Aurich, D. Kołodyńska, *Ocena wpływu kwasu cytrynowego na proces adsorpcji jonów La(III), Nd(III) i Ho(III)*, w: Nauka i przemysł – metody spektroskopowe w praktyce, nowe wyzwania i możliwości (red. Z. Hubicki), Wydawnictwo UMCS, Lublin 2021, ISBN 978-83-227-9504-0, str. 351-355.
5. **K. Burdzy**, D. Kołodyńska, *IDHA – zielona alternatywa w procesie adsorpcji pierwiastków ziem rzadkich*, w: Nauka i przemysł – lubelskie spotkania studenckie (red. D. Kołodyńska), Wydawnictwo UMCS, Lublin 2022, ISBN 978-83-227-9603-0, str. 262-265.
6. **K. Burdzy,** D. Ogórek, D. Kołodyńska, *Adsorpcja kompleksów lantanu(III) z kwasem iminodibursztynowym metodą kolumnową*, w: Nauka i przemysł – metody spektroskopowe w praktyce, nowe wyzwania i możliwości (red. Z. Hubicki), Wydawnictwo UMCS, Lublin 2022, ISBN 978-83-227-9602-3, str. 424-427.
7. **K. Burdzy**, D. Kołodyńska, *GLDA - wysoce efektywny i biodegradowalny czynnik kompleksujący w procesie adsorpcji pierwiastków ziem rzadkich*, w: Nauka i przemysł – lubelskie spotkania studenckie (red. D. Kołodyńska), Wydawnictwo UMCS, Lublin 2023, ISBN 978-83-227-9701-3, str. 250-253.
8. **K. Burdzy**, D. Kołodyńska, *Badania potencjometryczne kompleksów lantanowców z kwasem glutaminodioctowym*, w: Nauka i przemysł – metody spektroskopowe w praktyce, nowe wyzwania i możliwości (red. Z. Hubicki), Wydawnictwo UMCS, Lublin 2023, ISBN 978-83-227-9700-6, str. 247-250.

Wystąpienia konferencyjne:

1. **K. Araucz**, D. Fila, D. Kołodyńska, *Ocena efektywności sorpcji jonów lantanu(III) i niklu(II) na jonitach Purolite S957 i Diphonix*, VII Ogólnopolskie Sympozjum „Nauka i przemysł – lubelskie spotkania studenckie", Lublin, 24.06.2019 r. (poster).
2. **K. Araucz**, A. Aurich, D. Kołodyńska, *Kwas cytrynowy jako czynnik kompleksujący w procesie sorpcji jonów La(III)*, Interdyscyplinarna Konferencja Naukowa „Green Week 2020: Nowy początek dla ludzkości i natury", Lublin, 21.10.2020 r. (poster).
3. **K. Araucz**, A. Aurich, D. Kołodyńska, *Zastosowanie anionitów akrylowych w procesie odzysku lantanowców w obecności kwasu cytrynowego*, Interdyscyplinarna Konferencja Naukowa „Green Week 2020: Nowy początek dla ludzkości i natury", Lublin, 21.10.2020 r. (poster).

4. **K. Araucz**, A. Aurich, D. Kołodyńska, *Sorpcja kompleksów La(III) z kwasem cytrynowym na jonitach chelatujących*, Interdyscyplinarna Konferencja Naukowa „Green Week 2020: Nowy początek dla ludzkości i natury", Lublin, 21.10.2020 r. (poster).
5. **K. Araucz**, A. Aurich, D. Kołodyńska, *Zastosowanie kwasu cytrynowego jako naturalnego czynnika kompleksującego w procesie adsorpcji pierwiastków ziem rzadkich*, II Interdyscyplinarna Konferencja Doktorantów Nauk Biologicznych „BIO-IDEA 2021", Lublin, 15.05.2021 r. (komunikat).
6. **K. Araucz**, A. Aurich, D. Kołodyńska, *Ocena wpływu kwasu cytrynowego na proces adsorpcji jonów La(III), Nd(III) i Ho(III)*, XIV Ogólnopolskie Sympozjum „Nauka i przemysł – metody spektroskopowe w praktyce, nowe wyzwania i możliwości", Lublin, 29-30.06.2021 r. (poster).
7. **K. Araucz**, A. Aurich, D. Kołodyńska, *Citric acid as a natural complexing agent in the rare earth elements recovery process*, 15th International interdisciplinary conference "Current Environmental Issues-2021", Białystok, 22-24.09.2021 r. (poster).
8. **K. Burdzy**, A. Aurich, D. Kołodyńska, *Green complexing agent - citric acid in the adsorption process*, 13th International Conference on Agrophysics: Agriculture in changing climate, Lublin, 15-16.11.2021 r. (poster).
9. **K. Burdzy**, D. Kołodyńska, *IDHA - biodegradable complexing agent in the adsorption of rare earth elements*, 9th International Conference on Sustainable Solid Waste Management, Corfu, Greece, 15-18.06.2022 r. (poster).
10. **K. Burdzy**, D. Kołodyńska, *IDHA - zielona alternatywa w procesie adsorpcji pierwiastków ziem rzadkich*, X Ogólnopolskie Sympozjum „Nauka i przemysł – lubelskie spotkania studenckie", Lublin, 27.06.2022 r. (komunikat).
11. **K. Burdzy**, D. Ogórek, D. Kołodyńska, *Adsorpcja kompleksów lantanu(III) z kwasem iminodibursztynowym metodą kolumnową*, XV Ogólnopolskie Sympozjum „Nauka i Przemysł - metody spektroskopowe w praktyce, nowe wyzwania i możliwości", Lublin, 28-29.06.2022 r. (poster).
12. **K. Burdzy**, D. Kołodyńska, *Optymalizacja procesu adsorpcji pierwiastków ziem rzadkich w obecności kwasu iminodibursztynowego*, 64. Zjazd Naukowy Polskiego Towarzystwa Chemicznego, Lublin, 11-16.09.2022 r. (komunikat).
13. **K. Burdzy**, D. Kołodyńska, *Proces adsorpcji kompleksów lantanu(III) z kwasem glutaminodioctowym z zastosowaniem metody dynamicznej*, 46. Międzynarodowe

Seminarium Naukowo-Technicznego „Chemistry for Agriculture”, Karpacz, 20-23.11.2022 r. (poster).

14. **K. Burdzy**, D. Kołodyńska, *Zastosowanie kwasu glutaminodioctowego w procesie usuwania jonów lantanowców*, 46. Międzynarodowe Seminarium Naukowo-Technicznego „Chemistry for Agriculture”, Karpacz, 20-23.11.2022 r. (poster).
15. **K. Burdzy**, D. Kołodyńska, *GLDA - wysoce efektywny i biodegradowalny czynnik kompleksujący w procesie adsorpcji pierwiastków ziem rzadkich*, XI Ogólnopolskie Sympozjum „Nauka i przemysł – lubelskie spotkania studenckie”, Lublin, 26.06.2023 r. (komunikat).
16. **K. Burdzy**, D. Kołodyńska, *Badania potencjometryczne kompleksów lantanowców z kwasem glutaminodioctowym*. XVI Ogólnopolskie Sympozjum „Nauka i Przemysł - metody spektroskopowe w praktyce, nowe wyzwania i możliwości”, Lublin, 27-29.06.2023 r. (poster).

Projekty badawcze:

1. Projekt badawczy Narodowego Centrum Badań i Rozwoju „Nowe związki kompleksowe lantanowców dla technologii światłowodów do laserów włóknowych i wzmacniaczy optycznych” - akronim projektu REEPHOT” w ramach Działania 4.1 Poddziałanie 4.1.1. Strategiczne programy badawcze dla gospodarki Programu Operacyjnego Inteligentny Rozwój 2014-2020, Wspólne Przedsięwzięcie z Województwem Lubelskim w obszarze technologii fotonicznych, na podstawie umowy o dofinansowanie nr POIR.04.01.01-00-0040/17-00 z dnia: 07.12.2018 r., uczestnictwo w projekcie w okresie 18.03.2019 r. – 01.08.2019 r. oraz 23.10.2019 r. – 30.09.2020 r.
2. Projekt „Inkubator Innowacyjności 4.0” realizowany przez konsorcjum Uniwersytetu Marii Curie-Skłodowskiej w Lublinie oraz Uniwersytetu Medycznego w Lublinie w ramach programu „Inkubator Innowacyjności 4.0”, Wsparcie zarządzania badaniami naukowymi i komercjalizacja wyników prac B+R w jednostkach naukowych i przedsiębiorstwach, współfinansowanego z Programu Operacyjnego Inteligentny Rozwój 2014-2020 (Działanie 4.4), uczestnictwo w projekcie w okresie 01.07.2022 r. – 30.11.2022 r.

Nagrody:

1. III miejsce w konkursie na najlepszy plakat naukowy na Ogólnopolskim Sympozjum „Nauka i przemysł - lubelskie spotkania studenckie”, Lublin, 24.06.2019 r.
2. Stypendium dla najlepszych doktorantów z Własnego Funduszu Stypendialnego UMCS na rok akademicki 2022/2023.

Staże i szkolenia:

1. Staż naukowy w Zakładzie Chemii Koordynacyjnej Uniwersytetu im. Adama Mickiewicza w Poznaniu w okresie 08-14.12.2019 r.
2. Staż naukowy w Zakładzie Fizykochemii Materiałów Porowatych Instytutu Agrofizyki im. Bohdana Dobrzańskiego Polskiej Akademii Nauk w Lublinie w okresie 24.11.2021 r. - 24.12.2021 r.
3. Staż naukowy w Wydziale Laboratorium Chemicznego Kawęczyn PGNiG TERMIKA SA w Warszawie w okresie 20-31.03.2023 r.

Dorobek naukowy niewchodzący w skład rozprawy doktorskiej:

Wykaz publikacji naukowych w czasopismach indeksowanych w bazie JCR:

1. D. Kołodyńska, **K. Araucz**, *New titanium oxide sorbent for As(V) and Cr(VI) removal as well as La(III) and Nd(III) recovery*, Journal of Molecular Liquids, 315 (2020) 113720, doi:10.1016/j.molliq.2020.113720, IF_{2020} 5,065, 100 pkt MEiN.
2. **K. Burdzy**, Y.-G. Chen, G.-Y. Lv, S.-H. Chen, D. Kołodyńska, *Application of ion exchangers with the N-methyl-D-glucamine groups in the V(V) ions adsorption process*, Materials, 15 (2022) 1026, doi:10.3390/ma15031026, IF_{2022} 3,748, 140 pkt MEiN.
3. D. Kołodyńska, **K. Burdzy**, S. Hunger, A. Aurich, Y. Ju, *Green extractants in assisting recovery of REEs: A case study*, Molecules, 28 (2023) 965, doi:10.3390/molecules28030965, IF_{2022} 4,927, 100 pkt MEiN.

Rozdziały w monografiach:

1. **K. Araucz**, D. Kołodyńska, *Pozyskiwanie pierwiastków ziem rzadkich – przerób bastnezytu i monacytu*, w: Nauka i przemysł – metody spektroskopowe w praktyce, nowe wyzwania i możliwości (red. Z. Hubicki), Wydawnictwo UMCS, Lublin 2019, ISBN 978-83-227-9219-3, str. 584-592.
2. D. Fila, **K. Araucz**, Z. Hubicki, *Metody odzysku pierwiastków ziem rzadkich ze źródeł pierwotnych i wtórnych*, w: Nauka i przemysł – metody spektroskopowe w praktyce, nowe wyzwania i możliwości (red. Z. Hubicki), Wydawnictwo UMCS, Lublin 2019, ISBN 978-83-227-9219-3, str. 593-601.
3. P. Gierszewska, K. Głowacka, **K. Araucz**, W. Sofińska-Chmiel, Z. Hubicki, *Parametry adsorpcyjne jonów wanadu na anionitach – badania kinetyczne*, w: Nauka i przemysł – metody spektroskopowe w praktyce, nowe wyzwania i możliwości (red. Z. Hubicki), Wydawnictwo UMCS, Lublin 2020, ISBN 978-83-227-9369-5, str. 516-520.

Wystąpienia konferencyjne:

1. D. Fila, **K. Araucz**, Z. Hubicki, *Wymiana jonowa jako skuteczna metoda odzysku pierwiastków ziem rzadkich*, VI Ogólnopolska Konferencja Naukowa „Innowacje w praktyce", Lublin, 04-05.04.2019 r. (poster).
2. D. Fila, **K. Araucz**, Z. Hubicki, *Ocena możliwości wykorzystania jonitów chelatujących o ugrupowaniach aminofosfonowych w procesie odzysku jonów metali ze zużytych akumulatorów niklowo-wodorkowych (Ni-MH)*, VI Ogólnopolska Konferencja Naukowa „Innowacje w praktyce", Lublin, 04-05.04.2019 r. (komunikat).
3. D. Fila, **K. Araucz**, Z. Hubicki, *Odzysk jonów La(III) z roztworów pochodzących z ługowania baterii niklowo-wodorkowych za pomocą jonitów o ugrupowaniach iminodioctowych*, Ogólnopolska Konferencja Naukowa „Ochrona środowiska – rozwiązania i perspektywy", Lublin, 17.05.2019 r. (poster).
4. D. Fila, **K. Araucz**, Z. Hubicki, *Usuwanie jonów Ni(II) z roztworów kwaśnych za pomocą procesu wymiany jonowej*, Ogólnopolska Konferencja Naukowa „Ochrona środowiska – rozwiązania i perspektywy", Lublin, 17.05.2019 r. (poster).
5. **K. Araucz**, D. Fila, D. Kołodyńska, J. Gęga, Z, Hubicki, *Ługowanie jonów metali ciężkich ze szczególnym uwzględnieniem pierwiastków ziem rzadkich ze źródeł*

odpadowych, 54. Konferencja Mikrobiologiczna „Mikroorganizmy różnych środowisk", Lublin, 20-21.09.2021 r. (wykład plenarny).

6. J. Bąk, **K. Burdzy**, D. Fila, A. Gładysz-Płaska, Z. Hubicki, D. Kołodyńska, M. Wawrzkiewicz, A. Wołowicz, G. Wójcik, *Usuwanie zanieczyszczeń z wód i ścieków z zastosowaniem procesu adsorpcji*, 64. Zjazd Naukowy Polskiego Towarzystwa Chemicznego, Lublin, 11-16.09.2022 r. (poster).

Projekty badawcze:

1. Projekt badawczy Narodowego Centrum Nauki „Badanie wpływu starzenia biowęgli na ich właściwości oraz oddziaływanie z zanieczyszczeniami organicznymi i nieorganicznymi w kontekście ich toksyczności", na podstawie umowy o dofinansowanie UMO-2017/25/B/NZ8/02191 w ramach konkursu „OPUS 13" z dnia: 01.02.2018 r., uczestnictwo w projekcie w okresie 01.03.2018 r. – 31.01.2020 r.
2. Projekt badawczy Narodowego Centrum Nauki „Projektowanie i wytwarzanie funkcjonalnych matryc nieorganicznych metodami in situ oraz przez neutralizację odpadowych ścieków zawierających wanadany: właściwości, oddziaływania powierzchniowe, testy katalityczne i elektrochemiczne" na podstawie umowy o dofinansowanie UMO-2018/29/B/ST8/01122 w ramach konkursu „OPUS 15" z dnia: 01.03.2019 r., uczestnictwo w projekcie w okresie 01.11.2019 r. – 31.10.2021 r.

Staże i szkolenia:

1. Staż z projektu „Wiza na rynku pracy" w laboratorium chemicznym Biowet Puławy sp. z o.o. 03.07.2017 r. – 29.09.2017 r.
2. Szkolenie „Metody spektroskopowe w praktyce (FT-IR/Raman)" w dniach 13.05-16.05.2019 r. w ramach projektu „Zintegrowany UMCS", projekt realizowany w ramach Programu Operacyjnego Wiedza Edukacja Rozwój Oś III. Szkolnictwo wyższe dla gospodarki i rozwoju, Działanie 3.5 Kompleksowe programy szkół wyższych, na podstawie umowy o dofinansowanie nr POWR.03.05.00-00-Z012/17-00 w ramach zadania nr 2.

3. Kurs analiz chromatograficznych (GC/HPLC) w dniach 07.05-15.06.2019 r. w ramach projektu „Zintegrowany UMCS", projekt realizowany w ramach Programu Operacyjnego Wiedza Edukacja Rozwój Oś III. Szkolnictwo wyższe dla gospodarki i rozwoju, Działanie 3.5 Kompleksowe programy szkół wyższych, na podstawie umowy o dofinansowanie nr POWR.03.05.00-00-Z012/17-00 w ramach zadania nr 2.
4. Seminarium „Analiza wielopierwiastkowa (ASA, ICP-OES, ICP-MS), mikrofalowe i ekstrakcyjne techniki przygotowania próbek do analiz oraz spektroskopia molekularna (UV-Vis, FT-IR, spektroskopia Ramana i fluorescencyjna)" organizowane przez Perlan Technologies w Warszawie w dniu 22.11.2019 r.
5. Webinarium „Atomowa spektroskopia absorpcyjna oraz emisyjna spektrometria z wzbudzeniem w plazmie mikrofalowej w analizie pierwiastkowej" organizowane przez Perlan Technologies w dniu 02.07.2020 r.
6. Webinarium „High-End UV-VIS/NIR Spectroscopy: Application examples & tips and tricks for the use of integrating spheres" organizowane przez Perlan Technologies w dniu 29.10.2020 r.
7. Webinarium „Walidacja procesów czyszczenia" organizowane przez Perlan Technologies w dniu 01.12.2020 r.
8. Webinarium „Różne zastosowania spektroskopii molekularnej w badaniach naukowych" organizowane przez MS Spectrum w dniu 02.12.2020 r.
9. Webinarium „Spektrometria ICP-MS: eleganckie narzędzie w analizie wielopierwiastkowej" organizowane przez Perlan Technologies w dniu 10.12.2020 r.
10. Webinarium „Techniki emisyjne w oznaczeniach pierwiastków" organizowane przez Perlan Technologies w dniu 15.12.2020 r.
11. Webinarium „Analiza pierwiastkowa za pomocą spektrometrów ICP-MS firmy Analytik Jena" organizowane przez MS Spectrum w dniu 29.04.2021 r.
12. Webinarium „Spektrometria mas wybranych jonów z reakcyjną komorą przepływową – technologia SIFT-MS" organizowane przez Perlan Technologies w dniu 05.11.2021 r.
13. Webinarium „Analiza pierwiastkowa za pomocą spektrometrii atomowej i emisyjnej Analytik Jena" organizowane przez MS Spectrum w dniu 07.04.2022 r.

Oryginalne prace naukowe wraz z oświadczeniami

[D1] K. Araucz, A. Aurich, D. Kołodyńska, *Novel multifunctional ion exchangers for metal ions removal in the presence of citric acid*, Chemosphere, 251 (2020) 126331.

IF_{2020}: 7,086 **Punkty MEiN**: 100

Chemosphere 251 (2020) 126331

Contents lists available at ScienceDirect

Chemosphere

journal homepage: www.elsevier.com/locate/chemosphere

Novel multifunctional ion exchangers for metal ions removal in the presence of citric acid

Katarzyna Araucz [a], Andreas Aurich [b], Dorota Kołodyńska [a, *]

[a] Department of Inorganic Chemistry, Faculty of Chemistry, Maria Curie-Skłodowska University, M. Curie Skłodowska Sq. 2, 20-031, Lublin, Poland
[b] Environmental and Biotechnology Centre, Department Umwelt und Biotechnologisches Zentrum (UBZ), Helmholtz-Centre for Environmental Research-UFZ, Permoserstr. 15, 04318, Leipzig, Germany

HIGHLIGHTS

- Citric acid for NiMH recycling was proposed.
- A ion exchange process was developed for removal of REEs and HMs ions from battery leaching solution.
- Multifunctional ion exchangers Purolite S957 and Diphonix Resin® can be used to this aim.

GRAPHICAL ABSTRACT

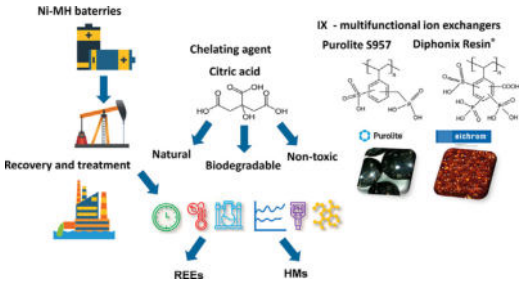

ARTICLE INFO

Article history:
Received 17 November 2019
Received in revised form
20 February 2020
Accepted 23 February 2020
Available online 26 February 2020

Handling Editor: Y. Yeomin Yoon

Keywords:
La(III)
Ni(II)
Citric acid
Purolite S957
Diphonix Resin®
Remediation
Sorption
Spent batteries

ABSTRACT

The present study deals with the potential application of Purolite S957 and Diphonix Resin® for the removal of rare earth elements from aqueous liquors as a result of the extraction of spent Ni-MH batteries in the presence of citric acid. The effects of the metal ion and the citric acid ratio, pH, ion exchanger dose, contact time, initial concentration and temperature were studied using the batch technique. The Langmuir and Freundlich adsorption isotherm models were used for the description of the adsorption process. The equilibrium adsorption data were fitted using the pseudo first order, pseudo second order, intraparticle diffusion, Boyd, film diffusion and Dumwald-Wagner models. The maximum adsorption capacity q_0 obtained from the Langmuir isotherm was found to be 46.63 mg/g for Ni(II) and 60.75 mg/g for La(III) on Purolite S957 as well as 46.55 mg/g for Ni(II) and 60.12 mg/g for La(III) on Diphonix Resin®. The kinetics followed the pseudo second order reaction. Based on the Weber-Morris model the adsorption process proved to proceed in two stages. Based on the Boyd model the rate controlling steps were film and intraparticle diffusions. The adsorption process was spontaneous and endothermic in nature. Reusability of ion exchangers in the desorption studies was also evaluated as a sustainable approach. The physicochemical properties of Purolite S957 and Diphonix Resin® were studied using the ASAP analysis, optical and scanning electron microscopy, potentiometric titration, pH_{PZC} and FT-IR as well as XPS analysis.

1. Introduction

Several methods can be used to remove rare earth elements (REEs) from the secondary sources such as waste electronic and

* Corresponding author.
E-mail address: d.kolodynska@poczta.umcs.lublin.pl (D. Kołodyńska).

https://doi.org/10.1016/j.chemosphere.2020.126331
0045-6535/

electrical equipment (WEEEs), mine coal combustion products (CCPs) and acid mine drainages (AMDs) and these are precipitation, ion exchange and extraction. A critical review on secondary wastes has been provided in (Binnemans et al., 2013) including a summary of different components containing REEs and heavy metal ions (HMs). It is well known that using 2 M H_2SO_4 it is possible to recover Ni(II) and other metal ions from Ni-MH batteries. After neutralization by NaOH (pH about 1.2) the lanthanides precipitate, however, the highest efficiency for La(III) can be obtained. After leaching, Fe(III) ions are usually the most predominant impurities and can be present at high concentrations (Agarwal et al., 2019). At pH 3.5 it is also possible to remove Fe(III) ions at a temperature higher than 353 K (increasing pH and temperature reduced the solubility of iron hydroxide) (Izadi et al., 2017). As follows from the literature data 2-ethylhexylphosphonic acid mono 2-ethylhexyl ester (PC88A) and bis(2,4,4-trimethylpentyl) phosphinic acid (Cyanex 272) have the potential to remove impurities like Fe(III), Cd(II) and Mn(II) whereas di-2-ethylheyxl phosphoric acid (D2EHPA) can be used for removal of Zn(II), Al(III) and Mn(II) at low pH values from leachates of spent Ni-MH. Typically Ni(II) and Co(II) ions are further separated by Cyanex 272. However, it should be pointed out that the REEs separation process and mechanism depend on the state in which REEs occur in the aqueous solutions (Akcil et al., 2018).

In the ion exchange process the presence of ligands in a solution changes both the mechanism and capacity of sorption due to the modification of metal speciation. In the recovery process, the complexing agents such as ethylenediaminetetraacetic (EDTA) and nitrilotriacetic (NTA) acids are used. However, despite their very good chelating properties these synthetic compounds have some disadvantages such as poor biodegradability. 2-hydroxy-1,2,3-propanotricarboxylic acid also known as 3-hydroxy-3-carboxy-pentanodiacetic acid or simply citric acid is a common organic acid containing three carboxyl and one hydroxyl groups. Therefore it is well known for its ability to form quite strong complexes with uranium. It is also known to remove metal ions from soils and wastewaters effectively. It is environmentally friendly, exhibits relatively consistent removal efficiency and is cost-effective. Citric acid forms different types of complexes with the transition metals, lanthanides and actinides (Rajan and Martell, 1965; Zabiszak et al., 2018). It has been used to extract plutonium from contaminated soils, to decontaminate the components of nuclear reactors and to extract metals and radionuclides, such as As(III,V), Ba(II), Cd(II), Cs(I), Co(II), Cu(II), Cr(III,V), Pb(II), Ni(II), Zn(II), Sr(II), Th(IV) and U(VI) from contaminated soils, wastes and municipal solid waste ashes. Exemplary, the extraction procedure using citric acid in combination with dithionite followed by the ammonium carbonate extraction allows to decrease U(VI) amounts from 450 to 540 mg/kg to less than 50 mg/kg (Francis et al., 1999). Citrates were used to chelate Fe(III) ions and prevent its precipitation, however, the efficiency is largely dependent on pH. Citric acid has several advantages as an extracting agent; (i) it biodegrades rapidly to carbon dioxide and water, making the treatment and disposal of the effluent more environmentally friendly, (ii) it is inexpensive and can be obtained as an industrial waste product and (iii) it offers a buffered system in contrast to sulphuric acid. One possible solution to obtain citric acid during the biosynthesis, as proposed in the INCOVER project whose aim is to develop innovative and sustainable added-value technologies for a resource recovery-based treatment of wastewater, is using smart operation monitoring and control methodologies (Aurich et al., 2017; Förster et al., 2007; Kamzolova et al., 2005). It is important because in the EU the citric acid consumption is 530,000 t/year, the annual import is about 200,000 t and the demand is expected to increase by 5% every year. Citric acid is used in many industrial processes as a cleaner, decalcifier, colour-stabilizer, acidulant and flavour enhancer. Citric acid is safe and can be used as food additives (Soccol et al., 2006).

The main objective of this study was to develop the strategy of heavy metals (HMs) and rare earth elements (REEs) removal from liquors obtained from the extraction of spent Ni-MH batteries as WEEEs. As follows form the literature the overall cost to process 1 t of Ni-MH batteries is at maximum US$ 50.00 and this produces 316 kg of Ni worth at least US$ 680.00 (Bertuol et al., 2006; Dvořák and Vu, 2015; Tenório and Espinosa, 2002). Obtaining the Ni(II) salts is well described, however, REEs, which can be obtained by the ion exchange separation, are also valuable. The assumption for this was the fact that the strong cation ion exchangers with the sulphonic functional groups were ineffective for selective uptake of useful rare earth metal ions. Therefore, for their preparation the ion exchangers with di- and trifunctional groups were used. The introduction of different functional groups improves the effectiveness of separation, adsorption kinetics and elution processes (Alexandratos, 2007; Smolik et al., 2014). Within this type of ion exchangers there can be distinguished: Purolite S957 which contains the phosphonic and sulphonic functional groups as well as Diphonix Resin® with 1,1-diphosphonic, sulphonic and carboxylic ones. The adsorption capacity was investigated by changing different parameters such as the different ratio of metal ions and citric acid solution, pH, ion exchanger dose, contact time as well as the initial concentration and temperature. Moreover, the adsorption mechanisms were examined studying kinetic and isotherm models. The reusability of ion exchangers was also evaluated as a sustainable approach.

2. Materials and methods

2.1. Materials characterization

Ni(II) and La(III) stock solutions were prepared using $Ni(NO_3)_2 \cdot 6H_2O$ and $La(NO_3)_3 \cdot H_2O$, respectively by dissolving a suitable amount of salt. The final concentration was estimated by the ICP-OES method. Ni(II) and La(III) working solutions were prepared by diluting stock solutions with deionized water before the use. Citric acid $C_6H_8O_7 \cdot H_2O$ was purchased from Chempur Company (Poland).

The chelating ion exchanger Purolite S957 produced by Purolite Ltd (Germany) contains the phosphonic and sulphonic functional groups. Diphonix Resin® produced by EiChrom Industries (France) contains geminally substituted diphosphonic, sulphonic and carboxylic acid groups covalently bonded to the polymer matrix (Silva et al., 2018). Both of them were used for the sorption of Ni(II) and La(III). Typical properties of both ion exchangers are collected in Table 1.

To avoid the changes of acidity during the studies the initial Na^+ form of the ion exchangers was converted to the H^+ one (Izadi et al., 2017). The changes of the pH during equilibration in the DI water are presented in Table 1. For both ion exchangers the additional physicochemical properties were determined.

Ion exchange capacity (IEC) represents the totality of active sites or functional groups responsible for the ion exchange process which was determined by the titration method (Contescu et al., 1997). The functional groups content was determined using the potentiometric titration methods. Purolite S957 and Diphonix Resin® were converted to the H^+ form, i.e. all acid groups obtain H^+ as counter ions and were titrated with 0.1 M NaOH. The titrations were made at room temperature with the variation ±1 °C. For this purpose the 907 Titrando titrator equipped with the 800 Dosino type dosing systems, 801 type magnetic stirrer, high performance unitrode and Pt 1000 temperature sensor (Metrohm) were used.

Point of zero charge (abbreviated as PZC) of ion exchangers was

Table 1
Physical and chemical properties of Purolite S957 and Diphonix Resin®.

Properties	Purolite S957	Diphonix Resin®
Manufacturer	Purolite (Germany)	EiChrom Industries (France)
Appearance	Dark brown with some cream-coloured spherical beads	Beige small spherical beads
Structure	macroporous	gel
Matrix	PS-DVB	PS-DVB
Functional Group	phosphonic, sulphonic	diphosphonic, sulphonic, carboxylic
Bead size	0.55-0.75 (mm)	0.074–0.150 (mm)
Ionic form as shipped	H^+	H^+
Total capacity	8.0 (meq/g) 18 Fe (g/dm^3)	5.6 (meq/g)
Density	1.12 (g/cm^3)	1.05-1.11 (g/cm^3)
Moisture content	55-70 %	70 %
Specific surface area S_{BET}	14.9 (m^2/g)	0.2 (m^2/g)
Average pore diameter D_{BJH}	34.1 (nm)	4.52 (nm)
Micropore volume V_{micro}	0.0007 (cm^3/g)	0.0001
Optical microscope images (magnification 6x)		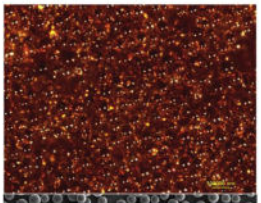
SEM images (magnification 80x)	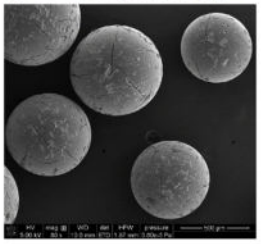	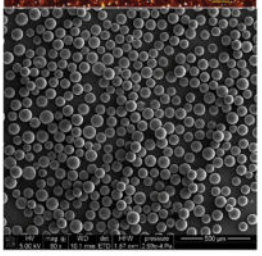
Particle size distribution	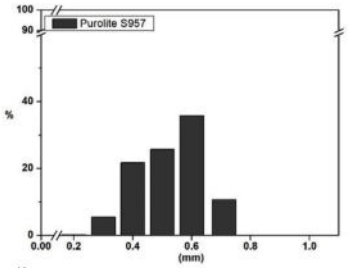	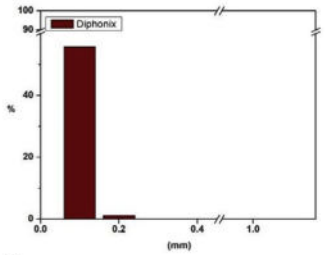
Changes of the pH during equilibration in the DI water	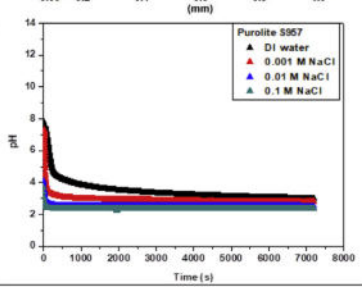	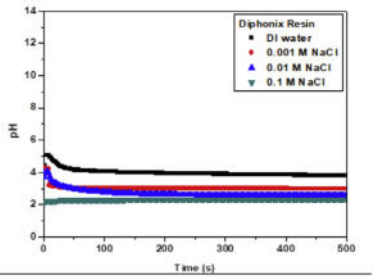

determined using the pH drift method based on the curve pH_0 vs. ΔpH (pH_1-pH_0) (Lopez-Ramon et al., 1999). To this end 0.5 g of ion exchanger was added into a flask containing 50 cm^3 of the pH-adjusted solution of 0.01 M NaCl. The initial pH was adjusted to a value from 2 to 12. The flasks were stoppered and stirred for 24 h. The final pH values were measured (pH_1). The potentiometric titrations in the presence of sodium chloride NaCl at 0.1, 0.01 and 0.001 M were also conducted. 0.5 g of Diphonix Resin® or Purolite S957 and 50 cm^3 of NaCl solutions were added to the 50 cm^3 beaker and stirred. As for potentiometric titrations the standard 0.1 M HCl and 0.1 M NaOH solutions were used. After each addition the suspension pH was measured. As previously the 907 Titrando titrator was used for this purpose.

The parameters of the porous structure of Purolite S957 and Diphonix Resin® were determined measuring the N_2 adsorption/desorption isotherms at 77 K. The accelerated surface area and porosimetry system, ASAP 2420 M (Micromeritics Instrument Corporation, USA) were used to this end. Before measurements the samples were degassed at 378 K. The Brunauer-Emmett-Teller (BET) method was used for the surface area calculation and the Barrett-Joyner-Halenda (BJH) method was applied to determine the pore size distribution.

SEM images of Purolite S957 and Diphonix Resin® were also made. To this end the Quanta 3D FEG (FEI Corporation) instrument was used.

Purolite S957 and Diphonix Resin® were analysed using an attenuated total reflection Fourier transform infrared (ATR-FTIR) spectrometer (Agilent Cary 630, Agilent Technologies) under the ambient conditions. The spectra were recorded from 4000 to 644 cm^{-1}.

The X-ray photoelectron spectroscopy (XPS) method was used to study chemical compositions of the samples using the multi chamber ultra-high vapour XPS UVH (Prevac) equipped with the monochromatized AlK_α radiation. As for the charge neutralization of ion exchangers the flood gun source was applied. The binding-energy scale with the binding energy 285.0 eV was calibrated by means of the carbon line.

2.2. Kinetic and adsorption/desorption tests

The sorption process was studied for the three different metal ion to citric acid ratios 1:1, 1:2 and 2:1. Working solutions were prepared weighing the appropriate amounts of citric acid and stock solutions of Ni(II) and La(III).

Stock solutions of Ni(II) and La(III) ions at the concentration of 1000 mg/dm^3 were prepared from $NiCl_2 \cdot 6H_2O$ and $La(NO_3)_3 \cdot H_2O$ (Avantor Performance Materials Poland S.A.) and suitably diluted accordingly to various required initial concentrations. The appropriate amount of citric acid was also added. The concentration of metal ion corresponds to the content of Ni(II) and La(III) ions in the leachates from the spent Ni-MH batteries. The detailed procedure for their extraction by citric acid was not presented due to patent preparation.

Adsorption experiments in the single component systems were performed at 293 K using the batch (static) technique. Static sorption experiments were carried out in terms of the invariable solid to solution ratio. 50 cm^3 of metal ion solutions with the initial concentration of Ni(II) and La(III) in the presence of citric acid ranging from 25 to 200 mg/dm^3 were placed in 100 cm^3 conical flasks with 0.1 g ion exchanger samples and stirred at 180 rpm, in the time interval from 1 to 360 min using the laboratory shaker type 358A (Elpin Plus, Poland). The experiments were conducted at room temperature (298 K). The initial pHs of the solutions were adjusted to 5.0 using the 1 M HNO_3 or 1 M NaOH solution to avoid metal ions precipitation. The pHs of the solution during the sorption studies were not regulated. After stirring the samples were separated by filtration using the filter paper.

To determine the adsorption capacity of selected ion exchangers experiments were conducted with the various initial concentrations of metal ions in the presence of citric acid from 25 to 600 mg/dm^3. For the desorption process different eluting agents were proposed. The systems were performed as described previously.

The concentrations of Ni(II) and La(III) in the solutions were analysed by the Inductively Coupled Plasma Optical Emission Spectrometry (ICP-OES) using ICP-OES 720 (Varian, USA) at 216.555 nm for Ni(II) and 333.749 nm for La(III), respectively. The experiments were performed in triplicate and the average values were obtained.

Ni-MH batteries are composed mainly the $LaNi_5$ and/or $MnNi_5$ compounds combined with rare earth elements such as La(III), Ce(III), Pr(III) and Nd(III) as well as Fe(III), Ni(II), Co(II), Cu(II) and Zn(II) (Tenório and Espinosa, 2002). Therefore during the selectivity determination these elements were taken into account. Adsorption experiments were performed in the batch mode.

3. Results

3.1. Ion exchangers properties characterization

The ion exchangers can be used for removal of metallic impurities from complex solutions containing chlorides, fluorides, sulphates and phosphates as well as EDTA, citrate and tartrate ligands (Kołodyńska and Hubicki, 2012; Silva et al., 2018; Zhao et al., 2007). The properties of ion exchangers depend on the degree of cross-linking. With the increasing percent of divinylbenzene (%DVB), the resistance to oxidation and the differences in affinity grow, but the operating capacities and rate of kinetics diminish. With the increase of %DVB the water content also decreases. In our experiments it was found that the water content was equal to 53% for Purolite S957 and 67% for Diphonix Resin®. The pH changes during the equilibration in the DI water are presented in Table 1. Both Purolite S957 and Diphonix Resin® are characterized by the spherical shape.

Diphonix Resin® is the result of the investigations carried out at the Argonne National Laboratory and University of Tennessee. It was developed primarily for actinide separation in the acidic solutions. However, it also adsorbs strongly divalent transition metal cations at pH 1–2 and trivalent cations at pH 0–2. It is fine-grained as can be seen on the optical microscope scan (Table 1). Another important parameter is the particle size which ranges from 0.55 to 0.75 mm for Purolite S957 and from 0.074 to 0.15 mm for Diphonix Resin®. The sieve analysis shows that in the case of Diphonix Resin® the beads are monodispersive and for Purolite S957 slightly more than 40% mass beads have a coarse grain size 0.40–0.60 mm (Table 1). This is relevant taking into account the kinetic process proportional to the inverse of the square of the particle diameter. In the case of Purolite S957 the fraction of beads below 0.30 mm and above 0.71 mm which is about 4% by mass is comparable. The ion exchangers being tested have only about 1.5% of the mass fraction with a relatively small size. The analogous results were obtained in (Gargul et al., 2019). Diphonix Resin® is characterized by smaller particles and all of them are in the range of 0.1–0.2 mm. In the literature for the other commercial ion exchangers such as Lewatit TP 207 and Chelex 100 the bead size is 0.4–1.250 mm and 0.3–1.20 mm, respectively.

Purolite S957 and Diphonix Resin® are macroporous and gel types, respectively. Macroporous ion exchangers contain a network of pores within a gel matrix making them appear opaque in contrast to the gel resins with clear glassy beads that are fully translucent to light. As follows from the ASAP analysis for Purolite

S957 (Table 1, Fig. 1) the BET total surface area is equal to 14.9 m^2/g and the average pore diameter 34.1 nm. For Diphonix Resin® these values were 0.2 m^2/g and 4.52 nm, respectively (Fila et al., 2019). According to the IUPAC classification the average pore diameter is in the mesoporosity range (2–50 nm).

The obtained results were confirmed by the SEM analysis at the same magnification (Table 1). The porous structure with large voids and cavities can be seen only in the case of Purolite S957.

Another parameter characterizing ion exchangers is the capacity. The content of functional groups by the unit of mass or volume is expressed as the total exchange capacity in millimoles or milliequivalents i.e. mmol/g (meq/g) or mmol/cm^3 (meq/cm^3) (Nikoloski and Ang, 2014). The IEC value (meq/g) was determined using the following equation:

$$IEC = V_{NaOH} \times C_{NaOH/m} \quad (1)$$

where: V_{NaOH} is the volume of NaOH used for the titration (cm^3), m is the dry weight of the ion exchanger (g), C_{NaOH} is the NaOH concentration.

For Purolite S957 and Diphonix Resin® they are equal to 8.0 meq/g and 5.3 meq/g, respectively. However, under real operating conditions particularly the dynamic ones, the use of all functional groups is practically impossible. Therefore the working ion exchange capacity is a more useful unit characteristic of ion exchangers. It determines the number of ions that can be exchanged between the solution and the ion exchanger under the given operating conditions. It also determines the sorption mechanism. Based on the potentiometric titration Purolite S957 contains about 60% of sulphone groups. For Diphonix Resin® this content is 45% and about 5% for the carboxylic groups (titration is characterized by three distinct phases and the total amount of acidic groups can be determined from the second intersection point). The content of the diphosphonic group was determined as a subtraction result. Their presence was confirmed by the XPS analysis (Fig. 2).

For Purolite S957 the pH_{PZC} values obtained using the drift and potentiometric titration methods were equal to 1.95 and 1.99, respectively. For Diphonix Resin® previously determined by us the value was 2.18 (or 1.85 by the drift method) (Fila et al., 2019).

The Fourier transform infrared spectra with the ATR mode for Purolite S957 and Diphonix Resin® before and after Ni(II) and La(III) ions adsorption in the presence of citric acid are shown in Fig. 3.

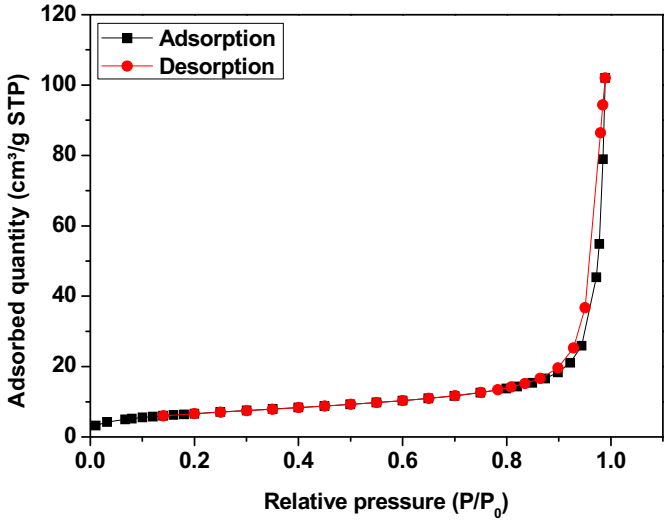

Fig. 1. ASAP analysis of Purolite S957.

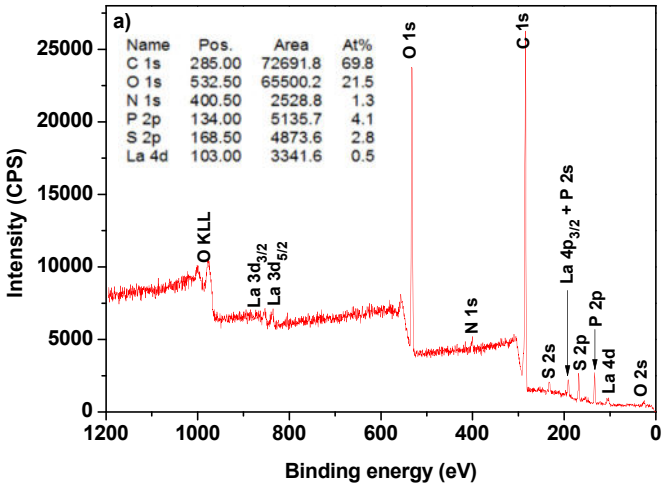

Fig. 2. XPS analysis of Purolite S957 after La(III) sorption.

The hydroxyl –OH stretching vibration broad band occurred at 3412 and 3436 cm^{-1} for Purolite S957 and Diphonix Resin®, respectively. After the sorption of Ni(II) and La(III) ions in the presence of citric acid its maximum is at 3420 and 3426 cm^{-1}. This band is characterized by not only the residual hydration water but also the presence of the sulphonic groups. A weak band at 1440-1395 cm^{-1} refers to the O–H deformation in the plane. The absorption band at 875-960 cm^{-1} has been ascribed to the OH–O out-of-plane deformation. The bands in the range from 2800 to 3000 cm^{-1} are characteristic of the polystyrene structure (Lazar et al., 2014; Zagorodni et al., 2002). The gel and macroporous styrene-divinylbenzene (ST-DVB) copolymer matrices correspond to the vibrations of the asymmetric ν_{as} and symmetric ν_s stretching vibrations of aliphatic –CH chains at 2960 cm^{-1} and 2920 cm^{-1} (double peaks). After the sorption of La(III) and Ni(II) ions in the presence of citric acid they are at 2968, 2931 as well as 2973 and 2929 cm^{-1}, respectively. The next are C–H bending vibrations in the side chain at 669, 703, 830 and 1029 cm^{-1}, $-CH_2$ scissoring at 1411 and 1449 cm^{-1} as well as δ_s CH_2 1470 cm^{-1} scissoring bands (Bogoczek and Surowiec, 1986; Ghosh et al., 2015). Additionally, the absorption peaks at 1627 and 1656 cm^{-1} correspond to the simple C=C bonds in the ST-DVB structure. For both ion exchangers the absorption bands in the 1200-900 cm^{-1} region are attributed to the S=O stretching vibrations in the $-SO_3^-$ groups i.e. at 1230 cm^{-1} asymmetric ν_{as} stretching, 1220 cm^{-1} symmetric ν_s stretching, 985 cm^{-1} stretching ν vibrations of single S–OH as well as P=O stretching vibrations in the $-PO_3^{2-}$ groups (Zagorodni et al., 2002). The absorption band of carbonyl C=O stretching and hydroxyl –OH deformation vibrations of the carboxylic groups is at about 1740 cm^{-1} and 1644 cm^{-1}, respectively. A peak around 1450 cm^{-1} is characterized of the symmetric C=O stretching vibrations. After metal ions sorption the stretching frequency of the carboxylate carbonyl is shifted to the lower wavelength of 1560 cm^{-1}. These functional groups can coordinate metal ions by the unidentate, bidentate and bridging complexes. The presence of the phosphonic group in Purolite S957 and Diphonix Resin® is confirmed by the bands at 2280 cm^{-1} which corresponds to the stretching vibrations of the P–OH groups. The bands at 1132 and 989 cm^{-1} correspond to the stretching vibrations of the P=O and P–O groups.

3.2. Physicochemical properties of citric acid and its complexes with metal ions

The main objective of this study was to develop the removal

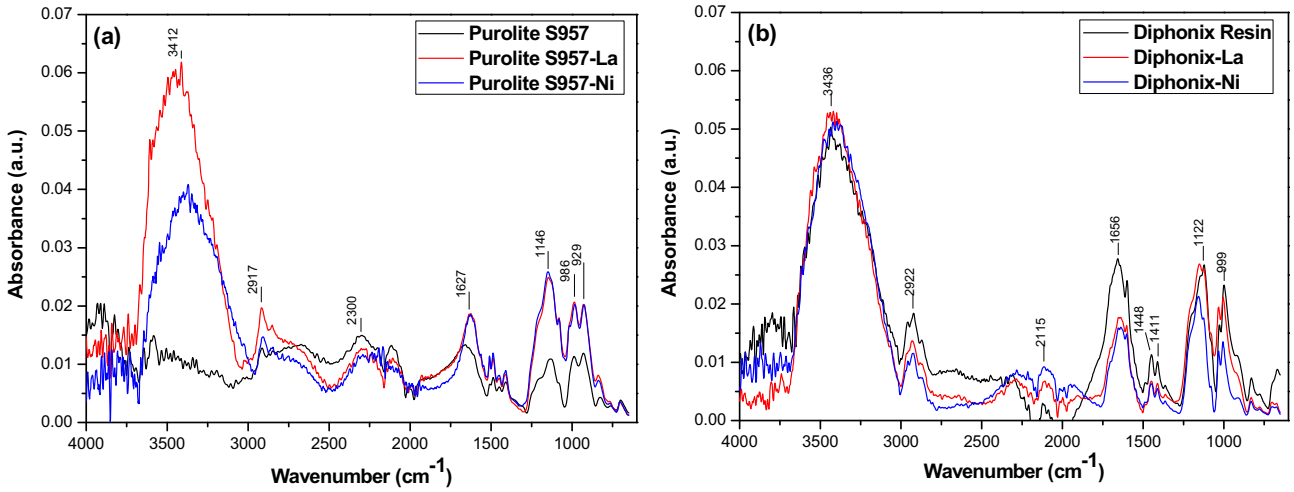

Fig. 3. FTIR spectra for a) Purolite S957 and b) Diphonix Resin® before and after the adsorption of Ni(II) and La(III) ions in the presence of citric acid.

strategy of heavy metal ions and rare earth elements represented by the Ni(II) and La(III) ions from the aqueous solutions containing citric acid based on the extraction of spent Ni-MH batteries. Technological progress with the increased demand for REEs resulted in the need to develop new methods of recovery of these elements from the secondary sources such as WEEEs, CCPs and AMDs. One of the solutions can be the use of non-toxic and biodegradable citric acid. It is obtained from many sources, commercially through the fermentation of waste potatoes after the starch extraction by mycological fermentation using *Candida* spp. or by the solvent extraction process from the *Aspergillus niger* fermentation solution (Huang et al., 2011). It occurs in living organisms playing a very important role in metabolism as a transitional product in the Krebs cycle in which it is isomerized to isocitric acid. It is generally recognized as safe approved by the Joint Food and Agriculture Organization and World Health Organization Expert Committee on Food Additives (Soccol et al., 2006). Citric acid has also been classified by the U.S. Food and Drug Administration as a nontoxic compound and approved for the general use as a food additive. In the EU it is designated by the E numbers: E330 (citric acid), E331-E333 (citrates). In the food industry it plays a variety of roles, for example, prevents spoilage of food caused by the presence of microorganisms, acts as an antioxidant, prevents changes in colour or taste and is used as a pH control agent and acidulant. In addition, iron ammonium citrate acts as an anti-caking agent added to loose products and prevents the absorption of moisture. Besides the food industry, citric acid is also used in the cosmetics, pharmaceutical, textile and many other industries (Dhillon et al., 2011; Soccol et al., 2006).

Citric acid (CA) is commonly considered to be a tribasic moderately strong organic acid, with the pK_a values extrapolated to the zero ionic strength of 2.92, 4.28 and 5.21 at 298 K. The percentage contents of the citric acid forms as a function of pH are presented in Table 2. The successive pK_a values for citric acid deprotonation at 293 K are $pK_{a1} = 3.15$, $pK_{a2} = 4.77$ and $pK_{a3} = 6.39$ (Aurich et al., 2017). The pK_a of the hydroxyl group has been found to be 14.4 by means of ^{13}C NMR spectroscopy. The speciation diagram shows that the citric acid solution is the buffer between the pH about 2 and 8 (or in the pH range 2.5–6.5 according to (Aurich et al., 2017)). In the biological systems at the pH about 7 the two species are the citrate ion and the monohydrogen citrate ion. At the zero ionic strength, the enthalpy change associated with two ionizations was reported to be 0.28 and −0.71 kcal/mol. The presence of active carboxyl and hydroxyl groups in the molecule makes citric acid a chelating agent of great complexation affinities not only for REEs but also for other elements. The comparison of the stability constants of REE complexes with various chelating agents is presented in Table 2.

The ability to coordinate metal ions for citric acid is not as high as for EDTA or DTPA but its undoubtful advantage is its biodegradability, particularly when more and more attention is paid to the environmental protection and the principles of green chemistry are widely used (Römkens et al., 2002).

The chelating properties of citric acid against heavy metals, e.g. Fe(III) and Cu(II) have also contributed to its use as a stabilizer of oils and fats as well as for cleaning of power station boilers. Mg(II) and Ca(II) ions complexation is used in the process of water softening (Begum et al., 2012; Kirimura et al., 2011).

The types of complexes formed by citric acid depend on the metal ions (Table 2). They can be mononuclear, binuclear or polynuclear as well as bi-, tri- and multidentate. For example with Ni(II) or Fe(II) it forms bidentate, mononuclear complexes with two carboxyl acid groups of the citric acid molecule and with Cu(II) and Cd(II) tridentatate, mononuclear complexes with two carboxyl acid groups and the hydroxyl group (Bassi et al., 2000; Huang et al., 2011). The general reaction of complex formation is as follows:

$$M^{2+} + cit^{3-} \rightleftarrows [M(cit)]^{-} \quad (2)$$

$$M^{3+} + cit^{3-} \rightleftarrows [M(cit)] \quad (3)$$

The citrate ligand binds tridentately with α-hydroxy or α-alkoxy, α-carboxy and one of β-carboxy groups. This is the most common coordination mode found for the transition metal citrates such as those with Ni(II) (Chen et al., 2012). Biodegradation of these complexes by *Pseudomonas fluorescens* revealed that this process is influenced by the type of the formed complex. According to (Francis et al., 1998) bidentate Ca(II), Fe(II), Ni(II), Zn(II) citrate complexes are readily degraded. Tridentate Cd(II), Cu(II), binuclear U(VI) and polynuclear U(VI) species are recalcitrants. Several metals such as Cr(III) with In(III), Cd(II) with Ni(II), Mn(II) or Zn(II), and U(VI) with Al(III), Cu(II), Fe(III) and In(III) formed mixed-metal complexes with citric acid.

In the paper (Ohyoshi et al., 1972) it was found that different lanthanide complexes are formed depending on pH of the solution. They can be as follows: $[Ln(Hcit)]^{+}$, $[Ln(cit)]$, $[Ln(cit)_2]^{3}$, $[Ln(OH)(cit)]^{-}$ (Svoronos et al., 1981). The mole fraction of La(III) species vs.

Table 2
Comparison of the percentage contents of the citric acid forms as a function of pH, the stability constants of REE complexes with various chelating agents of [LnL] type ($\mu = 0.1$; $T = 293$ K) and pH of REE precipitation from different solutions.

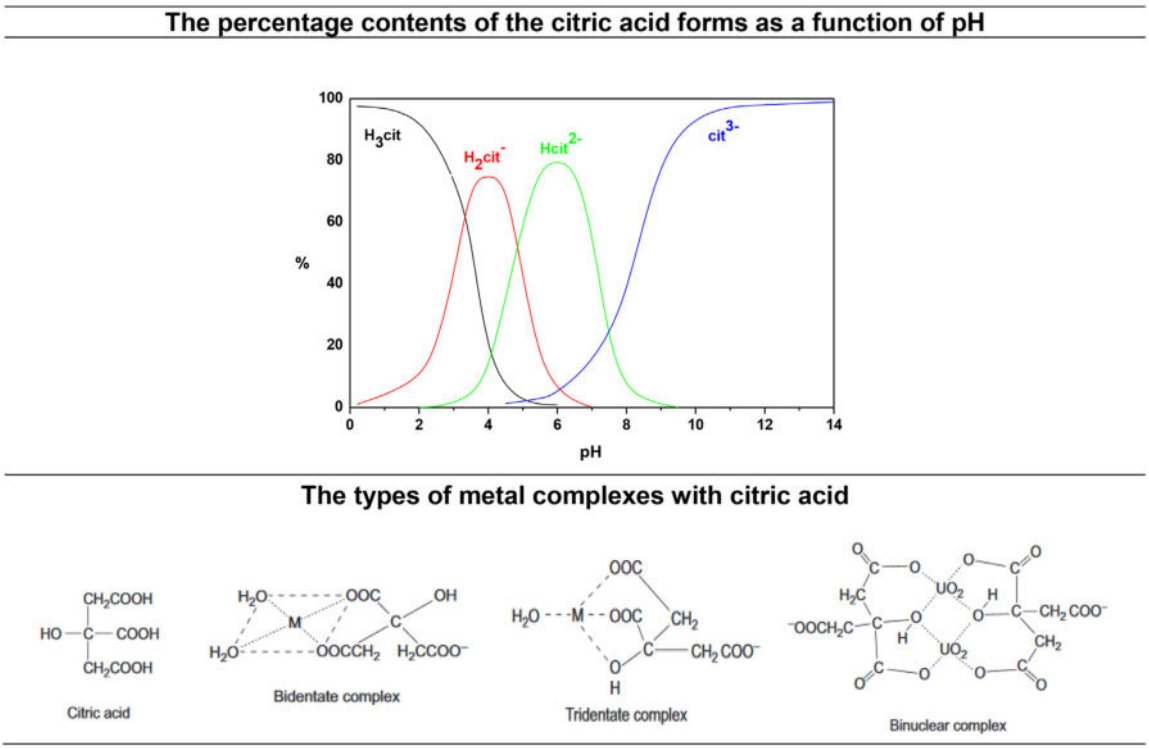

REE(III)	logK[LnL]				
	CA	EDTA	PDTA	HEDTA	DTPA
La	7.10	15.50	16.42	13.82	19.96
Ce	7.40	15.98	16.79	14.45	20.90
Pr	7.60	16.40	17.17	14.96	21.85
Nd	7.70	16.61	17.54	15.16	22.24
Pm	7.71	16.90	17.80	15.40	22.50
Sm	7.80	17.14	17.97	15.64	22.84
Eu	7.80	17.35	18.26	15.62	22.91
Gd	7.72	17.37	18.21	15.44	23.01
Tb	7.74	17.93	18.64	15.55	23.21
Dy	7.79	18.30	19.05	15.51	23.46
Ho	7.84	18.60	19.30	15.55	23.30
Er	7.86	18.85	19.61	15.61	23.18
Tm	8.00	19.32	20.08	16.00	22.97
Yb	8.05	19.51	20.25	16.17	23.01
Lu	8.07	19.83	20.56	16.25	23.00
pH **of REEs precipitation from different solution**					
	SO_4^{2-}	Cl^-	NO_3^-	CH_3COO^-	ClO_4^-
La	7.41/7.61	8.03	7.83/8.35/8.71	7.93	8.76/8.10
Ce	7.35/7.07	7.41	76/8.1	7.77	n.a.
Pr	7.17/6.98	7.05	7.35	7.66	7.40
Nd	6.95/6.73	7.02/7.40	7.00/7.31	7.59	7.6/7.3
Sm	6.70	6.83	6.92	7.40	7.57/7.13
Eu	6.68	n.a.	6.82	7.18	6.91
Gd	6.75	n.a.	6.83	7.10	7.45/6.81
Y	6.83	6.78	7.95/7.39	6.83	7.57/6.81
Er	6.50	n.a.	6.76	6.59	n.a.
Tm	6.21	n.a.	6.40	6.53	n.a.
Yb	6.18/6.16	n.a.	6.30	6.50	7.30/6.45
Lu	6.18	n.a.	6.30	6.46	6.45
Sc	n.a.	4.8	n.a.	6.1	n.a.

CA – citric acid, EDTA – ethylenediaminetetraacetate, PDTA – 3-propanediamine-tetraacetate, HEDTA – N-(2-hydroxyethyl)ethylenediaminetriacetate, DTPA – diethylenetriaminepentaacetate.

pH for the solution with citric acid can be calculated from the stability constant logarithms according to the reactions:

$$Ln^{3+} + cit^{3-} \rightleftarrows [Ln(cit)] \quad (4)$$

$$Ln^{3+} + Hcit^{2-} \rightleftarrows [Ln(Hcit)]^{+} \quad (5)$$

$$Ln^{3+} + H_2cit^{-} \rightleftarrows [Ln(H_2cit)]^{2+} \quad (6)$$

In the pH range 7–8, the precipitation of neutral complex of the Ln:cit = 1:1 system was observed. A small amount of $[Ln(H_2cit)]^{2+}$ of low stability is likely to form near pH 3 (Zhou et al., 2008). For $Hcit^{2-}$ the complexes are as follows:

$$Ln^{3+} + Hcit^{2-} \rightleftarrows [Ln(cit)] + H^{+} \quad (7)$$

3.3. Effect of the citric acid to metal ion ratio

In the preliminary studies the sorption process was examined for the three different metal ion to citric acid ratios 1:1, 1:2 and 2:1. The adsorption capacity (q_t) at time t, adsorption percentage *(S%)* as well as the partition coefficient of metal ions between the ion exchangers and solution (K_d) were calculated according to Eqs. (8)–(10):

$$q_t = (c_0 - c_t) \times \frac{V}{m} \quad (8)$$

$$S\% = \frac{(c_0 - c_t)}{c_t} \times 100 \quad (9)$$

$$K_d = \frac{(c_0 - c_e)}{c_e} \times \frac{V}{m} \quad (10)$$

where: q_t is the adsorption amount of Ni(II) or La(III) ions in the presence of citric acid at time t (mg/g), c_0 is the initial concentration of Ni(II) or La(III) in the solution in the presence of citric acid (mg/dm^3), c_t is the concentration of Ni(II) or La(III) in the presence of citric acid at time *t* (mg/dm^3), *V* is the volume of solution (dm^3), *m* is the mass of dry ion exchange sample (g), *S%* is the adsorption percentage (%). All the experiments were performed in triplicate and the general agreement of the obtained values was within 5%.

For *t* equal to the equilibrium contact time when c_t is equal to c_e and q_t is equal to q_e, the amount of M(II/III) adsorbed at equilibrium, q_e, can be calculated using Eq. (11):

$$q_e = (c_0 - c_e) \times \frac{V}{m} \quad (11)$$

The research results show that the optimal citric acid to metal(II/III) ion ratio in the sorption of Ni(II) and La(III) ions from the citrate solutions is 1:1 due the largest values of q_t (Fig. 4a). Therefore, subsequent studies were carried out for this ratio. For La(III) the neutral complexes with citric acid are supposed.

3.4. Ion exchangers mass effect

As for the ion exchanger mass effect, different quantities of Purolite S957 and Diphonix Resin® varying from 0.05, 0.1, 0.5 and 1 g were used. The results showed that the amount of La(III) ions sorbed on Diphonix Resin® decreased from 5.63 to 2.75 mg/g increasing the ion exchange amount (Fig. 4b). The analogous results for Ni(II) are as follows 4.92 and 2.60 mg/g. With decreasing the ion exchange amount, the number of ion exchange functional groups

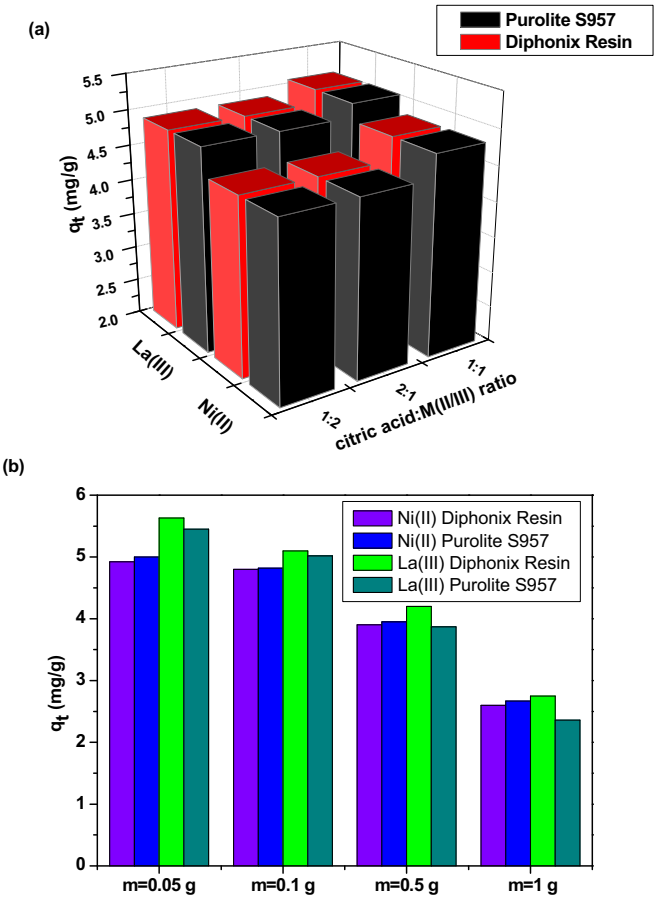

Fig. 4. The effect of a) the citric acid:metal ion ratio and b) the mass on the sorption of Ni(II) and La(III) ions in the presence of citric acid on Purolite S957 and Diphonix Resin® (the initial concentration of La(III) and Ni(II) 50 mg/dm^3).

also decreases. However, increasing the amount of resin the La(III) and Ni(II) removal efficiency (%S) increased from 55 to 99.9%. This is due to the fact that there are no available functional groups for complete removal of the metal ions/complexes from the solution. At a higher adsorbent dose the solution ion concentration drops to lower values and the system reaches equilibrium at lower values of q_t which indicates that the adsorption sites remain unsaturated. In addition, this phenomenon may be caused by the aggregation of sorbent particles at a larger mass which will reduce the chemically active sites.

3.5. pH effect

As for pH effects it was found that SACs such as these containing sulphonic groups and SBA with the quaternary ammonium can dissociate over the entire pH range. The sulphonic groups, which ionise even under strongly acidic conditions (pK_a~1), are not characterized by good selectivity towards metal ions. WACs are ionized at the solutions pH higher than the acid dissociation constant i.e. pK_a of the functional groups, so they operate when the solution pH is higher than the pK_a and the ion exchangers with higher pK_a are preferred. Therefore the ion exchangers containing carboxylic groups operate at pH higher than 4, whereas the ion exchangers with the amino groups operate at pH lower than 11. The phosphonic ion exchangers are characterized by intermediate acidity which results in greater selectivity than that of the sulphonic ion exchangers as well as much higher capacity than the

carboxylic ones at low pH (both studied ion exchangers contain the phosphonic groups). The influence of pH on the sorption of HMs and REEs has been extensively studied by many authors. The sorption of metal ions is low at very acidic pH and increases with the increasing pH to a certain value. This phenomenon can be explained by the surface charge of the adsorbent. At low pH the cations compete with the H^+ ions in the solution for the active sites which causes low adsorption. At high pH the adsorbent surface has a negative charge as a result of the complete dissociation of the functional groups, whereby it is easy for the positively charged ions to be adsorbed resulting in the higher adsorption. A very high pH value makes the adsorption process impossible due to formation of metal hydroxides and precipitation.

It can be assumed that basicity of rare earth elements increases successively from Sc(III) to La(III). Of all the elements with the III oxidation degree, lanthanides form the most basic hydroxides. This is confirmed by (i) the ease of hydroxides to dissolve in acids or ammonium salts solutions and (ii) their absorption of CO_2 from the atmosphere as well as (iii) great electrode potentials, tendency towards hydrogen removal from water and large heat of their oxides dissolution in acids.

The change of rare earth elements basicity, decreasing with the order number often constituted the basis for various methods of their separation. Another method of fractionation precipitation is the basic precipitation of hydroxides and basic salts based on precipitation in the order of increasing basic properties of lanthanides with the decrease of hydrogen ions concentration in the solution. The hitherto investigations show that precipitation of hydroxides of all lanthanides proceeds in a narrow range of pH values. The pH values, at which precipitation of lanthanide salts solutions begins, are presented in Table 2. Therefore further studies on the La(III) ions sorption on the ion exchangers Purolite S957 and Diphonix Resin® were carried out for the pH value 6.0. The discrepancies in the pH values of the precipitation threshold given by various authors are a result of different precipitation process conditions.

3.6. Kinetic studies

The kinetic parameters of La(III) or Ni(II) ions in the presence of citric acid on the ion exchange samples were compared and calculated based on the following models (Eqs.(12)–(18)) (Ho and McKay, 1999; Ho and McKay, 1998):

a) the pseudo first order (PFO)

$\frac{dq_t}{dt} = k_1(q_e - q_t)$ and the applying boundary conditions t = 0 to t = t and $q_t = 0$ to $q_t = q_t$,

$$\log(q_e - q_t) = \log(q_e) - \frac{k_1 t}{2.303} \tag{12}$$

b) the pseudo second order (PSO)

$\frac{dq_t}{dt} = k_2(q_e - q_t)^2$ and the applying boundary conditions t = 0 to t = t and $q_t = 0$ to $q_t = q_t$

$$\frac{t}{q_t} = \frac{1}{k_2 q_e^2} - \frac{t}{q_e} \tag{13}$$

with the initial sorption rate for $q_t/t \rightarrow 0$

$$h = k_2 q_e^2$$

c) the Weber-Morris model also known as the intraparticle diffusion model (IPD)

$$q_t = k_i t^{0.5} + C \tag{14}$$

d) the Boyd model (BM)

$$Bt = -0.497 - \ln(1 - F) \tag{15}$$

e) the film diffusion model (FD)

$$\ln(1 - F) = k_f t \tag{16}$$

f) the Dumwald-Wagner model (DW)

$$\log\left(1 - F^2\right) = -\frac{k_{DW}}{2.303t} \tag{17}$$

as well as

g) the pore and film diffusion coefficients:

$$D_p = 0.03\frac{r^2}{t_{1/2}} \text{ and } D_f = 0.23\frac{r\delta q_e}{t_{1/2}c_0} \tag{18}$$

where: q_e, q_t were defined as previously, k_1 is the pseudo first order rate constant (dm^3/min), k_2 is the pseudo second order rate constant (g/mg·min), k_i is the intraparticle diffusion rate constant (mg/g·$min^{0.5}$), C is the intercept called the Weber-Morris diffusion constant, F is the fraction of solute adsorbed at any time (fractional attainment of equilibrium at time t equal to $F=q_t/q_e$), for F > 0.85 B is the diffusion constant, k_f is the film diffusion model rate constant (1/min), k_{DW} is the Dumwald-Wagner model rate constant (1/min), r is the mean radius of the sorbent (cm), δ is the film thickness equal to 1×10^{-3} cm, $t_{1/2}$ is the time at which the half of the maximal sorption was achieved (s), c_0 is the initial concentration of Ni(II) or La(III) ions in the presence of citric acid (mg/dm^3).

It was found that the removal of Ni(II) and La(III) increased rapidly during the first 10–15 min caused by the strong forces of Ni(II) and La(III) and the ion exchangers and then more slowly until the equilibrium. The %sorption increased from 10% to 100%. However, when the initial concentration of metal ions increased from 25 to 200 mg/dm^3 it decreased. The results showed that the removal efficiency increased rapidly from 40% to 100% and thereafter it remained almost constant at a lower concentration particularly in the case of Diphonix Resin®. This is due to the fact that the removal efficiency depends more upon the concentration of the solution and less upon the dose larger than the optimal. Moreover, the greater the concentration of the ion in the solution, the greater is the ion exchange process. It is obvious that for the ion exchanger with a low percentage of cross-linking, the solution passes quickly through the matrix and the kinetics is fast. With the increase of the cross-linking diffusion of the exchangeable ions is hindered by the dense matrix and the kinetics is slow. However, those with the low cross-linking are characterized by the tendency towards swelling which confines their physical strength. For the applied ion exchangers %DVB was equal to 10.

In the case of the ion exchange process metal ions transfer is usually characterized by either external mass transfer (boundary layer diffusion) or intraparticle diffusion or both. The most commonly used technique to identify the sorption mechanism and to predict the rate controlling step is fitting the experimental data

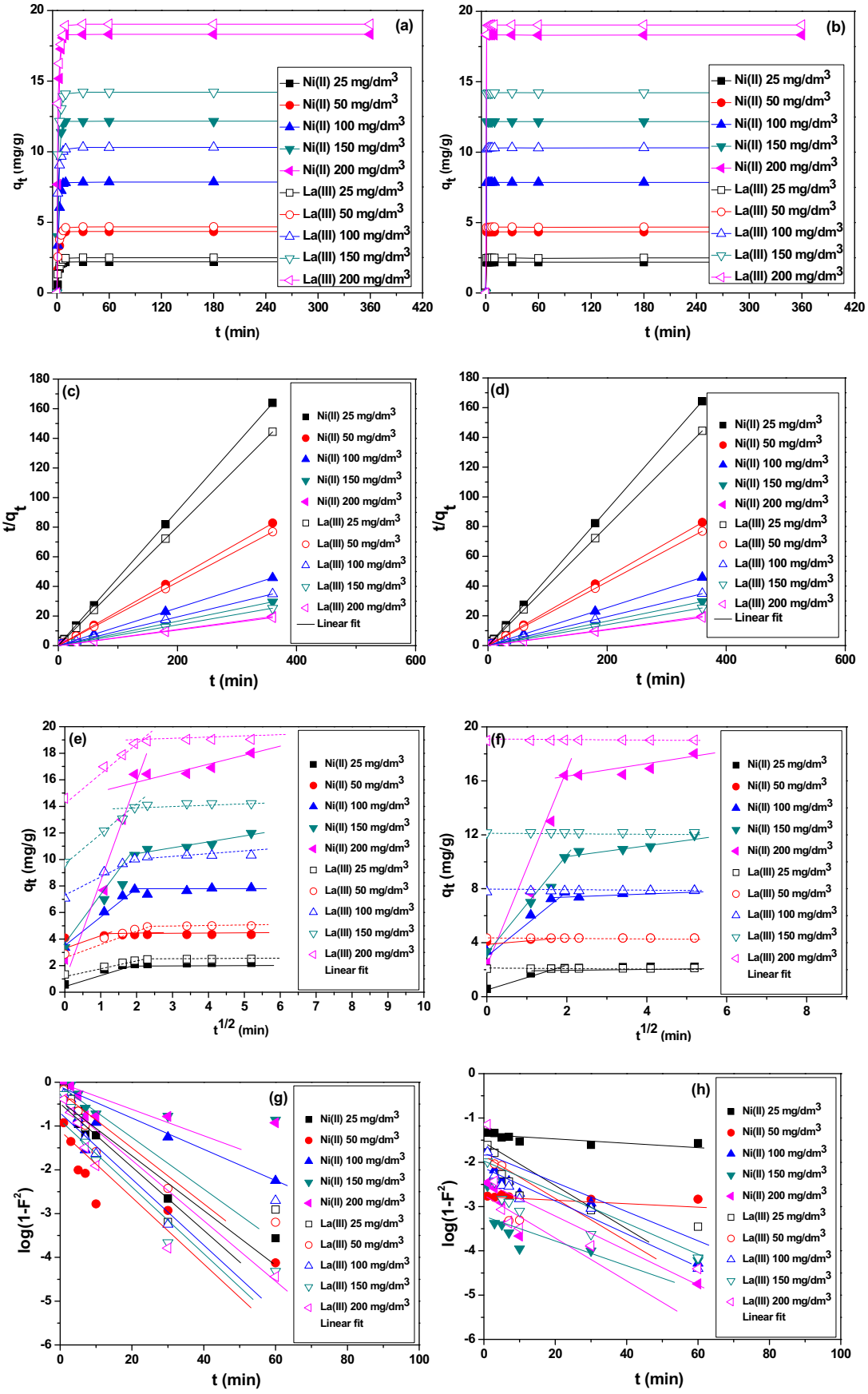

Fig. 5. a-b) Effect of the phase contact time, c-d) the pseudo-second-order kinetic plots, e-f) the intraparticle kinetic plots and g-h) the Dumwald-Wagner kinetic plots for the sorption of Ni(II) and La(III) complexes with citric acid on Purolite S957 and Diphonix Resin®.

in an intraparticle diffusion plot. Therefore the obtained results were analysed by different kinetic models. The kinetic parameters and other values were estimated based on Fig. 5a–b and they are listed in Table 3.

Practically all kinetic theories (except for the PSO equation) lead to dependence of the exponential type $F = 1\text{-}exp(-k_1 t)$ described by the Boyd model. In the PFO the parameter $k_1(q_e\text{-}q_t)$ does not represent the number of available sites. The expression of $q_e\text{-}q_t$ represents the fraction of available functional groups at time *t*. Additionally, $log(q_e)$ is an adjustable parameter and often not equal to the intercept of a plot of $log(q_e\text{-}q_t)$ *vs. t* (Douven et al., 2015; Ho and McKay, 1998). Moreover, the PFO equation does not adjust the whole range of contact time and generally is applicable over the initial 10–20 min of the sorption process (Fig. 5c–d). During the kinetic experiments in which adsorption phenomena are important in addition to the intramolecular diffusion, a gradual shift in the impact of individual phenomena from pure diffusion (*c=0, high constant Kd*) to pure adsorption (*high c, low Kd*) is evidently observed. Therefore, the nature of kinetic phenomena can be indirectly identified using the empirical Weber-Morris equation. However, it should be remembered that in this case this equation can be treated as only a comparative tool. If the diffusion is rate controlling, the slope of the plots based on the PFO will vary inversely with the particle size, the film thickness and the distribution coefficient k_1. If the sorption rate controlling step is chemical exchange, the slope is independent of particle diameter and depends only on the concentration of the sorbate in solution and the temperature.

Table 3
The kinetic parameters for the sorption of Ni(II) and La(III) on Purolite S957 and Diphonix Resin® for the selected models.

Parameter/Model	Purolite S957		Diphonix	
	Ni(II)	La(III)	Ni(II)	La(III)
$q_{e,exp}$ (mg/g)	18.32	19.04	18.33	19.04
PFO				
$q_{e,cal}$ (mg/g)	0.42	0.46	0.01	0.02
k_1	0.04	0.04	0.03	0.03
R^2	0.955	0.984	0.803	0.979
PSO model				
$q_{e,cal}$ (mg/g)	18.34	19.06	18.33	19.04
k_2	0.017	0.239	8.808	4.705
h	5.72	94.42	93.66	132.92
R^2	0.999	1.000	1.000	1.000
IPD model				
k_{i1}	6.38	2.98	6.02	4.41
C_1	2.403	10.710	18.280	18.068
R^2	0.910	0.971	0.970	0.756
k_{i2}	0.27	0.11	0.00	0.00
R^2	0.958	0.964	0.992	0.947
Boyd model				
B	7.05×10^{-8}	1.67×10^{-7}	4.29×10^{-7}	3.96×10^{-7}
R^2	0.855	0.984	0.926	0.979
FD model				
k_f	0.322	0.314	0.392	0.321
R^2	0.955	0.984	0.911	0.979
DW model				
k_{DW}	0.027	0.059	0.079	0.085
R^2	0.9645	0.9863	0.9031	0.980
log K_d				
Fe(III)	3.75		5.88	
Ni(II)	3.94		5.96	
Co(II)	3.20		5.65	
Cu(II)	3.18		5.51	
Zn(II)	3.04		5.23	
La(III)	4.35		6.66	
Ce(III)	3. 74		6.31	
Pr(III)	3.62		5.90	
Nd(III)	3.60		5.78	

According to (Płaziński and Rudziński, 2011) for PFO the difference $(q_e\text{-}q_t)$ becomes smaller and the value $ln(q_e\text{-}q_t)$ greater and greater. The effect of random errors will grow proportionally to the reverse of the factor $(q_e\text{-}q_t)$. As for PSO the plot of t/q_t vs. *t* should give a linear relationship, based on which q_2, k_2 and *h* can be determined from the slope and intercept of the plot. The PSO equation can be used for extrapolation of the kinetic data q_t and estimation of the value q_e corresponding to them. It should be mentioned that extrapolation confinement to the points measured for the states close to equilibrium is $q_t > 80\%\ q_e$.

In our studies the better R^2 values were observed for the PSO kinetic model which indicates that this model fits the adsorption kinetic data best. The kinetic data of Ni(II) and La(III) were plotted with the excellent correlation coefficients 0.999 for Ni(II) and 1.000 for La(III). It was found that the equilibrium adsorbed amounts calculated from the PSO kinetics ($q_{e,cal}$) are also close to the experimental amounts adsorbed at equilibrium ($q_{e,exp}$). The PSO constant k_2 decreased with the increase of Ni(II) and La(III) concentration. It also increased with the decrease in the particle size of Diphonix Resin® compared to Purolite S957. The values of the rate constant were found to decrease from 0.564, 0.632, 0.175, 0.026 to 0.017 g/mg·min for Ni(II) on Purolite S957 as well as from 20.918, 14.419, 10.334, 9693 to 8.804 g/mg·min for Ni(II) on Diphonix Resin®. For La(III) on Purolite S957 they were as follows from: 0.782, 0.437, 0.359, 0.247 to 0.239 g/mg·min as well as on Diphonix Resin® from 14.462, 13.206, 10.344, 9668 to 4.705 g/mg·min with the increase of the initial concentration from 25 to 200 mg/dm^3. As for *h* these values were as follows: 1.09, 1.19, 2.75, 3.63 and 5.72 mg/g·min for Ni(II) on Purolite S957 and 35.25, 54.27, 63.69, 74.58, and 93.66 mg/g·min for Ni(II) on Diphonix Resin®, for La(III) on Purolite S957 4,91, 11.00, 38.37, 50.15 and 94.42 mg/g·min as well as 100.99, 103.75, 116.52, 129.66, 132.92 mg/g·min on Diphonix Resin®.

As for the Weber-Morris model (Fig. 5 e-f) it is known that the intraparticle diffusion is the only rate limiting step when the plot q_t vs. $t^{0.5}$ is linear and passes through the origin. If the plot does not pass through the origin, this indicates that the adsorption processes do not follow only the intraparticle diffusion but also the film diffusion (connected with the thickness of the boundary layer). The external mass transfer is significant, particularly in the initial reaction phase. The IPD plots can be sometimes divided into steps. The initial stages of sorption are connected with the boundary layer diffusion effect (diffusion/convection in the bulk solution and boundary layer diffusion) and the later stages (linear portion of the curve) due to the intraparticle diffusion (diffusion into pores) and approaching the equilibrium state. This kind of multilinearity was also reported in the recent studies (Fila et al., 2019). The intercept of the plot reflects the boundary layer effect. The larger is the intercept, the greater is the surface sorption contribution in the rate controlling step. In our studies the slope of the first and second portions is defined as the intraparticle diffusion parameter k_i displayed in Table 3. The values of C_i and R^2 are also listed in this table. For the C_i parameter there was found the following relation: $C_1 > C_2$. They indicate that the resistance to the external mass transfer decreases as the intercept decreases. Additionally, the intraparticle diffusion parameter k_i (mg/g·min$^{0.5}$) is proportional to the initial concentration due to the greater deriving force with the increasing initial concentration.

After determination of q_e value, the fractional attainment of equilibrium at time *t* (min) equal to $F=q_t/q_e$ can be used for the identification of the slowest step of sorption process according to the Boyd model. If the plots *Bt* (where *Bt* is a function of *F*) vs. *t* ($t < 120$ min) are linear and pass through the origin, the slowest step in the adsorption process is the internal diffusion. The plot of *Bt* vs. *t* is linear with the distribution coefficients 0.885–0.994 indicating that sorption is controlled by the film diffusion connected

with the external mass transfer. The values of B, D_i and R^2 are listed in Table 3. In the case of Purolite S957 the calculated values of the effective diffusion coefficients D_i for Ni(II) were found to be 1.09×10^{-7}, 1.37×10^{-7}, 2.41×10^{-7}, 6.56×10^{-8} and 7.05×10^{-8} m^2/min for the initial concentration of 25, 50, 100, 150 and 200 mg/dm^3, respectively. The analogous values for Diphonix Resin® are as follows: 1.64×10^{-7}, 1.85×10^{-7}, 3.19×10^{-7}, 3.27×10^{-7} and 4.29×10^{-7} m^2/min. For La(III) they are equal to: 1.40×10^{-7}, 1.43×10^{-7}, 1.47×10^{-7}, 1.56×10^{-7} and 1.67×10^{-7} m^2/min for Purolite S957 and 3.24×10^{-7}, 3.33×10^{-7}, 3.65×10^{-7}, 3.89×10^{-7} and 3.96×10^{-7} m^2/min for Diphonix Resin®.

As for the film diffusion (FD) model it was found that the k_f parameters were as follows for Ni(II): 0.072, 0.241, 0.276, 0.330 and 0.322 1/min on Purolite S957 and 0.148, 0.247, 0.298, 0.381 and 0.392 1/min on Diphonix Resin®. For La(III) they are equal to: 0.268, 0.209, 0.272, 0.304 and 0.314 1/min on Purolite S957 as well as 0.259, 0.264, 0.276, 0.302 and 0,321 1/min on Diphonix Resin®.

The Dumwald-Wagner model assumes that for the linearity the plots do not intersect the origin, the rate limiting step is an intra-particle diffusion process, otherwise that is a film diffusion. Furthermore, the higher intercept indicates that the film diffusion rate control step has greater influence on the rate limiting step (Fig. 5g–h).

It should be concluded that the rate limiting step is not a sole intraparticle diffusion process and there can be also the film diffusion. The adsorption of Ni(II) and La(III) ions proceeds in the presence of citric acid on Purolite S957 and Diphonix Resin® by a complex mechanism consisting of both film adsorption and intra-particle transport. Some limitations could be also due to the structure of the applied ion exchangers. The macroporous ion exchanger Purolite S957 is characterized by the much more heterogeneity than Diphonix Resin®.

In the presented studies the adsorption kinetics is mainly connected with the film diffusion as well as the internal diffusion. Both these steps can take considerable time. The external mass transfer is several times as important as the migration of the metal species through the pore volume. The obtained results confirm that the film diffusion is the rate controlling step because the film diffusion coefficients D_f are in the range 10^{-6}–10^{-8} cm^2/s. If pore diffusion is to be rate controlling, the pore diffusion coefficient D_p should be in the range 10^{-11}–10^{-13} cm^2/s.

3.7. Partition coefficient determination

In the separation processes the partition between two phases is described by the partition coefficient (K_d). As metal ions occur in different forms, the more appropriate is the use of the distribution ratio (D). K_d and D are identical if the solute has only one chemical form in each phase. If the solute exists in more than one chemical form in both the solution and solid phase, then Kd and D have usually different values, however, D changes depending on the operating conditions (Fryxell et al., 2004; Shaibu et al., 2006). The high values of K_d indicate that the majority of the metal ions are adsorbed on the ion exchangers, however, this does not indicate the strength of the process. It should be noted that it provides only indirect information on the type of surface interactions taking place. Often these values are determined over a range of concentrations at a constant temperature. Plotting of $logK_d$ as a function of pH (or acid concentration) provides some information about the mechanism involved in the ion exchange process i.e. the number of protons exchanged during the process referring to the chemical equation. Taking into account their values in our studies it was established that they increase with the increasing concentration of the complexes. In Table 3 the comparison of the distribution coefficients ($logK_d$) for the sorption of metal ion complexes with citric acid on Purolite S957 and Diphonix Resin® is presented. The highest values were obtained for La(III) and the smallest in the case of Zn(II) complexes with citric acid. These values were referred to those reported in the literature. Even at low concentrations the majority of REEs reported are in the III oxidation state in the acid leaching solutions. Therefore compared to Fe(III) the selective sorption is a challenging task.

Strong cationic ion exchangers with the sulphonic functional groups sorb Fe(III) and other HMs quickly (Silva et al., 2018) due to fast diffusion/convection in the solution bulk. As presented in (Canner et al., 2018) U(VI), Cu(II), Ni(II) and Co(II) follow the chelating mechanism with respect to the iminodiacetate functional groups. For Fe(III) partial hydrolysis occurs. However, the pure anion exchange mechanism was observed for REEs. In malic acid buffer the ion exchanger Purolite S910 shows a preference towards the medium REEs. Unlike Purolite S910, Amberlite IRC86 with the carboxylic functional group exhibits a definite selectivity towards the light REEs with La(III) and Ce(III) showing the highest adsorption (Bezzina et al., 2018). It was found that the ion exchange process involves the ion exchange with a slight difference between La(III) and Gd(III), increase in the case of Tb(III) and constant value for Lu(III). An unusual behaviour of Y(III) is observed. The slope gradient from this plot for the Y(III) ion indicates a process involving the transfer of another proton.

3.8. Adsorption isotherm determination

The influence of the concentration of selected metal ions on the sorption capacity was analysed. The adsorption data of La(III) or Ni(II) in the presence of citric acid on Purolite S957 and Diphonix Resin® were analysed using the Langmuir (Eq. (19)) and Freundlich (Eq. (20)) isotherm models:

$$q_e = \frac{q_0 K_L c_e}{1 + K_L c_e} \tag{19}$$

$$q_e = K_F {c_e}^{1/n} \tag{20}$$

where: q_e, c_e were defined as previously, q_0 is the maximum amount of metal complexes sorbed per unit mass of adsorbent to form a complete monolayer on the surface of ion exchanger (mg/g), K_L is the Langmuir constant related to the affinity of the binding sites (dm^3/mg), K_F is the Freundlich adsorption capacity (mg/g), $1/n$ is the Freundlich constant related to the surface heterogeneity. The above mentioned parameters can be calculated from the linearized plots of c_e/q_e vs. c_e and $\log q_e$ vs. $\log c_e$, respectively. Moreover, the obtained results can be described with the separation factor R_L as well as $1/n$. R_L and $1/n$ are dimensionless and R_L is defined as follows:

$$R_L = \frac{1}{1 + K_L c_0} \tag{21}$$

The Langmuir and Freundlich models are two isotherm models generally used for quantitative description of the adsorption equilibrium between the ion exchanger and the solution phase (Nikoloski and Ang, 2014). The shape of the obtained isotherm is indicative of adsorption processes.

The Langmuir isotherm can be used for quantitative determination and comparison of different sorbents (Deepatana et al., 2006; Escudero et al., 2008). At first it was elaborated for description of adsorption of gases on active carbon. Its application was extended to the empirical description of the equilibrium between the liquid and solid phases. The model is based on the assumptions:

(i) the adsorbent possesses active sites on its surface called active centres (these may be lattice defects or interfaces), (ii) the adsorption process proceeds on the active centres, (iii) each centre can adsorb only one molecule, thus a monomolecular layer is formed on the adsorbent surface, (iv) the adsorbed molecules in the active sites do not interact and the adsorption process is characterized by the dynamic equilibrium between the sorption and desorption. This equation describes particularly well the chemical adsorption when the adsorbed substance forms a monomolecular layer on the solid phase surface.

The Freundlich isotherm is the earliest known relationship describing the sorption equation. This fairly satisfactory empirical isotherm can be used for non-ideal sorption that involves heterogeneous surface energy systems. In general, as the K_F value increases the adsorption capacity of adsorbent for a given adsorbate increases. Additionally, n is indicative of adsorption preference. The value of 1/n below one indicates the Langmuir isotherm while 1/n above one is indicative of cooperative adsorption. The plot of $logq_e$ vs. $logc_e$ gives a straight line with the slope of $1/n$ and the intercept of the values of K_F. The evaluated constants are given in Table 4. Comparing the parameters of isotherms (Fig. 6a-d, Table 4) it can be stated that the value of R^2 from the Langmuir isotherm is the highest indicating a good fit to the experimental data. In addition, the values of R_L from 0 to 1 indicate favourable adsorption nature. The results also showed that the adsorption was enhanced upon increasing temperature, suggesting that the adsorption process could be more likely chemical adsorption rather than physical one.

Table 4
Adsorption isotherm parameters for the sorption of Ni(II) and La(III) complexes with citric acid on Purolite S957 and Diphonix Resin®.

Parameter	Purolite S957		Diphonix Resin®	
	Ni(II)	La(III)	Ni(II)	La(III)
	293 K			
$q_{e,exp}$ (mg/g)	41.29	58.29	41.83	58.59
Langmuir isotherm				
q_0 (mg/g)	40.14	60.35	41.81	60.15
K_L (dm^3/mg)	1.121	5.623	1.206	9.121
R^2	0.9968	0.9941	0.9937	0.9944
Freundlich isotherm				
K_F (dm^3/mg)	17.24	45.25	15.97	102.35
n	3.979	2.375	2.929	1.716
R^2	0.9191	0.6893	0.6911	0.6536
	313 K			
$q_{e,exp}$ (mg/g)	43.26	58.33	43.22	59.07
Langmuir isotherm				
q_0 (mg/g)	45.11	62.29	45.30	63.00
K_L (dm^3/mg)	0.951	5.465	0.899	0.911
R^2	0.9899	0.9962	0.9996	0.9999
Freundlich isotherm				
K_F (dm^3/mg)	16.29	46.99	16.12	38.32
n	2.334	2.137	2.266	2.227
R^2	0.7485	0.8903	0.7178	0.8899
	333 K			
$q_{e,exp}$ (mg/g)	44.09	58.35	44.14	60.01
Langmuir isotherm				
q_o (mg/g)	46.63	60.75	46.55	60.12
K_L (dm^3/mg)	0.896	4.648	0.856	3.789
R^2	0.9979	0.9943	0.9968	0.9999
Freundlich isotherm				
K_F (dm^3/mg)	17.18	45.59	16.76	35.55
n	2.146	2.078	2.119	2.011
R^2	0.7485	0.8813	0.7507	0.8898
Thermodynamic parameters				
ΔG° at 293	−16.96	−23.31	−17.35	−26.53
ΔG° at 313	−20.06	−25.13	−19.99	−33.11
ΔG° at 333	−22.92	−26.91	−23.06	−38.46
ΔH° (kJ/mol)	26.77	23.06	24.43	61.01
ΔS° (J/mol K)	91.9	32.6	84.9	24.0

3.9. Temperature effect

The nature of the sorption process can be estimated by thermodynamic parameters such as the change in free energy (ΔG°), enthalpy (ΔH°) and entropy (ΔS°). These parameters can be estimated considering the equilibrium constants at different temperatures. Thermodynamic parameters of the adsorption were calculated from the variations of the thermodynamic equilibrium constant K_d determined by plotting $\ln(q_e/c_e)$ vs. q_e and extrapolating to zero q_e. The standard free energy change ΔG° can be calculated using Eqs.(22)–(24):

$$\ln K_d = \frac{\Delta S^o}{R} - \frac{\Delta H^o}{RT} \tag{22}$$

$$\Delta G^o = -RT \ln K_d \tag{23}$$

$$\Delta G^o = \Delta H^o - T\Delta S^o \tag{24}$$

where: ΔG° is the standard free energy change of the ion exchange (kJ/mol), R is the universal gas constant (8.314 J/mol K), T is the absolute temperature (K), ΔH° is the enthalpy (kJ/mol), ΔS° is the entropy (J/mol K).

The values of enthalpy ΔH° and entropy ΔS° were obtained from the slope and intercept of $\ln K_d$ vs. $1/T$ plots. The Gibbs free energy ΔG° was calculated using the K_d value. The values of the thermodynamic parameters for the sorption of Ni(II) and La(III) ions on Purolite S957 and Diphonix Resin® are given in Table 4. The positive value of enthalpy change ΔH° shows that the adsorption of Ni(II) and La(III) ions is of an endothermic nature. An adsorption process is generally considered as physical if ΔH° < 20 kJ/mol and as chemical when ΔH° > 40 kJ/mol. The negative value of ΔG° decreases with an increase in temperature, indicating that the reaction is spontaneous and demonstrating that the higher temperatures facilitate the adsorption. The obtained positive values of ΔS° showed the affinity of Purolite S957 and Diphonix Resin® for Ni(II) and La(III) and the increasing randomness. The positive value of ΔH° indicated the endothermic nature of adsorption process. On the other hand, either change in the pore size of the ion exchangers causing intraparticle diffusion within the pores or enhancement in the chemical affinity of Ni(II) and La(III) ions for the functional groups leading to some chemical interactions takes place during the adsorption process.

The Arrhenius equation was applied to evaluate the activation energy of adsorption representing the minimum energy that reactants must have for the reaction to proceed, as shown by the following relationship:

$$\ln k_2 = \ln A - \frac{E_a}{RT} \tag{25}$$

where: k_2 (g/mg min) is the rate constant obtained from the pseudo second-order kinetic model, E_a (kJ/mol) is the Arrhenius activation energy of adsorption and A is the Arrhenius factor (g/mg min). When $\ln k_2$ is plotted against $1/T$, a straight line with the slope of $-E_a/R$ is obtained.

The activation energy values were found to be: 0.47 kJ/mol for Ni(II) on Purolite S957, 0.83 kJ/mol for La(III) on Purolite S957 as well as 68.1 kJ/mol for Ni(II) on Diphonix Resin®, 76.5 kJ/mol for La(III) on Diphonix Resin®. It is evident that there is an apparent relationship between the E_a and the relevant structural parameters of the ion exchangers (gel and macroporous). It is also known that the value < 50 kJ/mol generally indicates a film and particle diffusion controlled process, whereas higher values represent chemical reaction processes. In similar studies, E_a values for Amberlite IRA-

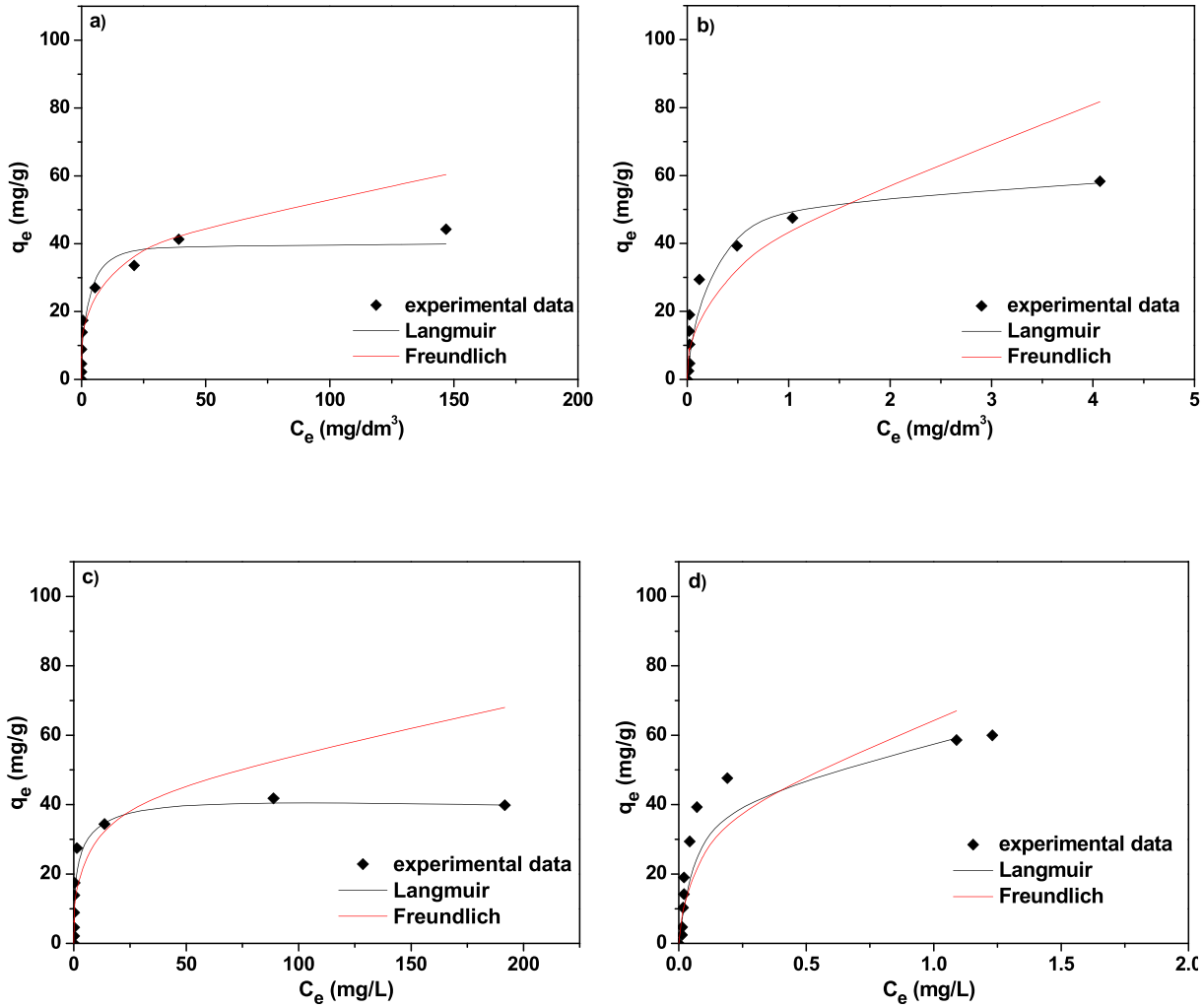

Fig. 6. Non-linear fitting of the isotherms to the experimental data for sorption of a) and c) Ni(II) as well as b) and d) La(III) ions on Purolite S957 (a–b) and Diphonix Resin® (c–d).

743 and XSC-800 ion exchangers were reported to be 4.952 kJ/mol (Ohyoshi et al., 1972) and 20.38 kJ/mol (Canner et al., 2018), respectively.

The comparison of the obtained results with those by other researchers is presented in Table 5. In our studies the obtained results were not compared to those of the ion exchangers with the sulphonic functional groups although they are mainly used in metal separation processes without specific adsorption requirements. This group of resins shows the strongest adsorption capacity of the cation exchangers but poor metal selectivity and difficulties of the

Table 5
Comparison of the obtained results with those by other researchers for the Ni(II) and La(III) sorption.

Metal ion	Adsorbent	$q_{e,max}$ (mg/g)	Ref.
Ni(II)	Purolite S957	44.09	This work
	Diphonix Resin®	44.14	This work
	Purolite S930	10.43	Deepatana et al. (2006)
	Purolite S950	18.42	
	Coffee wastes	7.25	Escudero et al. (2008)
	Grape stalk	38.31	
	Lignin	5.99	Guo et al. (2008)
	Brewer's spent grain	1.64	Wierzba and Kłos (2019)
	Magnetic peptide resins with glycine (MGLY)	391.00	Hamza and Abdel-Rahman (2015)
La(III)	Purolite S957	58.35	This work
	Diphonix Resin®	60.01	This work
	Amberlite IRC86	40.60	Bezzina et al. (2018)
	Lewatit TP 207	114.70	Esma et al. (2014)
	Lewatit TP 260	106.70	
	polyaminophosphonic acid sorbent (PPA-PGMA)	109.59	Galhoum et al. (2019)
	Iron oxide loaded Ca-alginate beads	123.50	Wu et al. (2010)
	Fe_3O_4@DTPA superparamagnetic nanoparticles	62.00	Almeida and Toma (2016)

adsorbed metal ions elution. Additionally, it depends on the ion exchanger form. For example in the wastewater treatment from inorganic industrial streams such ion exchanger as Dowex 50Wx8 in the Na^+ form shows a 10% higher metal loading capacity than in the H^+ form.

3.10. Desorption and mechanism description

As for desorption studies two eluents were applied e.g. hydrochloric and nitric acids at a concentration 0.5, 1.0 and 2.0 mol/dm^3 (Fig. 7).

Since using 2.0 mol/dm^3 nitric acid resulted in the highest leaching of lanthanide ions, it was proposed for desorption. Generally, the HMs ions such Ni(II) are more readily desorbed than REEs such as La(III). As follows from the literature data there is the strict relationship between the functional groups and their metal ions removal. The presence of sulphonic functional groups determines better hydrophilic properties of Purolite S957 and Diphonix Resin® compared to the traditional ion exchangers such as Lewatit SP112 (Kołodyńska, 2010). The sulphonic acid groups increase the hydrophilicity of ion exchanger, metal accessibility and ensures fast kinetics:

$$2R-SO_3H+M^{2+}\rightleftarrows(R-SO_3)_2^{2-}\rightarrow M^{2+}+2H^+ \quad (26)$$

For M^{3+} this reaction should be analogous.

Moreover, the diphosphonic acid groups determine selectivity of the resin with $pK_1 = 1.27$, $pK_2 = 2.41$, $pK_3 = 6.67$ and $pK4 = 10.04$. They also ensure high selectivity and low desorption for Fe(III) over the divalent cations M(II) in the acid solutions as well as high affinity for lanthanides, actinides and polyvalent cations over a wide range of acid concentrations. The complexation reaction can be as follows:

$$R-(PO_3H_2)_2^{2-}+M^{2+}\rightleftarrows R-(PO_3H_2)_2^{2-}\rightarrow M^{2+} \quad (27)$$

In the case of metal ions with the additional charge (M^{3+}), it can be neutralized by the sulphonate functional groups. It was found that phosphoryl oxygen and acidic oxygen cannot be simultaneously coordinated to the metal ion. In acidic solutions, for example the neutral metal-nitrate(V) species may be bound to the phosphoryl groups of diphosphonic acid.

However, in the case of the carboxylic groups, the resin has strong affinity for protons (above a low acid concentration, ion exchangers are completely converted to the free acid and do not react with neutral salts) (Höll, 1984). WAC sorbs metal ions only when protons are neutralized by co-ions of the solution:

$$R-COOH+NaOH\rightleftarrows R-COONa+H_2O \quad (28)$$

$$2R-COONa+M^{2+}\rightleftarrows 2(R-COO^-)\rightarrow M^{2+}+2Na^+ \quad (29)$$

Such groups have a great ability to remove REEs from solution due to their ability to form the strongest complexes with O-donor ligands (Bezzina et al., 2018).

In the case of Purolite S957 containing only sulphonic and phosphonic functional groups the selectivity series at low pH follows the order of Fe(III) > Al(III) > Mn(II) = Cu(II) = Zn(II) = Co(II) = Ni(II), therefore it preferentially extracts trivalent metal cations below pH 1. It should be added that the sulfonic acid resin Bio-Rad™ AG MP-50 displayed much lower selectivity at these higher proton concentrations. These combined properties provide high selectivity for Fe(III) and other transitional metals in the acidic solutions (Canner et al., 2018). To describe the mechanism of metal ion sorption it should be known that according to the Pearson Hard and Soft Acids and Bases (HSAB) theory, the ligands of the functional groups in ion exchangers behave as electron donors (bases) and the metal ions as electron acceptors (acids) following the Lewis theory. Hard acids are ions with low electronegativity, non-polarizable, have the high charge to ionic radius ratio and are attracted to hard bases of high electronegativity. On the other hand, soft acids are polarizable ions with the low charge to ionic radius ratio and with relatively high electronegativity that matches the relatively low electronegativity of soft bases. Thus ion exchangers with the phosphonic, phosphinic, phosphonic, carboxylic groups (hard base) can interact with hard acids like Fe(III), Al(III), Sc(III) and Ln(III). When high selectivity between two hard or soft acids (metal ions) is required a base group containing the number of donor atoms similar to the oxidation state of the target acid ion is preferred e.g. carboxylic groups with two electron donor atoms favour the interactions with metal ions with II over III the oxidation state.

The characterization of selected ion exchangers requires the determination of both their equilibrium and kinetic properties. Acidity of a solution has two effects on metal sorption. Under the acidic conditions protonation of the binding chelating functional groups is observed, however, hydroxide ions in the basic solution complexed and precipitated metal ions. Therefore, pH of a solution is the first parameter which should be optimized. At pH of the solution equal to pH_{PZC}, the surface charge of the ion exchangers is neutral and therefore the negligible sorption of La(III) and Ni(II) or their complexes with citric acid is observed. When pH is lower than pH_{PZC}, the surface charge of the ion exchangers is positive. There is an electrostatic repulsion between La(III) and Ni(II) and low sorption efficiency. In the case of negative metal ions complexes with citric acid they are supposed to be adsorbed, however, in this pH region they do not exist. At pH greater than pH_{PZC} this value is negative which produces the attraction of metal ions. Generally, the lower pH_{PZC} is, the more metal ions are attracted. Maximum sorption is likely to occur at pH values greater than PZC when adsorbents have a net negative charge. In the case of the citric acid in the solution, the carboxylic groups act with La(III) and Ni(II) to form complexes by releasing protons. This indicates that the ion exchange reaction increases acidity of solution as described in (Lu et al., 2009). The negligible effect of the increased ionic strength on the REEs cation extraction suggests chelating interactions of the phosphonic acid functionality with La(III) and not strong interactions with Ni(II) ions. However, this mechanism is rather complicated.

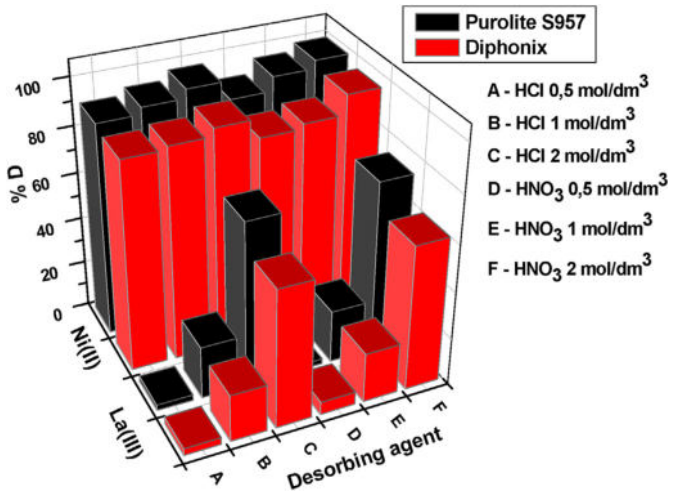

Fig. 7. The effect of desorbing agents for the desorption of Ni(II) and La(III) from Purolite S957 and Diphonix Resin®.

4. Conclusions

The use of ion exchange resins is constantly evolving and new areas are emerging. In this study, the removal of Ni(II) and La(III) ions from the citrate solutions onto the ion exchangers Diphonix Resin® and Purolite S957 was investigated under different experimental conditions varying such parameters as solution pH, contact time, ion exchanger dose, different ratio of ion exchanger and the initial concentration of metal ions. The optimal sorption process conditions were determined. The adsorption mechanisms were examined studying kinetic and isotherm models. Based on the obtained results, it can be concluded that the phase contact time, concentration and citric acid to metal ion ratio affect the sorption process. The results show that the sorption of Ni(II) and La(III) ions on the tested ion exchangers is very fast. The equilibrium is determined after 10–20 min for Diphonix Resin® and Purolite S957. Moreover, the adsorbents exhibit excellent adsorption of Ni(II) and La(III) ions from the citric solutions achieving removal of almost 100%. The suitability of the pseudo first order, pseudo second order, intraparticle diffusion, Boyd, film diffusion and Dumwald-Wagner kinetic models for the adsorption is also discussed. The pseudo second order kinetic model agrees very well with the adsorption behaviour over the studied range of metal ions concentration. The Langmuir model was found to provide the best fit to the data, as evidenced by the highest correlation coefficient. The obtained results have practical significance in the process of removing heavy metal ions and lanthanide ions from the solutions after the extraction of the Ni-MH batteries. The experimental results of this study demonstrate that Purolite S957 and Diphonix Resin® are suitable for adsorption of Ni(II) and La(III) ions from solutions. Moreover, citric acid can be proposed as an alternative chelating agent to EDTA, having the advantage of low price and high biodegradability. Both ion exchangers can be used for pretreatment of the acidic liquors to remove less valuable iron and to maximize further stages of exchange columns usage.

Declaration of competing interest

The authors declare that they have no known competing financial interests or personal relationships that could have appeared to influence the work reported in this paper.

CRediT authorship contribution statement

Katarzyna Araucz: Investigation, Data curation, Visualization, Writing - original draft. **Andreas Aurich:** Conceptualization, Methodology, Writing - review & editing. **Dorota Kołodyńska:** Conceptualization, Methodology, Writing - original draft, Investigation.

Acknowledgments

The authors are grateful for the financial support from the National Centre of Research and Development within Project No. POIR.04.01.01-00-0040/17–00.

References

Agarwal, V., Khalid, M.K., Porvali, A., Wilson, B.P., Lundström, M., 2019. Recycling of spent NiMH batteries: integration of battery leach solution into primary Ni production using solvent extraction. Sustain. Mater. Technol, e00121. https://doi.org/10.1016/j.susmat.2019.e00121.

Akcil, A., Akhmadiyeva, N., Abdulvaliyev, R., Meshram, A.P., 2018. Overview on extraction and separation of rare earth elements from red mud: focus on Scandium. Miner. Process. Extr. Metall. Rev. 39, 145–151. https://doi.org/10.1080/08827508.2017.1288116.

Alexandratos, S.D., 2007. New polymer-supported ion-complexing agents : design, preparation and metal ion affinities of immobilized ligands. J. Hazard Mater. 139, 467–470. https://doi.org/10.1016/j.jhazmat.2006.02.042.

Almeida, S.D.N., Toma, H.E., 2016. Neodymium(III) and lanthanum(III) separation by magnetic nanohydrometallurgy using DTPA functionalized magnetite nanoparticles. Hydrometallurgy 161, 22–28. https://doi.org/10.1016/j.hydromet.2016.01.009.

Aurich, A., Hofmann, J., Oltrogge, R., Wecks, M., Gläser, R., Blömer, L., Mauersberger, S., Müller, R.A., Sicker, D., Giannis, A., 2017. Improved isolation of microbiologically produced (2R,3S)-isocitric acid by adsorption on activated carbon and recovery with methanol. Org. Process Res. Dev. 21, 866–870. https://doi.org/10.1021/acs.oprd.7b00090.

Bassi, R., Prasher, S.O., Simpson, B.K., 2000. Extraction of metals from a contaminated sandy soil using citric acid. Environ. Prog. 19, 275–282. https://doi.org/10.1002/ep.670190415.

Begum, Z.A., Rahman, I.M.M., Tate, Y., Egawa, Y., Maki, T., Hasegawa, H., 2012. Formation and stability of binary complexes of divalent ecotoxic ions (Ni, Cu, Zn, Cd, Pb) with biodegradable aminopolycarboxylate chelants (dl-2-(2-carboxymethyl)nitrilotriacetic acid, GLDA, and 3-hydroxy-2,2′- iminodisuccinic acid, HIDS) in aqueous solu. J. Solut. Chem. 41, 1713–1728. https://doi.org/10.1007/s10953-012-9901-9.

Bertuol, D.A., Bernardes, A.M., Tenório, J.A.S., 2006. Spent NiMH batteries: characterization and metal recovery through mechanical processing. J. Power Sources 160, 1465–1470. https://doi.org/10.1016/j.jpowsour.2006.02.091.

Bezzina, J.P., Ogden, M.D., Moon, E.M., Soldenhoff, K.L., 2018. REE behavior and sorption on weak acid resins from buffered media. J. Ind. Eng. Chem. 59, 440–455. https://doi.org/10.1016/j.jiec.2017.11.005.

Binnemans, K., Jones, P.T., Blanpain, B., Van Gerven, T., Yang, Y., Walton, A., Buchert, M., 2013. Recycling of rare earths: a critical review. J. Clean. Prod. 51, 1–22. https://doi.org/10.1016/j.jclepro.2012.12.037.

Bogoczek, R., Surowiec, J., 1986. Chemical modification of styrene-divinylbenzene copolymers by dialkyl phosphites. Polymer 27, 631–634. https://doi.org/10.1016/0032-3861(86)90252-1.

Canner, A.J., Pepper, S.E., Hayer, M., Ogden, M.D., 2018. Removal of radionuclides from a HCl steel decontamination stream using chelating ion exchange resins – initial studies. Prog. Nucl. Energy 104, 271–279. https://doi.org/10.1016/j.pnucene.2017.10.007.

Chen, M.L., Gao, S., Zhou, Z.H., 2012. Isolations and characterization of highly water-soluble dimeric lanthanide citrate and malate with ethylenediaminetetraacetate. Dalton Trans. 41, 1202–1209. https://doi.org/10.1039/c1dt11466b.

Contescu, A., Contescu, C., Putyera, K., Schwarz, J.A., 1997. Surface acidity of carbons characterized by their continuous pK distribution and Boehm titration. Carbon N. Y. 35, 83–94. https://doi.org/10.1016/S0008-6223(96)00125-X.

Deepatana, A., Tang, J.A., Valix, M., 2006. Comparative study of chelating ion exchange resins for metal recovery from bioleaching of nickel laterite ores. Miner. Eng. 19, 1280–1289. https://doi.org/10.1016/j.mineng.2006.04.015.

Dhillon, G.S., Brar, S.K., Verma, M., Tyagi, R.D., 2011. Recent advances in citric acid bio-production and recovery. Food Bioprocess Technol. 4, 505–529. https://doi.org/10.1007/s11947-010-0399-0.

Douven, S., Paez, C.A., Gommes, C.J., 2015. The range of validity of sorption kinetic models. J. Colloid Interface Sci. 448, 437–450. https://doi.org/10.1016/j.jcis.2015.02.053.

Dvořák, P., Vu, H.N., 2015. Obtaining nickel and cobalt from spent NiMH batteries. Inz. Miner 1–6, 2015.

Escudero, C., Gabaldón, C., Marzal, P., Villaescusa, I., 2008. Effect of EDTA on divalent metal adsorption onto grape stalk and exhausted coffee wastes. J. Hazard Mater. 152, 476–485. https://doi.org/10.1016/j.jhazmat.2007.07.013.

Esma, B., Omar, A., Amine, D.M., 2014. Comparative study on lanthanum(III) sorption onto Lewatit TP 207 and Lewatit TP 260. J. Radioanal. Nucl. Chem. 299, 439–446.

Fila, D., Hubicki, Z., Kołodyńska, D., 2019. Recovery of metals from waste nickel-metal hydride batteries using multifunctional Diphonix resin. Adsorption 25, 367–382. https://doi.org/10.1007/s10450-019-00013-9.

Förster, A., Aurich, A., Mauersberger, S., Barth, G., 2007. Citric acid production from sucrose using a recombinant strain of the yeast *Yarrowia lipolytica*. Appl. Microbiol. Biotechnol. 75, 1409–1417. https://doi.org/10.1007/s00253-007-0958-0.

Francis, C.W., Timpson, M.E., Lee, S.Y., Elless, M.P., Wilson, J.H., 1998. The use of carbonate lixiviants to remove uranium from uranium-contaminated soils. J. Radioanal. Nucl. Chem. 228, 15–21. https://doi.org/10.1007/bf02387292.

Francis, C.W., Timpson, M.E., Wilson, J.H., 1999. Bench- and pilot-scale studies relating to the removal of uranium from uranium-contaminated soils using carbonate and citrate lixiviants. J. Hazard Mater. 66, 67–87. https://doi.org/10.1016/S0304-3894(98)00209-X.

Fryxell, G.E., Wu, H., Lin, Y., Shaw, W.J., Birnbaum, J.C., Linehan, J.C., Nie, Z., Kemner, K., Kelly, S., 2004. Lanthanide selective sorbents: self-assembled monolayers on mesoporous supports (SAMMS). J. Mater. Chem. 14, 3356–3363. https://doi.org/10.1039/b408181a.

Galhoum, A.A., Elshehy, E.A., Tolan, D.A., El-Nahas, A.M., Taketsugu, T., Nishikiori, K., Akashi, T., Morshedy, A.S., Guibal, E., 2019. Synthesis of polyaminophosphonic acid-functionalized poly(glycidyl methacrylate) for the efficient sorption of La(III) and Y(III). Chem. Eng. J. 375, 121932. https://doi.org/10.1016/j.cej.2019.121932.

Gargul, K., Boryczko, B., Bukowska, A., Jarosz, P., Małecki, S., 2019. Leaching of lead and copper from flash smelting slag by citric acid. Arch. Civ. Mech. Eng. 19, 648–656. https://doi.org/10.1016/j.acme.2019.02.001.

Ghosh, S., Dhole, K., Tripathy, M.K., Kumar, R., Sharma, R.S., 2015. FTIR spectroscopy in the characterization of the mixture of nuclear grade cation and anion exchange resins. J. Radioanal. Nucl. Chem. 304, 917–923. https://doi.org/10.1007/s10967-014-3906-3.

Guo, X., Zhang, S., Shan, X., 2008. Adsorption of metal ions on lignin. J. Hazard Mater. 151, 134–142. https://doi.org/10.1016/j.jhazmat.2007.05.065.

Hamza, M.F., Abdel-Rahman, A.A.H., 2015. Extraction studies of some hazardous metal ions using magnetic peptide resins. J. Dispersion Sci. Technol. 36, 411–422. https://doi.org/10.1080/01932691.2014.905955.

Ho, Y.S., McKay, G., 1999. Pseudo-second order model for sorption processes. Process Biochem. 34, 451–465.

Ho, Y.S., McKay, G., 1998. A comparison of chemisorption kinetic models applied to pollutant removal on various sorbents. Process Saf. Environ. Protect. 76, 332–340. https://doi.org/10.1205/095758298529696.

Höll, W., 1984. Optical verification of ion exchange mechanisms in weak electrolyte resins. React. Polym. 2, 93–101.

Huang, K., Inoue, K., Harada, H., Kawakita, H., Ohto, K., 2011. Leaching of heavy metals by citric acid from fly ash generated in municipal waste incineration plants. J. Mater. Cycles Waste Manag. 13, 118–126. https://doi.org/10.1007/s10163-011-0001-5.

Izadi, A., Mohebbi, A., Amiri, M., Izadi, N., 2017. Removal of iron ions from industrial copper raffinate and electrowinning electrolyte solutions by chemical precipitation and ion exchange. Miner. Eng. 113, 23–35. https://doi.org/10.1016/j.mineng.2017.07.018.

Kamzolova, S.V., Morgunov, I.G., Aurich, A., Perevoznikova, O.A., Shishkanova, N.V., Stottmeister, U., Finogenova, T.V., 2005. Lipase secretion and citric acid production in *Yarrowia lipolytica* yeast grown on animal and vegetable fat. Food Technol. Biotechnol. 43, 113–122.

Kirimura, K., Honda, Y., Hattori, T., 2011. Citric acid. In: Comprehensive Biotechnology. Elsevier B.V., pp. 135–142. https://doi.org/10.1016/B978-0-08-088504-9.00169-0

Kołodyńska, D., 2010. Diphonix Resin® in sorption of heavy metal ions in the presence of the biodegradable complexing agents of a new generation. Chem. Eng. J. 159, 27–36. https://doi.org/10.1016/j.cej.2010.02.017.

Kołodyńska, D., Hubicki, Z., 2012. Investigation of sorption and separation of lanthanides on the ion exchangers of various types. Ion Exch. Technol. 8, 193–240. https://doi.org/10.5772/50857.

Lazar, L., Bandrabur, B., Tataru-Fărmuş, R., Drobot, M., Bulgariu, L., Gutt, G., 2014. FTIR analysis of ion exchange resins with application in permanent hard water softening. Environ. Eng. Manag. J. 13, 2145–2152.

Lopez-Ramon, M.V., Stoeckli, F., Moreno-Castilla, C., Carrasco-Marin, F., 1999. On the characterization of acidic and basic surface sites on carbons by various techniques. Carbon N. Y. 37, 1215–1221. https://doi.org/10.1016/S0008-6223(98)00317-0.

Lu, D., Cao, Q., Cao, X., Luo, F., 2009. Removal of Pb(II) using the modified lawny grass: mechanism, kinetics, equilibrium and thermodynamic studies. J. Hazard Mater. 166, 239–247. https://doi.org/10.1016/j.jhazmat.2008.11.018.

Nikoloski, A.N., Ang, K.L., 2014. Review of the application of ion exchange resins for the recovery of platinum-group metals from hydrochloric acid solutions. Miner. Process. Extr. Metall. Rev. 35, 369–389. https://doi.org/10.1080/08827508.2013.764875.

Ohyoshi, A., Ohyoshi, E., Ono, H., Yamakawa, S., 1972. A study of citrate complexes of several lanthanides. J. Inorg. Nucl. Chem. 34, 1955–1960.

Płaziński, W., Rudziński, W., 2011. Kinetyka adsorpcji na granicy faz roztwór/ciało stałe. Znaczenie równań pseudo-first order oraz pseudo-second order. Wiadomości Chem. 65, 11–12.

Rajan, K.S., Martell, A.E., 1965. Equilibrium studies of uranyl complexes. III. Interaction of uranyl ion with ctric acid. Inorg. Chem. 44, 462–469.

Römkens, P., Bouwman, L., Japenga, J., Draaisma, C., 2002. Potentials and drawbacks of chelate-enhanced phytoremediation of soils. Environ. Pollut. 116, 109–121. https://doi.org/10.1016/S0269-7491(01)00150-6.

Shaibu, B.S., Reddy, M.L.P., Bhattacharyya, A., Manchanda, V.K., 2006. Evaluation of Cyanex 923-coated magnetic particles for the extraction and separation of lanthanides and actinides from nuclear waste streams. J. Magn. Magn Mater. 301, 312–318. https://doi.org/10.1016/j.jmmm.2005.07.005.

Silva, R.A., Hawboldt, K., Zhang, Y., 2018. Application of resins with functional groups in the separation of metal ions/species–a review. Miner. Process. Extr. Metall. Rev. 39, 395–413. https://doi.org/10.1080/08827508.2018.1459619.

Smolik, M., Siepietowski, Ł., Jakóbik-Kolon, A., 2014. The effects of concentrations of zirconium(IV) sulphate and sulphuric acid on sorption of zirconium(IV) and hafnium(IV) on Purolite S-957 resin. Adsorption isotherms of zirconium(IV) and hafnium(IV) ions. Solvent Extr. Ion Exch. 32, 437–446. https://doi.org/10.1080/07366299.2014.884889.

Soccol, C.R., Vandenberghe, L.P.S., Rodrigues, C., Pandey, A., 2006. New perspectives for citric acid production and application. Food Technol. Biotechnol. 44, 141–149.

Svoronos, D.R., Boulhassa, S., Guillaumont, R., Quarton, M., 1981. Citric complexes and neodymium citrate: NdCit, 3H2O. J. Inorg. Nucl. Chem. 43, 1541–1545. https://doi.org/10.1016/0022-1902(81)80333-8.

Tenório, J.A.S., Espinosa, D.C.R., 2002. Recovery of Ni-based alloys from spent NiMH batteries. J. Power Sources 108, 70–73. https://doi.org/10.1016/S0378-7753(02)00007-1.

Wierzba, S., Kłos, A., 2019. Heavy metal sorption in biosorbents – using spent grain from the brewing industry. J. Clean. Prod. 225, 112–120. https://doi.org/10.1016/j.jclepro.2019.03.286.

Wu, D., Zhao, J., Zhang, L., Wu, Q., Yang, Y., 2010. Lanthanum adsorption using iron oxide loaded calcium alginate beads. Hydrometallurgy 101, 76–83.

Zabiszak, M., Nowak, M., Taras-Goslinska, K., Kaczmarek, M.T., Hnatejko, Z., Jastrzab, R., 2018. Carboxyl groups of citric acid in the process of complex formation with bivalent and trivalent metal ions in biological systems. J. Inorg. Biochem. 182, 37–47. https://doi.org/10.1016/j.jinorgbio.2018.01.017.

Zagorodni, A.A., Kotova, D.L., Selemenev, V.F., 2002. Infrared spectroscopy of ion exchange resins: chemical deterioration of the resins. React. Funct. Polym. 53, 157–171.

Zhao, X., Wang, L., Liu, D., 2007. Effect of several factors on peracetic acid pretreatment of sugarcane bagasse for enzymatic hydrolysis. J. Chem. Technol. Biotechnol. 82, 1115–1121. https://doi.org/10.1002/jctb.

Zhou, R.S., Song, J.F., Yang, Q.F., Xu, X.Y., Xu, J.Q., Wang, T.G., 2008. Syntheses, structures and magnetic properties of a series of 2D and 3D lanthanide complexes constructed by citric ligand. J. Mol. Struct. 877, 115–122. https://doi.org/10.1016/j.molstruc.2007.07.027.

[D2] K. Burdzy, A. Aurich, S. Hunger, R. Jastrząb, M. Zabiszak, D. Kołodyńska, *Green citric acid in the sorption process of rare earth elements*, Chemical Engineering Journal, 437 (2022) 135366.

IF_{2020}: 16,744 **Punkty MEiN**: 200

Chemical Engineering Journal 437 (2022) 135366

Contents lists available at ScienceDirect

Chemical Engineering Journal

journal homepage: www.elsevier.com/locate/cej

Green citric acid in the sorption process of rare earth elements

Katarzyna Burdzy [a,*], Andreas Aurich [b], Steffi Hunger [b], Renata Jastrząb [c], Michał Zabiszak [c], Dorota Kołodyńska [a,*]

[a] Department of Inorganic Chemistry, Faculty of Chemistry, Maria Curie-Skłodowska University, M. Curie Skłodowska Sq. 2, 20-031 Lublin, Poland
[b] Department Centre for Environmental Biotechnology (UBZ), Helmholtz-Centre for Environmental Research-UFZ, Permoserstrasse 15, 04318 Leipzig, Germany
[c] Faculty of Chemistry, Adam Mickiewicz University, Uniwersytetu Poznańskiego 8, 61-614 Poznan, Poland

ARTICLE INFO

Keywords:
Rare earth elements
Chelating agents
Green citric acid
Ion exchangers
Adsorption

ABSTRACT

In this study the effects of citric acid (CA) as a biodegradable complexing agent in the sorption process of La(III), Nd(III) and Ho(III) ions (single component systems) on various types of ion exchangers (chelating ion exchangers, cation exchanger, strongly and weakly basic polystyrene and polyacrylate anion exchangers) were investigated. The effects of pH, Ln(III):CA molar ratio, phase contact time and initial concentrations as well as temperature on the adsorption capacity were analysed. The optimal process conditions were also determined which varied depending on the ion exchanger and the metal ion. The process was fast in all systems (up to 60 min). The sorption data was analysed using the pseudo-first order (PFO), pseudo-second order (PSO), intraparticle diffusion (IPD), Boyd and Dumwald–Wagner (DW) kinetic models as well as the Langmuir, Freundlich, and Temkin isotherm models. Among the studied adsorbents, the highest adsorption capacity was obtained for the Purolite S957 chelating ion exchanger which was 162.04 mg/g for the La(III) complexes, 142.65 mg/g for the Nd(III) complexes and 180.26 mg/g for the Ho(III) complexes. Reusability of ion exchangers in the desorption studies was also evaluated as a sustainable approach. Moreover, dynamic experiments were performed using the columns set. The Thomas, Adams–Bohart, Yoon–Nelson and Wolborska models were applied to the experimental data to predict the dynamic behaviour of fixed bed columns. The physicochemical properties of adsorbents were characterized by scanning electron microscopy (SEM), pH_{pzc}, and Fourier transform infrared spectroscopy (FTIR). The binary complexes of Ln(III) ions with CA at various metal:ligand ratios were investigated using the potentiometric method. The overall stability constants of the complexes were determined.

1. Introduction

Nowadays when highly developed technology accompanies the life of almost every human being, it is difficult to imagine life without it. However, when using our everyday electronic gadgets, we do not always realize that it would not be possible without the extremely important metals, which are rare earth elements (REEs). Due to their unique physical and chemical properties, REEs are essential in the production of batteries, capacitors, magnets, superconductors, catalysts, pharmaceuticals, for clean energy technologies (including lighting, wind turbines, electrified vehicles) or in military applications (e.g. defense missiles) [1–3]. Such a wide application of REEs meant that the demand for these elements increased rapidly over the last two decades with the development of high-tech products. Most REEs are not as rare as the name suggests, for example cerium, which is the most abundant REE in the earth's crust, is more common than copper or lead [4]. The main sources of REEs in nature are the mineral deposits of bastnasite, monazite, xenotime as well as loparite and apatite [5]. Among them, bastnasite is the most abundant. The largest resources are in China, USA, Australia, India and Russia. However, there are several challenges to mining, processing and global REEs availability. This is, among others, their geological distribution. REE minerals are rarely concentrated which makes them difficult to exploit. In addition, REEs, due to similar physicochemical properties, often occur together in the same deposits which further complicates the process. Another fact that does not facilitate the extraction of these elements is that they often occur together with the radioactive decay chains of uranium or thorium. All these factors cause that many countries, even those with REEs deposits on their territories, rely heavily on imports. This has led to a situation where one country, China, has played a dominant role in the global extraction of REEs since 1990. Up till 2010 China controlled 97% of the global REEs production [6]. The dangerous situation on the REEs market, caused by the market

* Corresponding authors.
E-mail addresses: katarzyna.araucz@poczta.umcs.lublin.pl (K. Burdzy), d.kolodynska@poczta.umcs.lublin.pl (D. Kołodyńska).

https://doi.org/10.1016/j.cej.2022.135366
Received 28 December 2021; Received in revised form 16 February 2022; Accepted 17 February 2022
Available online 21 February 2022

monopoly, fears of a sharp increase in prices and limited supplies, resulted in the resumption of production in the United States, supplemented by new or increased production in Australia, Burma (Myanmar) and Burundi as well as the start of searching for alternative sources of their recovery. For example, according to the Mineral Commodity Summaries 2020 report in the United States, domestic production of mineral concentrates increased to 26,000 tons, which is a 44% increase compared to 2018 [7]. However, the undeniable fact is that the global resources of REEs are shrinking, and in conjunction with the constantly growing demand, it becomes necessary to develop new methods of obtaining them. A promising alternative to the traditional extraction of REEs is their recovery from the secondary sources. However, at present only limited quantities of REEs from batteries, permanent magnets, and fluorescent lamps are recycled [7]. The development of optimal recovery methods for REEs, apart from securing their reserves, would also contribute to reducing the amount of toxic waste in the environment. One of the most effective methods of separating and recovering metal ions is adsorption which successfully uses ion exchangers with various functional groups [8–11]. Recently the literature has reported many adsorbents used in the recovery of REEs. Esma et al. [8] carried out the research on the La(III) ions adsorption using the commercial macroporous resins containing iminodiacetic (Lewatit TP 207) and aminomethylphosphonic acid groups (Lewatit TP 260). In their paper Galhoum et al. [12] described the synthesis and application of cysteine-functionalized chitosan magnetic nano-based particles in the recovery of La(III), Nd(III) and Yb(III) while Liao et al. [13] used the prepared graphitic-C_3N_4 nanosheets in the adsorption process of Eu(III), La(III), Nd(III) and Th(IV) ions. In the series of publications Javadian et al. [14–17] described the synthesis of the magnetic nanocomposites: calcium alginate carrying poly(pyrimidine-thiophene-amide), calcium alginate/carboxymethyl chitosan containing $Ni_{0.2}Zn_{0.2}Fe_{2.6}O_4$, CMC bionanocomposite carboxymethyl chitosan/poly(pyrimidine-thiopheneidine-amide)/$Ni_{0.2}Zn_{0.2}Fe_{2.6}O_4$ and Ca-alginate/carboxymethyl chitosan/$Ni_{0.2}Zn_{0.2}Fe_{2.6}O_4$, which they used in the adsorption process of Nd(III), Tb(III) and Dy(III) ions.

It is well-known that the eluting agents based on the inorganic substances are not suitable for separation of REEs [18,19]. Therefore, to this aim organic substances forming complexing compounds of varying stability with Ln(III) were proposed. In the sixties of the last century citric acid (CA) solutions neutralized to various pH values were studied first. Then the obtained results show that the separation efficiency of the citrate solutions increases with the decreasing values of pH and the increasing time of separation. The 5% CA solutions or its ammonium salts with the pH gradient from 3.5 to 3.9 were typically used to separate Sc, La and Y or Ce-group using the citrate-acetate mixture. For example, the separation factors were for the pairs of Lu(III)-Yb(III) 1.31, Yb(III)-Tm(III) 1.52, Tm(III)-Er(III) 1.60, Er(III)-Ho(III) 1.50, Ho(III)-Dy(III) 1.37, Dy(III)-Tb(III) 1.40, Tb(III)-Gd(III) 1.37, Gd(III)-Eu(III) 1.12, Eu(III)-Sm(III) 1.19, Sm(III)-Pm(III) 1.38, Pm(III)-Nd(III) 1.09, Nd(III)-Pr(III) 1.18, Pr(III)-Ce(III) 1.69 at 360 K. Therefore this was proved to be very valuable in developing separation techniques and has found several applications in radiochemistry.

Nowadays, however, a new perspective is associated with the use of CA originated from the fermentation process as green CA. As for the amount of production and utility, citric acid is one of the most important bioproducts. It has been used not only as a complexing agent in metal treatment but also as a monomer for the polymers production, a softener as the effect of its organic acid chelating and buffering properties [20]. It exists in human plasma at a concentration of 0.1 mM. It is an important intermediate in the Krebs cycle and is involved in the metalloenzyme systems, such as aconitase and $NifV^-$ nitrogenase in the nitrogen fixation [21]. In addition, rare earth citrates can be used to prepare homogeneous gels of metal oxides by the solvent evaporation. This causes a rapid increase in viscosity which reduces the diffusion of complexes and thus prevents phase separation and allows for obtaining such oxides as $(La_{1-x}Sr_x)CoO_3$, $(Bi,La)_4Ti_3O_{12}$ [22,23]. Citrates are used in food industry for production of soft drinks, as food additives, acidity regulators, buffers, antioxidants, preservatives and stabilizing agents, in dietary supplements against zinc, copper, iron etc. They are also used in producing medicaments, cosmetics, plastics and in oral rehydration treatment [24,25].

CA is produced biotechnologically on a large industrial scale using the fungus *Aspergillus niger*, sugars (glucose, sucrose) and sugar molasses as substrates [20,26]. The use of these substrates for the bioprocesses is in competition with their essential application as food and feed. As an advantage, the yeast *Yarrowia lipolytica* has a broader variety in terms of the substrates for the production of CA, e.g. carbohydrates, (raw) glycerol, ethanol, fatty acids, plant oils, and by-products like waste frying oil (WFO) [27–29]. In particular, the use of waste products such as WFO allows the production of CA in a sustainable, green way without competition to the food supply [30].

On the other hand, lanthanide(III) ions and their complexes are used in medicine because of their anti-cancer, anti-inflammatory, anti-coagulating and anti-allergic properties. Gadolinium(III) complexes with their magnetic properties have been used in the magnetic resonance imaging method [31].

Due to its significant impact on the development of separation techniques and applicability of CA, in this paper we will discuss the possibility of the use of its green form obtained in the fermentation process in the REE sorption and separation using different types of ion exchangers (the most commercially common) with the phosphonic and sulphonic, aminophosphonic, sulphonic as well as quaternary ammonium functional groups of types I and II as well as with the different types of polymer matrix (polystyrene and polyacrylate). The focus will be made on presenting the applicability of varying parameters of the effectiveness of La(III), Nd(III) and Ho(III) sorption process in the presence of CA.

2. Materials and methods

2.1. Materials

In this study there were used the following adsorbents: Purolite S957, Purolite S950, Lewatit Monoplus SP112, Lewatit MonoPlus M500, Lewatit MonoPlus M600, Lewatit MonoPlus MP500, Amberjet 4200, Amberjet 4400, Amberjet 4600, Amberlite IRA 458, Amberlite IRA 958 and Amberlite IRA 67. The details of the studied ion exchangers are given in the Supplementary Materials.

Citric acid (CA) containing the biomass-free fermentation solution derived from a non-sterile bioprocess with the yeast *Yarrowia lipolytica* H181 using waste frying oil as a substrate was obtained by the Helmholtz-Centre for Environmental Research-UFZ (Germany). The details of the yeast cultivation process are presented in the Supplementary Materials.

$La(NO_3)_3{\cdot}6H_2O$, $Ce(NO_3)_3{\cdot}6H_2O$, $Pr(NO_3)_3{\cdot}6H_2O$, $Nd(NO_3)_3{\cdot}6H_2O$, $Sm(NO_3)_3{\cdot}6H_2O$, $Ho(NO_3)_3{\cdot}5H_2O$ were obtained from Sigma-Aldrich and were used without further purification.

2.2. Apparatus and instruments

All apparatus and equipment used in this study are presented in the Supplementary Materials.

2.3. Potentiometric measurements

Before each measurement series, the pH-meter indication was calibrated with two buffer solutions at pH 4.00 and 9.00. Potentiometric titrations were made in the atmosphere of neutral gas (helium 5.0) at 293 ± 1 K and with the constant ionic strength (μ = 0.1 M KNO_3). Measurements were made in the pH range from 2.5 to 11.0. The CO_2-free NaOH solution at the concentration of 0.1940 M was used as a titrant. The concentration of the complexing agent (CA) in the sample

was 1.0×10^{-3} M. The selection of the model as well as the protonation constants for the used ligand and the stability constants for the complexes were studied on the basis of the points obtained from the titration curve using the HYPERQUAD2008 program. The determined ionic product for water was $pK_w = 13.77$. The calculations were made using 150–350 points for each job. The hydrolysis constants of metal ions were also determined and included in the computer analysis of potentiometric data.

2.4. Adsorption studies - static method

The stock solution of Ln(III) ions at the concentration of 1×10^{-2} M was prepared by dissolving appropriate amounts of $La(NO_3)_3{\cdot}6H_2O$, $Nd(NO_3)_3{\cdot}6H_2O$ or $Ho(NO_3)_3{\cdot}5H_2O$ in the deionised water. The solutions of the Ln(III) ions and CA system with the various required initial concentrations were prepared by adding the equimolar amounts of metal ions solution to the CA solutions. The final concentration of Ln(III) was estimated by the ICP-OES method.

To find out the optimal conditions for the sorption of Ln(III) complexes with CA on the selected ion exchangers the batch method was used in the single component systems. To test the influence of the initial pH of the solution for Ln(III)-CA on Purolite S957, Purolite S950, Lewatit SP112, Lewatit M500, Lewatit M600, Lewatit MP500, Amberjet 4200, Amberjet 4400 and Amberjet 4600 as well as Amberlite IRA 458, Amberlite IRA 958 and Amberlite IRA 67 the 20 mL solution of 1.0×10^{-3} M concentration in the pH range 2.0–12.0 and 0.05 g of the selected ion exchanger were used. In this research stage 1 M HNO_3 or 1 M NaOH solutions were used to adjust the initial pHs of the solution. The effect of the Ln(III):CA ratio of 1:1, 1:2 and 1:4 on the adsorption efficiency was also investigated. To evaluate the kinetics of the sorption process the 10 mL solution of 1.0×10^{-3}–2.5×10^{-3} M concentration and 0.1 g of the ion exchanger were placed in the 100 mL conical flasks and shaken in the time interval from 1 to 240 min. The above experiments were performed at 293 K with a shaking speed of 180 rpm. The influence of temperature in the range from 293 to 333 K on the Ln(III) adsorption efficiency was also evaluated. After shaking all samples were separated by filtration using the filter paper. The sorption isotherm studies were carried out analogously at the initial concentrations of the studied solutions in the range 1.0×10^{-3}–1.3×10^{-2} M.

2.5. Desorption studies

The desorption studies were also carried out to evaluate the regeneration abilities of the adsorbents. Hydrochloric and nitric(V) acids in the concentrations of 0.5, 1 and 2 M were used as the desorbing agents. Prior to testing, the Ln(III)-CA complexes were adsorbed on a given ion exchanger using an initial concentration of 1.0×10^{-3} M and a phase contact time of 240 min. After the sorption process, the prepared samples were allowed to dry. The desorption tests were carried out using an adsorbent dose of 10 g/L and a temperature of 293 K. The reusability studies of ion exchangers were carried out on the example of adsorption/desorption of La(III)-CA complexes in the same way for the best desorbing agent in five sorption/desorption cycles. The experiments were performed in triplicate, therefore the obtained results were averaged.

2.6. Adsorption studies – Dynamic method

The studies with the dynamic method were carried out only for the La(III) complexes with CA. For this purpose, the solution of La(III)-CA complexes with a concentration of 1.0×10^{-3} M, pH values equal to 8.0 and La(III):CA ratio 1:1 for the chelating ion exchangers and the cation exchanger and 1:2 for the anion exchangers were used. The pH values of the solutions were adjusted with 1 M HNO_3 or 1 M NaOH. These studies were carried out at room temperature (293 K). The dynamic experiments were performed using glass columns with a diameter of 1.5 cm and a height of 25 cm packed with 10 mL of swollen ion exchanger. The flow rate of the solution through the bed was 0.6 mL/min. The effluent was collected in defined volume fractions and analysed by the ICP-OES method. The column experiments were conducted until the concentration of La(III) ions in the effluent reached the initial concentration.

2.7. The equations

2.7.1. Static method

Based on the experiments the basic parameters such as the amount of Ln(III) adsorbed per amount of ion exchanger at the equilibrium q_e [mg/g], the amount of adsorbed Ln(III) at the time t q_t [mg/g], the adsorption effectiveness $\%S$ and the desorption percentage $\%D$ as well as the distribution coefficients K_d were estimated using the following equations (Eqs.(1)–(5)):

$$q_e = (C_0 - C_e) \times \frac{V}{m} \tag{1}$$

$$q_t = (C_0 - C_t) \times \frac{V}{m} \tag{2}$$

$$\%S = \frac{(C_0 - C_t)}{C_t} \times 100\% \tag{3}$$

$$\%D = \frac{C_{des}}{C_0} \times 100\% \tag{4}$$

$$K_d = \frac{(C_0 - C_e)}{C_e} \times \frac{V}{m} \tag{5}$$

where C_0 is the initial concentration of Ln(III) in the solution [mg/L], C_e is the equilibrium concentration of Ln(III) in the solution [mg/L], C_t is the concentration of Ln(III) at the time t [mg/L], V is the solution volume [L], m is the mass of the ion exchanger [g] and C_{des} is the Ln(III) ions concentration after the desorption process [mg/L].

In order to study the adsorption kinetics five kinetic models were applied to fit the adsorption kinetic data:

a) pseudo-first order kinetic equation [32]

$$q_t = q_e(1 - exp(-k_1 t)) \tag{6}$$

b) pseudo-second order kinetic equation [33]

$$q_t = \frac{k_2 q_e^2 t}{1 + k_2 q_e t} \tag{7}$$

c) intraparticle diffusion kinetic model (Weber-Morris model) [34]

$$q_t = k_i t^{0.5} + C \tag{8}$$

d) Boyd kinetic model [35]

$$B_t = -0.4977 - ln(1 - F) \tag{9}$$

e) Dumwald-Wagner model [36]

$$log(1 - F^2) = -\frac{k}{2.303t} \tag{10}$$

where q_e, q_t were defined as previously, k_1 is the pseudo-first order rate constant [1/min], k_2 is the pseudo-second order rate constant [g/mg min], k_i is the intraparticle diffusion rate constant [mg/g $min^{1/2}$], C is the value of intercept related to the boundary layer thickness, F is the Ln (III) adsorbed fraction at the time t ($F = q_t/q_e$), k is the Dumwald-Wagner model rate constant [1/min].

The adsorption data were also analysed using the following isotherm models:

a) Langmuir model [37]

$$q_e = \frac{q_0 K_L C_e}{1 + K_L C_e} \tag{11}$$

b) Freundlich model [38]

$$q_e = K_F C_e^{1/n} \tag{12}$$

c) Temkin model [39]

$$q_e = BlnA + BlnC_e \tag{13}$$

where q_e, C_e were defined as previously, q_0 is the maximum monolayer adsorption capacity of the ion exchanger [mg/g], K_L is the Langmuir constant related to the affinity of the binding sites [L/mg], K_F is the Freundlich adsorption capacity [mg/g], n is the Freundlich constant related to the adsorption intensity, A is the Temkin constant related to the maximum binding energy [L/g], B is related to the adsorption heat [J/mol] and can be expressed as $B = RT/b_T$ where R is the gas constant (8.314 J/mol K), T is the absolute temperature [K], and b_T is the Temkin isotherm constant.

Thermodynamic parameters such as the Gibbs free energy change ΔG° [kJ/mol], the enthalpy change ΔH° [kJ/mol] and the entropy change ΔS° [J/mol K] were determined to evaluate the nature of the adsorption process based on the following equations [40]:

$$\Delta G^o = -RTlnK_c \tag{14}$$

$$\Delta G^o = \Delta H^o - T\Delta S^o \tag{15}$$

$$lnK_c = \frac{\Delta S^o}{R} - \frac{\Delta H^o}{RT} \tag{16}$$

where R is the universal gas constant (8.314 J/mol K), T is the absolute temperature [K], K_c is the thermodynamic equilibrium constant which is determined by plotting $\ln(q_e/c_e)$ vs. q_e and extrapolating to zero q_e.

Additionally, the error function - the Chi-square (χ^2) was used for the isotherm models fitting:

$$\chi^2 = \sum \frac{(q_{e,exp} - q_{e,cal})^2}{q_{e,cal}} \tag{17}$$

where $q_{e,\mathrm{exp}}$ is the adsorption capacity determined experimentally and $q_{e,cal}$ is the adsorption capacity according to the given model.

2.7.2. Dynamic method

On the basis of the breakthrough curves obtained in the dynamic tests, the basic parameters such as the working exchange capacity C_w [mg/mL], the mass distribution coefficient D_g and the volume distribution coefficient D_v were determined using the following equations:

$$C_w = \frac{U \times C_0}{V_j} \tag{18}$$

$$D_g = \frac{\overline{U} - U_0 - V}{m_j} \tag{19}$$

$$D_v = \frac{\overline{U} - U_0 - V}{V_j} \tag{20}$$

where: C_0 is the initial La(III) ions concentration [mg/mL], U is the effluent volume to the break point [L], V_j is the bed volume [mL], m_j is the dry ion exchanger mass [g], $\bar{U}$ is the volume of the leakage equal $C/C_0 = 0.5$ [mL], U_0 is the dead volume in the column [mL] and V is the empty space volume between the resin beads equal 0.4 mL.

Several mathematical models have been developed to predict the dynamic behaviour of the column. The following models were used to determine the breakthrough performance as well as to calculate the column kinetic parameters and adsorption capacity of the fixed bed column:

a) the Thomas model

$$ln\left(\frac{C_0}{C} - 1\right) = \frac{k_{Th} q_0 m}{Q} - \frac{k_{Th} C_0}{Q} V \tag{21}$$

b) the Adams-Bohart model

$$ln\left(\frac{C}{C_0}\right) = k_{AB} C_0 t - k_{AB} q \frac{H}{v} \tag{22}$$

c) the Yoon-Nelson model

$$ln\left(\frac{C}{C_0 - C}\right) = k_{YN} t - k_{YN} \tau \tag{23}$$

d) the Wolborska model

$$ln\left(\frac{C}{C_0}\right) = \frac{\beta_a C_0}{q} t - \frac{\beta_a H}{v} \tag{24}$$

$$\beta_a = \frac{v^2}{2D}\left(\sqrt{1 + \frac{4\beta_0 D}{v^2}} - 1\right) \tag{25}$$

where C is the outlet concentration [mg/L], C_0 is the initial concentration [mg/L], k_{Th} is the Thomas rate constant [mL/mg min], q_0 is the adsorption capacity [mg/g], m is the mass of the adsorbent in the column [g], Q is the flow rate [mL/min], V is the effluent volume [L], k_{AB} is the Adams-Bohart rate constant [L/mg min], t is the time [min], q is the adsorption capacity [mg/L], H is the bed depth of the fixed bed column [cm], v is the linear velocity calculated by dividing the flow rate by the column section area [cm/min], k_{YN} is the Yoon-Nelson rate constant [1/min], τ is the time required for 50% adsorbate breakthrough [min], β_a is the kinetic coefficient of the external mass transfer [1/min] and D is the axial diffusion coefficient [cm^2/min], β_0 is the external mass transfer coefficient with a negligible axial dispersion coefficient D.

3. Results and discussion

3.1. Materials characterization

3.1.1. Citric acid

Citric acid is a tricarboxylic organic compound (Fig. 1). CA has a hydroxyl group and three carboxyl functional groups which allow for the formation of thermodynamically stable complexes with many metal ions, e.g. Ca(II), Sr(II), Mn(II), Co(II), Ni(II), Cu(II), Fe(II), La(III) [41–45]. This contributes to the increasing solubility of metal ions and at the same time their bioavailability facilitating the ions adsorption in the biological systems [46]. The X-ray crystallographic patterns proved that the central hydroxyl and carboxyl groups lie in a plane perpendicular to the backbone plane [47].

In the acidic and neutral solutions CA dissociates readily in three stages [46]:

$$H_3Cit + H_2O \rightleftarrows H_2Cit^- + H_3O^+ \tag{26}$$

$$K_{a1} = \frac{[H_2Cit^-][H_3O^+]}{[H_3Cit]}$$

$$H_2Cit^- + H_2O \rightleftarrows HCit^{2-} + H_3O^+ \tag{27}$$

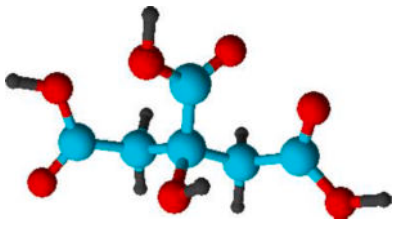

Fig. 1. Structure of CA.

$$K_{a2} = \frac{[HCit^{2-}][H_3O^+]}{[H_2Cit^-]}$$

$$HCit^{2-} + H_2O \rightleftarrows Cit^{3-} + H_3O^+ \quad (28)$$

$$K_{a3} = \frac{[Cit^{3-}][H_3O^+]}{[HCit^{2-}]}$$

At 298 K the respective equilibrium constants pK_{a1}, pK_{a2}, and pK_{a3} are 3.13, 4.76, and 6.4 [48]. However, in the strongly basic solutions, CA can also split off the hydroxyl proton with a pK_{a4} equal 11.6 [49]. Due to the high pK_{a4} value, hydroxyl citrate ionization can be neglected in most cases of complex formation, therefore most speciation studies treat CA as having only three ionisable groups. For this reason, citrates act as tridentate ligands [46].

The relatively low protonation constants of CA cause deprotonation of carboxyl groups to occur at low pH values, therefore in the biological systems where the pH oscillates around 7.0, these compounds are present in a completely deprotonated form (Table 1).

The solid-phase studies proved that at first CA loses the proton of the central carboxyl group and then those from the terminal carboxyl groups [47,50]. Based on the examination of the NMR spectra, a similar dissociation pattern can be expected in the solution (Fig. 2).

Bastug et al. [51] determined the protonation constants of CA and the stability constants of the 1:1 binary complexes of CA with Cu(II), Ni (II), Co(II), Mn(II) and Ce(III) potentiometrically at the temperatures of 288, 298 and 308 K and the ionic strength of 0.10 mol/L ($NaClO_4$). The thermodynamic parameters for the complex formation reaction were also given. It was found that all the three protonation constants of CA increased with the increasing temperature, proving that the process is endothermic. Therefore, a higher temperature is favourable for all protonation reactions of the ligand in the aqueous solution. Oxygen atoms act as electron donors and each of them can serve as a metal ligand. CA tends to form various types of complexes with metal ions. These include weak complexes with alkali metal ions and alkaline earth metal ions and very strong ones with heavy metal ions and lanthanides.

Among the complexes of CA depending on the complexed metal ion, one can distinguish mononuclear, binuclear, or polynuclear and bi-, tri- as well as multidentate complexes (Fig. 3). For example, metals such as Ca(II), Fe(II) and Ni(II) form bidentate, mononuclear complexes with two carboxyl groups of the CA molecule. Cu(II), Cd(II) and Pb(II) form tridentate, mononuclear complexes, involving two carboxyl groups and the hydroxyl group [52]. U(VI) complexes with CA are an example of the binuclear complexes with two uranyl ions and two CA molecules involving four carboxylic acid groups and two hydroxyl groups [53].

NMR study of the Ln(III) complexes with CA at the ratio 1:2 and at pH 7.4 was carried out and the possible coordination geometry of Ln $(cit)_2$ complex was proposed [54]. It was found that one lanthanide ion is coordinated by two citrate ligands through a central hydroxyl group and a central carboxylate group, forming a coordination center involving some water molecules (Fig. 4). Two terminal carboxylate groups are not directly involved in the complexation but are directed to the coordination center due to the hydrogen bond interactions between the carboxylate groups and the coordinated water molecules.

The stability constants of REE complexes with CA as a chelating agent of [LnL] type (μ=0.1; T = 293 K) are equal to 7.10, 7.40, 7.60, 7.70, 7.71, 7.80, 7.80, 7.72, 7.74, 7.79, 7.84, 7.86, 8.00, 8.05, 8.07 for La(III), Ce(III), Pr(III), Nd(III), Pm(III), Sm(III), Eu(III), Gd(III), Tb(III), Dy(III), Ho(III), Er(III), Tm(III), Yb(III), Lu(III), respectively [48].

Table 1
The protonation constants for CA.

Overall protonation constants (logβ)	SD	Protonation equilibria	Successive protonation constants (log$K$)
12.64	0.04	$H_2Cit^- + H_3O^+ \rightleftarrows H_3Cit$	3.16
9.48	0.04	$HCit^{2-} + H_3O^+ \rightleftarrows H_2Cit^-$	4.12
5.36	0.04	$Cit^{3-} + H_3O^+ \rightleftarrows HCit^{2-}$	5.36

This paper presents the results of the analysis of the potentiometric data of the binary systems of CA with La(III), Ce(III), Pr(III), Nd(III), Sm (III), Ho(III) during the formation of complexes. The results of the potentiometric titrations of solutions containing La(III), Ce(III), Pr(III), Nd(III), Sm(III) and Ho(III) and CA at the various metal:ligand ratios are presented in Fig. 5, Fig. S1 and Table 2.

The obtained data were used for the modelling of the reactions of soluble complexes formation. The positively charged Ln(III) ions can interact with the negatively charged CA. The overall protonation constants of H_3Cit are equal to 12.64, 9.48 and 5.36 (logβ). These reactions are pH dependent. Therefore the conditional constant gives the relationship between the concentration of formed complexes and the unreacted Ln(III) ions as well as the complexing agent (H_3Cit). The protonated complexes of LnH_xL type, LnL and LnL_2 types as well as hydroxycomplexes of $LnL(OH)_x$ type were identified in all systems. The complex formation starts with the formation of the protonated species. Almost the whole CA introduced into the system at all studied ratios was coordinated by Ln(III) ions. Interestingly, the species made of CA and Sm (III) ions exhibit the slightly lower equilibrium constants of complex formation which is a consequence of the gadolinium break effect (Table 2).

Under the thermodynamic conditions especially in the equilibrium the complexes formation reaction is selective and only those metal ions with the highest values of the stability constant are formed first.

For La(III), Ce(III), Pr(III), Nd(III), Sm(III) and Ho(III) and L (CA) in the 1:1 system, for the LnHL complexes they are: 4.16, 4.49, 4.28, 4.59, 4.46 and 5.43; for LnL 6.15, 6.68, 6.69, 6.73, 6.67 and 7.14 as well as for LnL(OH) 6.60, 8.12, 8.26, 7.41, 7.69 and 7.90, respectively. In the 1:2 system these values are: for the LnHL complexes: 4.08, 4.34, 4.50, 4,86, 3.85 and 5.52; for LnL 6.19, 6.61, 6.84, 7.11, 6.81 and 7.42 as well as for LnL(OH) 7.94, 8.60, 8.85, 8.69, 8.85 and 7.64, respectively. For La(III), Ce(III), Nd(III), Sm(III) and Ho(III) and L (CA) in the 2:1 system, for the LnHL complexes they are: 4.05, 3.74, 4.53, 4,39 and 8.72; while for LnL 6.11, 6.38, 6.25, 6.84, 6.83 and 10.85 as well as for LnL(OH) 7.61, 7.56, 8.20, 8.70, 8.58 and 7.65, for La(III), Ce(III), Pr(III), Nd(III), Sm(III) and Ho(III) and L (CA), respectively.

3.1.2. Ion exchangers

The morphology of ion exchangers surface was studied by means of the SEM method. The images were taken before and after the La(III) complexes adsorption process and are presented in Fig. S2. The obtained SEM images show the difference between the structure of macroporous and gel ion exchangers. As follows from the Fig. S2 the surface of macroporous ion exchangers (Purolite S957, Purolite S950, Lewatit SP112, Lewatit MP500, Amberlite IRA 958) is rather homogeneous and porous which is confirmed by the presence of pores in their structure which are the site for the sorption of metal ions. In the case of gel ion exchangers (Lewatit M500, Lewatit M600, Amberjet 4200, Amberjet 4400, Amberjet 4600, Amberlite IRA 458, Amberlite IRA 67), a homogeneous surface is also observed.

After the sorption process the surface of macroporous ion exchangers does not change significantly. The SEM images of gel ion exchangers show that their surface became denser after the sorption process than before. The most visible changes are in the case of Amberlite IRA 67 where the surface became much rougher and irregular.

In order to characterize the porous structure of the ion exchangers, a review of the literature was made. Table 3 shows the specific surface area (S_{BET}) and the average pore diameter (D) of the tested adsorbents obtained by other researchers. In all cases the surface area as well as the pore size were calculated using the Brunauer–Emmett–Teller (BET) and the Barrett–Joyner–Halenda (BJH) methods, respectively.

It can be noticed that the specific surface area of the ion exchangers

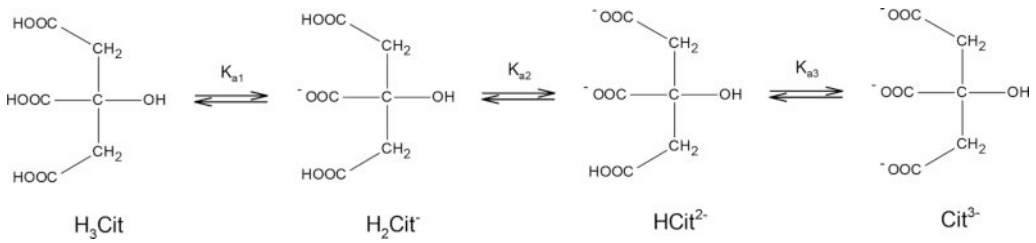

Fig. 2. Dissociation equilibria of CA.

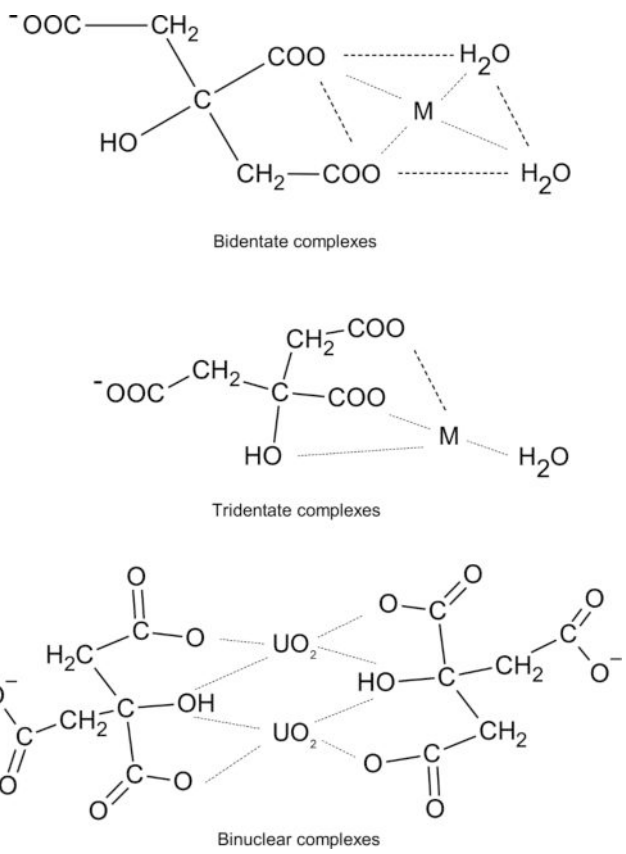

Fig. 3. Types of metal citrate complexes.

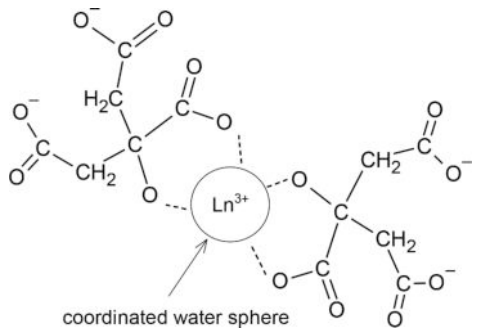

Fig. 4. Possible coordination geometry of $Ln(cit)_2$ complex in the pH 7.4 solution.

selected for the study was quite diverse but it had small values in the range of 0.45–14.98 m^2/g. The average pore size was in the range of 2.84–34.10 nm which indicates the presence of mesopores (2–50 nm) in the structure of the ion exchangers.

The point of zero charge (pH_{pzc}) of the ion exchangers, i.e. the pH value of the solution at which the adsorbent surface is electrically neutral, was determined using the potentiometric titration and drift methods. Table 3 summarizes the pH_{pzc} values obtained by both methods. As follows from the comparison of the two methods, similar values were obtained. It is known that if the pH < pH_{pzc}, the surface of the ion exchangers is positively charged. In this case the electrostatic repulsion occurs between the Ln(III) ions and the adsorbent surface which is the cause of low sorption efficiency. In this pH range, negative complexes of Ln(III) with CA could be easily adsorbed but they do not exist at low pH values. If pH > pH_{pzc} the surface is negatively charged which results in the attraction of metal ions and the repulsion of negatively charged Ln(III)-CA complexes. However, our studies showed a different effect of pH on the adsorption process than that described here which suggests that apart from the electrostatic attraction, other mechanisms are involved in the process of Ln(III)-CA complexes adsorption.

The FTIR spectra of the investigated ion exchangers recorded before and after the sorption of Ln(III) complexes with CA are presented in Fig. 6.

A broad, intensive peak present in each recorded spectrum in the range of 3500–3300 cm^{-1} is characteristic of the hydroxyl or hydroxyl and amino groups. The peaks originating from the ion exchanger matrix (cross-linked polystyrene or polyacrylic) are also clearly visible. The bands at about 3020 cm^{-1} and 2920 cm^{-1} are ascribed to the asymmetric and the corresponding symmetric stretching vibrations of the $–CH_2$ groups. The asymmetric, stretching vibrations of the carbon–carbon bonds in the ring ($\nu_{as}(C = C)$) and the asymmetric, scissoring vibrations of the methylene groups ($\delta_{as}(–CH_2)$) exist at the frequencies in the range of 1480–1470, 1420–1410, and 1380–1370 cm^{-1}. The deformation vibrations of 1,4-disubstituted benzene rings were confirmed and they are visible in the case of the polystyrene-divinylbenzene matrix in the wave number range 975–823 cm^{-1}.

In the case of the ion exchangers with a polyacrylic matrix, the characteristic peaks appearing in the frequency range 1650–1550, 1460–1370 and 1260 cm^{-1} were assigned to the C–C stretching, C–H deformation, and C–N stretching bonds, respectively [61]. Besides the peaks from the matrix, those confirming the presence of functional groups are also visible.

The presence of the phosphonic and sulfonic functional groups in Purolite S957 is confirmed by the bands at 2283 and 2112 cm^{-1} corresponding to the stretching vibrations of the P-OH and S-OH groups, respectively. The bands at 1123 and 988 cm^{-1} correspond to the stretching vibrations of the P = O, P-O, S = O and S-O groups [62–64]. In the Purolite S950 spectrum, the bands at 2312 cm^{-1} indicate the stretching vibrations of the P-OH groups. At 1081 and 973 cm^{-1} the presence of the P = O and P-O groups in the phosphonic group was observed. Moreover, in the range of 1530–1400 cm^{-1} there are weaker bands corresponding to the N–H deformation vibrations [63].

The four peaks observed in the Lewatit SP112 spectrum at 1176, 1124, 1037 and 1008 cm^{-1} are attributed to the presence of sulfonic groups. These peaks arise as a result of the stretching vibrations of the S = O and S-O groups in the $-SO_3$ group.

Comparing the FTIR spectra of the ion exchangers obtained before and after the sorption of the Ln(III) complexes with CA, some changes in

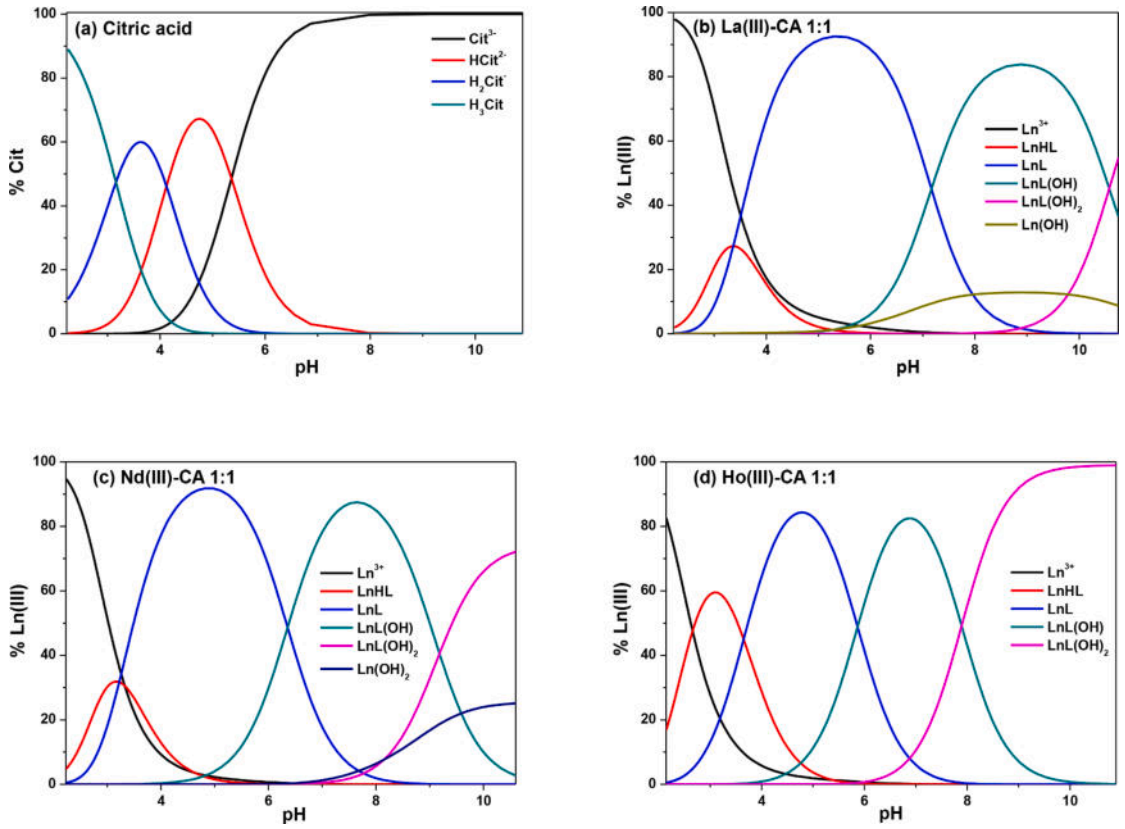

Fig. 5. Percentage of CA individual forms depending on the pH values (a) and the distribution diagrams for the Ln(III)-L systems (where Ln = La(III), Nd(III), Ho(III) and L = citric acid, CA) at the Ln(III):L ratio 1:1 (b-d).

the spectra were observed. The peak shifts and intensity changes were found in the characteristic bands of the functional groups. After the sorption process of Ln(III) complexes with CA, the peaks from the phosphonic and/or sulfonic functional groups in the spectra of the chelating ion exchangers were shifted towards higher wave numbers. This suggests that these groups are involved in the Ln(III) ion binding. After the sorption the FTIR spectra of the anion exchangers exhibit two strong bands at 1565 and 1370 cm^{-1} which can be assigned to the asymmetric and symmetric stretchings of the COO^- groups, respectively ($\nu_{as}(COO^-)$ and $\nu_s(COO^-)$) [65].

3.2. Adsorption studies - static method

3.2.1. Effect of initial pH

It is well-recognized that the solution pH has a significant influence on the behaviour of the adsorption process due to its effect on the chemical speciation of the adsorbate in the aqueous solution and the surface charge of the adsorbent by ionization of resin functional groups [66]. To determine the optimal pH values for the adsorption of La(III), Nd(III) and Ho(III) ions in the presence of CA with the use of the tested adsorbents, the experiments were conducted in the pH range of 2.0–12.0 by adjusting with 1 M HNO_3 or 1 M NaOH. In this research stage, the ratio between the Ln(III) ions and CA was maintained at 1:1 for the chelating ion exchangers and the cation exchanger and 1:2 for the anion exchangers.

The obtained results for the La(III)-CA complexes are demonstrated in Fig. 7 and for the Nd(III) and Ho(III) complexes in Figs. S3 and S4.

It can be seen that changing the solution pH influences the sorption process in a different way, depending on the adsorbent and the metal ion. In the case of La(III) complexes adsorption on the chelating ion exchangers (Purolite S957, Purolite S950) and the cation exchanger (Lewatit SP112), the obtained sorption capacity is almost constant and independent of the solution pH. Only in a very alkaline environment a decrease in the sorption efficiency can be observed.

Similar results were obtained for the sorption of Nd(III) and Ho(III) complexes on Purolite S957 and for Ho(III) complexes sorption on Purolite S950. The studies of the Nd(III) complexes adsorption on Purolite S950 and Lewatit SP112 as well as Ho(III) complexes on Lewatit SP112 showed that in these cases, as the solution pH increases, the sorption efficiency decreases which indicates that ion exchangers bind the uncomplexed form of metal ions more easily. A similar relationship was observed for the weakly basic anion exchanger Amberlite IRA 67 where the highest adsorption capacity was recorded at pH 4.0 while a further increase in pH resulted in a decreasing sorption efficiency.

A completely different behaviour, regardless of the tested metal, is shown by the strongly basic anionic ion exchangers (Lewatit M500, Lewatit M600, Lewatit MP500, Amberjet 4200, Amberjet 4400, Amberjet 4600, Amberlite IRA 458, Amberlite IRA 958), the sorption capacity of which depends largely on the pH value of the solution. The potentiometric measurements showed that at pH 2.0, free Ln(III) ions and the protonated species H_3Cit are the dominant forms in the solution therefore probability of Ln(III)-CA chelates formation is not sufficient. The repulsion between the Ln(III) cations and the positively charged active sites of the anionic ion exchangers can be considered the reason for the insignificant removal obtained at the studied pH lower value. On the other hand, free Ln(III) ions are easily removed by the chelating ion exchangers and the cation exchanger. As the pH increases, the proportion of Ln(III) complex forms in the solution also increases being more easily trapped by the functional groups of anionic ion exchangers. The decrease in the sorption capacity at high pH values may result from the competition between the OH^- and Ln(III)-CA complexes for adsorption on the positively charged active sites of the adsorbent.

Therefore for the further studies of Ln(III) ions sorption in the presence of CA there were selected the following pH values of the

Table 2
The overall stability constants (logβ) and the equilibrium constants of complex formation ($logK_e$) in the systems of Ln(III)-L (where Ln = La(III), Ce(III), Pr(III), Nd(III), Sm(III), Ho(III) and L = citric acid, CA) for various metal:ligand ratios.

Species	1:1			1:2			2:1		
	logβ	SD	logK_e	logβ	SD	logK_e	logβ	SD	logK_e
La(III)-CA									
LnHL	9.52	0.03	**4.16**	9.44	0.06	**4.08**	9.41	0.05	**4.05**
LnL	6.15	0.01	**6.15**	6.19	0.03	**6.19**	6.11	0.02	**6.11**
LnL(OH)	−1.01	0.04	**6.60**	0.36	0.07	**7.94**	−0.05	0.06	**7.61**
$LnL(OH)_2$	−7.59	0.05	**7.19**	–	–	**–**	−6.10	0.03	**7.73**
LnL_2	–	–	**–**	10.16	0.06	**3.98**	–	–	**–**
Ce(III)-CA									
LnHL	9.85	0.06	**4.49**	9.70	0.05	**4.34**	9.10	0.10	**3.74**
LnL	6.68	0.03	**6.68**	6.61	0.02	**6.61**	6.38	0.02	**6.38**
LnL(OH)	1.03	0.06	**8.12**	1.44	0.05	**8.60**	0.17	0.10	**7.56**
$Ln(OH)_2$	−7.53	0.07	**5.21**	−6.86	0.07	**5.47**	−5.30	0.03	**8.31**
LnL_2	–	–	**–**	10.58	0.06	**3.97**	–	–	**–**
Pr(III)-CA									
LnHL	9.63	0.10	**4.28**	9.86	0.06	**4.50**	–	–	**–**
LnL	6.69	0.03	**6.69**	6.84	0.03	**6.84**	6.25	0.07	**6.25**
LnL(OH)	1.18	0.06	**8.26**	1.92	0.06	**8.85**	0.68	0.06	**8.20**
$LnL(OH)_2$	−7.07	0.07	**5.52**	−5.80	0.08	**6.05**	−5.71	0.05	**7.38**
LnL_2	–	–	**–**	10.94	0.07	**4.10**	–	–	**–**
Ln_2L	–	–	**–**	–	–	**–**	9.69	0.09	**3.44**
Nd(III)-CA									
LnHL	9.95	0.04	**4.59**	10.22	0.03	**4.86**	9.89	0.08	**4.53**
LnL	6.73	0.02	**6.73**	7.11	0.02	**7.11**	6.84	0.04	**6.84**
LnL(OH)	0.37	0.04	**7.41**	2.03	0.04	**8.69**	1.77	0.08	**8.70**
$LnL(OH)_2$	−8.81	0.07	**4.59**	−6.05	0.05	**5.70**	−4.45	0.08	**7.55**
LnL_2	–	–	**–**	11.30	0.04	**4.19**	–	–	**–**
Sm(III)-CA									
LnHL	9.82	0.04	**4.46**	9.21	0.12	**3.85**	9.75	0.04	**4.39**
LnL	6.67	0.02	**6.67**	6.81	0.02	**6.81**	6.83	0.02	**6.83**
LnL(OH)	0.59	0.04	**7.69**	1.89	0.05	**8.85**	1.64	0.04	**8.58**
$LnL(OH)_2$	−8.33	0.05	**4.85**	−5.65	0.05	**6.23**	−4.63	0.03	**7.51**
LnL_2	–	–	**–**	10.93	0.05	**4.13**	–	–	**–**
Ho(III)-CA									
LnH_2L	–	–	**–**	–	–	**–**	17.09	0.05	**7.61**
LnHL	10.79	0.02	**5.43**	10.88	0.02	**5.52**	14.08	0.06	**8.72**
LnL	7.14	0.02	**7.14**	7.42	0.02	**7.42**	10.85	0.04	**10.85**
LnL(OH)	1.28	0.03	**7.90**	1.29	0.02	**7.64**	4.73	0.03	**7.65**
$LnL(OH)_2$	−6.62	0.04	**5.88**	−6.92	0.02	**5.56**	–	–	**–**
LnL_2	–	–	–	11.22	0.03	**3.80**	–	–	**–**

Table 3
The textural parameters [55–60] and pH_{pzc} of adsorbents.

Adsorbent	S_{BET} [m^2/g]	D [nm]	pH_{pzc}	
			PTM*	DM*
Purolite S957	14.90	34.10	1.96	1.60
Purolite S950	14.90	30.90	9.81	9.82
Lewatit SP112	14.98	32.72	6.06	6.43
Lewatit M500	2.38	2.84	5.06	4.25
Lewatit M600	0.45	19.22	6.31	6.26
Lewatit MP500	1.87	9.60	7.35	7.08
Amberjet 4200	5.27	9.03	6.42	6.72
Amberjet 4400	1.96	6.14	6.41	6.25
Amberjet 4600	1.47	17.53	6.78	6.60
Amberlite IRA 458	2.03	3.60	6.33	6.55
Amberlite IRA 958	2.03	6.46	5.99	6.41
Amberlite IRA 67	4.05	7.10	9.50	9.67

PTM* - the potentiometric titration method, DM* - the drift method.

solutions: pH 8.0 for La(III) on all tested ion exchangers except Amberlite IRA 67 where the pH value was 4.0, pH 8.0 for Nd(III) on Purolite S957 and strongly basic anion exchangers, pH 4.0 for Nd(III) on Purolite S950, Lewatit SP112 and Amberlite IRA 67, pH 8.0 for Ho(III) on Purolite S957, Purolite S950 and strongly basic anion exchangers, pH 2.0 for Ho(III) on Lewatit SP112 and pH 4.0 for Ho(III) on Amberlite IRA 67.

3.2.2. *Effect of Ln(III):CA molar ratio*

The sorption process was examined for the three different Ln(III) to CA ratios 1:1, 1:2 and 1:4. The initial Ln(III) ions concentration of 1.0×10^{-3} M, the initial solution pH 8.0 (La(III) on all tested ion exchangers except Amberlite IRA 67, Nd(III) on Purolite S957 and strongly basic anion exchangers, Ho(III) on Purolite S957, Purolite S950 and strongly basic anion exchangers), pH 4.0 (La(III) on Amberlite IRA 67, Nd(III) on Purolite S950, Lewatit SP112, Amberlite IRA 67 and Ho(III) on Amberlite IRA 67), pH 2.0 (Ho(III) on Lewatit SP112), the adsorbent dose of 10 g/L and the temperature of 293 K remained constant.

The effect of La(III):CA molar ratios on the adsorption efficiency onto the tested adsorbents is shown in Fig. 8. Similar results were obtained for the Nd(III) and Ho(III) complexes (Fig. S5, Fig. S6).

As follows from Fig. 8 the concentration of CA has a significant impact on the sorption capacity of the tested cation exchanger and anion exchangers. For example, increasing the concentration of CA from 1.0 ×

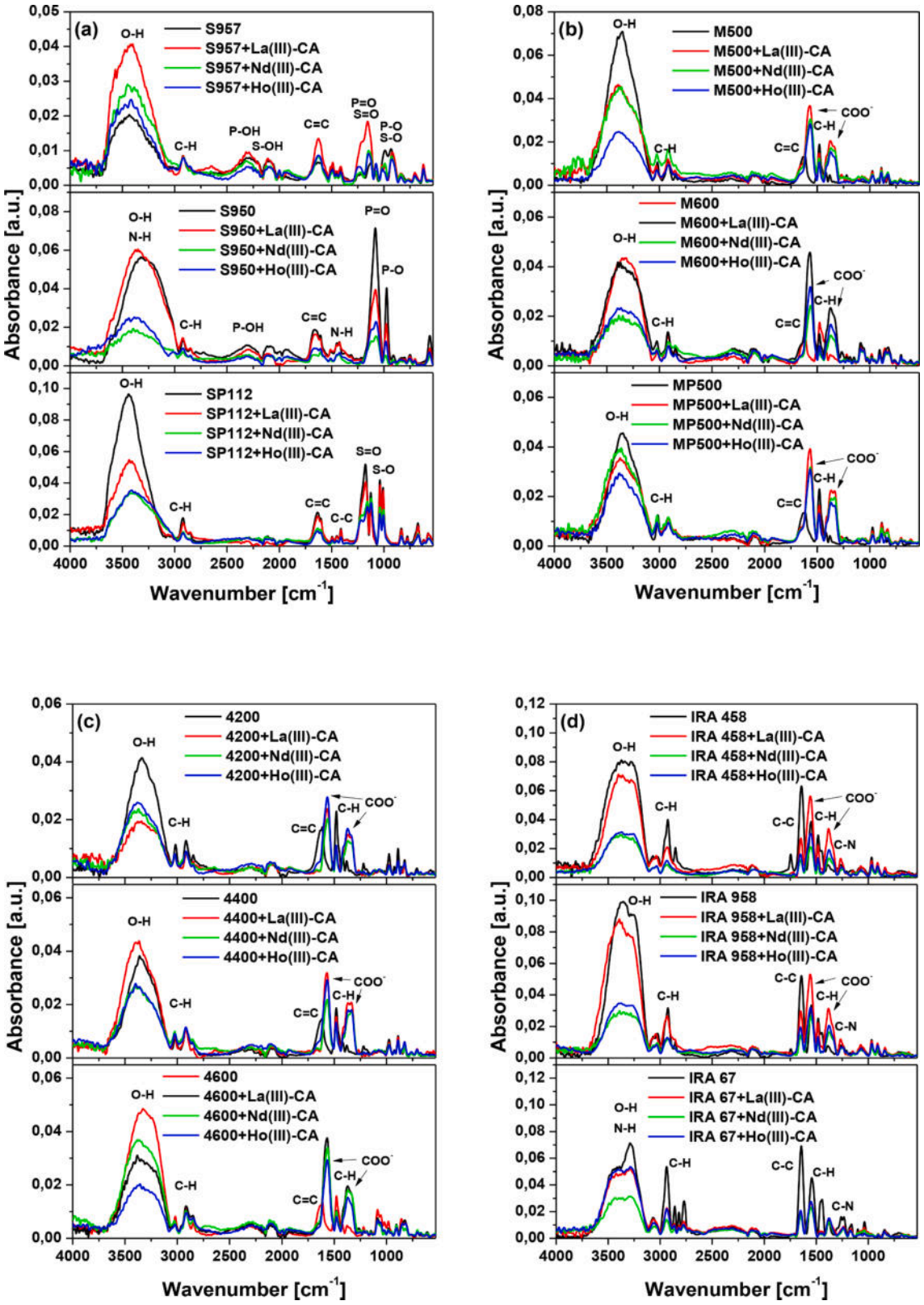

Fig. 6. FTIR spectra for (a) Purolite S957, Purolite S950, Lewatit SP112, (b) Lewatit M500, Lewatit M600, Lewatit MP500, (c) Amberjet 4200, Amberjet 4400, Amberjet 4600 and (d) Amberlite IRA 458, Amberlite IRA 958, Amberlite IRA 67 before and after the adsorption of La(III), Nd(III) and Ho(III) ions in the presence of CA.

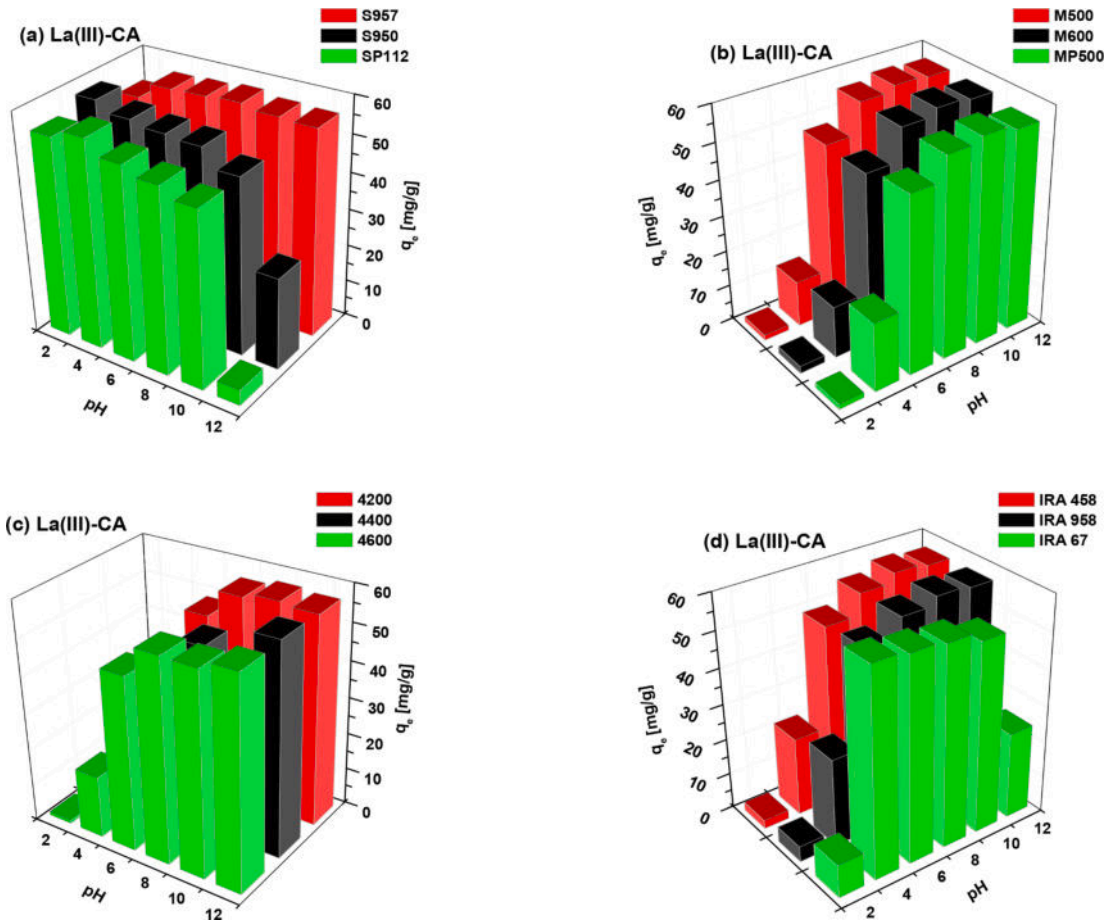

Fig. 7. The effect of pH on the sorption of La(III)-CA complexes on (a) Purolite S957, Purolite S950, Lewatit SP112, (b) Lewatit M500, Lewatit M600, Lewatit MP500, (c) Amberjet 4200, Amberjet 4400, Amberjet 4600 and (d) Amberlite IRA 458, Amberlite IRA 958, Amberlite IRA 67.

10^{-3} M to 4.0×10^{-3} M decreased the amount of adsorbed La(III) ions from 13.37 to 7.37 mg/g for Lewatit SP112.

In the case of strongly basic anion exchangers, the increase in the CA concentration increased the sorption capacity from 8.14 to 13.82 mg/g for Lewatit M500, 9.78 to 13.80 mg/g for Lewatit M600, 8.52 to 13.85 mg/g for Lewatit MP500, 8.43 to 13.83 mg/g for Amberjet 4200, 8.08 to 13.84 mg/g for Amberjet 4400, 7.81 to 13.80 mg/g for Amberjet 4600, 6.57 to 13.76 mg/g for Amberlite IRA 458 and 6.39 to 13.73 mg/g for Amberlite IRA 958.

Moreover, the change of the La(III):CA ratio from 1:1 to 1:2 influenced significantly the amount of adsorbed La(III) ions while a further increase in CA did not cause great changes in the sorption capacity. For Amberlite IRA 67, an increase from 1.0×10^{-3} M to 2.0×10^{-3} M caused an increase in the sorption capacity in relation to the La(III) complexes from 13.05 to 14.02 mg/g while a further increase from 2.0×10^{-3} M to 4.0×10^{-3} M reduced the sorption capacity to 12.02 mg/g.

The studies with the use of chelating ion exchangers proved that the sorption capacity does not change significantly and is around 14 mg/g for Purolite S957 and Purolite S950 regardless of the CA concentration.

In the case of Nd(III) and Ho(III) ions adsorption in the presence of CA, the same relationships were observed, however, for the Ho(III) ions the changes in the concentration of CA had a smaller impact on the values of sorption capacity (Fig. S6). In connection with the above considerations, further studies were carried out with the Ln(III):CA ratio 1:1 for the chelating ion exchangers and the cation exchanger and 1:2 for the anion exchangers.

3.2.3. Kinetic studies

One of the basic factors affecting the metal uptake from the solution is the phase contact time. The effect of contact time on the sorption capacity of ion exchangers was investigated at the previously determined optimal pH values, the Ln(III):CA ratio 1:1 for the chelating ion exchangers and the cation exchanger and 1:2 for the anion exchangers and at a temperature of 293 K. Fig. 9a-d shows an example of the La(III)-CA complexes adsorption at a concentration of 2.5×10^{-3} M on the tested ion exchangers within 240 min.

In the studied systems the rate of complexes adsorption is rapid at the beginning of the process and then gradually slows down until it reaches an equilibrium state where there is no significant increase in the complexes removal. In less than about 60 min, over 90% of the adsorption process is completed. This phenomenon can be explained by the saturation of the available active sites of the ion exchangers. Moreover, an increase in the initial concentration from 1.0×10^{-3} M to 2.5×10^{-3} M resulted in a longer time for the system to equilibrate (not presented here). The increase in the initial concentration of metal ions increases the sorption capacity. For example, for the La(III)-CA complexes, as the initial concentration increases from 1.0×10^{-3} M to 2.5×10^{-3} M, the sorption capacity increases from 13.76 to 35.22 mg/g for Purolite S957, from 14.27 to 36.87 mg/g for Purolite S950, from 13.94 to 22.22 mg/g for Lewatit SP112, from 14.05 to 36.87 mg/g for Lewatit M500, 14.00 to 36.99 mg/g for Lewatit M600, 13.75 to 35.56 mg/g for Lewatit MP500, 12.14 to 34.07 mg/g for Amberjet 4200, 12.59 to 33.76 mg/g for Amberjet 4400, 11.90 to 33.80 mg/g for Amberjet 4600, 14.40 to 37.20 mg/g for Amberlite IRA 458, 13.45 to 37.20 mg/g for Amberlite IRA 958 and 14.43 to 36.75 mg/g for Amberlite IRA 67.

The adsorption capacity is of great importance when choosing the best ion exchanger. However, for a pilot application the kinetic characteristics of a given adsorbent are also important. Based on the kinetic

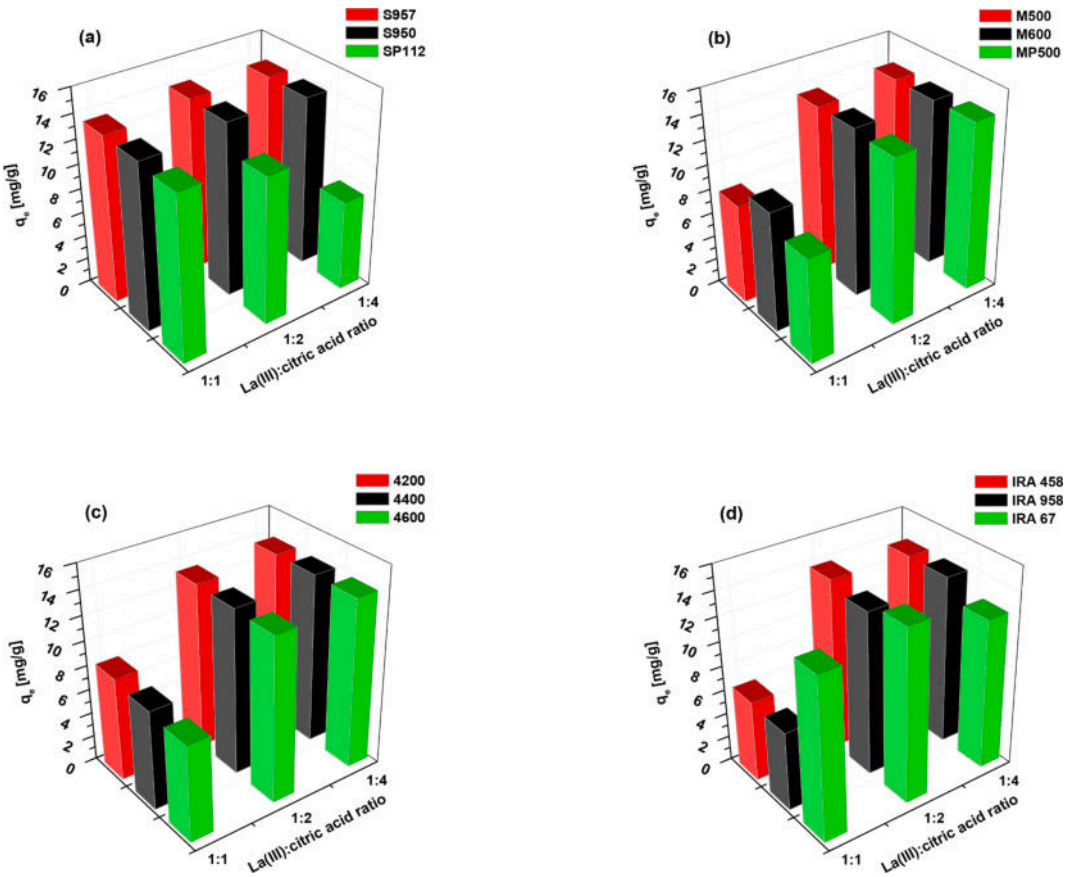

Fig. 8. The effect of the La(III):CA molar ratio on the sorption of La(III)-CA complexes on (a) Purolite S957, Purolite S950, Lewatit SP112, (b) Lewatit M500, Lewatit M600, Lewatit MP500, (c) Amberjet 4200, Amberjet 4400, Amberjet 4600 and (d) Amberlite IRA 458, Amberlite IRA 958, Amberlite IRA 67.

analysis, it is possible to determine the adsorbate uptake rate, which determines the time required to complete the process. There are several mathematical models describing the kinetics of the adsorption process which can generally be classified as the adsorption reaction models and the adsorption diffusion models. However, these models are of a completely different nature.

The adsorption diffusion models are always constructed based on the following steps: (1) the bulk phase transport of the metal ions to the external surface, (2) the transport across the boundary layer (external mass transfer), (3) the diffusion in the liquid contained in the pores and/or along the pore walls (intraparticle diffusion), and (4) the adsorption and desorption between the adsorbate and the active sites [67]. However, the models of adsorption reactions are based on the entire adsorption process without taking into account the above-mentioned steps.

The kinetic parameters of the sorption process were determined and matched to the pseudo-first order (PFO), pseudo-second order (PSO), Weber-Morris intraparticle diffusion, Boyd, and Dumwald-Wagner kinetic models. The calculated kinetic parameters for a La(III)-CA concentration of 2.5×10^{-3} M are presented in Table 4. The experimental data fitting for the La(III)-CA complexes sorption for the kinetic models and at the La(III)-CA concentration of 2.5×10^{-3} M is shown in Fig. 9. Additionally, the kinetic parameters for Nd(III) and Ho(III) as well as for the initial concentrations of 1.0×10^{-3}-2.0×10^{-3} M are presented in Tables S2-S10.

The pseudo-first order (PFO) model was used as the first to describe the Ln(III)-CA complexes adsorption process. It does not adjust the whole range of contact time and generally is applicable over the initial 10–20 min of the sorption process. The obtained values of the correlation coefficients R^2 are very high (0.927–1.000), however, the values of the adsorption capacity ($q_{1,cal}$) calculated on the basis of the model are different from those obtained experimentally. This condition must be met for the model that describes the experimental data best.

The use of the pseudo-second order (PSO) model allowed to obtain the best fit of the experimental amounts adsorbed at equilibrium ($q_{e,\exp}$) to the calculated values. This is also confirmed by the values of the correlation coefficients R^2, which in most cases are equal to 1. Considering the constant rate values (k_2), it was observed that the rate constant decreases when the initial concentration of Ln(III)-CA complexes increases. With a higher amount of complexes in the solution and the same mass of ion exchanger i.e. the same number of available active sites, the sorption sites are quickly exchanged and the kinetic rate decreases [68]. For example, for the La(III)-CA complexes, the values of the rate constant decreased from 0.110 to 0.036 g/mg min for Purolite S957, from 0.008 to 0.002 g/mg min for Purolite S950, from 0.018 to 0.007 g/mg min for Lewatit SP112, from 0.061 to 0.028 g/mg min for Lewatit M500, from 0.037 to 0.025 g/mg min for Lewatit M600, from 0.049 to 0.012 g/mg min for Lewatit MP500, from 0.052 to 0.020 g/mg min for Amberjet 4200, from 0.027 to 0.004 g/mg min for Amberjet 4400, from 0.043 to 0.016 g/mg min for Amberjet 4600, from 0.042 to 0.029 g/mg min for Amberlite IRA 458, from 0.121 to 0.049 g/mg min for Amberlite IRA 958 and from 0.042 to 0.010 g/mg min for Amberlite IRA 67 with the increase of the initial concentration from 1.0×10^{-3} M to 2.5×10^{-3} M. The constant rate values (k_2) for the Nd(III) and Ho(III) complexes adsorption are presented in Tables S5 and S8. The experimental data fitting of the sorption process of La(III)-CA complexes to the pseudo-first order and pseudo-second order models is presented in Fig. 9a–d.

In the next stage of the description of the Ln(III)-CA complexes sorption process kinetics, the adsorption diffusion models (Weber-Morris intraparticle diffusion, Boyd, and Dumwald-Wagner models) were used. The Weber-Morris intraparticle diffusion model assumes that if the adsorption process is controlled by the intraparticle diffusion, then

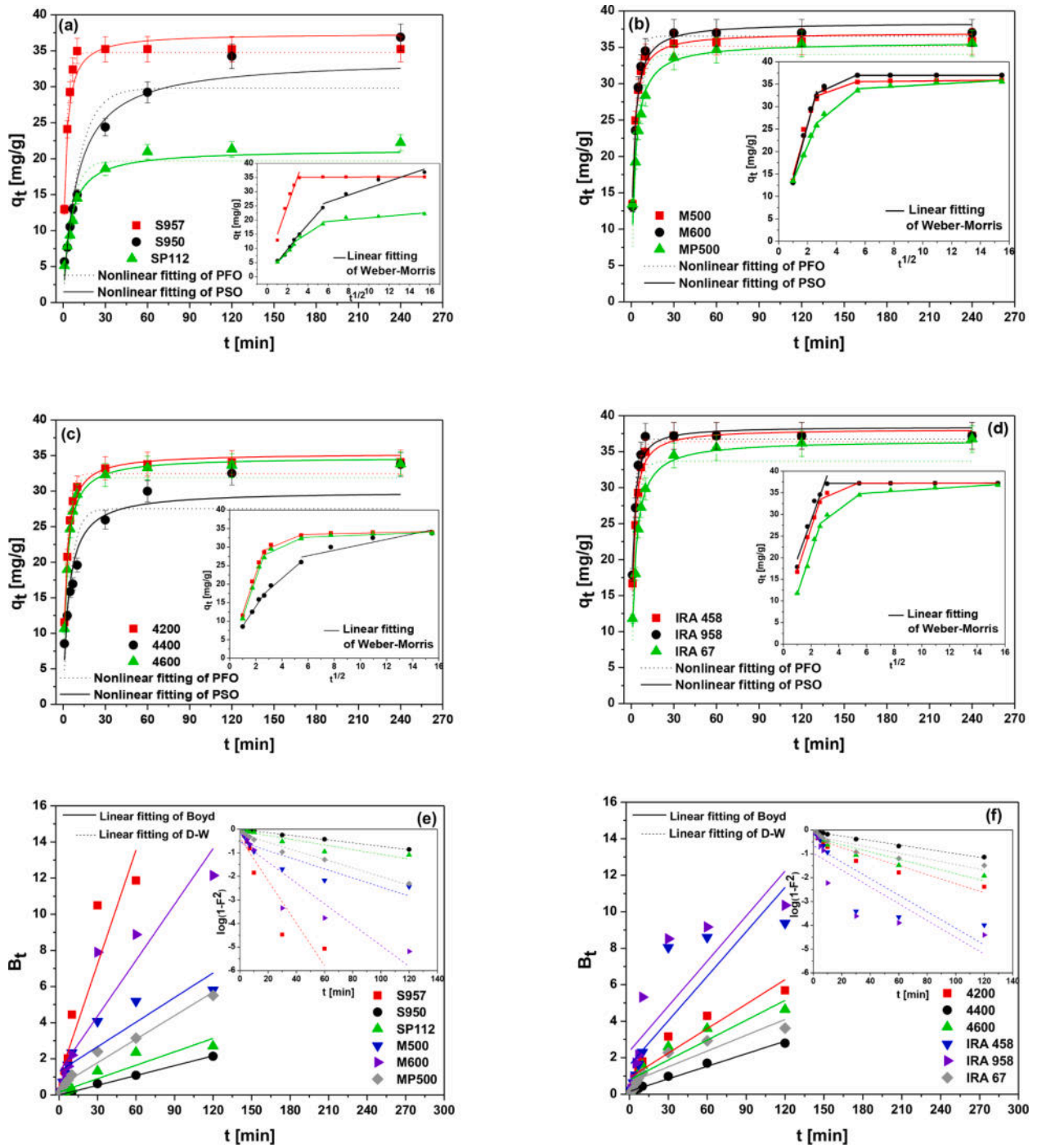

Fig. 9. Experimental data fitting for the La(III)-CA complexes sorption on Purolite S957, Purolite S950, Lewatit SP112, Lewatit M500, Lewatit M600, Lewatit MP500, Amberjet 4200, Amberjet 4400, Amberjet 4600, Amberlite IRA 458, Amberlite IRA 958, Amberlite IRA 67 for the (a-d) pseudo-first order, pseudo-second order, Weber-Morris intraparticle diffusion, (e-f) Boyd, and Dumwald-Wagner (D-W) kinetic models ($C_0 = 2.5 \times 10^{-3}$ M).

the plot of q_t vs. $t^{1/2}$ should give a straight line which goes through the origin of the coordinate system. When the plot does not pass through the origin, the intraparticle diffusion is not the only rate limiting step but also other kinetic processes can control the adsorption rate [69]. In the case when different mechanisms with different rate constants are involved in sorption, the plot is multilinear. Then the multiple linear regressions should be applied: one for each linear region [70]. The fitting of the experimental data to the Weber-Morris model on the example of the La(III)-CA complexes adsorption is shown in Fig. 9a–d. On the basis of the obtained dependencies q_t vs. $t^{1/2}$, it can be concluded that the kinetics of the Ln(III)-citric acid complexes adsorption process is a two or three-step process, depending on the adsorbent and metal ion. For example, for the La(III)-CA complexes adsorption, it was shown that the process is three-stage when using the Purolite S950, Lewatit SP112, Lewatit M500, Lewatit M600, Lewatit MP500, Amberjet 4200, Amberjet 4400, Amberjet 4600, Amberlite IRA 458, Amberlite IRA 67 ion exchangers, while for Purolite S957 and Amberlite IRA 958 ion exchangers the process proceeds in two steps. These are external (first, the steeply sloping portion) and intraparticle diffusion (the steady adsorption stage) as well as the equilibrium establishing one where the intraparticle diffusion starts to slow down due to the extremely low adsorbate concentrations in the solution [71]. Such multilinearity was also reported in

Table 4
Kinetic parameters for the La(III)-CA complexes sorption on Purolite S957, Purolite S950, Lewatit SP112, Lewatit M500, Lewatit M600, Lewatit MP500, Amberjet 4200, Amberjet 4400, Amberjet 4600, Amberlite IRA 458, Amberlite IRA 958, Amberlite IRA 67 ($C_0 = 2.5 \times 10^{-3}$ M).

Model		Pseudo-First Order					Pseudo-Second Order		
Adsorbent	$q_{e.exp}$ [mg/g]	$q_{1.cal}$ [mg/g]		k_1 [1/min]	R^2		$q_{2.cal}$ [mg/g]	k_2 [g/mg min]	R^2
Purolite S957	35.22	31.38		0.340	0.999		35.38	0.036	1.000
Purolite S950	36.87	28.17		0.020	0.984		38.59	0.002	0.998
Lewatit SP112	22.22	16.16		0.052	0.954		22.70	0.007	1.000
Lewatit M500	35.85	25.93		0.259	0.991		36.04	0.028	1.000
Lewatit M600	36.99	28.70		0.252	0.993		37.22	0.025	1.000
Lewatit MP500	35.56	23.93		0.125	0.989		35.96	0.012	1.000
Amberjet 4200	34.07	25.35		0.208	0.986		34.32	0.020	1.000
Amberjet 4400	33.76	25.90		0.630	0.974		34.53	0.004	0.999
Amberjet 4600	33.80	25.29		0.184	0.989		34.08	0.016	1.000
Amberlite IRA 458	37.20	26.30		0.248	0.998		37.40	0.029	1.000
Amberlite IRA 958	37.20	26.69		0.343	0.985		37.32	0.049	1.000
Amberlite IRA 67	36.75	27.99		0.146	0.986		37.11	0.010	1.000
	k_{i1}[mg/g $min^{1/2}$]	C_1	R^2	k_{i2} [mg/g $min^{1/2}$]	C_2	R^2	k_{i3} [mg/g $min^{1/2}$]	C_3	R^2
Purolite S957	11.91	2.00	0.978	0.01	35.04	0.394	–	–	–
Purolite S950	4.46	0.73	0.964	4.04	2.25	1.000	1.22	19.03	0.926
Lewatit SP112	3.72	1.33	0.993	2.31	6.11	0.930	0.32	17.61	0.795
Lewatit M500	11.17	3.54	0.959	1.15	29.35	0.848	0.35	35.39	0.764
Lewatit M600	11.93	1.92	0.984	1.46	29.13	0.910	0.00	36.97	0.738
Lewatit MP500	7.67	5.88	0.996	2.60	19.47	0.976	0.19	32.94	0.800
Amberjet 4200	10.50	1.70	0.986	1.47	25.25	0.925	0.08	32.98	0.729
Amberjet 4400	5.30	3.37	0.986	3.05	9.36	0.986	0.73	23.26	0.858
Amberjet 4600	9.68	2.18	0.992	1.61	23.58	0.909	0.14	31.85	0.780
Amberlite IRA 458	9.81	7.22	0.996	1.37	29.85	0.891	0.00	37.19	0.933
Amberlite IRA 958	10.52	8.15	0.966	0.01	37.12	0.425	–	–	–
Amberlite IRA 67	9.65	1.94	0.993	2.38	21.55	0.965	0.21	33.61	0.911
	Boyd				**Dumwald-Wagner**				
	B_t		R^2		K		intercept		R^2
Purolite S957	11.87		0.873		0.208		0.37		0.875
Purolite S950	2.14		0.998		0.016		0.01		0.998
Lewatit SP112	2.70		0.886		0.022		0.10		0.891
Lewatit M500	5.81		0.790		0.044		0.52		0.799
Lewatit M600	12.14		0.866		0.102		0.51		0.869
Lewatit MP500	5.51		0.972		0.042		0.19		0.977
Amberjet 4200	2.79		0.894		0.044		0.36		0.904
Amberjet 4400	2.79		0.988		0.021		0.07		0.990
Amberjet 4600	4.63		0.882		0.035		0.31		0.893
Amberlite IRA 458	9.38		0.732		0.080		0.65		0.734
Amberlite IRA 958	10.35		0.702		0.081		0.97		0.706
Amberlite IRA 67	3.62		0.852		0.027		0.25		0.863

our recent studies [55]. Additionally, the values of intercept (*C*) give an idea about the thickness of the boundary layer. The larger is the intercept, the greater is the surface sorption contribution in the rate controlling step. For the *C* parameter there was found the following relation: $C_3 > C_2 > C_1$. With the increasing initial concentration of the solution the values of C_1, C_2 and C_3 increased, as a result of the greater influence of the boundary layer on the process rate. In our studies the slope of the successive portions is defined as the intraparticle diffusion parameter k_i. The values of parameters k_{i1}, k_{i2} and k_{i3} decreased in the series $k_{i1} > k_{i2} > k_{i3}$ and increased with the increasing initial metal concentrations due to the greater deriving force with the increasing initial concentration.

Another adsorption diffusion model is the Boyd model. This model also allows to define the actual rate controlling step of the sorption process. The Boyd model is based on the dependence $B_t = -0.4977 - \ln(1-(q_t/q_e))$ vs. *t*, which is shown in Fig. 9e-f. on the example of La(III) complexes adsorption. If the plot of B_t vs. *t* is linear and passes through the origin, then the actual slowest step in the adsorption is the intraparticle diffusion. However, the plots obtained by us are linear only for the adsorption of La(III)-CA complexes on Purolite S950 and Amberjet 4400. For the other metal ions and ion exchangers the plots are nonlinear. Moreover, for all the tested systems, the plots do not pass through the origin of the coordinate systems. This indicates that the studied process of Ln(III)-CA complexes adsorption on the selected chelating ion exchangers, cation exchanger and anion exchangers is a complex process including both intraparticle and boundary layer diffusions.

Finally, to confirm the mechanism of Ln(III)-CA complexes adsorption, the Dumwald-Wagner model was used. It assumes that if the plot of $\log(1-F^2)$ vs. *t* is linear and passes through the origin, the rate limiting step is the intraparticle diffusion process, otherwise it is the film diffusion. Furthermore, the higher intercept indicates that the film diffusion rate control step has greater influence on the rate limiting step [72]. The Dumwald-Wagner kinetic plots for the La(III)-CA complexes sorption are presented in Fig. 9e-f. The obtained results show that, according to the Dumwald-Wagner model, the stage controlling the adsorption process of La(III) ions on the Purolite S957, Lewatit SP112, Lewatit M500, Lewatit M600, Lewatit MP500, Amberjet 4200, Amberjet 4400, Amberjet 4600, Amberlite IRA 458, Amberlite IRA 958 as well as the Amberlite IRA 67 ion exchangers and Nd(III) and Ho(III) ions on all tested adsorbents is film diffusion as evidenced by the fact that the straight lines do not pass through the origin. In the case of La(III) ions adsorption in the presence of CA on Purolite S950, a straight line was obtained for which the intercept value was 0.01. This suggests that unlike other studied systems this process can be mainly controlled by the intraparticle diffusion. Additionally, for the remaining systems the obtained intercept values (Tables 4, S4, S7, S10) indicate that the film diffusion has the greatest

impact on the sorption of La(III)-CA complexes onto the Amberlite IRA 958 ion exchanger.

Summing up, the obtained results indicate that the pseudo-second order model is the best one describing the sorption process of La(III), Nd(III) as well as Ho(III) complexes in the presence of CA on the Purolite S957, Purolite S950, Lewatit SP112, Lewatit M500, Lewatit M600, Lewatit MP500, Amberjet 4200, Amberjet 4400, Amberjet 4600, Amberlite IRA 458, Amberlite IRA 958 and Amberlite IRA 67 ion exchangers. Additionally, these processes were found to be complex including both intraparticle and boundary layer diffusions. However, when the Purolite S950 ion exchanger is used for the adsorption of La (III) ions, the rate controlling step of the process is mainly the intraparticle diffusion.

3.2.4. Equilibrium studies

The adsorption mechanism depends on many factors, including the type of adsorbent, adsorbate and their mutual affinity, properties of the sorbent surface or those of the aqueous solutions [73]. For the solid–liquid adsorption systems, the adsorption isotherms are important models explaining the adsorbent and adsorbate interactions. When the adsorption reaction reaches the equilibrium state, the adsorption isotherms can indicate the distribution of adsorbate between the solution and the adsorbent. Therefore, it is important to identify the model that describes the process under study in the best way.

For the best determination of the isotherm model, sorption experiments of Ln(III)-CA complexes on various adsorbents were conducted under the optimal conditions at the concentrations ranging from 1.0×10^{-3} M to 1.3×10^{-2} M. The Langmuir, Freundlich and Temkin isotherm models were employed to investigate the adsorption behaviour. Fig. 10a–c presents the fit of the experimental data to different models of adsorption isotherms on the example of the La(III)-CA complexes adsorption.

The calculated values of isotherm models parameters at the temperature of 293 K as well as the correlation coefficient (R^2) and error function Chi-square (χ^2) are listed in Table S11. The adsorption isotherms parameters for higher temperatures (313 and 333 K) are summarized in Tables S12-S14. The Langmuir model is used to describe the monolayer adsorption process on the homogeneous adsorbent surface where there are no significant interactions between the adsorbed species. The Freundlich isotherm model is the earliest known empirical equation used to describe the multilayer adsorption on the heterogeneous surface. The Temkin isotherm model is based on the assumption that there are adsorbent-adsorbate interactions that cause the heat of adsorption to decrease linearly with the coverage. In this model the chemical adsorption is regarded as electrostatic interactions. By analysing the obtained correlation coefficient (R^2) and error function Chi-square (χ^2) values, it can be concluded that for most of the studied systems the Langmuir model is the best one to describe the adsorption process. The exceptions were the processes of Nd(III) complexes adsorption on the Lewatit SP112 ion exchanger and La(III) and Ho(III) complexes adsorption on the Amberlite IRA 67 ion exchanger, for which a better fit to the Freundlich model was obtained, indicating adsorption

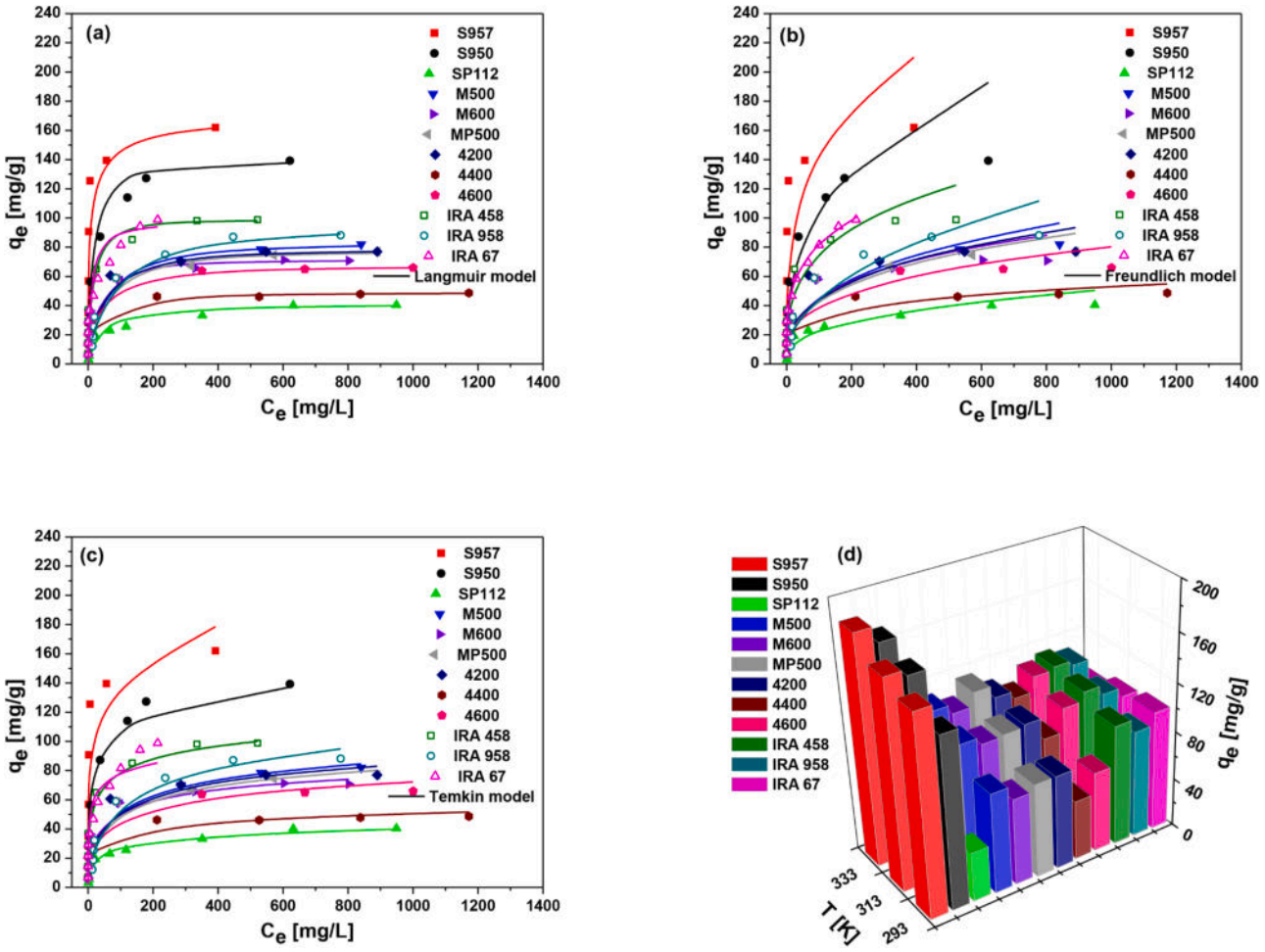

Fig. 10. Non-linear fitting of (a) Langmuir, (b) Freundlich and (c) Temkin isotherms to the experimental data for the sorption of La(III)-CA complexes on Purolite S957, Purolite S950, Lewatit SP112, Lewatit M500, Lewatit M600, Lewatit MP500, Amberjet 4200, Amberjet 4400, Amberjet 4600, Amberlite IRA 458, Amberlite IRA 958, Amberlite IRA 67 and (d) comparison of the maximum sorption capacity of adsorbents in relation to the La(III)-CA complexes for different temperatures.

on the heterogeneous surfaces.

On the basis of the calculated Langmuir constants K_L, the affinity of the tested Ln(III) complexes for the adsorbents was determined. The higher value of the K_L parameter, the stronger the interactions between the adsorbent and the adsorbate. For the chelating ion exchangers, the affinity for the Ln(III)-CA complexes increases according to the following series: Nd(III) < La(III) < Ho(III) for Purolite S957 and Ho(III) < Nd(III) < La(III) for Purolite S950, for the cation exchanger Lewatit SP112 and all anion exchangers this series has the form: La(III) < Nd(III) < Ho(III). Moreover, the determined values of K_L increase with the increasing temperature for all adsorbents except Amberlite IRA 67 for which this parameter decreases. This proves that the affinity of Ln(III) complexes for the ion exchanger depends on the temperature. Using the Langmuir model, the parameter of the maximum surface coverage (maximum monolayer capacity, q_0) was also determined for each ion exchanger in relation to the tested Ln(III) complexes. For the La(III)-CA complexes, the q_0 values for the ion exchangers increased in the following series: Lewatit SP112 < Amberjet 4400 < Amberjet 4600 < Lewatit M600 < Amberjet 4200 < Lewatit MP500 < Lewatit M500 < Amberlite IRA 958 < Amberlite IRA 458 < Amberlite IRA 67 < Purolite S950 < Purolite S957. The highest maximum adsorption capacity in relation to the La(III) complexes was obtained for the Purolite S957 chelating ion exchanger which was 163.27 mg/g. For the Nd(III)-CA complexes, the series was as follows: Amberjet 4400 < Amberjet 4600 < Lewatit M600 < Amberjet 4200 < Lewatit MP500 < Lewatit M500 < Lewatit SP112 < Amberlite IRA 958 < Purolite S950 < Amberlite IRA 458 < Amberlite IRA 67 < Purolite S957. In this case the highest maximum adsorption capacity was also obtained for the Purolite S957 chelating ion exchanger which was 142.65 mg/g. Whereas for the Ho(III) complexes the series was as follows: Amberjet 4400 < Amberjet 4600 < Purolite S950 < Lewatit M600 < Lewatit MP500 < Lewatit M500 < Amberlite IRA 958 < Amberjet 4200 < Amberlite IRA 458 < Amberlite IRA 67 < Lewatit SP112 < Purolite S957. In relation to the Ho (III) complexes, the highest maximum adsorption capacity was also obtained for Purolite S957 being 180.26 mg/g.

The use of the Freundlich model allowed to determine the dimensionless parameter n which indicates the intensity of the sorption process. The obtained values of the parameter n in the range from 1 to 10 indicate that the adsorption process in the tested systems was favourable and efficient. Moreover, based on the inverse of the n parameter, the degree of diversity of the sorption sites on the sorbent surface can be predicted. In our paper the values of $1/n$ in the range from 0.137 to 0.473 were obtained satisfying the condition: $0 < 1/n < 1$. The obtained values are closer to zero than one which proves the surface heterogeneity [74].

Another applied isotherm model was the Temkin model. On its basis the parameter A related to the maximum binding energy and the parameter B related to the adsorption heat were determined. The B parameter values were smaller than 8 kJ/mol. This result suggests the weak interactions between the Ln(III) complexes and the adsorbents. In most of the tested systems, except for the systems with the Amberlite IRA 67 ion exchanger, the value of the parameter A increased with the increasing temperature, which confirms that the binding capacity increased as the temperature increased in the adsorption process.

The obtained adsorption capacities of the studied ion exchangers were compared with various adsorbents described in the literature and are presented in Table S15.

3.2.5. *Effect of temperature and thermodynamic parameters*

Temperature is an important parameter influencing the adsorption process. The reason for this is that the temperature of the solution can affect the solid/liquid interfaces, the swelling property of adsorbents and the mobility of metal ions [75]. In our paper, the influence of temperature on the adsorption of La(III), Nd(III) and Ho(III) complexes with CA on different adsorbents was examined at 293, 313 and 333 K. The comparison of the maximum sorption capacity of adsorbents in relation to the La(III)-CA complexes for different temperatures is shown in Fig. 10d. Moreover, the parameters of adsorption isotherms for higher temperatures (313 and 333 K) were also calculated and are summarized in Tables S12-S14.

As follows from the obtained results, it can be concluded that the increase in the temperature caused an increase in the sorption capacity in most of the tested systems. This increase in the adsorption capacity can be explained by a decrease in the thickness of the boundary layer surrounding the ion exchange beads with the increasing temperature which results in reduction in the mass transfer resistance of the molecules in the boundary layer. This may also be a result of an increase in the mobility of the complex molecules with an increase in their kinetic energy and an increased rate of intramolecular diffusion of the adsorbate with an increase in the temperature. However, there were exceptions to this dependency. In the case of the La(III) complexes adsorption on the Lewatit SP112 ion exchanger, the temperature increase from 293 K to 333 K caused a slight decrease in the sorption capacity from 40.40 to 38.61 mg/g. The decrease in the sorption efficiency with the increasing temperature is also visible in the adsorption processes on the weakly basic anion exchanger Amberlite IRA 67 regardless of the tested Ln(III) ions (from 98.79 to 88.12 mg/g for the La(III) complexes, from 119.35 to 116.62 mg/g for the Nd(III) complexes and from 123.07 to 122.15 mg/g for the Ho(III) complexes). A possible explanation for this phenomenon may be the weak interactions between the molecules of the complexes and weakly basic Amberlite IRA 67 at these temperatures which results in the escape of the adsorbate from the solid phase to the bulk phase again with the increasing temperature [76].

Thermodynamic considerations of the sorption process are necessary to understand the nature of the adsorption process. The values of thermodynamic parameters for the sorption of La(III)-CA complexes are listed in Table 5. The thermodynamic parameters for the sorption of Nd (III) and Ho(III) complexes are presented in Tables S16 and S17. The linear plots of $\ln K_c$ vs. $1/T$ are presented in Fig. S7. As can be seen from the obtained results, the negative values of Gibbs free energy (ΔG°) for all tested systems at different temperatures indicate that the adsorption process occurs spontaneously and is thermodynamically favourable. On the basis of the ΔG° value, one can conclude about the nature of the interactions between the adsorbent and the adsorbate. If ΔG° is in the range from −20 to 0 kJ/mol, this can indicate a significant contribution of physical interactions in the adsorption process (electrostatic interactions). On the other hand, if the values of ΔG° are in the range from −80 to −400 kJ/mol, then chemisorption (coordination bonds) is dominant [77]. The values of enthalpy change (ΔH°) obtained in our research were mainly positive which proves that the process was endothermic. However, in the case of the systems in which the Amberlite IRA 67 ion exchanger was used as the adsorbent and for the La(III)-CA-Lewatit SP112 system, negative values were obtained, indicating the

Table 5
Thermodynamic parameters for the sorption of the La(III)-CA complexes on Purolite S957, Purolite S950, Lewatit SP112, Lewatit M500, Lewatit M600, Lewatit MP500, Amberjet 4200, Amberjet 4400, Amberjet 4600, Amberlite IRA 458, Amberlite IRA 958 and Amberlite IRA 67.

Adsorbent	ΔH° [kJ/mol]	ΔS° [J/mol K]	ΔG° [kJ/mol]		
			293 K	313 K	333 K
Purolite S957	20.79	62.84	−14.67	−16.35	−19.55
Purolite S950	20.61	58.35	−13.18	−15.93	−17.78
Lewatit SP112	−1.32	−30.81	−9.14	−9.61	−10.21
Lewatit M500	14.41	30.11	−11.15	−13.18	−14.63
Lewatit M600	18.04	41.93	−10.91	−13.42	−14.84
Lewatit MP500	19.34	45.67	−10.86	−12.95	−14.99
Amberjet 4200	14.02	28.02	−10.86	−13.08	−14.24
Amberjet 4400	25.32	60.44	−9.08	−11.90	−13.75
Amberjet 4600	22.54	55.01	−10.20	−13.13	−14.64
Amberlite IRA 458	9.59	19.11	−12.77	−14.51	−15.82
Amberlite IRA 958	11.03	19.68	−11.52	−13.20	−14.59
Amberlite IRA 67	−10.44	−41.86	−14.94	−15.45	−15.55

exothermic nature of the adsorption process. In addition, the ΔH° value below 40 kJ/mol indicates the physical nature of the adsorption while chemisorption is characterized by the ΔH° values ranging from 40 to 120 kJ/mol [78]. In our studies the values of both ΔG° and ΔH° for all tested systems were in the range of physisorption which suggests that adsorption of Ln(III) complexes with CA on the applied ion exchangers was driven by a physisorption process. Another determined thermodynamic parameter was the entropy change (ΔS°). The positive values of ΔS° for most systems indicate an increase in the randomness during the adsorption of Ln(III) complexes while the negative values in the case of the systems with the Amberlite IRA 67 ion exchanger and for the La(III)-CA-Lewatit SP112 system indicate a decrease in the randomness at the solid/solution interface [79].

3.3. Desorption studies

When assessing the adsorbent, apart from the adsorption efficiency, the possibility of its regeneration should be also taken into account. For this purpose, the desorption process was carried out. Three different concentrations, i.e. 0.5, 1 and 2 M of hydrochloric acid and nitric acid(V) as eluents were used in this study in the recovery process. Fig. 11 shows the obtained desorption results on the example of La(III) ions. The results for the Nd(III) and Ho(III) ions are shown in Figs. S8 and S9. It can be easily noticed that the desorption process proceeded with different efficiency depending on the tested ion exchanger.

The best regenerative properties were obtained for the polystyrene anion exchangers while the lowest desorption ability was demonstrated for the chelating ion exchangers and the cation exchanger. This may be due to the greater affinity of the chelating ion exchangers and the cation exchanger for Ln(III) ions compared to the anion exchangers. For the chelating ion exchangers and the cation exchanger, significant influence of the eluent on the desorption process was demonstrated. It was observed that in the case of these ion exchangers, an increase in the concentration of the desorbing agent increases the desorption process efficiency. Desorption of Ln(III) ions from both strongly basic and weakly basic anion exchangers proceeded with satisfactory efficiency, regardless of the desorbing agent. Taking into account the studied rare earth elements ions, the desorption process from the anion exchangers is the most effective for Nd(III) ions for which *%D* was achieved in the range of 86–100%, then for Ho(III) ions where *%D* was obtained in the range of 68–94%, the lowest desorption capacity was recorded for La (III) ions where *%D* was in the range of 54–84%.

On the example of La(III) ions, five sorption/desorption cycles were also performed to evaluate the possibility of reusing and recycling sorbents. For this purpose there were selected the following desorbing agents: 2 M HNO_3 for Purolite S957 and Lewatit SP112, 2 M HCl for Purolite S950 and 0.5 M HCl for all anion exchangers. Table S18 shows the obtained results. After five cycles, the changes in the sorption efficiency of La(III) complexes on the polystyrene ion exchangers did not vary more than 10%. In the case of the polyacrylic ion exchangers, a decrease in the adsorption efficiency of up to 66% was observed. Thus the polystyrene ion exchangers show a better regeneration ability

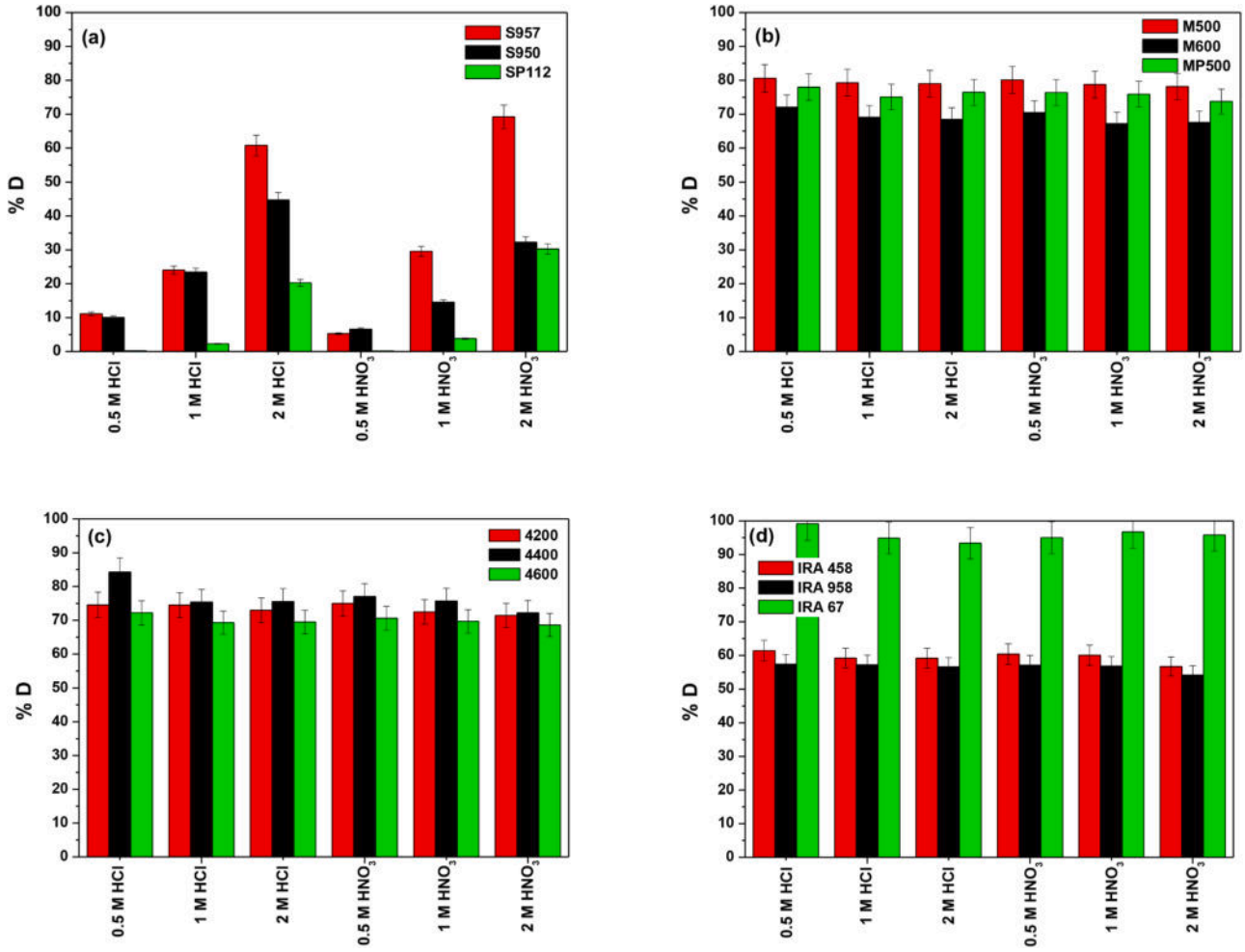

Fig. 11. Dependence of La(III) ions desorption capacity on (a) Purolite S957, Purolite S950, Lewatit SP112, (b) Lewatit M500, Lewatit M600, Lewatit MP500, (c) Amberjet 4200, Amberjet 4400, Amberjet 4600 and (d) Amberlite IRA 458, Amberlite IRA 958, Amberlite IRA 67 using the desorption agents: HCl and HNO_3 at various concentrations.

compared to the polyacrylic ones, and therefore they can be used many times in adsorption processes.

3.4. Adsorption studies - dynamic method

The adsorption process can be conducted using various methods. Among them the static and dynamic methods can be distinguished. The dynamic method is available in several varieties but the most preferred method in the industry is the dynamic method on a fixed bed. This method is easy, inexpensive, allows for the purification of large amounts of solutions because the adsorbate is in a continuous contact with the fresh adsorbent and also allows to shorten the process time. Therefore, the research was also carried out using the dynamic method, selecting La (III) as a representative of rare earth elements. The La(III) complexes sorption process was examined for the pH values equal to 8.0, the La(III): CA ratio 1:1 for the chelating ion exchangers and the cation exchanger, 1:2 for the anion exchangers, and the initial concentration equal to 1.0×10^{-3} M.

Based on the breakthrough curves (C/C_0 vs. V) (Fig. 12), the basic parameters such as the working exchange capacity C_w, the mass distribution coefficient D_g and the volume distribution coefficient D_v were determined and are presented in Table 6.

The typical "S" shaped breakthrough curves were obtained in almost all cases. Only for the weakly basic polyacrylate anion exchanger Amberlite IRA 67 sorption of different types of complexes is evident. The obtained results allowed to present the affinities series towards the La (III)-CA complexes on the tested adsorbents which was as follows: Amberlite IRA 958 < Lewatit MP500 < Amberlite IRA 458 < Lewatit M600 < Amberjet 4600 < Amberjet 4400 < Lewatit M500 < Amberjet 4200 < Lewatit SP112 < Purolite S950 < Purolite S957. The highest value of the working exchange capacity was obtained for the Purolite S957 chelating ion exchanger which is consistent with the previous batch experiments.

The adsorption process studied by the dynamic method is influenced by the axial dispersion as well as the internal and external mass transfer resistances. Therefore there were developed the mathematical correlations for description of these processes as accurately as possible. There are many mathematical models that can be used to evaluate the column performance. The Thomas model, Adams-Bohart model, Yoon-Nelson model and Wolborska model were used in this study.

The Thomas model is one of the most general and commonly used models to interpret the fixed bed column adsorption data. It is based on the assumption that the process follows the Langmuir isotherm model without the axial dispersion. Moreover, it assumes a constant separation factor and that the rate driving force obeys the second-order reversible reaction kinetics [80]. This model describes best the systems in which the internal and external diffusion resistances are small, which is particularly relevant for adsorption in most liquid systems and therefore is the most important for adsorption in the aqueous environment [81].

Table 6
Dynamic studies parameters of La(III)-CA complexes adsorption (pH = 8.0, $C_0 = 1.0 \times 10^{-3}$ M).

Adsorbent	U [mL]	Ū [mL]	C_w [mg/mL]	D_g	D_v	%D
Purolite S957	7700	10,800	102.96	2528.24	1079.56	99.65
Purolite S950	4500	6900	60.17	1824.23	689.56	99.24
Lewatit SP112	3250	6100	43.46	1618.50	609.56	92.06
Lewatit M500	2700	3370	38.12	1012.94	336.56	95.35
Lewatit M600	2500	3150	35.30	896.34	314.56	96.31
Lewatit MP500	1650	2400	23.30	958.05	239.56	81.59
Amberjet 4200	2750	3480	38.83	955.94	347.56	97.66
Amberjet 4400	2650	3300	37.42	830.67	329.56	94.44
Amberjet 4600	2650	3250	37.42	897.72	324.56	95.26
Amberlite IRA 458	2100	3080	29.65	818.85	307.56	95.54
Amberlite IRA 958	1300	2010	18.36	618.82	200.56	62.40
Amberlite IRA 67	–	–	–	–	–	97.42

Another widely used model is the Yoon-Nelson model, developed to investigate the adsorption and breakthrough of gaseous adsorbate in the activated carbons. This model assumes that the probability of the adsorbate breakthrough on the adsorbent and the adsorbate adsorption are proportional to the rate of the decrease in the probability of adsorption of each adsorbate molecule [84,85]. The Yoon-Nelson model does not require such detailed data as adsorbate characteristics, adsorbent type or physical properties of the adsorption bed. It is applicable for a single component system [80].

The Wolborska model is a model used to describe the adsorption dynamics developed on the basis of the analysis of the p-nitrophenol adsorption on the activated carbon. It is used to describe the initial segment of the breakthrough curve (for low concentration range) and

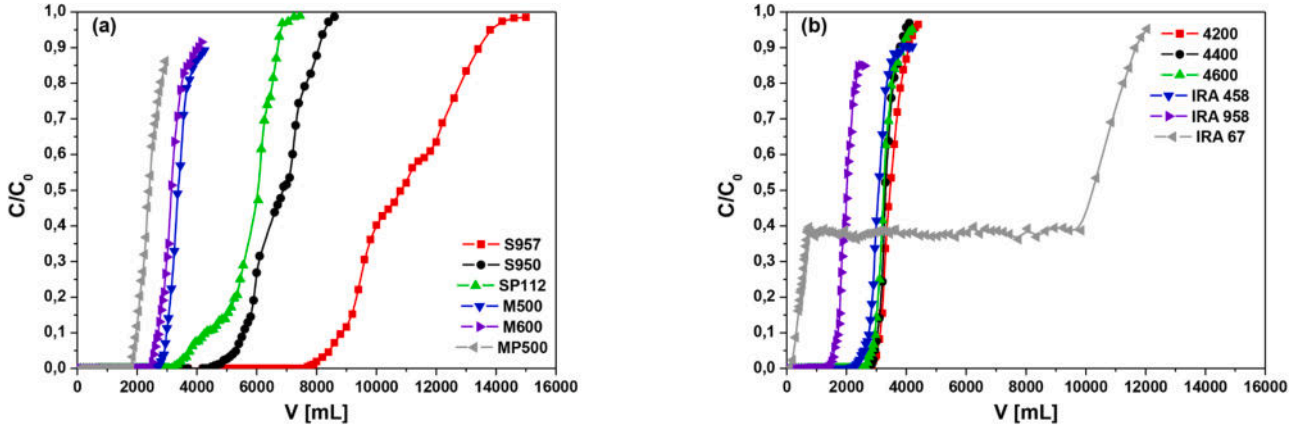

Fig. 12. Breakthrough curves of La(III)-CA complexes sorption on (a) Purolite S957, Purolite S950, Lewatit SP112, Lewatit M500, Lewatit M600, Lewatit MP500, (b) Amberjet 4200, Amberjet 4400, Amberjet 4600, Amberlite IRA 458, Amberlite IRA 958, Amberlite IRA 67 (pH = 8.0, $C_0 = 1.0 \times 10^{-3}$ M).

applies the mass transfer phenomenon for the diffusion mechanism. The model describes the adsorption process controlled by the film diffusion with the constant kinetic coefficient. The concentration profile moves steadily at a constant velocity through the bed depth at a nearly constant width [86]. It was also observed that generally the axial diffusion can be neglected when the bed height is short or when the flow rate of influent through the column is high, then $\beta_a = \beta_0$. The expression describing the Wolborska model is equivalent to the expression from the Adams-Bohart model if the k_{AB} coefficient is equal to β_a/q [87].

The experimental data were fitted with the Thomas model, Adams-Bohart model, Yoon-Nelson model and Wolborska model in order to investigate the behaviour of the La(III)-CA complexes adsorption on the columns. The parameters of the models were evaluated from the plots of $\ln(C_0/C)$-t vs. V, $\ln(C/C_0)$ vs. t, $\ln(C/C_0\text{-}C)$ vs. t and $\ln(C/C_0)$ vs. t for the Thomas, Adams-Bohart, Yoon-Nelson and Wolborska models, respectively, and are listed in Table S19. It should be noted that when the Adams-Bohart and Wolborska models were used, only the initial part of the curve (the concentration $C/C_0 < 0.5$) was taken into account.

The use of the Thomas model made it possible to determine the Thomas rate constants (k_{Th}) and the maximum solid-phase concentrations (adsorption capacities - q_0). The values of the correlation coefficient R^2 for this model are in the range of 0.911–0.980 which indicates a good fit to the experimental data. Only in the case of the system with Amberlite IRA 67 the correlation coefficient is very low and equals 0.377 which can be explained by a completely different shape of the breakthrough curve, probably caused by the adsorption of only selected types of complexes.

On the basis of the Adams-Bohart model, the parameters of column performance, such as the maximum saturation concentration of the metals (adsorption capacities - q) and the Adams-Bohart rate constant (k_{AB}) were determined. In this case, the obtained values of the correlation coefficient R^2 were in the range of 0.870–0.985 (except for Amberlite IRA 67 where the R^2 value was equal to 0.097). The Adams-Bohart model described the experimental data quite well but only in the initial parts of the breakthrough curves.

The Yoon-Nelson model which is a simple theoretical model that does not require much detailed data, allowed to determine the Yoon-Nelson rate constant (k_{YN}) and the time required for 50% adsorbate breakthrough (τ). It can be observed that the τ value obtained for the Purolite S957 chelating ion exchanger was 18506.58 min and was over three times higher than the τ value for the anion exchanger (τ = 3398.99–6014.75 min), being also significantly higher than the values obtained for the second chelating ion exchanger Purolite S950 and the cation exchanger Lewatit SP112. This means that the column filled with the Purolite S957 ion exchanger could work more than three times longer compared to that of the tested anion exchangers and twice longer compared to the tested chelating and cation exchangers to achieve 50% adsorption capacity. The values of the correlation coefficient R^2 for this model are in the range of 0.911–0.980 which indicates a good fit to the experimental data.

The Wolborska model like the Adams-Bohart model was used to describe only the initial part of the curve (the concentration $C/C_0 < 0.5$). On its basis, the kinetic coefficient of the external mass transfer (β_a) and the maximum saturation concentration of the metals (adsorption capacities - q) were determined. The results showed that the model described the experimental data satisfactorily with the correlation coefficient R^2 ranging from 0.870 to 0.985 (except for Amberlite IRA 67 where the R^2 value was equal to 0.097).

Comparing the parameters obtained on the basis of the four models used in this paper, it can be concluded that all of them were acceptable to describe the whole or a part of the dynamic behaviour of the column. The Thomas and Yoon-Nelson models described the experimental data best for the columns filled with the Purolite S957, Purolite S950, Lewatit SP112, Lewatit M600, Lewatit MP500, Amberlite IRA 958, and Amberlite IRA 67 ion exchangers while for the Lewatit M500, Amberjet 4200, Amberjet 4400, Amberjet 4600 and Amberlite IRA 458 ion exchangers, a slightly better fit was obtained for the Adams-Bohart and Wolborska models.

After the columns were exhausted, the desorption studies were carried out using 2 M HNO_3 for the chelating ion exchangers and the cation exchanger, and 0.5 M HCl for the anion exchangers as the eluents. As shown in Table 6 the La(III) ions desorption was highly efficient (62.40–99.65%) and much higher compared to the results obtained using the static method. This may be due to different process conditions, e.g. the amount of the desorbing agent.

4. Conclusions

This paper investigated the sorption process of rare earth elements representatives ions (La(III), Nd(III), Ho(III)) in the presence of CA on various types of ion exchangers by conducting batch and column experiments. In the first stage the formation of binary complexes containing rare earth elements ions and CA was studied using the potentiometric methods. In the tested systems the formation of protonated complexes of LnH_xL type, LnL type and hydroxy complexes of the $LnL(OH)_x$ type was found. Then in the main part of the research the effect of different pHs, Ln(III):CA molar ratio, contact time, initial concentrations, and temperature on the adsorption capacity of ion exchangers was analysed. These studies made it possible to conclude that the sorption process is highly dependent on these factors and made it possible to determine the optimal process parameters which sometimes differed significantly depending on the tested metal-adsorbent system. The sorption process in all systems was fast. The sorption equilibrium was established within 60 min. The kinetic studies suggested that the sorption of rare earth elements complexes followed the pseudo-second order kinetic model (R^2 close to 1). Based on the determined isotherm parameters, it was found that for most of the studied systems the Langmuir model is the best one to describe the adsorption process. In the case of Nd(III) complexes adsorption on the Lewatit SP112 ion exchanger and La(III) and Ho(III) complexes on the Amberlite IRA 67 ion exchanger, a better fit was obtained for the Freundlich model. The maximum equilibrium capacities were obtained for the Purolite S957 chelating ion exchanger which were equal to 162.04 mg/g for the La(III) complexes, 142.65 mg/g for the Nd(III) complexes, and 180.26 mg/g for the Ho(III) complexes. The results of the desorption process of the ion exchangers showed the possibility of their reuse. The column tests were the confirmation of the very good adsorption capacity of the ion exchangers. The experimental results of this study demonstrate that the studied ion exchangers are suitable for adsorption of rare earth elements complexes with CA from the solutions. Moreover, CA can be proposed as an alternative chelating agent for the currently used poorly biodegradable synthetic compounds.

Declaration of Competing Interest

The authors declare the following financial interests/personal relationships which may be considered as potential competing interests:

Kolodynska Dorota reports financial support was provided by National Centre for Research and Development.

Acknowledgments

The authors are grateful for the financial support from the National Centre of Research and Development under Project No. POIR.04.01.01-00-0040/17-00.

Appendix A. Supplementary data

Supplementary data to this article can be found online at https://doi.org/10.1016/j.cej.2022.135366.

References:

[1] M.R. Ganjali, V.K. Gupta, F. Faridbod, P. Norouzi, Applications of the lanthanide series in human life, Lanthanides Ser. Determ. Var. Anal. Methods (2016) 37–58, https://doi.org/10.1016/b978-0-12-804704-0.00002-5.

[2] T. Dutta, K.H. Kim, M. Uchimiya, E.E. Kwon, B.H. Jeon, A. Deep, S.T. Yun, Global demand for rare earth resources and strategies for green mining, Environ. Res. 150 (2016) 182–190, https://doi.org/10.1016/j.envres.2016.05.052.

[3] C. Tunsu, M. Petranikova, M. Gergorić, C. Ekberg, T. Retegan, Reclaiming rare earth elements from end-of-life products: a review of the perspectives for urban mining using hydrometallurgical unit operations, Hydrometallurgy. 156 (2015) 239–258, https://doi.org/10.1016/j.hydromet.2015.06.007.

[4] S.B. Castor, J.B. Hedrick, Rare earth elements, Soc. Mining, Metall. Explor. (2006) 769–792.

[5] M.K. Jha, A. Kumari, R. Panda, J. Rajesh Kumar, K. Yoo, J.Y. Lee, Review on hydrometallurgical recovery of rare earth metals, Hydrometallurgy 165 (2016) 2–26.

[6] A.R. Chakhmouradian, F. Wall, Rare earth elements: Minerals, mines, magnets (and more), Elements 8 (2012) 333–340.

[7] U.S. Geological Survey, Mineral Commodity Summaries, 2020. https://pubs.usgs.gov/periodicals/mcs2020/mcs2020.pdf.

[8] B. Esma, A. Omar, D.M. Amine, Comparative study on lanthanum(III) sorption onto Lewatit TP 207 and Lewatit TP 260, J. Radioanal. Nucl. Chem. 299 (1) (2014) 439–446, https://doi.org/10.1007/s10967-013-2766-6.

[9] Z. He, S. Tian, P. Ning, Adsorption of arsenate and arsenite from aqueous solutions by cerium-loaded cation exchange resin, J. Rare Earths. 30 (6) (2012) 563–572, https://doi.org/10.1016/S1002-0721(12)60092-1.

[10] D. Lakherwal, Adsorption of heavy metals: a review, Int. J. Environ. Res. Dev. 4 (2014) 2249–3131, https://doi.org/10.1007/s11270-007-9401-5.

[11] X. Hérès, V. Blet, P. Di Natale, A. Ouaattou, H. Mazouz, D. Dhiba, F. Cuer, Selective extraction of rare earth elements from phosphoric acid by ion exchange resins, Metals (Basel) 8 (2018) 682, https://doi.org/10.3390/met8090682.

[12] A.A. Galhoum, M.G. Mafhouz, S.T. Abdel-Rehem, N.A. Gomaa, A.A. Atia, T. Vincent, E. Guibal, Cysteine-functionalized chitosan magnetic nano-based particles for the recovery of light and heavy rare earth metals: uptake kinetics and sorption isotherms, Nanomaterials 5 (2015) 154–179, https://doi.org/10.3390/nano5010154.

[13] Q. Liao, D. Zou, W. Pan, W. Linghu, R. Shen, X. Li, A.M. Asiri, K.A. Alamry, G. Sheng, L. Zhan, X. Wu, Highly efficient capture of Eu(III), La(III), Nd(III), Th(IV) from aqueous solutions using g-C_3N_4nanosheets, J. Mol. Liq. 252 (2018) 351–361, https://doi.org/10.1016/j.molliq.2017.12.145.

[14] H. Javadian, M. Ruiz, M. Taghvai, A.M. Sastre, Novel magnetic nanocomposite of calcium alginate carrying poly(pyrimidine-thiophene-amide) as a novel green synthesized polyamide for adsorption study of neodymium, terbium, and dysprosium rare-earth ions, Colloids Surfaces A Physicochem. Eng. Asp. 603 (2020) 125252, https://doi.org/10.1016/j.colsurfa.2020.125252.

[15] H. Javadian, M. Ruiz, A.M. Sastre, Response surface methodology based on central composite design for simultaneous adsorption of rare earth elements using nanoporous calcium alginate/carboxymethyl chitosan microbiocomposite powder containing $Ni_{0.2}Zn_{0.2}Fe_{2.6}O_4$ magnetic nanoparticles: Batch, Int. J. Biol. Macromol. 154 (2020) 937–953, https://doi.org/10.1016/j.ijbiomac.2020.03.131.

[16] H. Javadian, M. Ruiz, M. Taghavi, A.M. Sastre, Synthesis of magnetic CMC bionanocomposite containing a novel biodegradable nanoporous polyamide selectively synthesized in ionic liquid as green media: Investigation on Nd^{+3}, Tb^{+3}, and Dy^{+3} rare earth elements adsorption, J. Mol. Liq. 308 (2020) 113017, https://doi.org/10.1016/j.molliq.2020.113017.

[17] H. Javadian, M. Ruiz, T.A. Saleh, A.M. Sastre, Ca-alginate/carboxymethyl chitosan/$Ni_{0.2}Zn_{0.2}Fe_{2.6}O_4$ magnetic bionanocomposite: Synthesis, characterization and application for single adsorption of Nd^{+3}, Tb^{+3}, and Dy^{+3} rare earth elements from aqueous media, J. Mol. Liq. 306 (2020) 112760, https://doi.org/10.1016/j.molliq.2020.112760.

[18] M. Marhol, Ion exchangers in analytical chemistry: Their properties and use in inorganic chemistry, Elsevier Scientific Publishing Company, Academia, Prague, 1982.

[19] F. Helfferich, R. Kunin, Ion exchange, J. Electrochem. Soc. 110 (6) (1963) 121C, https://doi.org/10.1149/1.2425793.

[20] R. Ciriminna, F. Meneguzzo, R. Delisi, M. Pagliaro, Citric acid: emerging applications of key biotechnology industrial product, Chem. Cent. J. 11 (2017) 1–9, https://doi.org/10.1186/s13065-017-0251-y.

[21] M. Dakanali, E.T. Kefalas, C.P. Raptopoulou, A. Terzis, T. Mavromoustakos, A. Salifoglou, Synthesis and spectroscopic and structural studies of a new cadmium (II)-citrate aqueous complex. Potential relevance to cadmium(II)-citrate speciation and links to cadmium toxicity, Inorg. Chem. 42 (8) (2003) 2531–2537, https://doi.org/10.1021/ic0205029.

[22] A.n. Hardy, G. Vanhoyland, M. Van Bael, J. Mullens, L. Van Poucke, A statistical approach to the identification of determinant factors in the preparation of phase pure $(Bi,La)_4Ti_3O_{12}$ from an aqueous citrate gel, J. Eur. Ceram. Soc. 24 (9) (2004) 2575–2581, https://doi.org/10.1016/j.jeurceramsoc.2003.09.018.

[23] G. Vanhoyland, J. Pagnaer, J. D'Haen, S. Mullens, J. Mullens, Characterization and structural study of lanthanum citrate trihydrate $[La(C_6H_5O_7)(H_2O)_2]\cdot H_2O$, J. Solid State Chem. 178 (1) (2005) 166–171, https://doi.org/10.1016/j.jssc.2004.10.042.

[24] A. Apelblat, A. Apelblat, Physicochemical properties of inorganic citrates, Citric Acid (2014) 267–357, https://doi.org/10.1007/978-3-319-11233-6_5.

[25] S. Krukowski, M. Karasiewicz, W. Kolodziejski, Convenient UV-spectrophotometric determination of citrates in aqueous solutions with applications in the pharmaceutical analysis of oral electrolyte formulations, J. Food Drug Anal. 25 (3) (2017) 717–722, https://doi.org/10.1016/j.jfda.2017.01.009.

[26] L. Yang, M. Lübeck, P.S. Lübeck, *Aspergillus* as a versatile cell factory for organic acid production, Fungal Biol. Rev. 31 (1) (2017) 33–49, https://doi.org/10.1016/j.fbr.2016.11.001.

[27] E. Cavallo, H. Charreau, P. Cerrutti, M.L. Foresti, *Yarrowia lipolytica*: A model yeast for citric acid production, FEMS Yeast Res. 17 (2017) 1–16, https://doi.org/10.1093/femsyr/fox084.

[28] D.T.H. Do, C.W. Theron, P. Fickers, Organic wastes as feedstocks for non-conventional yeast-based bioprocesses, Microorganisms 7 (2019) 1–22, https://doi.org/10.3390/microorganisms7080229.

[29] I. Morgunov, S. Kamzolova, J. Lunina, Citric acid production by *Yarrowia lipolytica* Yeast on different renewable raw materials, Fermentation 4 (2) (2018) 36, https://doi.org/10.3390/fermentation4020036.

[30] M.-Y. Becker, N. Kohlheb, S. Hunger, S. Eschrich, R. Müller, A. Aurich, Early-stage sustainability assessment of biotechnological processes: a case study of citric acid production, Eng. Life Sci. 20 (3-4) (2020) 90–103, https://doi.org/10.1002/elsc.201800198.

[31] M. Zabiszak, M. Nowak, M. Gabryel, K. Ogawa, M.T. Kaczmarek, Z. Hnatejko, R. Jastrzab, New coordination compounds of citric acid and polyamines with lanthanide ions - potential application in monitoring the treatment of cancer diseases, J. Inorg. Biochem. 198 (2019) 110715, https://doi.org/10.1016/j.jinorgbio.2019.110715.

[32] S. Lagergren, About the theory of so-called adsorption of soluble substances, K. Sven. Vetenskapsakademiens Handl. 24 (1898) 1–39.

[33] Y.S. Ho, G. McKay, Pseudo-second order model for sorption processes, Process Biochem. 34 (5) (1999) 451–465, https://doi.org/10.1016/S0032-9592(98)00112-5.

[34] W.J. Weber, J.C. Morris, Kinetics of adsorption on carbon from solution, J. Sanit. Eng. Div. 89 (2) (1963) 31–59.

[35] G.E. Boyd, A.W. Adamson, L.S. Myers, The exchange adsorption of ions from aqueous solutions by organic zeolites II. Kinetics, J. Am. Chem. Soc. 69 (1947) 2836–2848.

[36] H.X. Zhu, X.J. Cao, Y.C. He, Q.P. Kong, H. He, J. Wang, Removal of Cu^{2+} from aqueous solutions by the novel modified bagasse pulp cellulose: kinetics, isotherm and mechanism, Carbohydr. Polym. 129 (2015) 115–126, https://doi.org/10.1016/j.carbpol.2015.04.049.

[37] I. Langmuir, The adsorption of gases on plane surfaces of glass, mica and platinum, J. Am. Chem. Soc. 40 (1918) 1361–1403, https://doi.org/10.1021/ja01340a008.

[38] H.M.F. Freundlich, Over the adsorption in solution, J. Phys. Chem. 57 (1906) 385–471.

[39] M.I. Temkin, V. Pyzhev, Kinetics of ammonia synthesis on promoted iron catalysts, Acta Physicochim. URSS. 12 (1940) 327–356.

[40] F. Reguyal, A.K. Sarmah, W. Gao, Synthesis of magnetic biochar from pine sawdust via oxidative hydrolysis of $FeCl_2$ for the removal sulfamethoxazole from aqueous solution, J. Hazard. Mater. 321 (2017) 868–878.

[41] B. Sheldrick, Calcium hydrogen citrate trihydrate, Acta Crystallogr. Sect. B Struct. Crystallogr. Cryst. Chem. 30 (8) (1974) 2056–2057.

[42] D.E. Zacharias, J.P. Glusker, Structure of strontium citrate pentahydrate, Acta Crystallogr. C. 49 (1993) 1732–1735, https://doi.org/10.1107/s0108270193000964.

[43] D. Wyrzykowski, L. Chmurzyński, Thermodynamics of citrate complexation with Mn^{2+}, Co^{2+}, Ni^{2+} and Zn^{2+} ions, J. Therm. Anal. Calorim. 102 (1) (2010) 61–64, https://doi.org/10.1007/s10973-009-0523-4.

[44] A.C. Bertoli, R. Carvalho, M.P. Freitas, T.C. Ramalho, D.T. Mancini, M.C. Oliveira, A. De Varennes, A. Dias, Structural determination of Cu and Fe-Citrate complexes: theoretical investigation and analysis by ESI-MS, J. Inorg. Biochem. 144 (2015) 31–37, https://doi.org/10.1016/j.jinorgbio.2014.12.008.

[45] J.C. Barnes, P.A. Bristow, Lanthanum citrate complexes in acid solutions, J. Less-Common Met. 22 (4) (1970) 463–465.

[46] D. Wyrzykowski, J. Czupryniak, T. Ossowski, L. Chmurzyński, Thermodynamic interactions of the alkaline earth metal ions with citric acid, J. Therm. Anal. Calorim. 102 (1) (2010) 149–154, https://doi.org/10.1007/s10973-010-0970-y.

[47] J.P. Glusker, Citrate conformation and chelation: enzymatic implications, Acc. Chem. Res. 13 (1980) 345–352, https://doi.org/10.1021/ar50154a002.

[48] R.M. Smith, A.E. Martell (Eds.), Critical Stability Constants, Springer US, Boston, MA, 1989.

[49] A.M.N. Silva, X. Kong, R.C. Hider, Determination of the pK_a value of the hydroxyl group in the α-hydroxycarboxylates citrate, malate and lactate by 13C NMR: implications for metal coordination in biological systems, Biometals 22 (5) (2009) 771–778, https://doi.org/10.1007/s10534-009-9224-5.

[50] A. Rammohan, J.A. Kaduk, Crystal structures of alkali metal (Group 1) citrate salts, Acta Crystallogr. Sect. B Struct. Sci. Cryst. Eng. Mater. 74 (2) (2018) 239–252, https://doi.org/10.1107/S2052520618002330.

[51] A.S. Bastug, S. Göktürk, T. Sismanoglu, 1:1 Binary complexes of citric acid with some metal ions: Stability and thermodynamic parameters, Asian J. Chem. 20 (2008) 1269–1278.

[52] R. Bassi, S.O. Prasher, B.K. Simpson, Extraction of metals from a contaminated sandy soil using citric acid, Environ. Prog. 19 (4) (2000) 275–282, https://doi.org/10.1002/ep.670190415.

[53] A.J. Francis, C.J. Dodge, J.B. Gillow, Biodegradation of metal citrate complexes and implications for toxic-metal mobility, Nature 356 (6365) (1992) 140–142.

[54] Y. Chunbo, L. Juzheng, Z. Daqing, W.u. Yijie, N.i. Jiazuan, Lanthanide-induced shift and relaxation rate studies of the aqueous complexation of citrate, Polyhedron 14 (23-24) (1995) 3579–3583, https://doi.org/10.1016/0277-5387(95)00172-O.

[55] K. Araucz, A. Aurich, D. Kołodyńska, Novel multifunctional ion exchangers for metal ions removal in the presence of citric acid, Chemosphere 251 (2020) 126331, https://doi.org/10.1016/j.chemosphere.2020.126331.
[56] D. Kołodyńska, D. Fila, Z. Hubicki, Static and dynamic studies of lanthanum(III) ion adsorption/desorption from acidic solutions using chelating ion exchangers with different functionalities, Environ. Res. 191 (2020) 110171, https://doi.org/10.1016/j.envres.2020.110171.
[57] D. Kołodyńska, D. Fila, Z. Hubicki, Recovery of lanthanum(III) and nickel(II) ions from acidic solutions by the highly effective ion exchanger, Molecules 25 (2020) 3718, https://doi.org/10.3390/molecules25163718.
[58] D. Kołodyńska, H. Hubicka, Z. Hubicki, Sorption of heavy metal ions from aqueous solutions in the presence of EDTA on monodisperse anion exchangers, Desalination 227 (1-3) (2008) 150–166, https://doi.org/10.1016/j.desal.2007.06.022.
[59] D. Kołodyńska, Green complexing agent - EDDS in removal of heavy metal ions on strongly basic anion exchangers, Desalination 280 (1-3) (2011) 44–57, https://doi.org/10.1016/j.desal.2011.06.060.
[60] D. Kołodyńska, Cu(II), Zn(II), Ni(II), and Cd(II) complexes with HEDP removal from industrial effluents on different ion exchangers, Ind. Eng. Chem. Res. 49 (5) (2010) 2388–2400.
[61] S. Nagireddi, A.K. Golder, R. Uppaluri, Combinatorial optimality of functional groups, process parameters, and Pd(II) adsorption–desorption characteristics for commercial anion exchange resins-synthetic electroless plating systems, Environ. Sci. Pollut. Res. 27 (20) (2020) 24614–24626, https://doi.org/10.1007/s11356-019-05941-1.
[62] N.A. Nekrasova, V.M. Gelis, V.V. Milyutin, N.A. Budantseva, E.A. Kozlitin, M. V. Logunov, Y.E. Pristinskii, Sorption of Th, U, and Am on phosphorus-containing ion-exchange materials, Radiochemistry 52 (1) (2010) 71–75.
[63] S.D. Alexandratos, X. Zhu, ATR-FTIR spectroscopy as a probe for metal ion binding onto immobilized ligands, Mater. Chem. Phys. 218 (2018) 196–203, https://doi.org/10.1016/j.matchemphys.2018.07.026.
[64] L. Lazar, B. Bandrabur, R.-E. Tataru-Farmus, M. Drobota, L. Bulgariu, G. Gutt, FTIR analysis of ion exchange resins with application in permanent hard water softening, Environ. Eng. Manag. J. 13 (9) (2014) 2145–2152.
[65] G. Socrates, Infrared and Raman characteristic group frequencies. Tables and Charts, Third Edition, John Wiley & Sons Ltd, England, 2001.
[66] S. Iqbal, J.-I. Yun, EDTA-functionalized mesoporous silica for the removal of corrosion products: adsorption studies and performance evaluation under gamma irradiation, Microporous Mesoporous Mater. 248 (2017) 149–157, https://doi.org/10.1016/j.micromeso.2017.04.028.
[67] H. Qiu, L.u. Lv, B.-C. Pan, Q.-J. Zhang, W.-M. Zhang, Q.-X. Zhang, Critical review in adsorption kinetic models, J. Zhejiang Univ. Sci. A. 10 (5) (2009) 716–724, https://doi.org/10.1631/jzus.A0820524.
[68] G. Darracq, J. Baron, M. Joyeux, Kinetic and isotherm studies on perchlorate sorption by ion-exchange resins in drinking water treatment, J. Water Process Eng. 3 (2014) 123–131, https://doi.org/10.1016/j.jwpe.2014.06.002.
[69] J. Nastaj, A. Przewłocka, M. Rajkowska-Myśliwiec, Biosorption of Ni(II), Pb(II) and Zn(II) on calcium alginate beads: equilibrium, kinetic and mechanism studies, Polish J Chem. Technol. 18 (2016) 81–87, https://doi.org/10.1515/pjct-2016-0052.
[70] E.G. Deze, S.K. Papageorgiou, E.P. Favvas, F.K. Katsaros, Porous alginate aerogel beads for effective and rapid heavy metal sorption from aqueous solutions: effect of porosity in Cu^{2+} and Cd^{2+} ion sorption, Chem. Eng. J. 209 (2012) 537–546.
[71] M. Arthy, M.P. Saravanakumar, Isotherm modeling, kinetic study and optimization of batch parameters for effective removal of Acid Blue 45 using tannery waste, J. Mol. Liq. 187 (2013) 189–200, https://doi.org/10.1016/j.molliq.2013.06.019.
[72] A.L.I. Omnia, S. Mohamed, Adsorption of copper ions and alizarin red S from aqueous solutions onto a polymeric nanocomposite in single and binary systems, Turkish J. Chem. 41 (2017) 967–986, https://doi.org/10.3906/kim-1703-72.
[73] P. Staroń, J. Chwastowski, M. Banach, Sorption and desorption studies on silver ions from aqueous solution by coconut fiber, J. Clean. Prod. 149 (2017) 290–301.
[74] P. Nautiyal, K.A. Subramanian, M.G. Dastidar, Adsorptive removal of dye using biochar derived from residual algae after in-situ transesterification: alternate use of waste of biodiesel industry, J. Environ. Manage. 182 (2016) 187–197.
[75] L. Zhang, Y. Zeng, Z. Cheng, Removal of heavy metal ions using chitosan and modified chitosan: a review, J. Mol. Liq. 214 (2016) 175–191, https://doi.org/10.1016/j.molliq.2015.12.013.
[76] M. Greluk, Z. Hubicki, Comparison of the gel anion exchangers for removal of Acid Orange 7 from aqueous solution, Chem. Eng. J. 170 (1) (2011) 184–193, https://doi.org/10.1016/j.cej.2011.03.052.
[77] W. Konicki, M. Aleksandrzak, E. Mijowska, Equilibrium, kinetic and thermodynamic studies on adsorption of cationic dyes from aqueous solutions using graphene oxide, Chem. Eng. Res. Des. 123 (2017) 35–49, https://doi.org/10.1016/j.cherd.2017.03.036.
[78] V.O. Shikuku, F.F. Donato, C.O. Kowenje, R. Zanella, O.D. Prestes, A comparison of adsorption equilibrium, kinetics and thermodynamics of aqueous phase clomazone between faujasite X and a natural zeolite from Kenya, South African J. Chem. 68 (2015) 245–252, https://doi.org/10.17159/0379-4350/2015/v68a33.
[79] S. Sohni, R. Hashim, H. Nidaullah, J. Lamaming, O. Sulaiman, Chitosan/nano-lignin based composite as a new sorbent for enhanced removal of dye pollution from aqueous solutions, Int. J. Biol. Macromol. 132 (2019) 1304–1317, https://doi.org/10.1016/j.ijbiomac.2019.03.151.
[80] M.S. Podder, C.B. Majumder, Biological detoxification of As(III) and As(V) using immobilized bacterial cells in fixed-bed bio-column reactor: prediction of kinetic parameters, Groundw. Sustain. Dev. 6 (2018) 14–42, https://doi.org/10.1016/j.gsd.2017.10.004.
[81] S. Chatterjee, S. Mondal, S. De, Design and scaling up of fixed bed adsorption columns for lead removal by treated laterite, J. Clean. Prod. 177 (2018) 760–774, https://doi.org/10.1016/j.jclepro.2017.12.249.
[82] I. Kavianinia, P.G. Plieger, N.G. Kandile, D.R.K. Harding, Fixed-bed column studies on a modified chitosan hydrogel for detoxification of aqueous solutions from copper(II), Carbohydr. Polym. 90 (2) (2012) 875–886, https://doi.org/10.1016/j.carbpol.2012.06.014.
[83] H. Zeng, S. Sun, Y. Yu, J. Zhang, D. Li, Column studies on the adsorption of As(V) by granular chitosan adsorbent prepared with backwashing iron-containing sludge, Colloids Surfaces A Physicochem. Eng. Asp. 627 (2021) 127247, https://doi.org/10.1016/j.colsurfa.2021.127247.
[84] E. Sundhararasu, S. Tuomikoski, H. Runtti, T. Hu, T. Varila, T. Kangas, U. Lassi, Alkali-activated adsorbents from slags: column adsorption and regeneration study for nickel(II) removal, ChemEngineering. 5 (2021) 1–15, https://doi.org/10.3390/chemengineering5010013.
[85] A.D. Dorado, X. Gamisans, C. Valderrama, M. Solé, C. Lao, Cr(III) removal from aqueous solutions: a straightforward model approaching of the adsorption in a fixed-bed column, J. Environ. Sci. Heal. - Part A Toxic/Hazardous Subst. Environ. Eng. 49 (2) (2014) 179–186, https://doi.org/10.1080/10934529.2013.838855.
[86] A. Katsigiannis, C. Noutsopoulos, J. Mantziaras, M. Gioldasi, Removal of emerging pollutants through Granular Activated Carbon, Chem. Eng. J. 280 (2015) 49–57, https://doi.org/10.1016/j.cej.2015.05.109.
[87] B. Preetha, T. Viruthagiri, Batch and continuous biosorption of chromium(VI) by *Rhizopus arrhizus*, Sep. Purif. Technol. 57 (1) (2007) 126–133, https://doi.org/10.1016/j.seppur.2007.03.015.

Supplementary Materials

Green citric acid in the sorption process of rare earth elements

Katarzyna Burdzy[a]*, Andreas Aurich[b], Steffi Hunger[b], Renata Jastrząb[c], Michał Zabiszak[c], Dorota Kołodyńska[a]*

[a]Department of Inorganic Chemistry, Faculty of Chemistry, Maria Curie-Skłodowska University, M. Curie Skłodowska Sq. 2, 20-031 Lublin, Poland,

[b]Environmental and Biotechnology Centre, Department Umwelt und Biotechnologisches Zentrum (UBZ), Helmholtz-Centre for Environmental Research-UFZ, Permoserstr. 15, 04318 Leipzig, Germany,

[c]Faculty of Chemistry, Adam Mickiewicz University, Uniwersytetu Poznańskiego 8, 61-614 Poznan, Poland

1. Ion exchangers

Purolite S957 with the phosphonic and sulphonic functional groups and Purolite S950 with the aminophosphonic functional groups are commercially available chelating ion exchangers manufactured by Purolite Ltd. (Germany). Lewatit Monoplus SP112 cation exchanger with the sulphonic functional groups was supplied by Lanxess (Germany). Lewatit MonoPlus M500, Lewatit MonoPlus M600, Lewatit MonoPlus MP500 (Lanxess, Germany) and Amberjet 4200, Amberjet 4400, Amberjet 4600 (Rohm and Haas, France) are strongly basic polystyrene anion exchangers with the quaternary ammonium functional groups (M500, MP500, 4200, 4400 – type I and M600, 4600 – type II). Amberlite IRA 458, Amberlite IRA 958 and Amberlite IRA 67 are polyacrylate anion exchangers obtained from Rohm and Haas (France). Amberlite IRA 458 and Amberlite IRA 958 are strongly basic anion exchangers of type I, while Amberlite IRA 67 is a weak base anion exchanger with the tertiary amine functional groups. All ion exchangers were washed several times with distilled water to remove impurities and dried at room temperature.

2. Apparatus and instruments

The laboratory shakers Elpin type 357 and Elpin type 358A (Elpin Plus, Poland) were used in the sorption process by the static method. The pH values were measured at the start and end of each study by pHmeter pHM82 (Radiometer, Copenhagen).

The concentrations of Ln(III) ions were analysed by the inductively coupled plasma optical emission spectrometry using ICP-OES 720-ES (Varian, USA) at 333.749 nm for La(III), 401.224 nm for Nd(III) and 345.600 nm for Ho(III). The ICP-OES instrument has been calibrated using the ICP standards. To avoid matrix interference, ultrapure nitric acid was used for preparation of all standards and blank samples. The relative

standard deviation (RSD) for the triplicate analysis was within 5%.

Scanning electron microscopy (SEM) was used to study the surface morphology of ion exchangers. All samples were gold sputtered prior to the analysis with the CCU-010 sputter (Safematic, Switzerland). The SEM images were recorded using a Phenom Pro X scanning electron microscope operating at 5 kV at the magnifications of 10000x.

Point of zero charge (pH_{pzc}) of the ion exchangers was determined using the potentiometric titration method for the three ionic strengths (0.1, 0.01 and 0.001 M NaCl). The suspensions of the resin (0.5 g) and NaCl solution (50 mL) were mixed using a magnetic stirrer and titrated with the standard solutions (0.1 M HCl and 0.1 M NaOH). To this end the Dosino and Titrando kit (Metrohm) was used. pH_{pzc} was also determined using the drift method. For this purpose 0.2 g of ion exchanger and 20 mL of the pH-adjusted 0.1 M NaCl solution were added into a flask and stirred with the rate of 180 rpm for 24 h. The initial pH (pH_0) of the solution was in the range from 2.0 to 12.0. The solution was separated from the sorbent by filtration. The final pH (pH_1) values were measured. Based on the curve pH_0 vs. ΔpH $(pH_1\text{-}pH_0)$ pH_{pzc} was determined as the point of intersection with the x axis.

The Fourier transform infrared (FTIR) spectroscopy was used to confirm the presence of the expected functional groups. To this end the Cary 630 spectrophotometer with the attenuated total reflectance mode (ATR-FTIR) (Agilent Technologies) was used. FTIR spectra were recorded over the interval 4000–530 cm^{-1}.

The 907 Titrando titrator equipped with the 800 Dosino type dosing systems, 801 type magnetic stirrer, high performance unitrode and Pt 1000 temperature sensor (Metrohm) was used to perform potentiometric measurements.

3. Yeast strain, media and cultivation conditions

The strain *Yarrowia lipolytica* H181 obtained from the strain collection of the Helmholtz Centre for Environmental Research - UFZ (Leipzig, Germany) was used for the production of citric acid. This strain is able to produce citric acid with the high concentration from 95 to 198 g/L from triglycerides like plant oils and waste frying oil [S1, S2]. For pre-cultivation the yeast was incubated at Reader agar plates at 30°C for 48 h.

The sterile pre-culture of *Y. lipolytica* H181 was grown in 500 mL shaking flasks with baffles and a working volume of 100 mL being incubated for 51 h at 30°C on a rotary shaker at 135 rpm. The medium was composed of: 3.0 g/L NH_4Cl, 0.7 g/L KH_2PO_4, 0.35 g/L $MgSO_4 \cdot 7H_2O$, 0.1 g/L NaCl, 0.13 g/L $CaCl_2 \cdot 2H_2O$, 3.5 mg/L $FeSO_4 \cdot 7H_2O$ and 1 mg/L thiamine hydrochloride. The concentrations of trace elements were: 20 mg/L $CuSO_4 \cdot 5H_2O$, 20 mg/L $MnSO_4 \cdot 5H_2O$, 10.5 mg/L $ZnCl_2$, 2.5 mg/L $CoSO_4 \cdot 7H_2O$ and 28.5 g/L H_3BO_3. All components were dissolved in the running water. 3 mL of sunflower oil as the carbon source was added into each flask at the beginning and after the 21 h cultivation. After 21 h and 51 h (end) the pH was measured and adjusted with 40% NaOH to be 5-6.

The medium of the pre-culture was used for the non-sterile main culture in the bioreactors too except for NH_4Cl which was substituted with 3.7 g/L $(NH_4)_2SO_4$.

The waste frying oil (WFO, based on brand “Amphora de Risso”, Cargill, Germany) was added as the sole carbon after its two-day use for deep-frying of french fries. The WFO was composed of: 5.4% myristic acid (14:0), 0.2% palmitic acid (16:0), 1.6% stearic acid (18:0), 58.7% oleic acid (18:1, w9c), 3.5% vaccenic acid (18.1, w7c), 19.6% linoleic acid (18:2), 8.7% linolenic acid (18:3), 0.4% arachidonic acid (20:0), 0,9% eiocsenic acid (20:1, w9c) and 1.0% other fatty acids.

The non-sterile CA production process (166 h) was performed as a fed-batch mode in a 20-L stirred tank reactor (ISF215, Infors AG, Switzerland) with an initial working volume of 9 L. The bioreactor was inoculated with 10% (v/v) pre-culture of *Y. lipolytica* H181. The initial WFO concentration was 20 g/L and 1,500 g was added over the first 95 h of cultivation. The optimized process conditions for the CA production were determined with pH at 5.0 by 40% NaOH, temperature at 30°C and a dissolved oxygen concentration DOC > 20% using a stirrer speed of 800 rpm and an airflow of 4 L/min. All added substances were completely non-sterile.

4. Analytical methods (CA production)

The determination of organic acids, inorganic anions and cations was carried out using the ion chromatography (IC) system ICS 5000^{+} DP (Thermo Fisher Scientific, Germany). For the anion separation a IonPac AS19 (2 mm diameter, 250 mm length) analytical column was used. The separation of anionic components was made under the following conditions: the sample injection volume, 5 µL; the eluent flow rate, 0.2 mL/min; the KOH eluent gradient: isocratic at 10 mM hold for 5 min, linear to 40 mM from 5 to 15 min, linear to 60 mM from 15 to 28 min and isocratic at 10 mM hold for 28-40 min. For the cation separation the IonPac CS12A (2 mm diameter, 250 mm length) analytical column was used. The separation of cationic components was made under the following conditions: the sample injection volume, 5 µL; the eluent flow rate, 0.25 mL/min; the methanesulfonic acid eluent gradient: isocratic at 5 mM hold for 12.5 min, linear to 20 mM from 12.5 to 27.5 min and isocratic at 5 mM hold for 27.5-30 min. The organic acids were quantified with the software Chromeleon 7.2.4 (Thermo Fisher Scientific, Germany) using the calibration curves.

5. Separation of yeast biomass and WFO

The Sartoflow® Alpha crossflow microfiltration equipment (Sartorius, Göttingen, Germany) was used to separate the yeast biomass (15.5 g/L) and the residual waste frying oil (12.7 g/L) completely from the final culture broth. The microfiltration process was conducted by the Hydrosart® type membranes (Sartorius) with 0.2 μm pore sizes and the total filtration area of 0.1 m^2.

After separation of the yeast biomass and the waste frying oil residues, the concentrations of the ionic components (Table S1) were measured in the permeate. The sustainable form of CA solution was used in all experiments on the sorption of rare earth elements.

Table S1. Composition of yeast based citric acid solution after removing the yeast biomass and the residual waste frying oil.

Ionic component	Concentration [g/L]
Citric acid	186.74
Isocitric acid	8.5
Cl^-	0.36
Ca^{2+}	0.63
K^+	0.08
Na^+	23.19
Mg^{2+}	0.03
SO_4^{2-}	2.04

6. Potentiometric measurements

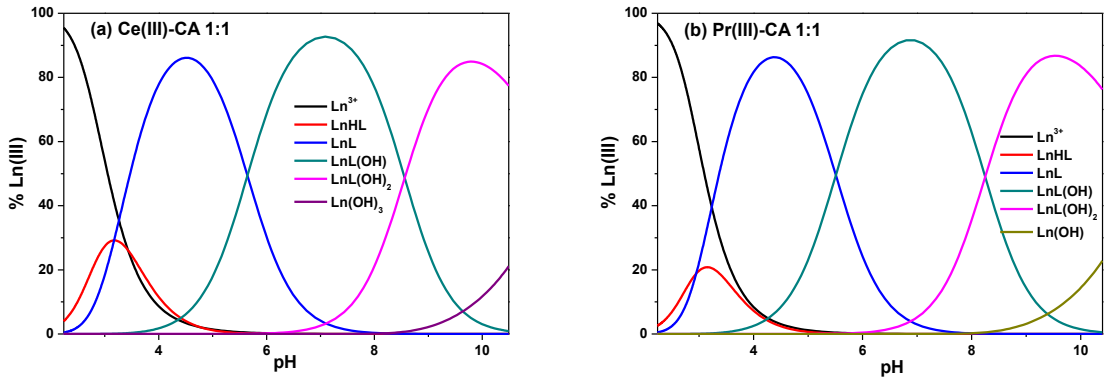

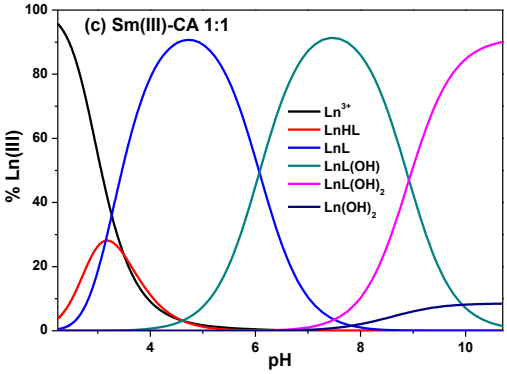
(c) Sm(III)-CA 1:1
% Ln(III)
pH
Ln3+
LnHL
LnL
LnL(OH)
LnL(OH)2
Ln(OH)2

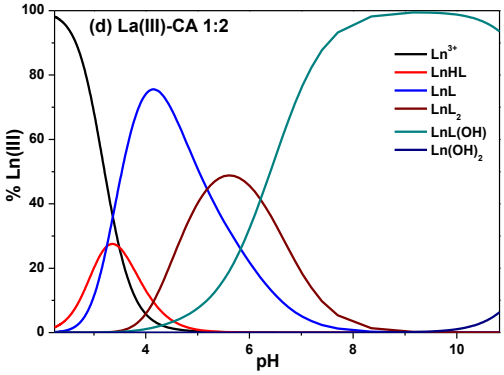
(d) La(III)-CA 1:2
% Ln(III)
pH
Ln3+
LnHL
LnL
LnL2
LnL(OH)
Ln(OH)2

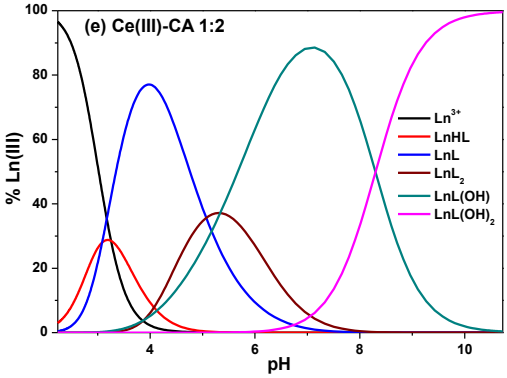
(e) Ce(III)-CA 1:2
% Ln(III)
pH
Ln3+
LnHL
LnL
LnL2
LnL(OH)
LnL(OH)2

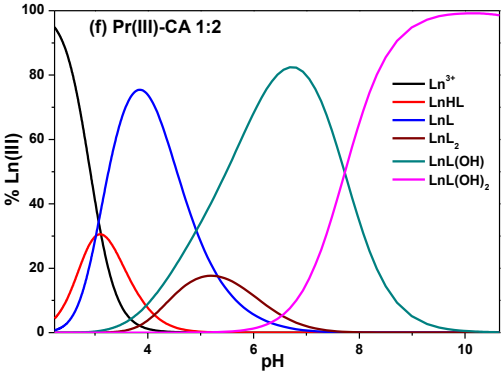
(f) Pr(III)-CA 1:2
% Ln(III)
pH
Ln3+
LnHL
LnL
LnL2
LnL(OH)
LnL(OH)2

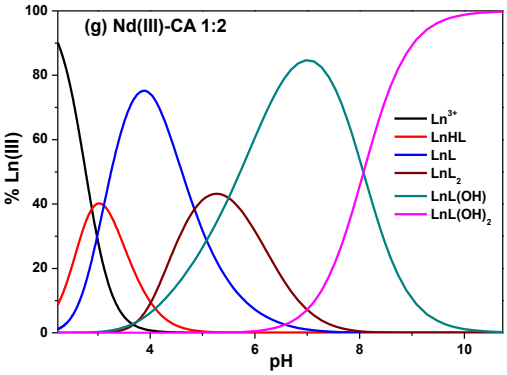
(g) Nd(III)-CA 1:2
% Ln(III)
pH
Ln3+
LnHL
LnL
LnL2
LnL(OH)
LnL(OH)2

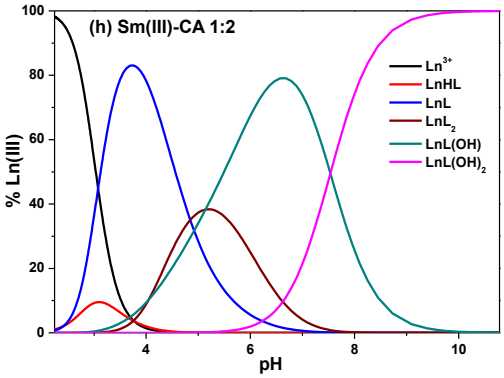
(h) Sm(III)-CA 1:2
% Ln(III)
pH
Ln3+
LnHL
LnL
LnL2
LnL(OH)
LnL(OH)2

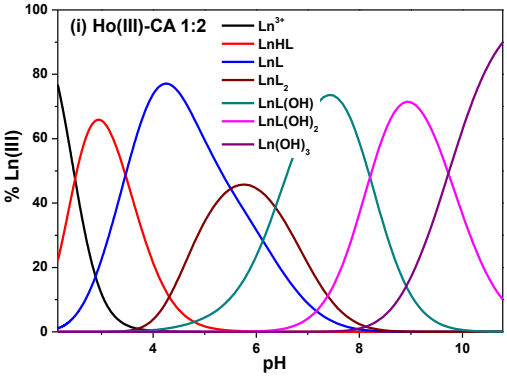
(i) Ho(III)-CA 1:2
% Ln(III)
pH
Ln3+
LnHL
LnL
LnL2
LnL(OH)
LnL(OH)2
Ln(OH)3

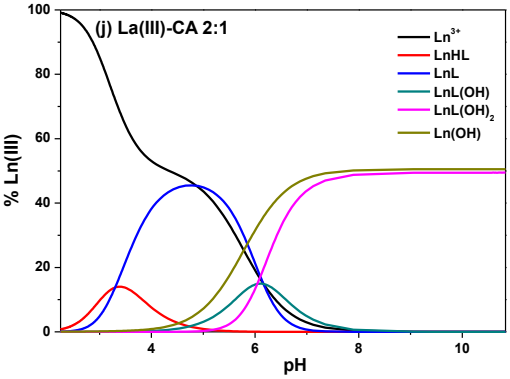
(j) La(III)-CA 2:1
% Ln(III)
pH
Ln3+
LnHL
LnL
LnL(OH)
LnL(OH)2
Ln(OH)

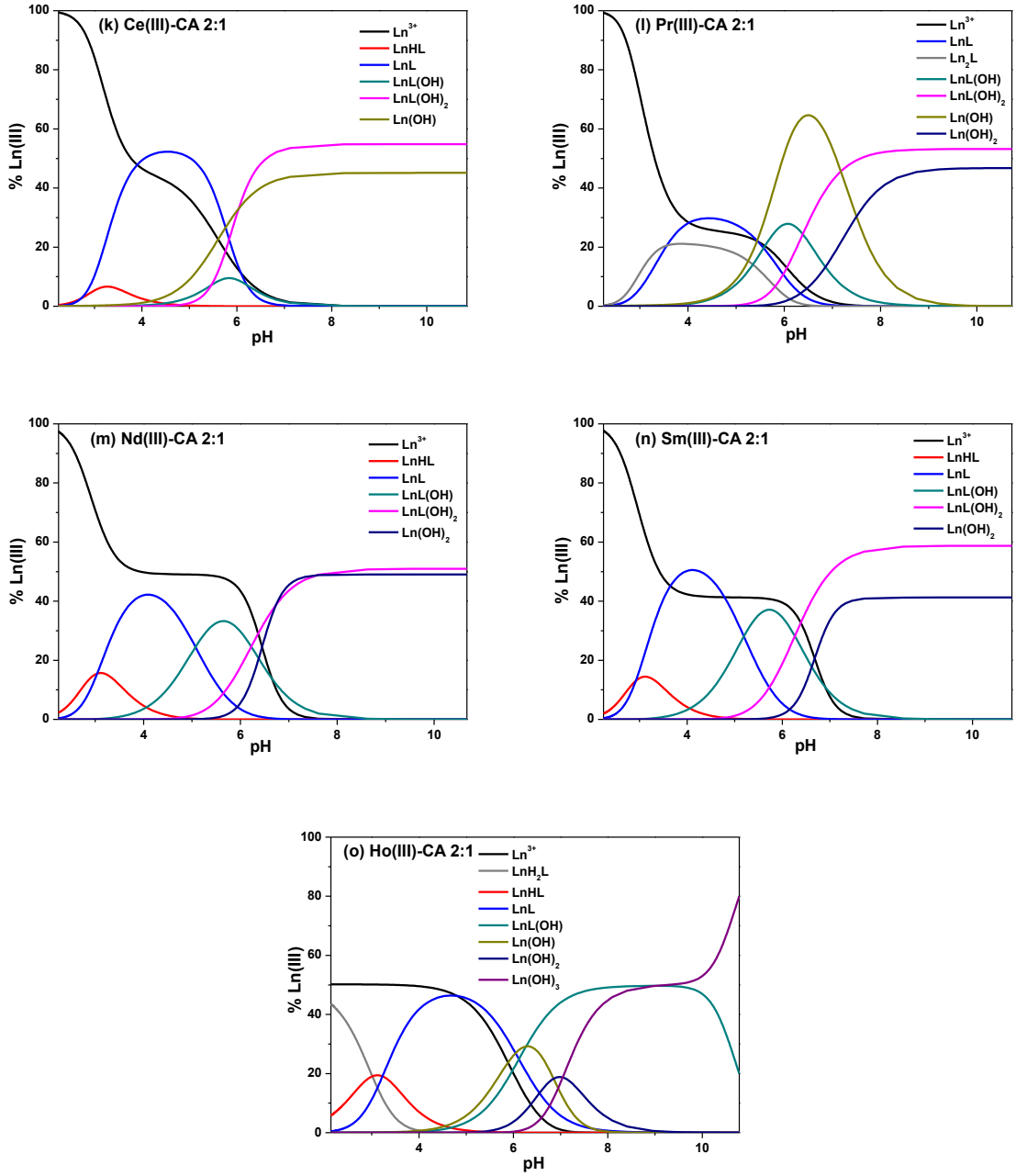

Fig.S1. Distribution diagrams for the Ln(III)-L systems (where Ln=La(III), Ce(III), Pr(III), Nd(III), Sm(III), Ho(III) and L=citric acid, CA): (a-c) Ln(III)-L 1:1, (d-i) Ln(III)-L 1:2, (j-o) Ln(III)-L 2:1.

7. The morphology of ion exchangers surface

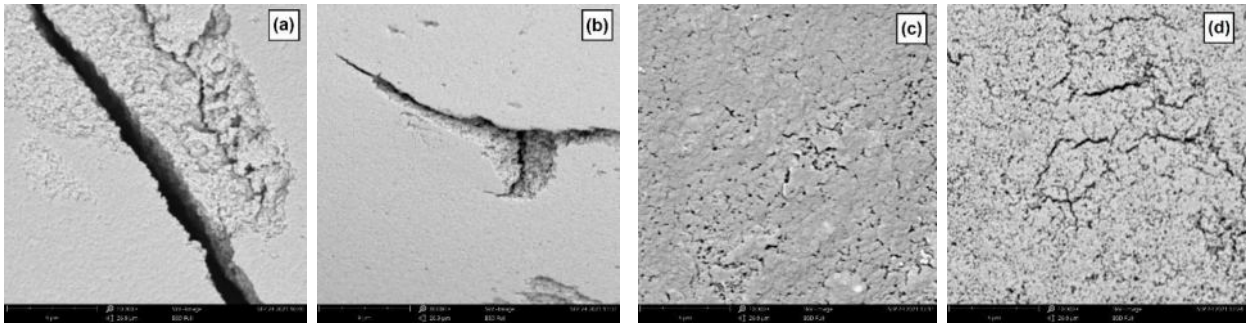

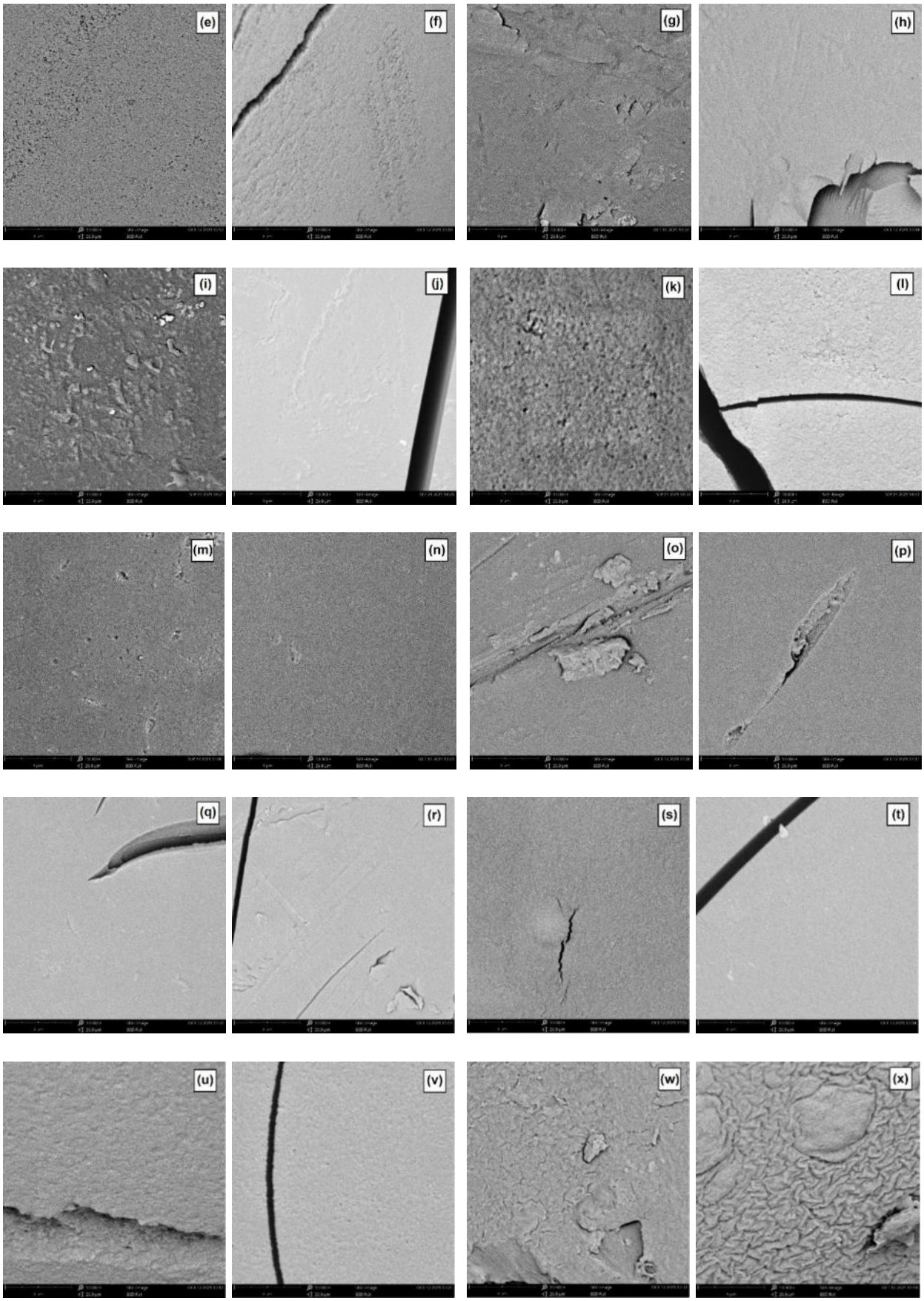

Fig.S2. SEM images of (a,b) Purolite S957, (c,d) Purolite S950, (e,f) Lewatit SP112, (g,h) Lewatit M500, (i,j) Lewatit M600, (k,l) Lewatit MP500, (m,n) Amberjet 4200, (o,p) Amberjet 4400, (q,r) Amberjet 4600,

(s,t) Amberlite IRA 458, (u,v) Amberlite IRA 958, and (w,x) Amberlite IRA 67 (a,c,e,g,i,k,m,o,q,s,u,w) before and (b,d,f,h,j,l,n,p,r,t,v,x) after the adsorption of La(III) ions in the presence of CA (magnification × 10000).

8. Kinetic and adsorption studies

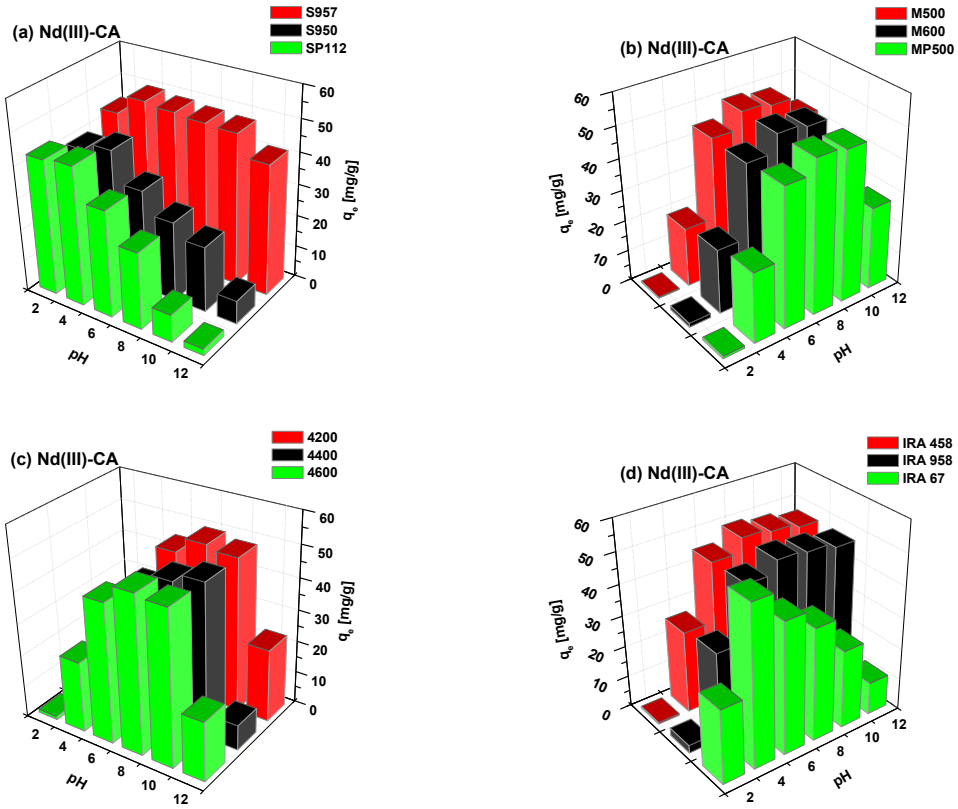

Fig.S3. The effect of pH on the sorption of Nd(III)-CA complexes on (a) Purolite S957, Purolite S950, Lewatit SP112, (b) Lewatit M500, Lewatit M600, Lewatit MP500, (c) Amberjet 4200, Amberjet 4400, Amberjet 4600 and (d) Amberlite IRA 458, Amberlite IRA 958, Amberlite IRA 67.

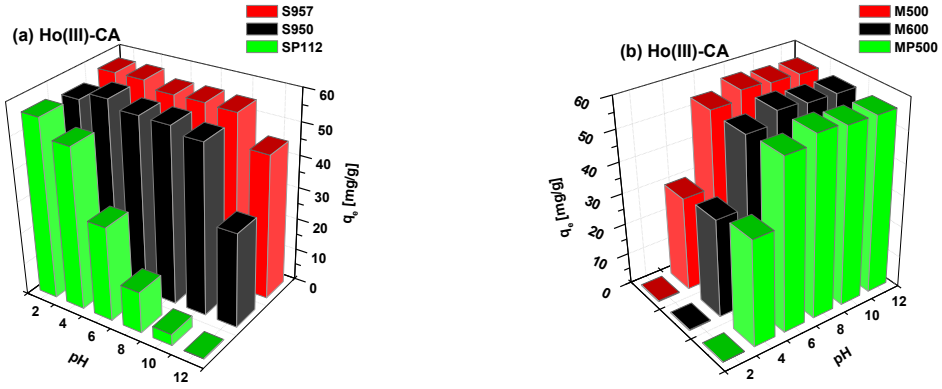

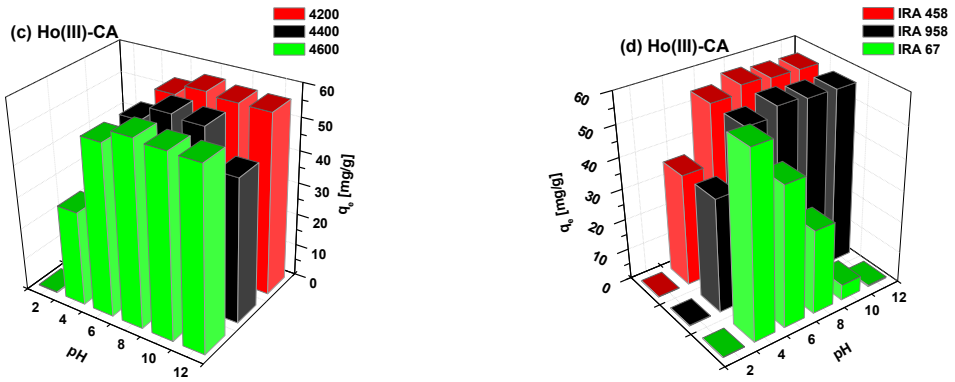

Fig.S4. The effect of pH on the sorption of Ho(III)-CA complexes on (a) Purolite S957, Purolite S950, Lewatit SP112, (b) Lewatit M500, Lewatit M600, Lewatit MP500, (c) Amberjet 4200, Amberjet 4400, Amberjet 4600 and (d) Amberlite IRA 458, Amberlite IRA 958, Amberlite IRA 67.

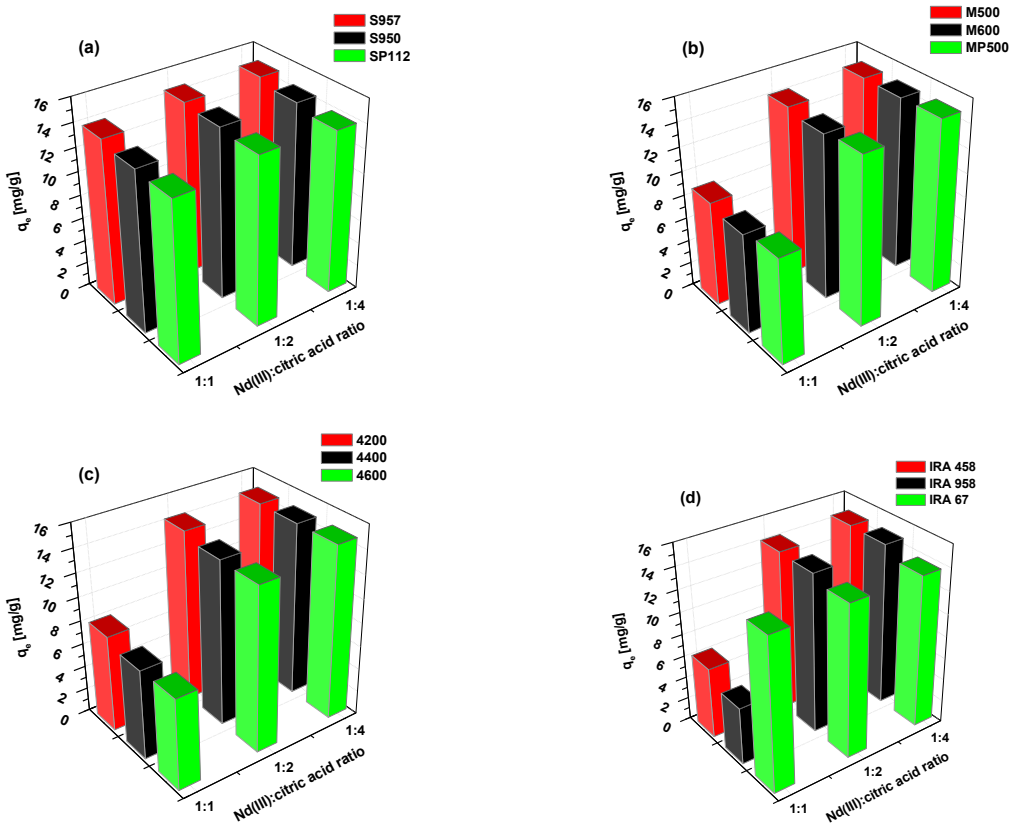

Fig.S5. The effect of molar ratio on the sorption of Nd(III)-CA complexes on (a) Purolite S957, Purolite S950, Lewatit SP112, (b) Lewatit M500, Lewatit M600, Lewatit MP500, (c) Amberjet 4200, Amberjet 4400, Amberjet 4600 and (d) Amberlite IRA 458, Amberlite IRA 958, Amberlite IRA 67.

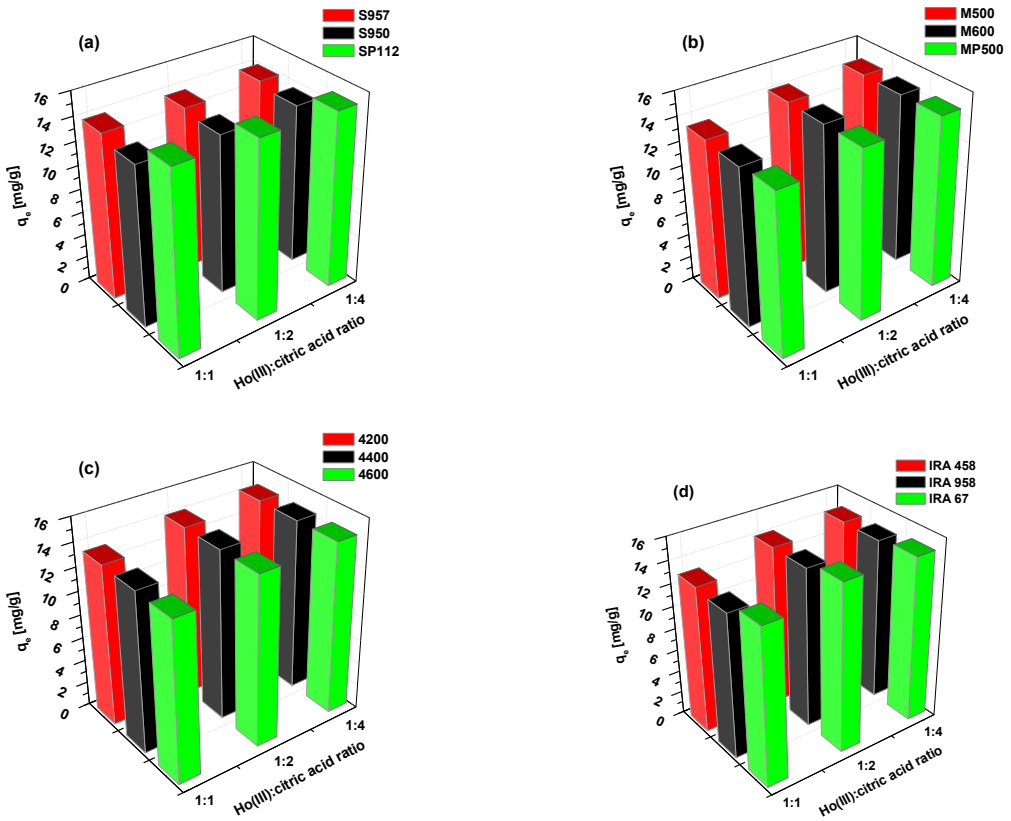

Fig.S6. The effect of molar ratio on the sorption of Ho(III)-CA complexes on (a) Purolite S957, Purolite S950, Lewatit SP112, (b) Lewatit M500, Lewatit M600, Lewatit MP500, (c) Amberjet 4200, Amberjet 4400, Amberjet 4600 and (d) Amberlite IRA 458, Amberlite IRA 958, Amberlite IRA 67.

Table S2. Kinetic parameters for the pseudo-first order and pseudo-second order kinetic models for the La(III)-CA complexes sorption on Purolite S957, Purolite S950, Lewatit SP112, Lewatit M500, Lewatit M600, Lewatit MP500, Amberjet 4200, Amberjet 4400, Amberjet 4600, Amberlite IRA 458, Amberlite IRA 958, Amberlite IRA 67 (C_0=1.0×10^{-3} M - 2.0×10^{-3} M).

Model			**Pseudo-First Order**			**Pseudo-Second Order**		
Adsorbent	C_o ×10^{-3} [M]	$q_{e.exp}$ [mg/g]	$q_{1.cal}$ [mg/g]	k_1 [1/min]	R^2	$q_{2.cal}$ [mg/g]	k_2 [g/mg min]	R^2
Purolite S957	1.0	13.76	12.93	0.407	0.998	13.81	0.110	1.000
	1.5	20.90	20.01	0.432	0.996	20.98	0.076	1.000
	2.0	28.40	27.44	0.423	0.999	28.50	0.056	1.000
Purolite S950	1.0	14.27	12.00	0.045	0.999	14.90	0.008	0.999
	1.5	21.11	15.60	0.026	0.985	22.00	0.004	0.999
	2.0	28.71	21.71	0.023	0.987	30.00	0.003	0.998
Lewatit SP112	1.0	13.94	9.42	0.072	0.956	14.17	0.018	1.000
	1.5	17.51	12.30	0.056	0.964	17.86	0.010	1.000
	2.0	18.78	14.52	0.056	0.996	19.26	0.008	1.000
Lewatit M500	1.0	14.05	10.84	0.237	0.996	14.15	0.061	1.000
	1.5	21.26	15.40	0.246	0.986	21.38	0.044	1.000
	2.0	28.59	19.81	0.248	0.988	28.74	0.036	1.000

Lewatit M600	1.0	14.00	11.36	0.210	0.996	14.13	0.037	1.000
	1.5	21.34	16.60	0.216	0.988	21.50	0.033	1.000
	2.0	29.25	24.31	0.268	0.995	29.44	0.031	1.000
Lewatit MP500	1.0	13.75	8.16	0.173	0.941	13.83	0.049	1.000
	1.5	21.02	12.33	0.174	0.949	21.14	0.033	1.000
	2.0	28.34	18.70	0.162	0.983	28.57	0.020	1.000
Amberjet 4200	1.0	12.14	9.13	0.200	0.959	12.23	0.052	1.000
	1.5	19.75	16.04	0.244	0.991	19.89	0.039	1.000
	2.0	27.03	21.33	0.215	0.993	27.24	0.024	1.000
Amberjet 4400	1.0	12.59	9.08	0.138	0.946	12.73	0.027	1.000
	1.5	19.91	14.12	0.140	0.944	20.11	0.019	1.000
	2.0	26.91	19.79	0.096	0.960	27.33	0.009	1.000
Amberjet 4600	1.0	11.90	9.07	0.177	0.985	12.00	0.043	1.000
	1.5	20.07	14.97	0.170	0.976	20.27	0.022	1.000
	2.0	26.89	25.11	0.255	0.981	27.10	0.024	1.000
Amberlite IRA 458	1.0	14.40	12.31	0.243	0.994	14.51	0.042	1.000
	1.5	21.39	15.88	0.207	0.992	21.55	0.031	1.000
	2.0	29.39	23.31	0.257	0.999	29.57	0.032	1.000
Amberlite IRA 958	1.0	13.45	9.52	0.329	0.994	13.49	0.121	1.000
	1.5	20.74	18.16	0.388	0.987	20.81	0.075	1.000
	2.0	29.39	28.19	0.469	0.984	29.48	0.068	1.000
Amberlite IRA 67	1.0	14.43	11.59	0.214	0.996	14.55	0.042	1.000
	1.5	21.50	17.80	0.178	0.990	21.70	0.020	1.000
	2.0	29.30	22.09	0.155	0.986	29.56	0.014	1.000

Table S3. Kinetic parameters for the Weber-Morris intraparticle diffusion kinetic model for the La(III)-CA complexes sorption on Purolite S957, Purolite S950, Lewatit SP112, Lewatit M500, Lewatit M600, Lewatit MP500, Amberjet 4200, Amberjet 4400, Amberjet 4600, Amberlite IRA 458, Amberlite IRA 958, Amberlite IRA 67 (C_0=1.0×10^{-3} M - 2.0×10^{-3} M).

Model	**Weber-Morris Intraparticle Diffusion**									
	C_o ×10^{-3} [M]	k_{i1} [mg/g min$^{1/2}$]	C_1	R^2	k_{i2} [mg/g min$^{1/2}$]	C_2	R^2	k_{i3} [mg/g min$^{1/2}$]	C_3	R^2
Purolite S957	1.0	4.81	0.91	0.961	0.01	13.66	0.431	-	-	-
	1.5	7.35	1.50	0.952	0.02	20.64	0.393	-	-	-
	2.0	9.97	1.87	0.970	0.00	28.34	0.401	-	-	-
Purolite S950	1.0	2.09	0.32	0.967	1.81	1.19	0.999	0.28	10.46	0.675
	1.5	2.88	0.52	0.980	2.64	1.38	1.000	0.52	13.66	0.885
	2.0	3.61	0.63	0.952	3.14	2.83	0.994	0.87	16.18	0.904
Lewatit SP112	1.0	3.22	0.21	0.955	1.22	6.15	0.971	0.11	12.40	0.823
	1.5	3.52	0.52	0.987	1.67	5.92	0.991	0.24	14.07	0.907

	2.0	3.11	1.06	0.999	2.33	3.23	1.000	0.24	15.34	0.748
Lewatit M500	1.0	4.24	1.13	0.993	0.59	10.79	0.902	0.01	13.95	0.676
	1.5	6.72	1.70	0.973	0.73	17.12	0.909	0.02	20.98	0.838
	2.0	8.57	3.58	0.949	0.97	23.13	0.859	0.02	28.26	0.636
Lewatit M600	1.0	4.41	0.11	0.986	0.43	10.70	0.655	0.09	12.78	0.623
	1.5	6.85	0.38	0.987	1.03	15.57	0.938	0.02	21.03	0.793
	2.0	9.92	0.38	0.987	1.07	23.49	0.899	0.00	29.25	0.724
Lewatit MP500	1.0	3.68	2.27	0.954	0.56	10.15	0.969	0.05	12.97	0.876
	1.5	5.48	3.88	0.962	0.81	15.74	0.968	0.08	19.84	0.833
	2.0	7.06	4.47	0.986	1.46	19.13	0.934	0.12	26.60	0.810
Amberjet 4200	1.0	3.95	0.04	0.994	0.55	8.85	0.994	0.02	11.80	0.812
	1.5	6.47	0.40	0.993	0.72	15.56	0.895	0.03	19.33	0.724
	2.0	8.40	0.90	0.994	1.21	19.93	0.910	0.05	26.27	0.783
Amberjet 4400	1.0	3.45	0.52	0.974	0.59	7.91	0.920	0.14	10.68	0.758
	1.5	5.61	0.78	0.989	0.99	12.71	0.996	0.17	17.49	0.851
	2.0	5.93	1.87	0.984	2.17	11.57	0.987	0.33	22.18	0.847
Amberjet 4600	1.0	3.50	0.38	0.984	0.71	7.67	0.929	0.04	11.36	0.921
	1.5	5.79	0.91	0.999	0.80	14.22	0.949	0.16	17.91	0.811
	2.0	7.90	1.38	0.996	1.22	19.86	0.648	0.06	26.06	0.851
Amberlite IRA 458	1.0	4.11	1.25	0.998	0.35	11.65	0.423	0.08	13.29	0.585
	1.5	6.34	1.55	0.984	0.85	16.03	0.880	0.07	20.48	0.638
	2.0	8.76	2.92	0.983	1.20	22.95	0.834	0.00	29.38	0.794
Amberlite IRA 958	1.0	3.77	2.95	0.969	0.01	13.37	0.963	-	-	-
	1.5	6.39	3.21	0.986	0.01	20.58	0.627	-	-	-
	2.0	8.97	5.47	0.988	0.00	29.38	0.820	-	-	-
Amberlite IRA 67	1.0	4.49	0.37	0.987	0.62	10.65	0.860	0.04	13.82	0.777
	1.5	5.80	1.02	0.973	1.14	14.19	0.900	0.11	19.90	0.907
	2.0	8.07	1.29	0.992	1.88	17.66	0.955	0.14	27.18	0.972

Table S4. Kinetic parameters for the Boyd and Dumwald-Wagner kinetic models for the La(III)-CA complexes sorption on Purolite S957, Purolite S950, Lewatit SP112, Lewatit M500, Lewatit M600, Lewatit MP500, Amberjet 4200, Amberjet 4400, Amberjet 4600, Amberlite IRA 458, Amberlite IRA 958, Amberlite IRA 67 (C_0=1.0×10^{-3} M - 2.0×10^{-3} M).

Model		**Boyd**		**Dumwald-Wagner**		
	C_o ×10^{-3} [M]	B_t	R^2	k	intercept	R^2
Purolite S957	1.0	10.67	0.780	0.077	1.21	0.548
	1.5	13.20	0.680	0.108	0.99	0.682
	2.0	11.27	0.674	0.093	1.07	0.677
Purolite S950	1.0	5.15	0.997	0.041	-0.06	0.995
	1.5	2.90	0.995	0.023	0.01	0.996

	2.0	2.51	0.997	0.019	0.01	0.997
Lewatit SP112	1.0	3.78	0.912	0.030	0.16	0.921
	1.5	3.05	0.945	0.024	0.11	0.952
	2.0	3.01	0.895	0.026	0.09	0.900
Lewatit M500	1.0	6.86	0.819	0.056	0.47	0.826
	1.5	5.17	0.728	0.040	0.52	0.735
	2.0	6.71	0.847	0.053	0.50	0.855
Lewatit M600	1.0	6.70	0.972	0.050	0.22	0.977
	1.5	6.46	0.870	0.051	0.38	0.879
	2.0	13.66	0.898	0.114	0.48	0.901
Lewatit MP500	1.0	4.45	0.875	0.032	0.37	0.887
	1.5	4.57	0.883	0.033	0.38	0.894
	2.0	4.77	0.916	0.035	0.30	0.925
Amberjet 4200	1.0	5.35	0.857	0.041	0.36	0.867
	1.5	9.55	0.973	0.072	0.26	0.976
	2.0	5.50	0.868	0.042	0.37	0.878
Amberjet 4400	1.0	4.14	0.962	0.030	0.19	0.969
	1.5	3.90	0.934	0.028	0.23	0.943
	2.0	3.59	0.969	0.027	0.13	0.975
Amberjet 4600	1.0	4.56	0.853	0.035	0.31	0.864
	1.5	7.17	0.954	0.052	0.14	0.953
	2.0	5.39	0.844	0.040	0.38	0.856
Amberlite IRA 458	1.0	5.12	0.873	0.039	0.34	0.883
	1.5	7.41	0.974	0.057	0.27	0.980
	2.0	10.20	0.784	0.087	0.59	0.787
Amberlite IRA 958	1.0	6.35	0.602	0.043	0.82	0.608
	1.5	5.86	0.549	0.041	0.85	0.555
	2.0	14.49	0.812	0.106	0.99	0.817
Amberlite IRA 67	1.0	7.07	0.962	0.053	0.26	0.967
	1.5	3.89	0.845	0.029	0.28	0.857
	2.0	3.68	0.829	0.027	0.28	0.840

Table S5. Kinetic parameters for the pseudo-first order and pseudo-second order kinetic models for the Nd(III)-CA complexes sorption on Purolite S957, Purolite S950, Lewatit SP112, Lewatit M500, Lewatit M600, Lewatit MP500, Amberjet 4200, Amberjet 4400, Amberjet 4600, Amberlite IRA 458, Amberlite IRA 958, Amberlite IRA 67 (C_0=1.0×10^{-3} M - 2.5×10^{-3} M).

Model			**Pseudo-First Order**			**Pseudo-Second Order**		
Adsorbent	C_o ×10^{-3} [M]	$q_{e.exp}$ [mg/g]	$q_{1.cal}$ [mg/g]	k_1 [1/min]	R^2	$q_{2.cal}$ [mg/g]	k_2 [g/mg min]	R^2
Purolite S957	1.0	13.87	14.96	0.395	0.996	13.94	0.072	1.000

	1.5	21.55	23.40	0.404	0.999	21.67	0.051	1.000
	2.0	27.48	27.97	0.339	0.998	27.64	0.033	1.000
	2.5	34.58	29.90	0.233	0.993	34.87	0.020	1.000
Purolite S950	1.0	14.12	8.00	0.026	0.927	14.22	0.011	0.998
	1.5	22.51	13.26	0.045	0.980	22.81	0.010	1.000
	2.0	29.75	17.92	0.043	0.988	30.28	0.007	1.000
	2.5	36.41	21.27	0.035	0.976	37.13	0.005	1.000
Lewatit SP112	1.0	14.85	13.44	0.265	0.998	14.96	0.053	1.000
	1.5	22.86	19.99	0.276	0.992	23.01	0.038	1.000
	2.0	29.73	23.82	0.244	0.996	29.93	0.027	1.000
	2.5	35.93	27.20	0.233	0.977	36.18	0.022	1.000
Lewatit M500	1.0	13.91	11.06	0.218	0.993	14.02	0.043	1.000
	1.5	21.32	16.78	0.257	0.993	21.43	0.041	1.000
	2.0	28.37	21.50	0.254	0.995	28.53	0.034	1.000
	2.5	34.30	26.13	0.256	0.992	34.49	0.028	1.000
Lewatit M600	1.0	13.51	10.42	0.217	0.992	13.59	0.047	1.000
	1.5	21.09	16.59	0.248	0.992	21.22	0.041	1.000
	2.0	28.34	21.25	0.232	0.986	28.53	0.029	1.000
	2.5	34.39	25.68	0.216	0.990	34.65	0.022	1.000
Lewatit MP500	1.0	13.79	8.55	0.206	0.967	13.88	0.063	1.000
	1.5	21.38	13.66	0.188	0.996	21.50	0.032	1.000
	2.0	28.70	20.07	0.124	0.998	29.05	0.015	1.000
	2.5	34.57	24.48	0.103	0.999	35.08	0.010	1.000
Amberjet 4200	1.0	14.12	12.60	0.242	0.995	14.22	0.048	1.000
	1.5	21.58	18.61	0.230	0.997	21.76	0.031	1.000
	2.0	28.98	24.66	0.233	0.999	29.21	0.024	1.000
	2.5	35.15	27.43	0.209	0.993	35.41	0.018	1.000
Amberjet 4400	1.0	13.71	10.58	0.173	0.987	13.84	0.035	1.000
	1.5	19.96	10.61	0.033	0.949	20.37	0.011	1.000
	2.0	28.50	21.32	0.031	0.995	29.57	0.004	0.999
	2.5	34.43	27.31	0.020	0.995	36.08	0.002	0.994
Amberjet 4600	1.0	13.64	10.68	0.215	0.991	13.74	0.051	1.000
	1.5	19.91	15.39	0.202	0.978	20.08	0.032	1.000
	2.0	28.66	23.01	0.205	0.990	28.90	0.021	1.000
	2.5	34.81	26.89	0.185	0.991	35.12	0.016	1.000
Amberlite IRA 458	1.0	13.93	10.05	0.216	0.989	13.97	0.046	1.000
	1.5	21.25	13.89	0.229	0.992	21.35	0.047	1.000
	2.0	28.31	18.20	0.243	0.990	28.45	0.041	1.000
	2.5	34.09	21.62	0.251	0.998	34.25	0.036	1.000

Amberlite IRA 958	1.0	13.85	20.10	0.506	0.967	13.91	0.092	1.000
	1.5	21.40	23.07	0.375	0.984	21.51	0.048	1.000
	2.0	28.88	24.80	0.318	0.999	29.03	0.037	1.000
	2.5	34.96	31.36	0.312	0.993	35.16	0.029	1.000
Amberlite IRA 67	1.0	14.28	11.21	0.264	0.982	14.37	0.065	1.000
	1.5	21.93	18.58	0.299	0.995	22.05	0.044	1.000
	2.0	29.25	24.04	0.232	0.993	29.47	0.024	1.000
	2.5	35.29	28.93	0.195	0.998	35.62	0.016	1.000

Table S6. Kinetic parameters for the Weber-Morris intraparticle diffusion kinetic model for the Nd(III)-CA complexes sorption on Purolite S957, Purolite S950, Lewatit SP112, Lewatit M500, Lewatit M600, Lewatit MP500, Amberjet 4200, Amberjet 4400, Amberjet 4600, Amberlite IRA 458, Amberlite IRA 958, Amberlite IRA 67 (C_0=1.0×10^{-3} M - 2.5×10^{-3} M).

Model	**Weber-Morris Intraparticle Diffusion**									
	C_o ×10^{-3} [M]	k_{i1} [mg/g min$^{1/2}$]	C_1	R^2	k_{i2} [mg/g min$^{1/2}$]	C_2	R^2	k_{i3} [mg/g min$^{1/2}$]	C_3	R^2
Purolite S957	1.0	4.58	0.37	0.924	0.02	13.60	0.618	-	-	-
	1.5	7.04	0.88	0.915	0.03	21.25	0.428	-	-	-
	2.0	8.61	1.23	0.955	0.06	26.69	0.567	-	-	-
	2.5	9.42	3.01	0.985	0.16	32.61	0.420	-	-	-
Purolite S950	1.0	2.17	2.23	0.979	0.69	7.05	0.987	0.24	10.31	0.982
	1.5	3.70	3.54	0.999	1.38	11.27	0.949	0.14	20.33	0.883
	2.0	4.32	5.62	0.990	2.03	13.14	0.953	0.19	26.91	0.980
	2.5	5.10	7.13	0.980	2.24	16.78	0.972	0.35	31.33	0.825
Lewatit SP112	1.0	4.77	0.28	0.998	0.61	11.53	0.830	0.01	14.78	0.629
	1.5	7.38	0.88	0.991	0.77	18.65	0.862	0.01	22.74	0.728
	2.0	9.19	1.81	0.988	1.22	22.87	0.844	0.03	29.30	0.783
	2.5	11.33	2.02	0.991	1.27	28.51	0.967	0.05	35.25	0.768
Lewatit M500	1.0	4.45	0.20	0.986	0.55	10.46	0.852	0.05	13.21	0.879
	1.5	6.58	1.70	0.991	0.75	17.12	0.878	0.02	21.05	0.913
	2.0	8.49	3.05	0.992	1.04	22.69	0.888	0.01	28.22	0.964
	2.5	10.36	3.50	0.989	1.24	27.50	0.891	0.01	34.13	0.901
Lewatit M600	1.0	4.18	0.63	0.991	0.57	10.15	0.917	0.03	13.03	0.957
	1.5	6.82	0.89	0.989	0.80	16.61	0.910	0.01	20.91	0.747
	2.0	9.08	1.34	0.981	1.10	22.01	0.919	0.03	27.89	0.607
	2.5	10.40	2.39	0.991	1.46	25.89	0.921	0.06	33.61	0.644
Lewatit MP500	1.0	3.75	2.43	0.984	0.47	10.87	0.957	0.03	13.36	0.676
	1.5	4.99	4.86	0.999	0.83	16.12	0.902	0.07	20.34	0.859
	2.0	5.49	5.54	0.989	2.44	14.45	0.968	0.08	27.62	0.531
	2.5	6.39	5.76	0.996	3.40	14.32	0.988	0.16	32.38	0.750

Amberjet 4200	1.0	4.33	0.39	0.999	0.65	10.53	0.865	0.01	13.97	0.981
	1.5	6.68	0.44	0.999	0.98	15.96	0.876	0.03	21.19	0.594
	2.0	8.94	0.91	0.998	1.34	21.46	0.863	0.03	28.56	0.761
	2.5	10.91	1.07	0.986	1.76	25.15	0.922	0.05	34.33	0.969
Amberjet 4400	1.0	3.89	0.62	0.999	0.72	9.17	0.963	0.06	12.90	0.824
	1.5	3.98	0.97	0.994	2.02	6.72	0.985	0.21	16.96	0.829
	2.0	4.07	1.65	0.997	2.90	4.79	1.000	0.75	17.97	0.816
	2.5	3.74	1.85	0.994	2.92	4.23	1.000	1.42	14.01	0.905
Amberjet 4600	1.0	4.24	0.47	0.994	0.65	9.96	0.947	0.01	13.43	0.938
	1.5	6.13	0.64	0.998	0.96	14.35	0.980	0.03	19.50	0.762
	2.0	8.61	1.02	0.990	1.45	20.27	0.926	0.05	27.88	0.817
	2.5	10.25	1.28	0.993	2.04	23.01	0.943	0.07	33.77	0.865
Amberlite IRA 458	1.0	3.99	1.57	0.997	0.50	10.83	0.921	0.04	13.29	0.828
	1.5	5.48	4.43	0.973	0.85	16.51	0.837	0.02	21.00	0.853
	2.0	7.63	5.72	0.981	0.99	22.92	0.905	0.01	28.19	0.868
	2.5	8.06	9.52	0.987	1.07	28.21	0.841	0.02	33.87	0.729
Amberlite IRA 958	1.0	4.02	1.88	0.953	0.01	13.78	0.514	-	-	-
	1.5	6.24	2.37	0.964	0.03	20.98	0.675	-	-	-
	2.0	8.09	4.13	0.946	0.07	28.00	0.565	-	-	-
	2.5	9.72	4.73	0.960	0.08	33.96	0.495	-	-	-
Amberlite IRA 67	1.0	4.88	0.28	0.986	0.44	11.77	0.937	0.01	14.14	0.646
	1.5	7.56	0.50	0.986	0.58	18.67	0.825	0.02	21.66	0.890
	2.0	9.36	0.53	0.984	1.36	21.58	0.851	0.04	28.75	0.827
	2.5	10.57	0.58	0.992	2.18	23.03	0.901	0.05	34.62	0.780

Table S7. Kinetic parameters for the Boyd and Dumwald-Wagner kinetic models for the Nd(III)-CA complexes sorption on Purolite S957, Purolite S950, Lewatit SP112, Lewatit M500, Lewatit M600, Lewatit MP500, Amberjet 4200, Amberjet 4400, Amberjet 4600, Amberlite IRA 458, Amberlite IRA 958, Amberlite IRA 67 (C_0=1.0×10^{-3} M - 2.5×10^{-3} M).

Model		**Boyd**		**Dumwald-Wagner**		
	C_o ×10^{-3} [M]	B_t	R^2	k	intercept	R^2
Purolite S957	1.0	5.94	0.679	0.042	0.67	0.690
	1.5	7.63	0.693	0.060	0.76	0.699
	2.0	5.88	0.729	0.043	0.57	0.740
	2.5	7.56	0.819	0.062	0.43	0.824
Purolite S950	1.0	1.88	0.892	0.014	0.13	0.896
	1.5	2.70	0.834	0.022	0.16	0.838
	2.0	3.28	0.939	0.026	0.12	0.945
	2.5	3.67	0.994	0.028	0.08	0.996
Lewatit SP112	1.0	7.46	0.815	0.062	0.47	0.821

	1.5	7.00	0.801	0.056	0.51	0.808
	2.0	6.61	0.874	0.051	0.42	0.883
	2.5	7.29	0.931	0.055	0.37	0.939
Lewatit M500	1.0	4.87	0.874	0.035	0.35	0.887
	1.5	4.91	0.683	0.038	0.53	0.691
	2.0	6.28	0.750	0.049	0.54	0.756
	2.5	6.86	0.787	0.054	0.53	0.794
Lewatit M600	1.0	3.79	0.677	0.027	0.43	0.686
	1.5	5.71	0.737	0.046	0.51	0.744
	2.0	6.18	0.833	0.050	0.44	0.841
	2.5	8.77	0.977	0.068	0.27	0.981
Lewatit MP500	1.0	8.86	0.981	0.066	0.29	0.984
	1.5	4.30	0.826	0.031	0.39	0.838
	2.0	6.39	0.908	0.054	0.21	0.913
	2.5	5.01	0.937	0.040	0.17	0.944
Amberjet 4200	1.0	5.07	0.691	0.040	0.47	0.697
	1.5	7.59	0.930	0.061	0.32	0.937
	2.0	6.23	0.849	0.049	0.39	0.858
	2.5	4.90	0.787	0.037	0.40	0.796
Amberjet 4400	1.0	4.76	0.905	0.036	0.28	0.915
	1.5	3.84	0.964	0.030	0.10	0.970
	2.0	3.60	0.993	0.028	-0.01	0.990
	2.5	2.23	0.987	0.017	-0.01	0.986
Amberjet 4600	1.0	5.54	0.801	0.043	0.41	0.809
	1.5	7.31	0.943	0.057	0.30	0.950
	2.0	5.63	0.877	0.044	0.34	0.887
	2.5	5.28	0.868	0.041	0.32	0.877
Amberlite IRA 458	1.0	3.22	0.598	0.022	0.45	0.606
	1.5	5.24	0.726	0.040	0.53	0.733
	2.0	7.79	0.841	0.060	0.53	0.847
	2.5	7.12	0.837	0.055	0.55	0.844
Amberlite IRA 958	1.0	8.05	0.688	0.062	0.82	0.695
	1.5	5.97	0.716	0.045	0.61	0.725
	2.0	7.40	0.866	0.054	0.52	0.876
	2.5	8.96	0.886	0.073	0.50	0.892
Amberlite IRA 67	1.0	9.54	0.959	0.074	0.37	0.964
	1.5	6.10	0.797	0.045	0.53	0.808
	2.0	5.33	0.788	0.042	0.43	0.797
	2.5	5.76	0.849	0.046	0.34	0.857

Table S8. Kinetic parameters for the pseudo-first order and pseudo-second order kinetic models for the Ho(III)-CA complexes sorption on Purolite S957, Purolite S950, Lewatit SP112, Lewatit M500, Lewatit M600, Lewatit MP500, Amberjet 4200, Amberjet 4400, Amberjet 4600, Amberlite IRA 458, Amberlite IRA 958, Amberlite IRA 67 (C_0=1.0×10^{-3} M - 2.5×10^{-3} M).

Model			**Pseudo-First Order**			**Pseudo-Second Order**		
Adsorbent	C_o ×10^{-3} [M]	$q_{e.exp}$ [mg/g]	$q_{1.cal}$ [mg/g]	k_1 [1/min]	R^2	$q_{2.cal}$ [mg/g]	k_2 [g/mg min]	R^2
Purolite S957	1.0	15.10	15.63	0.367	0.994	15.19	0.067	1.000
	1.5	22.36	21.04	0.343	1.000	22.48	0.048	1.000
	2.0	28.14	26.10	0.270	0.991	28.34	0.028	1.000
	2.5	37.30	28.08	0.182	0.994	37.63	0.017	1.000
Purolite S950	1.0	14.50	12.96	0.018	0.981	16.17	0.002	0.973
	1.5	21.20	18.51	0.015	0.997	23.54	0.002	0.973
	2.0	26.29	23.41	0.020	0.998	29.04	0.001	0.986
	2.5	35.01	28.39	0.021	0.999	37.43	0.002	0.991
Lewatit SP112	1.0	15.59	12.44	0.338	0.998	15.65	0.089	1.000
	1.5	23.36	17.57	0.336	0.998	23.44	0.064	1.000
	2.0	29.17	23.24	0.334	1.000	29.29	0.047	1.000
	2.5	37.29	28.59	0.337	1.000	37.43	0.040	1.000
Lewatit M500	1.0	14.36	15.21	0.407	0.992	14.43	0.088	1.000
	1.5	21.65	21.38	0.386	0.990	21.74	0.062	1.000
	2.0	28.74	26.19	0.378	0.988	28.86	0.049	1.000
	2.5	36.11	37.04	0.388	0.987	36.28	0.035	1.000
Lewatit M600	1.0	14.36	14.47	0.397	0.995	14.43	0.092	1.000
	1.5	21.65	20.81	0.346	0.998	21.76	0.052	1.000
	2.0	28.74	29.71	0.369	0.986	28.89	0.039	1.000
	2.5	36.11	34.03	0.334	0.998	36.31	0.030	1.000
Lewatit MP500	1.0	14.36	11.58	0.369	0.995	14.41	0.106	1.000
	1.5	21.65	18.93	0.249	0.979	21.80	0.035	1.000
	2.0	28.74	22.67	0.138	0.995	29.12	0.015	1.000
	2.5	36.11	28.29	0.105	1.000	36.75	0.008	1.000
Amberjet 4200	1.0	14.63	13.78	0.319	0.998	14.71	0.068	1.000
	1.5	22.15	19.50	0.292	1.000	22.28	0.043	1.000
	2.0	29.18	27.59	0.310	0.996	29.36	0.033	1.000
	2.5	37.02	33.72	0.290	0.997	37.26	0.024	1.000
Amberjet 4400	1.0	14.63	12.86	0.290	0.997	14.72	0.063	1.000
	1.5	22.14	12.92	0.185	0.983	22.29	0.038	1.000
	2.0	29.18	22.52	0.159	0.998	29.50	0.017	1.000
	2.5	37.02	27.27	0.084	0.997	37.72	0.008	1.000
Amberjet 4600	1.0	14.63	12.83	0.248	0.997	14.74	0.051	1.000

	1.5	22.14	19.05	0.250	0.997	22.31	0.035	1.000
	2.0	29.18	25.95	0.250	0.998	29.40	0.025	1.000
	2.5	37.02	32.42	0.240	1.000	37.31	0.019	1.000
Amberlite IRA 458	1.0	14.35	14.53	0.482	0.975	14.40	0.112	1.000
	1.5	21.63	21.30	0.460	0.997	21.71	0.076	1.000
	2.0	28.72	30.93	0.444	0.997	28.84	0.050	1.000
	2.5	36.09	32.60	0.406	0.994	36.24	0.040	1.000
Amberlite IRA 958	1.0	14.36	13.28	0.444	0.992	14.41	0.103	1.000
	1.5	21.64	23.11	0.489	0.971	21.72	0.070	1.000
	2.0	28.74	34.84	0.492	0.991	28.85	0.049	1.000
	2.5	36.11	37.86	0.451	0.956	36.23	0.043	1.000
Amberlite IRA 67	1.0	15.72	15.26	0.315	0.992	15.82	0.058	1.000
	1.5	23.77	22.84	0.288	0.991	23.93	0.033	1.000
	2.0	31.83	29.52	0.272	0.988	32.07	0.023	1.000
	2.5	39.31	34.36	0.246	0.996	39.61	0.018	1.000

Table S9. Kinetic parameters for the Weber-Morris intraparticle diffusion kinetic model for the Ho(III)-CA complexes sorption on Purolite S957, Purolite S950, Lewatit SP112, Lewatit M500, Lewatit M600, Lewatit MP500, Amberjet 4200, Amberjet 4400, Amberjet 4600, Amberlite IRA 458, Amberlite IRA 958, Amberlite IRA 67 (C_0=1.0×10^{-3} M - 2.5×10^{-3} M).

Model	**Weber-Morris Intraparticle Diffusion**									
	C_o ×10^{-3} [M]	k_{i1} [mg/g min$^{1/2}$]	C_1	R^2	k_{i2} [mg/g min$^{1/2}$]	C_2	R^2	k_{i3} [mg/g min$^{1/2}$]	C_3	R^2
Purolite S957	1.0	4.70	0.99	0.934	0.02	14.80	0.572	-	-	-
	1.5	6.65	2.26	0.939	0.04	21.84	0.485	-	-	-
	2.0	7.89	2.46	0.989	0.09	26.97	0.435	-	-	-
	2.5	8.94	5.31	0.985	0.27	34.03	0.415	-	-	-
Purolite S950	1.0	1.26	0.05	0.976	0.07	13.42	1.000	-	-	-
	1.5	1.83	0.09	0.985	0.04	20.53	1.000	-	-	-
	2.0	2.38	0.15	0.993	0.04	25.61	1.000	-	-	-
	2.5	2.90	3.40	0.993	0.03	34.52	1.000	-	-	-
Lewatit SP112	1.0	4.01	3.48	0.939	0.03	15.25	0.461	-	-	-
	1.5	5.79	5.91	0.931	0.04	22.86	0.476	-	-	-
	2.0	7.44	6.58	0.941	0.05	28.54	0.463	-	-	-
	2.5	9.18	9.52	0.937	0.06	36.55	0.450	-	-	-
Lewatit M500	1.0	4.14	2.02	0.949	0.02	14.16	0.551	-	-	-
	1.5	5.79	4.15	0.959	0.02	21.37	0.412	-	-	-
	2.0	7.79	5.49	0.914	0.03	28.35	0.476	-	-	-
	2.5	9.93	6.02	0.965	0.04	35.59	0.456	-	-	-
Lewatit M600	1.0	4.99	0.72	0.974	0.25	13.02	0.675	0.00	14.35	0.979

	1.5	7.32	0.91	0.990	0.55	18.75	0.726	0.00	21.64	0.975
	2.0	9.65	1.35	0.978	0.72	24.97	0.643	0.00	28.73	0.974
	2.5	12.19	1.41	0.986	1.01	30.74	0.722	0.00	36.10	0.992
Lewatit MP500	1.0	4.20	2.79	0.959	0.23	13.08	0.610	0.01	14.24	0.917
	1.5	5.64	2.88	0.994	1.07	15.85	0.744	0.01	21.51	0.918
	2.0	6.36	2.96	0.979	2.80	13.45	0.969	0.01	28.60	0.940
	2.5	7.28	3.13	0.996	4.18	12.16	0.988	0.09	34.86	0.504
Amberjet 4200	1.0	4.88	0.50	0.994	0.43	12.33	0.746	0.00	14.58	0.817
	1.5	7.25	0.95	0.991	0.75	18.12	0.795	0.00	22.09	0.845
	2.0	9.47	1.27	0.996	0.92	24.23	0.750	0.01	29.10	0.719
	2.5	11.96	1.43	0.992	1.37	29.67	0.758	0.01	36.92	0.668
Amberjet 4400	1.0	5.01	0.14	0.991	0.47	12.06	0.838	0.00	14.57	0.616
	1.5	7.41	0.24	0.990	0.85	17.51	0.871	0.00	22.08	0.686
	2.0	8.38	0.51	0.970	2.39	16.04	0.971	0.02	28.97	0.538
	2.5	7.19	3.86	0.990	4.16	11.62	0.998	0.21	34.18	0.515
Amberjet 4600	1.0	4.73	0.11	0.999	0.64	11.16	0.895	0.00	14.57	0.592
	1.5	7.16	0.37	0.998	0.94	17.02	0.895	0.01	22.07	0.557
	2.0	9.26	0.50	0.996	1.33	21.98	0.859	0.01	29.08	0.628
	2.5	11.65	0.60	0.997	1.81	27.17	0.857	0.01	36.82	0.736
Amberlite IRA 458	1.0	5.23	0.79	0.965	0.02	14.11	0.607	-	-	-
	1.5	6.25	3.71	0.880	0.01	21.47	0.497	-	-	-
	2.0	8.38	4.24	0.920	0.02	28.46	0.493	-	-	-
	2.5	10.51	5.64	0.856	0.03	35.67	0.471	-	-	-
Amberlite IRA 958	1.0	5.40	0.44	0.920	0.15	13.47	0.488	0.01	14.21	0.921
	1.5	8.05	0.70	0.949	0.24	20.29	0.461	0.01	21.49	0.966
	2.0	10.49	0.92	0.977	0.25	27.34	0.527	0.01	28.57	0.993
	2.5	11.22	5.55	0.915	0.57	33.03	0.472	0.01	35.90	0.991
Amberlite IRA 67	1.0	5.35	0.12	0.998	0.43	13.36	0.800	0.01	15.64	0.764
	1.5	7.75	0.34	0.989	0.86	18.97	0.696	0.03	23.41	0.827
	2.0	10.28	0.41	0.963	1.15	25.29	0.801	0.04	31.32	0.823
	2.5	12.38	0.91	0.996	1.59	30.22	0.860	0.05	38.56	0.855

Table S10. Kinetic parameters for the Boyd and Dumwald-Wagner kinetic models for the Ho(III)-CA complexes sorption on Purolite S957, Purolite S950, Lewatit SP112, Lewatit M500, Lewatit M600, Lewatit MP500, Amberjet 4200, Amberjet 4400, Amberjet 4600, Amberlite IRA 458, Amberlite IRA 958, Amberlite IRA 67 (C_0=1.0×10^{-3} M - 2.5×10^{-3} M).

Model	**Boyd**			**Dumwald-Wagner**		
	C_o ×10^{-3} [M]	B_t	R^2	k	intercept	R^2
Purolite S957	1.0	5.85	0.682	0.043	0.64	0.691
	1.5	6.21	0.696	0.047	0.64	0.704

	2.0	6.27	0.718	0.051	0.52	0.723
	2.5	6.50	0.769	0.055	0.41	0.773
Purolite S950	1.0	3.33	0.919	0.025	-0.09	0.916
	1.5	4.18	0.874	0.031	-0.13	0.871
	2.0	4.39	0.904	0.033	-0.13	0.899
	2.5	5.00	0.904	0.037	-0.13	0.898
Lewatit SP112	1.0	6.20	0.662	0.046	0.72	0.668
	1.5	6.48	0.706	0.048	0.71	0.714
	2.0	6.60	0.710	0.050	0.69	0.717
	2.5	6.66	0.690	0.051	0.73	0.696
Lewatit M500	1.0	8.09	0.809	0.062	0.66	0.817
	1.5	8.86	0.735	0.070	0.75	0.740
	2.0	8.63	0.799	0.069	0.69	0.805
	2.5	10.16	0.878	0.078	0.60	0.885
Lewatit M600	1.0	8.28	0.702	0.065	0.78	0.707
	1.5	8.69	0.717	0.071	0.71	0.721
	2.0	8.96	0.712	0.073	0.74	0.716
	2.5	8.94	0.703	0.074	0.72	0.706
Lewatit MP500	1.0	5.88	0.695	0.041	0.71	0.704
	1.5	6.18	0.752	0.050	0.48	0.759
	2.0	6.36	0.753	0.056	0.33	0.756
	2.5	6.52	0.878	0.058	0.16	0.881
Amberjet 4200	1.0	7.12	0.761	0.057	0.59	0.768
	1.5	7.45	0.761	0.061	0.58	0.767
	2.0	7.63	0.780	0.062	0.57	0.786
	2.5	7.66	0.784	0.063	0.54	0.790
Amberjet 4400	1.0	7.02	0.763	0.058	0.56	0.768
	1.5	7.37	0.779	0.061	0.52	0.784
	2.0	7.19	0.813	0.064	0.33	0.817
	2.5	6.57	0.954	0.056	0.08	0.957
Amberjet 4600	1.0	7.38	0.794	0.063	0.47	0.799
	1.5	7.92	0.803	0.068	0.48	0.807
	2.0	7.93	0.820	0.067	0.46	0.825
	2.5	7.65	0.851	0.063	0.42	0.857
Amberlite IRA 458	1.0	6.88	0.684	0.045	0.83	0.696
	1.5	7.56	0.685	0.055	0.87	0.693
	2.0	7.55	0.702	0.056	0.80	0.710
	2.5	7.83	0.745	0.059	0.78	0.752
Amberlite IRA 958	1.0	6.06	0.662	0.039	0.79	0.674

	1.5	6.12	0.599	0.040	0.85	0.609
	2.0	6.00	0.584	0.040	0.83	0.592
	2.5	5.83	0.584	0.040	0.81	0.590
Amberlite IRA 67	1.0	7.11	0.802	0.056	0.54	0.810
	1.5	5.96	0.810	0.046	0.46	0.820
	2.0	5.94	0.823	0.046	0.44	0.834
	2.5	5.72	0.833	0.044	0.41	0.844

Table S11. Adsorption isotherm parameters for the sorption of La(III), Nd(III) and Ho(III) complexes with CA on Purolite S957, Purolite S950, Lewatit SP112, Lewatit M500, Lewatit M600, Lewatit MP500, Amberjet 4200, Amberjet 4400, Amberjet 4600, Amberlite IRA 458, Amberlite IRA 958 and Amberlite IRA 67 at the temperature of 293 K.

Model			**Langmuir**			
Adsorbent	**REE**	$q_{e.exp}$ [mg/g]	q_0 [mg/g]	K_L [L/mg]	R^2	χ^2
Purolite S957	La(III)	162.04	163.27	0.264	1.000	0.001
	Nd(III)	142.65	143.25	0.182	1.000	0.001
	Ho(III)	180.26	179.57	0.437	0.999	0.086
Purolite S950	La(III)	139.15	140.00	0.123	0.998	0.015
	Nd(III)	103.71	111.57	0.098	0.987	0.006
	Ho(III)	101.75	103.76	0.091	0.998	0.007
Lewatit SP112	La(III)	40.40	41.47	0.027	0.994	0.006
	Nd(III)	97.47	94.34	0.078	0.968	0.737
	Ho(III)	177.55	180.34	0.154	1.000	0.001
Lewatit M500	La(III)	81.88	83.93	0.031	0.999	0.015
	Nd(III)	92.88	96.85	0.057	0.998	0.010
	Ho(III)	108.33	106.74	0.231	0.988	0.172
Lewatit M600	La(III)	70.72	71.49	0.094	0.999	0.001
	Nd(III)	87.47	90.87	0.053	0.998	0.009
	Ho(III)	104.31	102.30	0.255	0.991	0.150
Lewatit MP500	La(III)	76.96	78.51	0.035	0.999	0.011
	Nd(III)	90.41	94.75	0.048	0.994	0.011
	Ho(III)	105.61	103.78	0.254	0.991	0.146
Amberjet 4200	La(III)	76.94	79.26	0.040	0.999	0.001
	Nd(III)	89.55	92.05	0.094	0.998	0.001
	Ho(III)	108.62	106.82	0.322	0.992	0.134
Amberjet 4400	La(III)	48.70	49.02	0.059	1.000	0.003
	Nd(III)	52.25	53.47	0.057	0.999	0.001
	Ho(III)	74.88	74.21	0.258	0.999	0.021
Amberjet 4600	La(III)	65.86	67.37	0.044	1.000	0.001
	Nd(III)	81.43	83.24	0.071	0.999	0.007

	Ho(III)	99.15	97.68	0.261	0.994	0.086
Amberlite IRA 458	La(III)	98.79	99.17	0.183	0.998	0.004
	Nd(III)	104.24	108.25	0.090	0.997	0.018
	Ho(III)	114.65	113.24	0.335	0.991	0.182
Amberlite IRA 958	La(III)	88.14	95.94	0.016	0.996	0.008
	Nd(III)	97.67	103.36	0.053	0.997	0.009
	Ho(III)	108.56	106.24	0.300	0.991	0.185
Amberlite IRA 67	La(III)	98.79	98.05	0.106	0.981	0.251
	Nd(III)	119.35	122.55	0.456	0.974	0.301
	Ho(III)	123.07	127.43	0.619	0.965	0.702

		Freundlich				**Temkin**			
		K_F [mg/g]	n	R^2	χ^2	A [L/g]	B [J/mol]	R^2	χ^2
Purolite S957	La(III)	30.83	2.59	0.790	70.717	8.70	21.96	0.894	1.538
	Nd(III)	74.09	7.27	0.696	4.537	320.29	13.43	0.798	1.666
	Ho(III)	64.96	5.06	0.869	2.167	14.82	22.17	0.957	0.205
Purolite S950	La(III)	23.21	3.04	0.951	14.934	7.53	16.24	0.974	0.027
	Nd(III)	12.65	2.11	0.773	10.761	1.06	20.97	0.971	0.236
	Ho(III)	21.53	2.79	0.919	9.265	6.12	14.98	0.990	0.076
Lewatit SP112	La(III)	4.55	2.85	0.891	1.968	1.18	5.68	0.978	0.007
	Nd(III)	19.83	3.47	0.963	0.063	10.55	10.56	0.913	2.770
	Ho(III)	59.38	4.74	0.867	5.028	8.15	23.68	0.948	1.016
Lewatit M500	La(III)	10.41	3.02	0.911	2.213	0.58	13.68	0.990	0.093
	Nd(III)	10.58	2.30	0.857	10.844	1.03	16.56	0.967	0.120
	Ho(III)	36.81	4.53	0.960	0.323	310.62	8.77	0.941	1.745
Lewatit M600	La(III)	13.43	3.55	0.864	3.458	4.10	9.14	0.979	0.145
	Nd(III)	10.26	2.40	0.816	9.565	1.01	15.37	0.934	0.174
	Ho(III)	37.47	4.87	0.872	0.598	378.85	8.49	0.969	0.748
Lewatit MP500	La(III)	11.39	3.29	0.853	1.757	0.77	12.29	0.961	0.130
	Nd(III)	10.48	2.40	0.742	7.397	0.89	16.41	0.941	0.160
	Ho(III)	32.92	4.07	0.910	1.867	89.96	10.07	0.980	0.503
Amberjet 4200	La(III)	11.49	3.24	0.819	2.900	0.76	12.76	0.936	0.453
	Nd(III)	14.59	2.73	0.744	10.612	2.11	14.61	0.933	0.552
	Ho(III)	40.08	4.64	0.939	1.216	408.53	8.91	0.969	0.903
Amberjet 4400	La(III)	12.68	4.83	0.775	0.684	3.04	6.31	0.885	0.162
	Nd(III)	10.73	3.73	0.604	1.837	2.51	7.48	0.817	0.278
	Ho(III)	31.15	6.18	0.819	1.266	1088.10	5.69	0.976	0.001
Amberjet 4600	La(III)	11.00	3.48	0.801	2.587	0.83	10.73	0.904	0.552
	Nd(III)	11.88	2.70	0.770	8.799	1.51	13.43	0.927	0.398
	Ho(III)	34.58	4.72	0.858	1.598	200.27	8.73	0.980	0.188

Amberlite IRA 458	La(III)	23.41	3.78	0.899	4.563	19.68	10.83	0.998	0.015
	Nd(III)	14.40	2.30	0.807	12.824	1.65	18.47	0.974	0.148
	Ho(III)	30.53	3.05	0.901	5.108	19.67	14.29	0.993	0.252
Amberlite IRA 958	La(III)	6.43	2.33	0.862	4.983	0.20	18.76	0.971	0.477
	Nd(III)	9.98	2.13	0.826	12.668	0.80	18.90	0.983	0.208
	Ho(III)	39.62	4.69	0.946	0.760	481.92	8.63	0.963	1.261
Amberlite IRA 67	La(III)	24.59	3.82	0.969	0.020	33.32	9.62	0.918	2.111
	Nd(III)	34.58	2.41	0.924	2.169	15.09	17.83	0.952	1.301
	Ho(III)	40.48	2.20	0.915	0.818	14.51	20.54	0.948	1.838

Table S12. Adsorption isotherm parameters for the sorption of La(III)-CA complexes on Purolite S957, Purolite S950, Lewatit SP112, Lewatit M500, Lewatit M600, Lewatit MP500, Amberjet 4200, Amberjet 4400, Amberjet 4600, Amberlite IRA 458, Amberlite IRA 958 and Amberlite IRA 67 at the temperature of 313 K and 333 K.

Model			**Langmuir**			
Adsorbent	T [K]	$q_{e.exp}$ [mg/g]	q_0 [mg/g]	K_L [L/mg]	R^2	χ^2
Purolite S957	313	169.58	170.81	0.377	1.000	0.001
	333	185.37	187.30	0.493	0.999	0.001
Purolite S950	313	165.06	166.54	0.153	0.997	0.013
	333	173.09	174.63	0.325	1.000	0.001
Lewatit SP112	313	38.82	39.61	0.034	0.996	0.003
	333	38.61	39.18	0.044	0.996	0.003
Lewatit M500	313	101.77	105.61	0.035	0.999	0.004
	333	110.12	114.47	0.043	1.000	0.001
Lewatit M600	313	95.86	96.35	0.098	0.997	0.017
	333	102.68	104.12	0.126	0.998	0.001
Lewatit MP500	313	98.21	101.30	0.045	0.999	0.001
	333	114.77	118.47	0.048	0.999	0.008
Amberjet 4200	313	100.16	103.14	0.048	1.000	0.001
	333	104.72	106.88	0.059	0.999	0.005
Amberjet 4400	313	81.64	82.83	0.069	0.999	0.001
	333	97.82	99.62	0.082	0.999	0.001
Amberjet 4600	313	101.02	103.46	0.045	0.999	0.010
	333	110.18	113.43	0.059	1.000	0.001
Amberlite IRA 458	313	109.53	109.96	0.262	0.999	0.003
	333	113.48	114.05	0.434	1.000	0.001
Amberlite IRA 958	313	101.94	112.40	0.017	0.996	0.011
	333	109.63	121.08	0.019	0.997	0.010
Amberlite IRA 67	313	95.13	94.00	0.051	0.960	0.720
	333	88.12	90.10	0.031	0.956	0.463

		Freundlich				Temkin			
	T [K]	K_F [mg/g]	n	R^2	χ^2	A [L/g]	B [J/mol]	R^2	χ^2
Purolite S957	313	36.28	2.58	0.773	83.796	12.02	22.90	0.905	1.956
	333	44.39	2.46	0.768	77.185	15.45	25.55	0.932	0.993
Purolite S950	313	28.90	2.76	0.940	26.023	9.33	19.82	0.980	0.102
	333	36.50	2.65	0.898	59.040	14.21	21.66	0.968	0.240
Lewatit SP112	313	5.30	3.11	0.898	1.894	2.07	5.08	0.979	0.001
	333	6.81	3.56	0.902	1.482	5.61	4.43	0.977	0.007
Lewatit M500	313	10.99	2.63	0.947	5.518	0.59	17.85	0.986	0.174
	333	12.17	2.56	0.946	7.878	0.71	19.37	0.985	0.281
Lewatit M600	313	17.77	3.36	0.922	3.550	6.61	11.58	0.992	0.009
	333	19.09	3.20	0.942	6.356	7.14	12.71	0.983	0.007
Lewatit MP500	313	12.65	2.86	0.885	5.362	0.79	16.72	0.982	0.427
	333	13.51	2.61	0.869	7.187	0.80	20.12	0.981	0.323
Amberjet 4200	313	12.79	2.81	0.909	6.397	0.843	16.90	0.970	0.409
	333	14.66	2.89	0.872	6.693	1.147	17.01	0.951	0.406
Amberjet 4400	313	15.69	3.68	0.945	2.720	2.29	11.36	0.992	0.212
	333	17.12	3.28	0.940	5.804	2.19	14.31	0.977	0.433
Amberjet 4600	313	13.01	2.86	0.943	4.618	0.90	16.44	0.992	0.130
	333	14.45	2.73	0.926	8.774	1.09	18.28	0.967	0.417
Amberlite IRA 458	313	26.70	3.62	0.902	7.185	23.75	12.14	0.997	0.039
	333	30.28	3.63	0.900	11.023	35.50	12.45	0.995	0.192
Amberlite IRA 958	313	6.20	2.09	0.875	9.133	0.20	22.96	0.973	0.717
	333	6.66	2.04	0.888	10.622	0.22	24.55	0.976	0.659
Amberlite IRA 67	313	15.42	3.10	0.883	0.138	3.66	11.90	0.910	2.393
	333	10.75	2.74	0.938	0.001	1.42	12.49	0.914	1.768

Table S13. Adsorption isotherm parameters for the sorption of Nd(III)-CA complexes on Purolite S957, Purolite S950, Lewatit SP112, Lewatit M500, Lewatit M600, Lewatit MP500, Amberjet 4200, Amberjet 4400, Amberjet 4600, Amberlite IRA 458, Amberlite IRA 958 and Amberlite IRA 67 at the temperature of 313 K and 333 K.

Model		Langmuir				
Adsorbent	T [K]	$q_{e.exp}$ [mg/g]	q_0 [mg/g]	K_L [L/mg]	R^2	χ^2
Purolite S957	313	147.84	147.36	0.291	1.000	0.005
	333	159.09	157.81	0.312	1.000	0.024
Purolite S950	313	111.18	112.97	0.253	0.995	0.071
	333	115.88	119.60	0.403	0.997	0.046
Lewatit SP112	313	98.68	95.12	0.093	0.970	0.707
	333	101.14	98.48	0.114	0.975	0.506
Lewatit M500	313	96.68	98.68	0.088	0.997	0.032

	333	104.58	106.99	0.101	0.996	0.058
Lewatit M600	313	94.72	96.41	0.071	0.997	0.071
	333	100.38	103.70	0.085	0.999	0.018
Lewatit MP500	313	95.97	98.37	0.070	0.997	0.050
	333	100.49	103.67	0.095	0.997	0.011
Amberjet 4200	313	97.92	99.24	0.117	0.996	0.029
	333	103.82	106.02	0.142	0.996	0.012
Amberjet 4400	313	73.60	74.72	0.056	0.997	0.026
	333	85.49	87.44	0.104	0.999	0.001
Amberjet 4600	313	93.51	95.50	0.072	0.996	0.043
	333	101.53	103.96	0.089	0.997	0.051
Amberlite IRA 458	313	105.15	107.94	0.116	0.997	0.024
	333	108.41	110.80	0.126	0.996	0.061
Amberlite IRA 958	313	98.18	101.62	0.064	0.997	0.044
	333	101.00	104.46	0.087	0.998	0.015
Amberlite IRA 67	313	118.41	120.56	0.247	0.946	0.871
	333	116.62	126.75	0.123	0.954	0.348

		Freundlich				**Temkin**			
	T [K]	K_F [mg/g]	n	R^2	χ^2	A [L/g]	B [J/mol]	R^2	χ^2
Purolite S957	313	78.86	7.38	0.640	4.552	486.62	13.49	0.740	1.507
	333	82.04	6.68	0.678	4.749	288.44	15.42	0.791	1.174
Purolite S950	313	24.87	2.57	0.916	8.013	6.92	16.80	0.991	0.053
	333	29.94	2.27	0.890	13.465	7.87	19.66	0.980	0.001
Lewatit SP112	313	23.15	3.82	0.966	0.150	24.42	9.63	0.903	3.115
	333	25.59	3.91	0.939	0.075	34.12	9.74	0.906	2.786
Lewatit M500	313	14.40	2.57	0.838	8.809	1.98	15.63	0.992	0.061
	333	15.43	2.40	0.811	10.397	1.99	17.70	0.980	0.044
Lewatit M600	313	12.29	2.45	0.851	8.509	1.43	15.78	0.973	0.019
	333	13.23	2.30	0.850	14.125	1.53	17.55	0.970	0.161
Lewatit MP500	313	12.56	2.44	0.792	8.438	1.34	16.49	0.968	0.075
	333	15.05	2.47	0.781	11.494	1.89	17.15	0.974	0.247
Amberjet 4200	313	18.41	2.91	0.660	6.511	3.34	15.01	0.914	0.202
	333	19.94	2.75	0.662	9.828	3.61	16.52	0.908	0.352
Amberjet 4400	313	11.95	3.09	0.659	3.098	1.69	11.31	0.877	0.121
	333	15.55	2.98	0.700	8.276	2.73	13.26	0.914	0.574
Amberjet 4600	313	12.76	2.52	0.786	8.469	1.47	15.70	0.952	0.100
	333	14.18	2.38	0.776	11.318	1.63	17.67	0.958	0.148
Amberlite IRA 458	313	16.77	2.45	0.798	12.060	2.36	17.67	0.984	0.147
	333	17.42	2.39	0.803	11.342	2.49	18.32	0.986	0.053

Amberlite IRA 958	313	11.41	2.26	0.837	10.690	1.09	17.71	0.981	0.074
	333	13.78	2.33	0.803	13.533	1.58	17.77	0.959	0.225
Amberlite IRA 67	313	26.57	2.35	0.948	0.180	8.50	17.57	0.913	2.990
	333	17.97	2.01	0.946	1.832	2.78	20.66	0.933	1.561

Table S14. Adsorption isotherm parameters for the sorption of Ho(III)-CA complexes on Purolite S957, Purolite S950, Lewatit SP112, Lewatit M500, Lewatit M600, Lewatit MP500, Amberjet 4200, Amberjet 4400, Amberjet 4600, Amberlite IRA 458, Amberlite IRA 958 and Amberlite IRA 67 at the temperature of 313 K and 333 K.

Model				**Langmuir**					
Adsorbent	T [K]	$q_{e.exp}$ [mg/g]	q_0 [mg/g]	K_L [L/mg]	R^2	χ^2			
Purolite S957	313	195.43	193.25	0.814	0.999	0.073			
	333	199.56	196.65	1.083	0.998	0.106			
Purolite S950	313	110.83	113.26	0.374	0.999	0.010			
	333	115.45	118.17	0.600	0.998	0.041			
Lewatit SP112	313	182.04	183.56	0.224	0.999	0.003			
	333	185.60	186.65	0.304	0.999	0.004			
Lewatit M500	313	109.87	108.44	0.309	0.991	0.126			
	333	112.00	110.42	0.313	0.991	0.160			
Lewatit M600	313	107.64	105.21	0.279	0.990	0.198			
	333	110.54	107.95	0.290	0.989	0.240			
Lewatit MP500	313	110.81	109.05	0.325	0.992	0.151			
	333	113.03	111.93	0.347	0.992	0.122			
Amberjet 4200	313	111.78	109.06	0.350	0.990	0.231			
	333	112.98	111.12	0.350	0.990	0.175			
Amberjet 4400	313	99.25	98.46	0.279	0.996	0.047			
	333	108.85	107.81	0.267	0.991	0.112			
Amberjet 4600	313	107.06	106.05	0.270	0.993	0.093			
	333	112.50	109.07	0.328	0.988	0.332			
Amberlite IRA 458	313	115.58	113.84	0.357	0.991	0.218			
	333	116.63	114.49	0.373	0.990	0.278			
Amberlite IRA 958	313	109.02	106.34	0.277	0.988	0.238			
	333	109.93	107.61	0.265	0.989	0.227			
Amberlite IRA 67	313	122.71	129.39	0.334	0.915	1.368			
	333	122.15	150.64	0.123	0.831	1.060			
			Freundlich				**Temkin**		
	T [K]	K_F [mg/g]	n	R^2	χ^2	A [L/g]	B [J/mol]	R^2	χ^2
Purolite S957	313	96.79	5.90	0.828	4.289	187.13	20.03	0.925	0.473
	333	108.98	6.71	0.902	1.799	1111.12	17.02	0.925	0.001
Purolite S950	313	27.57	2.51	0.873	16.130	8.26	17.73	0.970	0.250

	333	34.51	2.36	0.854	13.624	11.27	19.61	0.986	0.118
Lewatit SP112	313	68.99	5.24	0.871	4.119	20.77	21.76	0.955	0.707
	333	78.13	5.72	0.935	3.751	62.77	19.63	0.971	0.393
Lewatit M500	313	38.95	4.46	0.971	0.980	355.09	9.00	0.951	1.372
	333	39.45	4.40	0.974	0.533	353.11	9.13	0.939	1.906
Lewatit M600	313	38.35	4.70	0.877	0.503	332.51	8.91	0.968	0.980
	333	38.47	4.51	0.894	0.310	275.06	9.30	0.957	1.422
Lewatit MP500	313	34.93	3.83	0.914	2.384	80.23	11.00	0.980	0.585
	333	36.76	3.82	0.931	2.094	100.65	11.00	0.969	0.847
Amberjet 4200	313	41.29	4.58	0.942	0.661	420.01	9.12	0.964	1.422
	333	41.77	4.53	0.943	0.551	419.47	9.23	0.950	1.614
Amberjet 4400	313	36.29	4.90	0.876	1.665	328.30	8.36	0.981	0.198
	333	38.28	4.55	0.898	0.635	267.34	9.24	0.954	1.015
Amberjet 4600	313	35.92	4.35	0.875	1.208	146.75	9.76	0.964	0.563
	333	37.47	4.19	0.869	0.412	135.00	10.37	0.958	1.249
Amberlite IRA 458	313	31.47	3.06	0.900	4.426	21.76	14.27	0.992	0.354
	333	32.35	3.08	0.913	3.306	24.91	14.10	0.984	0.636
Amberlite IRA 958	313	39.53	4.75	0.944	0.359	522.49	8.50	0.955	1.617
	333	39.61	4.75	0.944	0.174	539.67	8.49	0.942	1.967
Amberlite IRA 67	313	32.75	2.25	0.928	0.308	11.12	19.08	0.868	4.919
	333	20.42	1.80	0.958	0.219	3.22	22.98	0.835	5.460

Table S15. Comparison of adsorption capacities of the selected adsorbents in the REE(III) ions sorption.

Adsorbent	Optimal pH	Adsorbed element	q_e [mg/g]	Refs.
Purolite S957	8.0	La, Nd, Ho	162.04 (La) 142.65 (Nd) 180.26 (Ho)	This study
Purolite S950	8.0 (La) 4.0 (Nd)	La, Nd, Ho	139.15 (La) 103.71 (Nd) 101.75 (Ho)	
Lewatit SP112	8.0 (La) 4.0 (Nd) 2.0 (Ho)	La, Nd, Ho	40.40 (La) 97.47 (Nd) 177.55 (Ho)	
Lewatit M500	8.0	La, Nd, Ho	81.88 (La) 92.88 (Nd) 108.33 (Ho)	
Lewatit M600	8.0	La, Nd, Ho	70.72 (La) 87.47 (Nd) 104.31 (Ho)	
Lewatit MP500	8.0	La, Nd, Ho	76.96 (La) 90.41 (Nd) 105.61 (Ho)	

Amberjet 4200	8.0	La, Nd, Ho	76.94 (La) 89.55 (Nd) 108.62 (Ho)	
Amberjet 4400	8.0	La, Nd, Ho	48.70 (La) 52.25 (Nd) 74.88 (Ho)	
Amberjet 4600	8.0	La, Nd, Ho	65.86 (La) 81.43 (Nd) 99.15 (Ho)	
Amberlite IRA 458	8.0	La, Nd, Ho	98.79 (La) 104.24 (Nd) 114.65 (Ho)	
Amberlite IRA 958	8.0	La, Nd, Ho	88.14 (La) 97.67 (Nd) 108.56 (Ho)	
Amberlite IRA 67	4.0	La, Nd, Ho	98.79 (La) 119.35 (Nd) 123.07 (Ho)	
ADSORBSIA™ As500	6.0	La, Nd	24.77 (La) 22.23 (Nd)	[S3]
Magnetic nanoparticles $CuFe_2O_4$	7.0-8.0	La, Ce, Nd	42.0 (La) 40.2 (Ce) 51.0 (Nd)	[S4]
Lewatit TP 207	1.5 - 4.6	La	114.7 (La)	[S5]
Lewatit TP 260	5.2	La	106.7 (La)	
Cysteine-functionalized chitosan magnetic nano-based particles	5.0	La, Nd, Yb	17.9 (La) 17.6 (Nd) 19.3 (Yb)	[S6]
Graphitic-C_3N_4 powder	8.0	La, Nd, Eu, Th	122.3 (La) 132.5 (Nd) 155.0 (Eu) 185.6 (Th)	[S7]
CA/CMC/$Ni_{0.2}Zn_{0.2}Fe_{2.6}O_4$ magnetic nanocomposite	5.5	Nd, Tb, Dy	23.15 (Nd) 24.41 (Tb) 25.24 (Dy)	[S8]
CA-P(P-T-A)-$Ni_{0.2}Zn_{0.2}Fe_{2.6}O_4$ magnetic nanocomposite	5.5	Nd, Tb, Dy	72.49 (Nd) 108.82 (Tb) 113.08 (Dy)	[S9]
CMC/P(PTA)/$Ni_{0.2}Zn_{0.2}Fe_{2.6}O_4$ magnetic nanocomposite	5.5	Nd, Tb, Dy	39.82 (Nd) 50.32 (Tb) 48.23 (Dy)	[S10]
Raw bark powder of *M. indica*	2.5	Ho	4.68 (Ho)	[S11]
Acid-treated bark powder of *M. indica*	8.5	Ho	10.40 (Ho)	
Sulfonic-functionalized algal/polyethyleneimine beads	5.0	Sc, Ce, Ho	142.06 (Sc) 99.48 (Ce) 100.61 (Ho)	[S12]
TVEX–PHOR resin	3.5	Ho, Pr	50.4 (Ho) 49.0 (Pr)	[S13]

Table S16. Thermodynamic parameters for the sorption of Nd(III)-CA complexes on Purolite S957, Purolite S950, Lewatit SP112, Lewatit M500, Lewatit M600, Lewatit MP500, Amberjet 4200, Amberjet 4400, Amberjet 4600, Amberlite IRA 458, Amberlite IRA 958 and Amberlite IRA 67.

Adsorbent	**ΔH°**	**ΔS°**	**ΔG° [kJ/mol]**

	[kJ/mol]	[J/mol K]	293 K	313 K	333 K
Purolite S957	11.88	31.01	-14.15	-15.54	-17.72
Purolite S950	28.13	91.76	-15.65	-18.42	-21.63
Lewatit SP112	4.22	7.10	-14.73	-15.90	-17.32
Lewatit M500	11.30	27.76	-13.77	-15.13	-17.21
Lewatit M600	11.20	25.99	-13.25	-14.91	-16.59
Lewatit MP500	9.01	19.45	-13.52	-15.05	-16.60
Amberjet 4200	13.26	33.71	-13.44	-15.28	-17.09
Amberjet 4400	22.34	54.55	-10.40	-12.89	-14.85
Amberjet 4600	16.84	43.49	-12.71	-14.78	-16.75
Amberlite IRA 458	5.15	11.43	-15.09	-16.26	-17.86
Amberlite IRA 958	3.21	2.10	-14.28	-15.31	-16.67
Amberlite IRA 67	-14.39	-36.73	-20.40	-21.00	-21.21

Table S17. Thermodynamic parameters for the sorption of Ho(III)-CA complexes on Purolite S957, Purolite S950, Lewatit SP112, Lewatit M500, Lewatit M600, Lewatit MP500, Amberjet 4200, Amberjet 4400, Amberjet 4600, Amberlite IRA 458, Amberlite IRA 958 and Amberlite IRA 67.

Adsorbent	ΔH° [kJ/mol]	ΔS° [J/mol K]	ΔG° [kJ/mol]		
			293 K	313 K	333 K
Purolite S957	22.78	73.90	-15.56	-18.64	-20.78
Purolite S950	33.17	108.51	-15.50	-18.67	-22.15
Lewatit SP112	5.47	11.95	-14.86	-16.25	-17.63
Lewatit M500	5.57	15.13	-15.72	-17.08	-18.63
Lewatit M600	8.27	22.36	-15.12	-16.68	-18.31
Lewatit MP500	10.99	32.46	-15.30	-17.27	-18.88
Amberjet 4200	6.95	20.28	-15.77	-17.47	-18.87
Amberjet 4400	30.37	88.17	-12.18	-15.46	-17.97
Amberjet 4600	16.99	49.88	-14.46	-16.58	-18.75
Amberlite IRA 458	4.48	15.79	-16.99	-18.41	-19.93
Amberlite IRA 958	1.95	2.98	-15.76	-16.92	-18.18
Amberlite IRA 67	-10.43	-17.31	-22.15	-23.05	-23.74

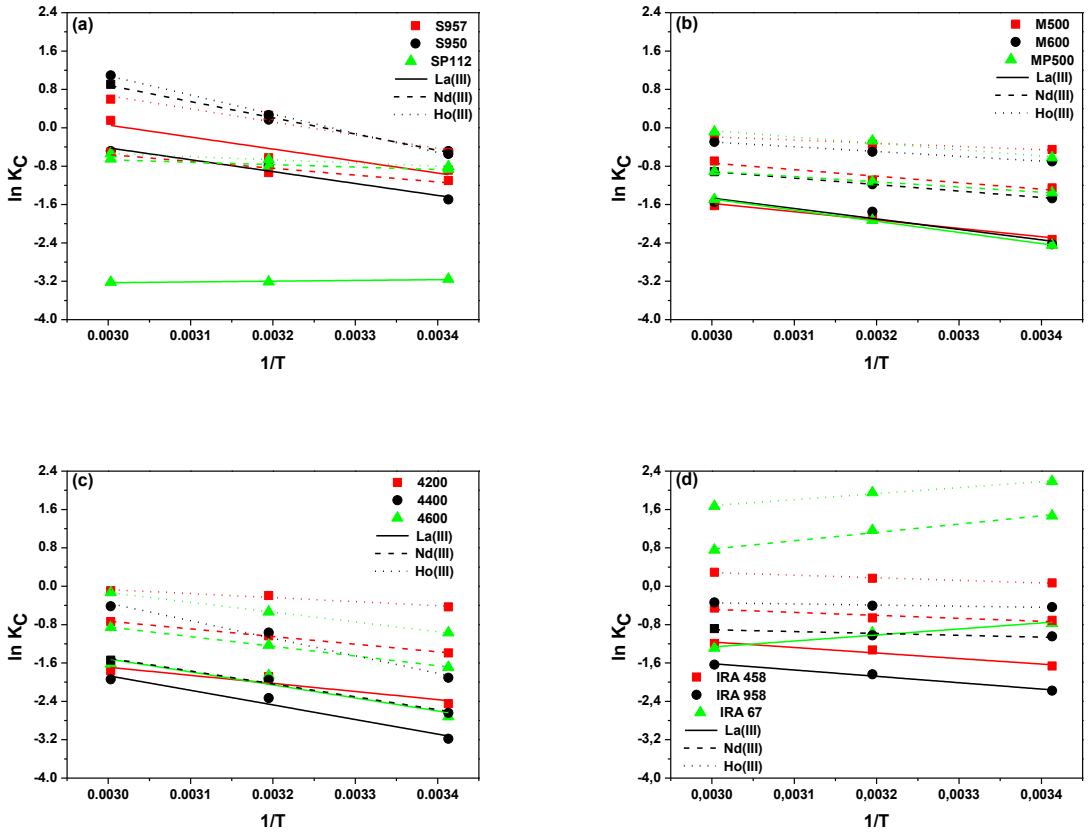

Fig.S7. Plots of $\ln K_C$ as a function of reciprocal of temperature (1/T) for the sorption of La(III), Nd(III) and Ho(III) complexes with CA on (a) Purolite S957, Purolite S950 and Lewatit SP112, (b) Lewatit M500, Lewatit M600 and Lewatit MP500, (c) Amberjet 4200, Amberjet 4400 and Amberjet 4600, (d) Amberlite IRA 458, Amberlite IRA 958 and Amberlite IRA 67.

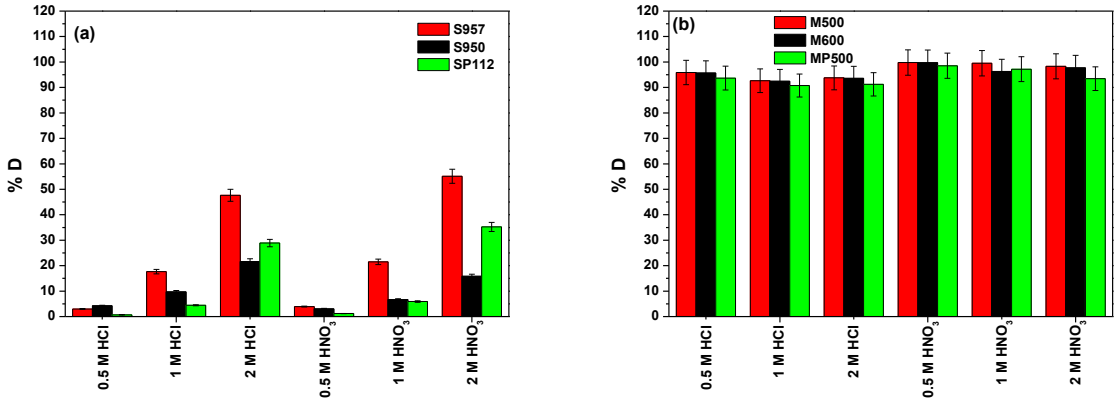

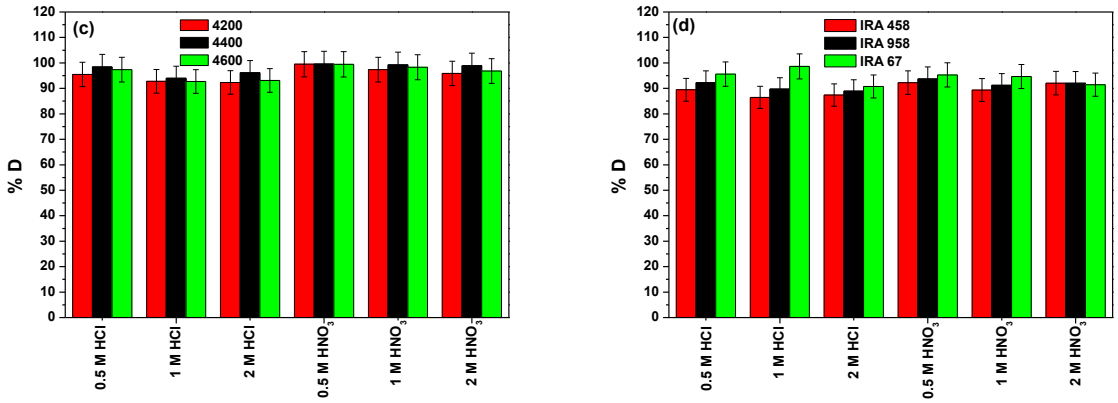

Fig.S8. Dependence of Nd(III) ions desorption capacity on (a) Purolite S957, Purolite S950, Lewatit SP112, (b) Lewatit M500, Lewatit M600, Lewatit MP500, (c) Amberjet 4200, Amberjet 4400, Amberjet 4600 and (d) Amberlite IRA 458, Amberlite IRA 958, Amberlite IRA 67 using the desorption agents: HCl and HNO_3 at various concentrations.

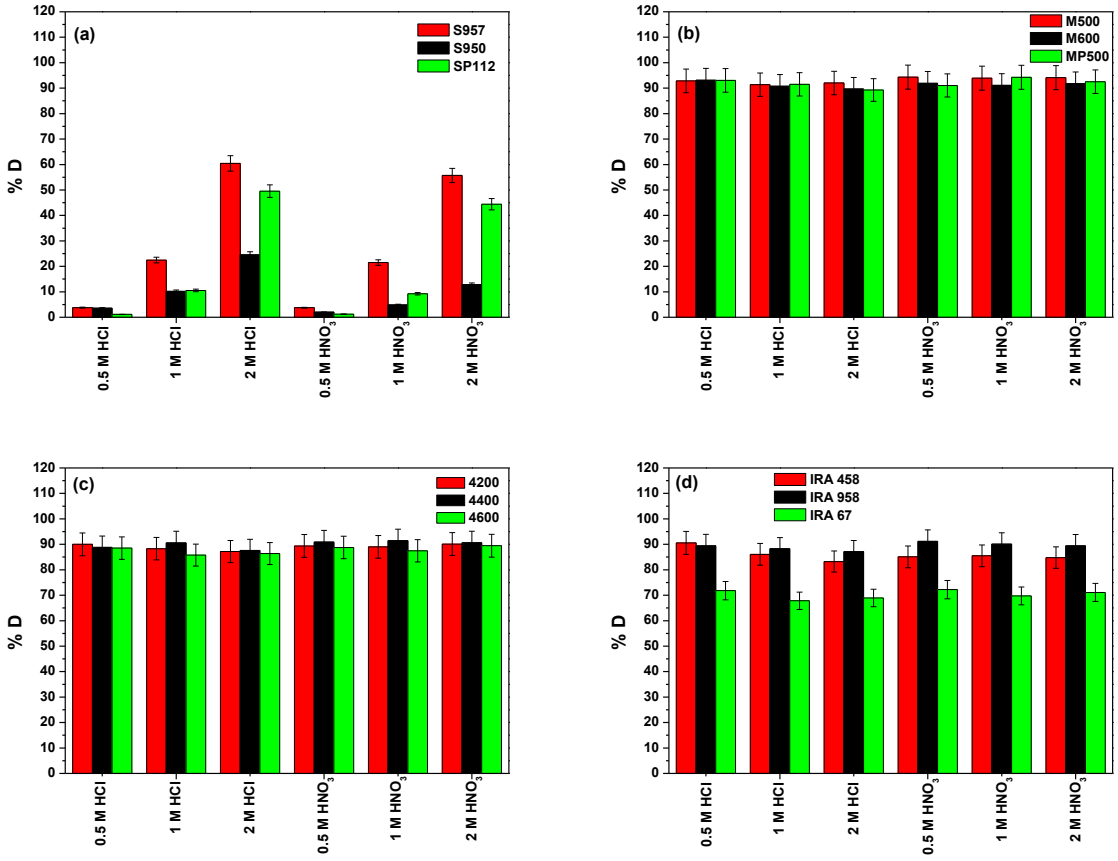

Fig.S9. Dependence of Ho(III) ions desorption capacity on (a) Purolite S957, Purolite S950, Lewatit SP112, (b) Lewatit M500, Lewatit M600, Lewatit MP500, (c) Amberjet 4200, Amberjet 4400, Amberjet 4600 and (d) Amberlite IRA 458, Amberlite IRA 958, Amberlite IRA 67 using the desorption agents: HCl and HNO_3 at various concentrations.

Table S18. Reusability studies of adsorbents on the example of the adsorption/desorption of La(III)-CA complexes.

Number of cycles	Purolite S957		Purolite S950		Lewatit SP112	
	%S	%D	%S	%D	%S	%D
1	97.89	69.23	93.03	44.68	95.86	30.29
2	99.07	68.55	99.87	50.13	99.97	35.27
3	98.63	86.08	99.96	75.19	99.79	54.67
4	99.39	99.89	99.99	97.49	99.98	77.19
5	99.73	97.28	98.43	98.44	99.92	97.83
Number of cycles	**Lewatit M500**		**Lewatit M600**		**Lewatit MP500**	
	%S	%D	%S	%D	%S	%D
1	87.42	80.13	83.61	72.07	89.05	78.01
2	86.04	51.86	86.54	49.96	80.25	46.34
3	90.77	52.62	91.75	53.23	86.45	50.20
4	88.40	54.72	85.40	51.72	83.15	49.94
5	92.15	65.85	88.58	61.67	81.74	56.22
Number of cycles	**Amberjet 4200**		**Amberjet 4400**		**Amberjet 4600**	
	%S	%D	%S	%D	%S	%D
1	88.26	74.58	86.28	84.29	83.61	72.21
2	84.90	50.97	81.10	60.27	82.99	46.86
3	91.56	57.29	87.62	63.06	89.12	56.52
4	86.86	54.05	85.46	61.19	83.91	50.10
5	87.98	61.37	86.91	71.28	85.40	57.08
Number of cycles	**Amberlite IRA 458**		**Amberlite IRA 958**		**Amberlite IRA 67**	
	%S	%D	%S	%D	%S	%D
1	82.81	61.44	82.68	57.38	97.11	99.18
2	56.66	25.46	56.28	29.97	35.93	35.34
3	59.53	34.62	62.81	35.93	32.74	35.67
4	54.58	30.38	55.77	34.50	32.74	40.60
5	55.43	40.96	52.71	42.28	31.76	42.62

Table S19. Breakthrough fitting models results for the adsorption of La(III)-CA acid complexes.

Model	**Thomas**			**Adams–Bohart**		
Adsorbent	$k_{Th} \times 10^3$ [mL/mg min]	q_0 [mg/g]	R^2	$k_{AB} \times 10^6$ [L/mg min]	q [mg/L]	R^2
Purolite S957	5.06	347.71	0.944	6.46	116211.44	0.903
Purolite S950	9.03	240.79	0.980	8.96	74143.50	0.945
Lewatit SP112	8.65	199.55	0.943	5.58	69628.50	0.870
Lewatit M500	20.01	150.33	0.911	30.01	38538.89	0.930

Lewatit M600	15.67	131.74	0.940	20.48	36705.10	0.927
Lewatit MP500	18.85	138.39	0.971	19.30	28564.77	0.941
Amberjet 4200	22.01	140.15	0.961	30.61	39559.19	0.981
Amberjet 4400	29.29	122.79	0.956	39.18	38003.23	0.973
Amberjet 4600	20.21	132.23	0.947	26.21	37990.61	0.985
Amberlite IRA 458	22.26	120.18	0.953	26.87	35365.44	0.969
Amberlite IRA 958	29.08	88.85	0.952	32.04	23236.55	0.948
Amberlite IRA 67	0.77	261.99	0.377	0.32	211657.82	0.097
	Yoon–Nelson			**Wolborska**		
	k_{YN} [1/min]	τ [min]	R^2	β [1/min]	q [mg/L]	R^2
Purolite S957	0.0007	18506.58	0.944	0.751	116211.44	0.903
Purolite S950	0.0012	11345.04	0.980	0.664	74143.50	0.945
Lewatit SP112	0.0012	9367.43	0.943	0.389	69628.50	0.870
Lewatit M500	0.0028	5895.72	0.911	1.157	38538.89	0.930
Lewatit M600	0.0022	5457.17	0.940	0.752	36705.10	0.927
Lewatit MP500	0.0027	4084.60	0.971	0.551	28564.77	0.941
Amberjet 4200	0.0031	6014.75	0.961	1.211	39559.19	0.981
Amberjet 4400	0.0041	5750.40	0.956	1.489	38003.23	0.973
Amberjet 4600	0.0029	5643.16	0.947	0.996	37990.61	0.985
Amberlite IRA 458	0.0031	5328.13	0.953	0.950	35365.44	0.969
Amberlite IRA 958	0.0041	3398.99	0.952	0.745	23236.55	0.948
Amberlite IRA 67	0.0001	11383.35	0.377	0.068	211657.82	0.097

References:

[S1] A. Aurich, A. Förster, S. Mauersberger, G. Barth, U. Stottmeister, Citric acid production from renewable resources by *Yarrowia lipolytica*, Biotechnol. Adv. 21 (2003) 454–455.

[S2] M.Y. Becker, N. Kohlheb, S. Hunger, S. Eschrich, R. Müller, A. Aurich, Early-stage sustainability assessment of biotechnological processes: A case study of citric acid production, Eng. Life Sci. 20 (2020) 90–103. https://doi.org/10.1002/elsc.201800198.

[S3] D. Kołodyńska, K. Araucz, New titanium oxide sorbent for As(V) and Cr(VI) removal as well as La(III) and Nd(III) recovery, J. Mol. Liq. 315 (2020) 113720. https://doi.org/10.1016/j.molliq.2020.113720.

[S4] Y.-J. Tu, C.T. Johnston, Rapid recovery of rare earth elements in industrial wastewater by $CuFe_2O_4$ synthesized from Cu sludge, J. Rare Earths. 36 (2018) 513–520.

https://doi.org/10.1016/j.jre.2017.11.009.

[S5] B. Esma, A. Omar, D.M. Amine, Comparative study on lanthanum(III) sorption onto Lewatit TP 207 and Lewatit TP 260, J. Radioanal. Nucl. Chem. 299 (2014) 439–446. https://doi.org/10.1007/s10967-013-2766-6.

[S6] A.A. Galhoum, M.G. Mafhouz, S.T. Abdel-Rehem, N.A. Gomaa, A.A. Atia, T. Vincent, E. Guibal, Cysteine-functionalized chitosan magnetic nano-based particles for the recovery of light and heavy rare earth metals: uptake kinetics and sorption isotherms, Nanomaterials. 5 (2015) 154–179. https://doi.org/10.3390/nano5010154.

[S7] Q. Liao, D. Zou, W. Pan, W. Linghu, R. Shen, X. Li, A.M. Asiri, K.A. Alamry, G. Sheng, L. Zhan, X. Wu, Highly efficient capture of Eu(III), La(III), Nd(III), Th(IV) from aqueous solutions using g-C_3N_4nanosheets, J. Mol. Liq. 252 (2018) 351–361. https://doi.org/10.1016/j.molliq.2017.12.145.

[S8] H. Javadian, M. Ruiz, A.M. Sastre, Response surface methodology based on central composite design for simultaneous adsorption of rare earth elements using nanoporous calcium alginate/carboxymethyl chitosan microbiocomposite powder containing $Ni_{0.2}Zn_{0.2}Fe_{2.6}O_4$ magnetic nanoparticles: Batch , Int. J. Biol. Macromol. 154 (2020) 937–953. https://doi.org/10.1016/j.ijbiomac.2020.03.131.

[S9] H. Javadian, M. Ruiz, M. Taghvai, A.M. Sastre, Novel magnetic nanocomposite of calcium alginate carrying poly(pyrimidine-thiophene-amide) as a novel green synthesized polyamide for adsorption study of neodymium, terbium, and dysprosium rare-earth ions, Colloids Surfaces A Physicochem. Eng. Asp. 603 (2020) 125252. https://doi.org/10.1016/j.colsurfa.2020.125252.

[S10] H. Javadian, M. Ruiz, M. Taghavi, A.M. Sastre, Synthesis of magnetic CMC bionanocomposite containing a novel biodegradable nanoporous polyamide selectively synthesized in ionic liquid as green media: Investigation on Nd^{+3}, Tb^{+3}, and Dy^{+3} rare earth elements adsorption, J. Mol. Liq. 308 (2020) 113017. https://doi.org/10.1016/j.molliq.2020.113017.

[S11] P.M. Mishra, L. Barick, A.P. Devi, K.K. Swain, Biospecific separation of holmium(III)

using raw and chemically treated bark powder of *Mangifera indica*: kinetics, isotherm and thermodynamic studies, Environ. Technol. 42 (2019). https://doi.org/10.1080/09593330.2019.1645741.

[S12] M.F. Hamza, K.A.M. Salih, A.A.H. Abdel-Rahman, Y.E. Zayed, Y. Wei, J. Liang, E. Guibal, Sulfonic-functionalized algal/PEI beads for scandium, cerium and holmium sorption from aqueous solutions (synthetic and industrial samples), Chem. Eng. J. 403 (2021) 126399. https://doi.org/10.1016/j.cej.2020.126399.

[S13] S.I. El-Dessouky, E.A. El-Sofany, J.A. Daoud, Studies on the sorption of praseodymium(III), holmium(III) and cobalt(II) from nitrate medium using TVEX-PHOR resin, J. Hazard. Mater. 143 (2007) 17–23. https://doi.org/10.1016/j.jhazmat.2006.08.070.

[D3] K. Burdzy, Y. Ju, D. Kołodyńska, *Iminodisuccinic acid (IDHA) as an effective biodegradable complexing agent in the adsorption process of La(III), Nd(III) and Ho(III) ions*, Chemical Engineering Journal, 461 (2023) 142059.

IF_{2022}: 16,744 **Punkty MEiN**: 200

Chemical Engineering Journal 461 (2023) 142059

Contents lists available at ScienceDirect

Chemical Engineering Journal

journal homepage: www.elsevier.com/locate/cej

Iminodisuccinic acid (IDHA) as an effective biodegradable complexing agent in the adsorption process of La(III), Nd(III) and Ho(III) ions

Katarzyna Burdzy [a,*], Yongming Ju [b,c,d], Dorota Kołodyńska [a,*]

[a] Department of Inorganic Chemistry, Faculty of Chemistry, Maria Curie-Skłodowska University, M. Curie Skłodowska Sq. 2, 20-031 Lublin, Poland
[b] South China Institute of Environmental Sciences, Ministry of Environmental Protection, Guangzhou 510655, China
[c] Laboratory of Pesticide Environmental Assessment and Pollution Control, Nanjing Institute of Environmental Sciences, Ministry of Ecology and Environment (MEE), Nanjing 210042, China
[d] The Key Laboratory of Water and Air Pollution Control of Guangdong Province, South China Institute of Environmental Sciences, Ministry of Ecology and Environment (MEE), Guangzhou 510655, China

ARTICLE INFO

Keywords:
Chelating agents
Rare earth elements
IDHA
Ion exchangers
Adsorption

ABSTRACT

Environmental pollution and the continued depletion of many deposits have made the recycling of used materials an urgent need. An important aspect of this topic is the development of alternative compounds with a more favourable environmental profile compared to those currently in use. Indeed, when designing such processes, the negative human impact on the environment should be mitigated as much as possible. This paper presents the results of a study on the application of biodegradable complexing agent iminodisuccinic acid (IDHA) for the recovery of La(III), Nd(III) and Ho(III) by adsorption (single-component systems, static and dynamic methods) using various types of ion exchangers. The results obtained allow to determine the optimal process conditions and show that the chelating ion exchanger Purolite S957 has the highest adsorption capacity related to the La(III) complexes (142.29 mg/g), while the Nd(III) and Ho(III) complexes adsorb with the highest efficiency (161.04 mg/g for Nd(III) and 201.74 mg/g for Ho(III)) in the cation exchanger Lewatit SP112. According to the desorption studies the adsorbents are characterized by a large regeneration capability. This paper also presents the characterization of the physicochemical properties of the applied ion exchangers and the analysis of the binary systems (Ln(III)-IDHA) to determine the overall stability constants of the complexes using the potentiometric methods. Biodegradable IDHA was used to this aim.

1. Introduction

Complexing agents are molecules that can be electron donors for metal atoms or ions, thereby forming coordination bonds. When a complexing agent contains two or more electron donor atoms, it can be called a chelating agent [1]. They have been widely applied for many years. They are used, among others, as components in detergents, fertilizers, or water treatment products, in the food industry, in medicine, as well as in the oil and gas industry. In chemical analysis, the complexing agents are used for the direct and indirect determination of many cations, anions, and organic compounds as well as for masking interfering cations. In hydrometallurgical processes, they are applied at each stage of ore processing, from flotation through leaching, enrichment, and separation (extraction, ion exchange) to obtaining pure metal (electrolysis, electrorefining). They are also used in the paper, textile, and cosmetic industries [2,3]. Due to the ability of complexing agents to form stable chelates soluble in water with many metal ions, they can be used in the metal removal process, in the treatment of toxic metal-contaminated solid waste materials and sewages as well as in the recovery of valuable metals from secondary sources [4–7].

Aminopolycarboxylic acids (APCA) are a group of complexing agents which include commonly known compounds such as ethylenediaminetetraacetic acid (EDTA), nitrilotriacetic acid (NTA), N,N,N', N'',N''-diethylenetriaminepentaacetic acid (DTPA), N-(2-hydroxyethylo)ethylenediamine-N,N',N'-triacetic acid (HEDTA) or iminodiacetic acid (IMDA). The compounds belonging to this group contain one or more nitrogen atoms linked by carbon atoms to two or more carboxyl groups. This group also includes new compounds such as N-(1,2-dicarboxyethyl)-D,L-aspartic acid (IDHA), N,*N*-bis(carboxymethyl)-L-glutamic acid (GLDA), ethylenediamine-N,N′-disuccinic acid (EDDS), and

* Corresponding authors.
E-mail addresses: katarzyna.araucz@poczta.umcs.lublin.pl (K. Burdzy), d.kolodynska@poczta.umcs.lublin.pl (D. Kołodyńska).

https://doi.org/10.1016/j.cej.2023.142059
Received 11 December 2022; Received in revised form 14 February 2023; Accepted 19 February 2023
Available online 22 February 2023

methylglycinediacetic acid (MGDA) which have high biodegradability compared to those mentioned above. This feature is particularly important in view of the studies carried out for the complexing agents, which showed that entering surface waters and remaining there in high concentrations for a long time they can cause remobilization of heavy metals, leading to potential negative effects on humans and the environment [2,8].

As already mentioned, a properly selected complexing agent can find application in the field of metal removal and recovery, especially in processes based on adsorption which, due to its high efficiency, simplicity, low cost of operation of the process and the fact that it does not generate toxic by-products, is a leading method and at the same time environmentally friendly [9,10]. Many examples of studies on the effect of complexing agents on metal adsorption can be found in the literature. Dudzińska and Clifford [11] carried out the research on the removal of Pb(II) complexes with EDTA using anion exchange resins. Juang et al. [12] used EDTA, NTA, and citrate in the removal of Co(II), Ni(II), Mn(II), Sr(II) on the strongly acidic Amberlite IR-120 ion exchange resin. Escudero et al. [13] removed Cu(II) and Ni(II) from the aqueous solutions in the presence of EDTA using grape stalks and exhausted coffee waste as adsorbents, while Kržišnik et al. [14] analysed the removal of Zn(II) complexes with EDTA and citric acid by zerovalent iron nanoparticles. However, there are few literature reports on the use of complexing agents, especially highly biodegradable ones, in the adsorption of such valuable metals as rare earth elements (REEs).

REEs include 17 elements: scandium (Sc), yttrium (Y) and 15 lanthanides (La-Lu). The unique optical, luminescent, fluorescent, and magnetic properties promoted the REEs use in many everyday products. Electronic equipment, hybrid cars, polishing powders, magnets, fiber optics, lasers, and superconductors are just some of the applications of REEs [15–17]. Today the technological process aims at developing products with better performance and durability, smaller size and energy consumption. However, this development may become impossible when the necessary raw materials are in short supply. Therefore, in order to draw attention to the global problem, since 2011 the European Commission has been issuing lists of critical raw materials, i.e. mineral raw materials that are essential for the modern economy and the integrity of modern industrial systems however at the same time they are largely hazardous in terms of supply availability. In the first list 14 raw materials can be found. Unfortunately, the constantly growing demand increased the list to 30 items in 2020 [18]. The critical raw materials include antimony, beryllium, bismuth, cobalt, gallium, germanium, magnesium, scandium, tantalum, phosphorus, vanadium as well as light and heavy rare earth elements. Therefore, recycling of rare earths has become an extremely important issue.

Knowledge about the adsorption processes of REE complexes, their type and stability is important for their use in the REE recovery and separation. Today, many examples are well documented but the area remains active for research and improvement, especially regarding the biodegradable complexing agents of the new generation such as iminodisuccinic acid (IDHA). Therefore, in the presented paper the REEs complexes (La(III), Ce(III), Pr(III), Nd(III), Sm(III), Ho(III)) with the biodegradable complexing agent IDHA were studied by the potentiometric method to determine their stability constants and then the adsorption studies were carried out for La(III), Nd(III) and Ho(III) complexes with IDHA using 12 common commercially available ion exchangers of different types (different matrix, functional groups, and structure). To optimize the process, the effects of such conditions as ion exchanger mass, Ln(III):IDHA molar ratio, solution pH, contact time, initial concentrations, and temperature were investigated. The kinetics of the sorption process were analysed using pseudo-first order, pseudo-second order, intraparticle diffusion, Boyd and Dumwald-Wagner models, while Langmuir, Freundlich, and Temkin models were used to evaluate equilibrium results. In the column studies, the mathematical models of Thomas, Adams-Bohart, Yoon-Nelson and Wolborska were applied to assess the dynamics of the adsorption process. The ion exchangers have been subjected to physicochemical as well as adsorption and desorption processes characterization.

2. Materials and methods

2.1. Materials

In the study there were employed the following ion exchangers: chelating ion exchangers (Purolite S957, Purolite S950), cation exchanger (Lewatit Monoplus SP112), strongly basic anion exchangers (Lewatit MonoPlus M500, Lewatit MonoPlus M600, Lewatit MonoPlus MP500, Amberjet 4200, Amberjet 4400, Amberjet 4600, Amberlite IRA 458, Amberlite IRA 958) and weakly basic anion exchanger (Amberlite IRA 67). Our previous paper includes more details about these ion exchangers [19].

IDHA (tetrasodium salt of N-(1,2-dicarboxyethyl)-D,L-aspartic acid, iminodisuccinic acid), produced by the Lanxess, Bayer AG Leverkusen, Germany as a Baypure CX 100 was used as a complexing agent.

The lanthanide salts ($La(NO_3)_3{\cdot}6H_2O$, $Nd(NO_3)_3{\cdot}6H_2O$, $Ho(NO_3)_3{\cdot}5H_2O$ for the adsorption studies and additionally $Ce(NO_3)_3{\cdot}6H_2O$, $Pr(NO_3)_3{\cdot}6H_2O$, $Sm(NO_3)_3{\cdot}6H_2O$ for the potentiometric studies) employed in this paper were purchased from Sigma-Aldrich and used without additional purification.

2.2. Apparatus and instruments

The Supplementary Materials lists all equipment and apparatus applied in this study.

2.3. Potentiometric measurements

The potentiometric titrations were conducted using a 907 Titrando titrator equipped with the 800 Dosino type dosing systems with the combined pH electrode Metrohm 6.0259.100. The pH-meter was calibrated with two buffer solutions at pH 4.00 and pH 9.00 before each measurement series. The potentiometric titrations were performed at 293 ± 1 K in the neutral gas environment (helium 5.0) and with the constant ionic strength (μ = 0.1 M KNO_3). The potentiometric measurements were made in the pH range from 2.5 to 11.0. The titrant was the CO_2-free NaOH solution at the concentration of 0.1945 M. The experiments were performed with the metal to ligand molar ratios of 1:1, 1:2 and 2:1. The concentration of metal ions in the sample was 1.0×10^{-3} M. The HYPERQUAD2008 program was used to determine the protonation constants for the employed ligand as well as the stability constants for the studied complexes. The calculations were made using 150–350 points for each titration. The metal ions hydrolysis constants and the ionic product for water (pK_w = 13.78) were included in the computer analysis of the potentiometric data.

2.4. Adsorption studies - static method

By dissolving suitable amounts of $La(NO_3)_3{\cdot}6H_2O$, $Nd(NO_3)_3{\cdot}6H_2O$ or $Ho(NO_3)_3{\cdot}5H_2O$ in the deionized water, a stock solution of Ln(III) ions with the concentration of 1×10^{-2} M was obtained. The solutions of Ln(III) complexes with IDHA with varying required initial concentrations and metal to ligand molar ratios were prepared by adding appropriate volumes of metal ion stock solution to the IDHA solutions. The inductively coupled plasma optical emission spectroscopy (ICP-OES) method was used to estimate the final concentration of Ln(III) ions.

The static adsorption studies in the single-component systems were carried out to optimize the adsorption parameters of Ln(III)-IDHA complexes on the selected ion exchangers. In the study there was used the following procedure (unless otherwise stated): 0.1 g of the relevant ion exchanger was placed in 100 cm^3 conical flasks, 10 mL of Ln(III)-IDHA complexes solution was added, and then shaken for 4 h at 293 K at the shaking speed of 180 rpm. After shaking the samples were

separated by filtration using the filter paper. The experiments were performed in triplicate, therefore the obtained results were averaged.

In the first step, the effect of the ion exchanger mass in the range from 0.1 to 0.2 g was examined using the 1.0×10^{-3} M concentration solutions. Next the influence of molar ratios of Ln(III):IDHA (1:1, 1:2, 1:4) on the adsorption efficiency was investigated. The concentration of metal ions in the sample was 1.0×10^{-3} M. The first two steps were conducted without pH adjustment. To evaluate the impact of the initial solution pH for the Ln(III)-IDHA complexes adsorption 0.05 g of the selected ion exchanger and 20 mL solution of 1.0×10^{-3} M concentration in the pH range 2.0–12.0 was applied. The solutions pH values were adjusted using the 1 M HNO_3 or 1 M NaOH solutions. The kinetic studies were carried out for five initial concentrations in the range of 0.5×10^{-3}-2.5×10^{-3} M, with the time intervals ranging from 1 to 240 min. The adsorption isotherm studies were performed for the initial concentrations in the range of 0.5×10^{-3}-1.4×10^{-2} M at the temperatures of 293, 313 and 333 K.

The basic parameters such as adsorption capacities at the equilibrium q_e [mg/g], adsorption capacities at any time q_t [mg/g], and adsorption effectiveness *%S* were calculated using Equations 1–3.

$$q_e = (C_0 - C_e) \times \frac{V}{m} \tag{1}$$

$$q_t = (C_0 - C_t) \times \frac{V}{m} \tag{2}$$

$$\%S = \frac{(C_0 - C_t)}{C_0} \times 100\% \tag{3}$$

where C_0 and C_e are the initial and equilibrium concentrations of Ln(III) in the solution [mg/L], C_t is the concentration of Ln(III) in the solution after the adsorption process conducted at the time t [mg/L], V is the volume of the Ln(III) solution [L], m is the mass of the ion exchanger [g].

2.5. Kinetic and isotherm models

To describe the experimental data obtained from the kinetic studies there were used the following models:

a) the pseudo-first order kinetic equation [20]

$$q_t = q_e(1 - \exp(-k_1 t)) \tag{4}$$

b) the pseudo-second order kinetic equation [21]

$$q_t = \frac{k_2 q_e^2 t}{1 + k_2 q_e t} \tag{5}$$

c) the intraparticle diffusion kinetic model (Weber-Morris model) [22]

$$q_t = k_i t^{0.5} + C \tag{6}$$

d) the Boyd kinetic model [23]

$$F = 1 - \frac{6}{\pi^2} \sum_{n=1}^{\infty} \frac{1}{n^2} \exp(-n^2 B_t) \tag{7}$$

$$F = \frac{q_t}{q_e} \tag{8}$$

$$B_t = (\sqrt{\pi} - \sqrt{\pi - \frac{\pi^2 \mathrm{F}}{3}})^2, \text{ for F values} < 0.85 \tag{9}$$

$$B_t = -0.4977 - \ln(1 - F), \text{ for F values} > 0.85 \tag{10}$$

e) the Dumwald-Wagner model [24]

$$\log(1 - F^2) = -\frac{k}{2.303 t} \tag{11}$$

where q_e, q_t were defined as previously, k_1 is the rate constant of the PFO equation [1/min], k_2 is the rate constant of the PSO equation [g/mg min], k_i is the rate constant of the intraparticle diffusion model [mg/g $\mathrm{min}^{1/2}$], C is the value of intercept related to the boundary layer thickness, F is the fractional attainment of equilibrium at time t, n is the integer that defines the infinite series solution, B_t is the mathematical function of F, k is the rate constant of the Dumwald-Wagner model [1/min].

The adsorption data of Ln(III) complexes were analysed by three different isotherm models:

a) the Langmuir model [25]

$$q_e = \frac{q_0 K_L C_e}{1 + K_L C_e} \tag{12}$$

b) the Freundlich model [26]

$$q_e = K_F C_e^{1/n} \tag{13}$$

c) the Temkin model [27]

$$q_e = B\ln A + B\ln C_e \tag{14}$$

where q_e, C_e were defined as previously, q_0 is the maximum theoretical quantity adsorbed to provide a full monolayer [mg/g], K_L is the Langmuir constant [L/mg], K_F is the Freundlich constant [mg/g], n is the Freundlich intensity parameter which denotes the surface heterogeneity or the magnitude of the adsorption driving force, A is the Temkin constant related to the maximum binding energy [L/g], B is the constant related to the adsorption heat [J/mol] and can be expressed as $B = RT/b_T$ where R is the gas constant (8.314 J/mol K), T is the absolute temperature [K], and b_T is the Temkin isotherm constant.

To determine the best fit of the experimental data to the kinetic and isotherm models, the coefficient of determination (R^2) and the Chi-square (χ^2) were used. The Chi-square (χ^2) is defined as follows:

$$\chi^2 = \sum \frac{(q_{e,\exp} - q_{e,cal})^2}{q_{e,cal}} \tag{15}$$

where $q_{e,\exp}$ is the adsorption capacity determined experimentally and $q_{e,cal}$ is the adsorption capacity according to the given model. The kinetic and equilibrium parameters for the nonlinear forms of the equations were calculated using the OriginPro 8 software.

2.6. Thermodynamic study

The thermodynamics of the adsorption process was described using such parameters as the Gibbs free energy change ΔG° [kJ/mol], the enthalpy change ΔH° [kJ/mol] and the entropy change ΔS° [J/mol K]. As illustrated by Equation (16), the change in free energy (ΔG°) is dependent on the thermodynamic equilibrium constant K_c (dimensionless). Multiplying the distribution coefficient K_d [L/g] by the factor of 1000, the equilibrium constant K_c can be calculated.

$$\Delta G^o = -RT\ln K_c \tag{16}$$

$$K_d = \frac{q_e}{C_e} \tag{17}$$

where R is the universal gas constant (8.314 J/mol K), T is the absolute temperature [K], q_e, C_e were defined as previously. The values of ΔH° and ΔS° can be calculated from the slope and intercept of $\ln K_c$ vs $1/T$ plot (Equation (18)).

$$\ln K_c = \frac{\Delta S^o}{R} - \frac{\Delta H^o}{RT} \tag{18}$$

2.7. Desorption studies

The desorption experiments were conducted to assess the ion exchangers regeneration abilities. In this study, different concentrations

(0.5, 1 and 2 M) of hydrochloric and nitric(V) acids were used as desorbing agents for the recovery process. Complexes-loaded ion exchangers were dried, weighed at 0.1 g, and shaken at 180 rpm at 293 K in 100 mL conical flasks with 10 mL of eluents. The reusability of the ion exchangers was determined by running five sorption/desorption cycles of La(III)-IDHA complexes sequentially for the optimal eluent. The desorption percentage (*%D*) was determined using Equation (19):

$$\%D = \frac{C_{des}}{C_0} \times 100\% \tag{19}$$

where C_{des} is the Ln(III) ions concentration after the desorption process [mg/L].

2.8. Adsorption studies – Dynamic method

The dynamic method studies were performed for the La(III)-IDHA complexes. The tests were conducted under the optimal conditions selected during the static adsorption studies: for the chelating ion exchangers pH 8.0 and the La(III):IDHA molar ratio 1:1, for the cation exchanger SP112 pH 4.0 and the ratio 1:1, for the anion exchangers pH 10.0 and the ratio 1:2, for IRA 67 pH 4.0 and the ratio 1:2. The concentration of La(III) ions was 1.0×10^{-3} M. The pH values were adjusted with 1 M HNO_3 or 1 M NaOH. The studies were carried out at room temperature (293 K). The process was carried out in glass columns of 1.5 cm diameter and 25 cm height packed with 10 mL of swollen ion exchanger. The solution flowed through the bed at the constant rate of 0.6 mL/min. To obtain the breakthrough curve, the effluent was collected in defined volume fractions, and concentration of metal ions was analysed by the ICP-OES method. The column studies were terminated when the column was exhausted (the concentration of La(III) ions in the effluent reached the initial concentration).

The results of the column studies allowed the determination of the basic dynamic parameters: the capacity of the ion exchanger at the exhaustion point q_e [mg/g], the working exchange capacity C_w [mg/mL], the total exchange capacity C_t [mg/mL], the mass distribution coefficient D_g and the volume distribution coefficient D_v (Equations 20–24).

$$q_e = \frac{1}{m_j}\int_0^{V_k} (C_0 - C)dV \tag{20}$$

$$C_w = \frac{U \times C_0}{V_j} \tag{21}$$

$$C_t = \frac{\overline{U} \times C_0}{V_j} \tag{22}$$

$$D_g = \frac{\overline{U} - U_0 - V}{m_j} \tag{23}$$

$$D_v = \frac{\overline{U} - U_0 - V}{V_j} \tag{24}$$

where C_0 is the initial concentration of La(III) ions [mg/mL], C is the concentration of La(III) ions in the effluent [mg/mL], V_k is the volume of solution necessary for the bed exhaustion [mL], m_j is the dry ion exchanger mass [g], U is the effluent volume necessary to reach the break point [mL], V_j is the bed volume [mL], $\bar{U}$ is the effluent volume until $C/C_0 = 0.5$ [mL], U_0 is the dead volume in the column [mL] and V is the empty space volume between the resin beads equal 0.4 mL.

The following mathematical models were applied to the experimental data to evaluate the dynamics of the adsorption process and predict the breakthrough curves:

a) the Thomas model [28]

$$\ln\left(\frac{C_0}{C} - 1\right) = \frac{k_{Th}q_0 m}{Q} - \frac{k_{Th}C_0}{Q}V \tag{25}$$

b) the Adams-Bohart model [29]

$$\ln\left(\frac{C}{C_0}\right) = k_{AB}C_0 t - k_{AB}q\frac{H}{v} \tag{26}$$

c) the Yoon-Nelson model [30]

$$\ln\left(\frac{C}{C_0 - C}\right) = k_{YN}t - k_{YN}\tau \tag{27}$$

d) the Wolborska model [31]

$$\ln\left(\frac{C}{C_0}\right) = \frac{\beta C_0}{q}t - \frac{\beta H}{v} \tag{28}$$

$$\beta = \frac{v^2}{2D}\left(\sqrt{1 + \frac{4\beta_0 D}{v^2}} - 1\right) \tag{29}$$

where C_0 is the initial concentration of La(III) ions [mg/L], C is the concentration of La(III) ions in the effluent [mg/L], k_{Th} is the Thomas rate constant [mL/mg min], q_0 is the adsorption capacity [mg/g], m is the mass of the ion exchanger in the column [g], Q is the flow rate [mL/min], V is the effluent volume [L], k_{AB} is the Adams-Bohart rate constant [L/mg min], t is the time [min], q is the adsorption capacity of the ion exchanger per unit volume of the bed [mg/L], H is the bed depth of the fixed bed column [cm], v is the linear velocity [cm/min], k_{YN} is the Yoon-Nelson rate constant [1/min], τ is the time required for 50% adsorbate breakthrough [min], β is the kinetic coefficient of the external mass transfer [1/min] and D is the axial diffusion coefficient [cm^2/min], β_0 is the external mass transfer coefficient with the negligible axial dispersion coefficient D.

3. Results and discussion

3.1. Materials characterization

3.1.1. Iminodisuccinic acid

Iminodisuccinic acid (IDHA, N-(1,2-dicarboxyethyl)-D,L-aspartic acid, also known as Baypure CX 100) is a chelating agent from the

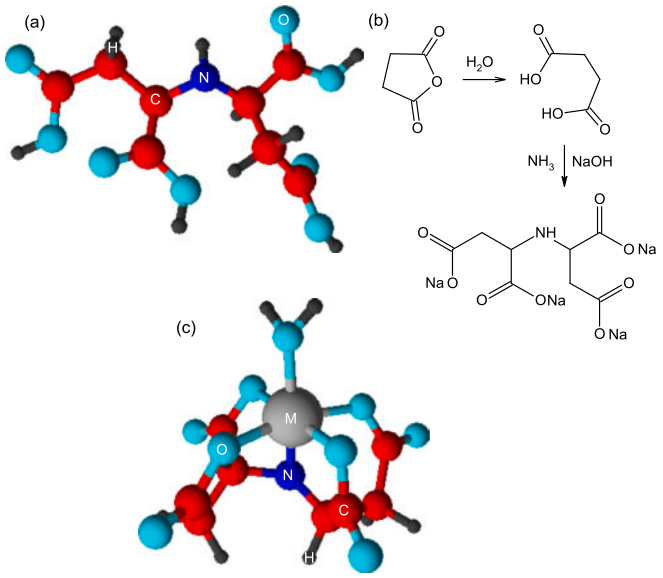

Fig. 1. (a) The structure of iminodisuccinic acid, (b) the synthesis of tetrasodium salt of iminodisuccinic acid, and (c) the structure of the iminodisuccinate complex with metal ion.

aminopolycarboxylic acid group. The IDHA is composed of four carboxyl groups and a nitrogen atom (Fig. 1a) and occurs in the form of stereoisomers [R,R], [R,S]/[S,R] and [S,S] [32].

IDHA is also characterized by great biodegradability using standardized tests [33]. Cokesa et al. [34] tested the biodegradability of all IDHA stereoisomers using the *Agrobacterium tumefaciens* BY6 strain. Easy biodegradation of all IDHA isomers was demonstrated with levels reaching approximately that of the reference compound, sodium benzoate (90%) with biodegradation of the [R,R] isomer beginning to a significant extent only after three days.

Due to the presence of four carboxyl groups and a nitrogen atom in the molecule, IDHA is called the pentadentate N, O donor ligand. With many metal ions, it can form the octahedral structure if the sixth coordination position is occupied by a water molecule (Fig. 1c). Sillanpää et al. [35] studied the complexation of metal ions by IDHA. The small size of the ligand causes the metal ion in the complex to be significantly exposed to the solvent.

The ability to form complexes with many metal ions with the simultaneous large biodegradability induced IDHA to be used as an alternative to poorly biodegradable complexing agents. Lucena et al. [36] compared the efficacy of IDHA and EDTA in providing various metals (Fe, Mn, Zn, Cu) to plants grown in greenhouses. Their results showed that IDHA can replace EDTA in hydroponics and fertigation cultures. IDHA was also proposed as a complexing agent for seed coating to increase nutrient salt adhesion [37].

Hasegawa et al. [38] used IDHA, in the recovery of indium from worn out liquid–crystal display panels. Wang et al. [39] showed that IDHA could replace the poorly biodegradable EDTA in the removal of Cd, Pb, and Zn.

Due to the presence of functional groups capable of dissociation IDHA occurs in different forms depending on the pH value of the solution. Potentiometric measurements at the ionic strength of 0.1 M at 293 ± 1 K were performed to determine the overall and successive protonation constants. The obtained data were analysed using the HYPERQUAD2008 program (Table 1). The IDHA protonation constants determined in paper are similar to the data presented by other researchers [32,40].

In the alkaline environment in the first protonation step (L^{4-} to HL^{3-}), the first proton attaches to the amine nitrogen atom ($\log K = 10.12$). HL^{3-} is the dominant form in the pH range from 5.5 to 9.2 (>90%). As the acidity of the solution increases, further protonation of the IDHA molecule occurs (HL^{3-} to H_4L) - protons attach to the oxygen atoms of the carboxyl groups which corresponds to the subsequent values of log*K* (4.56, 3.65, 3.30). In the case of the IDHA molecule, the attachment of the last proton to the oxygen atom occurs at pH equal to 2. The pH studied ranges from 2.5 to 11.0. The predicted protonation equilibria scheme for IDHA is presented in Fig. 2.

The percentage distributions of individual forms of IDHA are shown in Fig. 3a. In this paper the potentiometric measurements of the binary systems (IDHA with La(III), Ce(III), Pr(III), Nd(III), Sm(III) or Ho(III), respectively) were also made for better understanding of the complexation of rare earth elements by the complexing agent under study. The results of the potentiometric titrations at the various molar metal:ligand ratios in the systems Ln(III)-L = 1:1, 1:2, and 2:1 are shown in Fig. 3 a-d and S1 as well as Tables 2 and S1.

The LnL type complexes as well as the protonated complexes (LnH_xL) and hydroxycomplexes ($LnL(OH)_x$) were found in all systems. Furthermore, depending on the tested molar metal:ligand ratio, more complex forms ($LnHL_2$, LnL_2, Ln_2L, $Ln_2L(OH)_2$) also appeared. In order to determine the equilibrium constants of IDHA complexes with Ln(III) ions there were proposed the following reactions of their formation:

$$Ln^{3+} + H_2L^{2-} \rightleftarrows LnH_2L^{+} \quad (30)$$

$$Ln^{3+} + HL^{3-} \rightleftarrows LnHL \quad (31)$$

$$Ln^{3+} + L^{4-} \rightleftarrows LnL^{-} \quad (32)$$

$$LnL^{-} + H_2O \rightleftarrows LnL(OH)^{2-} + H^{+} \quad (33)$$

$$LnL(OH)^{2-} + H_2O \rightleftarrows LnL(OH)_2^{3-} + H^{+} \quad (34)$$

$$LnL^{-} + HL^{3-} \rightleftarrows LnHL_2^{4-} \quad (35)$$

$$Ln^{3+} + 2L^{4-} \rightleftarrows LnL_2^{5-} \quad (36)$$

$$2Ln^{3+} + L^{4-} \rightleftarrows Ln_2L^{2+} \quad (37)$$

$$Ln^{3+} + LnL(OH)^{2-} + H_2O \rightleftarrows Ln_2L(OH)_2 + H^{+} \quad (38)$$

In Ln(III)-IDHA systems, the complexation begins with the formation of the protonated species LnH_xL at pH around 3. For both systems with the equal amounts of metal and ligand and the double excess of IDHA, all Ln(III) ions introduced into the system were coordinated. In the systems with the molar metal:ligand ratio of 2:1, excess of Ln(III) remained uncomplexed due to the insufficient ligand amount. The calculated overall stability constants and the equilibrium constants of formation for the Ln(III)-IDHA complexes are summarized in Tables 2 and S1.

3.1.2. Ion exchangers

Scanning electron microscopy (SEM) was applied to investigate the internal structure and the surface physical morphology of the ion exchangers. Figures S2 a-l exhibit the SEM images recorded after the La(III)-IDHA complexes adsorption at the magnification of ×10,000. The ion exchangers selected for this study are beads with a rather homogeneous size and surface. However, these adsorbents differ in structure as confirmed by the SEM images. It can be seen (especially at the mechanical fracture sites) that the pores are randomly oriented and the pore shapes are spherical, semi-ellipsoidal or highly irregular. The gel ion exchangers (M500, M600, 4200, 4400, 4600, IRA 458, IRA 67) are characterized by a densely packed surface, while the surface of the macroporous ion exchangers (S957, S950, SP112, MP500, IRA 958) shows typical pores and cavities that are suitable sites for the adsorption of complexes (Figures S2 a, b, c, f, and j). The SEM images of the studied ion exchangers in pure form (before the adsorption process) were presented in our previous paper [19].

X-ray photoelectron spectroscopy (XPS) is one of the methods applied to obtain information about the physicochemical properties of a sample. In our study the XPS analysis was employed to confirm the presence of the assumed functional groups on the ion exchangers surface as well as to evaluate the Ln(III)-IDHA adsorption mechanism. XPS spectra of the ion exchangers were recorded before and after the adsorption of La(III)-IDHA complexes and are presented in Figures S3 a-l. The obtained elemental composition and binding energies are summarized in Tables 3 and S2.

XPS analysis of the ion exchangers revealed the presence of two main bands, C 1s and O 1s, derived from carbon and oxygen, which are the primary components of the ion exchanger matrix (Fig. S3 a-l). Bands with lower intensities and lower content in the test material were associated with the presence of phosphorus in phosphonic groups (P 2s, P 2p) (Fig. S3 a-b), sulfur in sulfonic groups (S 1s) (Fig. S3 c), and

Table 1
The protonation constants for IDHA.

Overall protonation constants (logβ)	SD	Protonation equilibria	Successive protonation constants (log*K*)
10.12	0.01	$IDHA^{4-} + H^{+} \rightleftarrows HIDHA^{3-}$	10.12
14.67	0.01	$HIDHA^{3-} + H^{+} \rightleftarrows H_2IDHA^{2-}$	4.56
18.32	0.01	$H_2IDHA^{2-} + H^{+} \rightleftarrows H_3IDHA^{-}$	3.65
21.63	0.01	$H_3IDHA^{-} + H^{+} \rightleftarrows H_4IDHA$	3.30

SD - standard deviation.

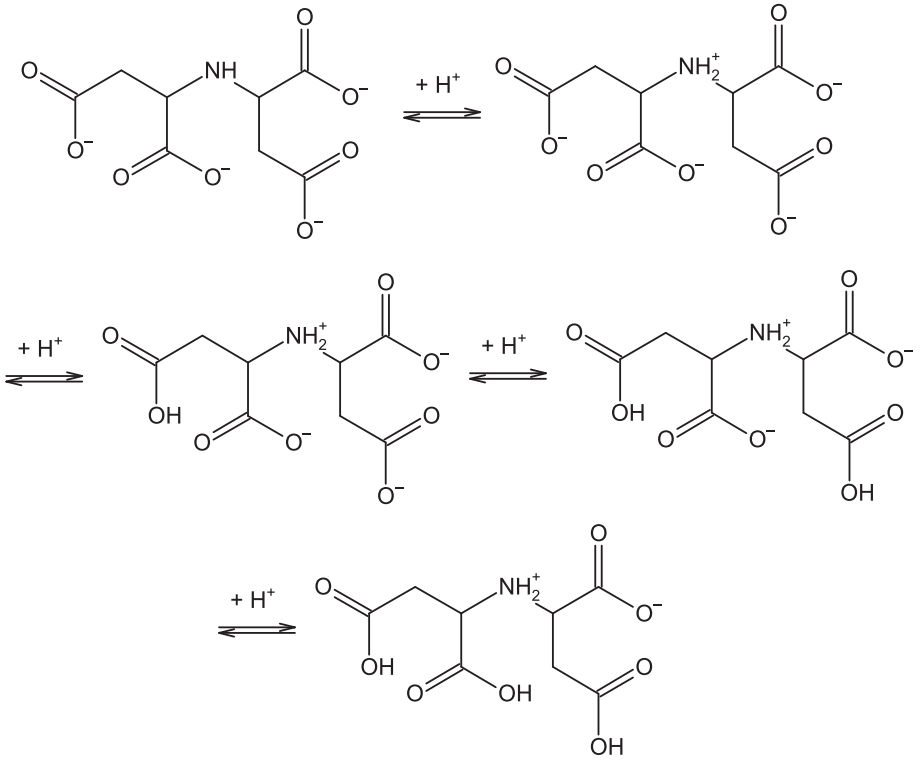

Fig. 2. Protonation equilibria of IDHA.

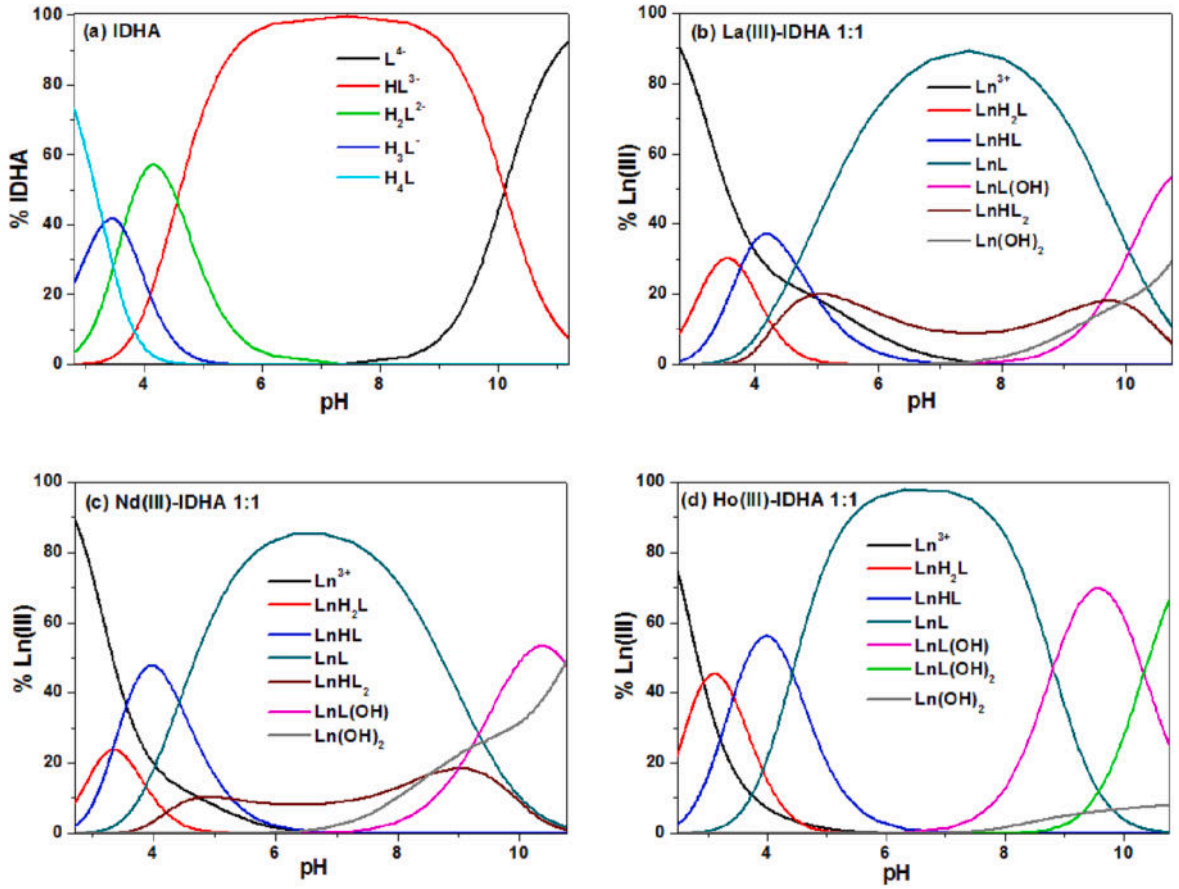

Fig. 3. (a) Percentage of IDHA individual forms depending on the pH values and (b-d) the distribution diagrams for the Ln(III)-L systems (where Ln = La(III), Nd(III), Ho(III) and L = IDHA) at the Ln(III):L ratio 1:1.

Table 2
The overall stability constants (logβ) and the equilibrium constants of complex formation (logK_e) in the systems of Ln(III)-L (where Ln = La(III), Nd(III), Ho(III) and L = IDHA) for various metal:ligand ratios.

Species	1:1			1:2			2:1		
	logβ	SD	logK_e	logβ	SD	logK_e	logβ	SD	logK_e
La(III)-IDHA									
LnH_2L	18.19	0.02	**3.51**	18.13	0.02	**3.46**	18.08	0.04	**3.41**
LnHL	14.41	0.01	**4.30**	14.42	0.01	**4.30**	14.52	0.02	**4.40**
LnL	9.75	0.01	**9.75**	9.83	0.02	**9.83**	10.30	0.02	**10.30**
LnL(OH)	0.31	0.02	**4.33**	0.89	0.03	**4.82**	2.80	0.04	**6.27**
$LnHL_2$	23.85	0.03	**3.98**	–	–	**–**	–	–	**–**
LnL_2	–	–	**–**	14.28	0.04	**4.45**	–	–	**–**
$Ln_2L(OH)_2$	–	–	**–**	–	–	**–**	1.31	0.03	**12.28**
Nd(III)-IDHA									
LnH_2L	18.33	0.02	**3.66**	18.12	0.03	**3.45**	18.19	0.07	**3.52**
LnHL	15.00	0.01	**4.88**	14.65	0.01	**4.53**	14.66	0.08	**4.54**
LnL	10.58	0.01	**10.58**	9.71	0.02	**9.71**	10.30	0.08	**10.30**
LnL(OH)	1.25	0.02	**4.44**	–	–	**–**	–	–	**–**
$LnHL_2$	24.47	0.03	**9.47**	–	–	**–**	–	–	**–**
LnL_2	–	–	**–**	14.91	0.04	**5.20**	–	–	**–**
Ln_2L	–	–	**–**	–	–	**–**	14.38	0.06	**4.08**
$Ln_2L(OH)_2$	–	–	**–**	–	–	**–**	2.18	0.04	**5.65**
Ho(III)-IDHA									
LnH_2L	19.31	0.01	**4.63**	19.37	0.02	**4.70**	19.57	0.02	**4.89**
LnHL	15.88	0.01	**5.76**	15.89	0.02	**5.78**	15.84	0.05	**5.72**
LnL	11.46	0.01	**11.46**	11.28	0.02	**11.28**	11.62	0.08	**11.62**
LnL(OH)	2.64	0.02	**4.95**	3.63	0.04	**6.13**	3.86	0.09	**6.01**
$LnL(OH)_2$	−7.71	0.02	**3.42**	−6.23	0.04	**3.91**	−5.04	0.04	**4.87**
Ln_2L	–	–	**–**	–	–	**–**	15.61	0.06	**3.99**
$Ln_2L(OH)_2$	–	–	**–**	–	–	**–**	3.85	0.04	**13.76**

SD - standard deviation.

Table 3
The elemental composition (C_{at}) and binding energies (E_B) for S957, S950, and SP112 before and after the adsorption of La(III) ions in the presence of IDHA obtained by XPS analysis.

Level	S957		S957 + La(III) -IDHA		S950		S950 + La(III) -IDHA		SP112		SP112 + La(III)-IDHA	
	E_B [eV]	C_{at} [%]	E_B [eV]	C_{at} [%]	E_B [eV]	C_{at} [%]	E_B [eV]	C_{at} [%]	E_B [eV]	C_{at} [%]	E_B [eV]	C_{at} [%]
C 1s	285.0	61.7	284.7	64.6	285.0	51.5	284.7	61.4	285.0	66.9	284.7	65.0
O 1s	533.0	23.0	531.5	24.2	530.5	25.1	530.7	23.4	532.0	20.5	532.2	21.7
N 1s	402.0	0.7	401.0	1.3	399.5	4.7	399.5	3.1	–	–	400.2	1.8
P 2p	134.5	7.9	133.2	5.9	133.5	9.9	132.5	8.0	–	–	–	–
S 2p	168.5	3.9	168.5	3.4	–	–	–	–	169.0	8.6	169.2	8.8
Al 2p	76.5	2.8	–	–	75.0	0.4	–	–	–	–	–	–
Na 1s	–	–	1070.7	0.5	1071.5	8.3	1070.7	3.1	1072.5	4.0	1071.5	2.1
La 3d	–	–	835.2	0.2	–	–	834.5	0.9	–	–	836.0	0.6

nitrogen in the amine and ammonium groups (N 1s) (Fig. S3 d-l). The Na 1s bands in the S957, S950 and SP112 (Fig. S3S a-c) confirm the sodium form of these ion exchangers, while the Cl 1s bands on the spectra of strongly basic anion exchangers confirm the chloride form (Fig. S3 d-k). The remaining bands (Si 2p, Al 2p, and Ca 2p) were not identified as corresponding to the components of the ion exchangers, so it can be assumed that they were introduced during production or processing. After the adsorption of La(III)-IDHA complexes, bands in the range of 833.0–836.7 eV appeared in the XPS spectra and they were assigned to the La 3d level. The La content on the surface of the adsorbents ranged from 0.1 to 0.9%. For the strongly basic anion exchangers, the bands originating from Cl (Cl^- form of the ion exchangers) were registered in the spectra before the adsorption process and disappeared after the process. This suggest the ion exchange mechanism (Cl^- anions are exchanged for complex anions). A similar situation occurs for the ion exchangers S950 and SP112 where the Na content (Na^+ form of the ion exchangers) also decreases but does not completely disappear.

The identification of functional groups in the ion exchangers structure was performed using the Fourier transform infrared spectroscopy (FTIR). The spectra recorded both before and after the adsorption process of La(III), Nd(III) and Ho(III) complexes with IDHA are shown in Figs. 4 and S4.

Ion exchangers with cross-linked polystyrene (S957, S950, SP112, M500, M600, MP500, 4200, 4400, 4600) and polyacrylic acid (IRA 458, IRA 958, IRA 67) matrixes were selected to study the adsorption process. The bands characteristic of the matrix-forming groups are present in the FTIR spectra. Typical bands corresponding to the stretching vibrations in the benzene ring as well as asymmetric and symmetric C—H stretching vibrations in the $–CH_2$ groups can be seen at about 3020 cm^{-1}, 2920 cm^{-1}, and 2850 cm^{-1} [41]. The presence of the aromatic ring in the matrix structure is indicated by the appearance of bands in the ranges of 1480–1470, 1420–1410, and 1380–1370 cm^{-1}, which can be attributed to the stretching vibrations between the carbon atoms in the ring and the asymmetric scissor vibrations of the methylene groups ($\delta_{as}(–CH_2)$) [42]. The spectra of the polyacrylate ion exchangers also clearly show a band at 1640 cm^{-1}, which corresponds to the stretching vibrations of the –C═O groups [43].

The intense band occurring on each spectrum at 3300–3500 cm^{-1} for the S957 and SP112 ion exchangers do not originate directly from the resin matrix but are related to the presence of moisture (O—H stretching vibrations). However in the case of S950 and anion exchangers with the quaternary ammonium and tertiary amine functional groups, this band

is also related to the N—H vibrations. The presence of water in the adsorbent phase is also confirmed by the bands at approximately 1635 cm^{-1} (δ(O—H) [44].

The ion exchangers investigated in this study have various functional groups on the surface, including phosphonic, sulphonic, amino-phosphonic, quaternary ammonium (types I and II) and tertiary amine ones. The bands characteristic of these groups were identified in the FTIR spectra. In Fig. 4 (S957) the bands at 2283 and 2112 cm^{-1} as well as at 1123 and 988 cm^{-1} are characteristic of phosphonic and sulfonic groups (stretching vibrations of P–OH and S–OH as well as P═O, P—O, S═O, and S—O groups). The analogous bands of phosphonic groups are present in the S950 spectrum (stretching vibrations of P–OH groups at 2312 cm^{-1} and of P═O and P—O groups at 1081 and 973 cm^{-1}). The recorded spectrum of the SP112 cation exchanger has bands at 1176, 1124, 1037, and 1008 cm^{-1}, which originate from the stretching vibrations of the S═O and S—O groups in the sulfonic groups. The FTIR spectra of the anion exchangers with the quaternary ammonium groups show a band at 975 cm^{-1} originating from quaternary nitrogen [45].

From the comparison of the spectra obtained before and after the adsorption process, there can be determined formation of new bonds, which facilitates the understanding of the mechanism of this process. The comparison of the recorded FTIR spectra, proved that after the adsorption process of La(III), Nd(III) and Ho(III) ions in the presence of IDHA, some bands shifted and their intensities changed. The bands originating from the phosphonic and sulfonic groups shifted toward higher wavelengths, suggesting the involvement of these groups in the adsorption process. In this case, the most probable mechanism of the process is the decomposition of complexes in the ion exchanger phase and the formation of bonds between metal ions and dissociated phosphonic or sulfonic groups. After adsorption of Ln(III)-IDHA complexes the additional bands at 1573 and 1368 cm^{-1}, representing asymmetric and symmetric stretching vibrations of carboxyl groups, respectively appeared on the spectra of the anion exchangers [46]. This confirms the presence of the complexes in the ion exchanger phase.

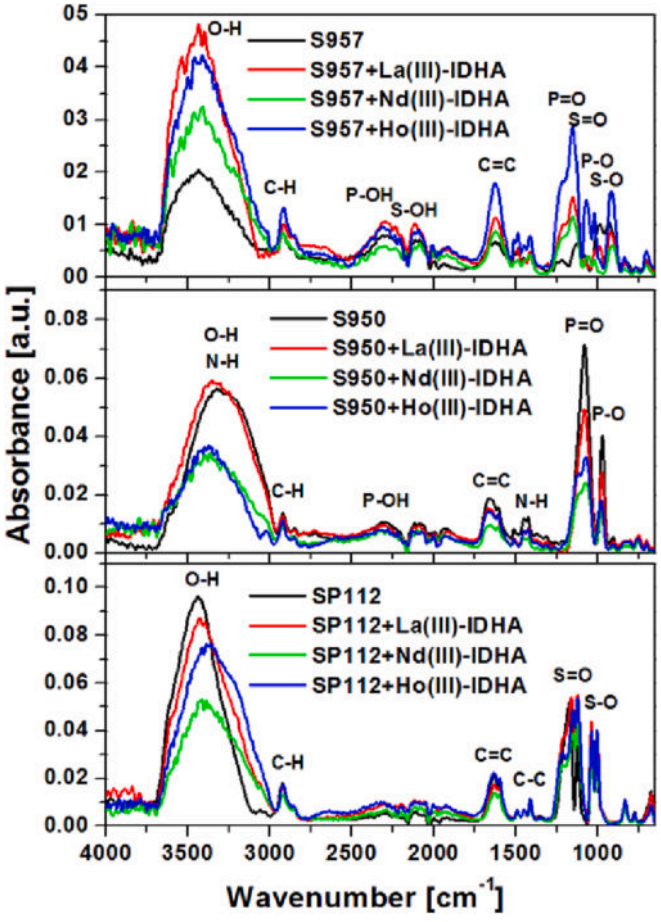

Fig. 4. FTIR spectra for S957, S950, and SP112 before and after the adsorption of La(III), Nd(III) and Ho(III) ions in the presence of IDHA.

The porous structure (specific surface area and the average pore diameter) as well as the point of zero charge of the studied ion exchangers were analysed in our previous paper [19]. The specific surface area of the ion exchangers was found to be in the range of 0.45–14.98 m^2/g, and the average pore size ranged of 2.84–34.10 nm, indicating the presence of mesopores.

3.2. Adsorption studies - static method

3.2.1. Effect of ion exchanger mass

The effect of ion exchanger mass in the range of 0.1–0.2 g on the La (III)-IDHA complex sorption process on the S957 and S950 chelating ion exchangers was investigated. Figure S5 depicts the relationship between the amount of La(III) complexes adsorbed and the ion exchanger mass.

It was found out that as the ion exchanger mass increases, the equilibrium absorption capacity decreases significantly. When the mass increased from 0.1 to 0.2 g, the adsorption capacity of the S957 decreased from 14.63 to 7.32 mg/g, while for the S950 from 14.50 to 7.23 mg/g. This can be explained by the unsaturation of adsorption sites during the adsorption process. Another reason can be the particle interactions, e.g. aggregation due to a high sorbent concentration that would reduce the total surface area of the adsorbent [47]. Therefore, the optimum ion exchanger dose for the sorption process was defined as being 0.1 g.

3.2.2. Effect of Ln(III):IDHA molar ratio

The choice of an appropriate molar ratio of metal to the complexing agent is an important issue in optimizing the adsorption process because of the type as well as the percentage of complex forms that will be formed. As shown by the results of the potentiometric measurements described in Section 3.1.1, changing the ligand concentration can result in the formation of additional forms of complexes: a low ligand concentration favours the formation of Ln_2L type forms while some of the Ln (III) ions remain uncomplexed. However, an excess of complexing agent results in the formation of LnL_2 type forms and guarantees complete complexation of the metal ions.

In order to analyse the effect of the metal:ligand molar ratio on the adsorption process of Ln(III)-IDHA complexes precisely the experiments were conducted using the solutions with the equal amounts of metal and ligand (molar ratio 1:1), and two- and fourfold excess of IDHA (molar ratio 1:2 and 1:4). The metal to ligand molar ratio of 2:1 was not tested due to the possibility of precipitation of uncomplexed Ln(III) ions at higher pH values. The concentration of Ln(III) ions in the samples was 1.0×10^{-3} M. In this stage of the study, solutions were prepared without pH adjustment. The results obtained for the La(III) complexes with IDHA are shown in Fig. 5. The results for the Nd(III) and Ho(III) complexes are summarized in Figures S6 and S7.

The studies allowed to conclude that the molar ratio of metal to ligand affects the adsorption process of Ln(III) ions with IDHA but this influence varies depending on the properties of the adsorbent used in the process, while being the same regardless of the studied metal ion. For the chelating ion exchangers, S957 and S950, the adsorption process proceeds with a large efficiency regardless of the IDHA concentration. When the adsorption process was conducted on the cation exchanger, SP112, the increase in the IDHA concentration from 1.0×10^{-3} M to 4.0×10^{-3} M caused a significant decrease in the adsorption capacities. For example, the adsorption capacity in relation to the La(III) complexes decreased from 13.41 to 2.25 mg/g. A different dependency was observed for the strongly basic anion exchangers (M500, M600, MP500, 4200, 4400, 4600, IRA 458, IRA 958) for which the highest adsorption capacities were observed at two- and fourfold excess of complexing

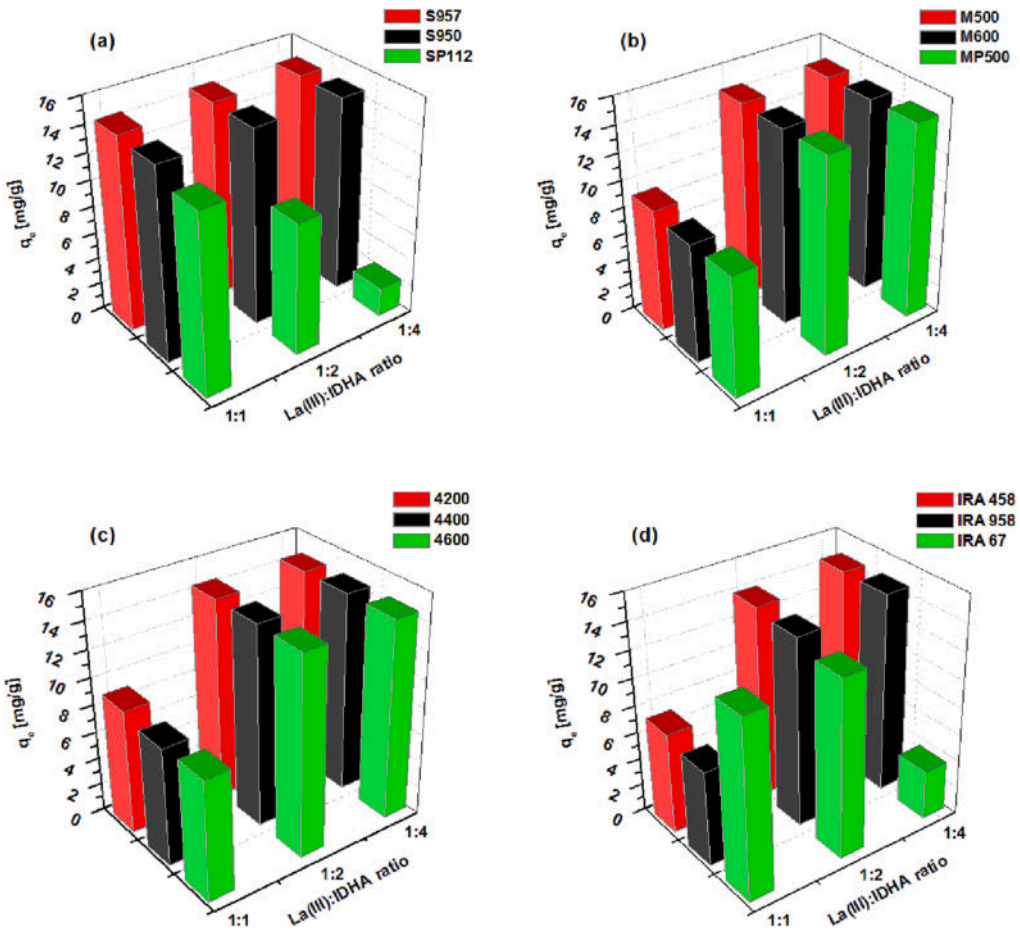

Fig. 5. The effect of the La(III):IDHA molar ratio on the sorption of La(III)-IDHA complexes on (a) S957, S950, SP112, (b) M500, M600, MP500, (c) 4200, 4400, 4600 and (d) IRA 458, IRA 958, IRA 67.

agent (the increase in the IDHA concentration from 1.0×10^{-3} M to 2.0×10^{-3} M resulted in the increasing amount of adsorbed complexes, and further increase in the IDHA concentration did not improve the process significantly). The last considered system was that containing the anion exchanger with the weakly basic functional groups, IRA 67, for which changing the metal:ligand ratio from 1:1 to 1:2 only improved the process efficiency marginally, while a further change from 1:2 to 1:4 definitely worsened it.

According to the above considerations, the values of 1:1 for the chelating ion exchangers and the cation exchanger and 1:2 for all anion exchangers were chosen as the optimal molar ratio of the metal to the complexing agent.

3.2.3. *Effect of initial pH*

The initial solution pH is an important parameter that can change sorption efficiency significantly. Positively charged metal ions form different types of complexes with the complexing agent. The type of the formed complex depends on the pH because it affects the ionization of the ligand. The solution pH also determines the surface charge of the adsorbent. In our studies the effect of the initial pH for the Ln(III) complexes adsorption in the pH range from 2.0 to 12.0 was evaluated and is presented in Fig. 6 for the La(III) complexes and for the Nd(III) and Ho(III) complexes in Figures S8 and S9.

The results obtained identified four types of relationships between the pH of the solution and the adsorption capacity that correspond to different ion exchanger groups. The first group are the chelating ion exchangers (S957, S950) for which the initial solution pH has no effect on the adsorption of Ln(III) ions in the presence of IDHA, and the adsorption capacity is almost stable over a very wide pH range (2.0–10.0). A decrease in adsorption efficiency is observed only at high pH values (12.0). This suggests that in this case the electrostatic attraction does not play a significant role in the adsorption mechanism of Ln(III) complexes with IDHA. For the system where the SP112 cation exchanger was used as an adsorbent a different relationship with increasing pH solution, the adsorption capacity decreased. The highest q_e values were obtained in the pH range 2.0–4.0 for the La(III)-IDHA complexes and for the Nd(III) and Ho(III) ones at pH 2.0. It should be noted, however, that in the low pH (<3.3) solution the IDHA molecules are mainly present in the completely protonated form (H_4IDHA) (Fig. 3a) and the metal ions are in the positive ions form (Ln^{3+}). This state of the system creates a small probability of forming a metal–ligand complex, so that only uncomplexed Ln(III) ions are adsorbed. Another effect of pH on the adsorption process was clearly visible for the third group of adsorbents, strongly basic anion exchangers, for which increasing the pH of the solution increased the adsorption capacity, reaching the highest values at pH 10.0. Analysis of the complex forms present in the metal–ligand system at different solution pH values also enables explanation of the dependence of the pH effect on the adsorption process for this group of ion exchangers. As the pH of the system increases, the proportion of negatively charged Ln(III)-IDHA complexes increases, and so does the adsorption capacity. The last considered case was a system containing the weakly basic anion exchanger IRA 67, for which the highest adsorption capacities were obtained at pH 4.0. Adsorption was negligible below this value, while an increase in the pH of the solution above 4.0 resulted in a gradual deterioration of the efficiency of the process. Such behaviour is typical of this type of ion exchanger. IRA 67 is a weakly basic anion exchanger that has tertiary amine groups. In neutral and alkaline environments, the free base form

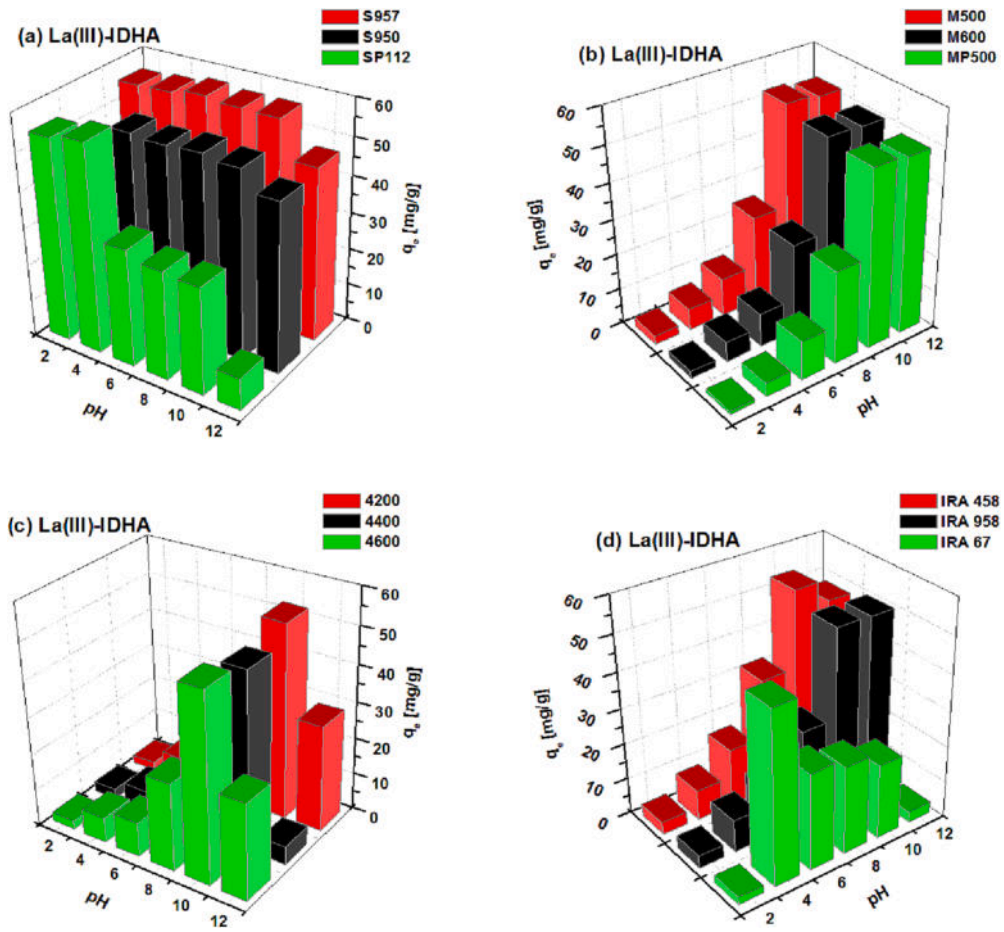

Fig. 6. The effect of pH on the sorption of La(III)-IDHA complexes on (a) S957, S950, SP112, (b) M500, M600, MP500, (c) 4200, 4400, 4600 and (d) IRA 458, IRA 958, IRA 67.

of the tertiary amine groups dissociates according to the following equation:

$$R\text{-}N(CH_3)_2\cdot H_2O \rightleftarrows R\text{-}^{+}NH(CH_3)_2OH^{-} \quad (39)$$

However, there is a poor dissociation process under these conditions, so anion uptake is not high. A significant increase in the adsorption capacity occurs in the acidic media where the hydrogen ion concentration is high enough to protonate the functional groups [48]. In our study, a large decrease in the solution pH value causes the breakdown of the Ln(III)-IDHA complexes, resulting in the uncomplexed free Ln^{3+} cations in the solution with no affinity for the protonated amine groups.

3.2.4. Kinetic studies

Kinetic studies of the adsorption process are a key step in determining the time required for the system to establish equilibrium, which is important primarily in industrial applications, and provide information on the mechanism and rate controlling steps of the process. The studies were carried out in the range of phase contact times from 1 to 240 min for different initial concentrations of Ln(III)-IDHA complexes (0.5×10^{-3}; 1.0×10^{-3}; 1.5×10^{-3}; 2.0×10^{-3}; 2.5×10^{-3} M) using optimal parameters (ion exchanger mass, metal:ligand molar ratio, solution pH) selected during the analysis of the results obtained in the previous steps. Fig. 7a-d present the adsorption of La(III) complexes with IDHA in the range of 0–240 min at the lowest tested concentration of 0.5×10^{-3} M.

As follows from the studies in the majority of the tested systems, the adsorption of Ln(III)-IDHA complexes is fast, reaching equilibrium in 30 min. For S957 and SP112 only 10 min was sufficient. It was also shown that adsorption of the complexes containing Ho(III) ions occurred faster compared to those with La(III) and Nd(III) ions (10 min for all systems except S950 and IRA 67). To establish equilibrium a slightly longer time was required for the systems with S950 and it was 60 min. An interesting case turned out to be the system containing the weakly basic ion exchanger IRA 67 for which the amount of adsorbed complexes increased during the first 120 min. Then the analysis of the samples, where the process took 240 min, showed the desorption occurrence. This phenomenon was observed only for the adsorption of La(III) and Nd(III) complexes with IDHA. The adsorption capacity decreased from 6.84 to 5.00 mg/g for the La(III)-IDHA complexes and from 6.77 to 4.08 mg/g for the Nd(III)-IDHA ones (initial concentration 0.5×10^{-3} M). In addition, increasing the concentration caused an increase in the time required to reach the system equilibrium while increasing the adsorption capacity.

In this paper the pseudo-first order (PFO), pseudo-second order (PSO), Weber-Morris intraparticle diffusion, Boyd, and Dumwald-Wagner (D-W) kinetic models were used to describe the adsorption kinetics of La(III), Nd(III), and Ho(III) complexes in the presence of IDHA. The quality of the models fit was assessed using the correlation coefficient (R^2) and the Chi-square (χ^2) analysis. Tables S3-S11 shows the calculated kinetic parameters for the adsorption of La(III), Nd(III) and Ho(III) complexes with IDHA at the initial concentrations ranging from 0.5×10^{-3} M to 2.5×10^{-3} M. Fig. 7a-d illustrate the obtained experimental data (points) and fitted kinetic models (lines) for the La(III)-IDHA complexes (initial concentration of 0.5×10^{-3} M).

The PFO and PSO models are the most frequently utilized models in the literature to characterize adsorption kinetics. The PFO model, first proposed by Lagergren, is the earliest empirical equation describing the

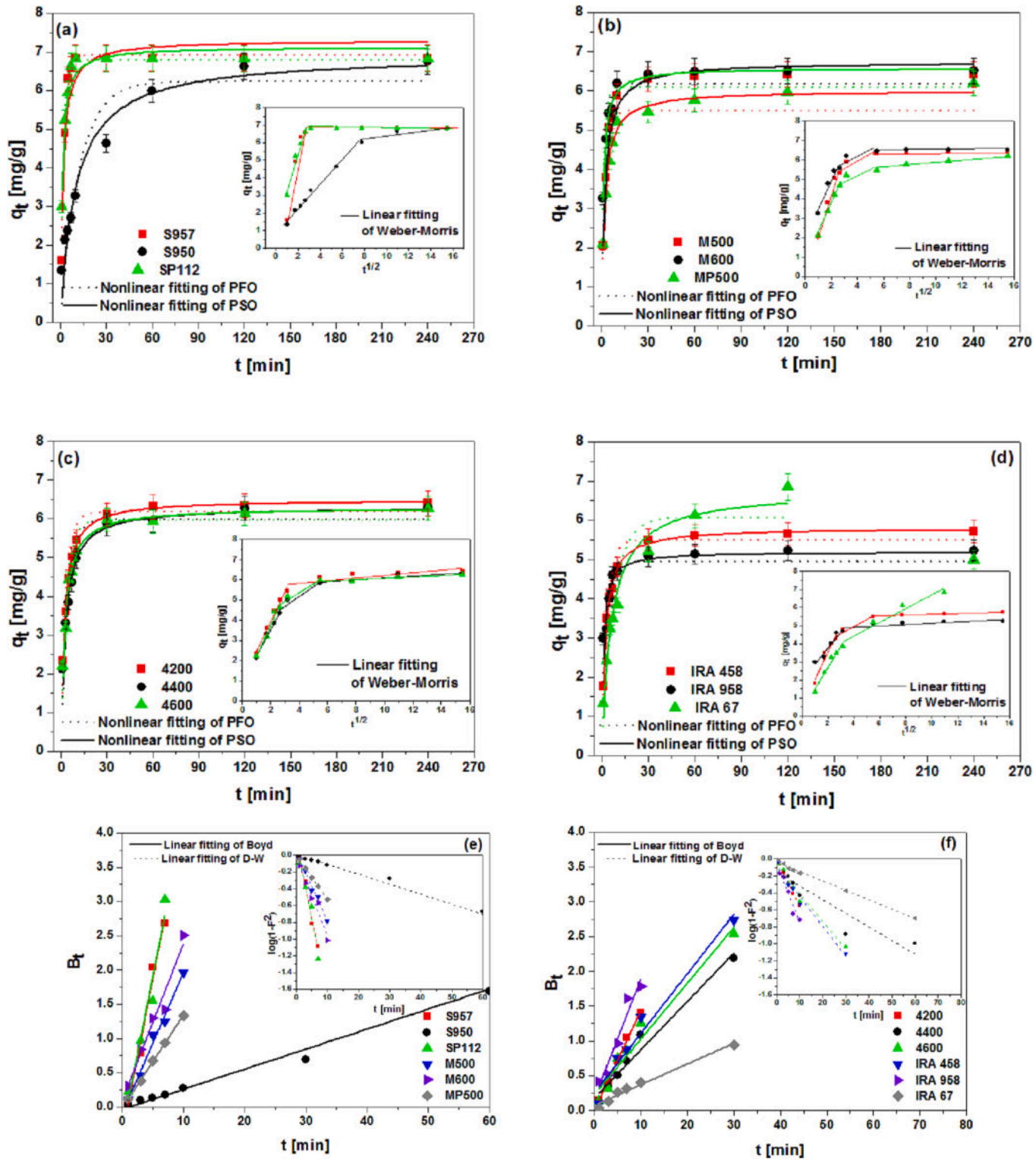

Fig. 7. Experimental data fitting for the La(III)-IDHA complexes sorption on S957, S950, SP112, M500, M600, MP500, 4200, 4400, 4600, IRA 458, IRA 958, IRA 67 for the (a-d) pseudo-first order, pseudo-second order, Weber-Morris intraparticle diffusion, (e-f) Boyd, and Dumwald-Wagner kinetic models ($C_0 = 0.5 \times 10^{-3}$ M).

rate of the adsorption process. It was initially used to explain the kinetics of carboxylic acid adsorption on charcoal in 1898 [20]. In 1984 Blanchard proposed an equation describing the rate of the adsorption process as a function of the difference between the equilibrium and the actual amount of adsorbate on the adsorbent surface, now known as the PSO model [21]. In many papers the linearized forms of these models are employed to determine the most suitable kinetic model for the adsorption process and for estimating kinetic parameters. However, it was found that the transformations of nonlinear equations to the linear form modify the error distribution, causing the model parameters to be distorted [49]. Therefore, in this study, nonlinear forms of models were applied to analyse the kinetic results (using the PFO and PSO models). The OriginPro 8 software was used for this purpose.

The analysis of the obtained R^2 and χ^2 values and the comparison of

the adsorption capacities values obtained experimentally ($q_{e,\exp}$) with those calculated from the models (q_{cal}) allowed to draw the conclusion that it is not possible to choose a single model that would describe all studied systems best, however, some relationships were observed. The adsorption process on the chelating ion exchanger S957 and the cation exchanger SP112, regardless of the adsorbed complex (containing La (III), Nd(III) or Ho(III)), followed the PFO model. The adsorption kinetics on S950 and IRA 67, regardless of the metal ion used in the system, were best described by the PSO model. In the case of strongly basic anion exchangers there was a correlation between the type of adsorbed complex and the best-fitting kinetic model: for the La(III)-IDHA complexes the PSO model was used, whereas changing the metal ion in the complex to Nd(III) or Ho(III) caused the adsorption process to follow the PFO model. The exception to this was the system with the M500 that, regardless of the metal ion, exhibited kinetics consistent with the PFO model. Fig. 7a-d show the nonlinear fit of the PFO and PSO models to the experimental data of the adsorption process of the La(III)-IDHA complexes.

Mass transfer processes in porous materials are essentially rate processes in which the mass transfer rate in influenced by a driving force and a resistance. The driving force is due mainly to concentration gradients for the material being transferred, and the resistance is due to the medium through which the material is being transferred and any interactions between them. This process is also directly affects the adsorption rate. Four basic steps can be considered in the solid–liquid adsorption process: transfer of the adsorbate from the solution phase to the external surface (bulk transport); the transport across the boundary layer (film diffusion); diffusion of the adsorbate through the adsorbent pores (intraparticle diffusion); and adsorption of the adsorbate on the active sites of the adsorbent [50]. The listed first and fourth steps are considered to be very fast and thus they do not determine the rate of the process. Moreover, the rate of adsorption depends on either the film diffusion or the intraparticle diffusion or both. The experimental data were fitted to the diffusion models commonly used in the literature (Weber-Morris intraparticle diffusion, Boyd, and Dumwald-Wagner models) in order to identify the step controlling the rate of the adsorption process.

Fig. 7a-d present the fitting of the experimental data for the adsorption process of the La(III)-IDHA complexes to the Weber-Morris model. The assumption of the Weber-Morris model is to obtain the plot of q_t vs $t^{1/2}$ as a straight line passing through the point (0,0) for the adsorption process in which the slowest step determining the rate of the whole process is the intraparticle diffusion. The analysis of the plots obtained for the adsorption process of Ln(III) ions in the presence of IDHA showed that they are characterized by a multilinear pattern, with two or three ranges of linearity. Such observations are very common in the literature [51–54]. This suggests that the intraparticle diffusion is not the only step that affects the process rate but is also dependent on other phenomena, characterized by different rate constants. The important parameter that can be obtained from the Weber-Morris model is the C parameter (intercept value), which indicates the thickness of the effect of the boundary layer on the particle diffusion. A larger value of the C parameter indicates that transport through the boundary layer has a greater effect on particle diffusion [55]. The intraparticle diffusion parameter k_i is defined as the slope of successive portions. The k_i value was discovered to increase with the increasing initial concentration of the Ln(III) complexes, possibly due to a larger driving force [56].

The Boyd model is another model used to describe the kinetics of the adsorption process which, based on the B_t vs t plot, allows one one to determine whether the rate controlling step of mass transfer is intraparticle diffusion (the plot is linear and passes through the origin) or film diffusion (the plot is not linear or does not pass through the origin) [57]. The Boyd plots for the adsorption of La(III) complexes with IDHA are shown in Fig. 7e-f (the points after establishing equilibrium of the system were not considered in the analysis). The determined values of the slope parameter of the linear segment in the plot B_t vs t are summarized in Tables S5, S8, and S11. For most of the systems studied, the plots were characterized by high linearity ($R^2 > 0.9$) but the obtained lines did not intersect the beginning of the coordinate system, which confirms the assumption that the diffusion is not the only stage that affects the rate of adsorption of Ln(III)-IDHA complexes.

The experimental data were fitted to the Dumwald-Wagner model which can also help to understand the mechanism of the adsorption process. The Dumwald-Wagner model performs an analogous plot analysis to the Weber-Morris and Boyd models, but in this case the log(1-F^2) vs t relationship is considered. Fig. 7e-f depict the fit of the obtained results to this model using the adsorption process of La(III)-IDHA complexes as an example. The calculated Dumwald-Wagner model rate constants and the intercept values are presented in Tables S5, S8, and S11. As can be seen from the presented values of intercept and correlation coefficients R^2, despite obtaining great linearity of Dumwald-Wagner plots, straight lines do not pass through the origin of the coordinate system, which confirms the conclusions obtained during the analysis of fits of the previous models that the adsorption processes of La (III), Nd(III) and Ho(III) complexes with IDHA studied in this paper were controlled not only by interparticle diffusion but represent a more complex mechanism.

3.2.5. Equilibrium studies

Using adsorption isotherms determined for optimal process conditions, the correlation between the concentration of Ln(III)-IDHA complexes in the solution and the degree of their accumulation on the ion exchanger surface was measured. This provided the information regarding the maximum adsorption capacity of the adsorbents as well as better understanding of the adsorption mechanism. The equilibrium data obtained in this study were analysed using the Langmuir, Freundlich, and Temkin isotherm models to find the best fit. Fig. 8a-c depict the fit of the nonlinear forms of isotherms to the experimental data using the adsorption of La(III)-IDHA complexes at 293 K as an example.

The Langmuir isotherm is a model widely used by many authors to describe the adsorption process of heavy metal ions, organic compounds, dyes, etc. It assumes that adsorption is a monolayer and takes place at specified locations on the homogeneous adsorbent surface known as active centres, with adsorbed particles not interacting with one another. The Freundlich model is the first known equation explaining the adsorption process. Adsorption following the Freundlich model is considered to be a multilayer process, where the energy of the active sites changes exponentially. Its important limitation is that the adsorption capacity is not limited. This means that as the adsorbate concentration increases, the theoretical amount of adsorbed adsorbate can go to infinity [58]. The Temkin model takes into account the effect of interactions between adsorbate molecules and adsorbent assuming that due to this the heat of adsorption of all particles in the layer will decrease linearly (rather than logarithmically) with coverage [59].

The values of the isotherm models parameters as well as the correlation coefficients (R^2) and error functions Chi-square (χ^2) were calculated using the OriginPro 8 software and are presented in Table S12 for 293 K and Tables S13-S15 for higher temperatures. A detailed analysis of the parameters evaluating the quality of the isotherm models fitting to the experimental data of the adsorption process of Ln(III) complexes with IDHA revealed that a single universal model cannot be used to describe the studied process, which suggests significant differences in the adsorption mechanism depending on the ion exchanger and metal forming the adsorption system.

For the adsorption process using the chelating ion exchangers S957 and S950 and the cation exchanger SP112, great agreement of the obtained data with the Temkin model was observed. The S957-La(III)-IDHA system with the better fit for the Langmuir model deviated from this observation. The Langmuir model described the processes occurring on strongly basic anion exchangers (M500, M600, MP500, 4200, 4400, 4600, IRA 458, IRA 958) also the best. However, one exception was observed in this group of ion exchangers: the adsorption process of Nd

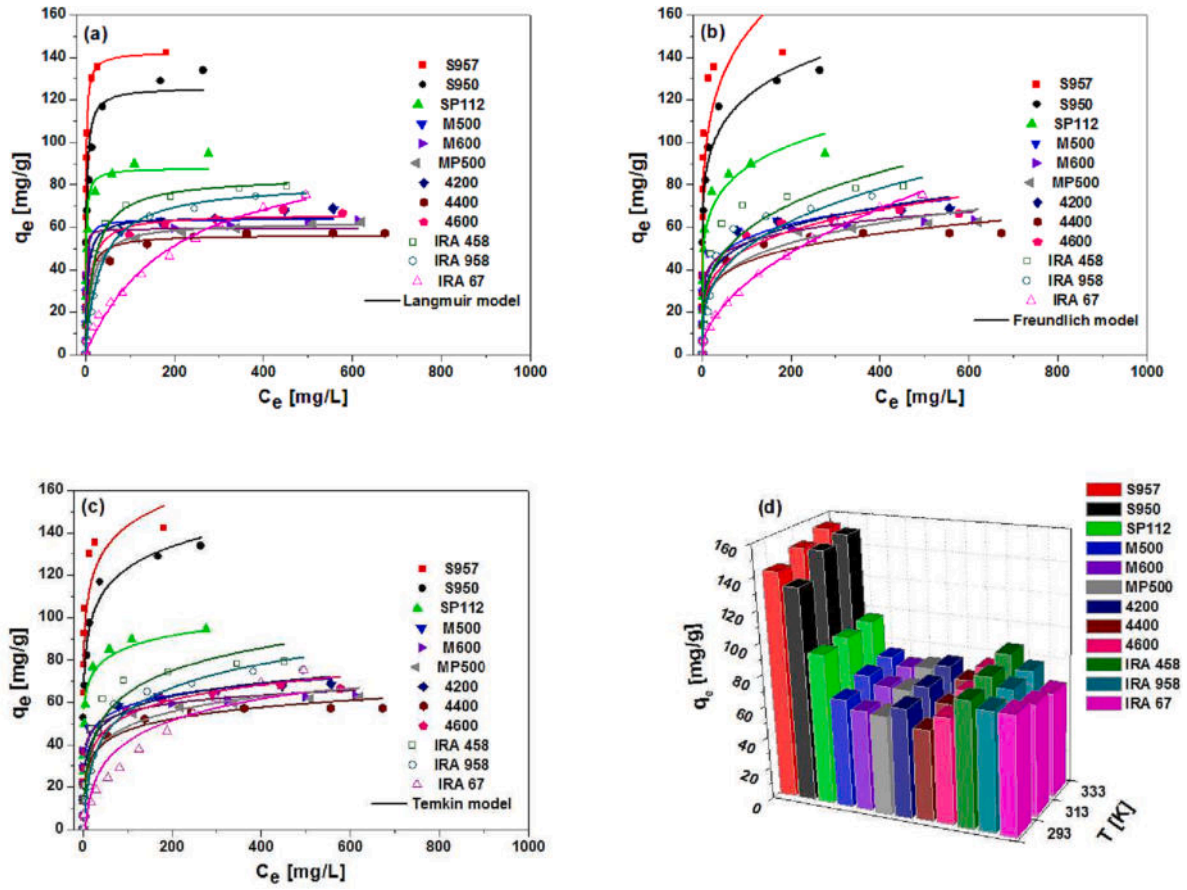

Fig. 8. Nonlinear fitting of (a) Langmuir, (b) Freundlich and (c) Temkin isotherms to the experimental data for the sorption of La(III)-IDHA complexes on S957, S950, SP112, M500, M600, MP500, 4200, 4400, 4600, IRA 458, IRA 958, IRA 67 and (d) comparison of the maximum sorption capacity of ion exchangers in relation to the La(III)-IDHA complexes for different temperatures.

(III)-IDHA complexes on IRA 458 followed the Temkin model rather than the Langmuir model. The system in which the weakly basic anion exchanger IRA 67 was used as an adsorbent, irrespective of the metal ion included in the adsorbed complex, was the only system that was consistent with the Freundlich model.

The obtained results enabled the formation of affinity series of the investigated ion exchangers for the Ln(III)-IHDA complexes and the selection of the best one for the adsorption process. S957, SP112 and all strongly basic anion exchangers showed increasing affinity for the Ln (III)-IDHA complexes according to the following series: La(III) < Nd (III) < Ho(III). For the other ion exchangers, the series was as follows: Nd (III) < Ho(III) < La(III) for S950, and Nd(III) < La(III) < Ho(III) for IRA 67. The maximum adsorption capacities of the ion exchangers obtained for the adsorption of La(III) complexes with IDHA increased in the following order: 4400 < MP500 < M600 < 4600 < M500 < 4200 < IRA 67 < IRA 958 < IRA 458 < SP112 < S950 < S957. The highest adsorption capacity (142.29 mg/g) towards La(III)-IDHA complexes was obtained for the S957 chelating ion exchanger. The series for the Nd(III)-IDHA complexes was as follows: 4400 < M600 < MP500 < 4600 < 4200 < IRA 67 < M500 < IRA 958 < IRA 458 < S950 < S957 < SP112. The highest affinity for the Nd(III)-IDHA complexes was exhibited by the SP112 cation exchanger for which the adsorption capacity of 161.04 mg/g was obtained. SP112 also showed the highest adsorption capacity (201.74 mg/g) towards the Ho(III) complexes as shown in the series: 4400 < 4600 < M600 < IRA 67 < MP500 < 4200 < IRA 958 < M500 < IRA 458 < S950 < S957 < SP112.

3.2.6. *Effect of temperature and thermodynamic parameters*

The temperature at which the adsorption process proceeds is an important parameter determining its efficiency. It is well-known that an increase in temperature can affect the process in two ways: by causing an increase in adsorption capacity (an endothermic process) or by causing a decrease (an exothermic process). Many studies reported in the literature proved that the adsorption processes using ion exchangers are endothermic, but even in such cases, too large an increase in temperature will result in a decrease in the adsorption efficiency due to the desorption process or damage of the adsorbent structure [60]. Furthermore, when applying the basic anion exchangers, there is also a significant risk of thermal degradation of the functional groups, which is already observed above 333 K. In the present study, the effect of temperature on the adsorption process of La(III), Nd(III), and Ho(III) complexes with the IDHA complexing agent was investigated on different ion exchangers at 293, 313 and 333 K. The effect of temperature on the maximum adsorption capacity of the ion exchangers with the exemplary La(III)-IDHA complexes is shown in Fig. 8d. Adsorption isotherms were also determined for the mentioned temperatures, and their parameters were calculated. These data are presented in Tables S13-S15.

As follows from the data, chelating ion exchangers, cation exchanger, and strongly basic anion exchangers in the adsorption of La(III)-IDHA complexes showed a typical trend of increasing adsorption capacity with the increasing temperature from 293 K to 333 K. However, these changes were very small for the systems of La(III)-IDHA-SP112 (from 94.77 to 97.11 mg/g) and La(III)-IDHA-IRA 958 (from 74.97 to 78.49 mg/g). This behavior of the adsorption system is associated with an increase in the kinetic energy of the adsorbate particles with the increasing temperature and thus an increase in their mobility toward the active sites. Furthermore, the rate of intramolecular diffusion is also accelerated. An additional phenomenon caused by increasing the

temperature is a reduction in the thickness of the boundary layer that surrounds the adsorbent particles, which contributes to a decrease in the mass transfer resistance [61]. The adsorption of Nd(III) and Ho(III) complexes showed an analogous relationship but the processes with the polyacrylic matrix ion exchangers (IRA 458, IRA 958) started to exhibit an exothermic character for these complexes. The weakly basic anion exchanger IRA 67 (also with the polyacrylic matrix), independently of the metal ion in the adsorbed complex, showed a decrease in the adsorption efficiency with the increasing process temperature. For these systems it can be concluded that the increase in the temperature enhanced the desorption process by weakening the adsorption forces between the active sites on the adsorbent surface and the Ln(III)-IDHA complexes [62].

The results obtained of the temperature effect on the adsorption process of the Ln(III)-IDHA complexes allowed the determination of the thermodynamic parameters that are presented in Table 4 for the La(III)-IDHA complexes and in Tables S16 and S17 for the Nd(III) and Ho(III) complexes. The linear plots of $\ln K_c$ vs $1/T$ are shown in Figure S10. From the analysis of the thermodynamic data, it is possible to infer the nature of the process under study. The determined Gibbs free energy values (ΔG°) provided information whether the investigated process is spontaneous and thermodynamically favourable (negative values) or, in contrast, non-spontaneous and thermodynamically unfavourable (positive values). Furthermore, it is known that for processes in which electrostatic interactions play a key role (physical adsorption), the ΔG° values are in the range of −20 to 0 kJ/mol. If on the other hand, this parameter is in the range of −80 to −400 kJ/mol, one should expect that the process is dominated by the chemical adsorption (coordination bond formation). The thermodynamic parameter ΔH° (enthalpy change) allows one to determine the energy effect of the process, taking into account positive values for the endothermic processes and negative values for the exothermic ones. At the same time, the ΔH° value can confirm the conclusions drawn from the analysis of the obtained ΔG° values regarding the main mechanism of the adsorption process: the ΔH° value below 40 kJ/mol suggests physical adsorption, while for chemical adsorption ΔH° is in the range of 40–120 kJ/mol. The value of entropy change (ΔS°), the last of the thermodynamic parameters, describes the randomness in the interactions between the adsorbent and the adsorbate.

Based on the results of the adsorption processes of the La(III), Nd(III), and Ho(III) ions in the presence of IDHA, it was found that the processes using all the studied ion exchangers were spontaneous and thermodynamically favourable (negative ΔG° values). In most of the studied systems, the adsorption processes were endothermic. The adsorption of La(III), Nd(III), and Ho(III) complexes on IRA 67 and the Nd(III) and Ho (III) complexes on IRA 458 and IRA 958 ion exchangers were identified as exothermic. The values of ΔG° and ΔH° parameters suggest that physical adsorption is the dominant mechanism. The positive entropy ΔS° values for all considered systems indicate increased randomness at the solid-solution interface during the Ln(III)-IDHA complex adsorption as well as significant affinity of adsorbent surfaces for these complexes.

Table 4
Thermodynamic parameters for the sorption of the La(III)-IDHA complexes on S957, S950, SP112, M500, M600, MP500, 4200, 4400, 4600, IRA 458, IRA 958 and IRA 67.

Ion exchanger	ΔH° [kJ/mol]	ΔS° [J/mol K]	ΔG° [kJ/mol]		
			293 K	313 K	333 K
S957	22.96	133.56	−16.23	−18.70	−21.59
S950	24.91	137.43	−15.17	−18.56	−20.61
SP112	2.28	56.31	−14.21	−15.35	−16.46
M500	4.64	55.95	−11.72	−12.95	−13.94
M600	4.94	55.51	−11.30	−12.49	−13.51
MP500	6.46	60.40	−11.23	−12.46	−13.64
4200	3.99	53.69	−11.74	−12.80	−13.89
4400	6.44	58.90	−10.82	−11.99	−13.18
4600	6.60	62.03	−11.57	−12.84	−14.05
IRA 458	5.85	62.86	−12.58	−13.80	−15.10
IRA 958	2.43	50.08	−12.23	−13.26	−14.23
IRA 67	−5.98	21.31	−12.23	−12.64	−13.09

3.3. Desorption studies

To assess the regeneration capacity of the investigated ion exchangers after adsorption of Ln(III)-IDHA complexes, the desorption process was carried out using 0.5, 1 and 2 M concentrations of hydrochloric and nitric(V) acids. The desorption process was conducted at 293 K for 240 min. The results obtained for the La(III) complexes are shown in Fig. 9 and for the Nd(III) and Ho(III) complexes in Figures S11 and S12. A very clear difference can be observed between the desorption process on the chelating ion exchangers and the cation exchangers and that occurring on the anion exchangers. It was shown that for the first group of adsorbents, the desorption process occurs much less efficiently in comparison with the group of anion exchangers. Furthermore, this process is dependent on the acid concentration (desorption efficiency increases with increasing acid concentration). This level of desorption capacity (22–69%) can indicate the high affinity of Ln(III)-IDHA complexes for this type of ion exchanger as well as the need to search for more optimal desorption conditions or change the desorbing agent. For the anion exchangers, no significant change in desorption efficiency with a change in the eluent concentration is observed.

For economical and environmental reasons, it is important that the adsorbents are used in the process many times. To determine whether the investigated ion exchangers have this ability with regard to the Ln (III)-IDHA complexes, we used La(III) as a representative of rare earth elements, and five adsorption/desorption cycles were performed. The eluents that produced the highest desorption efficiencies in the previous study (Fig. 9) were chosen as desorbing agents: 2 M HNO_3 for S957 and SP112, 2 M HCl for S950, and 1 M HCl for all anion exchangers except MP500, where 2 M HCl was used. The results are presented in Table S18. The chelating ion exchangers (S957, S950) and the cation exchanger (SP112) had the best reusability. In five adsorption/desorption cycles, their adsorption capacity remained close to 100%. Using polystyrene anion exchangers with the gel structure (M500, M600, 4200, 4400, 4600) in the process also provided good results. However, the adsorption efficiency dropped to 15%. The least satisfactory results were obtained for the polystyrene, macroporous, strongly basic anion exchanger MP500 and for the polyacrylic anion exchangers IRA 458, IRA 958, and IRA 67. For these ion exchangers during the second adsorption cycle, a significant decrease in the adsorption efficiency was observed. In the subsequent cycles *%S* remained at 40% for IRA 458, IRA 958, and 30% for MP500 and IRA 67.

3.4. Adsorption studies - dynamic method

In order to evaluate the applicability of the studied process in industry, experiments were carried out using the dynamic method on a fixed bed. This method, due to its simplicity and low cost, is the most frequently used in purification and separation processes. The experiments were carried out for the La(III) complexes with IDHA using the optimal conditions determined during the static method testing: the La (III):IDHA molar ratio 1:1 for S957, S950 and SP112, 1:2 for the anion exchangers, pH 8.0 for S957 and S950, 4.0 for the SP112 and IRA 67, and 10.0 for the strongly basic anion exchangers, the initial concentration equal to 1.0×10^{-3} M.

Fig. 10 depicts the obtained breakthrough curves for the adsorption of La(III)-IDHA complexes, which were used to calculate the dynamic parameters (the capacity of ion exchanger q_e, the working exchange capacity C_w, the total exchange capacity C_t, the mass distribution coefficient D_g and the volume distribution coefficient D_v) presented in Table 5.

The vast majority of the breakthrough curves shown in Fig. 10 are

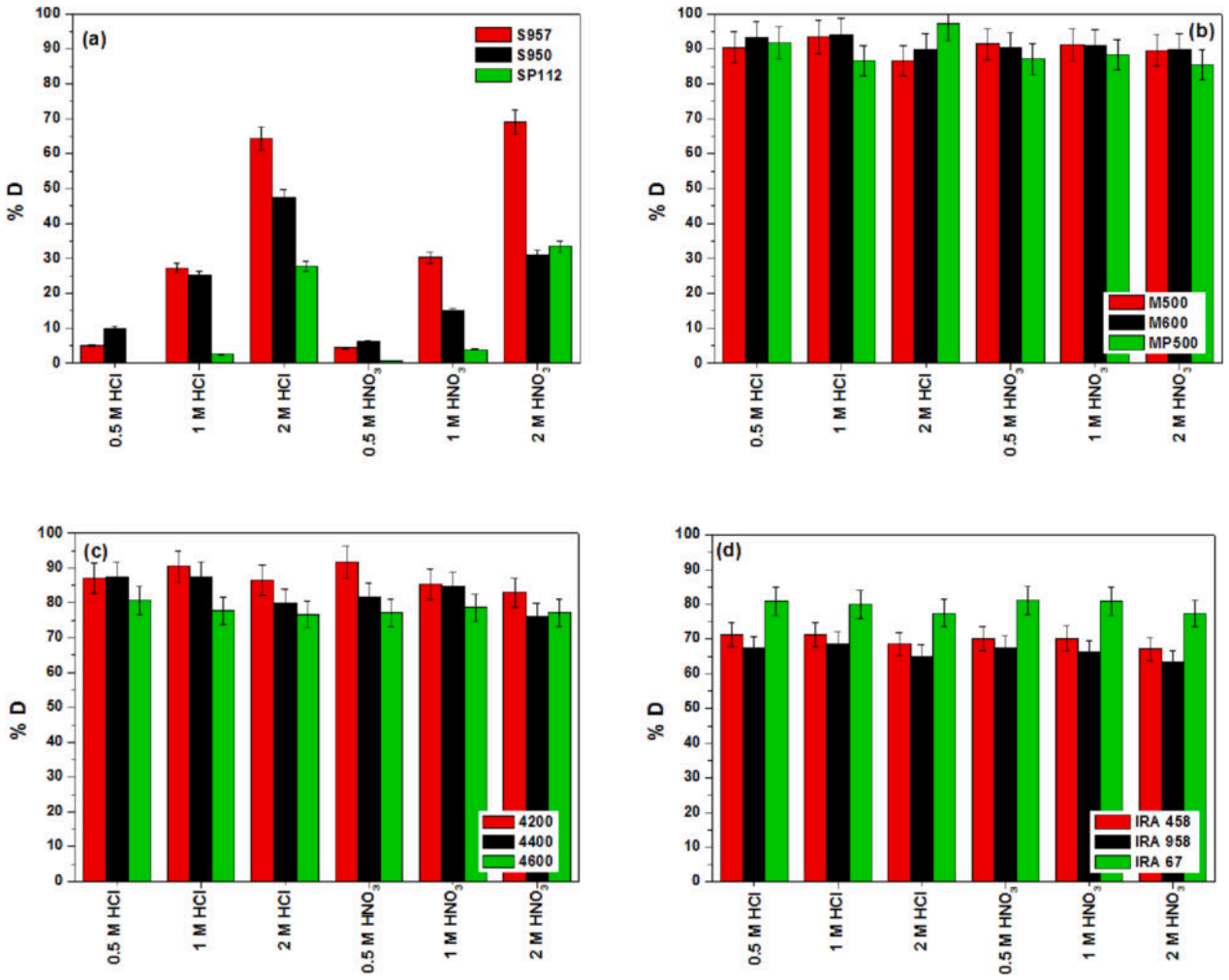

Fig. 9. Dependence of La(III) ions desorption capacity on (a) S957, S950, SP112, (b) M500, M600, MP500, (c) 4200, 4400, 4600 and (d) IRA 458, IRA 958, IRA 67 using the desorption agents: HCl and HNO_3 at various concentrations.

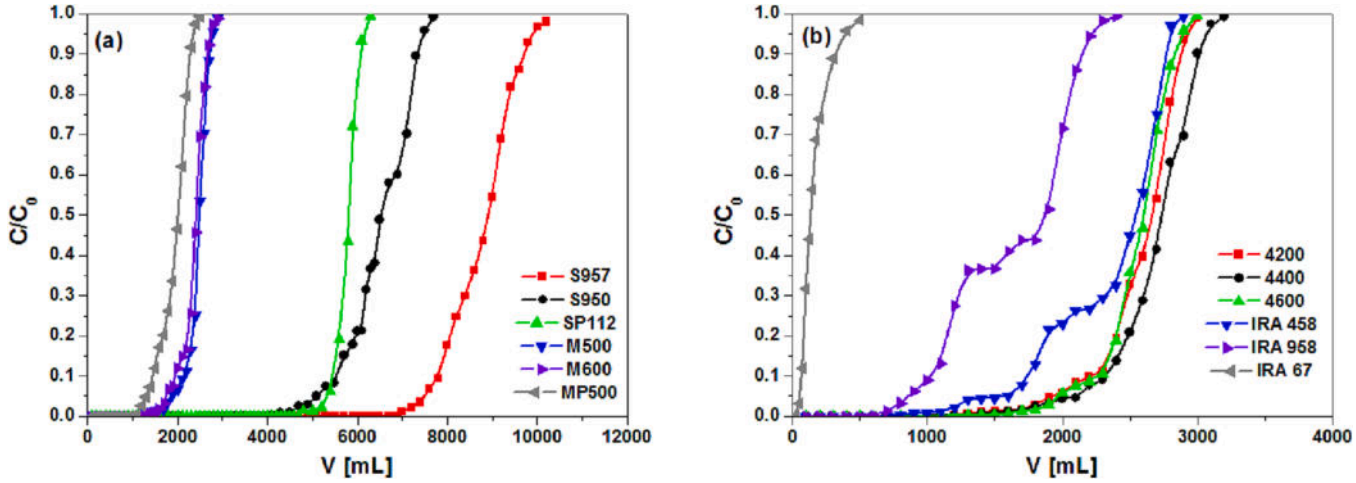

Fig. 10. Breakthrough curves of La(III)-IDHA complexes sorption on (a) S957, S950, SP112, M500, M600, MP500, (b) 4200, 4400, 4600, IRA 458, IRA 958, IRA 67 ($C_0 = 1.0 \times 10^{-3}$ M).

"S" shaped, which is characteristic of nearly ideal adsorption systems. For the columns using the polyacrylic anion exchangers (IRA 458, IRA 958) there were observed some deviations from the typical shape on the breakthrough curves. This may suggest the possibility of more than one type of complex formation. Furthermore, the sharper the shape of the breakthrough curve, the more effective the column system under study will be. This is evident for the pair of ion exchangers, S950 and SP112. S950 exhibited greater adsorption capacity towards La(III) complexes in

Table 5
Dynamic studies parameters of La(III)-IDHA complexes adsorption ($C_0 = 1.0 \times 10^{-3}$ M).

Ion exchanger	q_e [mg/g]	U [mL]	$\bar{U}$ [mL]	C_w [mg/mL]	C_t [mg/mL]	D_g	D_v	%D
S957	272.85	7000	8920	93.82	119.56	2087.96	891.56	99.17
S950	228.11	3900	6500	52.27	87.12	1718.41	649.56	92.16
SP112	211.55	4800	5840	67.99	82.73	1549.47	583.56	83.91
M500	102.65	1100	2500	15.58	35.41	751.10	249.56	99.85
M600	93.79	1200	2420	17.00	34.28	688.32	241.56	97.46
MP500	107.54	1000	2000	14.17	28.33	798.08	199.56	72.21
4200	98.73	1200	2680	17.00	37.96	735.90	267.56	98.69
4400	94.23	1100	2750	15.58	38.95	692.04	274.56	97.58
4600	98.16	1200	2600	17.00	36.83	717.93	259.56	97.29
IRA 458	87.66	800	2550	11.33	36.12	677.74	254.56	78.68
IRA 958	69.94	600	1900	8.50	26.91	584.88	189.56	65.41
IRA 67	5.70	25	138	0.36	2.01	36.29	13.36	76.10

the bath studies than SP112. Even in the column tests, the calculated adsorption capacity q_e for this ion exchanger is higher, but comparing the shapes of the breakthrough curves, it can be seen that the curve for SP112 is sharper and the breakthrough point appears later than that of S950, which means that in the industrial applications SP112 is more effective despite the lower q_e value. This is confirmed by the higher value of the working exchange capacity (C_w) for SP112.

The affinity of the investigated ion exchangers for the La(III)-IDHA complexes was also compared using the dynamic studies. The column bed was exhausted in the shortest time for the weakly basic anion exchanger IRA 67, indicating the lowest affinity for the La(III)-IDHA complexes. Higher adsorption capacity in the column systems was observed for the group of strongly basic anion exchangers. The affinity for the La(III)-IDHA complexes was similar in this group of ion exchangers. More than doubled adsorption capacities relative to the anion exchangers were possessed by the S950 and SP112, while the chelating ion exchanger S957 had the highest affinity, confirming the results obtained by the static method.

The Thomas, Adams-Bohart, Yoon-Nelson, and Wolborska mathematical models were used to describe the column performance. The first employed is the Thomas model, which is commonly used to describe adsorption in aqueous media because of its low internal and external diffusion resistance. Its basis is the assumption that adsorption follows the Langmuir model and second-order kinetics [63]. Furthermore, it excludes the occurrence of axial dispersion. The parameters of the Thomas model were determined from the $\ln(C_0/C)$-1 vs V plot and are presented in Table S19. Fitting the experimental data to the Thomas model yielded good agreement with the correlation coefficient R^2 ranging from 0.808 for the La(III)-IDHA-IRA 67 system to 0.990 for the La(III)-IDHA-S957 system. Furthermore, the values of adsorption capacities q_0 determined from the model were very close to the experimentally determined values.

Another frequently used model to describe the column behaviour is the Adams-Bohart model which assumes that the rate of the adsorption process in the column system is directly affected by the residual adsorbent capacity, i.e., the adsorbate capacity not used at a given time and the adsorbate concentration [64]. This linear model is used to describe the initial part of the breakthrough curve ($C/C_0 \ll 1$). The Adams-Bohart parameters were calculated on the basis of the $\ln(C/C_0)$ vs t plot and are listed in Table S19. The analysis of R^2 values showed a good agreement of the Adams-Bohart model with the experimental data. The best fit to the model was obtained for the systems with 4200, 4400 and 4600 anion exchangers ($R^2 = 0.986$).

A much simpler model to apply, due to the smaller amount of process data required for computation, is the Yoon-Nelson model. According to this model, the rate of decrease in the adsorption probability for each adsorbate particle was proportional to the adsorption probability of the adsorbate and the breakthrough probability of the adsorbate on the adsorbent [65]. Table S19 shows the parameters for this model determined from plotting the $\ln(C/C_0\text{-}C)$ vs t relationship. In most cases the R^2 correlation coefficients exceed 0.9. An important parameter that can be calculated from the Yoon-Nelson model is the time required for the 50% adsorbate breakthrough (τ). In our study, the τ value was the highest for the system with the S957 ion exchanger and was equal to 14595.54 min. This demonstrates the possibility of long-column operation as well as a high affinity for the La(III) complexes with IDHA. This is quite different in the system where the IRA 67 anion exchanger is used. The value of τ is 326.02 min, indicating very fast half-loading of the column with the adsorbate.

The linear form of the Wolborska model was also used to evaluate the data obtained using the column method. For this purpose, a graph of $\ln(C/C_0)$ versus t (analogous to the Adams-Bohart model) was created and the kinetic coefficient of the external mass transfer (β_a) as well as the adsorption capacity of the ion exchanger per unit volume of the bed (q) was determined (Table S17). In the Wolborska model, only the initial section of the breakthrough curve ($C/C_0 < 0.5$) was analysed, as in the Adams-Bohart model. The results analysis showed that the model adequately describes the experimental data (R^2 mainly above 0.9).

After completion of dynamic studies (bed exhaustion, $C/C_0 = 1$) the column regeneration was performed using as eluents in the desorption process the acids (2 M HNO_3 for S957 and SP112, 2 M HCl for S950, 1 M HCl for the anion exchangers) selected in Section 3.3 as optimal for this purpose. The results obtained from the desorption process are summarized in Table 5. As shown, the desorption process occurred very efficiently for the S957, S950, M500, M600, 4200, 4400, and 4600 ($\%D >$ 92%). For SP112 a slightly lower desorption efficiency of 83.91% was obtained, while the MP500, IRA 458, IRA 958, and IRA 67 anion exchangers were able to regenerate in the range of 65.41% – 78.68%, suggesting the need to look for stronger eluents.

4. Conclusions

Iminodisuccinic acid (IDHA), characterized by high biodegradability and ability to form complexes with many metal ions, was used as a complexing agent in the adsorption process of representatives of rare earth elements (La(III), Nd(III), Ho(III)) on various types of ion exchangers (chelating ion exchangers, cation exchanger, strongly and weakly basic polystyrene and polyacrylate anion exchangers). The study was carried out in single-component systems using static and dynamic methods. The main part of the experiment was preceded by potentiometric measurements to understand the complexation of rare earth elements by IDHA. The LnL type complexes as well as the protonated complexes (LnH_xL) and hydroxycomplexes ($LnL(OH)_x$) were identified in all systems. The adsorption process was optimised by investigating the effects of various factors (ion exchanger mass, Ln(III):IDHA molar ratio, solution pH, contact time, initial concentrations, and temperature) on the process efficiency. These were shown to have a significant effect on the adsorption process of Ln(III)-IDHA complexes. The optimal

process conditions were set as follows:

- ion exchanger mass: 0.1 g;
- metal:ligand molar ratio: 1:1 for the chelating ion exchangers and cation exchanger, 1:2 for all anion exchangers;
- solution pH: 4.0–10.0 for the Ln(III)-IDHA-S957/S950 systems, 2.0–4.0 for the La(III)-IDHA-SP112 system, 2.0 for the Nd(III)/Ho(III)-IDHA-SP112 systems, 10.0 for the Ln(III)-IDHA-strongly basic anion exchangers systems, 4.0 for the Ln(III)-IDHA-IRA 67 systems;
- phase contact time: 30 min (60–120 min for the systems with S950 and IRA 67).

The kinetics of the adsorption process in the Ln(III)-IDHA-S957/SP112 and the Nd(III)/Ho(III)-IDHA strongly basic anion exchanger systems were well described by the PFO model, while the PSO model provided the best fit to the experimental data obtained for the Ln(III)-IDHA-S950/IRA 67 systems and the La(III)-IDHA strongly basic anion exchanger systems. The determined adsorption isotherms allowed the fitting of isotherm models to the experimental data. The data obtained for the Ln(III)-IDHA-chelating ion exchanger systems were consistent with the Temkin model (exception: La(III)-IDHA-S957 - Langmuir model), for the Ln(III)-IDHA-strongly basic anion exchanger systems with the Langmuir model (exception: Nd(III)-IDHA-IRA 458 - Temkin model) and for the Ln(III)-IDHA-IRA 67 systems with the Freundlich model. The chelating ion exchanger S957 showed the highest adsorption capacity towards the La(III) complexes (142.29 mg/g) while the Nd(III) and Ho(III) complexes were best adsorbed by the SP112 cation exchanger (161.04 mg/g for Nd(III) and 201.74 mg/g for Ho(III)). The studies in the column systems confirm the feasibility of application of chelating ion exchangers, cation exchangers, and strongly basic anion exchangers in the adsorption of La(III), Nd(III), and Ho(III) in the presence of IDHA. Iminodisuccinic acid was shown to have very good complexation properties with rare earth elements and can replace poorly biodegradable ligands successfully.

Declaration of Competing Interest

The authors declare the following financial interests/personal relationships which may be considered as potential competing interests: Dorota Kołodyńska reports financial support was provided by NCBiR.

Data availability

No data was used for the research described in the article.

Acknowledgments

The authors are grateful for the financial support from the National Centre of Research and Development under Project No. POIR.04.01.01-00-0040/17-00.

Appendix A. Supplementary data

Supplementary data to this article can be found online at https://doi.org/10.1016/j.cej.2023.142059.

References

[1] L. Birch, R. Bachofen, Complexing agents from microorganisms, Experientia. 46 (1990) 827–834, https://doi.org/10.1007/BF01935533.
[2] B. Nowack, J.M. VanBriesen, Biogeochemistry of chelating agents, Washington, DC, 2005. https://doi.org/10.1021/bk-2005-0910.ch001.
[3] C.K. Schmidt, H.J. Brauch, Aminopolycarboxylate complexing agents, in: Org. Pollut. Water Cycle Prop. Occur. Anal. Environ. Relev. Polar Compd., 2006: pp. 155–180.
[4] F.C. Chang, S.L. Lo, C.H. Ko, Recovery of copper and chelating agents from sludge extracting solutions, Sep. Purif. Technol. 53 (2007) 49–56, https://doi.org/10.1016/j.seppur.2006.06.011.
[5] A.H.M. Veeken, H.V.M. Hamelers, Removal of heavy metals from sewage sludge by extraction with organic acids, Water Sci. Technol. 40 (1999) 129–136, https://doi.org/10.1016/S0273-1223(99)00373-X.
[6] G.P. Nayaka, J. Manjanna, K.V. Pai, R. Vadavi, S.J. Keny, V.S. Tripathi, Recovery of valuable metal ions from the spent lithium-ion battery using aqueous mixture of mild organic acids as alternative to mineral acids, Hydrometallurgy. 151 (2015) 73–77, https://doi.org/10.1016/j.hydromet.2014.11.006.
[7] S.M. Grimes, N.G. Yasri, A.J. Chaudhary, Recovery of critical metals from dilute leach solutions – Separation of indium from tin and lead, Inorganica Chim. Acta. 461 (2017) 161–166, https://doi.org/10.1016/j.ica.2017.02.002.
[8] R. Yang, C. Luo, G. Zhang, X. Li, Z. Shen, Extraction of heavy metals from e-waste contaminated soils using EDDS, J. Environ. Sci. 24 (2012) 1985–1994, https://doi.org/10.1016/S1001-0742(11)61036-X.
[9] D. Lakherwal, Adsorption of heavy metals: A Review, Int. J. Environ. Res. Dev. 4 (2014) 2249–3131, https://doi.org/10.1007/s11270-007-9401-5.
[10] N.H. Othman, N.H. Alias, M.Z. Shahruddin, N.F. Abu Bakar, N.R. Nik Him, W. J. Lau, Adsorption kinetics of methylene blue dyes onto magnetic graphene oxide, J. Environ Chem. Eng. 6 (2018) 2803–2811, https://doi.org/10.1016/j.jece.2018.04.024.
[11] M.R. Dudzinska, D.A. Clifford, Anion exchange studies of lead-EDTA complexes, React. Polym. 16 (1991) 71–80, https://doi.org/10.1016/0923-1137(91)90287-X.
[12] R.S. Juang, S.H. Lin, T.Y. Wang, Removal of metal ions from the complexed solutions in fixed bed using a strong-acid ion exchange resin, Chemosphere. 53 (2003) 1221–1228, https://doi.org/10.1016/S0045-6535(03)00578-2.
[13] C. Escudero, C. Gabaldón, P. Marzal, I. Villaescusa, Effect of EDTA on divalent metal adsorption onto grape stalk and exhausted coffee wastes, J. Hazard. Mater. 152 (2008) 476–485, https://doi.org/10.1016/j.jhazmat.2007.07.013.
[14] N. Kržišnik, A. Mladenovič, A.S. Škapin, L. Škrlep, J. Ščančar, R. Milačič, Nanoscale zero-valent iron for the removal of Zn^{2+}, Zn(II)-EDTA and Zn(II)-citrate from aqueous solutions, Sci. Total Environ. 476–477 (2014) 20–28, https://doi.org/10.1016/j.scitotenv.2013.12.113.
[15] V. Balaram, Rare earth elements: A review of applications, occurrence, exploration, analysis, recycling, and environmental impact, Geosci. Front. 10 (2019) 1285–1303, https://doi.org/10.1016/j.gsf.2018.12.005.
[16] S.B. Castor, J.B. Hedrick, Rare earth elements, in: Ind. Miner. Vol. 7th Ed. Soc. Mining, Metall. Explor. Littleton, Color., 2006: pp. 769–792. https://doi.org/10.1007/978-3-642-35458-8.
[17] S. Massari, M. Ruberti, Rare earth elements as critical raw materials: Focus on international markets and future strategies, Resour. Policy. 38 (2013) 36–43.
[18] E. Commission, Communication from the Commission to the European Parliament, the Council, the European Economic and Social Committee and the Committee of the Regions, Critical Raw Materials Resilience: Charting a Path towards greater Security and Sustainability (2020), https://doi.org/10.1007/978-3-030-40268-6_9.
[19] K. Burdzy, A. Aurich, S. Hunger, R. Jastrząb, M. Zabiszak, D. Kołodyńska, Green citric acid in the sorption process of rare earth elements, Chem. Eng. J. 437 (2022), 135366, https://doi.org/10.1016/j.cej.2022.135366.
[20] S. Lagergren, About the theory of so-called adsorption of soluble substances, K. Sven. Vetenskapsakademiens Handl. 24 (1898) 1–39.
[21] G. Blanchard, M. Maunaye, G. Martin, Removal of heavy metals from waters by means of natural zeolites, Water Res. 18 (1984) 1501–1507, https://doi.org/10.1016/0043-1354(84)90124-6.
[22] W.J. Weber, J.C. Morris, Kinetics of adsorption on carbon from solution, J. Sanit. Eng. Div. 89 (2) (1963) 31–59.
[23] G.E. Boyd, A.W. Adamson, L.S. Myers, The exchange adsorption of ions from aqueous solutions by organic zeolites II. Kinetics, J. Am. Chem. Soc. 69 (1947) 2836–2848.
[24] H.X. Zhu, X.J. Cao, Y.C. He, Q.P. Kong, H. He, J. Wang, Removal of Cu^{2+} from aqueous solutions by the novel modified bagasse pulp cellulose: Kinetics, isotherm and mechanism, Carbohydr. Polym. 129 (2015) 115–126, https://doi.org/10.1016/j.carbpol.2015.04.049.
[25] I. Langmuir, The adsorption of gases on plane surfaces of glass, mica and platinum, J. Am. Chem. Soc. 40 (1918) 1361–1403, https://doi.org/10.1021/ja01340a008.
[26] H.M.F. Freundlich, Over the adsorption in solution, J. Phys. Chem. 57 (1906) 385–471.
[27] M.I. Temkin, V. Pyzhev, Kinetics of ammonia synthesis on promoted iron catalysts, Acta Physicochim. URSS. 12 (1940) 327–356.
[28] H.C. Thomas, Heterogeneous ion exchange in a flowing system, J. Am. Chem. Soc. 66 (1944) 1664–1666, https://doi.org/10.1021/ja01238a017.
[29] G.S. Bohart, E.Q. Adams, Some aspects of the behavior of charcoal with respect to chlorine, J. Am. Chem. Soc. 189 (1920) 669, https://doi.org/10.1016/s0016-0032(20)90400-3.
[30] Y.H. Yoon, J.H. Nelson, Application of gas adsorption kinetics I. A theoretical model for respirator cartridge service life, Am. Ind. Hyg. Assoc. J. 45 (1984) 509–516, https://doi.org/10.1080/15298668491400197.
[31] A. Wolborska, Adsorption on activated carbon of p-nitrophenol from aqueous solution, Water Res. 23 (1989) 85–91, https://doi.org/10.1016/0043-1354(89)90066-3.
[32] H. Hyvönen, M. Orama, H. Saarinen, R. Aksela, Studies on biodegradable chelating ligands: Complexation of iminodisuccinic acid (ISA) with Cu(II), Zn(II), Mn(II) and Fe(III) ions in aqueous solution, Green Chem. 5 (2003) 410–414, https://doi.org/10.1039/b303372b.
[33] Organisation for economic cooperation and development, OECD Guidelines for the testing of chemicals, 1992.
[34] Z. Cokesa, H.J. Knackmuss, P.G. Rieger, Biodegradation of all stereoisomers of the EDTA substitute iminodisuccinate by *Agrobacterium tumefaciens* BY6 requires an

epimerase and a stereoselective C-N lyase, Appl. Environ. Microbiol. 70 (2004) 3941–3947, https://doi.org/10.1128/AEM.70.7.3941-3947.2004.
[35] A.J. Sillanpää, R. Aksela, K. Laasonen, Density functional complexation study of metal ions with (amino) polycarboxylic acid ligands, Phys. Chem. Chem. Phys. 5 (2003) 3382–3393, https://doi.org/10.1039/b303234p.
[36] J.J. Lucena, J.A. Sentís, M. Villén, T. Lao, M. Pérez-Sáez, IDHA chelates as a micronutrient source for green bean and tomato in fertigation and hydroponics, Agron. J. 100 (2008) 813–818, https://doi.org/10.2134/agronj2007.0257.
[37] R. Aksela, J. Peltonen, A. Weckman, Coated seed and method for coating seeds, WO 2004110961 (2003).
[38] H. Hasegawa, I.M.M. Rahman, Y. Egawa, H. Sawai, Z.A. Begum, T. Maki, S. Mizutani, Recovery of indium from end-of-life liquid-crystal display panels using aminopolycarboxylate chelants with the aid of mechanochemical treatment, Microchem. J. 106 (2013) 289–294, https://doi.org/10.1016/j.microc.2012.08.010.
[39] G. Wang, X. Pan, S. Zhang, Q. Zhong, W. Zhou, X. Zhang, J. Wu, M.G. Vijver, W.J.G.M. Peijnenburg, Remediation of heavy metal contaminated soil by biodegradable chelator–induced washing: Efficiencies and mechanisms, Environ. Res. 186 (2020), 109554, https://doi.org/10.1016/j.envres.2020.109554.
[40] L.N. Tolkacheva, V.M. Nikol'skii,, The thermodynamic characteristics of the formation of Al^{3+} ion complexes with iminodisuccinic acid in aqueous solutions, Russ. J. Phys. Chem. A. 86 (2012) 396–398, https://doi.org/10.1134/S0036024412030314.
[41] A. Traboulsi, N. Dupuy, C. Rebufa, M. Sergent, V. Labed, Investigation of gamma radiation effect on the anion exchange resin Amberlite IRA-400 in hydroxide form by Fourier transformed infrared and 13C nuclear magnetic resonance spectroscopies, Anal. Chim. Acta. 717 (2012) 110–121, https://doi.org/10.1016/j.aca.2011.12.046.
[42] G. Socrates, Infrared and Raman characteristic group frequencies., 2001.
[43] H. Uslu, Adsorption equilibria of formic acid by weakly basic adsorbent Amberlite IRA-67: Equilibrium, kinetics, thermodynamic, Chem. Eng. J. 155 (2009) 320–325, https://doi.org/10.1016/j.cej.2009.06.040.
[44] S. Nagireddi, A.K. Golder, R. Uppaluri, Combinatorial optimality of functional groups, process parameters, and Pd(II) adsorption–desorption characteristics for commercial anion exchange resins-synthetic electroless plating systems, Environ. Sci. Pollut. Res. 27 (2020) 24614–24626, https://doi.org/10.1007/s11356-019-05941-1.
[45] S.S. Muhammad, Uranium sorption using Lewatit MonoPlus M500 from sulphate media, Sci. J. Chem. 8 (2020) 7–19. https://doi.org/10.11648/j.sjc.20200801.12.
[46] D. Kołodyńska, Green complexing agent - EDDS in removal of heavy metal ions on strongly basic anion exchangers, Desalination. 280 (2011) 44–57, https://doi.org/10.1016/j.desal.2011.06.060.
[47] A. Shukla, Y.-H. Zhang, P. Dubey, J.L. Margrave, S.S. Shukla, The role of sawdust in the removal of unwanted materials from water, J. Hazard. Mater. B 95 (2002) 137–152, https://doi.org/10.1017/S0017089504001740.
[48] C. Stöhr, J. Horst, W.H. Höll, Application of the surface complex formation model to ion exchange equilibria - Part V. Adsorption of heavy metal salts onto weakly basic anion exchangers, React. Funct. Polym. 49 (2001) 117–132, https://doi.org/10.1016/S1381-5148(01)00067-0.
[49] M.E. González-López, C.M. Laureano-Anzaldo, A.A. Pérez-Fonseca, M. Arellano, J. R. Robledo-Ortíz, A critical overview of adsorption models linearization: methodological and statistical inconsistencies, Sep. Purif. Rev. 51 (2022) 358–372, https://doi.org/10.1080/15422119.2021.1951757.
[50] X. Cao, Q. Wang, S. Wang, R. Man, A novel polystyrene-poly(hydroxamic acid) interpenetrating polymer network and its adsorption towards rare earth ions, J. Rare Earths. 40 (2022) 127–134, https://doi.org/10.1016/j.jre.2020.11.017.
[51] B. Tanhaei, A. Ayati, M. Lahtinen, M. Sillanpää, Preparation and characterization of a novel chitosan/Al_2O_3/magnetite nanoparticles composite adsorbent for kinetic, thermodynamic and isotherm studies of Methyl Orange adsorption, Chem. Eng. J. 259 (2015) 1–10, https://doi.org/10.1016/j.cej.2014.07.109.
[52] G. Darracq, J. Baron, M. Joyeux, Kinetic and isotherm studies on perchlorate sorption by ion-exchange resins in drinking water treatment, J. Water Process Eng. 3 (2014) 123–131, https://doi.org/10.1016/j.jwpe.2014.06.002.
[53] X. Zhao, W. Wu, D. Pan, H. Wu, H. Du, Study on the behaviors and mechanism of Ni(II) adsorption at the hydroxyapatite-water interface: effect of particle size, Adsorpt. Sci. Technol. 2022 (2022) 1–9.
[54] R. Zaidi, S.U. Khan, I.H. Farooqi, A. Azam, Investigation of kinetics and adsorption isotherm for fluoride removal from aqueous solutions using mesoporous cerium-aluminum binary oxide nanomaterials, RSC Adv. 11 (2021) 28744–28760, https://doi.org/10.1039/d1ra00598g.
[55] S. Sahu, N. Bishoyi, R.K. Patel, Cerium phosphate polypyrrole flower like nanocomposite: A recyclable adsorbent for removal of Cr(VI) by adsorption combined with in-situ chemical reduction, J. Ind. Eng. Chem. 99 (2021) 55–67, https://doi.org/10.1016/j.jiec.2021.03.041.
[56] A. Özer, G. Dursun, Removal of methylene blue from aqueous solution by dehydrated wheat bran carbon, J. Hazard. Mater. 146 (2007) 262–269, https://doi.org/10.1016/j.jhazmat.2006.12.016.
[57] D. Kim, Y. Ren, M. Cui, Y. Lee, J. Kim, O. Kwon, W. Ji, J. Khim, Arsenic adsorption on two types of powdered and beaded coal mine drainage sludge adsorbent, Chemosphere. 272 (2021), 129560, https://doi.org/10.1016/j.chemosphere.2021.129560.
[58] A. Proctor, J.F. Toro-Vazquez, The Freundlich isotherm in studying adsorption in oil processing, J. Am. Oil Chem. Soc. 73 (1996) 1627–1633, https://doi.org/10.1016/B978-1-893997-91-2.50016-X.
[59] A.O. Dada, A.P. Olalekan, A.M. Olatunya, O. Dada, Langmuir, Freundlich, Temkin and Dubinin-Radushkevich isotherms studies of equilibrium sorption of Zn^{2+} unto phosphoric acid modified rice husk, IOSR J. Appl. Chem. 3 (2012) 38–45, https://doi.org/10.9790/5736-0313845.
[60] N.K. Soliman, A.F. Moustafa, Industrial solid waste for heavy metals adsorption features and challenges; a review, J. Mater. Res. Technol. 9 (2020) 10235–10253, https://doi.org/10.1016/j.jmrt.2020.07.045.
[61] Z. Aksu, A.I. Tatli, Ö. Tunç, A comparative adsorption/biosorption study of Acid Blue 161: Effect of temperature on equilibrium and kinetic parameters, Chem. Eng. J. 142 (2008) 23–39, https://doi.org/10.1016/j.cej.2007.11.005.
[62] A.E. Ofomaja, Y.S. Ho, Equilibrium sorption of anionic dye from aqueous solution by palm kernel fibre as sorbent, Dye. Pigment. 74 (2007) 60–66, https://doi.org/10.1016/j.dyepig.2006.01.014.
[63] H.S. Niasar, S. Das, C.(. Xu, M.B. Ray, Continuous column adsorption of naphthenic acids from synthetic and real oil sands process-affected water (OSPW) using carbon-based adsorbents, Chemosphere. 214 (2019) 511–518.
[64] B. Kiran, A. Kaushik, Cyanobacterial biosorption of Cr(VI): Application of two parameter and Bohart Adams models for batch and column studies, Chem. Eng. J. 144 (2008) 391–399, https://doi.org/10.1016/j.cej.2008.02.003.
[65] O. Hamdaoui, Dynamic sorption of methylene blue by cedar sawdust and crushed brick in fixed bed columns, J. Hazard. Mater. 138 (2006) 293–303, https://doi.org/10.1016/j.jhazmat.2006.04.061.

Supplementary Materials

Iminodisuccinic acid (IDHA) as an effective biodegradable complexing agent in the adsorption process of La(III), Nd(III) and Ho(III) ions

Katarzyna Burdzy[a]*, Yongming Ju[b], Dorota Kołodyńska[a]*

[a]Department of Inorganic Chemistry, Faculty of Chemistry, Maria Curie-Skłodowska University, M. Curie Skłodowska Sq. 2, 20-031 Lublin, Poland

[b]South China Institute of Environmental Sciences, Ministry of Environmental Protection, Guangzhou 510655, P. R. China; Laboratory of Pesticide Environmental Assessment and Pollution Control, Nanjing Institute of Environmental Sciences, Ministry of Ecology and Environment (MEE); Nanjing 210042, P. R. China; The Key Laboratory of Water and Air Pollution Control of Guangdong Province, South China Institute of Environmental Sciences, Ministry of Ecology and Environment (MEE), Guangzhou 510655, P. R. China

1. Apparatus and instruments

The static method of adsorption was performed using the laboratory shakers Elpin type 357 and Elpin type 358A (Elpin Plus, Poland). The pH of the solutions was measured by the pHmeter pHM82 (Radiometer, Copenhagen).

The Ln(III) ions concentration was analysed by the inductively coupled plasma optical emission spectrometry using ICP-OES 720-ES (Varian, USA) at 333.749 nm for La(III), 401.224 nm for Nd(III) and 345.600 nm for Ho(III). The calibration of the ICP-OES instrument was performed using the ICP standards. All standards and blank samples were prepared applying ultrapure nitric acid to avoid matrix interference. The relative standard deviation (RSD) for the triplicate analysis was within 5%.

The surface morphology of the ion exchangers was studied by the scanning electron microscopy (SEM) using the Quanta 3D FEG microscope with the EDS (Energy Dispersive Spectroscopy)/EBSD (Electron Backscatter Diffraction) system (FEI, USA). The SEM images were recorded at the magnifications of 10,000x.

The presence of the assumed functional groups on the surface of the ion exchangers was analyzed by the Fourier transform infrared (FTIR) spectroscopy (Cary 630 spectrometer with the attenuated total reflectance mode (ATR-FTIR), Agilent Technologies). FTIR spectra were recorded over the interval 4000-650 cm^{-1}.

The 907 Titrando titrator equipped with the 800 Dosino type dosing system with the combined pH electrode Metrohm 6.0259.100, 801 type magnetic stirrer and Pt 1000 temperature sensor (Metrohm) was used to perform potentiometric titrations.

2. Potentiometric measurements

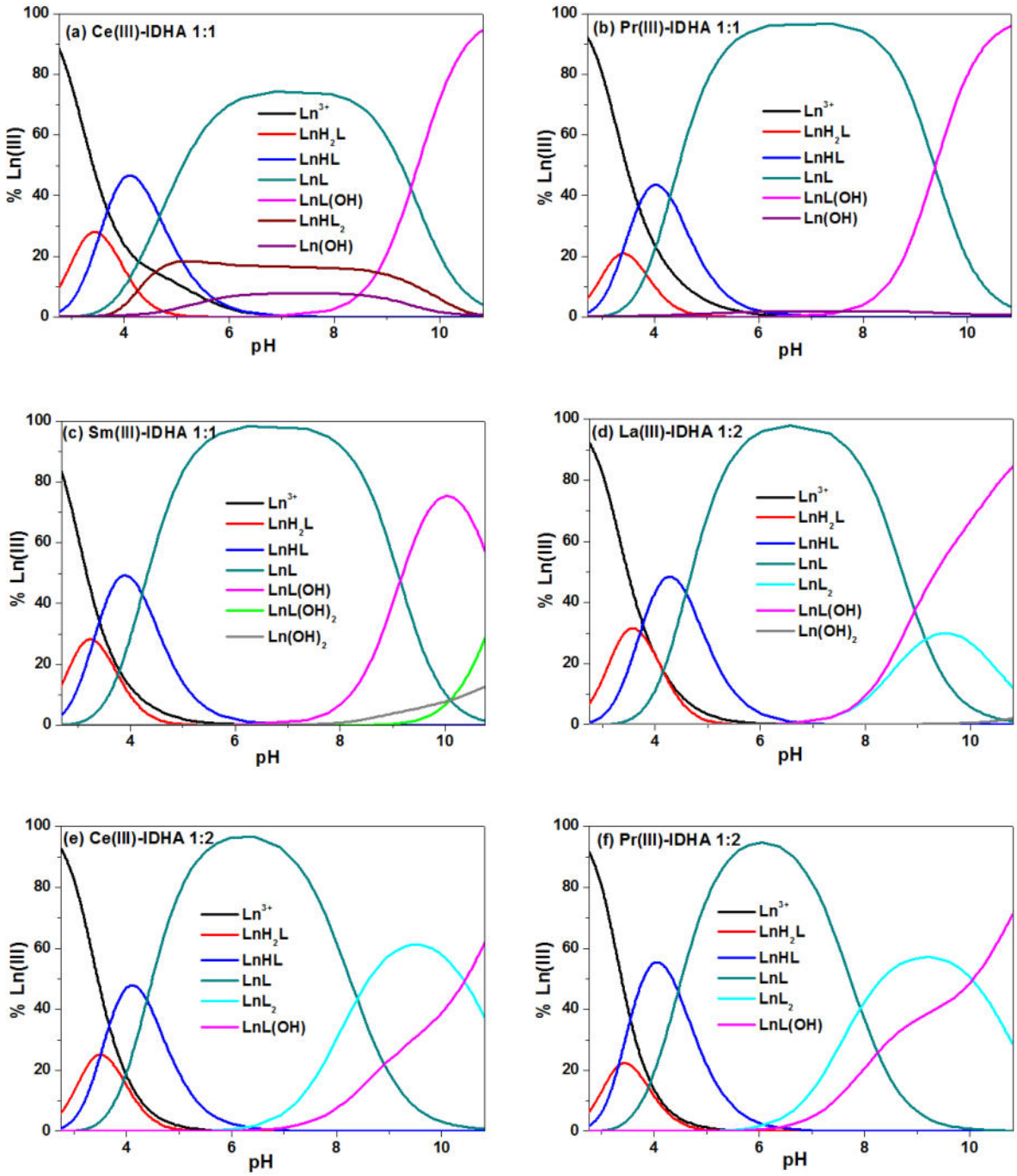

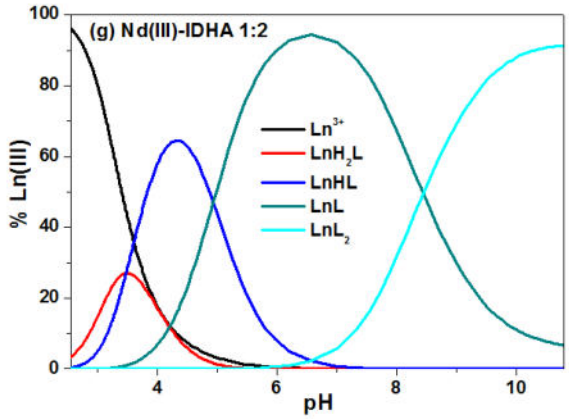
(g) Nd(III)-IDHA 1:2
% Ln(III)
pH
Ln3+
LnH2L
LnHL
LnL
LnL2

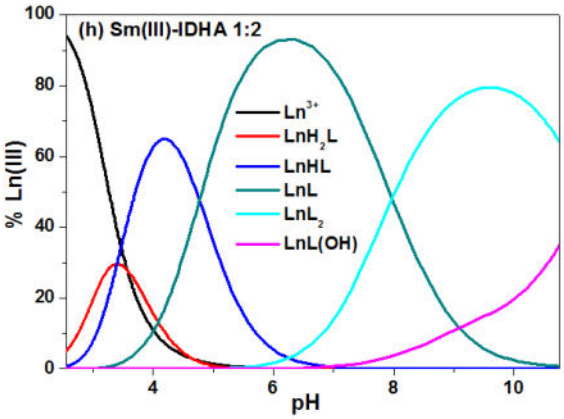
(h) Sm(III)-IDHA 1:2
% Ln(III)
pH
Ln3+
LnH2L
LnHL
LnL
LnL2
LnL(OH)

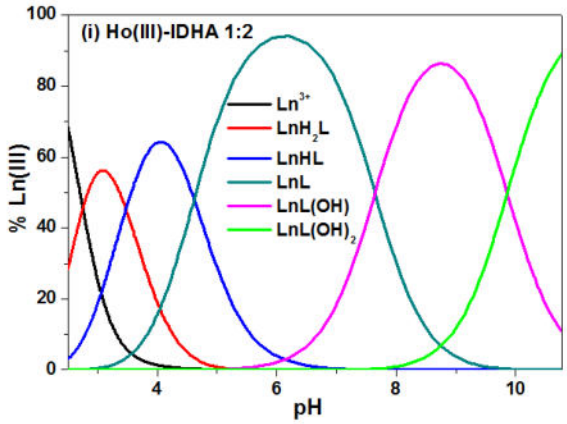
(i) Ho(III)-IDHA 1:2
% Ln(III)
pH
Ln3+
LnH2L
LnHL
LnL
LnL(OH)
LnL(OH)2

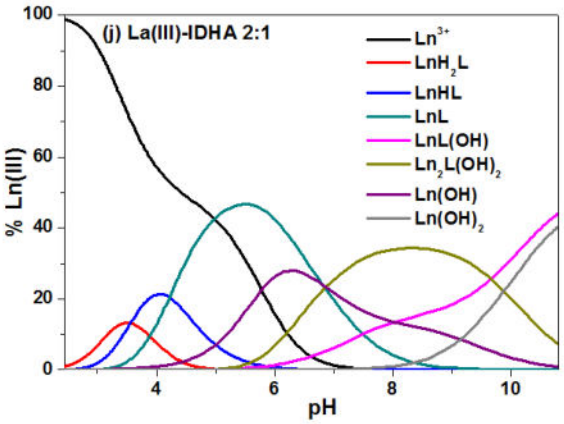
(j) La(III)-IDHA 2:1
% Ln(III)
pH
Ln3+
LnH2L
LnHL
LnL
LnL(OH)
Ln2L(OH)2
Ln(OH)
Ln(OH)2

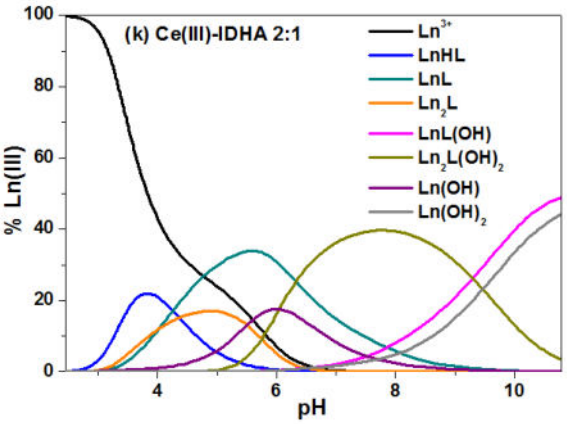
(k) Ce(III)-IDHA 2:1
% Ln(III)
pH
Ln3+
LnHL
LnL
Ln2L
LnL(OH)
Ln2L(OH)2
Ln(OH)
Ln(OH)2

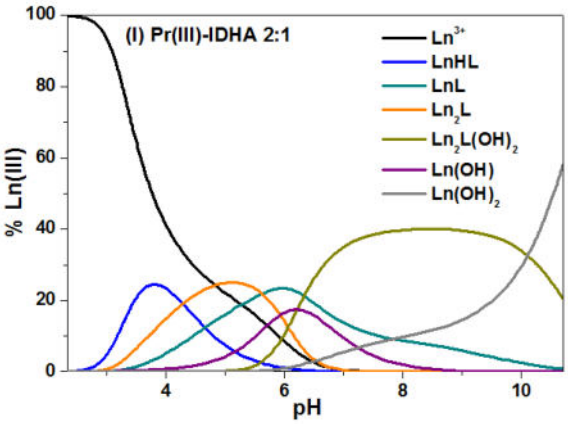
(l) Pr(III)-IDHA 2:1
% Ln(III)
pH
Ln3+
LnHL
LnL
Ln2L
Ln2L(OH)2
Ln(OH)
Ln(OH)2

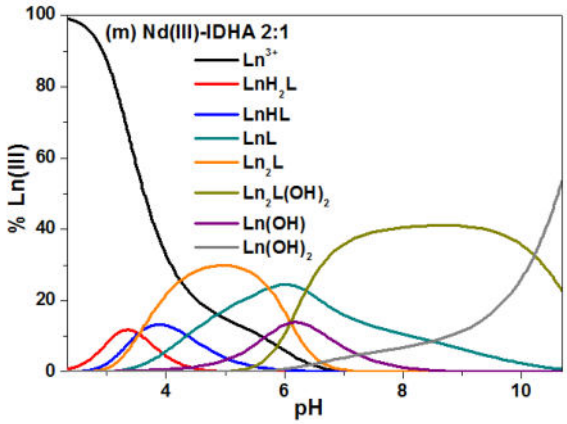
(m) Nd(III)-IDHA 2:1
% Ln(III)
pH
Ln3+
LnH2L
LnHL
LnL
Ln2L
Ln2L(OH)2
Ln(OH)
Ln(OH)2

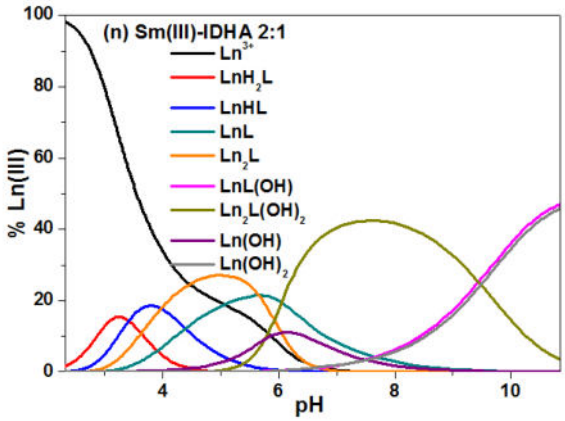
(n) Sm(III)-IDHA 2:1
% Ln(III)
pH
Ln3+
LnH2L
LnHL
LnL
Ln2L
LnL(OH)
Ln2L(OH)2
Ln(OH)
Ln(OH)2

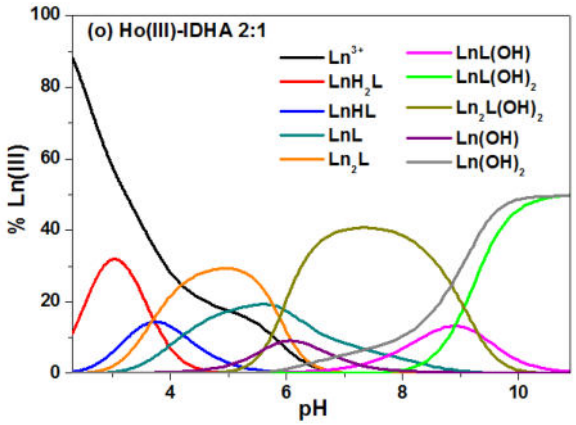

Figure S1. Distribution diagrams for the Ln(III)-L systems (where Ln=La(III), Ce(III), Pr(III), Nd(III), Sm(III), Ho(III) and L=IDHA): (a-c) Ln(III)-L 1:1, (d-i) Ln(III)-L 1:2, (j-o) Ln(III)-L 2:1.

Table S1. The overall stability constants (logβ) and the equilibrium constants of complex formation (logK_e) in the systems of Ln(III)-L (where Ln=Ce(III), Pr(III), Sm(III) and L=IDHA) for various metal:ligand ratios.

Species	1:1			1:2			2:1		
	logβ	SD	logK_e	logβ	SD	logK_e	logβ	SD	logK_e
Ce(III)-IDHA									
LnH_2L	18.27	0.02	**3.59**	18.05	0.06	**3.38**	-	-	-
LnHL	14.72	0.01	**4.61**	14.54	0.03	**4.42**	14.67	0.04	**4.55**
LnL	10.05	0.02	**10.05**	10.15	0.03	**10.15**	10.40	0.06	**10.40**
LnL(OH)	0.60	0.01	**4.32**	1.24	0.08	**4.86**	2.55	0.07	**5.92**
$LnHL_2$	24.08	0.05	**3.91**	-	-	-	-	-	-
LnL_2	-	-	-	15.38	0.08	**5.22**	-	-	-
Ln_2L	-	-	-	-	-	-	13.79	0.10	**3.39**
$Ln_2L(OH)_2$	-	-	-	-	-	-	2.29	0.05	**13.51**
Pr(III)-IDHA									
LnH_2L	18.15	0.02	**3.47**	18.06	0.04	**3.39**	-	-	-
LnHL	14.77	0.01	**4.66**	14.74	0.02	**4.62**	14.93	0.03	**4.81**
LnL	10.47	0.01	**10.47**	10.28	0.02	**10.28**	10.27	0.08	**10.27**
LnL(OH)	1.10	0.01	**4.39**	2.04	0.05	**5.53**	-	-	-
LnL_2	-	-	-	15.91	0.05	**5.63**	-	-	-
Ln_2L	-	-	-	-	-	-	14.14	0.06	**3.87**
$Ln_2L(OH)_2$	-	-	-	-	-	-	2.03	0.04	**5.53**
Sm(III)-IDHA									
LnH_2L	18.62	0.01	**3.94**	18.32	0.03	**3.64**	18.56	0.05	**3.88**
LnHL	15.32	0.01	**5.20**	14.92	0.02	**4.80**	15.14	0.04	**5.02**
LnL	11.09	0.01	**11.09**	10.15	0.03	**10.15**	10.75	0.07	**10.75**
LnL(OH)	1.95	0.01	**4.63**	1.05	0.08	**4.67**	3.08	0.05	**6.10**
$LnL(OH)_2$	-9.11	0.02	**2.71**	-	-	-	-	-	-

LnL_2	-	-	-	15.82	0.06	**5.67**	-	-	-
Ln_2L	-	-	-	-	-	-	14.65	0.06	**3.90**
$Ln_2L(OH)_2$	-	-	-	-	-	-	2.81	0.04	**13.50**

SD - standard deviation

3. The characterization of ion exchangers

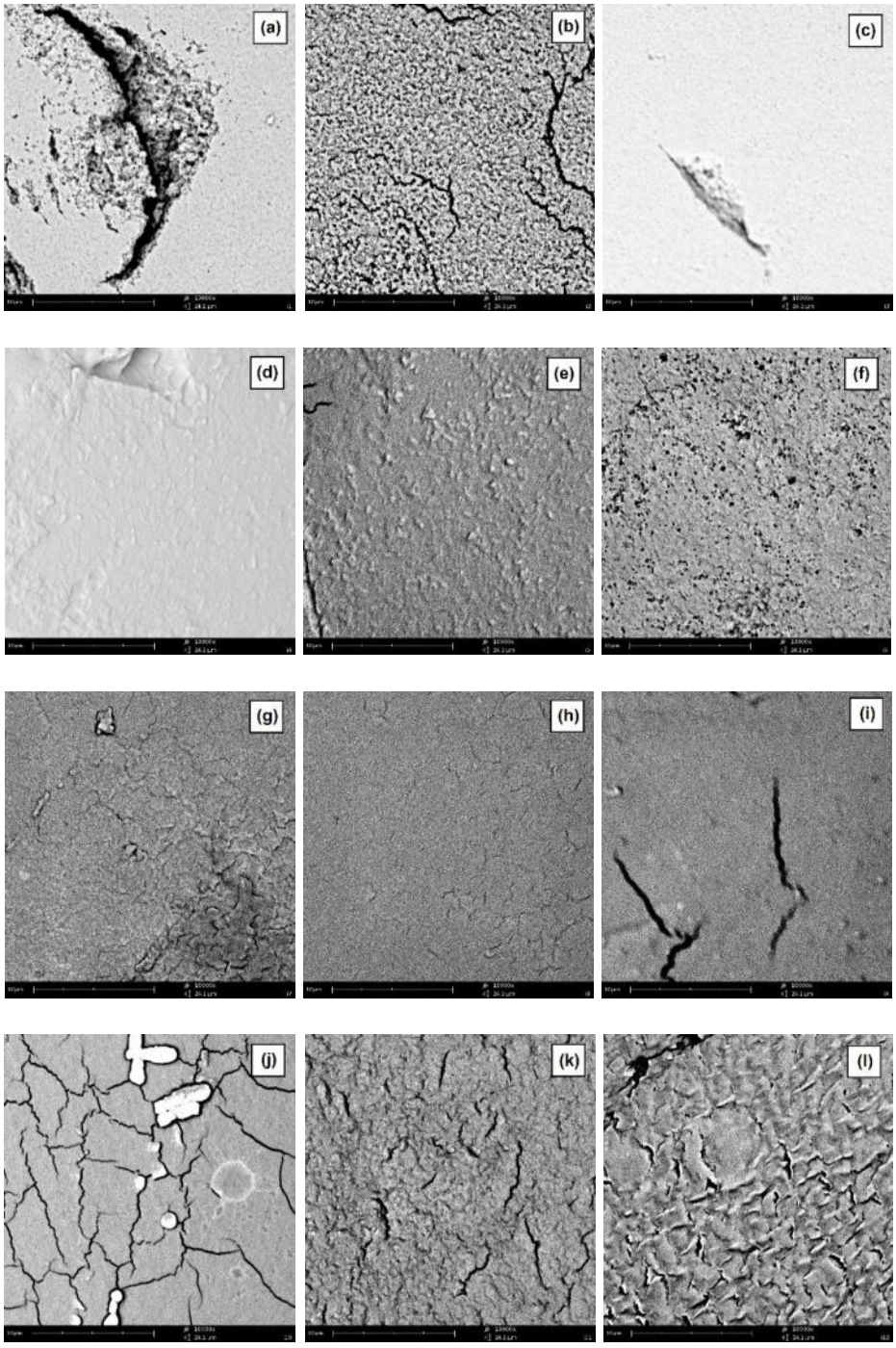

Figure S2. SEM images of (a) S957, (b) S950, (c) SP112, (d) M500, (e) M600, (f) MP500, (g) 4200, (h) 4400, (i) 4600, (j) IRA 458, (k) IRA 958, and (l) IRA 67 after the adsorption of La(III) ions in the presence of IDHA (magnification × 10,000).

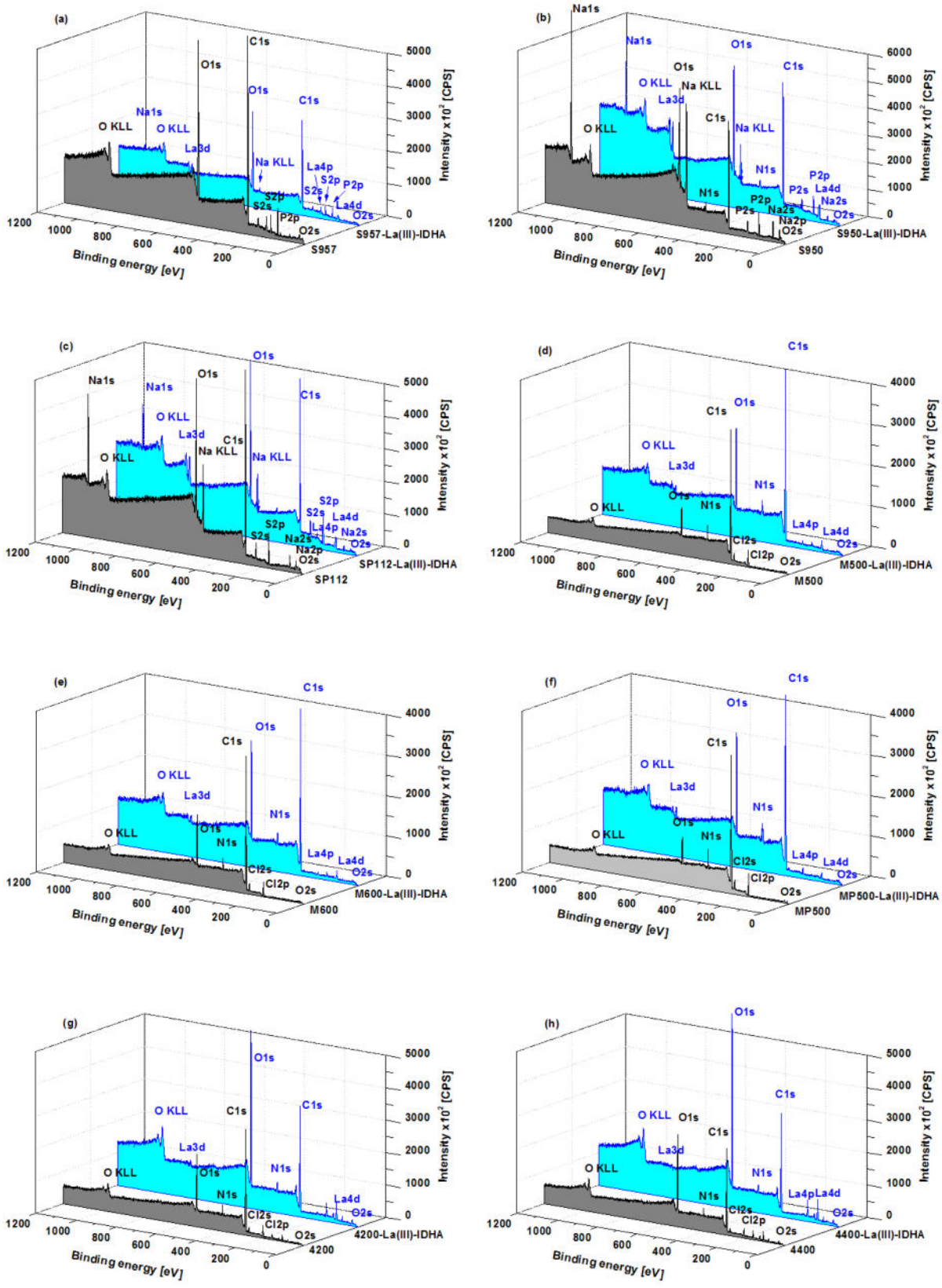
(a)
C1s
O1s
O1s
C1s
Na1s
O KLL
O KLL
La3d
Na KLL
La4p
S2p
P2p
S2s
S2p
La4d
S2s
O2s
P2p
O2s
S957
S957-La(III)-IDHA
(b)
Na1s
Na1s
O1s
O1s
C1s
O KLL
Na KLL
La3d
C1s
O KLL
Na KLL
N1s
P2p
N1s
P2s
P2p
La4d
P2s
Na2s
Na2p
O2s
O2s
S950
S950-La(III)-IDHA
(c)
O1s
Na1s
Na1s
O1s
C1s
O KLL
La3d
C1s
Na KLL
O KLL
Na KLL
S2p
S2s
La4d
S2p
La4p
Na2s
S2s
Na2s
O2s
Na2p
O2s
SP112
SP112-La(III)-IDHA
(d)
C1s
C1s
O1s
O KLL
La3d
N1s
O1s
N1s
O KLL
La4p
La4d
Cl2s
O2s
Cl2p
O2s
M500
M500-La(III)-IDHA
(e)
C1s
O1s
C1s
O KLL
La3d
N1s
O KLL
O1s
N1s
La4p
La4d
Cl2s
O2s
Cl2p
O2s
M600
M600-La(III)-IDHA
(f)
C1s
O1s
C1s
O KLL
La3d
N1s
O KLL
O1s
N1s
Cl2s
La4p
La4d
Cl2p
O2s
O2s
MP500
MP500-La(III)-IDHA
(g)
O1s
O KLL
C1s
C1s
La3d
O KLL
O1s
N1s
N1s
Cl2s
La4d
Cl2p
O2s
O2s
4200
4200-La(III)-IDHA
(h)
O1s
C1s
O KLL
O1s
C1s
La3d
O KLL
N1s
N1s
La4pLa4d
Cl2s
Cl2p
O2s
O2s
4400
4400-La(III)-IDHA
Intensity x10² [CPS]
Binding energy [eV]

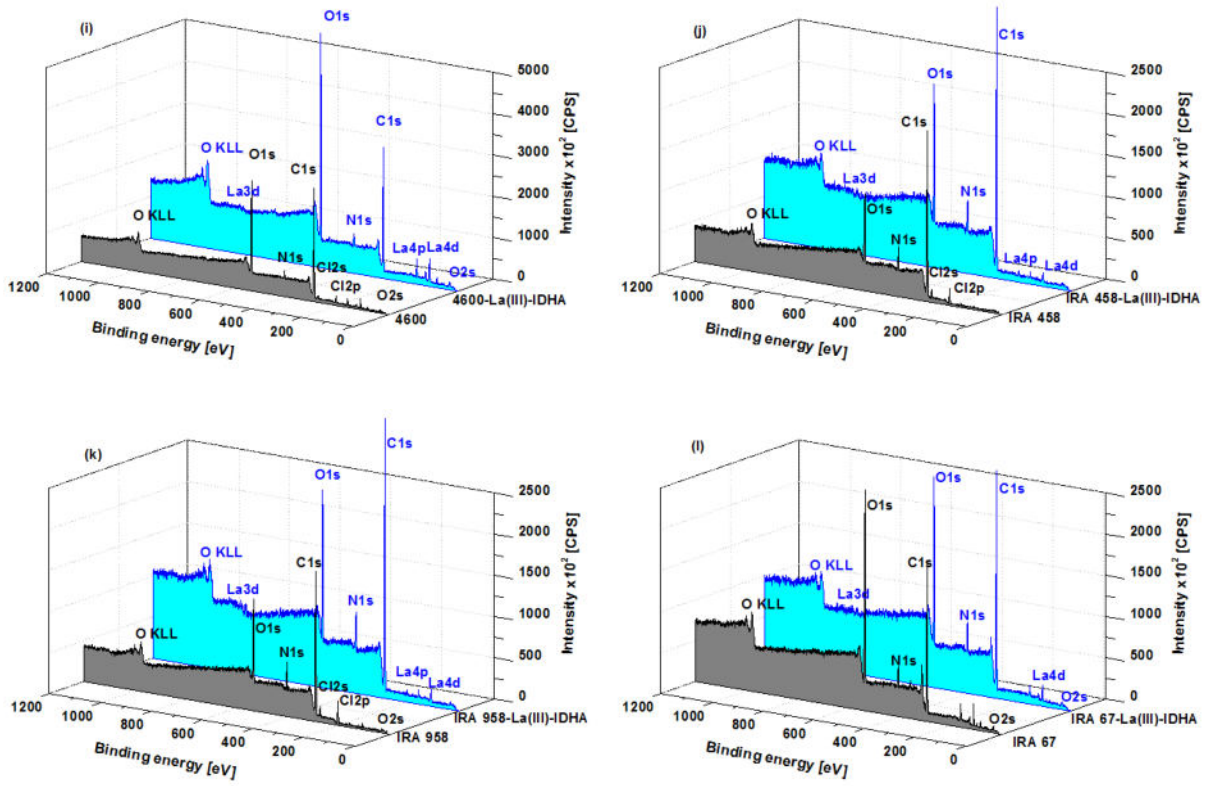

Figure S3. XPS spectra of (a) S957, (b) S950, (c) SP112, (d) M500, (e) M600, (f) MP500, (g) 4200, (h) 4400, (i) 4600, (j) IRA 458, (k) IRA 958, and (l) IRA 67 before and after the adsorption of La(III) ions in the presence of IDHA.

Table S2. The elemental composition (C_{at}) and binding energies (E_B) for M500, M600, MP500, 4200, 4400, 4600, IRA 458, IRA 958, and IRA 67 before and after the adsorption of La(III) ions in the presence of IDHA obtained by XPS analysis.

Level	M500		M500 + La(III)-IDHA		M600		M600 + La(III)-IDHA		MP500		MP500 + La(III)-IDHA	
	E_B [eV]	C_{at} [%]	E_B [eV]	C_{at} [%]	E_B [eV]	C_{at} [%]	E_B [eV]	C_{at} [%]	E_B [eV]	C_{at} [%]	E_B [eV]	C_{at} [%]
C 1s	284.7	83.0	284.7	78.1	284.7	79.8	284.7	76.2	284.7	81.2	284.7	76.7
O 1s	532.2	8.0	530.7	15.0	532.2	10.6	531.5	16.4	532.2	7.0	531.5	16.1
N 1s	402.5	4.0	401.7	4.8	402.5	4.7	401.7	4.8	402.5	5.6	402.5	6.9
Cl 2p	197.0	5.0	-	-	197.0	4.2	-	-	197.0	6.2	-	-
Si 2p	-	-	152.7	1.9	101.7	0.8	152.7	2.5	-	-	-	-
La 3d	-	-	854.0	0.2	-	-	834.5	0.1	-	-	834.5	0.3
Level	**4200**		**4200 + La(III)-IDHA**		**4400**		**4400 + La(III)-IDHA**		**4600**		**4600 + La(III)-IDHA**	
	E_B [eV]	C_{at} [%]	E_B [eV]	C_{at} [%]	E_B [eV]	C_{at} [%]	E_B [eV]	C_{at} [%]	E_B [eV]	C_{at} [%]	E_B [eV]	C_{at} [%]
C 1s	284.7	70.2	284.7	54.0	284.7	62.5	284.7	54.6	284.7	65.9	284.7	54.2
O 1s	531.5	16.2	531.5	26.2	532.2	22.3	531.5	30.4	532.2	20.8	531.5	29.4
N 1s	402.5	3.5	399.5	3.4	402.5	2.8	399.5	3.3	402.5	2.5	400.2	3.4
Cl 2p	197.0	3.4	-	-	197.0	2.7	-	-	197.7	1.9	-	-

Si 2p	101.7	5.0	153.5	7.5	103.0	6.1	152.7	9.7	102.5	6.1	152.7	8.8
Al 2p	74.0	1.7	74.0	8.8	74.7	3.6	74.0	1.9	74.0	2.8	74.0	3.4
Ca 2p	-	-	-	-	-	-	-	-	-	-	350.7	0.6
La 3d	-	-	836.7	0.1	-	-	833.0	0.2	-	-	835.2	0.2
Level	**IRA 458**		**IRA 458 + La(III)-IDHA**		**IRA 958**		**IRA 958 + La(III)-IDHA**		**IRA 67**		**IRA 67 + La(III)-IDHA**	
	E_B [eV]	C_{at} [%]	E_B [eV]	C_{at} [%]	E_B [eV]	C_{at} [%]	E_B [eV]	C_{at} [%]	E_B [eV]	C_{at} [%]	E_B [eV]	C_{at} [%]
C 1s	284.7	76.9	284.7	77.2	284.7	73.7	284.7	76.5	284.7	57.3	284.7	68.0
O 1s	531.5	13.4	530.7	16.2	531.5	14.9	530.7	15.9	531.5	26.4	531.5	18.7
N 1s	398.7	6.4	398.7	5.5	398.7	6.3	398.7	5.7	399.5	3.9	398.7	5.6
Cl 2p	196.2	2.6	-	-	196.2	4.0	-	-	-	-	-	-
Si 2p	101.0	0.7	152.7	1.0	101.0	1.2	152.7	1.8	101.7	9.2	153.5	3.3
Al 2p	-	-	-	-	-	-	-	-	74.0	2.6	-	-
Ca 2p	-	-	-	-	-	-	-	-	350.7	0.7	350.7	4.3
La 3d	-	-	833.7	0.1	-	-	833.7	0.1	-	-	834.5	0.1

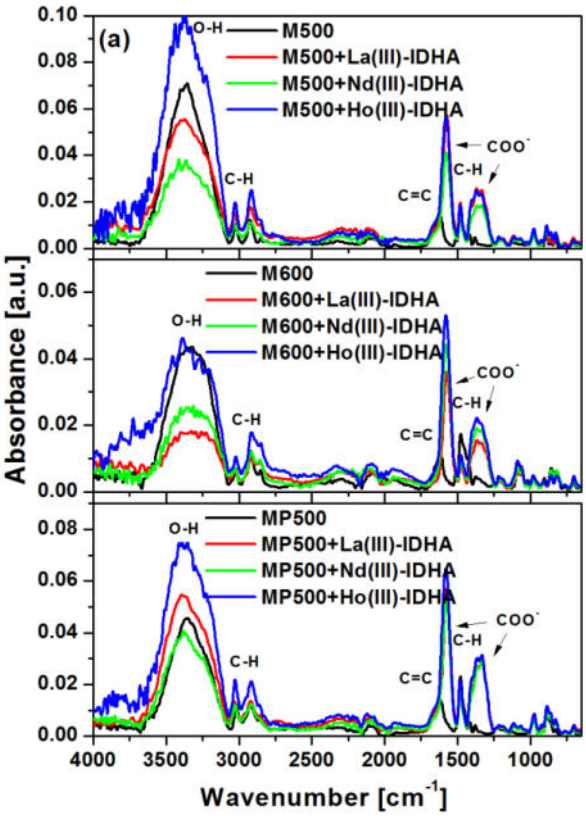

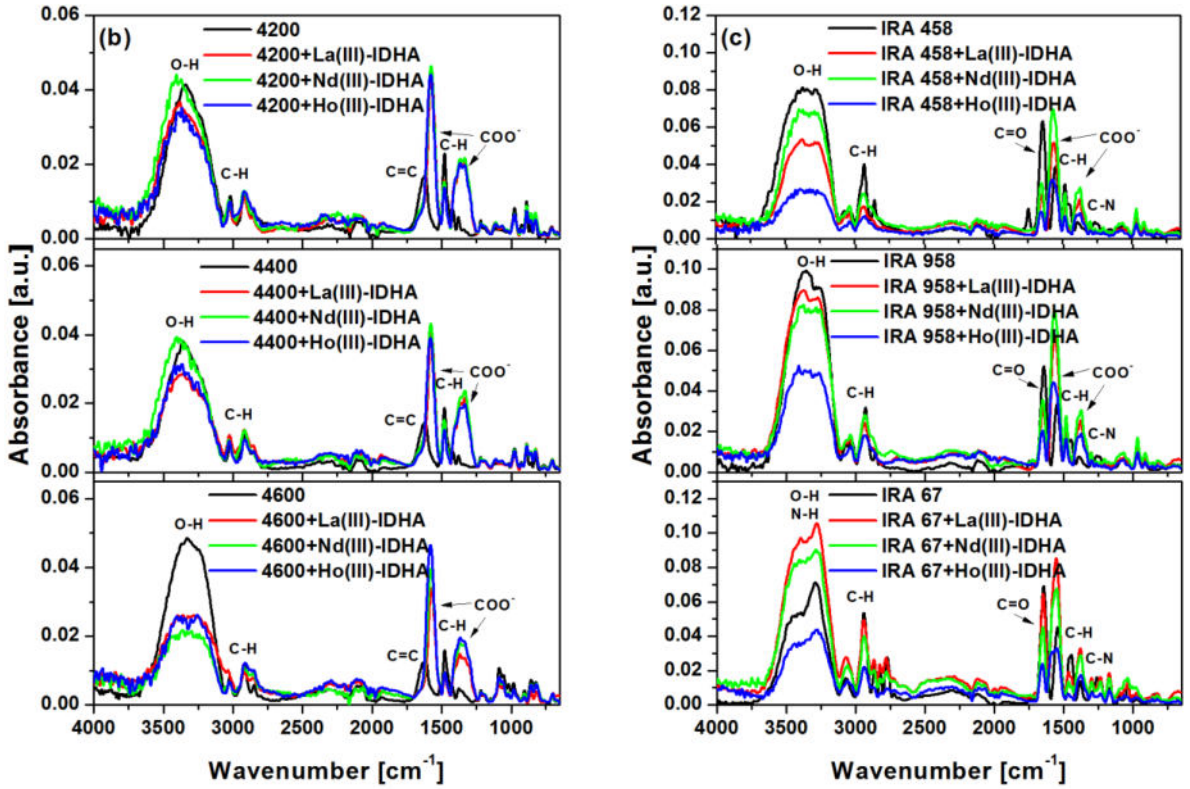

Figure S4. FTIR spectra for (a) M500, M600, MP500, (b) 4200, 4400, 4600 and (c) IRA 458, IRA 958, IRA 67 before and after the adsorption of La(III), Nd(III) and Ho(III) ions in the presence of IDHA.

4. Kinetic and adsorption studies

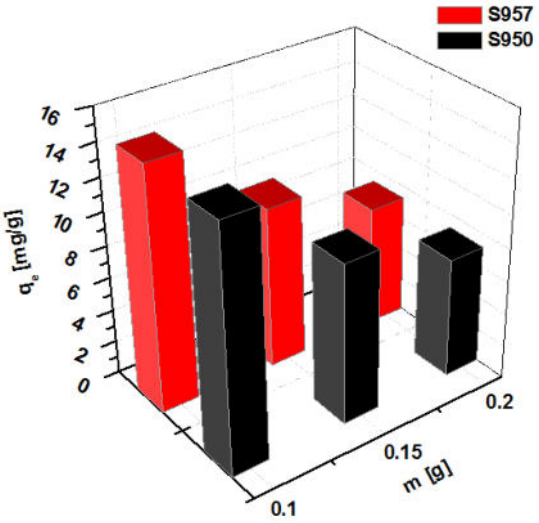

Figure S5. The effect of ion exchanger mass on the La(III)-IDHA complexes sorption on S957 and S950.

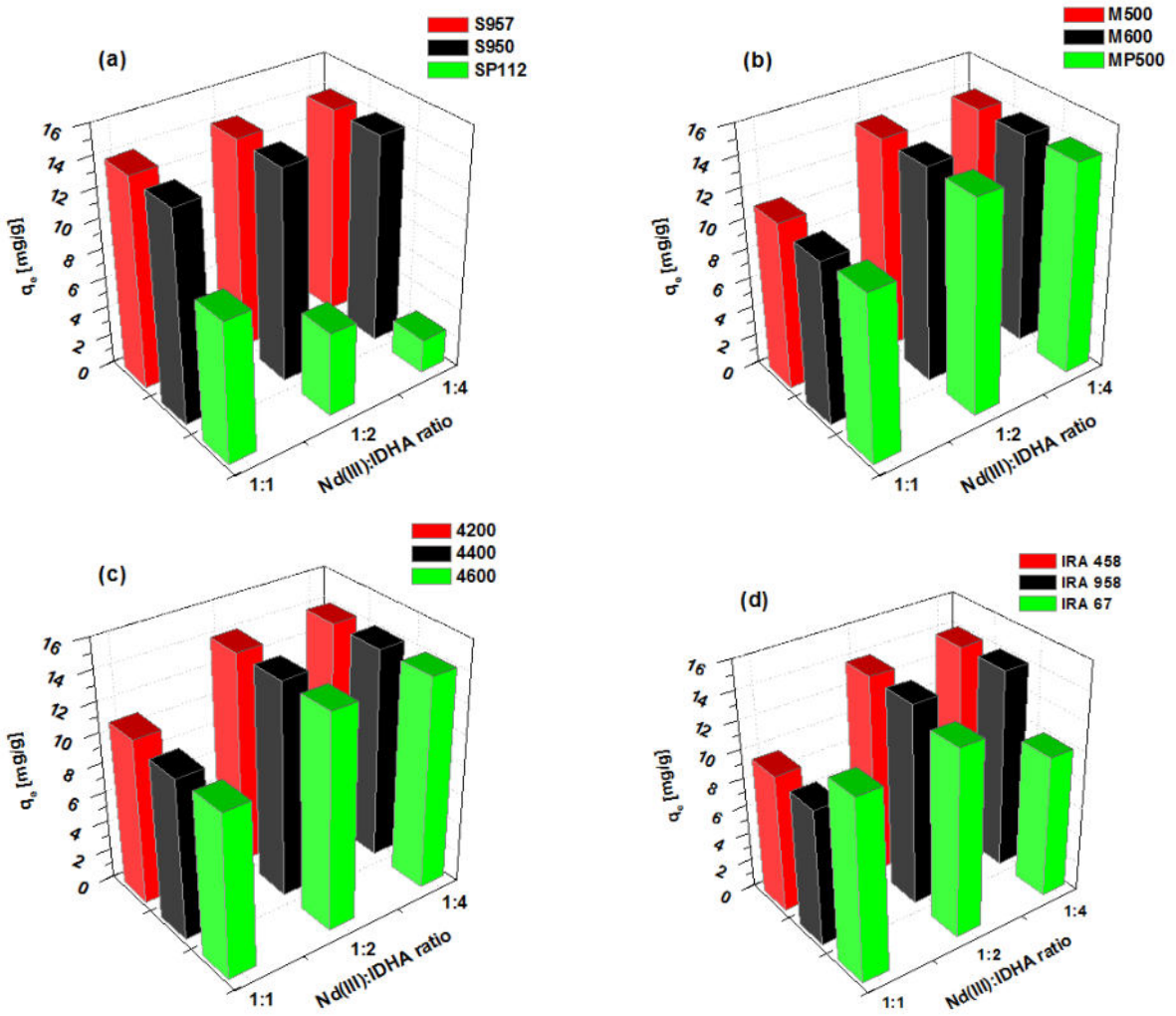

Figure S6. The effect of the Ln(III):IDHA molar ratio on the sorption of Nd(III)-IDHA complexes on (a) S957, S950, SP112, (b) M500, M600, MP500, (c) 4200, 4400, 4600 and (d) IRA 458, IRA 958, IRA 67.

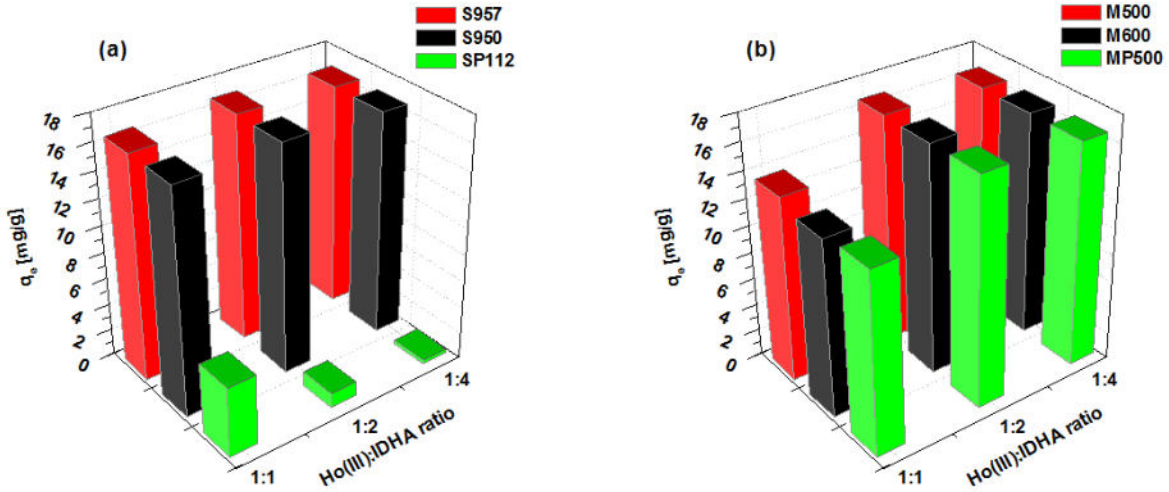

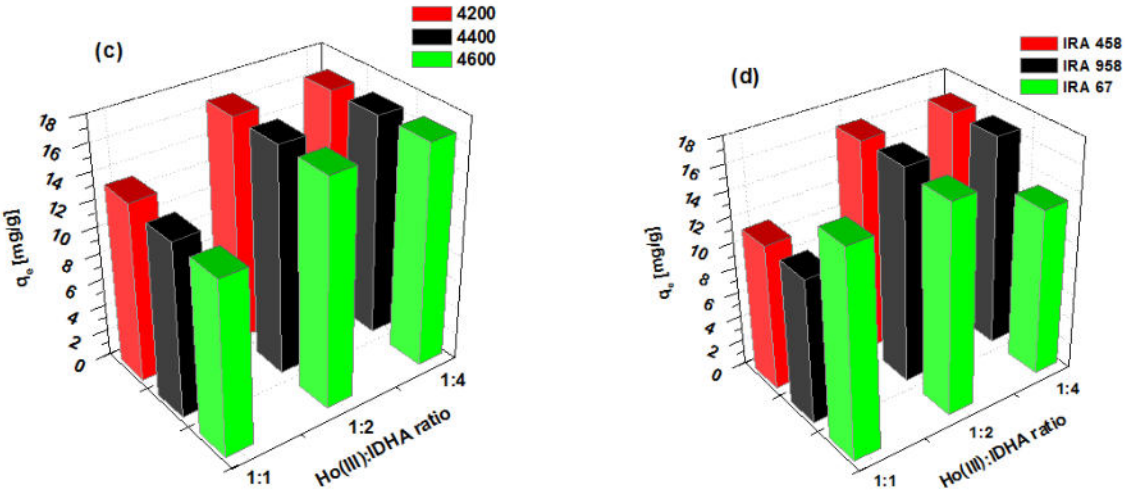

Figure S7. The effect of the Ln(III):IDHA molar ratio on the sorption of Ho(III)-IDHA complexes on (a) S957, S950, SP112, (b) M500, M600, MP500, (c) 4200, 4400, 4600 and (d) IRA 458, IRA 958, IRA 67.

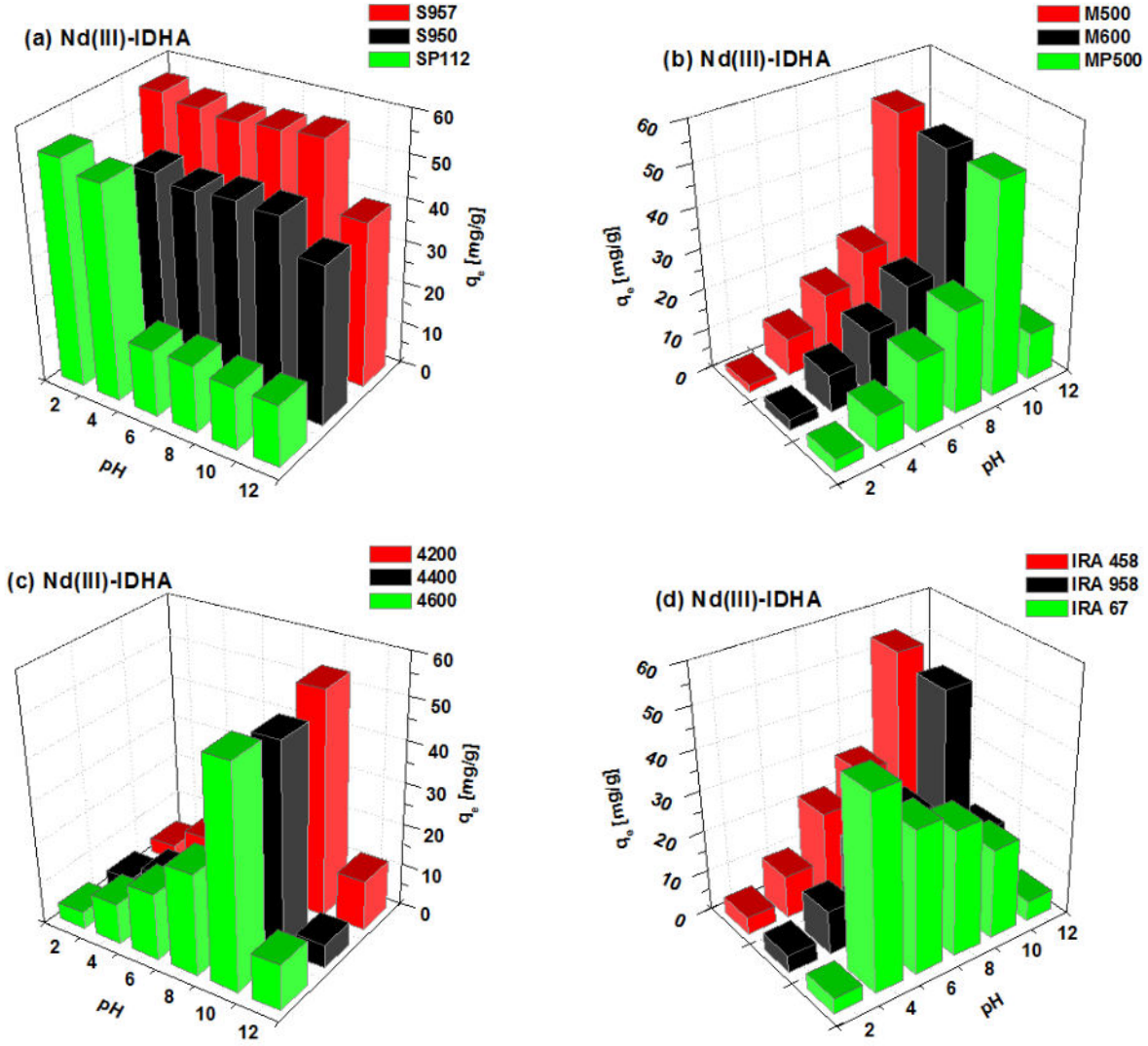

Figure S8. The effect of pH on the sorption of Nd(III)-IDHA complexes on (a) S957, S950, SP112, (b) M500, M600, MP500, (c) 4200, 4400, 4600 and (d) IRA 458, IRA 958, IRA 67.

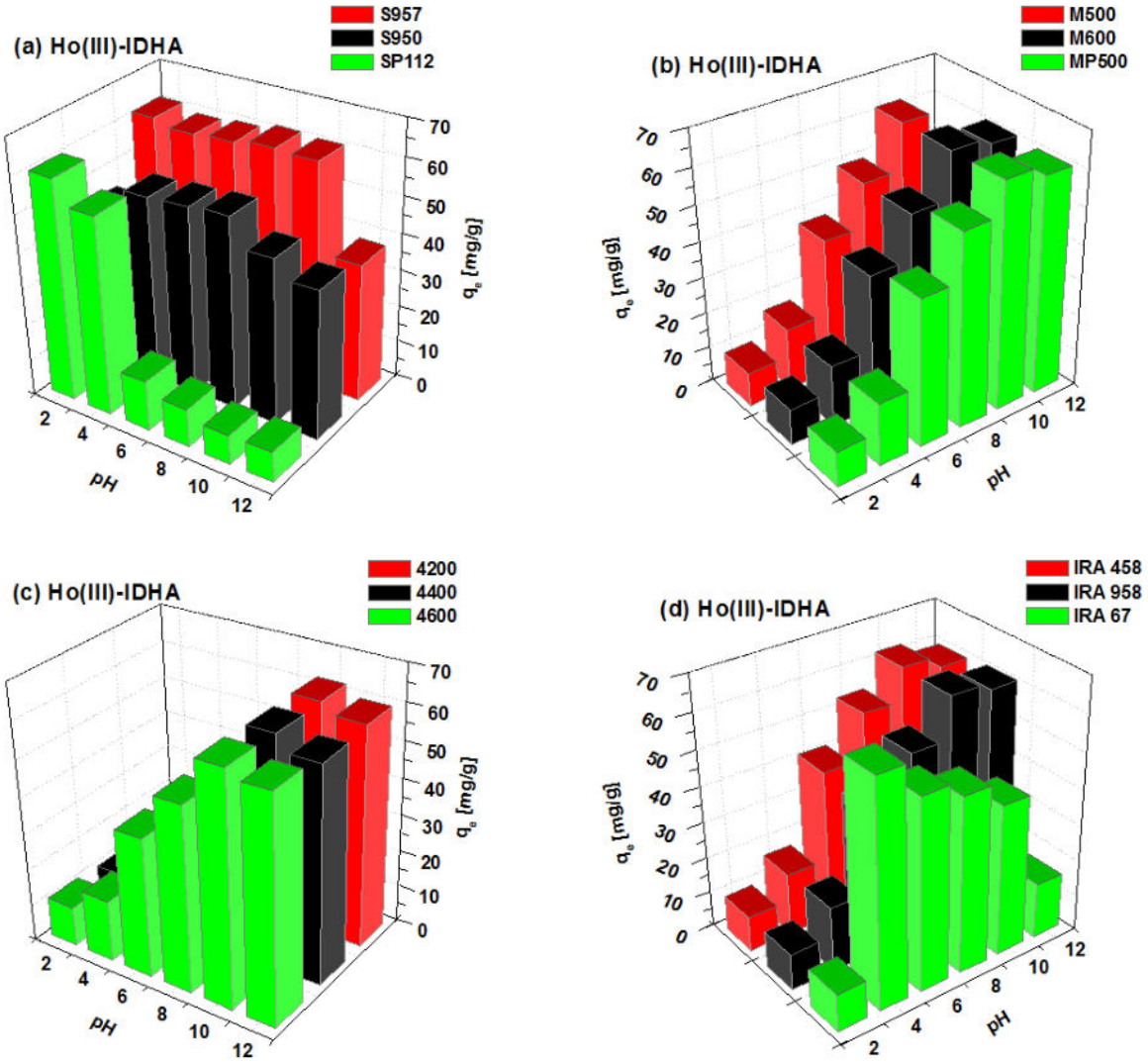

Figure S9. The effect of pH on the sorption of Ho(III)-IDHA complexes on (a) S957, S950, SP112, (b) M500, M600, MP500, (c) 4200, 4400, 4600 and (d) IRA 458, IRA 958, IRA 67.

Table S3. Kinetic parameters for the pseudo-first order and pseudo-second order kinetic models for the La(III)-IDHA complexes sorption on S957, S950, SP112, M500, M600, MP500, 4200, 4400, 4600, IRA 458, IRA 958, IRA 67 (C_0=0.5×10^{-3} M - 2.5×10^{-3} M).

Model			**Pseudo-First Order**				**Pseudo-Second Order**			
Ion exchanger	C_o ×10^{-3} [M]	$q_{e.exp}$ [mg/g]	$q_{1.cal}$ [mg/g]	k_1 [1/min]	R^2	χ^2	$q_{2.cal}$ [mg/g]	k_2 [g/mg min]	R^2	χ^2
S957	0.5	6.85	6.93	0.390	0.972	0.086	7.30	0.087	0.854	0.450
	1.0	13.11	13.06	0.504	0.973	0.162	13.67	0.067	0.932	0.415
	1.5	22.34	22.41	0.461	0.997	0.065	23.48	0.035	0.912	1.912
	2.0	29.01	29.17	0.442	0.988	0.451	30.55	0.026	0.899	3.877
	2.5	37.20	37.06	0.390	0.978	1.382	38.86	0.018	0.941	3.760
S950	0.5	7.65	6.95	0.118	0.803	0.843	7.55	0.021	0.904	0.409
	1.0	14.63	14.03	0.175	0.682	3.750	14.64	0.021	0.820	2.122

	1.5	23.18	22.64	0.172	0.811	6.361	23.71	0.012	0.900	3.348
	2.0	30.66	29.83	0.165	0.853	9.105	31.39	0.008	0.926	4.550
	2.5	37.34	36.01	0.164	0.843	14.100	38.02	0.007	0.928	6.517
	0.5	6.83	6.80	0.510	0.983	0.029	7.12	0.129	0.939	0.101
	1.0	14.28	14.24	0.422	0.960	0.338	14.89	0.052	0.934	0.550
SP112	1.5	20.68	20.70	0.417	0.994	0.116	21.70	0.034	0.930	1.367
	2.0	27.59	27.41	0.502	0.982	0.486	28.73	0.031	0.946	1.474
	2.5	34.74	34.63	0.457	0.986	0.684	36.28	0.023	0.940	2.882
	0.5	6.43	6.31	0.311	0.982	0.040	6.65	0.078	0.979	0.047
	1.0	14.23	13.95	0.324	0.983	0.181	14.71	0.036	0.982	0.192
M500	1.5	21.39	20.99	0.386	0.987	0.285	22.14	0.029	0.966	0.747
	2.0	29.37	29.05	0.368	0.971	1.187	30.49	0.021	0.949	2.073
	2.5	36.79	36.36	0.423	0.986	0.787	38.18	0.019	0.962	2.179
	0.5	6.51	6.26	0.541	0.859	0.170	6.60	0.142	0.988	0.015
	1.0	14.30	13.79	0.617	0.892	0.561	14.52	0.073	0.995	0.025
M600	1.5	21.47	20.78	0.688	0.890	1.133	21.83	0.055	0.991	0.090
	2.0	29.45	28.60	0.807	0.915	1.372	29.96	0.048	0.990	0.167
	2.5	36.88	35.67	0.933	0.856	2.929	37.28	0.045	0.992	0.169
	0.5	6.19	5.75	0.285	0.926	0.134	6.06	0.078	0.986	0.026
	1.0	13.87	13.19	0.303	0.932	0.637	13.93	0.036	0.998	0.018
MP500	1.5	20.77	19.91	0.344	0.945	1.124	21.06	0.027	0.994	0.123
	2.0	28.52	27.49	0.318	0.956	1.723	28.95	0.018	0.995	0.212
	2.5	35.82	34.22	0.258	0.903	6.164	35.90	0.012	0.977	1.462
	0.5	6.41	6.18	0.280	0.926	0.149	6.49	0.0733	0.991	0.019
	1.0	14.14	13.68	0.301	0.943	0.594	14.44	0.034	0.995	0.052
4200	1.5	21.32	20.82	0.317	0.964	0.830	21.92	0.024	0.984	0.373
	2.0	29.22	28.45	0.319	0.968	1.368	29.93	0.018	0.985	0.644
	2.5	36.60	35.76	0.325	0.969	2.046	37.57	0.015	0.979	1.399
	0.5	6.28	5.99	0.225	0.899	0.219	6.30	0.059	0.979	0.045
	1.0	13.98	13.15	0.260	0.893	1.098	13.91	0.030	0.988	0.124
4400	1.5	21.15	19.93	0.304	0.931	1.497	21.07	0.023	0.994	0.130
	2.0	28.97	27.25	0.306	0.943	2.257	28.76	0.018	0.989	0.442
	2.5	36.34	34.38	0.278	0.952	3.212	36.21	0.013	0.988	0.822
	0.5	6.27	5.97	0.260	0.922	0.158	6.28	0.069	0.979	0.043
	1.0	13.93	13.40	0.275	0.939	0.652	14.15	0.032	0.996	0.047
4600	1.5	21.02	20.23	0.281	0.950	1.153	21.33	0.022	0.993	0.165
	2.0	29.00	27.77	0.286	0.956	1.898	29.29	0.016	0.995	0.198
	2.5	36.31	34.72	0.288	0.953	3.174	36.56	0.013	0.984	1.050
IRA 458	0.5	5.73	5.50	0.281	0.937	0.110	5.80	0.080	0.995	0.009

	1.0	13.44	12.96	0.349	0.932	0.583	13.71	0.042	0.990	0.088
	1.5	20.61	20.01	0.380	0.961	0.720	21.11	0.030	0.991	0.168
	2.0	28.49	27.73	0.384	0.972	1.010	29.22	0.022	0.986	0.514
	2.5	35.87	35.02	0.384	0.979	1.199	36.83	0.018	0.979	1.195
IRA 958	0.5	5.23	4.96	0.478	0.616	0.288	5.19	0.174	0.873	0.095
	1.0	13.01	12.48	0.467	0.928	0.411	13.15	0.061	0.997	0.020
	1.5	20.08	19.25	0.527	0.903	1.161	20.29	0.045	0.995	0.064
	2.0	27.58	26.49	0.567	0.878	2.467	27.86	0.036	0.989	0.224
	2.5	34.69	33.67	0.579	0.934	2.179	35.33	0.029	0.975	0.813
IRA 67	0.5	6.84	6.07	0.130	0.896	0.363	6.76	0.024	0.967	0.116
	1.0	12.81	10.62	0.142	0.830	1.861	11.89	0.015	0.920	0.876
	1.5	18.57	15.31	0.157	0.828	3.712	17.00	0.012	0.916	1.801
	2.0	23.35	20.10	0.216	0.870	3.963	21.84	0.014	0.954	1.401
	2.5	25.00	23.06	0.257	0.917	2.777	24.75	0.016	0.986	0.456

Table S4. Kinetic parameters for the Weber-Morris intraparticle diffusion kinetic model for the La(III)-IDHA complexes sorption on S957, S950, SP112, M500, M600, MP500, 4200, 4400, 4600, IRA 458, IRA 958, IRA 67 (C_0=0.5×10^{-3} M - 2.5×10^{-3} M).

Model	**Weber-Morris Intraparticle Diffusion**									
Ion exchanger	C_o ×10^{-3} [M]	k_{i1} [mg/g min$^{1/2}$]	C_1	R^2	k_{i2} [mg/g min$^{1/2}$]	C_2	R^2	k_{i3} [mg/g min$^{1/2}$]	C_3	R^2
S957	0.5	2.42	0.04	0.859	0.00	6.85	0.938	-	-	-
	1.0	3.40	3.29	0.923	0.01	13.11	0.953	-	-	-
	1.5	6.47	3.91	0.902	0.01	22.34	0.918	-	-	-
	2.0	8.63	4.46	0.904	0.01	29.01	0.812	-	-	-
	2.5	10.61	5.27	0.943	0.03	36.85	0.393	-	-	-
S950	0.5	0.67	1.81	0.991	0.09	6.30	0.791	-	-	-
	1.0	1.68	4.45	0.985	0.07	13.59	0.770	-	-	-
	1.5	3.11	5.92	0.995	0.03	22.73	0.957	-	-	-
	2.0	4.19	7.17	0.992	0.10	29.22	0.814	-	-	-
	2.5	4.59	9.64	0.977	0.28	33.68	0.492	-	-	-
SP112	0.5	1.78	1.70	0.916	0.00	6.83	0.853	-	-	-
	1.0	3.94	2.62	0.966	0.00	14.28	0.873	-	-	-
	1.5	6.10	2.92	0.938	0.00	20.68	0.735	-	-	-
	2.0	7.15	6.79	0.925	0.00	27.59	0.982	-	-	-
	2.5	9.53	6.95	0.937	0.00	34.74	0.838	-	-	-
M500	0.5	2.06	0.12	0.969	0.30	4.69	0.818	0.01	6.27	0.810
	1.0	4.57	0.37	0.948	0.70	10.31	0.861	0.02	13.99	0.948
	1.5	7.24	0.86	0.940	0.78	16.96	0.912	0.02	21.05	0.899
	2.0	9.85	1.34	0.972	0.87	24.47	0.898	0.02	29.06	0.935

	2.5	11.94	3.50	0.974	0.79	32.36	0.701	0.02	36.44	0.904
M600	0.5	1.43	2.03	0.934	0.25	5.13	0.675	0.01	6.42	0.615
	1.0	3.31	4.58	0.937	0.43	11.87	0.829	0.01	14.18	0.509
	1.5	4.90	7.51	0.949	0.52	18.57	0.860	0.01	21.34	0.688
	2.0	6.45	11.68	0.925	0.49	26.64	0.891	0.02	29.23	0.719
	2.5	7.14	16.92	0.958	0.50	33.88	0.878	0.03	36.48	0.910
MP500	0.5	1.60	0.56	0.995	0.22	4.28	0.739	0.07	5.15	0.950
	1.0	3.80	1.21	0.947	0.82	8.73	0.985	0.07	12.84	0.961
	1.5	6.13	1.68	0.939	1.03	14.21	0.991	0.08	19.66	0.704
	2.0	8.37	2.05	0.988	1.24	20.50	0.974	0.11	26.93	0.768
	2.5	8.27	4.93	0.998	2.12	22.25	0.933	0.19	32.90	0.925
4200	0.5	1.65	0.72	0.998	0.06	5.57	0.625	-	-	-
	1.0	4.10	0.93	0.949	0.86	9.09	0.999	0.03	13.72	0.700
	1.5	6.62	1.00	0.980	1.06	15.18	0.989	0.03	20.85	0.874
	2.0	9.08	1.35	0.993	1.21	21.81	0.984	0.07	28.16	0.814
	2.5	11.35	1.94	0.992	1.44	28.00	0.934	0.08	35.43	0.957
4400	0.5	1.33	0.88	0.992	0.49	3.23	0.935	0.05	5.64	0.834
	1.0	3.54	1.26	0.942	0.95	7.54	1.000	0.12	12.36	0.782
	1.5	5.98	1.45	0.972	0.95	14.10	0.993	0.18	18.63	0.835
	2.0	8.37	1.66	0.994	0.95	21.03	0.968	0.27	25.03	0.910
	2.5	10.09	2.03	0.994	1.58	24.89	0.856	0.29	31.97	0.984
4600	0.5	1.57	0.63	0.966	0.43	3.63	0.940	0.03	5.74	0.885
	1.0	3.87	0.86	0.930	0.93	8.28	0.968	0.06	13.13	0.753
	1.5	6.07	1.05	0.992	0.93	14.49	0.965	0.12	19.33	0.629
	2.0	8.42	1.36	0.993	1.28	20.12	0.957	0.19	26.36	0.828
	2.5	10.59	1.70	0.996	1.44	26.05	0.960	0.25	32.76	0.913
IRA 458	0.5	1.53	0.49	0.925	0.40	3.37	0.920	0.02	5.42	0.912
	1.0	3.82	1.42	0.902	0.82	8.73	0.983	0.02	13.16	0.744
	1.5	6.28	1.96	0.962	0.87	15.50	0.998	0.03	20.17	0.792
	2.0	8.85	2.51	0.962	1.03	22.25	0.941	0.06	27.65	0.777
	2.5	11.27	2.97	0.976	1.11	29.22	0.851	0.07	34.81	0.990
IRA 958	0.5	1.00	1.81	0.911	0.04	4.75	0.664	-	-	-
	1.0	3.44	2.67	0.955	0.07	12.01	0.679	-	-	-
	1.5	5.18	4.87	0.975	0.13	18.43	0.606	-	-	-
	2.0	6.72	7.83	0.989	0.13	25.87	0.697	-	-	-
	2.5	9.44	8.61	0.983	0.13	32.99	0.753	-	-	-
IRA 67	0.5	1.19	0.31	0.961	0.41	2.65	0.960	-	-	-
	1.0	2.22	0.48	0.957	0.76	4.51	0.994	-	-	-
	1.5	3.27	0.95	0.955	1.01	7.28	0.995	-	-	-

	2.0	4.75	1.89	0.943	1.00	12.43	0.997	-	-	-
	2.5	5.63	2.90	0.968	0.79	17.00	0.937	-	-	-

Table S5. Kinetic parameters for the Boyd and Dumwald-Wagner kinetic models for the La(III)-IDHA complexes sorption on S957, S950, SP112, M500, M600, MP500, 4200, 4400, 4600, IRA 458, IRA 958, IRA 67 (C_0=0.5×10^{-3} M - 2.5×10^{-3} M).

Model		**Boyd**		**Dumwald-Wagner**		
Ion exchanger	C_o ×10^{-3} [M]	*slope*	R^2	*k* [1/min]	*intercept*	R^2
S957	0.5	0.457	0.984	0.426	-0.179	0.985
	1.0	0.436	0.987	0.407	-0.126	0.985
	1.5	0.512	0.976	0.481	-0.219	0.971
	2.0	0.534	0.974	0.502	-0.242	0.970
	2.5	0.395	0.949	0.374	-0.202	0.941
S950	0.5	0.030	0.998	0.028	0.017	0.997
	1.0	0.035	0.864	0.033	0.182	0.870
	1.5	0.043	0.766	0.041	0.246	0.770
	2.0	0.062	0.968	0.060	0.052	0.969
	2.5	0.051	0.867	0.049	0.128	0.867
SP112	0.5	0.450	0.954	0.422	-0.150	0.947
	1.0	0.412	0.923	0.383	-0.172	0.914
	1.5	0.402	0.977	0.373	-0.152	0.972
	2.0	0.396	0.987	0.368	-0.099	0.984
	2.5	0.388	0.989	0.360	-0.116	0.986
M500	0.5	0.205	0.987	0.188	-0.038	0.987
	1.0	0.199	0.995	0.183	-0.023	0.995
	1.5	0.219	0.959	0.202	0.013	0.964
	2.0	0.258	0.969	0.238	-0.038	0.973
	2.5	0.319	0.999	0.299	-0.086	0.997
M600	0.5	0.230	0.963	0.213	0.029	0.959
	1.0	0.228	0.981	0.212	0.083	0.984
	1.5	0.248	0.978	0.232	0.099	0.982
	2.0	0.268	0.974	0.252	0.138	0.980
	2.5	0.276	0.985	0.261	0.147	0.988
MP500	0.5	0.136	0.998	0.122	-0.021	0.998
	1.0	0.125	0.967	0.113	0.039	0.967
	1.5	0.140	0.923	0.126	0.056	0.925
	2.0	0.160	0.977	0.145	0.014	0.979
	2.5	0.132	0.992	0.118	-0.021	0.993
4200	0.5	0.143	0.997	0.129	0.015	0.997

	1.0	0.135	0.959	0.122	0.036	0.959
	1.5	0.172	0.955	0.156	0.011	0.958
	2.0	0.181	0.971	0.165	-0.013	0.973
	2.5	0.201	0.987	0.184	-0.023	0.989
4400	0.5	0.040	0.863	0.037	0.161	0.868
	1.0	0.042	0.950	0.039	0.155	0.956
	1.5	0.031	0.945	0.030	0.247	0.954
	2.0	0.025	0.890	0.024	0.276	0.903
	2.5	0.022	0.795	0.021	0.292	0.808
4600	0.5	0.080	0.964	0.075	0.089	0.970
	1.0	0.081	0.970	0.076	0.102	0.975
	1.5	0.065	0.866	0.060	0.153	0.876
	2.0	0.066	0.870	0.061	0.153	0.880
	2.5	0.029	0.889	0.028	0.286	0.902
IRA 458	0.5	0.086	0.971	0.080	0.098	0.976
	1.0	0.112	0.985	0.107	0.102	0.989
	1.5	0.109	0.954	0.104	0.163	0.962
	2.0	0.097	0.899	0.092	0.209	0.911
	2.5	0.104	0.872	0.099	0.221	0.884
IRA 958	0.5	0.171	0.931	0.157	0.069	0.931
	1.0	0.193	0.981	0.177	0.056	0.984
	1.5	0.183	0.898	0.168	0.103	0.901
	2.0	0.218	0.964	0.201	0.075	0.966
	2.5	0.258	0.923	0.241	0.070	0.925
IRA 67	0.5	0.028	0.994	0.026	0.038	0.994
	1.0	0.018	0.968	0.016	0.054	0.965
	1.5	0.016	0.936	0.015	0.070	0.932
	2.0	0.022	0.908	0.020	0.115	0.909
	2.5	0.039	0.942	0.036	0.149	0.949

Table S6. Kinetic parameters for the pseudo-first order and pseudo-second order kinetic models for the Nd(III)-IDHA complexes sorption on S957, S950, SP112, M500, M600, MP500, 4200, 4400, 4600, IRA 458, IRA 958, IRA 67 (C_0=0.5×10^{-3} M - 2.5×10^{-3} M).

Model			**Pseudo-First Order**				**Pseudo-Second Order**			
Ion exchanger	C_o ×10^{-3} [M]	$q_{e.exp}$ [mg/g]	$q_{1.cal}$ [mg/g]	k_1 [1/min]	R^2	χ^2	$q_{2.cal}$ [mg/g]	k_2 [g/mg min]	R^2	χ^2
S957	0.5	7.68	7.71	0.363	0.993	0.024	8.12	0.073	0.907	0.334
	1.0	15.00	15.04	0.353	0.997	0.040	15.83	0.037	0.918	1.124
	1.5	22.86	22.90	0.339	0.998	0.057	24.08	0.024	0.933	2.070
	2.0	29.92	29.90	0.293	0.988	0.659	31.39	0.016	0.952	2.551

	2.5	36.96	36.68	0.251	0.981	1.616	38.58	0.011	0.975	2.170
S950	0.5	7.55	7.49	0.092	0.961	0.240	8.17	0.015	0.963	0.220
	1.0	14.49	14.16	0.082	0.976	0.573	15.61	0.007	0.976	0.558
	1.5	22.49	21.52	0.086	0.960	2.097	23.73	0.005	0.985	0.795
	2.0	29.31	27.71	0.078	0.951	4.404	30.79	0.003	0.982	1.574
	2.5	35.91	33.62	0.072	0.953	6.299	37.56	0.002	0.983	2.316
SP112	0.5	7.72	7.77	0.356	0.995	0.019	8.16	0.073	0.908	0.327
	1.0	15.22	15.29	0.328	0.995	0.069	16.07	0.034	0.928	1.013
	1.5	22.42	22.43	0.347	0.999	0.029	23.62	0.024	0.932	2.012
	2.0	29.71	29.79	0.349	0.998	0.115	31.29	0.019	0.930	3.511
	2.5	36.52	36.54	0.346	0.997	0.239	38.44	0.015	0.932	5.268
M500	0.5	7.36	7.29	0.327	0.997	0.010	7.69	0.069	0.956	0.141
	1.0	14.51	14.39	0.338	0.997	0.038	15.18	0.036	0.951	0.601
	1.5	22.66	22.53	0.350	0.996	0.106	23.71	0.025	0.945	1.570
	2.0	29.61	29.39	0.346	0.997	0.124	30.92	0.019	0.953	2.226
	2.5	36.56	36.18	0.345	0.997	0.237	38.04	0.015	0.954	3.292
M600	0.5	7.38	7.19	0.427	0.992	0.010	7.57	0.097	0.988	0.025
	1.0	14.55	14.29	0.373	0.985	0.130	15.01	0.043	0.978	0.207
	1.5	22.72	22.45	0.385	0.983	0.392	23.58	0.028	0.963	0.877
	2.0	29.67	29.25	0.374	0.987	0.545	30.75	0.021	0.971	1.201
	2.5	36.61	36.00	0.372	0.985	0.934	37.83	0.017	0.969	1.923
MP500	0.5	7.41	7.35	0.508	0.989	0.022	7.70	0.118	0.945	0.107
	1.0	14.58	14.38	0.436	0.992	0.071	15.13	0.049	0.959	0.374
	1.5	22.76	22.43	0.413	0.988	0.276	23.61	0.030	0.962	0.881
	2.0	29.73	29.36	0.329	0.969	1.349	30.81	0.019	0.975	1.066
	2.5	36.68	35.91	0.233	0.951	3.929	37.75	0.010	0.983	1.363
4200	0.5	7.41	7.40	0.338	0.998	0.007	7.77	0.073	0.946	0.168
	1.0	14.58	14.57	0.307	0.988	0.155	15.29	0.034	0.943	0.718
	1.5	22.76	22.69	0.308	0.998	0.050	23.88	0.021	0.955	1.416
	2.0	29.71	29.71	0.312	0.992	0.409	31.23	0.017	0.942	3.108
	2.5	36.70	36.58	0.287	0.990	0.807	38.47	0.012	0.958	3.490
4400	0.5	7.40	7.28	0.349	0.967	0.086	7.64	0.079	0.978	0.056
	1.0	14.57	14.21	0.321	0.952	0.501	14.97	0.036	0.995	0.055
	1.5	22.75	22.38	0.314	0.965	0.913	23.51	0.023	0.978	0.584
	2.0	29.72	29.25	0.287	0.963	1.783	30.72	0.016	0.975	1.176
	2.5	36.68	35.85	0.235	0.961	3.184	37.72	0.010	0.988	1.004
4600	0.5	7.40	7.35	0.313	0.985	0.046	7.71	0.069	0.956	0.134
	1.0	14.56	14.46	0.288	0.981	0.231	15.19	0.032	0.964	0.447
	1.5	22.75	22.48	0.297	0.973	0.750	23.61	0.021	0.980	0.551

	2.0	29.71	29.53	0.270	0.962	1.944	30.95	0.015	0.961	2.006
	2.5	36.69	36.24	0.263	0.973	2.123	38.10	0.011	0.982	1.433
IRA 458	0.5	7.40	7.33	0.373	0.983	0.044	7.69	0.085	0.954	0.117
	1.0	14.57	14.51	0.368	0.994	0.070	15.27	0.040	0.929	0.829
	1.5	22.76	22.49	0.348	0.993	0.203	23.70	0.024	0.970	0.819
	2.0	29.73	29.58	0.357	0.997	0.160	31.09	0.020	0.953	2.150
	2.5	36.71	36.24	0.354	0.962	2.371	38.01	0.016	0.970	1.826
IRA 958	0.5	7.40	7.21	0.518	0.980	0.037	7.58	0.120	0.961	0.072
	1.0	14.50	14.27	0.457	0.987	0.108	15.02	0.052	0.963	0.314
	1.5	22.61	22.18	0.489	0.968	0.565	23.28	0.037	0.959	0.736
	2.0	29.53	29.22	0.472	0.989	0.358	30.69	0.027	0.954	1.542
	2.5	36.25	36.05	0.451	0.993	0.396	37.82	0.021	0.933	3.686
IRA 67	0.5	6.77	5.86	0.083	0.879	0.477	6.78	0.014	0.949	0.201
	1.0	12.29	10.37	0.156	0.859	1.500	11.54	0.017	0.938	0.653
	1.5	16.18	13.87	0.175	0.862	2.281	15.24	0.015	0.948	0.855
	2.0	19.89	17.64	0.195	0.906	2.282	19.18	0.014	0.976	0.580
	2.5	21.57	19.44	0.192	0.909	2.613	21.09	0.013	0.976	0.691

Table S7. Kinetic parameters for the Weber-Morris intraparticle diffusion kinetic model for the Nd(III)-IDHA complexes sorption on S957, S950, SP112, M500, M600, MP500, 4200, 4400, 4600, IRA 458, IRA 958, IRA 67 (C_0=0.5×10^{-3} M - 2.5×10^{-3} M).

Model	**Weber-Morris Intraparticle Diffusion**									
Ion exchanger	C_o ×10^{-3} [M]	k_{i1} [mg/g min$^{1/2}$]	C_1	R^2	k_{i2} [mg/g min$^{1/2}$]	C_2	R^2	k_{i3} [mg/g min$^{1/2}$]	C_3	R^2
S957	0.5	2.55	0.19	0.899	0.01	7.55	0.431	-	-	-
	1.0	4.97	0.31	0.920	0.02	14.72	0.596	-	-	-
	1.5	7.36	0.75	0.944	0.04	22.39	0.464	-	-	-
	2.0	9.18	0.88	0.979	0.09	28.89	0.406	-	-	-
	2.5	10.46	1.23	0.983	0.22	34.29	0.409	-	-	-
S950	0.5	1.27	0.14	0.989	0.03	7.09	0.936	-	-	-
	1.0	2.17	0.33	0.964	1.38	3.81	0.889	0.08	13.30	0.916
	1.5	3.46	0.57	0.989	2.03	5.89	0.965	0.17	19.99	0.788
	2.0	4.22	0.77	0.972	2.58	7.01	0.987	0.33	24.51	0.774
	2.5	4.71	1.24	0.969	3.18	7.70	0.967	0.54	27.86	0.875
SP112	0.5	2.59	0.16	0.938	0.00	7.66	0.959	-	-	-
	1.0	5.01	0.19	0.962	0.01	15.14	0.642	-	-	-
	1.5	7.21	0.79	0.924	0.04	21.92	0.432	-	-	-
	2.0	9.55	1.30	0.951	0.02	29.39	0.524	-	-	-
	2.5	11.59	1.68	0.930	0.08	35.53	0.425	-	-	-
M500	0.5	2.25	0.32	0.922	0.03	6.99	0.467	-	-	-

	1.0	4.43	0.77	0.910	0.06	13.75	0.458	-	-	-
	1.5	6.88	1.62	0.923	0.08	21.72	0.472	-	-	-
	2.0	8.91	2.21	0.941	0.08	28.53	0.499	-	-	-
	2.5	10.97	2.71	0.950	0.10	35.15	0.621	-	-	-
	0.5	2.11	1.16	0.941	0.27	5.86	0.914	0.00	7.32	0.951
	1.0	4.52	1.32	0.991	0.51	11.69	0.983	0.01	14.44	0.854
M600	1.5	7.52	1.41	0.979	0.66	19.08	0.858	0.01	22.55	0.930
	2.0	9.80	1.56	0.982	0.90	24.64	0.901	0.02	29.38	0.855
	2.5	12.04	1.97	0.987	1.04	30.61	0.887	0.04	35.95	0.876
	0.5	2.38	1.10	0.96	0.02	7.20	0.471	-	-	-
	1.0	4.89	1.18	0.953	0.35	12.60	0.904	0.01	14.45	0.842
MP500	1.5	7.70	1.44	0.962	0.65	19.09	0.975	0.01	22.59	0.933
	2.0	9.19	1.93	0.997	1.19	23.26	0.903	0.01	29.60	0.970
	2.5	9.57	2.35	0.995	2.57	21.74	0.936	0.10	35.34	0.762
	0.5	2.32	0.36	0.960	0.01	7.27	0.674	-	-	-
	1.0	4.56	0.42	0.972	0.03	14.22	0.517	-	-	-
4200	1.5	7.11	0.53	0.955	0.08	21.84	0.435	-	-	-
	2.0	9.36	0.76	0.954	0.09	28.67	0.415	-	-	-
	2.5	11.14	0.96	0.961	0.16	34.71	0.403	-	-	-
	0.5	1.98	1.06	0.973	0.02	7.11	0.541	-	-	-
	1.0	4.28	1.14	0.962	0.86	9.81	0.992	0.01	14.47	0.751
4400	1.5	6.97	1.29	0.993	0.97	17.20	0.924	0.03	22.38	0.565
	2.0	8.90	1.37	0.987	1.46	21.34	0.903	0.04	29.13	0.550
	2.5	9.91	1.65	1.000	2.38	22.57	0.927	0.12	35.05	0.771
	0.5	2.21	0.45	0.979	0.02	7.17	0.591	-	-	-
	1.0	4.23	0.79	0.975	0.06	13.80	0.448	-	-	-
4600	1.5	6.99	0.93	0.993	1.17	16.41	0.906	0.01	22.67	0.666
	2.0	8.89	1.05	0.988	1.51	21.59	0.877	0.00	29.67	0.686
	2.5	10.79	1.11	0.982	2.32	23.89	0.830	0.03	36.27	0.495
	0.5	2.11	0.95	0.967	0.01	7.24	0.756	-	-	-
	1.0	4.48	1.11	0.905	0.04	14.09	0.474	-	-	-
IRA 458	1.5	6.49	2.31	0.924	0.10	21.59	0.451	-	-	-
	2.0	8.87	2.67	0.945	0.07	28.91	0.446	-	-	-
	2.5	11.46	2.91	0.998	1.24	29.89	0.974	0.01	36.61	0.617
	0.5	1.79	1.99	0.890	0.02	7.12	0.870	-	-	-
	1.0	3.72	3.17	0.882	0.04	13.95	0.483	-	-	-
IRA 958	1.5	5.53	5.86	0.903	0.06	21.79	0.656	-	-	-
	2.0	7.72	6.58	0.906	0.04	28.98	0.536	-	-	-
	2.5	10.06	6.80	0.907	0.05	35.54	0.652	-	-	-

	0.5	1.01	0.01	0.943	0.50	1.51	0.989	-	-	-
	1.0	2.45	0.03	0.917	0.69	4.90	0.995	-	-	-
IRA 67	1.5	3.14	0.85	0.954	0.92	7.02	0.998	-	-	-
	2.0	4.18	1.18	0.973	1.08	9.91	0.989	-	-	-
	2.5	4.53	1.42	0.979	0.93	12.01	0.953	-	-	-

Table S8. Kinetic parameters for the Boyd and Dumwald-Wagner kinetic models for the Nd(III)-IDHA complexes sorption on S957, S950, SP112, M500, M600, MP500, 4200, 4400, 4600, IRA 458, IRA 958, IRA 67 (C_0=0.5×10^{-3} M - 2.5×10^{-3} M).

Model		**Boyd**		**Dumwald-Wagner**		
Ion exchanger	C_o ×10^{-3} [M]	*slope*	R^2	*k* [1/min]	*intercept*	R^2
	0.5	0.359	0.997	0.338	-0.143	0.997
	1.0	0.366	0.996	0.344	-0.171	0.993
S957	1.5	0.341	0.993	0.320	-0.158	0.991
	2.0	0.278	0.983	0.257	-0.134	0.981
	2.5	0.190	0.987	0.173	-0.067	0.986
	0.5	0.096	0.964	0.089	-0.117	0.963
	1.0	0.055	0.983	0.050	-0.047	0.984
S950	1.5	0.035	0.997	0.033	-0.021	0.999
	2.0	0.032	1.000	0.031	-0.016	0.999
	2.5	0.025	0.996	0.023	0.018	0.997
	0.5	0.512	0.965	0.489	-0.346	0.959
	1.0	0.481	0.906	0.459	-0.366	0.895
SP112	1.5	0.324	0.997	0.303	-0.131	0.995
	2.0	0.418	0.972	0.396	-0.252	0.966
	2.5	0.314	0.989	0.293	-0.110	0.991
	0.5	0.240	0.998	0.221	-0.055	0.999
	1.0	0.240	0.980	0.221	-0.038	0.982
M500	1.5	0.269	0.977	0.249	-0.058	0.981
	2.0	0.280	0.998	0.260	-0.088	0.998
	2.5	0.285	0.997	0.264	-0.100	0.996
	0.5	0.215	0.991	0.198	0.021	0.992
	1.0	0.220	0.972	0.202	-0.003	0.974
M600	1.5	0.268	0.991	0.249	-0.045	0.993
	2.0	0.254	0.995	0.235	-0.043	0.996
	2.5	0.254	0.993	0.235	-0.046	0.994
	0.5	0.394	0.998	0.374	-0.096	0.998
MP500	1.0	0.271	0.981	0.252	-0.015	0.985
	1.5	0.243	0.950	0.224	0.015	0.955

	2.0	0.231	0.995	0.212	-0.053	0.995
	2.5	0.101	0.983	0.095	0.046	0.987
4200	0.5	0.356	0.968	0.335	-0.198	0.961
	1.0	0.321	0.968	0.300	-0.179	0.963
	1.5	0.263	0.996	0.243	-0.099	0.996
	2.0	0.283	0.988	0.262	-0.112	0.989
	2.5	0.232	0.986	0.213	-0.077	0.987
4400	0.5	0.259	0.982	0.240	-0.084	0.978
	1.0	0.156	0.975	0.142	0.028	0.977
	1.5	0.205	0.991	0.187	-0.033	0.992
	2.0	0.192	0.992	0.175	-0.039	0.993
	2.5	0.148	0.993	0.133	-0.031	0.993
4600	0.5	0.298	0.969	0.277	-0.151	0.963
	1.0	0.233	0.990	0.214	-0.086	0.989
	1.5	0.203	0.997	0.186	-0.044	0.997
	2.0	0.216	0.983	0.198	-0.082	0.982
	2.5	0.134	0.983	0.128	0.033	0.987
IRA 458	0.5	0.351	0.979	0.330	-0.167	0.973
	1.0	0.292	0.972	0.272	-0.061	0.976
	1.5	0.231	0.995	0.213	-0.032	0.997
	2.0	0.305	0.996	0.284	-0.110	0.995
	2.5	0.236	0.977	0.217	-0.034	0.978
IRA 958	0.5	0.287	0.982	0.268	0.006	0.984
	1.0	0.259	0.970	0.240	0.021	0.974
	1.5	0.281	0.964	0.262	0.014	0.969
	2.0	0.340	0.997	0.321	-0.069	0.997
	2.5	0.369	0.976	0.348	-0.085	0.977
IRA 67	0.5	0.021	0.993	0.019	0.009	0.993
	1.0	0.021	0.968	0.019	0.060	0.965
	1.5	0.018	0.953	0.016	0.071	0.949
	2.0	0.018	0.908	0.016	0.089	0.905
	2.5	0.031	0.956	0.028	0.097	0.959

Table S9. Kinetic parameters for the pseudo-first order and pseudo-second order kinetic models for the Ho(III)-IDHA complexes sorption on S957, S950, SP112, M500, M600, MP500, 4200, 4400, 4600, IRA 458, IRA 958, IRA 67 (C_0=0.5×10^{-3} M - 2.5×10^{-3} M).

Model			**Pseudo-First Order**				**Pseudo-Second Order**			
Ion exchanger	C_o ×10^{-3} [M]	$q_{e.exp}$ [mg/g]	$q_{1.cal}$ [mg/g]	k_1 [1/min]	R^2	χ^2	$q_{2.cal}$ [mg/g]	k_2 [g/mg min]	R^2	χ^2
S957	0.5	7.65	7.67	0.338	0.998	0.006	8.08	0.069	0.925	0.271

	1.0	15.95	15.98	0.336	0.999	0.018	16.81	0.033	0.935	0.988
	1.5	23.93	24.01	0.328	0.989	0.373	25.22	0.022	0.924	2.577
	2.0	31.61	31.54	0.279	0.988	0.754	33.12	0.014	0.961	2.407
	2.5	40.59	40.25	0.239	0.964	3.646	42.27	0.009	0.973	2.816
	0.5	7.64	7.33	0.092	0.953	0.278	8.06	0.014	0.982	0.104
	1.0	15.93	15.53	0.086	0.967	0.920	17.10	0.006	0.978	0.612
S950	1.5	23.85	22.61	0.093	0.950	2.841	24.91	0.005	0.980	1.108
	2.0	31.45	29.73	0.079	0.956	4.574	33.02	0.003	0.984	1.628
	2.5	40.34	37.59	0.092	0.935	10.199	41.49	0.003	0.977	3.527
	0.5	8.08	8.09	0.316	0.997	0.012	8.50	0.062	0.942	0.228
	1.0	15.64	15.66	0.312	0.995	0.068	16.45	0.032	0.944	0.830
SP112	1.5	24.62	24.43	0.361	0.995	0.141	25.71	0.024	0.961	1.208
	2.0	32.32	32.20	0.346	0.990	0.556	33.79	0.018	0.953	2.527
	2.5	40.90	40.73	0.358	0.990	0.886	42.79	0.014	0.947	4.618
	0.5	8.36	8.27	0.524	0.992	0.021	8.68	0.108	0.940	0.148
	1.0	16.50	16.33	0.472	0.976	0.242	17.12	0.049	0.953	0.480
M500	1.5	24.92	24.74	0.467	0.996	0.091	26.00	0.031	0.940	1.546
	2.0	33.11	32.81	0.436	0.993	0.346	34.48	0.022	0.954	2.161
	2.5	41.40	41.04	0.426	0.993	0.553	43.15	0.017	0.956	3.266
	0.5	8.37	8.27	0.496	0.992	0.021	8.69	0.100	0.940	0.159
	1.0	16.50	16.39	0.448	0.994	0.078	17.24	0.044	0.933	0.815
M600	1.5	24.93	24.77	0.400	0.987	0.359	25.99	0.027	0.956	1.215
	2.0	33.12	32.78	0.426	0.989	0.519	34.50	0.021	0.954	2.242
	2.5	41.41	41.07	0.385	0.979	1.646	43.09	0.016	0.960	3.059
	0.5	8.36	8.31	0.604	0.990	0.021	8.69	0.128	0.917	0.174
	1.0	16.50	16.46	0.541	0.998	0.017	17.24	0.056	0.913	0.850
MP500	1.5	24.92	24.91	0.499	0.994	0.153	26.08	0.034	0.917	1.995
	2.0	33.11	32.99	0.419	0.986	0.672	34.57	0.022	0.944	2.671
	2.5	41.41	40.95	0.339	0.957	3.451	42.90	0.014	0.970	2.444
	0.5	8.36	8.34	0.409	0.998	0.007	8.75	0.081	0.934	0.218
	1.0	16.50	16.50	0.364	0.993	0.104	17.31	0.036	0.936	0.899
4200	1.5	24.93	24.87	0.358	0.996	0.116	26.12	0.023	0.943	1.862
	2.0	33.12	33.06	0.352	0.992	0.449	34.72	0.017	0.945	3.210
	2.5	41.41	41.34	0.343	0.993	0.642	43.40	0.013	0.949	4.706
	0.5	8.37	8.31	0.460	0.989	0.033	8.74	0.090	0.927	0.224
	1.0	16.51	16.45	0.384	0.996	0.058	17.28	0.038	0.941	0.799
4400	1.5	24.93	24.84	0.366	0.992	0.248	26.08	0.024	0.945	1.738
	2.0	33.11	33.03	0.355	0.994	0.370	34.68	0.018	0.949	2.882
	2.5	41.41	41.19	0.362	0.990	0.811	43.24	0.014	0.958	3.560

4600	0.5	8.36	8.32	0.390	0.988	0.040	8.73	0.078	0.942	0.192
	1.0	16.49	16.37	0.371	0.994	0.085	17.21	0.037	0.957	0.575
	1.5	24.92	24.86	0.354	0.991	0.292	26.09	0.023	0.947	1.697
	2.0	33.11	32.94	0.345	0.987	0.715	34.59	0.017	0.956	2.474
	2.5	41.41	41.16	0.346	0.988	1.018	43.22	0.014	0.961	3.437
IRA 458	0.5	8.37	8.31	0.439	0.994	0.019	8.73	0.086	0.937	0.198
	1.0	16.51	16.50	0.388	0.997	0.043	17.35	0.038	0.929	1.017
	1.5	24.94	24.89	0.372	0.996	0.117	26.14	0.024	0.943	1.811
	2.0	33.12	33.02	0.368	0.998	0.131	34.70	0.018	0.947	3.005
	2.5	41.42	41.35	0.364	0.986	1.237	43.38	0.015	0.937	5.530
IRA 958	0.5	8.37	8.32	0.560	0.996	0.010	8.71	0.116	0.922	0.182
	1.0	16.51	16.44	0.478	0.986	0.144	17.22	0.050	0.930	0.735
	1.5	24.93	24.79	0.527	0.997	0.070	26.00	0.036	0.928	1.621
	2.0	33.12	32.78	0.526	0.974	0.957	34.36	0.028	0.953	1.720
	2.5	41.41	41.19	0.473	0.974	1.686	43.12	0.020	0.941	3.790
IRA 67	0.5	7.97	7.60	0.225	0.900	0.370	8.028	0.045	0.985	0.054
	1.0	16.33	14.80	0.209	0.877	1.998	15.81	0.020	0.967	0.538
	1.5	24.21	20.86	0.200	0.834	5.592	22.40	0.013	0.937	2.112
	2.0	31.05	26.25	0.195	0.836	8.857	28.20	0.010	0.931	3.711
	2.5	35.40	31.19	0.232	0.884	7.551	33.17	0.011	0.964	2.369

Table S10. Kinetic parameters for the Weber-Morris intraparticle diffusion kinetic model for the Ho(III)-IDHA complexes sorption on S957, S950, SP112, M500, M600, MP500, 4200, 4400, 4600, IRA 458, IRA 958, IRA 67 (C_0=0.5×10^{-3} M - 2.5×10^{-3} M).

Model	**Weber-Morris Intraparticle Diffusion**									
Ion exchanger	C_o ×10^{-3} [M]	k_{i1} [mg/g min$^{1/2}$]	C_1	R^2	k_{i2} [mg/g min$^{1/2}$]	C_2	R^2	k_{i3} [mg/g min$^{1/2}$]	C_3	R^2
S957	0.5	2.54	0.08	0.936	0.01	7.51	0.512	-	-	-
	1.0	5.15	0.46	0.944	0.03	15.64	0.434	-	-	-
	1.5	7.73	0.63	0.950	0.04	23.46	0.458	-	-	-
	2.0	9.60	0.71	0.991	0.09	30.49	0.438	-	-	-
	2.5	11.71	0.92	0.992	2.58	26.46	0.967	0.01	40.44	0.699
S950	0.5	1.26	0.15	0.979	0.72	1.89	0.991	0.03	7.20	0.752
	1.0	2.55	0.27	0.941	1.43	4.73	0.970	0.05	15.19	0.704
	1.5	3.96	0.35	0.953	1.74	8.66	0.978	0.24	20.38	0.666
	2.0	4.71	0.46	0.964	2.69	8.21	0.985	0.35	26.31	0.816
	2.5	6.67	0.48	0.978	3.33	11.58	0.998	0.35	34.98	0.976
SP112	0.5	2.60	0.12	0.966	0.01	7.91	0.482	-	-	-
	1.0	5.00	0.28	0.969	0.02	15.36	0.422	-	-	-
	1.5	7.16	2.57	0.933	0.07	23.80	0.440	-	-	-

	2.0	9.58	2.91	0.964	0.06	31.53	0.447	-	-	-
	2.5	12.04	4.07	0.933	0.11	39.53	0.405	-	-	-
M500	0.5	2.14	2.16	0.892	0.00	8.28	0.901	-	-	-
	1.0	4.27	3.82	0.930	0.01	16.31	0.640	-	-	-
	1.5	6.81	4.96	0.891	0.02	24.60	0.505	-	-	-
	2.0	9.06	6.03	0.916	0.04	32.56	0.470	-	-	-
	2.5	11.38	7.22	0.915	0.07	40.59	0.413	-	-	-
M600	0.5	2.21	1.90	0.889	0.01	8.28	0.961	-	-	-
	1.0	4.65	2.81	0.881	0.01	16.33	0.656	-	-	-
	1.5	6.97	3.88	0.947	0.03	24.52	0.452	-	-	-
	2.0	9.14	5.62	0.906	0.04	32.58	0.461	-	-	-
	2.5	11.38	6.47	0.952	0.08	40.40	0.411	-	-	-
MP500	0.5	2.64	1.68	0.956	0.01	8.28	0.849	-	-	-
	1.0	5.59	2.24	0.945	0.02	16.28	0.464	-	-	-
	1.5	8.65	2.62	0.967	0.03	24.60	0.354	-	-	-
	2.0	9.35	5.45	0.950	0.01	32.96	0.790	-	-	-
	2.5	11.00	6.05	0.982	0.13	39.83	0.415	-	-	-
4200	0.5	2.48	1.08	0.929	0.01	8.28	0.885	-	-	-
	1.0	5.04	1.42	0.953	0.02	16.29	0.557	-	-	-
	1.5	7.61	1.99	0.950	0.03	24.48	0.510	-	-	-
	2.0	10.04	2.69	0.955	0.04	32.62	0.450	-	-	-
	2.5	12.52	3.14	0.959	0.08	40.45	0.409	-	-	-
4400	0.5	2.35	1.50	0.876	0.01	8.28	0.694	-	-	-
	1.0	4.92	1.81	0.937	0.02	16.27	0.643	-	-	-
	1.5	7.41	2.53	0.946	0.05	24.36	0.484	-	-	-
	2.0	9.97	2.88	0.961	0.03	32.68	0.483	-	-	-
	2.5	11.98	4.69	0.954	0.08	40.39	0.423	-	-	-
4600	0.5	2.44	1.08	0.950	0.01	8.25	0.877	-	-	-
	1.0	4.79	1.87	0.947	0.03	16.12	0.523	-	-	-
	1.5	7.46	2.26	0.959	0.04	24.45	0.485	-	-	-
	2.0	9.67	3.21	0.957	0.07	32.25	0.420	-	-	-
	2.5	12.00	4.20	0.962	0.10	40.24	0.423	-	-	-
IRA 458	0.5	2.38	1.36	0.901	0.01	8.28	0.953	-	-	-
	1.0	5.09	1.51	0.922	0.01	16.43	0.918	-	-	-
	1.5	7.56	2.32	0.948	0.02	24.63	0.578	-	-	-
	2.0	9.96	3.11	0.941	0.06	32.42	0.455	-	-	-
	2.5	12.34	4.19	0.943	0.08	40.50	0.443	-	-	-
IRA 958	0.5	2.72	1.38	0.945	0.01	8.21	0.578	-	-	-
	1.0	4.47	3.58	0.915	0.01	16.41	0.955	-	-	-

	1.5	6.49	6.31	0.874	0.01	24.78	0.946	-	-	-
	2.0	8.19	9.12	0.920	0.00	33.06	0.772	-	-	-
	2.5	10.97	9.37	0.939	0.02	41.20	0.615	-	-	-
	0.5	2.33	0.13	0.997	0.63	3.87	0.995	0.05	7.23	0.544
	1.0	4.10	0.35	0.947	0.83	8.48	0.996	0.17	13.86	0.841
IRA 67	1.5	5.55	0.74	0.962	1.01	12.22	0.978	0.64	14.83	0.930
	2.0	6.84	0.97	0.992	1.16	15.94	0.937	0.88	17.85	0.979
	2.5	8.92	1.10	1.000	1.26	21.17	0.994	0.70	24.74	0.980

Table S11. Kinetic parameters for the Boyd and Dumwald-Wagner kinetic models for the Ho(III)-IDHA complexes sorption on S957, S950, SP112, M500, M600, MP500, 4200, 4400, 4600, IRA 458, IRA 958, IRA 67 (C_0=0.5×10^{-3} M - 2.5×10^{-3} M).

Model		**Boyd**		**Dumwald-Wagner**		
Ion exchanger	C_o ×10^{-3} [M]	*slope*	R^2	*k* [1/min]	*intercept*	R^2
	0.5	0.357	0.992	0.335	-0.176	0.990
	1.0	0.341	0.990	0.320	-0.165	0.987
S957	1.5	0.352	0.987	0.330	-0.178	0.986
	2.0	0.271	0.966	0.250	-0.146	0.961
	2.5	0.170	0.979	0.154	-0.049	0.980
	0.5	0.048	0.984	0.045	-0.039	0.981
	1.0	0.053	0.994	0.049	-0.047	0.991
S950	1.5	0.033	0.994	0.030	0.010	0.994
	2.0	0.032	0.999	0.028	-0.021	0.999
	2.5	0.026	0.958	0.024	0.036	0.962
	0.5	0.339	0.977	0.318	-0.189	0.973
	1.0	0.344	0.958	0.323	-0.204	0.951
SP112	1.5	0.275	0.999	0.255	-0.074	0.999
	2.0	0.318	0.989	0.297	-0.138	0.986
	2.5	0.283	0.984	0.262	-0.070	0.986
	0.5	0.367	0.991	0.340	-0.047	0.993
	1.0	0.335	0.988	0.308	-0.054	0.988
M500	1.5	0.377	0.997	0.357	-0.111	0.995
	2.0	0.346	0.994	0.326	-0.107	0.991
	2.5	0.324	0.998	0.304	-0.085	0.996
	0.5	0.328	0.990	0.303	-0.028	0.993
	1.0	0.304	0.966	0.279	-0.024	0.968
M600	1.5	0.350	0.988	0.329	-0.139	0.984
	2.0	0.338	0.974	0.318	-0.112	0.969
	2.5	0.305	0.994	0.285	-0.094	0.993

	0.5	0.483	0.996	0.445	-0.097	0.994
	1.0	0.476	0.996	0.438	-0.117	0.995
MP500	1.5	0.518	0.984	0.487	-0.199	0.980
	2.0	0.349	0.990	0.322	-0.102	0.988
	2.5	0.257	0.990	0.238	-0.081	0.988
	0.5	0.363	0.992	0.335	-0.118	0.989
	1.0	0.331	0.985	0.304	-0.119	0.984
4200	1.5	0.355	0.985	0.334	-0.172	0.981
	2.0	0.360	0.969	0.339	-0.187	0.963
	2.5	0.319	0.992	0.298	-0.138	0.990
	0.5	0.343	0.981	0.317	-0.062	0.980
	1.0	0.312	0.989	0.286	-0.082	0.990
4400	1.5	0.328	0.995	0.307	-0.126	0.994
	2.0	0.377	0.960	0.355	-0.212	0.952
	2.5	0.309	0.995	0.288	-0.115	0.993
	0.5	0.320	0.989	0.294	-0.090	0.989
	1.0	0.277	0.998	0.301	-0.130	0.982
4600	1.5	0.347	0.985	0.325	-0.166	0.981
	2.0	0.299	0.986	0.279	-0.118	0.982
	2.5	0.293	0.993	0.273	-0.112	0.990
	0.5	0.316	0.996	0.291	-0.051	0.997
	1.0	0.308	0.980	0.282	-0.068	0.981
IRA 458	1.5	0.321	0.986	0.295	-0.106	0.983
	2.0	0.318	0.992	0.312	-0.133	0.993
	2.5	0.333	0.991	0.311	-0.125	0.991
	0.5	0.489	0.998	0.459	-0.133	0.996
	1.0	0.415	0.989	0.385	-0.118	0.988
IRA 958	1.5	0.400	0.992	0.372	-0.065	0.994
	2.0	0.340	0.983	0.313	-0.026	0.985
	2.5	0.503	0.975	0.481	-0.261	0.970
	0.5	0.060	0.973	0.055	0.084	0.975
	1.0	0.030	0.832	0.026	0.113	0.989
IRA 67	1.5	0.018	0.975	0.016	0.107	0.976
	2.0	0.014	0.951	0.013	0.113	0.952
	2.5	0.015	0.888	0.014	0.171	0.895

Table S12. Adsorption isotherm parameters for the sorption of La(III), Nd(III) and Ho(III) complexes with IDHA on S957, S950, SP112, M500, M600, MP500, 4200, 4400, 4600, IRA 458, IRA 958, and IRA 67 at the temperature of 293 K.

Model	**Langmuir**

Ion exchanger	REE	$q_{e.exp}$ [mg/g]	q_0 [mg/g]	K_L [L/mg]	R^2	χ^2
S957	La(III)	142.29	142.34	0.770	0.993	18.278
	Nd(III)	149.15	136.88	0.513	0.962	77.431
	Ho(III)	166.01	163.62	0.075	0.987	43.263
S950	La(III)	133.95	125.71	0.415	0.943	115.264
	Nd(III)	104.11	98.44	0.196	0.970	39.091
	Ho(III)	115.45	102.41	0.163	0.934	104.753
SP112	La(III)	94.77	90.29	0.449	0.984	17.287
	Nd(III)	161.04	141.94	0.318	0.875	123.108
	Ho(III)	201.74	187.38	0.822	0.960	170.487
M500	La(III)	68.55	63.61	0.570	0.975	15.803
	Nd(III)	71.56	69.27	0.467	0.975	17.209
	Ho(III)	92.27	87.36	2.923	0.985	17.839
M600	La(III)	63.27	59.13	1.691	0.972	15.492
	Nd(III)	65.66	62.83	0.849	0.975	14.664
	Ho(III)	85.26	81.92	3.062	0.988	12.176
MP500	La(III)	62.36	62.15	0.075	0.979	10.798
	Nd(III)	66.46	64.25	2.852	0.980	11.931
	Ho(III)	87.53	83.21	3.199	0.985	16.314
4200	La(III)	68.87	64.71	0.219	0.958	26.617
	Nd(III)	69.66	65.64	2.127	0.979	13.642
	Ho(III)	88.09	83.96	4.965	0.974	28.223
4400	La(III)	57.17	56.35	0.151	0.948	23.554
	Nd(III)	62.18	58.99	2.322	0.964	19.189
	Ho(III)	78.14	75.66	3.117	0.992	7.379
4600	La(III)	66.70	65.88	0.104	0.958	25.708
	Nd(III)	69.51	65.36	2.155	0.975	15.927
	Ho(III)	84.67	81.40	4.523	0.990	10.506
IRA 458	La(III)	79.21	83.40	0.053	0.985	12.802
	Nd(III)	82.15	72.45	1.754	0.932	59.809
	Ho(III)	99.02	93.14	2.718	0.983	22.642
IRA 958	La(III)	74.97	80.83	0.030	0.983	12.805
	Nd(III)	78.25	74.91	0.235	0.986	11.392
	Ho(III)	91.16	86.14	3.033	0.982	20.546
IRA 67	La(III)	75.20	101.78	0.005	0.984	10.329
	Nd(III)	70.40	119.31	0.003	0.989	6.184
	Ho(III)	86.60	85.06	0.019	0.864	114.070

	Freundlich				**Temkin**			
	K_F [mg/g]	n	R^2	χ^2	A [L/g]	B [J/mol]	R^2	χ^2

S957	La(III)	64.45	5.41	0.837	417.101	77.98	15.98	0.879	308.376
	Nd(III)	71.14	7.55	0.980	41.340	87.15	14.63	0.986	28.114
	Ho(III)	77.74	8.03	0.999	4.857	28.22	17.48	0.999	1.671
S950	La(III)	61.50	6.79	0.975	50.210	40.46	14.83	0.991	17.671
	Nd(III)	25.00	3.29	0.950	63.300	2.72	17.67	0.991	11.769
	Ho(III)	26.10	3.62	0.984	25.362	4.68	15.41	0.988	19.817
SP112	La(III)	49.13	8.01	0.986	15.148	101.27	9.57	0.995	5.861
	Nd(III)	96.12	9.67	0.957	112.054	2888.62	12.41	0.987	34.560
	Ho(III)	114.20	9.25	0.990	43.73	464.88	17.62	0.996	15.17
M500	La(III)	25.15	5.94	0.924	47.551	24.00	7.47	0.973	17.142
	Nd(III)	27.03	5.75	0.867	91.187	15.49	8.70	0.924	52.279
	Ho(III)	43.80	7.31	0.888	133.510	245.96	8.55	0.955	53.600
M600	La(III)	27.99	7.31	0.928	39.597	178.80	5.65	0.970	16.205
	Nd(III)	27.57	6.50	0.889	65.286	41.94	7.08	0.941	34.358
	Ho(III)	41.36	7.66	0.887	117.489	311.93	7.69	0.950	52.251
MP500	La(III)	15.45	4.33	0.895	55.045	1.27	10.01	0.954	24.246
	Nd(III)	35.81	8.98	0.878	74.277	263.01	5.08	0.919	49.721
	Ho(III)	42.10	7.64	0.893	115.142	364.05	7.69	0.952	51.361
4200	La(III)	20.63	4.94	0.911	56.323	4.95	9.08	0.957	27.430
	Nd(III)	32.70	7.35	0.922	51.172	254.21	6.29	0.973	17.599
	Ho(III)	45.15	8.23	0.891	119.529	906.00	7.25	0.954	50.674
4400	La(III)	17.74	5.14	0.878	54.949	3.76	7.86	0.921	35.429
	Nd(III)	29.24	7.51	0.898	53.992	195.17	5.72	0.940	31.973
	Ho(III)	38.93	8.23	0.870	113.224	439.35	6.72	0.930	60.946
4600	La(III)	17.32	4.38	0.898	62.426	1.84	10.32	0.947	32.297
	Nd(III)	32.43	7.34	0.917	53.846	244.41	6.27	0.966	22.383
	Ho(III)	42.48	8.11	0.871	131.936	537.79	7.25	0.930	71.216
IRA 458	La(III)	16.39	3.62	0.867	114.558	0.66	15.32	0.951	42.023
	Nd(III)	35.48	6.34	0.934	57.752	118.30	8.07	0.981	16.309
	Ho(III)	46.06	6.95	0.876	166.489	168.73	9.65	0.949	69.308
IRA 958	La(III)	11.83	3.17	0.890	83.209	0.33	15.97	0.965	26.379
	Nd(III)	25.55	4.93	0.931	54.611	10.10	9.82	0.976	18.523
	Ho(III)	43.03	7.33	0.895	122.013	263.58	8.33	0.957	50.121
IRA 67	La(III)	3.13	1.98	0.998	1.372	0.17	14.47	0.896	65.676
	Nd(III)	1.72	1.64	0.992	4.548	0.26	11.56	0.768	129.738
	Ho(III)	15.79	3.82	0.978	18.135	21.41	7.62	0.888	93.906

Table S13. Adsorption isotherm parameters for the sorption of La(III)-IDHA complexes on S957, S950, SP112, M500, M600, MP500, 4200, 4400, 4600, IRA 458, IRA 958, and IRA 67 at the temperature of 313 K and 333 K.

Model				Langmuir					
Ion exchanger	T [K]	$q_{e.exp}$ [mg/g]	q_0 [mg/g]	K_L [L/mg]	R^2	χ^2			
S957	313	149.58	149.43	1.750	0.994	23.129			
	333	154.13	151.56	4.269	0.995	18.061			
S950	313	148.57	137.60	0.456	0.948	124.723			
	333	151.57	145.88	0.999	0.980	59.780			
SP112	313	96.10	92.35	0.409	0.990	12.524			
	333	97.11	89.39	1.684	0.969	35.605			
M500	313	73.68	70.94	0.906	0.990	7.787			
	333	75.43	74.34	1.879	0.995	4.300			
M600	313	68.22	63.73	1.824	0.970	19.606			
	333	70.76	68.31	2.128	0.983	12.086			
MP500	313	67.87	65.16	0.305	0.976	15.395			
	333	72.18	68.77	1.240	0.973	19.195			
4200	313	71.92	67.80	0.357	0.972	19.941			
	333	74.85	72.75	1.394	0.974	20.887			
4400	313	62.33	60.38	0.501	0.987	6.852			
	333	67.03	65.60	1.047	0.972	17.775			
4600	313	72.34	67.56	0.448	0.975	17.299			
	333	76.55	72.54	1.145	0.974	21.367			
IRA 458	313	83.14	83.49	0.087	0.989	10.202			
	333	87.16	84.12	0.139	0.981	19.155			
IRA 958	313	77.14	80.61	0.040	0.993	5.271			
	333	78.49	80.32	0.048	0.992	6.030			
IRA 67	313	70.19	109.20	0.003	0.990	5.474			
	333	66.18	147.51	0.001	0.992	4.100			
			Freundlich				**Temkin**		
	T [K]	K_F [mg/g]	n	R^2	χ^2	A [L/g]	B [J/mol]	R^2	χ^2
S957	313	76.90	6.25	0.853	541.228	192.49	16.00	0.917	303.688
	333	89.02	5.69	0.859	534.211	281.95	17.65	0.927	276.936
S950	313	61.24	5.25	0.993	16.664	17.35	19.39	1.000	0.776
	333	87.66	7.87	0.988	37.331	241.38	15.41	0.991	26.285
SP112	313	54.32	9.29	0.992	10.229	269.64	8.80	0.996	4.823
	333	56.80	9.74	0.992	9.234	1263.77	7.80	0.998	2.424
M500	313	30.56	6.37	0.891	84.680	44.19	7.97	0.957	33.188
	333	35.85	7.44	0.825	144.053	154.27	7.32	0.894	87.198
M600	313	30.52	7.20	0.927	47.795	184.87	6.19	0.977	15.120
	333	32.99	7.50	0.867	94.127	198.18	6.50	0.921	55.668
MP500	313	24.80	5.82	0.927	46.052	20.87	7.60	0.981	12.050

	333	31.06	6.92	0.876	88.294	94.81	6.98	0.928	51.323
4200	313	24.28	5.36	0.911	63.122	10.11	8.87	0.966	24.274
	333	33.65	7.02	0.849	121.097	98.55	7.47	0.912	70.594
4400	313	25.05	6.44	0.901	54.030	30.30	6.80	0.961	21.015
	333	30.52	7.31	0.873	81.733	133.71	6.36	0.931	44.358
4600	313	26.18	5.77	0.933	47.365	22.27	8.02	0.986	9.816
	333	31.87	6.51	0.887	91.573	65.47	7.79	0.942	47.034
IRA 458	313	20.63	4.04	0.927	67.964	2.53	12.45	0.973	24.915
	333	23.83	4.30	0.943	56.170	6.40	11.22	0.962	37.986
IRA 958	313	14.41	3.47	0.917	65.443	0.76	13.66	0.964	28.204
	333	15.88	3.65	0.925	60.357	1.27	12.46	0.952	38.229
IRA 67	313	1.78	1.70	0.995	2.549	0.08	16.52	0.916	46.637
	333	0.72	1.40	0.995	2.266	0.05	17.23	0.891	53.439

Table S14. Adsorption isotherm parameters for the sorption of Nd(III)-IDHA complexes on S957, S950, SP112, M500, M600, MP500, 4200, 4400, 4600, IRA 458, IRA 958, and IRA 67 at the temperature of 313 K and 333 K.

Model			**Langmuir**			
Ion exchanger	T [K]	$q_{e.exp}$ [mg/g]	q_0 [mg/g]	K_L [L/mg]	R^2	χ^2
S957	313	160.84	156.51	0.268	0.985	52.140
	333	165.50	168.49	0.237	0.998	11.163
S950	313	111.31	100.57	0.748	0.968	45.690
	333	115.49	109.12	1.103	0.971	42.984
SP112	313	168.71	147.53	0.158	0.858	95.408
	333	172.93	149.60	0.592	0.868	81.675
M500	313	72.55	72.07	0.533	0.977	16.351
	333	73.22	72.53	1.310	0.973	20.142
M600	313	68.12	66.60	1.097	0.963	23.635
	333	69.23	67.31	1.252	0.957	28.100
MP500	313	69.75	66.29	3.508	0.974	16.885
	333	71.88	68.12	3.804	0.976	16.867
4200	313	71.17	67.68	2.817	0.982	12.777
	333	71.77	68.55	3.552	0.981	13.533
4400	313	64.56	62.07	2.450	0.979	12.189
	333	66.35	64.14	3.231	0.993	4.185
4600	313	70.71	66.79	2.369	0.982	11.958
	333	71.46	68.09	2.679	0.986	9.816
IRA 458	313	79.96	69.28	4.499	0.890	93.410
	333	78.72	67.36	5.876	0.865	111.462
IRA 958	313	76.95	74.71	0.194	0.990	8.056

	333	75.90		74.52	0.165		0.994		4.652
IRA 67	313	67.43		118.78	0.003		0.993		3.400
	333	65.29		145.94	0.002		0.997		1.407
			Freundlich					**Temkin**	
	T [K]	K_F [mg/g]	n	R^2	χ^2	A [L/g]	B [J/mol]	R^2	χ^2
S957	313	89.94	8.93	0.999	2.832	205.43	15.19	0.999	1.623
	333	99.57	9.38	0.999	0.054	291.61	15.82	1.000	0.051
S950	313	37.83	3.69	0.946	76.437	11.79	16.64	0.991	13.371
	333	46.99	3.28	0.942	86.673	15.88	19.49	0.992	12.411
SP112	313	100.55	9.08	0.964	99.420	2512.27	13.37	0.992	23.662
	333	104.02	8.95	0.966	97.730	2898.60	13.67	0.992	23.876
M500	313	29.99	6.23	0.807	138.975	23.46	8.60	0.875	90.175
	333	34.03	7.13	0.822	130.732	102.93	7.41	0.884	84.954
M600	313	30.70	7.04	0.827	109.470	74.91	6.98	0.879	76.554
	333	31.56	7.16	0.822	115.616	91.67	6.93	0.873	82.298
MP500	313	35.61	8.28	0.903	63.844	535.41	5.64	0.953	31.284
	333	36.98	8.28	0.898	71.355	556.20	5.85	0.952	33.868
4200	313	34.78	7.66	0.908	63.795	392.17	6.25	0.962	26.498
	333	36.58	8.05	0.893	75.565	623.07	6.11	0.953	33.143
4400	313	31.67	7.87	0.865	77.572	251.50	5.89	0.918	46.837
	333	33.66	8.22	0.858	85.838	423.32	5.80	0.915	51.519
4600	313	33.89	7.55	0.906	63.569	310.11	6.29	0.960	26.821
	333	35.32	7.77	0.897	71.564	429.24	6.23	0.954	31.728
IRA 458	313	36.25	6.74	0.951	41.884	275.62	7.19	0.989	9.241
	333	35.96	6.84	0.950	41.200	335.98	6.92	0.983	13.805
IRA 958	313	24.33	4.80	0.921	60.370	6.62	10.31	0.979	16.326
	333	23.12	4.66	0.911	66.818	4.44	10.82	0.977	17.307
IRA 67	313	1.32	1.57	0.999	0.628	0.07	16.21	0.901	50.021
	333	0.73	1.39	0.999	0.522	0.04	18.08	0.913	41.061

Table S15. Adsorption isotherm parameters for the sorption of Ho(III)-IDHA complexes on S957, S950, SP112, M500, M600, MP500, 4200, 4400, 4600, IRA 458, IRA 958, and IRA 67 at the temperature of 313 K and 333 K.

Model				**Langmuir**		
Ion exchanger	T [K]	$q_{e.exp}$ [mg/g]	q_0 [mg/g]	K_L [L/mg]	R^2	χ^2
S957	313	176.59	167.29	0.208	0.976	87.789
	333	185.55	177.33	0.306	0.978	90.061
S950	313	123.44	110.93	0.191	0.938	110.393
	333	129.34	114.79	0.304	0.931	133.156

SP112	313	204.40	188.94	1.016	0.960	172.217
	333	205.80	192.78	0.847	0.970	147.601
M500	313	93.49	88.44	3.831	0.984	19.049
	333	94.00	88.53	5.244	0.982	21.878
M600	313	86.75	83.05	5.551	0.979	22.408
	333	87.42	83.21	7.795	0.978	23.580
MP500	313	91.09	85.72	4.255	0.978	25.273
	333	92.63	86.88	5.407	0.973	32.305
4200	313	89.39	84.88	6.290	0.974	30.049
	333	90.97	85.34	9.784	0.968	37.118
4400	313	82.94	79.93	3.453	0.986	13.777
	333	85.26	81.61	3.965	0.983	17.422
4600	313	88.21	84.37	5.758	0.987	14.960
	333	88.83	84.45	7.917	0.978	24.599
IRA 458	313	98.35	93.93	1.871	0.989	14.373
	333	97.90	93.91	1.557	0.988	15.757
IRA 958	313	89.14	85.02	2.610	0.985	16.368
	333	88.44	84.93	1.998	0.987	14.549
IRA 67	313	80.21	103.45	0.004	0.901	67.347
	333	79.19	115.24	0.003	0.908	60.790

		Freundlich				**Temkin**			
	T [K]	K_F [mg/g]	n	R^2	χ^2	A [L/g]	B [J/mol]	R^2	χ^2
S957	313	95.26	9.66	0.998	6.175	255.93	15.22	0.999	4.836
	333	102.41	9.19	0.999	3.782	236.10	16.88	0.999	2.890
S950	313	29.76	3.53	0.985	26.269	6.24	16.53	0.986	24.292
	333	34.22	3.45	0.984	30.542	8.83	17.50	0.985	29.399
SP112	313	117.24	9.32	0.990	44.078	602.79	17.57	0.996	16.627
	333	124.58	9.47	0.998	10.846	1585.45	16.22	0.999	4.388
M500	313	45.43	7.56	0.878	148.176	357.10	8.37	0.943	68.896
	333	47.04	7.86	0.883	143.047	620.49	8.02	0.948	64.094
M600	313	44.01	8.19	0.871	137.606	713.66	7.26	0.928	76.652
	333	45.93	8.59	0.886	123.009	1469.18	6.91	0.947	57.791
MP500	313	44.95	7.84	0.897	118.264	590.26	7.71	0.959	47.457
	333	47.12	8.11	0.900	119.182	975.69	7.55	0.964	43.155
4200	313	46.64	8.32	0.892	123.285	1082.47	7.32	0.958	47.712
	333	48.63	8.65	0.895	122.584	1937.24	7.10	0.961	45.232
4400	313	41.94	8.17	0.886	112.341	586.66	7.06	0.952	47.599
	333	43.41	8.23	0.892	112.042	760.77	7.09	0.957	44.929
4600	313	45.19	8.17	0.875	138.575	713.56	7.46	0.940	66.892

	333	46.96	8.58	0.882	132.088	1426.49	7.09	0.947	59.754
IRA 458	313	44.50	6.72	0.864	181.410	103.95	10.08	0.939	81.179
	333	43.52	6.59	0.862	182.649	82.71	10.26	0.937	83.040
IRA 958	313	42.06	7.34	0.885	129.364	220.52	8.30	0.949	56.745
	333	40.65	7.10	0.877	136.914	138.21	8.62	0.943	63.863
IRA 67	313	4.88	2.33	0.970	20.679	0.80	10.31	0.846	104.575
	333	3.52	2.09	0.965	22.930	0.41	11.39	0.843	103.830

Table S16. Thermodynamic parameters for the sorption of Nd(III)-IDHA complexes on S957, S950, SP112, M500, M600, MP500, 4200, 4400, 4600, IRA 458, IRA 958, and IRA 67.

Ion exchanger	$\Delta H°$ [kJ/mol]	$\Delta S°$ [J/mol K]	$\Delta G°$ [kJ/mol]		
			293 K	313 K	333 K
S957	19.74	119.76	-15.27	-17.90	-20.04
S950	37.05	181.06	-16.14	-19.32	-23.42
SP112	12.33	94.80	-15.42	-17.40	-19.20
M500	1.24	46.42	-12.36	-13.30	-14.22
M600	2.57	49.27	-11.85	-12.89	-13.82
MP500	3.94	54.17	-11.92	-13.04	-14.08
4200	1.56	46.98	-12.20	-13.17	-14.07
4400	2.94	49.51	-11.56	-12.56	-13.54
4600	1.43	46.47	-12.18	-13.13	-14.04
IRA 458	-2.82	35.92	-13.36	-14.04	-14.80
IRA 958	-1.84	38.01	-12.98	-13.73	-14.50
IRA 67	-3.62	29.23	-12.20	-12.76	-13.37

Table S17. Thermodynamic parameters for the sorption of Ho(III)-IDHA complexes on S957, S950, SP112, M500, M600, MP500, 4200, 4400, 4600, IRA 458, IRA 958, and IRA 67.

Ion exchanger	$\Delta H°$ [kJ/mol]	$\Delta S°$ [J/mol K]	$\Delta G°$ [kJ/mol]		
			293 K	313 K	333 K
S957	11.11	87.62	-14.63	-16.17	-18.15
S950	18.60	114.36	-14.94	-17.13	-19.52
SP112	3.74	67.85	-16.12	-17.53	-18.83
M500	1.15	47.88	-12.87	-13.85	-14.78
M600	1.35	46.73	-12.34	-13.30	-14.21
MP500	3.28	53.97	-12.51	-13.65	-14.66
4200	1.83	49.05	-12.55	-13.51	-14.51
4400	4.31	55.16	-11.82	-13.00	-14.02
4600	2.62	51.01	-12.30	-13.42	-14.33
IRA 458	-0.79	43.11	-13.42	-14.28	-15.15
IRA 958	-1.75	37.63	-12.78	-13.49	-14.29

IRA 67	-4.56	26.71	-12.44	-12.79	-13.52

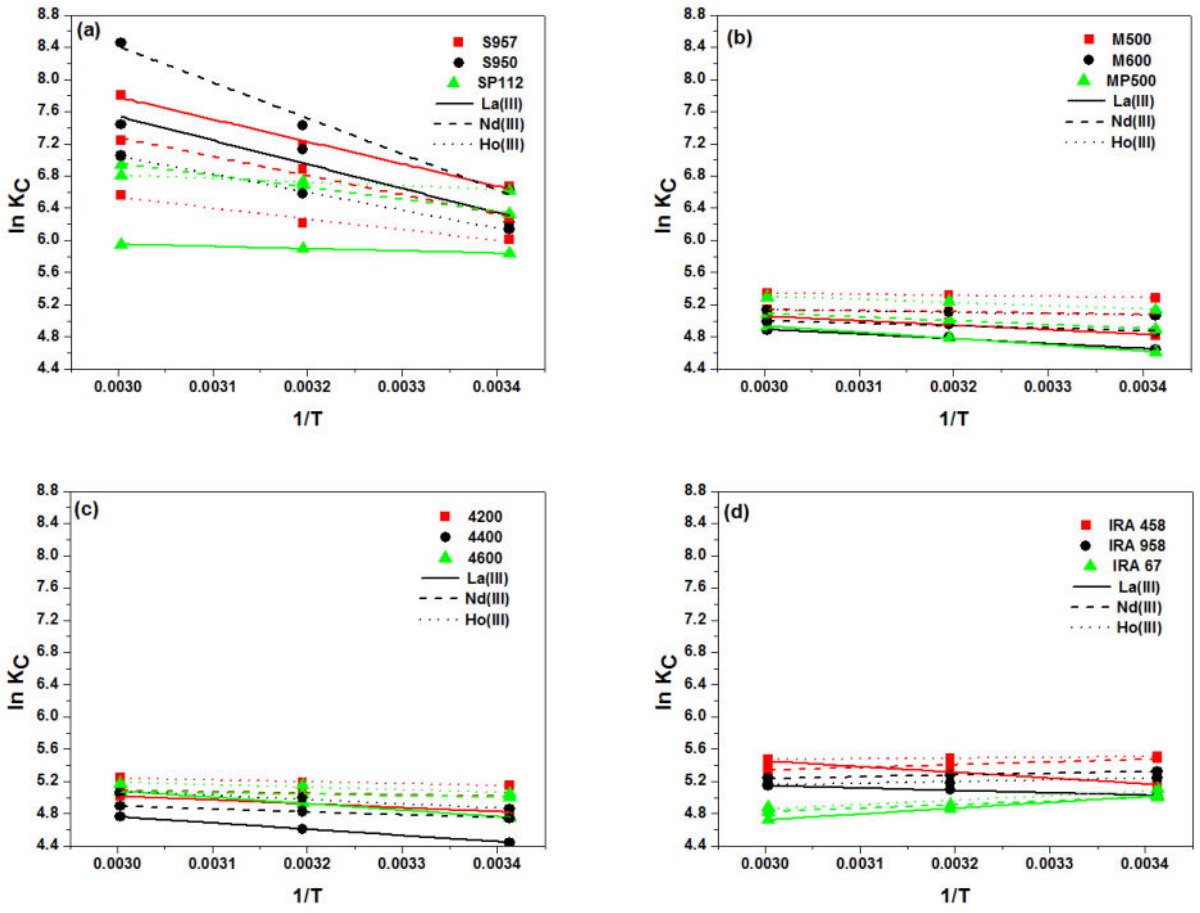

Figure S10. Plots of lnK_C as a function of reciprocal of temperature (1/T) for the sorption of La(III), Nd(III) and Ho(III) complexes with IDHA on (a) S957, S950 and SP112, (b) M500, M600 and MP500, (c) 4200, 4400 and 4600, (d) IRA 458, IRA 958 and IRA 67.

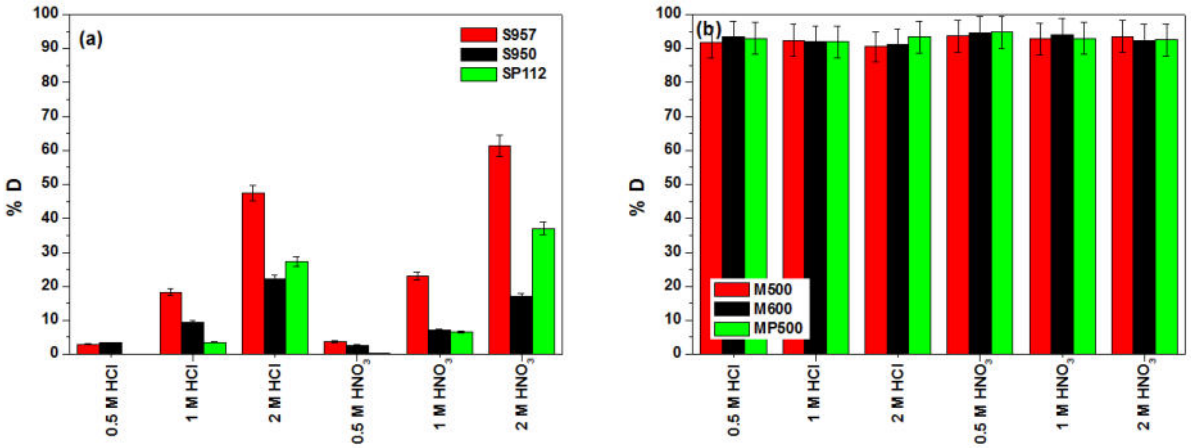

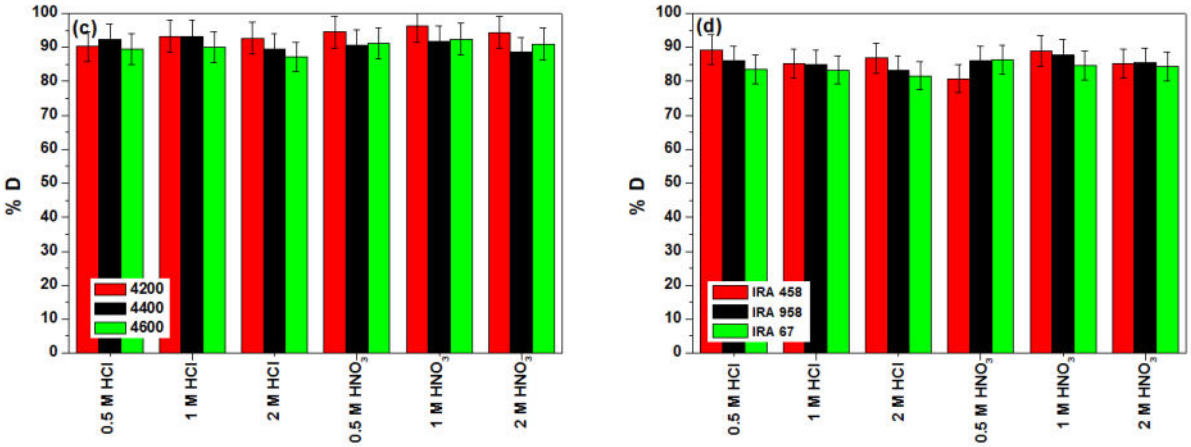

Figure S11. Dependence of Nd(III) ions desorption capacity on (a) S957, S950, SP112, (b) M500, M600, MP500, (c) 4200, 4400, 4600 and (d) IRA 458, IRA 958, IRA 67 using the desorption agents: HCl and HNO_3 at various concentrations.

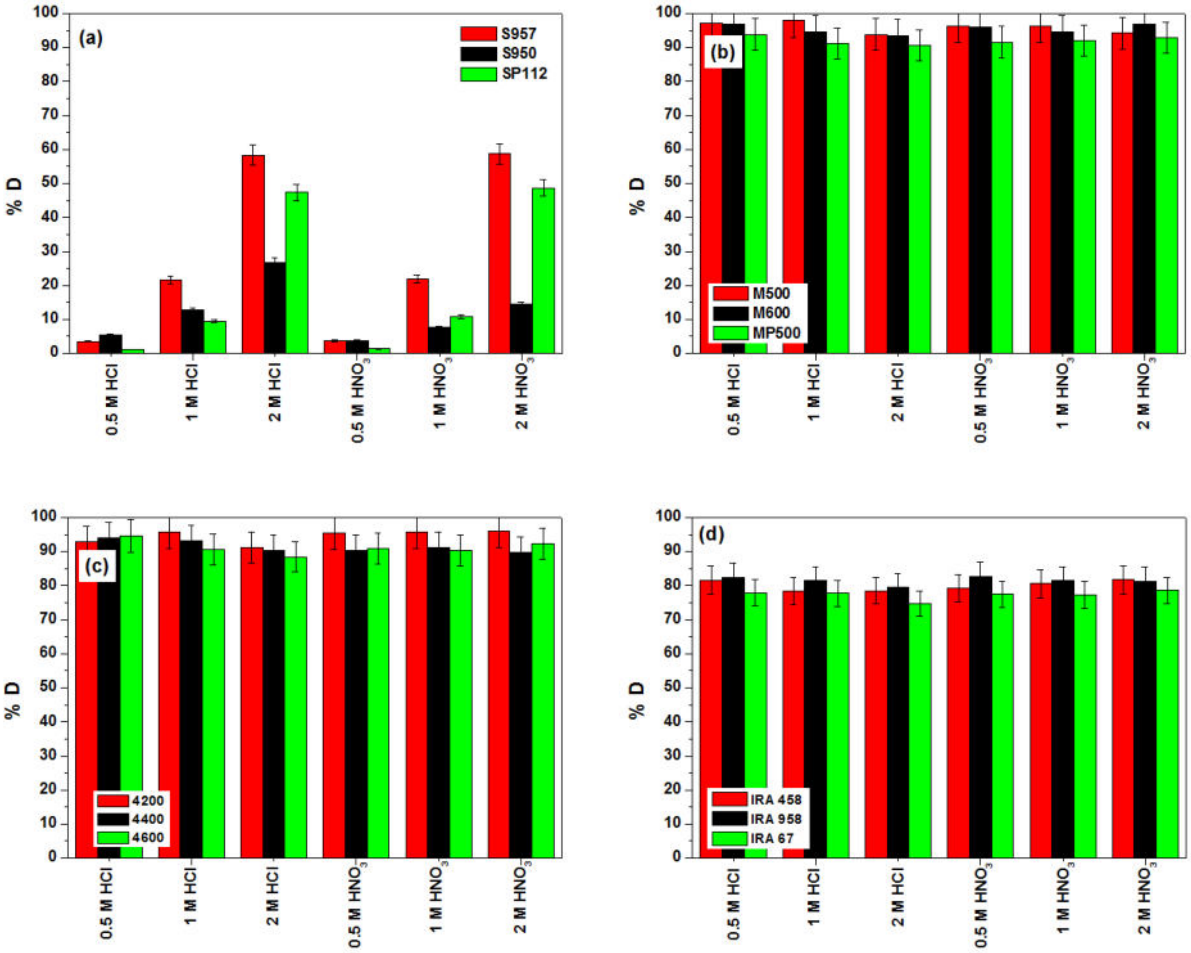

Figure S12. Dependence of Ho(III) ions desorption capacity on (a) S957, S950, SP112, (b) M500, M600, MP500, (c) 4200, 4400, 4600 and (d) IRA 458, IRA 958, IRA 67 using the desorption agents: HCl and HNO_3 at various concentrations.

Table S18. Reusability studies of the ion exchangers with the exemplary adsorption/desorption of La(III)-IDHA complexes.

Number of cycles	S957		S950		SP112	
	%S	*%D*	*%S*	*%D*	*%S*	*%D*
1	99.79	69.04	99.81	47.45	99.91	33.45
2	98.27	68.35	99.88	52.75	99.46	36.90
3	99.96	84.50	99.92	75.50	99.95	58.54
4	99.86	88.87	98.55	88.28	99.91	78.04
5	99.84	88.36	99.93	90.48	99.92	88.29
Number of cycles	**M500**		**M600**		**MP500**	
	%S	*%D*	*%S*	*%D*	*%S*	*%D*
1	98.25	93.42	98.82	94.11	98.85	97.32
2	84.94	59.97	91.96	78.90	17.60	8.82
3	91.34	75.56	94.46	82.09	27.74	7.25
4	90.47	84.51	93.96	84.83	29.63	1.67
5	92.26	13.10	95.39	73.50	33.28	1.28
Number of cycles	**4200**		**4400**		**4600**	
	%S	*%D*	*%S*	*%D*	*%S*	*%D*
1	99.09	90.51	98.67	87.30	98.96	77.72
2	87.41	76.76	84.03	49.39	96.80	63.78
3	84.55	82.53	90.10	63.99	98.69	66.04
4	84.92	88.67	91.35	70.35	95.13	62.47
5	83.56	62.88	92.05	59.00	93.96	54.75
Number of cycles	**IRA 458**		**IRA 958**		**IRA 67**	
	%S	*%D*	*%S*	*%D*	*%S*	*%D*
1	95.67	71.28	92.57	68.59	69.66	80.11
2	37.03	2.83	34.02	1.27	26.65	0.61
3	42.89	13.89	41.30	2.43	30.70	0.72
4	43.75	6.08	43.24	1.16	32.15	0.20
5	39.08	0.78	42.26	1.02	34.48	1.10

Table S19. Breakthrough fitting models results for the adsorption of La(III)-IDHA acid complexes.

Model	**Thomas**			**Adams–Bohart**		
Ion exchanger	$k_{Th} \times 10^3$ [mL/mg min]	q_0 [mg/g]	R^2	$k_{AB} \times 10^6$ [L/mg min]	q [mg/L]	R^2
S957	11.01	274.89	0.990	9.20	97678.56	0.961
S950	10.95	227.83	0.958	9.03	73195.88	0.969
SP112	26.65	214.78	0.926	15.85	69723.34	0.928

M500	22.05	102.28	0.934	15.67	31266.02	0.972
M600	24.12	93.39	0.964	17.69	29376.28	0.971
MP500	26.46	106.89	0.950	20.34	23487.10	0.902
4200	19.80	98.43	0.910	13.82	33071.25	0.985
4400	19.82	93.18	0.938	14.55	33758.96	0.986
4600	25.39	97.20	0.948	19.41	31195.61	0.986
IRA 458	16.65	86.07	0.893	12.26	29949.55	0.930
IRA 958	19.74	70.23	0.913	14.54	21134.93	0.788
IRA 67	72.19	7.74	0.808	209.04	1512.80	0.907
	Yoon–Nelson			**Wolborska**		
	k_{YN} [1/min]	τ [min]	R^2	β [1/min]	q [mg/L]	R^2
S957	0.0015	14595.54	0.990	0.899	97678.56	0.961
S950	0.0015	10708.42	0.958	0.661	73195.88	0.969
SP112	0.0038	9517.69	0.926	1.105	69723.34	0.928
M500	0.0031	3998.49	0.934	0.490	31266.02	0.972
M600	0.0034	3856.00	0.964	0.520	29376.28	0.971
MP500	0.0037	3144.66	0.950	0.478	23487.10	0.902
4200	0.0028	4210.84	0.910	0.457	33071.25	0.985
4400	0.0028	4349.60	0.938	0.491	33758.96	0.986
4600	0.0036	4134.94	0.948	0.605	31195.61	0.986
IRA 458	0.0024	3803.82	0.893	0.367	29949.55	0.930
IRA 958	0.0028	2677.92	0.913	0.307	21134.93	0.788
IRA 67	0.0105	326.02	0.808	0.316	1512.80	0.907

[D4] K. Burdzy, R. Jastrząb, D. Kołodyńska, *GLDA and ion exchangers: unlocking sustainable solutions for recovery of rare earth elements*, Sustainable Materials and Technologies (2023) – w recenzji

IF_{2022}: 10,681 **Punkty MEiN**: 200

GLDA AND ION EXCHANGERS: UNLOCKING SUSTAINABLE SOLUTIONS FOR RECOVERY OF RARE EARTH ELEMENTS

Katarzyna Burdzy[1], Renata Jastrząb[2], Dorota Kołodyńska[1]*

[1]Department of Inorganic Chemistry, Faculty of Chemistry, Maria Curie-Skłodowska University, M. Curie Skłodowska Sq. 2, 20-031 Lublin, Poland

[2]Faculty of Chemistry, Adam Mickiewicz University, Uniwersytetu Poznańskiego 8, 61-614 Poznań, Poland

Abstract

GLDA (tetrasodium salt of N,N-bis(carboxymethyl)-L-glutamic acid) was used for rare earth elements adsorption. Twelve commercial ion exchangers of different types were used as adsorbents in this process. They were characterized by describing the physicochemical properties: sieve analysis, scanning electron microscopy, X-ray photoelectron spectroscopy, and Fourier transform infrared spectroscopy. The stability constants of the Ln(III)-GLDA complexes in the binary systems at different Ln(III):GLDA molar ratios were determined by the potentiometric method. The effects of different process parameters (Ln(III):GLDA molar ratio, initial solution pH, phase contact time, initial solution concentrations, and temperature) on the adsorption of La(III), Nd(III), and Ho(III) ions in the presence of GLDA were investigated by the static method in the single-component systems. Kinetic, equilibrium, and thermodynamic parameters were calculated. The highest adsorption capacities were obtained for the Purolite S957 ion exchanger (139.57 mg/g for the La(III)-GLDA complexes, 152.72 mg/g for the Nd(III)-GLDA complexes, and 151.29 mg/g for the Ho(III)-GLDA complexes), Lewatit Monoplus SP112 ion exchanger (155.49 mg/g for the La(III)-

GLDA complexes, 150.23 mg/g for the Nd(III)-GLDA complexes, and 132.77 mg/g for the Ho(III)-GLDA complexes). The desorption process was performed to regenerate the ion exchangers. In addition, experiments were performed in the column systems.

Keywords: adsorption, chelating agents, GLDA, rare earth elements, ion exchangers

1. Introduction

GLDA (tetrasodium salt of N,N-bis(carboxymethyl)-L-glutamic acid) is a synthetic compound belonging to the group of aminopolycarboxylates (APCs), whose molecule is composed of two carboxymethyl groups attached to the nitrogen atom of glutamate (Fig. 1). The presence of one nitrogen atom in its molecule makes GLDA more readily biodegradable compared with conventional APCs (the presence of tertiary amines in, for example, EDTA or DTPA hinders their biodegradation) [1,2]. GLDA exists in two isomer forms of which, as shown in the study by Ginkel et al. [3], only the L-GLDA form is readily and completely degraded by microbial cultures. Borowiec et al. [4] compared the degree of biodegradation of GLDA and EDTA and found that GLDA was characterized by a high biodegradation rate of over 90%, while EDTA exhibited non-biodegradability. In addition, based on the Organization for Economic Development and Cooperation (OECD) screening tests, the officially recognized tests for assessing biodegradability, Ginkel and Geerts [5] found that GLDA is more than 60% biodegradable in less than 60 days and that its conversion to water, carbon dioxide, ammonium, and biomass is catalyzed by the *Rhizobium radiobacter* strain BG-1. This extremely valuable property of GLDA complexing agent, combined with its non-toxicity and safety of application, in contrast to conventional ligands, makes it an environmentally friendly compound. Another advantage of GLDA, that favours its increasing application, is its high solubility in both strongly acidic and strongly alkaline environments [6]. The thermal stability studies of GLDA showed that it is stable in the form of aqueous solutions up to 150^{o}C. Increasing the temperature to 170^{o}C resulted less than 12% degradation [7]. In the paper [8], the authors identified hydroxyglutaric acid and iminodiacetic acid as the primary degradation products of GLDA, while iminodiacetic acid is further decarboxylated to glycine and hydroxyacetic acid (Fig. 1).

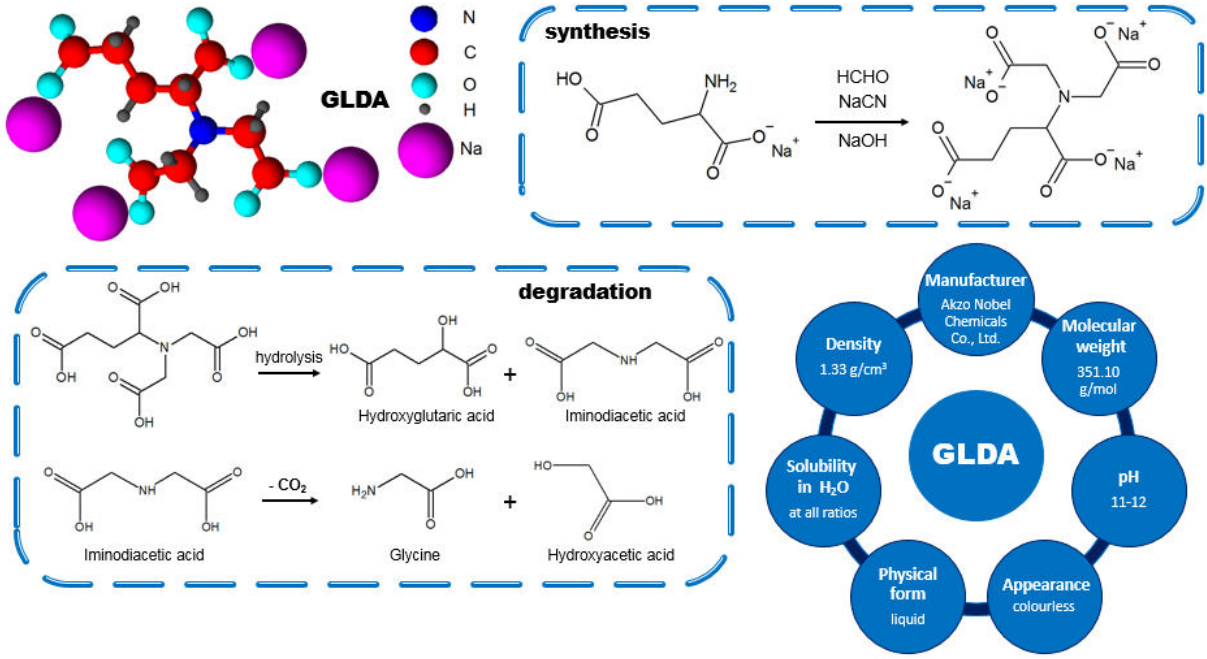

Fig. 1. Structure, synthesis, degradation, and properties of GLDA.

Due to the presence of the nitrogen atom and the four carboxyl groups in the molecule, GLDA as a pentadentate ligand forms very stable and soluble complexes with many metal ions [2,9–11]. Increased public awareness of the environment and its pollutants has led to a high demand for a chemical compound characterized by excellent complexing properties and, at the same time, high biodegradability since its entry into the market. Today, GLDA can be found in the composition of detergents along with citrates and carbonates [12]. As a water additive in the recirculating water systems, GLDA prevents precipitation of metals and inhibits deposition on metal surfaces [13]. It has also been proposed as a solvent for solid-deposits in oil wells, which, when deposited, disrupt oil production and cause large economic losses each year [14]. Salalá and Watanabe et al. [15,16] investigated the use of GLDA in geothermal systems for power generation through a process of chemical stimulation to increase the permeability of geothermal reservoirs. To protect cultural heritage, GLDA can be used in the cleaning and conservation of copper-alloy artifacts as an alternative

to chemical cleaning with EDTA [17]. The studies have shown that GLDA improves the mobility and availability of iron, an important nutrient for plant growth, resulting in more intensive plant growth [18]. In recent years, much research has been conducted on the use of GLDA in soil remediation. The complexation of metal ions into forms that can be better taken up by plants is used in phytoremediation processes. Yang et al. [19] studied the effect of complexing agents (including GLDA) on As(V) accumulation in *L. minor* plants by affecting Fe(III) deposition, which limits effective phytoremediation. They discovered that the addition of GLDA increased the accumulation of As(III) and As(V) ions while enhancing the uptake of other essential elements (phosphorus and iron). Similarly, Masoudi et al. [20] analysed the effect of GLDA on the removal of heavy metals from contaminated soils by corn using zinc and lead as examples. Guan et al. [21] compared the effects of GLDA and EDTA on phytoremediation of cadmium and lead by *Sedum hybridum* 'Immergrunchen'. GLDA increased the amount of metal ions removed from the soil in both cases. In recent years, a number of papers have also been published focusing on soil washing methods as a method to treat toxic pollutants [22–24]. They demonstrated the high effectiveness of both the pure complexing agent GLDA and its mixtures with citric acid, ascorbic acid, EDDS, or NTA, among others, in removing heavy metals while retaining most nutrients in the soil. The use of recycled GLDA for this purpose was also an important study, and its effectiveness was found to be comparable to that of the fresh solution [22]. The growing number of applications and the increasing prevalence of GLDA in the environment encouraged further research on this compound, such as the development of a direct determination method [25].

Complexing agents are used in metal recovery processes. A common method for this purpose is adsorption because it can achieve high process efficiency with ease

of use and low cost. There are numerous studies on the removal and recovery of metal ions by adsorption in the presence of EDTA (ethylenediaminetetraacetic acid) or DTPA (diethylenetriaminepentaacetic acid) [26–29]. However, the application of biodegradable complexing agents such as GLDA is under investigation. Of particular importance is the recycling of those elements whose deposits have been depleted or whose extraction poses many difficulties. This group includes the rare earth elements (REEs), whose unique magnetic, luminescent, fluorescent, and optical properties have led to their use in many high-tech products.

The aim of this paper was to study the complexes of REEs with the biodegradable complexing agent GLDA by a potentiometric method (determination of stability constants) and then to perform adsorption of the complexes on twelve different ion exchangers for the selected REE representatives (La(III), Nd(III) and Ho(III)). Among the ion exchangers selected for the experiments there were chelating ion exchangers (SAC-CIE), strongly cation exchanger (SAC), strongly basic anion exchangers (SBA), and weakly basic anion exchanger (WBA) which differed in the matrix, functional groups, structure, and bead size. A static method was used to investigate the effects of the Ln(III):GLDA molar ratio, initial solution pH, phase contact time, initial solution concentrations, and temperature on the adsorption of Ln(III)-GLDA complexes. Then the pseudo-first order, pseudo-second order, intraparticle diffusion, Boyd, Dumwald-Wagner kinetic and the Langmuir, Freundlich, and Temkin equilibrium models were used to describe the studied process. The thermodynamic parameters were determined. Adsorption was also performed using the dynamic method. The results were analysed using the Thomas, Adams-Bohart, Yoon-Nelson, and Wolborska models. In addition, the desorption process was carried out to regenerate the ion exchangers and their physicochemical characterization was performed.

2. Materials and Methods

2.1. Materials

The following ion exchangers were selected: Purolite S950, Purolite S957 (denoted as SAC-S950, SAC-S957), Lewatit Monoplus SP112 (denoted as SAC-SP112), Lewatit MonoPlus M500 (denoted as SBA-M500), Lewatit MonoPlus MP500, (denoted as SBA-MP500), Lewatit MonoPlus M600 (denoted as SBA-M600), Amberjet 4200 (denoted as SBA-4200), Amberjet 4400 (denoted as SBA-4400), Amberjet 4600, (denoted as SBA-4600), Amberlite IRA 958 (denoted as SBA-IRA 958), Amberlite IRA 458 (denoted as SBA-IRA 458) and Amberlite IRA 67 (denoted as WBA-IRA 67). More information on these ion exchangers is available in our previous paper [30].

The biodegradable complexing agent, GLDA (tetrasodium salt of N,N-bis(carboxymethyl)-L-glutamic acid), manufactured by Akzo-Nobel (Amsterdam, The Netherlands), was used as a ligand in the complexation of rare earth element ions. The product was an aqueous solution with a concentration of 38 wt% and was used without additional treatment.

The rare earth elements in the form of hydrated nitrate salts (i.e. $La(NO_3)_3 \cdot 6H_2O$, $Ce(NO_3)_3 \cdot 6H_2O$, $Pr(NO_3)_3 \cdot 6H_2O$, $Nd(NO_3)_3 \cdot 6H_2O$, $Sm(NO_3)_3 \cdot 6H_2O$, $Ho(NO_3)_3 \cdot 5H_2O$) were purchased from Sigma-Aldrich (Germany). La(III), Nd(III), and Ho(III) were selected as representative rare earth elements for the adsorption study.

2.2. Analytical methods

Elpin type 357 and Elpin type 358A laboratory shakers (Elpin Plus, Poland) were applied to perform the static adsorption. Measurements of the solution pH were done using the pHmeter pHM82 (Radiometer, Copenhagen).

The Ln(III) ion concentration was determined by inductively coupled plasma optical emission spectrometry using Varian 720-ES axial ICP-OES (Varian Inc., USA). Five standards with concentrations ranging from 0.25 to 20 mg/L and the blank solution were employed to create the calibration curves. To exclude matrix interference, all standards and blank samples were prepared with high purity HNO_3. La(III), Nd(III), and Ho(III) ions were measured at 333.749 nm, 401.224 nm, and 345.600 nm, respectively. The relative standard deviation (RSD) for the triple analysis was within 5%.

The bead size distribution of the ion exchangers was determined by the sieve analysis. For this purpose, 10 g of dry ion exchangers were sieved for 1 minute using laboratory sieves (Retsch, Poland) with a diameter of 200 × 50 mm and a mesh size of 100 to 900 μm.

The surface morphology of the ion exchanger beads was observed with a scanning electron microscope (SEM) using the Quanta 3D FEG (FEI, USA) with the EDS (Energy Dispersive Spectroscopy)/EBSD (Electron Backscatter Diffraction) system (FEI, USA). SEM were recorded at a magnification of 10,000x.

The X-ray photoelectron spectroscopy (XPS) was performed using ultra-high vacuum multi-chamber analytical system (Prevac, Poland) equipped with the monochromatic AlK_α radiation.

The FTIR spectra of the ion exchangers before and after the adsorption process were recorded using the Agilent Cary 630 ATR FT-IR spectrometer with the attenuated total reflectance mode (Agilent Technologies, Inc., USA) in the wavelength range 4000-650 cm^{-1} with a spectral resolution of 4 cm^{-1}. The spectra were collected using the MicroLab software (version B.04) and processed using Agilent Resolutions Pro software (version 5.2.0.861).

The potentiometric titrations were made with the 907 Titrando titrator equipped with dosing system (Metrohm, Switzerland). Prior to each measurement series, the display of the pH-meter was corrected with two standard buffer solutions of pH 4.00 and pH 9.00, and the operation conditions were as previously [30]. The protonation constants of the complexing agent (GLDA) and the stability constants of the rare earth element complexes with GLDA in the 1:1, 1:2, and 2:1 systems were calculated using the HYPERQUAD2008 program (Hyperquad Limited, Leeds, UK). The water ion product (pK_w) included in the computer analysis was 13.78.

2.3. Adsorption studies (static and dynamic methods)

The stock solutions of La(III), Nd(III), and Ho(III) ions with the 1×10^{-2} M concentration were prepared by dissolving appropriate amounts of hydrated rare earth nitrate salts ($La(NO_3)_3\cdot6H_2O$, $Nd(NO_3)_3\cdot6H_2O$ or $Ho(NO_3)_3\cdot5H_2O$) in deionized water. To prepare solutions for the adsorption studies with the desired concentrations and molar ratios of metal to ligand, appropriate volumes of the metal ion stock solution were added to the GLDA solutions. The ICP-OES spectroscopy was used to determine the final ion concentration.

The static adsorption experiments (single-component systems) were performed according to the following procedure: 0.1 g of the ion exchanger was added to 100 cm^3 Erlenmeyer flasks, then 10 mL of the Ln(III)-GLDA complexes solution was added and mechanically stirred at a shaking speed of 180 rpm and the amplitude of 8. After the indicated shaking time, the samples were separated with a filter paper. Each experiment was performed three times, and the presented results are their average. The influence of various factors on the Ln(III)-GLDA complexes adsorption was investigated. The studies on the molar Ln(III):GLDA ratio effect were performed at a metal ion concentration of 1.0×10^{-3} M and without pH adjustment. The influence of the

pH was also tested. The pH of the solutions was corrected to the desired value with 1 M HNO_3 or 1 M NaOH. The adsorption kinetic studies were performed for the contact time of the adsorbate with the adsorbent from 1 to 240 minutes and at the initial concentrations of 0.5×10^{-3}, 1.0×10^{-3}, and 1.5×10^{-3} M. The adsorption isotherms at the temperatures of 293, 313, and 333 K were determined using solutions with initial concentrations in the range of 0.5×10^{-3}-1.2×10^{-2} M. All experiments were conducted at 293 K (except for the adsorption isotherm studies at higher temperatures).

The desorption tests were carried out on the ion exchanger after the Ln(III)-GLDA complexes adsorption (prepared as described above). 0.1 g of the dried sample was weighed into 100 mL Erlenmeyer flasks and shaken at 180 rpm and 293 K with 10 mL of the desorbent media solution for 240 minutes. The effect of the desorbent agent (HCl or HNO_3) and the concentration (0.5, 1, and 2 M) was investigated.

The adsorption of La(III)-GLDA complexes on ion exchangers was also investigated in column systems, employing glass columns with a diameter of 1.5 cm and a height of 25 cm filled with 10 mL of swollen, suitable ion exchanger. In this stage, the optimal adsorption conditions for La(III)-GLDA complexes developed by the static method were applied: pH 8.0 and the La(III):GLDA ratio of 1:1 for SAC-S950 and SAC-S957, pH 2.0 and the La(III):GLDA ratio of 1:1 for SAC-SP112, pH 10.0 and the La(III):GLDA ratio of 1:2 for SBA-M500, SBA-MP500, SBA-M600, SBA-4200, SBA-4400, SBA-4600, SBA-IRA 958, SBA-IRA 458, and pH 4.0 and the La(III):GLDA ratio of 1:2 for WBA-IRA 67. The solution with a La(III) ion concentration of 1.0×10^{-3} M flowed through the bed at a constant rate of 0.6 mL/min at 293 K. After passing through the column, the effluent was collected in fractions and analysed by using the ICP-OES. The experiments in the column systems were terminated when the La(III) ions

concentration in the effluent was equal to the concentration of the solution entering the column.

2.4. Calculations

2.4.1. Static method: basic parameters

The adsorption capacities at the equilibrium q_e [mg/g] and at the defined time q_t [mg/g], the adsorption effectiveness *%S* and the desorption percentage *%D* were calculated from Eqs. 1-4.

$$q_e = (C_0 - C_e) \times \frac{V}{m} \quad (1)$$

$$q_t = (C_0 - C_t) \times \frac{V}{m} \quad (2)$$

$$\%S = \frac{(C_0 - C_t)}{C_0} \times 100\% \quad (3)$$

$$\%D = \frac{C_{des}}{C_0} \times 100\% \quad (4)$$

where C_0 is the initial concentration of Ln(III) [mg/L], C_e is the equilibrium concentration of Ln(III) [mg/L], C_t is the concentration of Ln(III) after time *t* [mg/L], *V* is the volume of the solution [L], *m* is the mass of ion exchanger [g], C_{des} is the concentration of Ln(III) after the desorption process [mg/L].

2.4.2. Dynamic method: basic parameters and mathematical models

Based on the results obtained in the column systems, using Eqs. 5-9, the values of the following parameters were determined: the adsorption capacity at the exhaustion point q_e [mg/g], the work exchange capacity C_w [mg/mL], the total exchange capacity C_t [mg/mL], the mass distribution coefficient D_g and the volume distribution coefficient D_v.

$$q_e = \frac{1}{m_j} \int_0^{V_k} (C_0 - C) dV \quad (5)$$

$$C_w = \frac{U \times C_0}{V_j} \quad (6)$$

$$C_t = \frac{\bar{U} \times C_0}{V_j} \quad (7)$$

$$D_g = \frac{\bar{U} - U_0 - V}{m_j} \quad (8)$$

$$D_v = \frac{\bar{U} - U_0 - V}{V_j} \quad (9)$$

where: C_0 is the concentration of Ln(III) ions in the solution entering the column [mg/mL], C is the concentration of Ln(III) ions in the leakage [mg/mL], V_k is the volume of solution required for the bed exhaustion [mL], m_j is the mass of the dry ion exchanger filling the column [g], U is the leakage volume required to reach the breakthrough point [mL], V_j is the volume of the ion exchanger placed in the column [mL], $\bar{U}$ is the leakage volume until C/C_0=0.5 [mL], U_0 is the dead volume in the column [mL] and V is the volume of empty space between the resin beads (0.4 mL).

The dynamics of the La(III)-GLDA adsorption process was estimated using the Thomas [31], Adams-Bohart [32], Yoon-Nelson [33], and Wolborska [34] models:

$$ln\left(\frac{C_0}{C} - 1\right) = \frac{k_{Th} q_0 m}{Q} - \frac{k_{Th} C_0}{Q} V \quad (10)$$

$$ln\left(\frac{C}{C_0}\right) = k_{AB} C_0 t - k_{AB} q \frac{H}{v} \quad (11)$$

$$ln\left(\frac{C}{C_0 - C}\right) = k_{YN} t - k_{YN} \tau \quad (12)$$

$$ln\left(\frac{C}{C_0}\right) = \frac{\beta C_0}{q} t - \frac{\beta H}{v} \quad (13)$$

$$\beta = \frac{v^2}{2D}\left(\sqrt{1 + \frac{4\beta_0 D}{v^2}} - 1\right) \quad (14)$$

where C_0 is the concentration of Ln(III) ions in the solution entering the column [mg/L], C is the concentration of Ln(III) ions in the leakage [mg/L], k_{Th} is the Thomas rate constant [mL/mg min], q_0 is the adsorption capacity of the ion exchanger filling the column [mg/g], m is the ion exchanger mass [g], Q is the flow rate [mL/min], V is the leakage volume [L], k_{AB} is the Adams-Bohart rate constant [L/mg min], t is the time [min], q is the adsorption capacity of the ion exchanger per unit volume of the bed [mg/L], v is the linear velocity [cm/min], H is the bed depth of the fixed bed column [cm], k_{YN} is the Yoon-Nelson rate constant [1/min], τ is the time necessary for 50% adsorbate breakthrough [min], β is the external mass transfer kinetic coefficient [1/min] and D is the axial diffusion coefficient [cm^2/min], β_0 is the external mass transfer coefficient with the negligible axial dispersion coefficient D.

2.4.3. Kinetic parameters

The kinetic data obtained in this paper for the Ln(III)-GLDA complexes adsorption were described using five commonly used models: pseudo-first order (PFO) [35], pseudo-second order (PSO) [36], Weber-Morris [37], Boyd [38], and Dumwald-Wagner (D-W) [39]:

$$q_t = q_e(1 - exp(-k_1 t)) \quad (15)$$

$$q_t = \frac{k_2 q_e^2 t}{1 + k_2 q_e t} \quad (16)$$

$$q_t = k_i t^{0.5} + C \quad (17)$$

$$F = 1 - \frac{6}{\pi^2}\sum_{n=1}^{\infty}\frac{1}{n^2} exp(-n^2 B_t) \quad (18)$$

$$F = \frac{q_t}{q_e} \quad (19)$$

$$B_t = (\sqrt{\pi} - \sqrt{\pi - \frac{\pi^2 F}{3}})^2 \text{, for F values < 0.85} \quad (20)$$

$B_t = -0.4977 - ln(1 - F)$, for F values > 0.85 *(21)*

$$log(1 - F^2) = -\frac{k}{2.303t} \quad (22)$$

where q_e, q_t were defined as previously, k_1 is the PFO rate constant [1/min], k_2 is the PSO rate constant [g/mg min], k_i is the Weber-Morris rate constant [mg/g $min^{1/2}$], C is the intercept value related to the boundary layer thickness, F is the fractional attainment of equilibrium at time t, n is the integer that defines the infinite series solution, B_t is the mathematical function of F, k is the Dumwald-Wagner model rate constant [1/min].

2.4.4. Isotherm parameters

There were examined the following adsorption isotherm models: Langmuir [40], Freundlich [41], Temkin [42] as regards their ability to describe the Ln(III)-GLDA complexes adsorption process accurately:

$$q_e = \frac{q_0 K_L C_e}{1 + K_L C_e} \quad (23)$$

$$q_e = K_F C_e^{1/n} \quad (24)$$

$$q_e = B ln A + B ln C_e \quad (25)$$

where q_e, C_e were defined as previously, q_0 is the maximum adsorption capacity [mg/g], K_L is the Langmuir constant [L/mg], K_F is the Freundlich constant [mg/g], n is the Freundlich intensity parameter, A [L/g] and B [J/mol] are the Temkin constants corresponding to the maximum binding energy and the adsorption heat, respectively. The Temkin constant B can be written as $B=RT/b_T$, where R is the gas constant (8.314 J/mol K), T is the absolute temperature [K], and b_T is the Temkin isotherm constant.

2.4.5. Thermodynamic parameters

The thermodynamic parameters (i.e. the Gibbs free energy change $\Delta G°$ [kJ/mol], the enthalpy change $\Delta H°$ [kJ/mol], and the entropy change $\Delta S°$ [J/mol K]) of the Ln(III)-GLDA adsorption on the studied ion exchangers were determined based on Eqs. 26 and 27.

$$\Delta G^o = -RT \ln K_c \quad (26)$$

$$\ln K_c = \frac{\Delta S^o}{R} - \frac{\Delta H^o}{RT} \quad (27)$$

To determine the thermodynamic parameters, it is necessary to get to know the value of the equilibrium constant K_c (dimensionless). It can be determined by multiplying the distribution coefficient K_d [L/g] [43].

2.4.6. Statistical analysis

In order to assess the accuracy of the fit of the obtained experimental data to different kinetic models and adsorption isotherm models, the correlation coefficient (R^2) and the Chi-square (χ^2) statistical test were used. The Chi-square test, which is the ratio of the sum of square differences between the experimental data and the data obtained from the models to the data from the models, is mathematically expressed as:

$$\chi^2 = \sum \frac{(q_{e,exp} - q_{e,cal})^2}{q_{e,cal}} \quad (28)$$

where $q_{e,exp}$ is the adsorption capacity determined from the experimental data and $q_{e,cal}$ is the adsorption capacity calculated from the model. The smallest Chi-square value indicates the best model fit. Using the OriginPro 8 software (OriginLab Corporation, USA), the kinetics and adsorption isotherm data were fitted to the nonlinear forms of models, and the corresponding parameters were calculated.

3. Results and Discussion

3.1. Materials characterization

3.1.1. GLDA as a high-potential complexing agent

Depending on the solution pH, the GLDA molecules are dissociated, the phases of which correspond to the protonation constants (overall and successive). The potentiometric measurements were made to determine their values using the HYPERQUAD2008 software at μ=0.1 M and T=293 K. The calculated protonation constant values are shown in Table 1, and the species distribution curves of GLDA are presented in Fig. 2a.

Table 1. The protonation constants for GLDA.

Overall protonation constants (log*β*)	**SD**	**Protonation equilibria**	**Successive protonation constants (log*K*)**
9.69	0.01	$GLDA^{4-} + H^{+} \rightleftarrows HGLDA^{3-}$	9.69
14.66	0.01	$HGLDA^{3-} + H^{+} \rightleftarrows H_2GLDA^{2-}$	4.97
18.27	0.01	$H_2GLDA^{2-} + H^{+} \rightleftarrows H_3GLDA^{-}$	3.61
20.88	0.02	$H_3GLDA^{-} + H^{+} \rightleftarrows H_4GLDA$	2.61

SD - standard deviation

The potentiometric studies at pH ranges from 2.5 to 11.0 have shown that GLDA exists as a fully protonated molecule (H_4GLDA) in strongly acidic solutions (pH=2). As the solution pH rises, protons begin to dissociate from the oxygen atoms in the carboxyl groups, corresponding to the successive log*K* values (2.61, 3.61, 4.97), and deprotonation takes place. When pH is 2.6, the dominant form becomes H_3GLDA^{-}, whose percentage reaches 61% at pH 3.1. The proton dissociation from another carboxyl group in the H_3GLDA^{-} molecule leads to the H_2GLDA^{2-} form formation, which is predominant at pH ranges from 3.6 to 5.0. $HGLDA^{3-}$ is the form found in the largest pH range (from 5.0 to 9.6), reaching 98.5%. Under strongly basic conditions, the last to dissociate is the proton from the amine nitrogen atom, forming a fully deprotonated form of $GLDA^{4-}$ (log*K*=9.69).

Understanding the GLDA complexation behaviour with metal ions is crucial in the design of many processes, such as industrial purification. Although there are the literature reports on the GLDA complexes with heavy metals (Ni, Cu, Zn, Cd, and Pb), Ca, Mg, Ba, and Y, little is known about their interaction with rare earth elements [9,11]. Therefore, the potentiometric measurements were conducted in the binary systems (GLDA with La(III), Ce(III), Pr(III), Nd(III), Sm(III), or Ho(III)) at different molar metal:GLDA ratios and presented in Figs. 2 and S1 and Table 2.

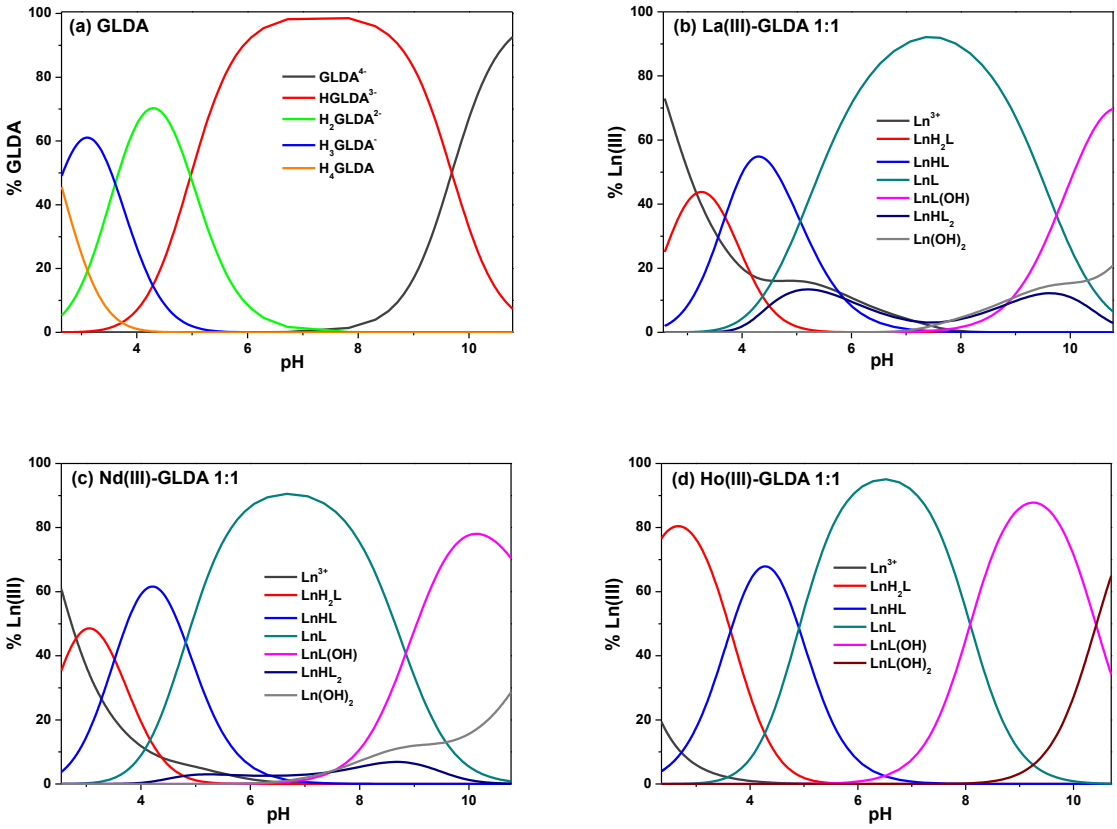

Fig. 2. (a) Percentage distribution of GLDA individual forms depending on the pH values and (b-d) distribution diagrams for the Ln(III)-GLDA systems at the Ln(III):GLDA ratio 1:1.

Table 2. The calculated values of the overall stability constants (logβ) and the equilibrium constants (logK_e) for the Ln(III)-GLDA systems for various Ln(III):GLDA ratios.

Species	1:1			1:2			2:1		
	logβ	SD	logK_e	logβ	SD	logK_e	logβ	SD	logK_e
La(III)-GLDA									
LnH_2L	18.70	0.02	**4.04**	18.53	0.02	**3.87**	18.30	0.04	**3.64**
LnHL	15.01	0.01	**5.33**	14.83	0.01	**5.15**	14.94	0.02	**5.25**

LnL	9.95	0.02	**9.95**	9.93	0.02	**9.93**	9.52	0.08	**9.52**
LnL(OH)	0.20	0.02	**4.02**	-	-	**-**	3.36	0.04	**7.60**
$LnL(OH)_2$	-	-	**-**	-	-	**-**	-6.35	0.05	**4.07**
$LnHL_2$	24.21	0.04	**4.57**	-	-	**-**	-	-	**-**
LnL_2	-	-	**-**	15.63	0.04	**5.70**	-	-	**-**
Ln_2L	-	-	**-**	-	-	**-**	13.71	0.05	**4.19**
Ce(III)-GLDA									
LnH_2L	19.14	0.01	**4.48**	19.70	0.02	**5.05**	-	-	**-**
LnHL	15.53	0.01	**5.84**	16.34	0.02	**6.65**	16.18	0.02	**6.49**
LnL	10.44	0.02	**10.44**	11.72	0.02	**11.72**	10.59	0.07	**10.59**
LnL(OH)	1.36	0.02	**4.69**	5.33	0.03	**7.38**	3.90	0.06	**7.07**
$LnL(OH)_2$	-	-	**-**	-4.65	0.03	**3.79**	-6.86	0.08	**3.02**
$LnHL_2$	24.54	0.05	**4.41**	-	-	**-**	-	-	**-**
Pr(III)-GLDA									
LnH_2L	18.83	0.01	**4.17**	-	-	**-**	19.94	0.05	**5.28**
LnHL	15.30	0.02	**5.61**	17.40	0.03	**7.71**	16.67	0.04	**6.98**
LnL	10.26	0.02	**10.26**	13.54	0.03	**13.54**	11.67	0.05	**11.67**
LnL(OH)	1.39	0.07	**4.89**	8.30	0.03	**8.53**	5.04	0.06	**7.14**
$LnL(OH)_2$	-	-	**-**	-0.82	0.04	**4.65**	-5.59	0.06	**3.14**
$LnHL_2$	24.18	0.02	**4.22**	-	-	**-**	-	-	**-**
Nd(III)-GLDA									
LnH_2L	19.08	0.01	**4.42**	19.68	0.03	**5.02**	19.88	0.06	**5.22**
LnHL	15.56	0.01	**5.87**	16.92	0.02	**7.24**	16.61	0.05	**6.92**
LnL	10.74	0.01	**10.74**	12.44	0.03	**12.44**	11.86	0.06	**11.86**
LnL(OH)	1.90	0.02	**4.92**	7.08	0.02	**8.41**	5.26	0.07	**7.17**
$LnL(OH)_2$	-	-	**-**	-2.31	0.03	**4.38**	-4.00	0.07	**4.50**
$LnHL_2$	24.21	0.09	**3.78**	25.50	0.04	**3.36**	-	-	**-**
Sm(III)-GLDA									
LnH_2L	19.29	0.02	**4.63**	-	-	**-**	-	-	**-**
LnHL	15.85	0.01	**6.16**	17.27	0.02	**7.58**	16.86	0.03	**7.17**
LnL	10.95	0.02	**10.95**	13.00	0.02	**13.00**	12.24	0.05	**12.24**
LnL(OH)	2.70	0.04	**5.51**	7.63	0.03	**8.41**	6.54	0.05	**8.07**
$LnL(OH)_2$	-	-	**-**	-2.71	0.03	**3.43**	-3.39	0.06	**3.84**
$LnHL_2$	-	-	**-**	26.02	0.05	**3.34**	-	-	**-**
LnL_2	19.93	0.06	**8.98**	-	-	**-**	-	-	**-**
Ho(III)-GLDA									
LnH_2L	20.60	0.03	**5.94**	-	-	**-**	-	-	**-**
LnHL	16.96	0.03	**7.27**	18.02	0.06	**8.33**	17.67	0.04	**7.98**
LnL	12.06	0.03	**12.06**	13.73	0.06	**13.73**	13.31	0.04	**13.31**
LnL(OH)	3.97	0.03	**5.69**	8.25	0.07	**8.29**	7.45	0.05	**7.91**

$LnL(OH)_2$	-6.45	0.03	**3.35**	-2.22	0.07	**3.30**	-2.33	0.05	**3.99**
$LnHL_2$	-	-	**-**	26.96	0.08	**3.54**	-	-	**-**

SD - standard deviation

Three basic forms of complexes were discovered in each studied system. These were: LnGLDA, LnH_xGLDA (the protonated complexes) and $LnGLDA(OH)_x$ (hydroxycomplexes). LnHGLDA and LnGLDA(OH) type complexes were identified in all systems. LnH_2GLDA and $LnGLDA(OH)_2$ type complexes were also discovered in more than half of the cases. The presence of redundant ligand molecules was manifested by the formation of $LnHGLDA_2$ type complexes. The forms of GLDA complexes with rare earth elements can be formed by the following reactions:

$$Ln^{3+} + H_2GLDA^{2-} \rightleftarrows LnH_2GLDA^{+} \quad (29)$$

$$Ln^{3+} + HGLDA^{3-} \rightleftarrows LnHGLDA \quad (30)$$

$$Ln^{3+} + GLDA^{4-} \rightleftarrows LnGLDA^{-} \quad (31)$$

$$LnGLDA^{-} + H_2O \rightleftarrows LnGLDA(OH)^{2-} + H^{+} \quad (32)$$

$$LnGLDA(OH)^{2-} + H_2O \rightleftarrows LnGLDA(OH)_2^{3-} + H^{+} \quad (33)$$

$$LnGLDA^{-} + HGLDA^{3-} \rightleftarrows LnHGLDA_2^{4-} \quad (34)$$

3.1.2. Ion exchangers

The physicochemical characterization of the ion exchangers was conducted by sieve analysis, scanning electron microscopy, X-ray photoelectron spectroscopy, and Fourier transform infrared spectroscopy.

To verify the ion exchanger bead size, the sieve analysis was made using the laboratory sieves with mesh sizes varying between 100 and 900 μm (Fig. 3). The results validated the information from the manufacturers on the beads dispersion. Among the twelve ion exchangers chosen for the study, there were both monodisperse and polydisperse ones. The SAC-SP112, SBA-M500, SBA-MP500, and SBA-M600 ion exchangers were recognized as having nearly uniform-sized (monodisperse) beads.

90% of the SAC-SP112 cation exchanger beads were 500 μm in size and 91% of the SBA-MP500 anion exchanger beads were 400 μm in size. The SBA-M500 and SBA-M600 anion exchangers had slightly greater diversity in bead size (81% and 72% of the 500 μm bead size, respectively). The other ion exchangers exhibited polydispersity, but the bead sizes estimated in the study differed a little from the data given by the manufacturers.

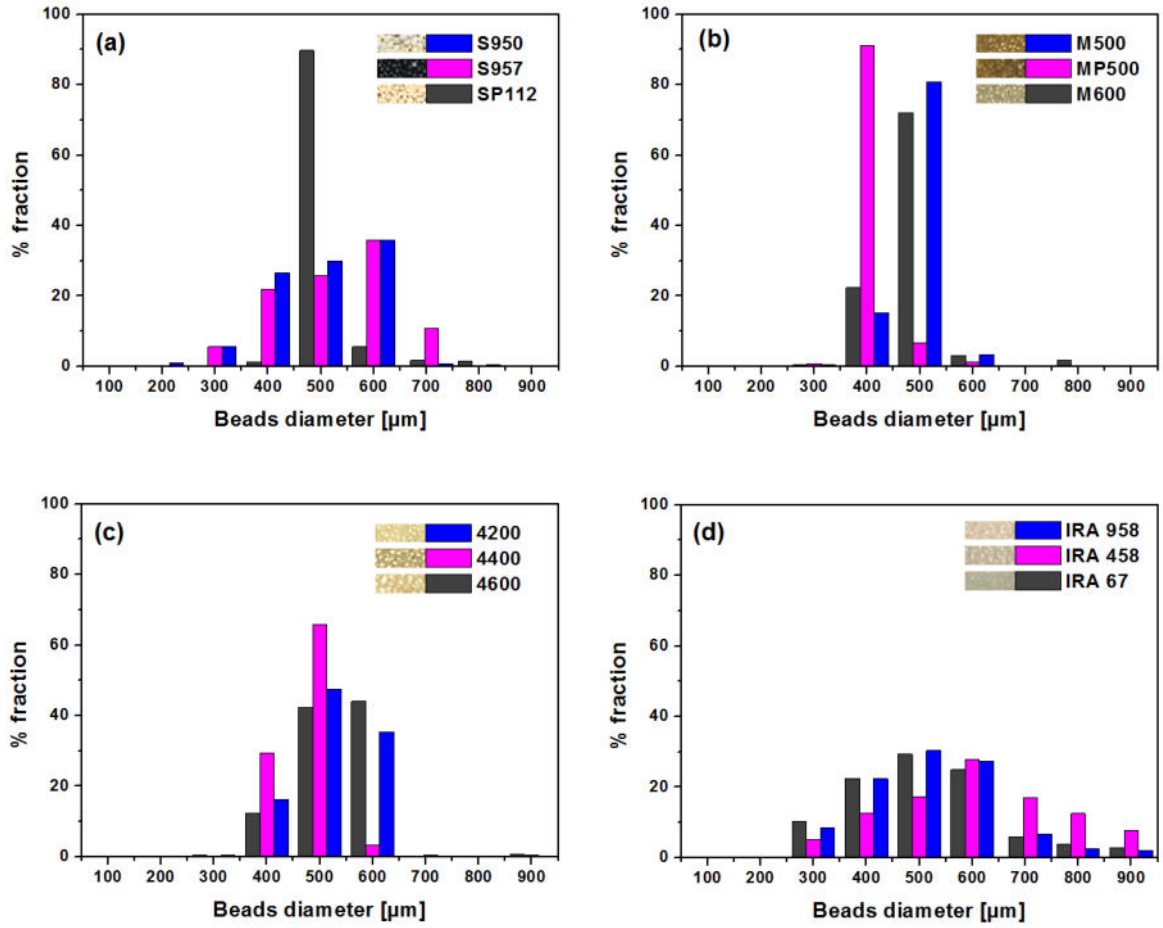

Figure 3. Bead size distribution diagrams for SAC ion exchangers (a) S950, S957, SP112, for SBA and WBA ion exchangers (b) M500, MP500, M600, (c) 4200, 4400, 4600, and (d) IRA 958, IRA 458, IRA 67, and the general appearance of the ion exchangers.

The surface morphology of the ion exchangers was examined by the scanning electron microscopy (SEM). The ion exchanger samples with La(III) ions adsorbed on the surface in the presence of GLDA were analysed (Fig. S2) and images were recorded at x10,000. All the ion exchangers are in the form of beads with a spherical

shape and homogeneous surface. In a few cases, cracks and fissures can be observed on the surface, which may be the result of mechanical damage. The SEM images of ion exchangers with a macroporous structure (SAC-S950, SAC-S957, SAC-SP112, SBA-MP500, SBA-IRA 958) show small cavities and pores typical of this structure, while the gel ion exchangers (SBA-M500, SBA-M600, SBA-4200, SBA-4400, SBA-4600, SBA-IRA 458, WBA-IRA 67) exhibit a more compact and packed surface. The last one, WBA-IRA 67, is characterized by a creased and irregular surface after adsorption. The SEM analysis of the ion exchangers before the adsorption process was presented in the paper [30].

The elemental composition of the ion exchanger surfaces was assessed using X-ray photoelectron spectroscopy (XPS), which also enables detecting the chemical state of the elements present there and consequently the Ln(III)-GLDA complexes adsorption mechanism. The analysis included the twelve pure ion exchangers as well as the ion exchangers after the La(III)-GLDA complexes adsorption under optimal conditions. Fig. 4 presents the wide-scan XPS spectra of samples before and after adsorption. The elemental compositions and binding energies obtained during the measurements are listed in Table S1.

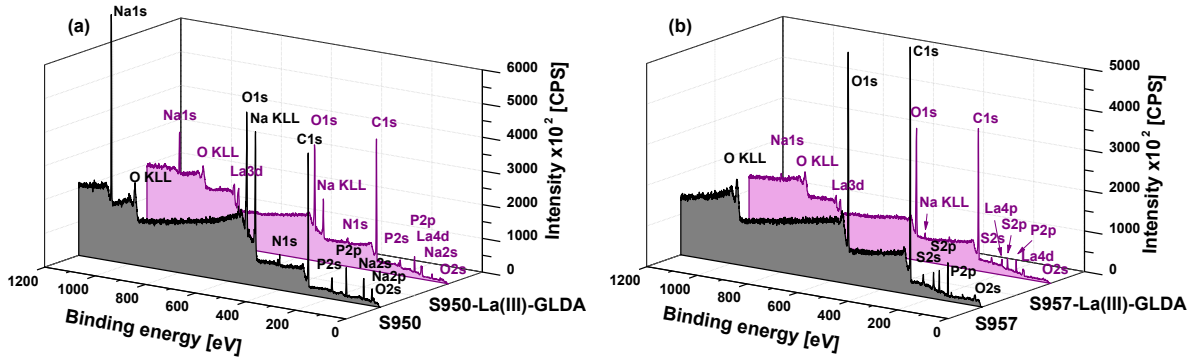

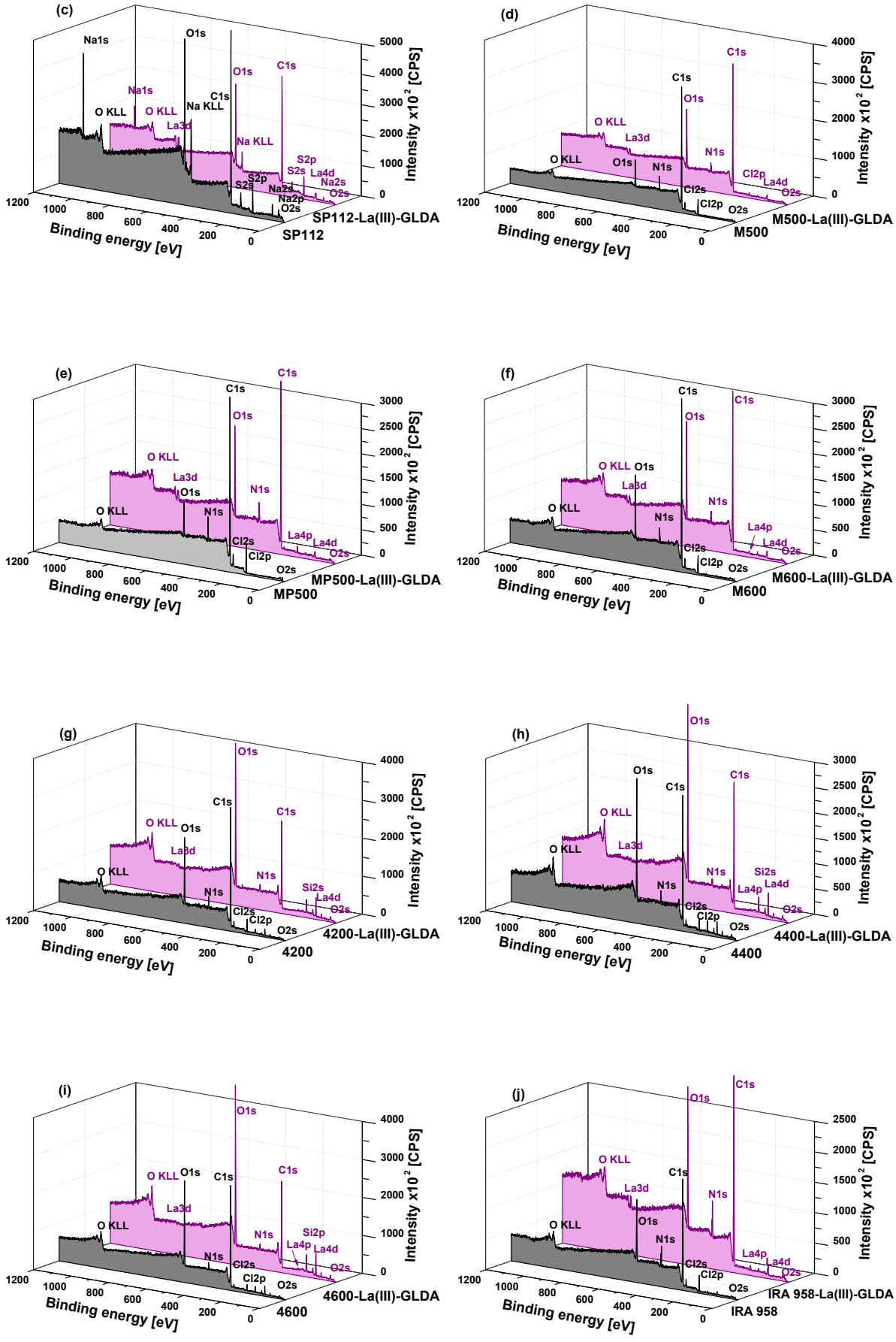
(c)
Na1s
O1s
C1s
O KLL
Na KLL
La3d
S2p
S2s
La4d
Na2s
Na2p
O2s
SP112
SP112-La(III)-GLDA
(d)
C1s
O1s
O KLL
La3d
N1s
Cl2p
Cl2s
O2s
M500
M500-La(III)-GLDA
(e)
MP500
MP500-La(III)-GLDA
(f)
M600
M600-La(III)-GLDA
(g)
4200
4200-La(III)-GLDA
(h)
Si2s
4400
4400-La(III)-GLDA
(i)
Si2p
4600
4600-La(III)-GLDA
(j)
IRA 958
IRA 958-La(III)-GLDA
Binding energy [eV]
Intensity x10 2 [CPS]

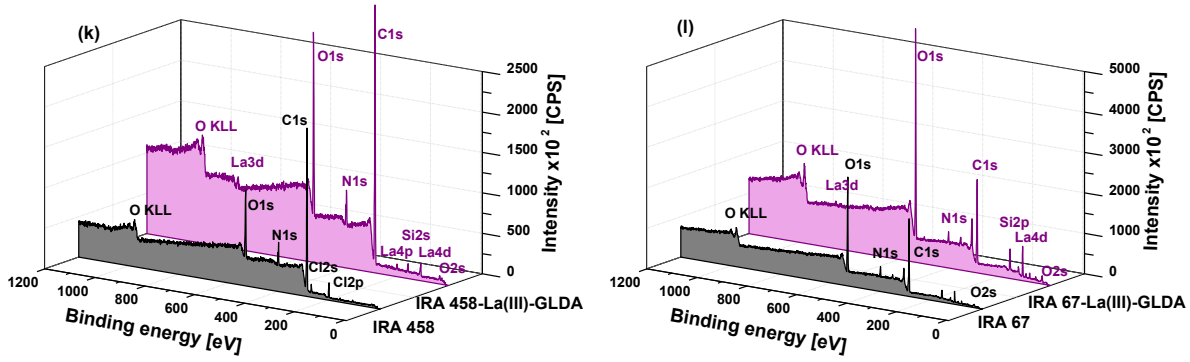

Fig. 4. XPS spectra of SAC ion exchangers (a) S950, (b) S957, (c) SP112, SBA ion exchangers (d) M500, (e) MP500, (f) M600, (g) 4200, (h) 4400, (i) 4600, (j) IRA 958, (k) IRA 458, and WBA ion exchangers (l) IRA 67 before and after the La(III)-GLDA complexes adsorption.

The XPS spectra recorded: C1s and O1s bands corresponding to the presence of carbon and oxygen atoms in the major matrix building blocks of ion exchangers; P2p bands in the SAC-S950 spectrum proving the presence of phosphonic groups; S2p bands in the SAC-SP112 spectrum derived from the sulfonic groups; and both (P2p and S2p) in the case of the SAC-S957 ion exchanger (phosphonic and sulfonic groups), as well as N1s bands corresponding to the amine and ammonium groups. The Na1s band originates from the sodium form of the ion exchangers SAC-S950, SAC-S957, and SAC-SP112, while the Cl2p band confirms the chloride form in which the SAC anion exchangers were present. Only WBA-IRA 67 had a free form. The appearance of unexpected Si2p, Al2p, and Ca2p bands can indicate additives or impurities introduced in the manufacturing or processing stage.

The spectra of ion exchangers after La(III)-GLDA complexes adsorption reveal bands originating from lanthanum atoms (La3d in the range of 833.7-836.7 eV), confirming effective adsorption. The lanthanum content ranged from 0.1 to 0.6%; nonetheless, it should be mentioned that this content, determined by the XPS technique, refers only to the surface layer of the ion exchanger and not the entire volume of the sample. The XPS spectra analysis of SBA anion exchangers in chloride

form after the adsorption showed complete disappearance of the Cl1s band. Similarly, the Na1s bands for the SAC-S950 and SAC-SP112 decreased. This suggests that the La(III)-GLDA complexes adsorption follows the ion exchange mechanism. Regarding anion exchangers, Cl^- ions are exchanged for the negatively charged La(III)-GLDA complexes, whereas Na^+ ions in the SAC-S950 and SAC-SP112 structures are replaced by La^{3+} ions released during the complex decomposition.

Fourier transform infrared spectroscopy (FTIR) was applied to confirm the functional groups of used ion exchangers. The spectra of the samples were recorded in the wavelength range of 4000 cm^{-1} to 650 cm^{-1} (Fig. 5).

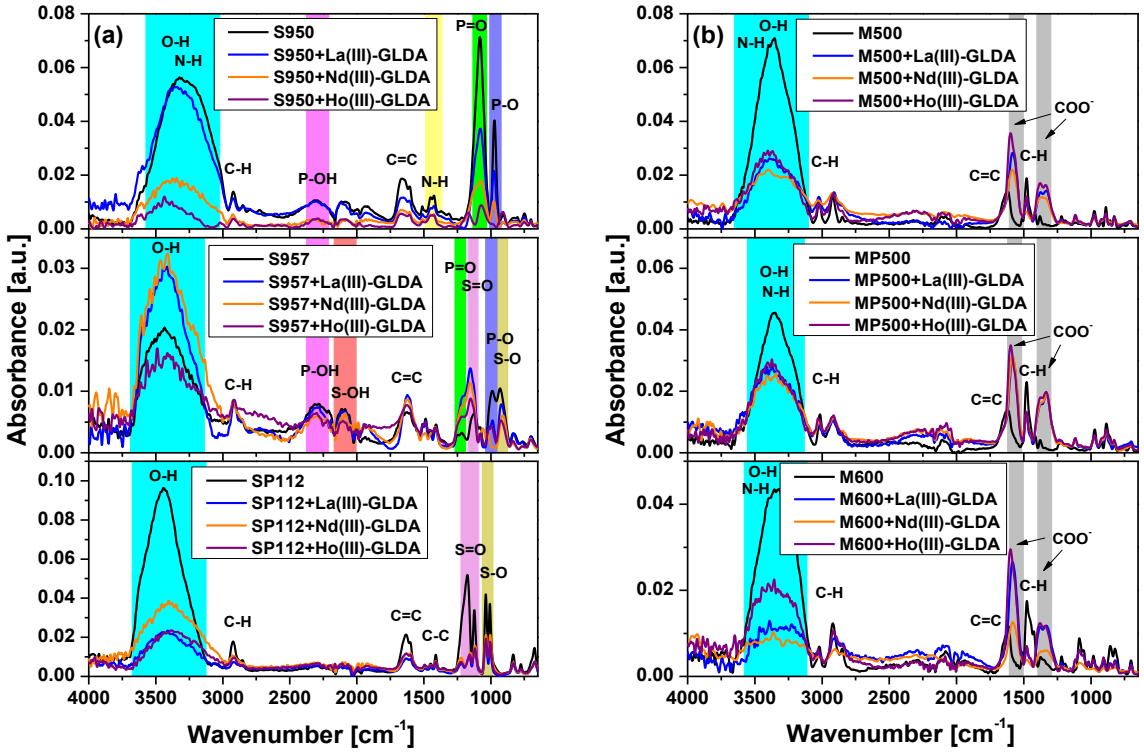

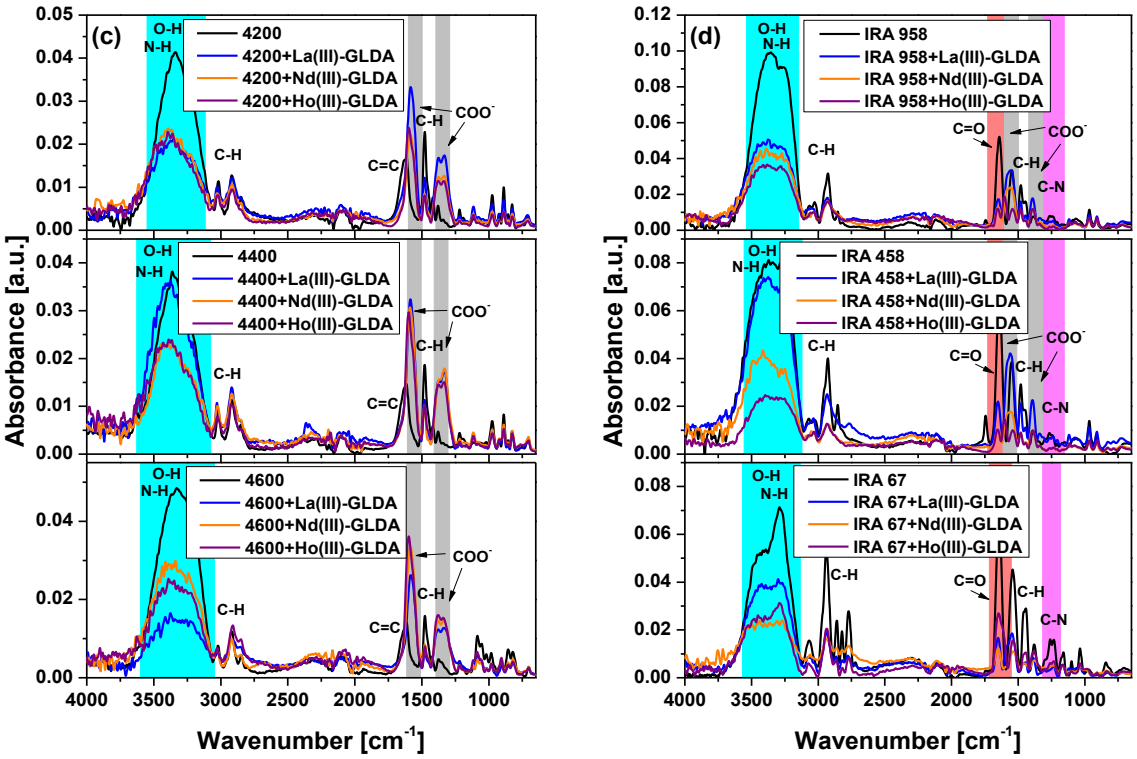

Fig. 5. FTIR spectra for SAC ion exchangers (a) S950, S957, SP112, for SBA and WBA ion exchangers (b) M500, MP500, M600, (c) 4200, 4400, 4600 and (d) IRA 958, IRA 458, IRA 67 before and after the Ln(III)-GLDA complexes adsorption.

The FTIR studies revealed the presence of multiple bands from both the ion exchanger matrix (divinylbenzene-crosslinked polystyrene or polyacrylic acid) and the various functional groups. The most prominent band present in each recorded spectrum is that in the range of 3500-3300 cm^{-1} attributed to the stretching vibrations of the O-H groups and the N-H groups [44]. Knowing the structures of SAC-S957 and SAC-SP112 (no groups containing nitrogen atoms), it is possible to conclude that the band originates from only the water content remaining in the ion exchanger phase and that there are only vibrations of O-H groups. In the other ten studied ion exchangers, where the quaternary ammonium, tertiary amine, or aminophosphonic groups are present, the vibrations of N-H groups also occur in this wavelength range. The bands in the 3050-3015 cm^{-1} range originate from the benzene ring and correspond to the C-

H stretching vibrations. In the range 2940-2840 cm^{-1}, there can be observed two bands derived from asymmetric and symmetric C-H stretching vibrations in the $-CH_2$ groups [45]. The aromatic ring presence in the ion exchanger structure is also confirmed by three bands at 1480-1470, 1420-1410, and 1380-1370 cm^{-1}, which are the result of asymmetric C=C stretching vibrations in the ring and asymmetric scissor vibrations in the methylene groups [46]. Furthermore, the band at 1640 cm^{-1} in the spectra of polyacrylate ion exchangers can be attributed to the stretching vibrations of -C=O groups [47].

The FTIR spectroscopic studies carried out on the SAC-S950 ion exchanger verified the existence of phosphonic groups. In Fig. 5a, at 2312 cm^{-1} as well as at 1083 and 973 cm^{-1}, there are clear bands of stretching vibrations of the P-OH, P=O, and P-O groups, respectively. The spectrum of SCA-SP112 revealed four bands characteristic of the sulfonic groups at 1177, 1123, 1037, and 1008 cm^{-1}, corresponding to the S=O and S-O groups stretching vibrations [48]. Meanwhile, the chelating ion exchanger SAC-S957, which has both phosphonic and sulfonic groups, exhibited all of the vibrations indicated above (at 2283, 2112, 1123, and 988 cm^{-1} - the stretching vibrations of P-OH and S-OH groups as well as P=O, P-O, S=O, and S-O groups) [49]. Quaternary nitrogen atoms in the anion exchangers with the ammonium groups give a characteristic band at 975 cm^{-1} [50].

The FTIR spectra recorded after the Ln(III)-GLDA complexes adsorption were compared to those obtained for the pure ion exchangers, allowing the mechanism driving the uptake of Ln(III) ions from the solution to be determined. The spectra of SAC-S950, SAC-S957, and SAC-SP112 (Fig. 5a) did not change significantly as for all the bands identified before the adsorption process, although a change in their intensity as well as slight shifts could be seen. For example, the bands of the sulfonic groups in

SAC-SP112 shifted from 1177, 1123, 1037, and 1008 cm^{-1} to 1156, 1121, 1035, and 1004 cm^{-1}, respectively, and those of the sulfonic and phosphonic groups in the SAC-S957 spectra shifted from 2283 cm^{-1} to 2299 cm^{-1} and from 1123 cm^{-1} to 1153 cm^{-1}. The change in the bands position for each group in the FTIR spectra suggests their involvement in the adsorption process. The contribution of the phosphonic and sulfonic groups (in the case of SAC-S950, SAC-S957, and SAC-SP112) to the removal of Ln(III)-GLDA complexes indicates that in the studied process, it is highly possible that the complexes decompose in favour of the formation of bonds between the dissociated phosphonic or sulfonic groups and Ln(III) ions. The anion exchanger spectra analysis after the Ln(III)-GLDA complexes adsorption revealed the appearance of new bands in the 1600-1580 cm^{-1} and 1380-1330 cm^{-1} regions, which can be attributed to the carboxyl groups stretching vibrations, originating from GLDA molecules, which is evidence of the presence of complexes in the ion exchanger phase [44].

3.2. GLDA in rare earth elements removal - Adsorption static method

3.2.1. Evaluation of the influence of different process conditions

In order for adsorption to occur with the highest possible effectiveness, besides choosing the appropriate adsorbent, it is also crucial to determine the optimal external conditions, such as the molar metal:ligand ratio, solution pH, process time, and temperature.

3.2.1.1. Ln(III):GLDA molar ratio

The analysis of the effect of individual conditions on the adsorption began with the selection of the appropriate metal to complexing agent molar ratio in the solution. It is commonly known that the types of complexes that occur, their quantity, and the degree of metal complexation depend on the amount of metal ions and ligand introduced into the solution. The experiments were conducted at the initial Ln(III) ions

concentration of 1.0×10^{-3} M, varying the GLDA concentration from 1.0×10^{-3} M to 4.0×10^{-3} M, which corresponded to the metal:ligand ratios of 1:1, 1:2, and 1:4, respectively (without modifying the original pH of the solution). The studies were not carried out in the systems with an underdose of GLDA (for example, the metal:ligand ratio 2:1), due to the Ln(III) hydroxides precipitation at higher values of pH. Fig. 6 demonstrates that increasing the GLDA concentration in the sample (change in the molar ratio from 1:1 to 1:4) had no impact on the adsorption capacities of SAC-S950 and SAC-S957 relative to the La(III) complexes; nonetheless, it had a significant effect on the other ion exchangers. The increase in the GLDA concentration from 1.0×10^{-3} M to 4.0×10^{-3} M in the system with SAC-SP112 caused a reduction in the adsorption effectiveness from 7.67 to 0.23 mg/g, while the inverse relationship was observed for the anion exchangers SBA-M500, SBA-MP500, SBA-M600, SBA-4200, SBA-4400, SBA-4600, SBA-IRA 958, and SBA-IRA 458, where the adsorption capabilities increased as the GLDA concentration increased. In the case of the aforementioned anion exchangers, a large increase in the q_e values was recorded when the ratio was altered from 1:1 to 1:2; further modifications no longer affected the system significantly. A significant overabundance of the complexing agent (Ln(III):GLDA ratio of 1:4) reduced adsorption capacities in the systems that contained the WBA-IRA 67. For the systems containing Nd(III) and Ho(III) ions, similar relationships were discovered (Figs. S3 and S4). Further research described in the paper were carried out at the Ln(III):GLDA ratios, which yielded the greatest capacity for adsorption but without unnecessary excess consumption of the complexing agent. These were the Ln(III):GLDA ratios of 1:1 for SAC-S950, SAC-S957, and SAC-SP112 and 1:2 for SBA-M500, SBA-MP500, SBA-M600, SBA-4200, SBA-4400, SBA-4600, SBA-IRA 958, SBA-IRA 458, and WBA-IRA 67.

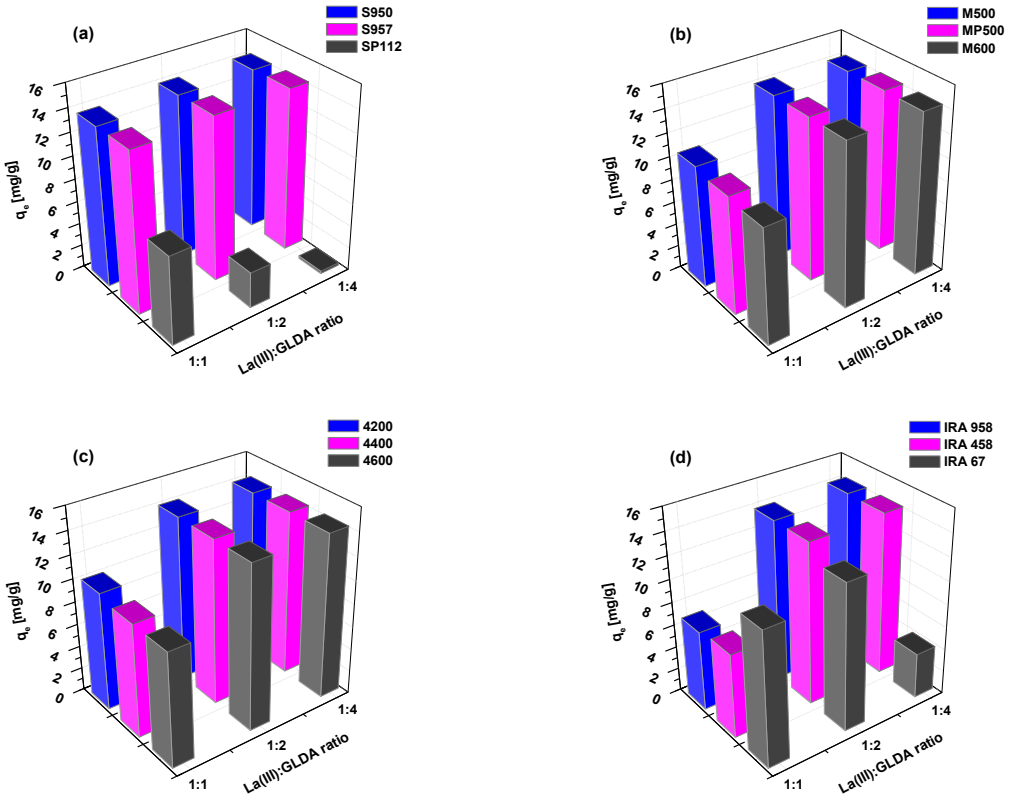

Fig. 6. Effect of the Ln(III):GLDA molar ratio on the La(III)-GLDA complexes adsorption on SAC ion exchangers (a) S950, S957, SP112, on SBA and WBA ion exchangers (b) M500, MP500, M600, (c) 4200, 4400, 4600 and (d) IRA 958, IRA 458, IRA 67.

3.2.1.2. The initial solution pH

It is commonly known that the solution pH has an impact both the adsorbent by changing its surface charge and the adsorbate by changing the form of the metal in the solution. In the aqueous solutions, La(III), Nd(III), and Ho(III) exist as Ln^{3+}, $Ln(OH)^{2+}$, $Ln(OH)_2^{+}$, and $Ln(OH)_3$. However, free cations capable of participating in the adsorption are present only in the solutions with the pH value below 6.0; more alkaline solutions cause hydroxide precipitation, which inhibits the process from proceeding. The addition of an appropriate amount of a ligand, such as GLDA, causes the formation of well-soluble complexes with metal ions, so that the process can be conducted over a considerably wider pH range, even up to pH 12.0. In addition, in the alkaline solutions rare earth elements form negatively charged complexes with GLDA (Fig. 2) which

provides the possibility of using a wide range of ion exchangers, such as the anion exchangers, in the adsorption process.

The effect of the initial solution pH on the Ln(III) ions adsorption with the complexing agent GLDA is investigated in this paper. The experiments were conducted in the pH range from 2.0 to 12.0 for the initial Ln(III) ions concentration of 1.0×10^{-3} M and the optimal molar metal:ligand ratios determined for each system in the previous stage of the study. The obtained q_e vs. initial pH dependencies for the adsorption of La(III)-GLDA complexes are shown in Fig. 7, and for the Nd(III)-GLDA and Ho(III)-GLDA complexes in Figs. S5 and S6.

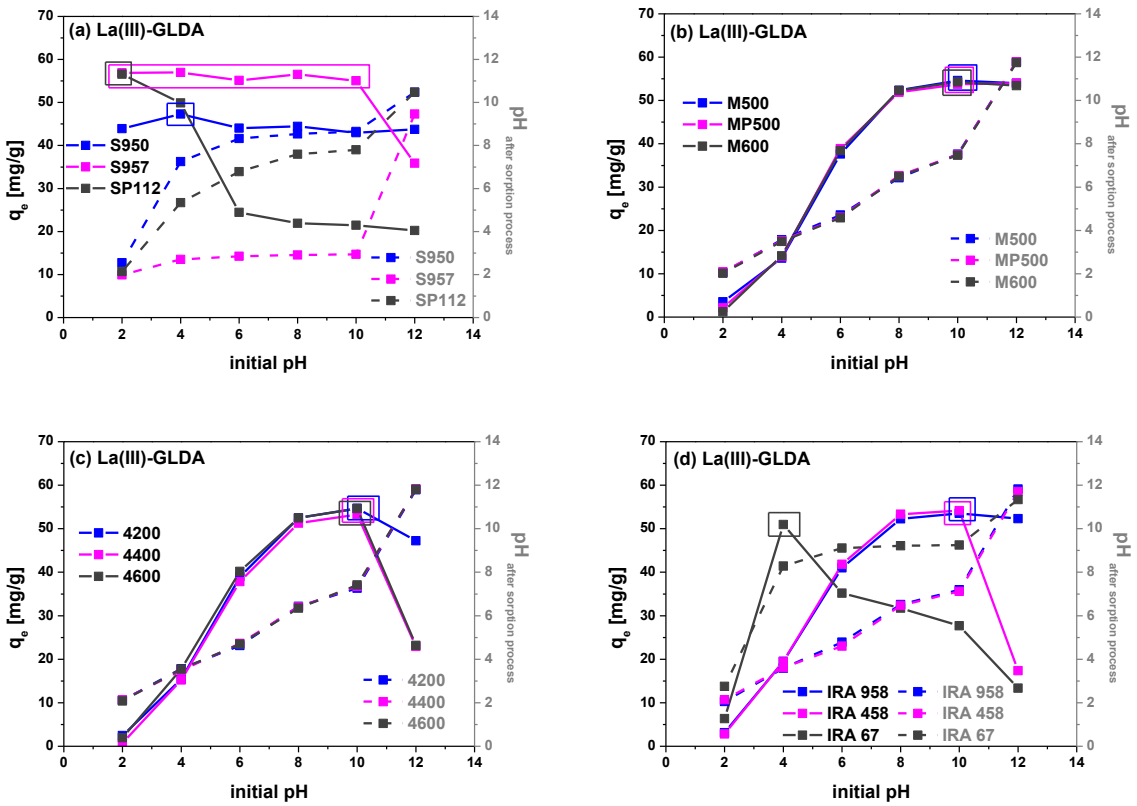

Fig. 7. Effect of the initial solution pH on the La(III)-GDLA complexes adsorption on SAC ion exchangers (a) S950, S957, SP112, on SBA and WBA ion exchangers (b) M500, MP500, M600, (c) 4200, 4400, 4600 and (d) IRA 958, IRA 458, IRA 67, and changes of solution pH after the process.

The results show that the studied correlation was significantly influenced by the type of ion exchanger used in the system, which is related to the presence of different

functional groups on their surface. Among the adsorbents selected for the experiments were the ion exchangers belonging to four groups: chelating ion exchangers (SAC-CIE), strongly cation exchangers (SAC), strongly basic anion exchangers (SBA), and weakly basic anion exchangers (WBA). For SAC-S950 and SAC-S957 (SAC-CIE), similar adsorption capacities were obtained over a very broad pH range from 2.0 to 10.0. During the La(III) complexes adsorption, the q_e values ranged from 42.98 to 47.31 mg/g for SAC-S950 and from 55.03 to 56.98 mg/g for SAC-S957, whereas the during Nd(III) complexes adsorption, the q_e values ranged from 35.75 to 40.94 mg/g for SAC-S950 and from 56.17 to 57.13 mg/g for SAC-S957. The q_e values for the SAC-S957-Ho(III)-GLDA system were also stable with the changes in pH (63.85-65.34 mg/g) but a different correlation was observed for the SAC-S950-Ho(III)-GLDA system; as pH increased, the adsorption capacity reduced from 44.88 to 24.63 mg/g. The SAC-SP112 cation exchanger showed the same behaviour. The maximum adsorption capacities (56.56 mg/g for La(III), 55.86 mg/g for Nd(III), and 64.30 mg/g for Ho(III)) were found here only in strongly acidic environments where the potentiometric measurements revealed free Ln^{3+} cations and fully protonated GLDA molecules incapable of forming complexes, and then dropped to barely 20.24 mg/g for La(III), 10.46 mg/g for Nd(III) and 13.19 mg/g for Ho(III) at pH 12.0. The optimal pH for the adsorption using SBA ion exchangers was determined to be 10.0. At this value this is directly related to the presence of negatively charged complexes in the solution that are readily captured by the quaternary ammonium groups of anion exchangers. WBA-IRA 67, having tertiary amine groups, which qualifies it to be in the WBA ion exchangers group, adsorbed the Ln(III)-GLDA complexes with the highest efficiency (50.97 mg/g for La(III), 51.96 mg/g for Nd(III), and 62.97 mg/g for Ho(III)) at pH 4.0. Both the decreasing pH value and its increase caused a significant reduction in the adsorption capacities. The anion

exchangers of this type are most effective in low pH solutions, i.e., at high hydrogen ion concentrations that allow protonation of their functional groups [51]. However, in too acidic an environment (pH=2), the metal ions remain uncomplexed (Ln^{3+}) and are not captured by the amine groups.

3.2.1.3. The phase contact time and the initial solution concentration

The studies on the impact of contact time between particular ion exchangers and the adsorbate (the solution of Ln(III)-GLDA complexes) were carried out analysing the systems in which adsorption proceeded for a period of 1 to 240 minutes. The experiment was conducted for the three initial concentrations of 0.5×10^{-3} M, 1.0×10^{-3} M, and 1.5×10^{-3} M. The obtained results for the exemplary La(III)-GLDA complexes of the concentration of 0.5×10^{-3} M are shown in Fig. S7a-d, and the determined adsorption capacities $q_{e.exp}$ are provided in Tables S2, S5, and S8. In all studied systems, efficiency was improved by lengthening the adsorption time until equilibrium was established and the process was complete. The results allowed to conclude that the adsorption of Ln(III)-GLDA complexes on the majority of the ion exchangers being used is very quick. The period of 30 minutes was sufficient for adsorption to occur with more than 95% efficiency. The exceptions were the systems with SAC-S950 and WBA-IRA 67 for which the period of time of up to 240 minutes was required at the concentration of Ln(III)-GLDA complexes of 1.5×10^{-3} M. The time needed for achieving adsorption equilibrium in the systems was dependent on the initial adsorbate concentration. At higher concentrations the period of time was longer. For example, for the SAC-S950-La(III)-GLDA system at the concentration of 0.5×10^{-3} M, the equilibrium was reached in 10 minutes, at the concentration of 1.0×10^{-3} M in 60 minutes, and at the concentration of 1.5×10^{-3} M in 120 minutes. An increase in the initial concentration also caused a reduction in the adsorption effectiveness (*%S*). However, in the studied

concentration range, *%S* did not decrease below 93% (the lowest *%S* value for the WBA-IRA 67-Nd(III)-GLDA system).

3.2.1.4. Temperature

Another important external parameter affecting adsorption efficiency is the temperature. In addition, the study of the temperature effect on the process is necessary to determine the thermodynamic parameters that allow a better understanding of its nature. In the current study, the adsorption of Ln(III)-GLDA complexes was performed at three different temperatures: 293 K, 313 K, and 333 K. The temperature effect on the maximum adsorption capabilities of ion exchangers towards the La(III)-GLDA complexes is shown in Fig. 8, and the experimentally determined q_e values are provided in Tables S11-S14.

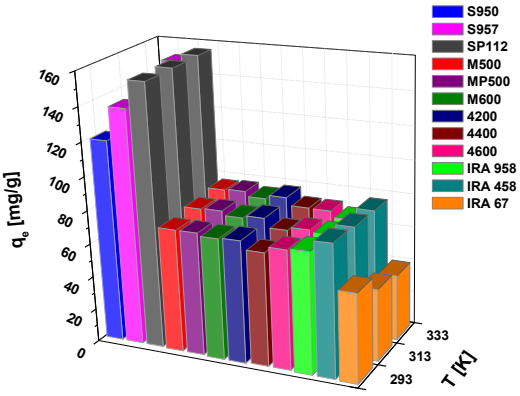

Fig. 8. Temperature effect on the La(III)-GLDA complexes adsorption on various ion exchangers.

The studies revealed that the ion exchangers chosen for adsorption can be divided into two groups with regard to the behaviour of their adsorption capacities with changes in the process temperature. Independent of the adsorbed complex (La(III)-GLDA, Nd(III)-GLDA, or Ho(III)-GLDA), the SAC-S950, SAC-S957, SAC-SP112, SBA-M500, SBA-MP500, SBA-M600, SBA-4200, SBA-4400, and SBA-4600 ion exchangers exhibited an increase in the adsorption capacity when the temperature was raised from 293 K to 333 K. Such behaviour for the ion exchangers is typical and often reported in

the literature [52–54]. This is because the adsorbate molecules are more easily transported to active sites, which is a result of an increase in their kinetic energy as well as an enhanced intraparticle diffusion rate. For these systems, changes in q_e were observed in varying ranges. The largest temperature influence on the adsorption was demonstrated for the SAC-S950-La(III)-GLDA system, where the q_e value increased from 120.10 to 135.40 mg/g, and the smallest for the SAC-SP112-La(III)-GLDA system where a change from 155.49 to 156.22 mg/g was registered. The completely opposite dependence was found for the second group which included the ion exchangers with polyacrylic matrix (SBA-IRA 958, SBA-IRA 458, and WBA-IRA 67). The adsorption effectiveness decreased with the rising temperature in the systems containing these ion exchangers. The largest reduction in the adsorption capacity (from 52.83 to 39.38 mg/g) was obtained for the WBA-IRA 67-La(III)-GLDA system.

3.2.2. Adsorption kinetics

The adsorption rates of Ln(III) complexes with GLDA on twelve different ion exchangers were determined by fitting the experimental data obtained by studying the phase contact time effect on the adsorption process to the pseudo-first order (PFO), pseudo-second order (PSO), Weber-Morris intraparticle diffusion, Boyd, and Dumwald-Wagner (D-W) kinetic models. For the analysis of the kinetics of adsorption with the PFO and PSO models, nonlinear versions of the equations were applied. Fitting was made using the OriginPro 8 software. The consistency of the experiment with the kinetic model was evaluated by applying the correlation coefficient (R^2) and the Chi-square (χ^2) statistical test. Table 3 presents the kinetic parameters determined for the La(III)-GLDA complexes adsorption at the 0.5×10^{-3} M initial concentration. The parameters obtained for higher concentrations and for Nd(III)/Ho(III)-GLDA complexes are summarized in Tables S2-S10. In addition, the fit of the kinetic models to the

experimental data obtained for the La(III)-GLDA complexes at the concentration of 0.5×10^{-3} M is illustrated in Fig. S7.

Table 3. Calculated kinetic parameters for the La(III)-GLDA complexes adsorption on SAC-S950, SAC-S957, SAC-SP112, SBA-M500, SBA-MP500, SBA-M600, SBA-4200, SBA-4400, SBA-4600, SBA-IRA 958, SBA-IRA 458, WBA-IRA 67 (C_0=0.5×10^{-3} M).

Model			**Pseudo-First Order**				**Pseudo-Second Order**		
Ion exchanger	$q_{e.exp}$ [mg/g]	$q_{1.cal}$ [mg/g]	k_1 [1/min]	R^2	χ^2	$q_{2.cal}$ [mg/g]	k_2 [g/mg min]	R^2	χ^2
SAC-S950	6.77	6.37	0.221	0.956	0.127	6.75	0.050	0.970	0.088
SAC-S957	6.89	6.90	0.447	0.998	0.004	7.24	0.108	0.910	0.194
SAC-SP112	6.85	6.68	0.204	0.976	0.082	7.07	0.044	0.973	0.090
SBA-M500	6.83	6.68	0.424	0.981	0.028	7.16	0.100	0.965	0.053
SBA-MP500	6.79	6.61	0.563	0.972	0.028	7.04	0.143	0.957	0.042
SBA-M600	6.83	6.74	0.369	0.992	0.014	7.23	0.085	0.955	0.082
SBA-4200	6.81	6.73	0.327	0.995	0.010	7.23	0.073	0.959	0.082
SBA-4400	6.81	6.62	0.351	0.982	0.030	7.10	0.082	0.965	0.059
SBA-4600	6.77	6.69	0.308	0.987	0.027	7.17	0.069	0.963	0.074
SBA-IRA 958	6.73	6.68	0.442	0.977	0.033	7.12	0.110	0.926	0.104
SBA-IRA 458	6.65	6.58	0.286	0.992	0.018	7.10	0.062	0.951	0.115
WBA-IRA 67	6.82	6.04	0.208	0.776	0.441	6.56	0.046	0.931	0.135
	Weber-Morris Intraparticle Diffusion								
	k_{i1} [mg/g min$^{1/2}$]	C_1	R^2	k_{i2} [mg/g min$^{1/2}$]	C_2	R^2	k_{i3} [mg/g min$^{1/2}$]	C_3	R^2
SAC-S950	1.80	0.03	0.978	0.16	5.01	1.000	0.06	5.86	0.934
SAC-S957	2.58	0.19	0.970	0.01	6.85	0.668	-	-	-
SAC-SP112	1.89	0.27	0.992	0.30	4.51	0.838	0.03	6.45	0.827
SBA-M500	2.58	0.18	0.968	0.81	3.99	0.983	0.02	6.63	0.347
SBA-MP500	2.42	0.97	0.988	0.38	5.22	0.789	0.01	6.75	0.743
SBA-M600	2.29	0.34	0.964	0.34	5.32	0.764	0.00	6.78	0.769
SBA-4200	2.24	0.17	0.974	0.34	5.21	0.962	0.01	6.74	0.617
SBA-4400	1.71	1.22	0.965	0.18	5.76	0.965	0.01	6.72	0.817
SBA-4600	1.92	0.60	0.970	0.17	5.85	0.929	0.00	6.75	0.655
SBA-IRA 958	2.54	0.32	0.993	0.67	4.53	0.973	0.00	6.67	0.272
SBA-IRA 458	2.04	0.09	0.933	0.27	5.24	0.865	0.00	6.61	0.856
WBA-IRA 67	1.60	0.55	0.936	0.64	2.57	0.975	0.18	4.55	0.764

	Boyd		**Dumwald-Wagner**		
	slope	R^2	k [1/min]	*intercept*	R^2
SAC-S950	0.135	0.973	0.122	-0.040	0.974
SAC-S957	0.558	0.985	0.536	-0.306	0.980

SAC-SP112	0.104	0.995	0.093	-0.017	0.996
SBA-M500	0.264	0.995	0.245	-0.020	0.996
SBA-MP500	0.286	0.985	0.268	0.044	0.988
SBA-M600	0.276	0.989	0.256	-0.070	0.989
SBA-4200	0.245	0.994	0.225	-0.065	0.995
SBA-4400	0.220	0.997	0.202	-0.033	0.997
SBA-4600	0.241	0.987	0.222	-0.086	0.985
SBA-IRA 958	0.384	0.989	0.363	-0.136	0.987
SBA-IRA 458	0.212	0.981	0.194	-0.056	0.983
WBA-IRA 67	0.058	0.941	0.053	0.049	0.937

On the basis of the PFO and PSO models fitting the experimental data, it can be concluded that both models were applicable in the studied process description. The PFO model provided an accurate description of adsorption kinetics in the systems containing SAC-S957, SAC-SP112, SBA-M500, SBA-MP500, SBA-M600, SBA-4200, SBA-4400, SBA-4600, SBA-IRA 958, or SBA-IRA 458, independently of the Ln(III) ions forming the complexes. This is evidenced by the obtained parameters determining the degree of fitting (R^2 and χ^2). Compared to the PSO model, the R^2 values were closer to unity and the χ^2 values were smaller. Additionally, the equilibrium adsorption capacities determined experimentally (q_{exp}) had greater agreement with the adsorption capacities calculated from the PFO model ($q_{1.cal}$) than with the adsorption capacities determined from the PSO model ($q_{2.cal}$). In the case of the Ln(III)-GLDA complexes adsorption on SAC-S950 and WBA-IRA 67, the process kinetics were more precisely represented by the PSO model, which was also confirmed by the values of R^2 and χ^2 as well as the agreement of q_{exp} and $q_{2.cal}$ values.

The PFO and PSO models are categorized as adsorption reaction models and are based on the overall adsorption process without considering its individual stages. When describing adsorption using these models, there is no possibility of getting to know the mechanism by which it occurs. Therefore, the Weber-Morris, Boyd, and

Dumwald-Wagner models, known as adsorption diffusion models, were developed to determine the process rate controlling step. During the adsorbate adsorption on the adsorbent, the adsorbate is transported in the solution phase in the first step. This stage proceeds quite rapidly and is called the bulk transport. Then the adsorbate passes the boundary layer (film diffusion) and diffuses through the pores of the adsorbent (intraparticle diffusion) so that it can be adsorbed onto the active sites of the adsorbent in the final step. The last adsorption phase is also regarded as quick, so only the film diffusion and/or intraparticle diffusion are included as factors affecting the adsorption rate [55].

According to the adsorption diffusion models, the adsorption mechanism can be estimated by determining first the q_t vs. $t^{1/2}$ plots for the Weber-Morris model, B_t vs. t plots for the Boyd model, and log(1-F^2) vs. t plots for the Dumwald-Wagner model. Then, the analysis of the resulting graphs reveals the process step that controls its rate. If the plot is a straight line passing through the origin, it should be inferred that the step is intraparticle diffusion; otherwise (when the line obtained is not straight and/or does not cross the origin), adsorption is a complex process influenced by both intraparticle diffusion and film diffusion [56–58]. In the present paper, such a procedure was employed for all experimental data and the resulting fits of the exemplary La(III)-GLDA complexes with the concentration of 0.5×10^{-3} M are shown in Fig. S7.

The application of the Weber-Morris model to describe the Ln(III)-GLDA complexes adsorption kinetics showed the multi-step process. The obtained plots of q_t vs. $t^{1/2}$ were not rectilinear and were characterized by the presence of two or three sections corresponding to the successive steps of adsorption that had various rate constants. Thus, it can be concluded that there are more steps beyond intraparticle diffusion affecting the Ln(III)-GLDA complexes adsorption rate. Additionally, the

boundary layer thickness effect on the adsorbate particles diffusion can be analysed based on the discussed model. This information is provided by the *C* parameter, which is the intercept value on the q_t vs. $t^{1/2}$ plot. The greater the boundary layer thickness influence, the greater the value of *C* [59]. Remarkable is the fact that the *C* values increase in the $C_1 < C_2 < C_3$ series as well as with the increasing initial Ln(III)-GLDA complexes concentration, suggesting a greater boundary layer effect (Tables 3, S3, S6, and S9). An increase in the initial concentration also caused an increase in the k_i values, which correspond to the slopes of the straight lines assigned to the subsequent adsorption steps.

The Boyd and Dumwald-Wagner plots (B_t vs. *t* and log(1-F^2) vs. *t*) are shown in Fig. S7e-f, and the determined parameters are summarized in Tables 3, S4, S7, and S10. It can be observed that the obtained graphs are characterized by great linearity, which is confirmed by the high R^2 values. The R^2 values for the Boyd model ranged from 0.893 to 0.998 for the La(III)-GLDA complexes adsorption, from 0.853 to 0.998 for the Nd(III)-GLDA complexes adsorption, and from 0.868 to 0.998 for the Ho(III)-GLDA complexes adsorption. As for the Dumwald-Wagner model the R^2 values ranged from 0.915 to 0.998 for the La(III)-GLDA complexes, from 0.846 to 0.998 for the Nd(III)-GLDA complexes and from 0.863 to 0.997 for the Ho(III)-GLDA complexes. However, in any case the straight lines obtained from the Boyd and Dumwald-Wagner plots did not intersect the point (0.0). The application of these models allowed to validate the conclusions obtained from the Weber-Morris model and confirmed the complexity of the Ln(III)-GLDA complexes adsorption mechanism.

3.2.3. Adsorption isotherms

Adsorption isotherms were determined to find the maximum adsorption capacities of the selected ion exchangers towards the Ln(III) complexes with the GLDA

complexing agent. These studies also allow for a better understanding of the adsorption mechanism by assessing the distribution of Ln(III)-GLDA complexes between the solution and the ion exchanger surface at equilibrium. The obtained experimental data were analysed using the Langmuir, Freundlich, and Temkin models. Isotherms were determined for the adsorption conducted under the optimal conditions at the temperatures of 293 K, 313 K, and 333 K. Fig. 9 depicts the nonlinear models fit to the data obtained during the adsorption of La(III)-GLDA complexes at 293 K.

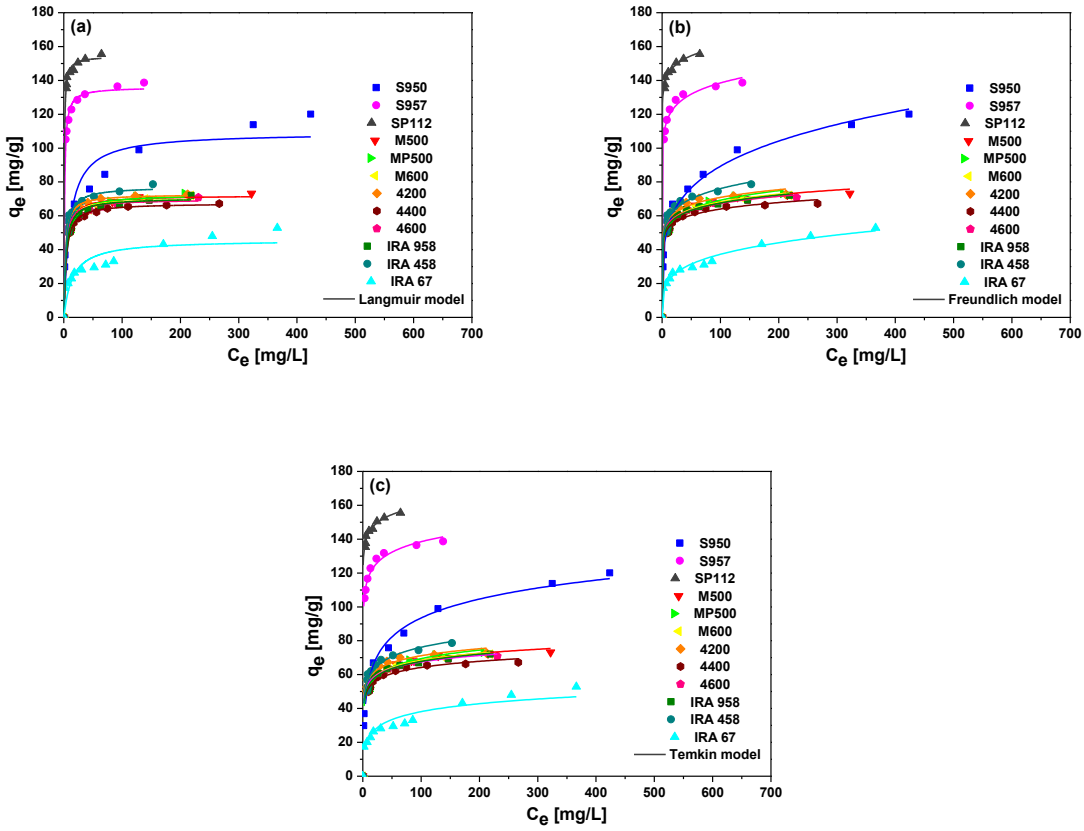

Fig. 9. Fitting the nonlinear form of (a) Langmuir, (b) Freundlich, and (c) Temkin adsorption isotherms to the experimental data of the La(III)-GLDA complexes adsorption on SAC, SBA, and WBA ion exchangers at 293 K.

The isotherm models chosen to analyse the experimental data differ significantly in their assumptions about the adsorption mechanism. The monolayer coverage of an energetically homogeneous adsorbent surface and the absence of interactions between the adsorbed particles are the Langmuir model assumptions. The Freundlich

model describes an entirely different adsorption mechanism in which adsorption occurs multilayered on the heterogeneous adsorbent surface and the adsorbate particles can interact with each other. The model that assumes the possibility of multilayer adsorption is also the Temkin model, which takes into consideration the interactions between the adsorbate and the adsorbent that cause a linear decrease in the adsorption heat with the coverage of the adsorbent surface.

The experimental data of adsorption isotherms of Ln(III) ions with GLDA on twelve ion exchangers were fitted to the nonlinear versions of isotherm models utilizing the OriginPro 8 software. The determined isotherm parameters as well as the R^2 and χ^2 values for the temperature of 293 K are summarized in Table S11, and for the temperatures of 313 K and 333 K in Tables S12-S14. From the obtained results, it is possible to infer the diversity of the adsorption mechanism depending on the ion exchanger used in the system. The adsorption of Ln(III)-GLDA complexes on SBA-M500, SBA-MP500, SBA-M600, SBA-4200, SBA-4400, SBA-4600, SBA-IRA 958, and SBA-IRA 458 was very well described by the Langmuir model. The adsorption data obtained using WBA-IRA 67 showed the best agreement with the Freundlich model, regardless of the Ln(III) ions present in the system. However, when SAC-S950, SAC-S957, or SAC-SP112 were used as adsorbents, the best isotherm fit was obtained for the Temkin model.

The determination of the maximum adsorption capacities of ion exchangers as regards the complexes under study provides an opportunity of developing an affinity series and identification of the adsorbent with the highest capability of capturing complexes from the solution. Twelve ion exchangers differing in the matrix, functional groups, structure, and bead size were ranked according to the increasing affinity for the Ln(III)-GLDA complexes:

- WBA-IRA 67 < SBA-4400 < SBA-4600 < SBA-M600 < SBA-IRA 958 < SBA-4200 < SBA-M500 < SBA-MP500 < SBA-IRA 458 < SAC-S950 < SAC-S957 < SAC-SP112 for the La(III)-GLDA complexes,

- WBA-IRA 67 < SBA-4400 < SBA-M600 < SBA-MP500 < SBA-M500 < SBA-4600 < SBA-IRA 958 < SBA-4200 < SAC-S950 < SBA-IRA 458 < SAC-SP112 < SAC-S957 for the Nd(III)-GLDA complexes,

- SAC-S950 < WBA-IRA 67 < SBA-4400 < SBA-MP500 < SBA-M600 < SBA-IRA 958 < SBA-M500 < SBA-4200 < SBA-4600 < SBA-IRA 458 < SAC-SP112 < SAC-S957 for the Ho(III)-GLDA complexes.

The studies presented in this paper proved that SAC-S957 and SAC-SP112 were characterized by the greatest adsorption capacities towards the complexes in focus. The adsorption capacities toward the La(III)-GLDA, Nd(III)-GLDA, and Ho(III)-GLDA complexes using SAC-S957 at 293 K were 139.57 mg/g, 152.72 mg/g, and 151.29 mg/g, respectively, while the values for SAC-SP112 were 155.49 mg/g, 150.23 mg/g, and 132.77 mg/g.

3.2.4. Adsorption thermodynamics

The basic thermodynamic parameters ($\Delta G°$, $\Delta H°$, and $\Delta S°$) of the Ln(III)-GLDA complexes adsorption on the twelve various ion exchangers were calculated for three temperatures (293 K, 313 K, and 333 K) and are presented in Tables 4, S15, and S16. The $\ln K_c$ vs. $1/T$ plots, from which the parameters were calculated, are shown in Fig. S8.

Table 4. Thermodynamic parameters for the La(III)-GLDA complexes adsorption on SAC, SBA, and WBA ion exchangers.

Ion exchanger	$\Delta H°$ [kJ/mol]	$\Delta S°$ [J/mol K]	$\Delta G°$ [kJ/mol]		
			293 K	313 K	333 K
SAC-S950	11.41	85.59	-13.76	-15.17	-17.21
SAC-S957	16.76	110.38	-15.62	-17.72	-20.05
SAC-SP112	2.50	73.26	-18.97	-20.41	-21.90

SBA-M500	3.95	58.58	-13.22	-14.39	-15.56
SBA-MP500	6.51	71.02	-14.29	-15.73	-17.13
SBA-M600	4.32	62.93	-14.13	-15.37	-16.64
SBA-4200	6.93	72.16	-14.22	-15.63	-17.11
SBA-4400	6.22	67.10	-13.47	-14.70	-16.16
SBA-4600	2.06	54.61	-13.95	-15.01	-16.14
SBA-IRA 958	-3.32	36.91	-14.13	-14.88	-15.60
SBA-IRA 458	-3.39	40.24	-15.20	-15.94	-16.82
WBA-IRA 67	-10.56	5.21	-12.11	-12.12	-12.33

The obtained negative $\Delta G°$ values for each system under study indicate the thermodynamically favourable and spontaneous nature of the Ln(III)-GLDA complexes adsorption. Moreover, the values varied between -20 kJ/mol and 0 kJ/mol, suggesting that the major mechanism is physical adsorption. This conclusion is validated by the values of the enthalpy change $\Delta H°$, which are less than 40 kJ/mol ($\Delta H°$ values above 40 kJ/mol are characteristic of chemical adsorption). Furthermore, the energy effect of adsorption can be inferred from $\Delta H°$. In the systems with the divinylbenzene-crosslinked polystyrene matrix ion exchangers (SAC-S950, SAC-S957, SAC-SP112, SBA-M500, SBA-MP500, SBA-M600, SBA-4200, SBA-4400, and SBA-4600), positive $\Delta H°$ values confirm the endothermic nature of the process while in the systems with the polyacrylate matrix ion exchangers (SBA-IRA 958, SBA-IRA 458, and WBA-IRA 67), negative $\Delta H°$ values were obtained, typical of exothermic processes. The positive entropy change $\Delta S°$ values indicate an increase in randomness at the phase boundary during the Ln(III)-GLDA complexes adsorption.

3.2.5. Desorption experiments

The desorption studies provide information on the extent of valuable metal ion recovery. They are also necessary to evaluate the possibility of regeneration and reuse of the adsorbent. Therefore, desorption is extremely important for the use of adsorbents in industrial processes where economical considerations play an important

role. Reusable adsorbents are also more suitable from an environmental perspective because they reduce the production of process waste. Accordingly, carrying out the research on the application of adsorbents in water and wastewater treatment processes and the recovery of various metals requires analysing the desorption process as well. In the present study, the desorption process was conducted using two desorbing agents with different concentrations. These were hydrochloric acid and nitric(V) acid at the concentrations of 0.5, 1, and 2 M. The obtained desorption efficiencies for the La(III)-GLDA complexes are shown in Fig. 10, and for the Nd(III)/Ho(III)-GLDA complexes in Figs. S9 and S10.

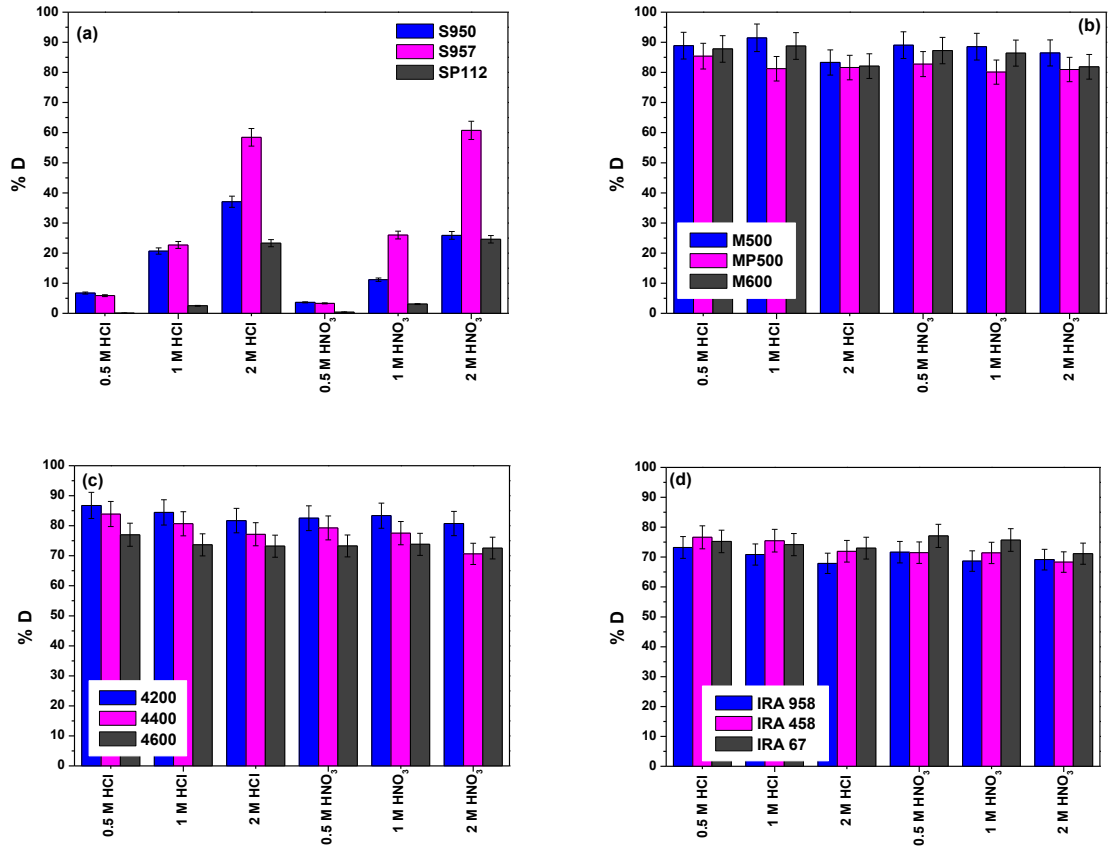

Fig. 10. Effect of the desorbing agent (type and concentration) on the desorption process of La(III) from the SAC ion exchangers (a) S950, S957, SP112, the SBA and WBA ion exchangers (b) M500, MP500, M600, (c) 4200, 4400, 4600, and (d) IRA 958, IRA 458, IRA 67.

Based on the presented results, it can be concluded that the desorption process on SAC-S950, SAC-S957, and SAC-SP112 is largely dependent on the concentration

of the used desorbing agent and that its effectiveness rises with the increasing eluent concentration. For example, in the desorption of La(III) from SAC-S957, changing the concentration of nitric(V) acid from 0.5 M to 2 M increased the desorption efficiency from 3.34% to 60.76%. The type of used desorbing agent was slightly less important compared to its concentration. Changing 2 M nitric(V) acid to 2 M hydrochloric acid increased the *%D* value from 25.90% to 37.07% during the desorption of La(III) from SAC-S950 but it resulted in a slight decrease from 24.60% to 23.29% during the desorption of La(III) from SAC-SP112. The other ion exchangers (anion exchangers) did not exhibit such correlations. Both the change of desorbing agent and its concentration affected marginally the process, with the obtained desorption efficiencies being greater compared to SAC-S950, SAC-S957, and SAC-SP112 (up to 94.38%). The results show that the Ln(III)-GLDA complexes have a higher affinity for SAC-S950, SAC-S957, and SAC-SP112 than for the anion exchangers.

3.3. GLDA in rare earth elements removal - Adsorption dynamic method

The adsorption studies using a static method enabled quick and easy determination of the effect of various factors on the Ln(III)-GLDA complexes adsorption. However, this method is suitable for the processes conducted on a smaller scale. In industry, the more preferred method of adsorption is the dynamic one, especially that on a fixed bed. Continuous passing of the solution through the immobilized adsorbent bed keeps the adsorbent in the constant contact with the fresh adsorbate solution, which makes it possible to achieve higher volumes of purified effluent.

The dynamic method was employed to study the La(III)-GLDA complexes adsorption at the concentrations of 1.0×10^{-3} M. The obtained results are illustrated as the breakthrough curves (C/C_o vs. V) in Fig. 11. On their basis, the fundamental

parameters describing the column system (q_e, C_w, C_t, D_g, and D_v) were calculated, which are summarized in Table 5.

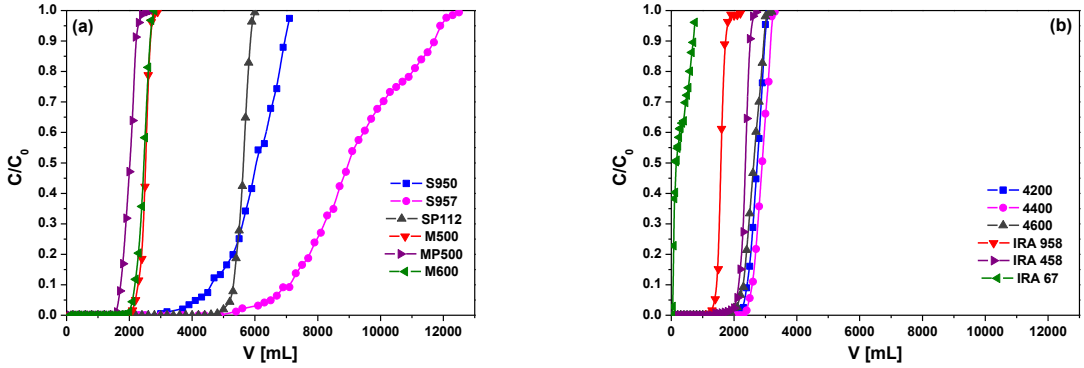

Fig. 11. Breakthrough curves of La(III)-GLDA complexes adsorption on SAC, SBA, and WBA ion exchangers (a) S950, S957, SP112, M500, MP500, M600, (b) 4200, 4400, 4600, IRA 958, IRA 458, IRA 67 (C_0=1.0×10^{-3} M).

Table 5. Dynamic studies parameters of the La(III)-GLDA complexes adsorption (C_0=1.0×10^{-3} M).

Ion exchanger	q_e [mg/g]	U [mL]	$\bar{U}$ [mL]	C_w [mg/mL]	C_t [mg/mL]	D_g	D_v	%D
SAC-S950	222.38	3000	6050	43.18	87.08	1599.37	604.56	94.04
SAC-S957	305.89	5400	9000	77.72	129.54	2106.70	899.56	99.03
SAC-SP112	211.94	4600	5640	66.21	81.18	1496.36	563.56	94.89
SBA-M500	104.34	2000	2520	28.33	35.70	757.12	251.56	93.67
SBA-MP500	110.22	1600	2020	22.66	28.61	806.08	201.56	98.36
SBA-M600	96.45	1700	2460	24.08	34.85	699.72	245.56	84.09
SBA-4200	103.86	1900	2750	26.91	38.95	755.16	274.56	98.20
SBA-4400	101.17	2400	2900	34.00	41.08	729.85	289.56	98.70
SBA-4600	100.53	1700	2620	24.08	37.11	723.46	261.56	99.71
SBA-IRA 958	67.14	1200	1590	17.00	22.52	489.23	158.56	99.37
SBA-IRA 458	86.39	1400	2360	19.83	33.43	627.16	235.56	99.95
WBA-IRA 67	10.25	50	150	0.68	2.03	39.55	14.56	94.24

The adsorption systems closest to the ideal are characterized by the breakthrough curves with a shape referred to as "S". The determined curves for the La(III)-GLDA complexes adsorption are characterized by this shape, however, they vary in steepness. The maximum adsorption capacities determined by the static

method and the affinity series formed from them are reflected in the results obtained using the column systems. It can be concluded that SAC-S957 showed the greatest uptake capacity of the La(III)-GLDA complexes among the tested ion exchangers. It was characterized by a very high value of the adsorption capacity q_e, equal to 305.89 mg/g as well as the other parameters crucial to the design of adsorption systems, such as the working exchange capacity C_w of 77.72 mg/mL and the total exchange capacity C_t of 129.54 mg/mL. Slightly lower adsorption efficiencies were reported for SAC-S950 and SAC-SP112 whose adsorption capacities obtained by the dynamic method were 222.38 mg/g and 211.94 mg/g, respectively. In the group of polystyrene anion exchangers (SBA-M500, SBA-MP500, SBA-M600, SBA-4200, SBA-4400, and SBA-4600), adsorption capacities ranged from 96.45 mg/g to 110.22 mg/g. The strongly basic polyacrylate anion exchangers SBA-IRA 958 and SBA-IRA 458 were slightly less efficient with the q_e values of 67.14 mg/g and 86.39 mg/g, respectively. The lowest adsorption capacity was determined for WBA-IRA 67, which is only 10.25 mg/g. For this column system, passing only 50 mL of solution through the column resulted in the column breakthrough, suggesting that WBA-IRA 67 is not suitable for the use as an adsorbent in the La(III)-GLDA complexes removal.

The experimental data of the La(III)-GLDA complexes adsorption in the column systems were analysed using four mathematical models (Thomas, Adams-Bohart, Yoon-Nelson, Wolborska models) to study the behaviour of the columns filled with the chosen ion exchangers. The obtained parameters from the models are summarized in Table S17.

The Thomas model is employed in the literature to describe column systems, assuming that the process follows the assumptions of the Langmuir isotherm and the second-order kinetic model omitting the axial dispersion [60]. The Adams-Bohart model

asserts that the adsorption rate depends mostly on the adsorbent capacity available at the moment for the adsorbate (called the residual adsorbent capacity) and on the adsorbate concentration [61]. The Yoon-Nelson model considers that the adsorption probability of adsorbate molecules, and thus the breakthrough on the adsorbent, is proportional to the rate of decrease in the adsorption probability of each adsorbate molecule [62]. While based on the Wolborska model, in the initial part of the breakthrough curve, the film diffusion with a constant kinetic coefficient is the adsorption controlling step [63]. The Thomas and Yoon-Nelson models are used to describe the breakthrough curves over their entire range. However, when applying the Adams-Bohart and Wolborska models, only the initial part of the curves should be analysed.

The Thomas model was adjusted to the experimental data by plotting $\ln(C_0/C)-1$ vs. V. The model allowed the Thomas rate constant k_{Th} and the adsorption capacities q_0 to be calculated. The q_0 values determined from the Thomas model exhibit good agreement with the adsorption capacities received by experiment (q_e in Table 5). The compatibility of the model with the experimental results was also assessed based on the R^2 value. The worst fit was characterized by the system with WBA-IRA 67, for which the R^2 was equal to 0.755. For the other ion exchangers, the values varied between 0.879 and 0.987, indicating a good match.

In the next step, linear plots of $\ln(C/C_0)$ vs. t were prepared to determine the Adams-Bohart model parameters (adsorption capacities per unit bed volume q and the Adams-Bohart rate constants k_{AB}). The greatest adsorption capacity of 130779.92 mg/L was obtained for SAC-S957. The R^2 values ranged from 0.422 for the system with WBA-IRA 67 to 0.974 for the system with SAC-SP112.

The time requisite to achieve a 50% adsorbate breakthrough (τ) and the Yoon-Nelson rate constant (k_{YN}) were computed using the intercept and slope of the Yoon-Nelson plot ($\ln(C/C_0-C)$ vs. t). The comparison of τ values gives crucial information about the possible column operating time before half depletion. According to the results, if SAC-S957 is used, the column will be half-occupied after 15275.70 minutes (254.6 hours of operation). This is almost four times longer compared to the SBA ion exchanger group, whose average τ value was 3909.73 minutes. For the column systems with SAC-S950 and SAC-SP112, τ is equal to 9851.82 and 9243.01 minutes were obtained, respectively. The column with WBA-IRA 67 reached the 50% breakthrough after only 438.41 minutes.

The last model chosen to describe the column systems was the Wolborska model. The model was based on the analogous dependence to the Adams-Bohart model ($\ln(C/C_0)$ vs. t), which was utilized to calculate the external mass transfer kinetic coefficients β_a and the adsorption capacities per unit bed volume q (Table S17). The R^2 values for fitting the Wolborska model to the La(III)-GLDA complexes adsorption experimental results in the column systems were 0.422 for the system with WBA-IRA 67 and from 0.707 to 0.974 for the other ion exchangers.

When the ion exchanger bed in all systems was depleted (C/C_0=1 in Fig. 11), the desorption process was conducted to recover La(III) and to regenerate the columns. Desorption was made by employing the following desorbing agents: 2 M HCl for the system with SAC-S950; 2 M HNO_3 for the systems with SAC-S957 and SAC-SP112; and 1 M HCl for the systems with anion exchangers. The results are shown in Table 5 as the *%D* values. The recovery of La(III) was incredibly high, ranging from 84.09% to 99.95%.

4. Conclusions

This study focused on the application of GLDA (tetrasodium salt of N,N-bis(carboxymethyl)-L-glutamic acid) as a biodegradable complexing agent in the adsorption of the rare earth element ions La(III), Nd(III), and Ho(III). The ion exchangers differing in the matrix, functional groups, structure and bead size as well as belonging to the groups of chelating ion exchangers, cation exchangers and strongly or weakly basic anion exchangers were selected as adsorbents. The experiments were performed using the static and dynamic methods in the single-component systems. Prior to the main part of the study, the potentiometric measurements were conducted to provide knowledge of the complex forms present in the solution depending on its pH. Moreover, the physicochemical characterization of ion exchangers was made. These studies promoted largely the explanation of adsorption mechanisms. In the Ln(III)-GLDA systems being investigated, the presence of LnGLDA complexes, the protonated complexes (LnH_xGLDA) and hydroxycomplexes ($LnGLDA(OH)_x$) was identified. The adsorption process was analysed in terms of the effects of the Ln(III):GLDA molar ratio, initial solution pH, phase contact time, initial concentrations, and temperature on its course. It was demonstrated that the adsorption of Ln(III)-GLDA complexes is dependent on the investigated factors, and that the ion exchanger used in the system has a significant effect on the selection of optimal parameters. The adsorption of Ln(III)-GLDA complexes was found to proceed with a great efficiency in 30 minutes; only in the systems containing SAC-S950 and WBA-IRA 67 the equilibrium took up to 240 minutes to establish. The adsorption kinetics on SAC-S950 and WBA-IRA 67 followed the PSO model, while the other systems were best characterized by the PFO model. The equilibrium studies allowed to conclude that both the Langmuir and Freundlich and

Temkin models were applicable in description of the Ln(III)-GLDA complexes adsorption (systems with SAC-S950, SAC-S957, and SAC-SP112 - the Temkin model; systems with the SBA ion exchangers - the Langmuir model; systems with WBA-IRA 67 - the Freundlich model). The greatest adsorption capacities were obtained for SAC-S957 and SAC-SP112, which were 139.57 mg/g and 155.49 mg/g for the La(III)-GLDA complexes, 152.72 mg/g and 150.23 mg/g for the Nd(III)-GLDA complexes, and 151.29 mg/g and 132.77 mg/g for the Ho(III)-GLDA complexes, respectively. However, in the case of SAC-SP112, a particular attention should be paid to the conditions under which these results were obtained. SAC-SP112 adsorbed with a satisfactory efficiency only in the very low pH range, in which according to the potentiometric measurements, mainly uncomplexed Ln^{3+} ions rather than complexes were present. Finally, the experiments performed by the dynamic method confirmed the good adsorption capacity of the ion exchangers towards the Ln(III)-GLDA complexes (with the exception of WBA-IRA 67). The results demonstrated in this paper indicate that GLDA has great complexing properties and can be applied as an alternative to the traditional, poorly biodegradable ligands.

Acknowledgments

The authors are grateful for the financial support from the National Centre for Research and Development under Project No. POIR.04.01.01-00-0040/17-00.

References:

[1] I.S.S. Pinto, I.F.F. Neto, H.M.V.M. Soares, Biodegradable chelating agents for industrial, domestic, and agricultural applications-a review, Environ. Sci. Pollut. Res. 21 (2014) 11893–11906. https://doi.org/10.1007/s11356-014-2592-6.

[2] F. Mechachti, S. Lakehal, A. Lakehal, C. Morell, L. Merzoud, H. Chermette, Predicted structure and selectivity of 3d transition metal complexes with glutamic: N,N-bis(carboxymethyl) acid, New J. Chem. 45 (2021) 18366–18378. https://doi.org/10.1039/d1nj03298d.

[3] C.G. van Ginkel, R. Geerts, P.D. Nguyen, Biodegradation of L-glutamatediacetate by mixed cultures and an isolate, in: Biogeochem. Chelating Agents, 2005: pp. 183–194.

[4] M. Borowiec, M. Huculak, K. Hoffmann, J. Hoffmann, Biodegradation of selected substances used in liquid fertilizers as an element of Life Cycle Assessment, Polish J. Chem. Technol. 11 (2009) 1–3. https://doi.org/10.2478/v10026-009-0001-6.

[5] C.G. van Ginkel, R. Geerts, Biodegradation of N,N-bis(carboxymethyl)-L-glutamate and its utilization as sole source of carbon, nitrogen, and energy by a *Rhizobium radiobacter* strain in seawater, Toxicol. Environ. Chem. 98 (2016) 26–35. https://doi.org/10.1080/02772248.2015.1113287.

[6] Akzo Nobel Chemicals Co. Ltd., Brochure of Dissolvine ® GL, 2020. https://chelates.akzonobel.com/siteassets/20170714-download-product-dissolvinegl-technicalbrochure.pdf.

[7] C.A. De Wolf, E. Bang, A. Bouwman, W. Braun, E. De Oliveira, H. Nasr.El-Din, Evaluation of environmentally friendly chelating agents for applications in the oil and gas industry, in: SPE - Eur. Form. Damage Conf. Proceedings, EFDC, 2014: pp. 311–325. https://doi.org/10.2118/168145-ms.

[8] K. Sokhanvarian, H.A. Nasr-El-Din, C.A. De Wolf, Thermal stability of oilfield aminopolycarboxylic acids/salts, SPE Prod. Oper. 31 (2016) 12–21. https://doi.org/10.2118/157426-PA.

[9] Z.A. Begum, I.M.M. Rahman, Y. Tate, Y. Egawa, T. Maki, H. Hasegawa, Formation

and stability of binary complexes of divalent ecotoxic ions (Ni, Cu, Zn, Cd, Pb) with biodegradable aminopolycarboxylate chelants (dl-2-(2-carboxymethyl)nitrilotriacetic acid, GLDA, and 3-hydroxy-2,2′- iminodisuccinic acid, HIDS) in aqueous solu, J. Solution Chem. 41 (2012) 1713–1728. https://doi.org/10.1007/s10953-012-9901-9.

[10] Z.A. Begum, I.M.M. Rahman, H. Sawai, Y. Tate, T. Maki, H. Hasegawa, Stability constants of Fe(III) and Cr(III) complexes with DL-2-(2-carboxymethyl)nitrilotriacetic acid (GLDA) and 3-hydroxy-2,2 ′-iminodisuccinic acid (HIDS) in aqueous solution, J. Chem. Eng. Data. 57 (2012) 2723–2732.

[11] Z.A. Begum, I.M.M. Rahman, H. Hasegawa, Complexation behavior of Sr^{II} and geochemically-related elements (Mg^{II}, Ca^{II}, Ba^{II}, and Y^{III}) with biodegradable aminopolycarboxylate chelators (GLDA and HIDS), J. Mol. Liq. 242 (2017) 1123–1130. https://doi.org/10.1016/j.molliq.2017.07.126.

[12] J. Jefferis, K. Zack, Detergent composition, WO2011100344A1, 2011.

[13] K.B. Charkhutian, B.L. Libutti, F. de Cordt, J.S. Ruffini, Process for inhibiting scale and fouling the metal surfaces exposed to an aqueous system, WO2004013055, 2004.

[14] M.H. Sulaiman, F. Adam, Z. Yaacob, M.Z. Mohd Noor, N. Abdullah, Evaluation of carboxylic acid and amine groups with $CaCO_3$, FeS and $BaSO_4$: Molecular dynamic simulations and experimental study, Arab. J. Sci. Eng. 47 (2022) 6693–6706. https://doi.org/10.1007/s13369-022-06647-2.

[15] L. Salalá, R. Takahashi, J. Argueta, J. Wang, N. Watanabe, N. Tsuchiya, Permeability enhancement and void formation by chelating agent in volcanic rocks (Ahuachapán and Berlín geothermal fields, El Salvador), Geothermics. 107 (2023). https://doi.org/10.1016/j.geothermics.2022.102586.

[16] N. Watanabe, K. Takahashi, R. Takahashi, K. Nakamura, Y. Kumano, K. Akaku,

T. Tamagawa, T. Komai, Novel chemical stimulation for geothermal reservoirs by chelating agent driven selective mineral dissolution in fractured rocks, Sci. Rep. 11 (2021) 1–11. https://doi.org/10.1038/s41598-021-99511-6.

[17] A. Macchia, I.A. Colasanti, L. Rivaroli, G. Favero, T. de Caro, L.P. Munoz, L. Campanella, M.F. La Russa, Natural based products for cleaning copper and copper alloys artefacts, Nat. Prod. Res. (2021). https://doi.org/doi.org/10.1080/14786419.2021.2000408.

[18] H. Hasegawa, M.A. Rahman, K. Saitou, M. Kobayashi, C. Okumura, Influence of chelating ligands on bioavailability and mobility of iron in plant growth media and their effect on radish growth, Environ. Exp. Bot. 71 (2011) 345–351. https://doi.org/10.1016/j.envexpbot.2011.01.004.

[19] G.L. Yang, M.X. Yang, S.M. Lv, A.J. Tan, The effect of chelating agents on iron plaques and arsenic accumulation in duckweed (*Lemna minor*), J. Hazard. Mater. 419 (2021) 126410. https://doi.org/10.1016/j.jhazmat.2021.126410.

[20] F. Masoudi, M. Shirvani, H. Shariatmadari, M.R. Sabzalian, Performance of new biodegradable chelants in enhancing phytoextraction of heavy metals from a contaminated calcareous soil, J. Environ. Heal. Sci. Eng. 18 (2020) 655–664. https://doi.org/10.1007/s40201-020-00491-y.

[21] H. Guan, L. Dong, Y. Zhang, S. Bai, L. Yan, GLDA and EDTA assisted phytoremediation potential of *Sedum hybridum* 'Immergrunchen' for Cd and Pb contaminated soil, Int. J. Phytoremediation. 24 (2022) 1395–1404. https://doi.org/doi.org/10.1080/15226514.2022.2031865.

[22] G. Wang, S. Zhang, X. Xu, Q. Zhong, C. Zhang, Y. Jia, T. Li, O. Deng, Y. Li, Heavy metal removal by GLDA washing: Optimization, redistribution, recycling, and changes in soil fertility, Sci. Total Environ. 569–570 (2016) 557–568.

https://doi.org/10.1016/j.scitotenv.2016.06.155.

[23] K. Wang, Y. Liu, Z. Song, Z.H. Khan, W. Qiu, Effects of biodegradable chelator combination on potentially toxic metals leaching efficiency in agricultural soils, Ecotoxicol. Environ. Saf. 182 (2019) 109399. https://doi.org/10.1016/j.ecoenv.2019.109399.

[24] D. Yan, Z. Guo, X. Xiao, C. Peng, Y. He, A. Yang, X. Wang, Y. Hu, Z. Li, Cleanup of arsenic, cadmium, and lead in the soil from a smelting site using N,N-bis(carboxymethyl)-L-glutamic acid combined with ascorbic acid: A lab-scale experiment, J. Environ. Manage. 296 (2021) 113174. https://doi.org/10.1016/j.jenvman.2021.113174.

[25] T. Murakami, R. Wakata, A. Mamorita, A.S. Mashio, K.H. Wong, S. Chinaka, H. Hasegawa, Direct analysis of biodegradable chelating agents based on liquid chromatography/electrospray ionization mass spectrometry using a metal-free hydrophilic interaction liquid chromatographic column, Anal. Sci. (2022) 10–12. https://doi.org/10.1007/s44211-022-00247-8.

[26] L. Karimzadeh, H. Lippold, M. Stockmann, C. Fischer, Effect of DTPA on europium sorption onto quartz – Batch sorption experiments and surface complexation modeling, Chemosphere. 239 (2020) 124771. https://doi.org/10.1016/j.chemosphere.2019.124771.

[27] L.J. Cajuste, J. Cruz-Díaz, C. García-Osorio, Extraction of heavy metals from contaminated soils: I. Sequential extraction in surface soils and their relationships to DTPA extractable metals and metal plant uptake, J. Environ. Sci. Heal. - Part A Toxic/Hazardous Subst. Environ. Eng. 35 (2000) 1141–1152. https://doi.org/10.1080/10934520009377024.

[28] P. Wu, J. Zhou, X. Wang, Y. Dai, Z. Dang, N. Zhu, P. Li, J. Wu, Adsorption of Cu-

EDTA complexes from aqueous solutions by polymeric Fe/Zr pillared montmorillonite: Behaviors and mechanisms, Desalination. 277 (2011) 288–295. https://doi.org/10.1016/j.desal.2011.04.043.

[29] J. Wang, M. Mao, S. Atif, Y. Chen, Adsorption behavior and mechanism of aqueous Cr(III) and Cr(III)-EDTA chelates on DTPA-chitosan modified Fe_3O_4@SiO_2, React. Funct. Polym. 156 (2020) 104720.

[30] K. Burdzy, A. Aurich, S. Hunger, R. Jastrząb, M. Zabiszak, D. Kołodyńska, Green citric acid in the sorption process of rare earth elements, Chem. Eng. J. 437 (2022) 135366. https://doi.org/10.1016/j.cej.2022.135366.

[31] K. Vijayaraghavan, Y.S. Yun, Polysulfone-immobilized *Corynebacterium glutamicum*: A biosorbent for Reactive black 5 from aqueous solution in an up-flow packed column, Chem. Eng. J. 145 (2008) 44–49. https://doi.org/10.1016/j.cej.2008.03.001.

[32] O. Hamdaoui, Removal of copper(II) from aqueous phase by Purolite C100-MB cation exchange resin in fixed bed columns: Modeling, J. Hazard. Mater. 161 (2009) 737–746. https://doi.org/10.1016/j.jhazmat.2008.04.016.

[33] Y.H. Yoon, J.H. Nelson, Application of gas adsorption kinetics I. A theoretical model for respirator cartridge service life, Am. Ind. Hyg. Assoc. J. 45 (1984) 509–516. https://doi.org/10.1080/15298668491400197.

[34] A. Wolborska, External film control of the fixed bed adsorption, Chem. Eng. J. 73 (1999) 85–92. https://doi.org/10.1016/S1385-8947(99)00049-2.

[35] Y.S. Ho, Citation review of Lagergren kinetic rate equation on adsorption reactions, Scientometrics. 59 (2004) 171–177. https://doi.org/10.1023/B:SCIE.0000013305.99473.cf.

[36] Y.S. Ho, Second-order kinetic model for the sorption of cadmium onto tree fern: A

comparison of linear and non-linear methods, Water Res. 40 (2006) 119–125. https://doi.org/10.1016/j.watres.2005.10.040.

[37] I. Tsibranska, E. Hristova, Comparison of different kinetic models for adsorption of heavy metals onto activated carbon from apricot stones, Bulg. Chem. Commun. 43 (2011) 370–377.

[38] A.E. Ofomaja, Kinetic study and sorption mechanism of methylene blue and methyl violet onto mansonia (*Mansonia altissima*) wood sawdust, Chem. Eng. J. 143 (2008) 85–95. https://doi.org/10.1016/j.cej.2007.12.019.

[39] I. Siminiceanu, N. Marchitan, G. Duca, A. Mereuta, Mathematical models based on thermodynamic equilibrium and kinetics of an ion exchange process, Rev. Chim. 61 (2010) 623–626.

[40] Y. Liu, Some consideration on the Langmuir isotherm equation, Colloids Surfaces A Physicochem. Eng. Asp. 274 (2006) 34–36. https://doi.org/10.1016/j.colsurfa.2005.08.029.

[41] P. Baláž, A. Aláčová, J. Briančin, Sensitivity of Freundlich equation constant 1/n for zinc sorption on changes induced in calcite by mechanical activation, Chem. Eng. J. 114 (2005) 115–121. https://doi.org/10.1016/j.cej.2005.08.017.

[42] X.S. Wang, Y. Qin, Equilibrium sorption isotherms for of Cu^{2+} on rice bran, Process Biochem. 40 (2005) 677–680. https://doi.org/10.1016/j.procbio.2004.01.043.

[43] O.A. Oyetade, V.O. Nyamori, S.B. Jonnalagadda, B.S. Martincigh, Removal of Cd^{2+} and Hg^{2+} from aqueous solutions by adsorption onto nitrogen-functionalized carbon nanotubes, Desalin. Water Treat. 108 (2018) 253–267. https://doi.org/10.5004/dwt.2018.21955.

[44] K.C. Lanigan, K. Pidsosny, Reflectance FTIR spectroscopic analysis of metal complexation to EDTA and EDDS, Vib. Spectrosc. 45 (2007) 2–9.

https://doi.org/10.1016/j.vibspec.2007.03.003.

[45] P.U. Singare, R.S. Lokhande, R.S. Madyal, Thermal degradation studies of some strongly acidic cation exchange resins, Open J. Phys. Chem. 1 (2011) 45–54. https://doi.org/10.4236/ojpc.2011.12007.

[46] O.C.S. Al Hamouz, S.A. Ali, Novel cross-linked polyphosphonate for the removal of Pb^{2+} and Cu^{2+} from aqueous solution, Ind. Eng. Chem. Res. 51 (2012) 14178–14187. https://doi.org/10.1021/ie301231k.

[47] T.H. Boyer, P.C. Singer, Stoichiometry of removal of natural organic matter by ion exchange, Environ. Sci. Technol. 42 (2008) 608–613. https://doi.org/10.1021/es071940n.

[48] S.D. Alexandratos, L.A. Hussain, Bifunctionality as a means of enhancing complexation kinetics in selective ion exchange resins, Ind. Eng. Chem. Res. 34 (1995) 251–254. https://doi.org/10.1021/ie00040a026.

[49] R. Liu, H. Tang, B. Zhang, Removal of Cu(II), Zn(II), Cd(III) and Hg(II) from waste water by poly(acrylaminophosphonic)-type chelating fiber, Chemosphere. 38 (1999) 3169–3179.

[50] S.S. Muhammad, Uranium sorption using Lewatit MonoPlus M500 from sulphate media, Sci. J. Chem. 8 (2020) 7–19. https://doi.org/10.11648/j.sjc.20200801.12.

[51] X Zhao, W.H. Höll, G. Yun, Elimination of cadmium trace contaminations from drinking water, Water Res. 36 (2002) 851–858. https://doi.org/10.1016/s0043-1354(01)00289-5.

[52] H. Simsek, M. Kobya, E. Khan, A.N. Bezbaruah, Removal of aqueous cyanide with strongly basic ion-exchange resin, Environ. Technol. 36 (2015) 1612–1622. https://doi.org/10.1080/09593330.2014.999829.

[53] C. Xiong, J. Zhu, C. Shen, Q. Chen, Adsorption and desorption of praseodymium

(III) from aqueous solution using D72 resin, Chinese J. Chem. Eng. 20 (2012) 823–830. https://doi.org/10.1016/S1004-9541(12)60405-4.

[54] K. Burdzy, Y.-G. Chen, G.-Y. Lv, S.-H. Chen, D. Kołodyńska, Application of ion exchangers with the N-methyl-D-glucamine groups in the V(V) ions adsorption process, Materials (Basel). 15 (2022) 1026.

[55] W.J. Weber, E.H. Smith, Simulation and design models for adsorption processes, Environ. Sci. Technol. 21 (1987) 1040–1050.

[56] R. Gayathri, K.P. Gopinath, P.S. Kumar, Adsorptive separation of toxic metals from aquatic environment using agro waste biochar: Application in electroplating industrial wastewater, Chemosphere. 262 (2021) 128031. https://doi.org/10.1016/j.chemosphere.2020.128031.

[57] A.C. Martins, O. Pezoti, A.L. Cazetta, K.C. Bedin, D.A.S. Yamazaki, G.F.G. Bandoch, T. Asefa, J. V. Visentainer, V.C. Almeida, Removal of tetracycline by NaOH-activated carbon produced from macadamia nut shells: Kinetic and equilibrium studies, Chem. Eng. J. 260 (2015) 291–299. https://doi.org/10.1016/j.cej.2014.09.017.

[58] M.M. Ali, S.A. Abedelmaksoud, M.H. Taha, A.M.A. El Naggar, A.S. Morshedy, A.A. Elzoghbi, Uranium separation from phosphoric acid using metallic carbonaceous structures as efficient adsorbents: an experimental and kinetic study, Radiochemistry. 62 (2020) 204–215. https://doi.org/10.1134/S1066362220020083.

[59] Y.R. Smith, D. Bhattacharyya, T. Willhard, M. Misra, Adsorption of aqueous rare earth elements using carbon black derived from recycled tires, Chem. Eng. J. 296 (2016) 102–111.

[60] M.T. Yagub, T.K. Sen, S. Afroze, H.M. Ang, Fixed-bed dynamic column adsorption study of methylene blue (MB) onto pine cone, Desalin. Water Treat. 55 (2015) 1026–

1039. https://doi.org/10.1080/19443994.2014.924034.

[61] N.E. Davila-Guzman, F.J. Cerino-Córdova, E. Soto-Regalado, M. Loredo-Cancino, J.A. Loredo-Medrano, R.B. García-Reyes, A mass transfer model for the fixed-bed adsorption of ferulic acid onto a polymeric resin: axial dispersion and intraparticle diffusion, Environ. Technol. 37 (2016) 1914–1922. https://doi.org/10.1080/09593330.2015.1135993.

[62] S. Selambakkannu, N.A.F. Othman, K.A. Bakar, Z.A. Karim, Adsorption studies of packed bed column for the removal of dyes using amine functionalized radiation induced grafted fiber, SN Appl. Sci. 1 (2019) 1–10. https://doi.org/10.1007/s42452-019-0184-2.

[63] Z. Xu, J.G. Cai, B.C. Pan, Mathematically modeling fixed-bed adsorption in aqueous systems, J. Zhejiang Univ. Sci. A. 14 (2013) 155–176. https://doi.org/10.1631/jzus.A1300029.

Supplementary Materials

GLDA AND ION EXCHANGERS: UNLOCKING SUSTAINABLE SOLUTIONS FOR RECOVERY OF RARE EARTH ELEMENTS

Katarzyna Burdzy[1], Renata Jastrząb[2], Dorota Kołodyńska[1]*

[1]Department of Inorganic Chemistry, Faculty of Chemistry, Maria Curie-Skłodowska University, M. Curie Skłodowska Sq. 2, 20-031 Lublin, Poland

[2]Faculty of Chemistry, Adam Mickiewicz University, Uniwersytetu Poznańskiego 8, 61-614 Poznań, Poland

1. Potentiometric measurements

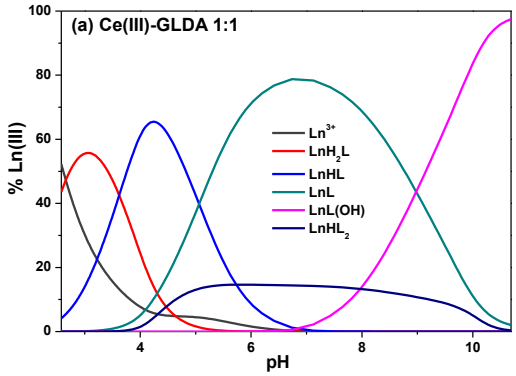

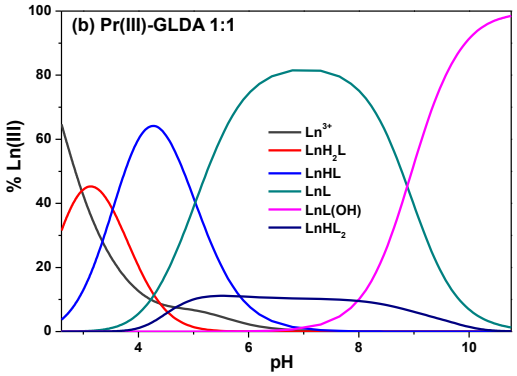

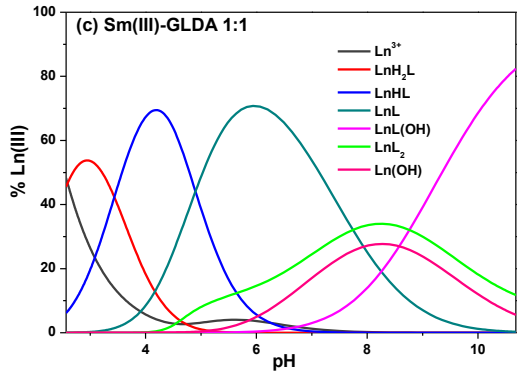

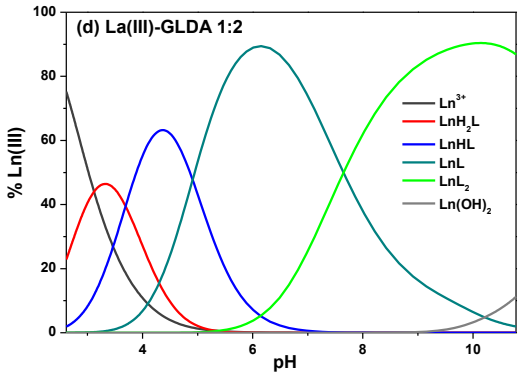

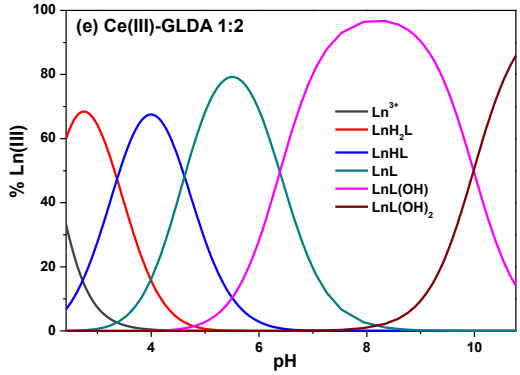

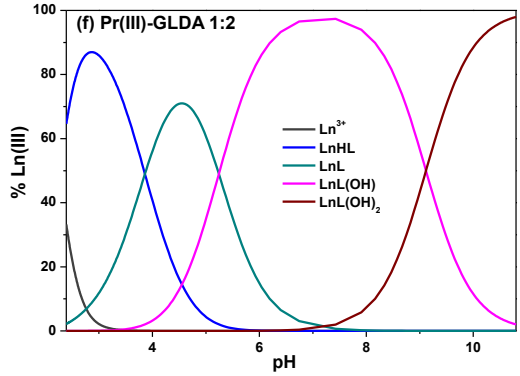

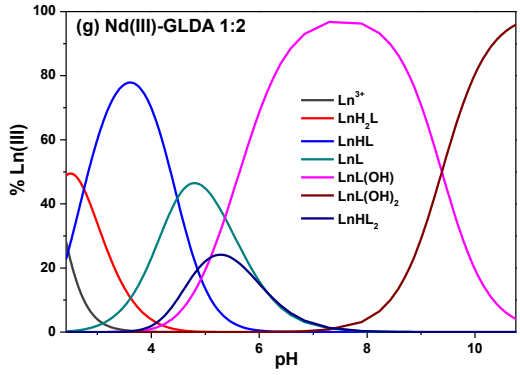

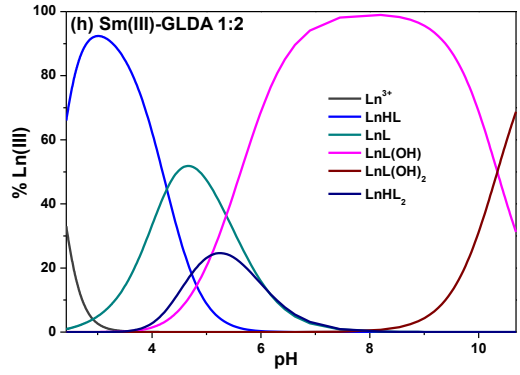

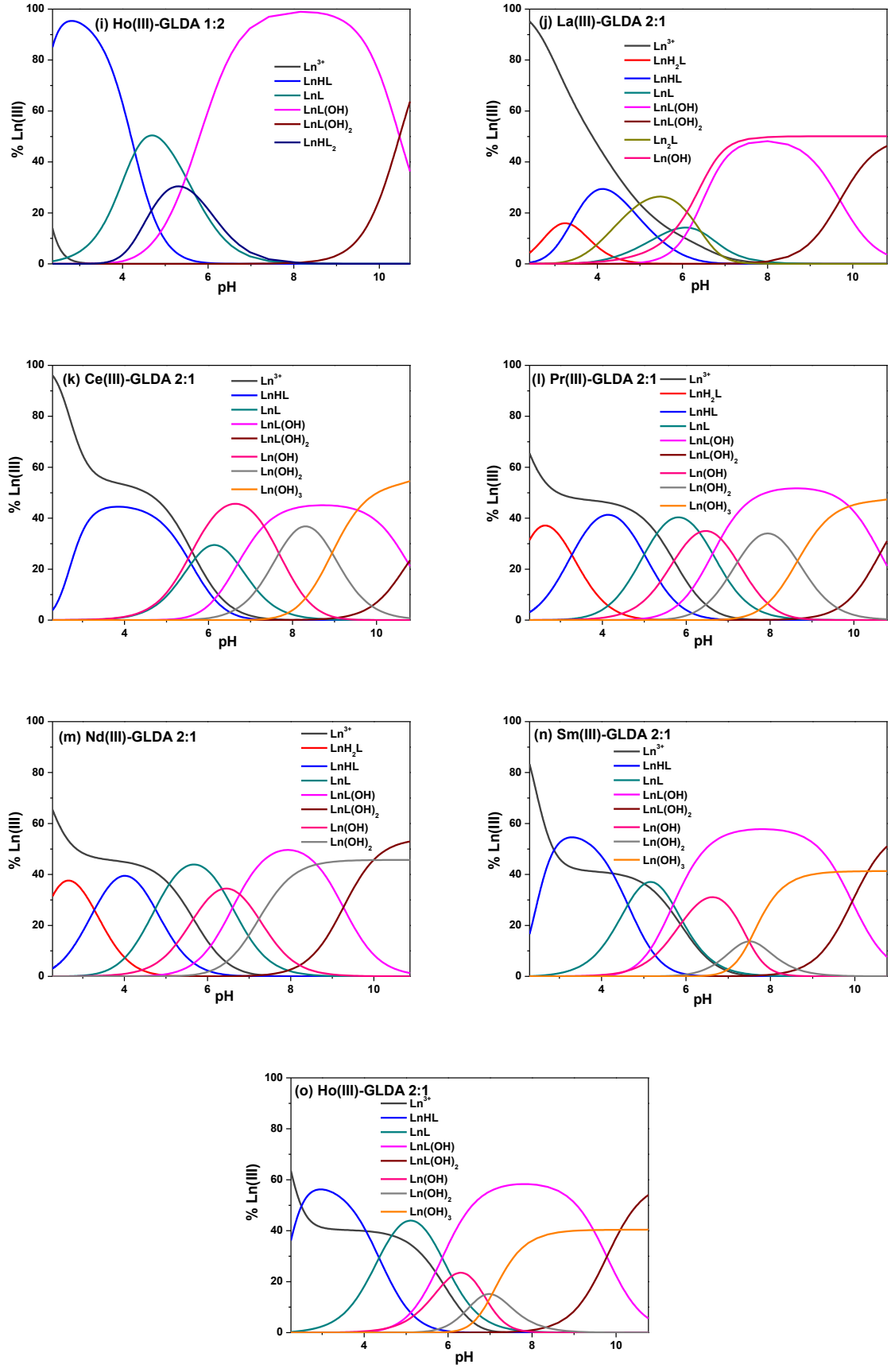

Fig. S1. Distribution diagrams for the Ln(III)-GLDA systems: (a-c) Ln(III)-GLDA 1:1, (d-i) Ln(III)-GLDA 1:2, (j-o) Ln(III)-GLDA 2:1.

2. The characterization of ion exchangers

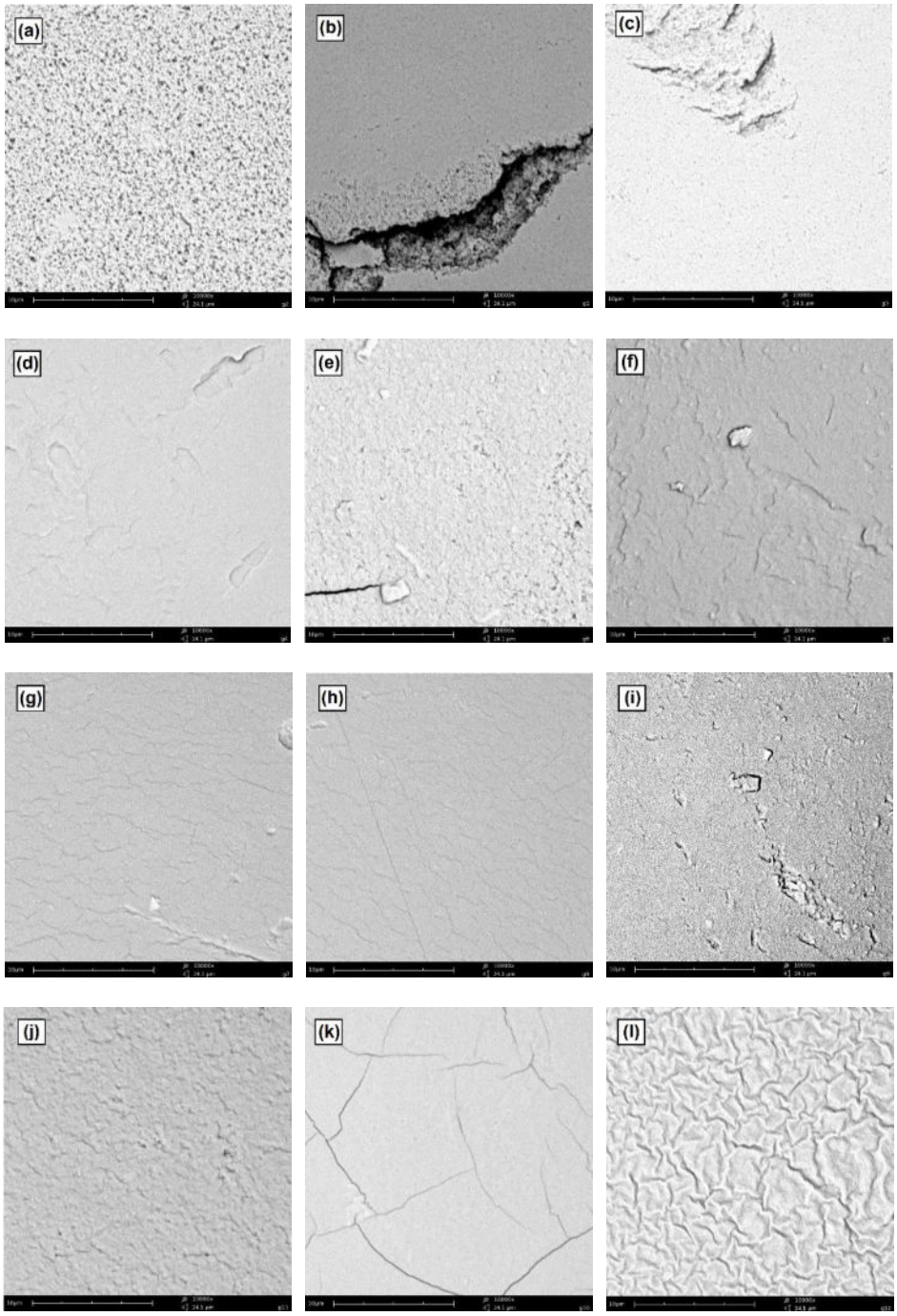

Fig. S2. SEM images of SAC ion exchangers (a) S950, (b) S957, (c) SP112, SBA ion exchangers (d) M500, (e) MP500, (f) M600, (g) 4200, (h) 4400, (i) 4600, (j) IRA 958, (k) IRA 458, and WBA ion exchanger (l) IRA 67 after the La(III)-GLDA complexes adsorption (magnification × 10,000).

Table 1. The elemental composition (C_{at}) and binding energies (E_B) for SAC, SBA, and WBA ion exchangers before and after the La(III)-GLDA complexes adsorption obtained by the XPS analysis.

Level	SAC-S950		SAC-S950 + La(III)-GLDA		SAC-S957		SAC-S957 + La(III)-GLDA		SAC-SP112		SAC-SP112 + La(III)-GLDA	
	E_B [eV]	C_{at} [%]	E_B [eV]	C_{at} [%]	E_B [eV]	C_{at} [%]	E_B [eV]	C_{at} [%]	E_B [eV]	C_{at} [%]	E_B [eV]	C_{at} [%]

C1s	285.0	51.6	284.7	66.4	285.0	61.7	284.7	66.4	285.0	66.9	284.7	67.9
O1s	530.5	25.1	531.5	20.5	533.0	23.0	532.2	22.7	532.0	20.5	531.5	20.9
N1s	399.5	4.7	399.5	2.2	402.0	0.7	401.0	1.6	-	-	399.5	1.3
P2p	133.5	9.9	133.2	7.3	134.5	7.9	134.0	5.6	-	-	-	-
S2p	-	-	-	-	168.5	3.9	168.5	3.1	169.0	8.6	168.5	7.6
Al2p	75.0	0.4	-	-	76.5	2.8	-	-	-	-	-	-
Na1s	1071.5	8.3	1070.7	3.0	-	-	1072.2	0.3	1072.5	4.0	1071.5	1.8
La3d	-	-	835.2	0.6	-	-	836.0	0.3	-	-	836.0	0.5
Level	**SBA-M500**		**SBA-M500 + La(III)-GLDA**		**SBA-MP500**		**SBA-MP500 + La(III)-GLDA**		**SBA-M600**		**SBA-M600 + La(III)-GLDA**	
	E_B [eV]	C_{at} [%]	E_B [eV]	C_{at} [%]	E_B [eV]	C_{at} [%]	E_B [eV]	C_{at} [%]	E_B [eV]	C_{at} [%]	E_B [eV]	C_{at} [%]
C1s	284.7	83.0	284.7	78.9	284.7	81.2	284.7	79.2	284.7	79.7	284.7	77.1
O1s	532.2	8.0	531.5	15.0	532.2	7.0	530.7	15.3	532.2	10.6	531.5	17.2
N1s	402.5	4.0	402.5	4.1	402.5	5.6	401.7	4.3	402.5	4.7	399.5	4.0
Cl2p	197.0	5.0	-	-	197.0	6.2	-	-	197.0	4.2	-	-
Si2p	-	-	154.2	1.9	-	-	152.7	1.0	101.7	0.8	152.7	1.6
La3d	-	-	833.7	0.1	-	-	851.0	0.2	-	-	836.7	0.1
Level	**SBA-4200**		**SBA-4200 + La(III)-GLDA**		**SBA-4400**		**SBA-4400 + La(III)-GLDA**		**SBA-4600**		**SBA-4600 + La(III)-GLDA**	
	E_B [eV]	C_{at} [%]	E_B [eV]	C_{at} [%]	E_B [eV]	C_{at} [%]	E_B [eV]	C_{at} [%]	E_B [eV]	C_{at} [%]	E_B [eV]	C_{at} [%]
C1s	284.7	70.2	284.7	55.5	284.7	62.5	284.7	56.8	284.7	65.9	284.7	51.7
O1s	531.5	16.2	531.5	29.1	532.2	22.3	531.5	28.3	532.2	20.8	531.5	30.9
N1s	402.5	3.5	402.5	2.8	402.5	2.8	399.5	2.4	402.5	2.5	399.5	2.0
Cl2p	197.0	3.4	-	-	197.0	2.7	-	-	197.7	1.9	-	-
Si2p	101.7	5.0	153.5	8.6	103.0	6.1	153.5	9.0	102.5	6.1	153.5	11.2
Al2p	74.0	1.7	74.0	3.9	74.7	3.6	74.0	3.4	74.0	2.8	74.0	4.1
La3d	-	-	835.2	0.1	-	-	836.0	0.1	-	-	836.0	0.1
Level	**SBA-IRA 958**		**SBA-IRA 958 + La(III)-GLDA**		**SBA-IRA 458**		**SBA-IRA 458 + La(III)-GLDA**		**WBA-IRA 67**		**WBA-IRA 67 + La(III)-GLDA**	
	E_B [eV]	C_{at} [%]	E_B [eV]	C_{at} [%]	E_B [eV]	C_{at} [%]	E_B [eV]	C_{at} [%]	E_B [eV]	C_{at} [%]	E_B [eV]	C_{at} [%]
C1s	284.7	73.6	284.7	72.7	284.7	76.9	284.7	72.7	284.7	57.2	284.7	44.1
O1s	531.5	14.9	530.7	17.8	531.5	13.4	531.5	18.3	531.5	26.4	531.5	34.8
N1s	398.7	6.3	399.5	8.0	398.7	6.4	399.5	6.3	399.5	3.9	399.5	3.0
Cl2p	196.2	4.0	-	-	196.2	2.6	-	-	-	-		
Si2p	101.0	1.2	152.7	1.3	101.0	0.7	152.7	2.6	101.7	9.2	153.5	12.4
Al2p	-	-	-	-	-	-	-	-	74.0	2.6	74.0	4.6
Ca2p	-	-	-	-	-	-	-	-	350.7	0.7	350.7	1.0
La3d	-	-	834.5	0.2	-	-	833.7	0.1	-	-	834.5	0.1

3. Kinetic and adsorption studies

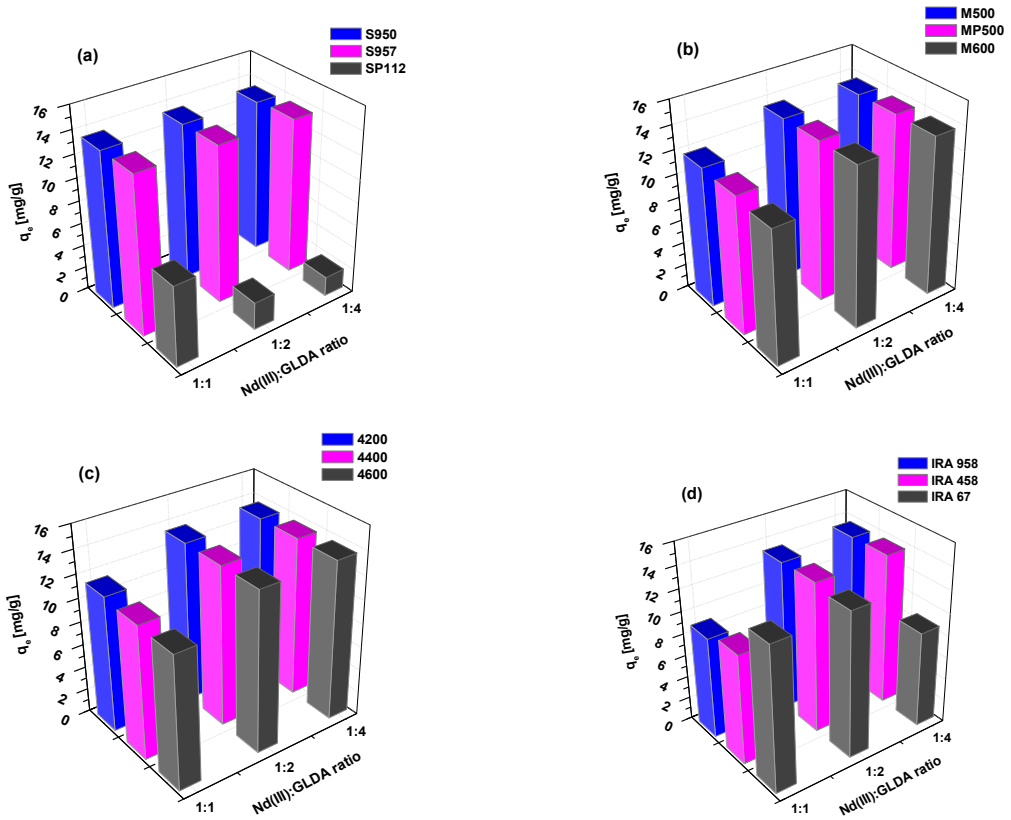

Fig. S3. Effect of the Ln(III):GLDA molar ratio on the Nd(III)-GLDA complexes adsorption on SAC ion exchangers (a) S950, S957, SP112, on SBA and WBA ion exchangers (b) M500, MP500, M600, (c) 4200, 4400, 4600 and (d) IRA 958, IRA 458, IRA 67.

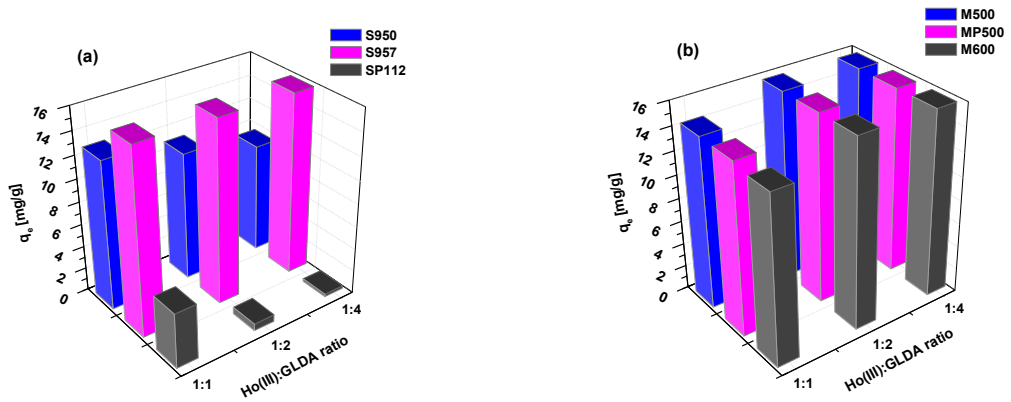

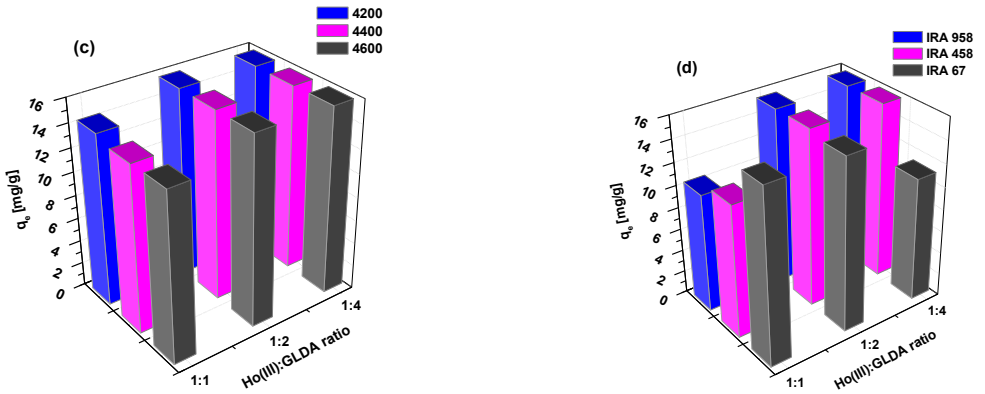

Fig. S4. Effect of the Ln(III):GLDA molar ratio on the Ho(III)-GLDA complexes adsorption on SAC ion exchangers (a) S950, S957, SP112, on SBA and WBA ion exchangers (b) M500, MP500, M600, (c) 4200, 4400, 4600 and (d) IRA 958, IRA 458, IRA 67.

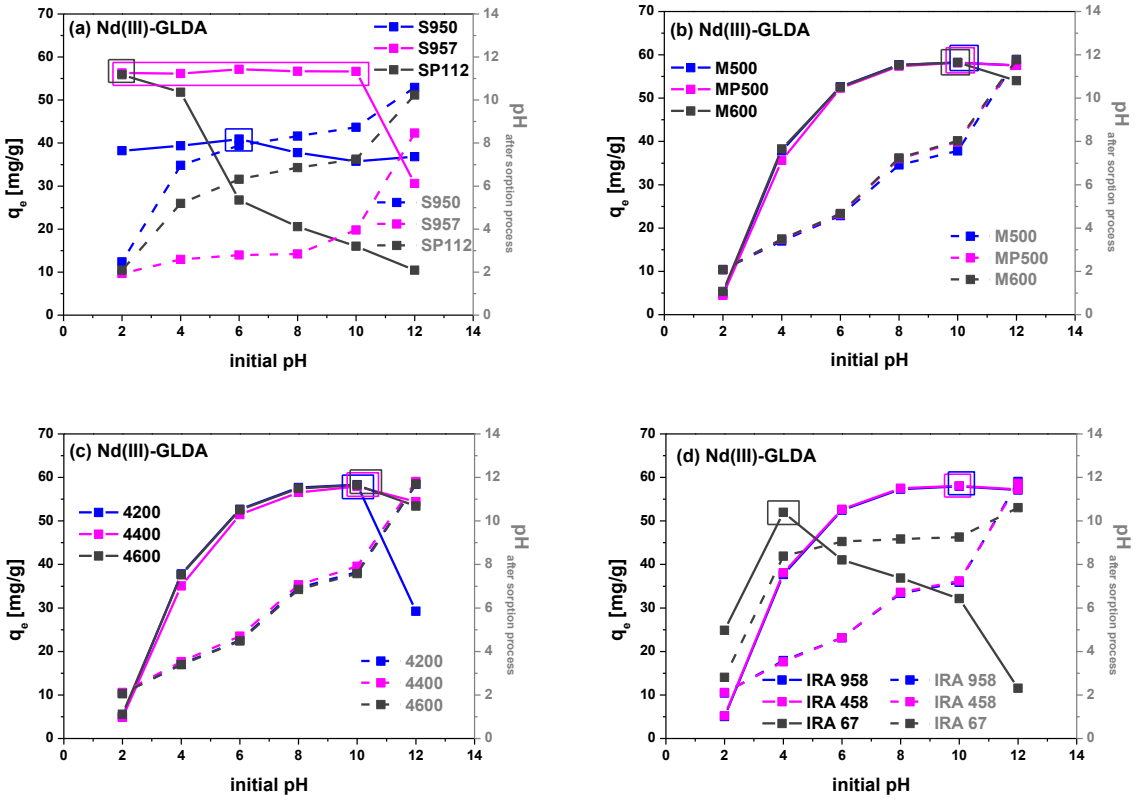

Fig. S5. Effect of the initial solution pH on the Nd(III)-GDLA complexes adsorption on SAC ion exchangers (a) S950, S957, SP112, on SBA and WBA ion exchangers (b) M500, MP500, M600, (c) 4200, 4400, 4600 and (d) IRA 958, IRA 458, IRA 67, and changes of solution pH after the process.

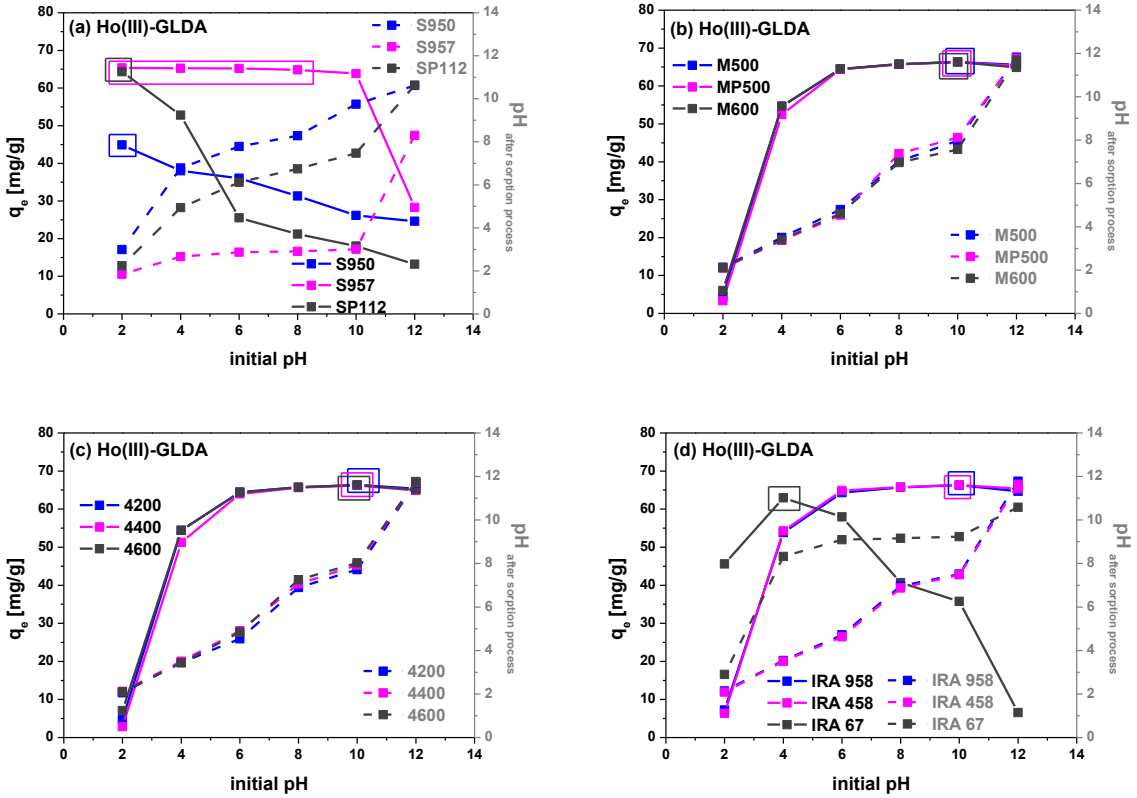

Fig. S6. Effect of the initial solution pH on the Ho(III)-GDLA complexes adsorption on SAC ion exchangers (a) S950, S957, SP112, on SBA and WBA ion exchangers (b) M500, MP500, M600, (c) 4200, 4400, 4600 and (d) IRA 958, IRA 458, IRA 67, and changes of solution pH after the process.

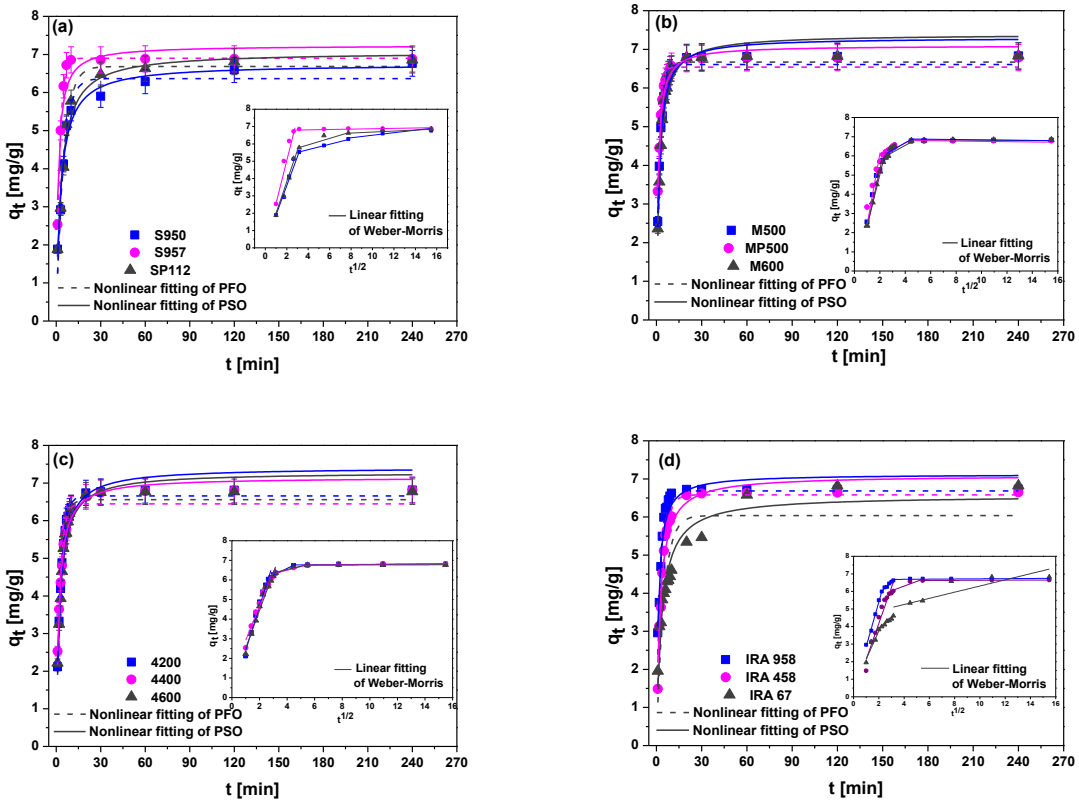

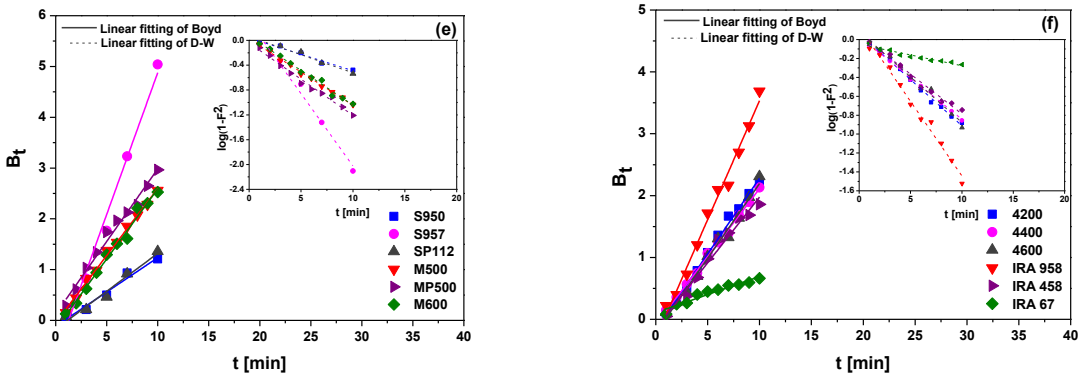

Fig. S7. (a-d) Influence of interaction time and fitting of the kinetic models: (a-d) pseudo-first order, pseudo-second order, Weber-Morris, (e-f) Boyd, and Dumwald-Wagner for the La(III)-GLDA complexes adsorption on SAC, SBA, and WBA ion exchangers (C_0=0.5×10^{-3} M).

Table S2. Kinetic parameters for the pseudo-first order and pseudo-second order kinetic models for the La(III)-GLDA complexes adsorption on SAC, SBA, and WBA ion exchangers (C_0=1.0×10^{-3} M and 1.5×10^{-3} M).

Model			**Pseudo-First Order**				**Pseudo-Second Order**			
Ion exchanger	C_o ×10^{-3} [M]	$q_{e.exp}$ [mg/g]	$q_{1.cal}$ [mg/g]	k_1 [1/min]	R^2	χ^2	$q_{2.cal}$ [mg/g]	k_2 [g/mg min]	R^2	χ^2
SAC-S950	1.0	13.86	13.22	0.185	0.962	0.512	14.06	0.019	0.984	0.216
	1.5	21.82	20.96	0.137	0.951	1.900	22.50	0.008	0.980	0.763
SAC-S957	1.0	14.25	14.06	0.706	0.975	0.111	14.56	0.088	0.898	0.450
	1.5	22.16	21.69	0.582	0.950	0.649	22.70	0.048	0.890	1.429
SAC-SP112	1.0	14.22	13.93	0.229	0.989	0.155	14.72	0.024	0.987	0.176
	1.5	21.14	20.73	0.217	0.985	0.455	21.88	0.016	0.984	0.486
SBA-M500	1.0	13.79	13.76	0.347	0.999	0.010	14.76	0.038	0.933	0.569
	1.5	19.75	19.42	0.389	0.991	0.133	20.82	0.031	0.959	0.582
SBA-MP500	1.0	13.73	13.46	0.496	0.980	0.101	14.38	0.060	0.952	0.243
	1.5	19.50	18.88	0.471	0.978	0.231	20.23	0.040	0.962	0.391
SBA-M600	1.0	13.79	13.66	0.375	0.991	0.066	14.62	0.043	0.947	0.380
	1.5	19.90	19.44	0.392	0.975	0.332	20.84	0.032	0.975	0.334
SBA-4200	1.0	13.78	13.70	0.291	0.993	0.064	14.71	0.031	0.947	0.505
	1.5	19.70	19.36	0.300	0.991	0.159	20.83	0.023	0.967	0.589
SBA-4400	1.0	13.76	13.49	0.323	0.989	0.092	14.51	0.036	0.966	0.274
	1.5	19.54	18.76	0.317	0.993	0.108	20.19	0.025	0.960	0.585
SBA-4600	1.0	13.73	13.52	0.325	0.975	0.193	14.50	0.037	0.958	0.327
	1.5	19.72	19.26	0.300	0.981	0.321	20.70	0.023	0.978	0.373
SBA-IRA 958	1.0	13.40	13.37	0.393	0.990	0.066	14.30	0.047	0.926	0.502
	1.5	19.72	19.45	0.474	0.923	0.786	20.66	0.042	0.922	0.800
SBA-IRA 458	1.0	13.30	13.24	0.308	0.986	0.124	14.23	0.034	0.929	0.619
	1.5	19.60	19.28	0.317	0.972	0.443	20.66	0.025	0.962	0.609

WBA-IRA 67	1.0	13.76	11.10	0.181	0.743	2.035	12.25	0.020	0.896	0.820
	1.5	19.64	14.93	0.189	0.709	4.313	16.59	0.015	0.863	2.037

Table S3. Kinetic parameters for the Weber-Morris kinetic model for the La(III)-GLDA complexes adsorption on SAC, SBA, and WBA ion exchangers (C_0=1.0×10^{-3} M and 1.5×10^{-3} M).

Model	**Weber-Morris Intraparticle Diffusion**									
Ion exchanger	C_o ×10^{-3} [M]	k_{i1} [mg/g min$^{1/2}$]	C_1	R^2	k_{i2} [mg/g min$^{1/2}$]	C_2	R^2	k_{i3} [mg/g min$^{1/2}$]	C_3	R^2
SAC-S950	1.0	13.86	0.07	0.989	0.53	9.21	0.981	0.08	12.68	0.962
	1.5	4.33	0.88	0.988	1.28	11.48	0.927	0.12	20.13	0.821
SAC-S957	1.0	2.81	5.86	0.936	0.02	14.05	0.676	-	-	-
	1.5	5.88	5.97	0.996	0.04	21.68	0.798	-	-	-
SAC-SP112	1.0	3.57	0.60	0.959	0.61	9.57	0.853	0.03	13.81	0.669
	1.5	5.35	0.72	0.982	0.88	14.48	0.902	0.03	20.60	0.668
SBA-M500	1.0	4.49	0.61	0.954	0.30	12.36	0.975	0.01	13.70	0.685
	1.5	5.66	2.84	0.944	0.41	17.49	0.961	0.01	19.62	0.845
SBA-MP500	1.0	5.16	1.04	0.982	0.62	11.06	0.825	0.01	13.63	0.631
	1.5	6.79	1.96	0.975	1.11	14.54	0.874	0.02	19.20	0.635
SBA-M600	1.0	4.11	1.63	0.960	0.45	11.71	1.000	0.01	13.71	0.770
	1.5	5.35	3.52	0.953	0.92	15.62	0.993	0.01	19.76	0.594
SBA-4200	1.0	4.23	0.39	0.966	0.38	11.71	0.915	0.01	13.66	0.728
	1.5	5.64	1.40	0.958	0.63	16.17	0.945	0.02	19.45	0.612
SBA-4400	1.0	3.83	1.44	0.944	0.39	11.54	0.938	0.01	13.58	0.757
	1.5	4.80	3.08	0.957	0.79	14.87	0.952	0.04	18.95	0.765
SBA-4600	1.0	3.79	1.62	0.957	0.36	11.80	0.878	0.01	13.64	0.786
	1.5	5.21	2.27	0.961	0.81	15.35	0.868	0.01	19.51	0.760
SBA-IRA 958	1.0	4.76	0.52	0.975	0.56	10.73	0.950	0.01	13.25	0.262
	1.5	5.63	4.16	0.974	0.74	17.53	0.901	0.03	19.40	0.462
SBA-IRA 458	1.0	4.09	0.54	0.931	0.28	11.49	0.918	0.00	13.25	0.536
	1.5	5.36	2.30	0.969	0.34	17.95	0.999	0.01	19.48	0.772
WBA-IRA 67	1.0	2.60	1.05	0.923	0.61	5.94	0.948	0.48	6.91	0.936
	1.5	3.65	1.24	0.963	1.61	6.02	0.986	0.72	8.77	0.989

Table S4. Kinetic parameters for the Boyd and Dumwald-Wagner kinetic models for the La(III)-GLDA complexes adsorption on SAC, SBA, and WBA ion exchangers (C_0=1.0×10^{-3} M and 1.5×10^{-3} M).

Model	**Boyd**			**Dumwald-Wagner**		
Ion exchanger	C_o ×10^{-3} [M]	*slope*	R^2	k [1/min]	*intercept*	R^2
SAC-S950	1.0	0.111	0.981	0.100	-0.034	0.983
	1.5	0.036	0.974	0.034	0.085	0.979

SAC-S957	1.0	0.377	0.995	0.359	-0.040	0.991
	1.5	0.355	0.975	0.336	-0.041	0.974
SAC-SP112	1.0	0.112	0.987	0.101	-0.021	0.986
	1.5	0.119	0.995	0.092	-0.013	0.995
SBA-M500	1.0	0.324	0.992	0.303	-0.147	0.990
	1.5	0.274	0.995	0.255	-0.054	0.996
SBA-MP500	1.0	0.294	0.980	0.275	0.012	0.983
	1.5	0.238	0.984	0.220	0.036	0.987
SBA-M600	1.0	0.292	0.985	0.271	-0.075	0.986
	1.5	0.236	0.984	0.217	-0.018	0.986
SBA-4200	1.0	0.252	0.988	0.232	-0.108	0.987
	1.5	0.217	0.998	0.199	-0.060	0.998
SBA-4400	1.0	0.221	0.994	0.203	-0.045	0.995
	1.5	0.172	0.994	0.157	-0.021	0.995
SBA-4600	1.0	0.245	0.985	0.226	-0.076	0.984
	1.5	0.191	0.994	0.174	-0.028	0.995
SBA-IRA 958	1.0	0.364	0.982	0.342	-0.146	0.981
	1.5	0.379	0.963	0.358	-0.116	0.960
SBA-IRA 458	1.0	0.255	0.962	0.235	-0.081	0.965
	1.5	0.213	0.987	0.194	-0.039	0.988
WBA-IRA 67	1.0	0.039	0.893	0.036	0.035	0.886
	1.5	0.039	0.919	0.036	0.026	0.915

Table S5. Kinetic parameters for the pseudo-first order and pseudo-second order kinetic models for the Nd(III)-GLDA complexes adsorption on SAC, SBA, and WBA ion exchangers (C_0=0.5×10^{-3} M-1.5×10^{-3} M).

Model			**Pseudo-First Order**				**Pseudo-Second Order**			
Ion exchanger	C_o ×10^{-3} [M]	$q_{e.exp}$ [mg/g]	$q_{1.cal}$ [mg/g]	k_1 [1/min]	R^2	χ^2	$q_{2.cal}$ [mg/g]	k_2 [g/mg min]	R^2	χ^2
SAC-S950	0.5	7.25	6.01	0.068	0.680	0.904	6.73	0.013	0.803	0.555
	1.0	14.25	11.48	0.096	0.626	3.613	12.77	0.009	0.782	2.105
	1.5	20.95	16.59	0.120	0.586	7.810	18.33	0.009	0.768	4.377
SAC-S957	0.5	7.37	7.33	0.405	0.996	0.007	7.84	0.088	0.937	0.126
	1.0	14.56	14.47	0.400	0.985	0.114	15.47	0.044	0.937	0.477
	1.5	21.49	21.35	0.402	0.987	0.216	22.82	0.030	0.938	1.004
SAC-SP112	0.5	7.37	7.25	0.456	0.978	0.035	7.74	0.102	0.958	0.067
	1.0	14.57	14.28	0.471	0.962	0.219	15.24	0.054	0.961	0.224
	1.5	21.49	21.11	0.448	0.962	0.496	22.52	0.035	0.956	0.572
SBA-M500	0.5	6.52	6.47	0.392	0.991	0.016	6.95	0.093	0.929	0.121
	1.0	13.42	13.28	0.343	0.997	0.026	14.26	0.039	0.952	0.375

	1.5	20.23	20.04	0.344	0.995	0.081	21.50	0.026	0.954	0.782
SBA-MP500	0.5	6.63	6.50	0.594	0.960	0.035	6.90	0.158	0.960	0.036
	1.0	13.47	13.13	0.564	0.968	0.126	14.00	0.072	0.965	0.140
	1.5	20.28	19.60	0.563	0.984	0.137	20.90	0.048	0.918	0.691
SBA-M600	0.5	6.58	6.50	0.429	0.990	0.015	6.95	0.105	0.939	0.089
	1.0	13.49	13.31	0.354	0.988	0.086	14.26	0.041	0.963	0.261
	1.5	20.34	19.91	0.380	0.975	0.357	21.33	0.030	0.973	0.382
SBA-4200	0.5	6.84	6.77	0.307	0.987	0.027	7.27	0.069	0.962	0.080
	1.0	13.78	13.61	0.271	0.994	0.058	14.65	0.029	0.966	0.335
	1.5	20.56	20.28	0.244	0.991	0.202	21.83	0.017	0.976	0.541
SBA-4400	0.5	6.84	6.77	0.321	0.994	0.013	7.27	0.071	0.958	0.088
	1.0	13.69	13.45	0.277	0.994	0.053	14.50	0.030	0.972	0.266
	1.5	20.46	19.93	0.251	0.989	0.237	21.50	0.018	0.982	0.377
SBA-4600	0.5	6.81	6.73	0.329	0.996	0.009	7.23	0.074	0.952	0.099
	1.0	13.73	13.58	0.280	0.989	0.104	14.58	0.030	0.962	0.350
	1.5	20.55	20.21	0.249	0.979	0.442	21.71	0.018	0.972	0.605
SBA-IRA 958	0.5	6.51	6.48	0.472	0.994	0.008	6.91	0.119	0.911	0.121
	1.0	13.19	13.12	0.446	0.991	0.050	13.99	0.056	0.926	0.415
	1.5	20.24	20.01	0.489	0.988	0.139	21.31	0.041	0.939	0.691
SBA-IRA 458	0.5	6.80	6.68	0.325	0.994	0.013	7.18	0.073	0.948	0.108
	1.0	13.51	13.38	0.336	0.994	0.047	14.36	0.038	0.947	0.425
	1.5	20.67	20.40	0.335	0.989	0.185	21.88	0.025	0.963	0.651
WBA-IRA 67	0.5	7.29	6.12	0.229	0.645	0.719	6.71	0.049	0.856	0.292
	1.0	13.90	10.67	0.229	0.576	2.883	11.82	0.026	0.790	1.424
	1.5	19.70	14.41	0.288	0.551	5.060	15.99	0.025	0.769	2.602

Table S6. Kinetic parameters for the Weber-Morris kinetic model for the Nd(III)-GLDA complexes adsorption on SAC, SBA, and WBA ion exchangers (C_0=0.5×10^{-3} M-1.5×10^{-3} M).

Model	**Weber-Morris Intraparticle Diffusion**									
Ion exchanger	C_o ×10^{-3} [M]	k_{i1} [mg/g min$^{1/2}$]	C_1	R^2	k_{i2} [mg/g min$^{1/2}$]	C_2	R^2	k_{i3} [mg/g min$^{1/2}$]	C_3	R^2
SAC-S950	0.5	0.34	1.60	0.971	0.38	1.83	0.942	-	-	-
	1.0	0.84	3.37	0.995	0.70	4.35	0.949	-	-	-
	1.5	1.43	5.26	0.967	0.92	7.79	0.942	-	-	-
SAC-S957	0.5	2.36	0.75	0.949	0.02	7.14	0.361	-	-	-
	1.0	4.25	2.16	0.947	0.03	14.26	0.349	-	-	-
	1.5	5.83	4.01	0.936	0.02	21.21	0.251	-	-	-
SAC-SP112	0.5	2.70	0.53	0.986	0.89	4.40	0.959	0.01	7.26	0.252
	1.0	4.24	2.82	0.971	0.94	11.08	0.886	0.02	14.29	0.251
	1.5	6.17	4.07	0.986	1.66	15.59	0.939	0.03	21.11	0.263

SBA-M500	0.5	2.35	0.13	0.934	0.78	3.92	0.994	0.01	6.43	0.450
	1.0	4.42	0.46	0.956	0.62	10.59	0.873	0.01	13.32	0.789
	1.5	6.17	1.61	0.959	0.52	17.54	0.892	0.02	20.18	0.819
SBA-MP500	0.5	2.29	1.18	0.987	0.35	5.28	0.682	0.01	6.60	0.995
	1.0	4.50	2.32	0.968	0.59	10.94	0.793	0.01	13.38	0.679
	1.5	5.74	5.04	0.977	1.06	15.71	0.746	0.02	20.05	0.583
SBA-M600	0.5	2.21	0.59	0.953	0.18	5.75	0.831	0.01	6.51	0.994
	1.0	3.88	1.61	0.961	0.51	11.15	0.887	0.01	13.43	0.698
	1.5	5.44	3.52	0.960	0.86	16.37	0.948	0.02	20.21	0.597
SBA-4200	0.5	2.19	0.18	0.984	0.42	4.98	0.974	0.01	6.84	0.626
	1.0	4.10	0.30	0.961	0.60	10.60	0.856	0.01	13.69	0.628
	1.5	5.91	0.33	0.982	1.02	15.06	0.886	0.02	20.35	0.757
SBA-4400	0.5	2.26	0.11	0.968	0.35	5.23	0.918	0.01	6.79	0.574
	1.0	3.99	0.50	0.958	0.56	10.60	0.891	0.02	13.47	0.674
	1.5	5.78	0.51	0.972	0.91	15.08	0.942	0.05	19.78	0.646
SBA-4600	0.5	1.99	0.58	0.950	0.14	6.04	0.819	0.01	6.72	0.925
	1.0	3.99	0.69	0.975	0.44	11.35	0.863	0.01	13.62	0.800
	1.5	5.73	0.85	0.988	0.86	15.77	0.943	0.02	20.28	0.670
SBA-IRA 958	0.5	2.65	0.06	0.957	0.64	4.50	0.822	0.01	6.42	0.769
	1.0	4.44	1.38	0.969	1.08	9.65	0.943	0.01	13.06	0.810
	1.5	6.31	3.41	0.965	1.43	15.48	0.983	0.02	19.97	0.843
SBA-IRA 458	0.5	2.03	0.44	0.954	0.12	6.05	0.999	0.01	6.62	0.976
	1.0	3.99	1.19	0.954	0.16	12.56	0.880	0.01	13.35	0.976
	1.5	5.77	2.47	0.961	0.52	17.91	0.829	0.01	20.55	0.999
WBA-IRA 67	0.5	1.62	0.80	0.928	0.44	3.23	0.984	0.23	4.26	0.814
	1.0	2.28	2.17	0.894	0.60	6.15	0.776	0.51	6.55	0.950
	1.5	3.24	3.35	0.949	0.61	9.74	0.975	0.69	9.20	0.989

Table S7. Kinetic parameters for the Boyd and Dumwald-Wagner kinetic models for the Nd(III)-GLDA complexes adsorption on SAC, SBA, and WBA ion exchangers (C_0=0.5×10^{-3} M-1.5×10^{-3} M).

Model		**Boyd**		**Dumwald-Wagner**		
Ion exchanger	C_o ×10^{-3} [M]	*slope*	R^2	*k* [1/min]	*intercept*	R^2
SAC-S950	0.5	0.008	0.989	0.008	0.030	0.989
	1.0	0.013	0.995	0.012	0.037	0.995
	1.5	0.016	0.954	0.014	0.044	0.951
SAC-S957	0.5	0.367	0.988	0.346	-0.155	0.985
	1.0	0.355	0.987	0.333	-0.144	0.984
	1.5	0.342	0.993	0.321	-0.121	0.992
SAC-SP112	0.5	0.316	0.988	0.297	-0.060	0.986

	1.0	0.297	0.989	0.278	-0.025	0.990
	1.5	0.311	0.993	0.291	-0.064	0.992
SBA-M500	0.5	0.338	0.984	0.318	-0.130	0.981
	1.0	0.266	0.996	0.246	-0.078	0.996
	1.5	0.270	0.998	0.249	-0.082	0.998
SBA-MP500	0.5	0.362	0.995	0.344	-0.029	0.995
	1.0	0.296	0.988	0.279	0.031	0.990
	1.5	0.273	0.998	0.256	0.030	0.998
SBA-M600	0.5	0.331	0.994	0.311	-0.089	0.994
	1.0	0.272	0.990	0.252	-0.086	0.988
	1.5	0.250	0.997	0.231	-0.042	0.997
SBA-4200	0.5	0.234	0.984	0.214	-0.070	0.984
	1.0	0.204	0.994	0.186	-0.065	0.995
	1.5	0.178	0.997	0.161	-0.060	0.997
SBA-4400	0.5	0.250	0.992	0.231	-0.081	0.991
	1.0	0.196	0.996	0.179	-0.052	0.997
	1.5	0.168	0.997	0.153	-0.045	0.997
SBA-4600	0.5	0.262	0.995	0.242	-0.088	0.995
	1.0	0.221	0.994	0.202	-0.084	0.994
	1.5	0.185	0.988	0.168	-0.069	0.987
SBA-IRA 958	0.5	0.438	0.985	0.417	-0.156	0.984
	1.0	0.424	0.980	0.403	-0.186	0.976
	1.5	0.408	0.996	0.388	-0.143	0.993
SBA-IRA 458	0.5	0.267	0.994	0.246	-0.105	0.993
	1.0	0.297	0.981	0.276	-0.134	0.977
	1.5	0.255	0.997	0.235	-0.077	0.996
WBA-IRA 67	0.5	0.045	0.872	0.041	0.067	0.865
	1.0	0.036	0.853	0.033	0.055	0.846
	1.5	0.039	0.873	0.035	0.059	0.868

Table S8. Kinetic parameters for the pseudo-first order and pseudo-second order kinetic models for the Ho(III)-GLDA complexes adsorption on SAC, SBA, and WBA ion exchangers (C_0=0.5×10^{-3} M-1.5×10^{-3} M).

Model			**Pseudo-First Order**				**Pseudo-Second Order**			
Ion exchanger	C_o ×10^{-3} [M]	$q_{e.exp}$ [mg/g]	$q_{1.cal}$ [mg/g]	k_1 [1/min]	R^2	χ^2	$q_{2.cal}$ [mg/g]	k_2 [g/mg min]	R^2	χ^2
SAC-S950	0.5	7.65	6.32	0.276	0.761	0.443	6.90	0.060	0.930	0.130
	1.0	15.77	12.94	0.242	0.739	2.164	14.11	0.025	0.913	0.718
	1.5	23.35	19.04	0.189	0.768	4.960	20.89	0.013	0.917	1.782
SAC-S957	0.5	7.86	7.86	0.406	0.999	0.003	8.42	0.081	0.917	0.200

	1.0	16.38	16.32	0.414	0.995	0.051	17.44	0.041	0.931	0.658
	1.5	24.53	24.42	0.394	0.996	0.095	26.14	0.025	0.933	1.534
SAC-SP112	0.5	7.87	7.87	0.304	0.995	0.016	8.47	0.057	0.931	0.226
	1.0	16.39	16.36	0.314	0.995	0.070	17.58	0.029	0.936	0.843
	1.5	24.54	24.47	0.308	0.994	0.173	26.24	0.019	0.948	1.473
SBA-M500	0.5	8.02	7.88	0.587	0.958	0.065	8.40	0.123	0.914	0.133
	1.0	15.88	15.65	0.488	0.977	0.156	16.69	0.052	0.953	0.320
	1.5	24.94	24.39	0.554	0.965	0.486	25.98	0.038	0.948	0.718
SBA-MP500	0.5	8.02	7.97	0.549	0.992	0.013	8.46	0.118	0.927	0.115
	1.0	15.88	15.77	0.538	0.994	0.041	16.78	0.058	0.925	0.485
	1.5	24.95	24.61	0.602	0.958	0.515	26.08	0.043	0.946	0.671
SBA-M600	0.5	8.02	7.87	0.493	0.965	0.065	8.42	0.101	0.939	0.112
	1.0	15.88	15.67	0.444	0.970	0.228	16.73	0.046	0.949	0.387
	1.5	24.95	24.52	0.425	0.955	0.823	26.14	0.029	0.937	1.151
SBA-4200	0.5	8.02	7.93	0.375	0.988	0.029	8.49	0.074	0.958	0.099
	1.0	15.88	15.69	0.367	0.983	0.156	16.80	0.037	0.962	0.361
	1.5	24.95	24.54	0.396	0.975	0.520	26.25	0.026	0.966	0.701
SBA-4400	0.5	8.02	7.98	0.336	0.995	0.015	8.57	0.064	0.941	0.171
	1.0	15.88	15.89	0.312	0.996	0.050	17.05	0.030	0.936	0.784
	1.5	24.94	24.77	0.336	0.990	0.258	26.53	0.021	0.953	1.222
SBA-4600	0.5	8.02	8.03	0.318	0.998	0.008	8.64	0.059	0.928	0.236
	1.0	15.88	15.89	0.310	0.999	0.016	17.08	0.029	0.935	0.828
	1.5	24.95	24.82	0.331	0.994	0.174	26.61	0.020	0.946	1.460
SBA-IRA 958	0.5	7.91	7.90	0.433	0.998	0.005	8.44	0.088	0.919	0.178
	1.0	16.03	15.97	0.416	0.997	0.030	17.07	0.042	0.931	0.627
	1.5	24.79	24.65	0.473	0.970	0.519	26.21	0.033	0.925	1.314
SBA-IRA 458	0.5	7.91	7.80	0.362	0.992	0.020	8.38	0.071	0.958	0.106
	1.0	16.03	15.78	0.364	0.983	0.162	16.92	0.036	0.963	0.359
	1.5	24.79	24.26	0.415	0.971	0.557	25.99	0.027	0.970	0.579
WBA-IRA 67	0.5	7.56	6.90	0.203	0.883	0.322	7.51	0.039	0.980	0.055
	1.0	16.37	13.50	0.223	0.719	2.869	14.85	0.021	0.893	1.090
	1.5	23.57	18.04	0.237	0.652	6.657	19.98	0.016	0.837	3.125

Table S9. Kinetic parameters for the Weber-Morris kinetic model for the Ho(III)-GLDA complexes adsorption on SAC, SBA, and WBA ion exchangers (C_0=0.5×10^{-3} M-1.5×10^{-3} M).

Model	**Weber-Morris Intraparticle Diffusion**									
Ion exchanger	C_o ×10^{-3} [M]	k_{i1} [mg/g min$^{1/2}$]	C_1	R^2	k_{i2} [mg/g min$^{1/2}$]	C_2	R^2	k_{i3} [mg/g min$^{1/2}$]	C_3	R^2
SAC-S950	0.5	1.72	0.86	0.975	0.23	4.50	0.943	-	-	-
	1.0	3.07	2.15	0.992	0.51	8.67	0.945	-	-	-

	1.5	4.18	2.51	0.988	0.81	11.77	0.959	-	-	-
SAC-S957	0.5	2.93	0.11	0.957	0.64	5.73	0.918	0.01	7.77	0.313
	1.0	5.72	1.03	0.979	1.21	12.23	0.922	0.01	16.23	0.311
	1.5	8.09	1.90	0.956	2.63	15.58	0.790	0.02	24.26	0.307
SAC-SP112	0.5	2.52	0.09	0.939	0.02	7.66	0.273	-	-	-
	1.0	5.08	0.70	0.948	0.04	15.94	0.302	-	-	-
	1.5	7.39	1.44	0.970	0.06	23.84	0.276	-	-	-
SBA-M500	0.5	2.28	2.02	0.823	0.56	6.11	0.956	0.01	7.94	0.255
	1.0	4.37	3.61	0.939	0.37	14.26	0.794	0.01	15.88	0.870
	1.5	5.70	8.30	0.921	0.31	23.37	0.865	0.02	24.94	0.655
SBA-MP500	0.5	3.28	0.52	0.987	0.38	6.61	0.590	0.01	8.01	0.373
	1.0	6.12	1.38	0.967	0.53	13.76	0.626	0.01	15.88	0.473
	1.5	7.94	5.54	0.984	0.87	21.54	0.603	0.02	24.94	0.944
SBA-M600	0.5	2.41	1.46	0.882	0.27	6.84	0.787	0.01	8.02	0.861
	1.0	4.21	3.51	0.938	0.35	14.34	0.735	0.01	15.87	0.354
	1.5	6.35	5.77	0.981	0.56	22.46	0.812	0.01	24.93	0.450
SBA-4200	0.5	2.46	0.84	0.971	0.30	6.70	0.930	0.00	8.02	0.890
	1.0	4.29	2.57	0.961	0.27	14.48	0.828	0.01	15.87	0.493
	1.5	6.36	5.23	0.955	0.46	22.58	0.834	0.01	24.94	0.577
SBA-4400	0.5	2.73	0.09	0.958	0.34	6.51	0.912	0.00	8.01	0.672
	1.0	4.94	0.67	0.962	0.23	14.70	0.855	0.01	15.88	0.580
	1.5	7.18	2.68	0.970	0.42	22.76	0.899	0.01	24.94	0.836
SBA-4600	0.5	2.58	0.17	0.944	0.12	7.40	0.827	0.01	8.01	0.527
	1.0	5.04	0.39	0.952	0.25	14.60	0.833	0.01	15.87	0.498
	1.5	7.32	2.28	0.956	0.52	22.27	0.849	0.02	24.94	0.535
SBA-IRA 958	0.5	3.05	0.13	0.974	0.61	5.88	0.891	0.01	7.84	0.383
	1.0	5.60	1.01	0.973	1.40	11.38	0.926	0.01	15.94	0.341
	1.5	7.89	3.89	0.983	1.55	19.60	0.999	0.01	24.64	0.284
SBA-IRA 458	0.5	2.18	1.12	0.923	0.19	6.92	0.830	0.00	7.90	0.789
	1.0	4.26	2.64	0.938	0.43	13.79	0.837	0.01	16.02	0.570
	1.5	6.11	5.75	0.938	0.51	22.12	0.854	0.01	24.78	0.537
WBA-IRA 67	0.5	1.89	0.23	0.957	0.50	3.69	0.985	0.02	7.32	0.999
	1.0	3.19	1.93	0.948	0.99	7.29	0.978	0.52	9.28	0.907
	1.5	4.45	2.55	0.957	0.47	12.40	0.866	0.83	11.38	0.978

Table S10. Kinetic parameters for the Boyd and Dumwald-Wagner kinetic models for the Ho(III)-GLDA complexes adsorption on SAC, SBA, and WBA ion exchangers (C_0=0.5×10^{-3} M-1.5×10^{-3} M).

Model		**Boyd**		**Dumwald-Wagner**		
Ion exchanger	C_o ×10^{-3} [M]	*slope*	R^2	*k* [1/min]	*intercept*	R^2

SAC-S950	0.5	0.065	0.946	0.059	0.052	0.943
	1.0	0.056	0.947	0.050	0.047	0.945
	1.5	0.046	0.971	0.042	0.031	0.968
SAC-S957	0.5	0.381	0.994	0.360	-0.147	0.994
	1.0	0.376	0.987	0.354	-0.145	0.985
	1.5	0.341	0.975	0.320	-0.120	0.973
SAC-SP112	0.5	0.275	0.990	0.254	-0.117	0.989
	1.0	0.282	0.991	0.261	-0.120	0.990
	1.5	0.276	0.990	0.255	-0.122	0.989
SBA-M500	0.5	0.338	0.979	0.321	0.019	0.981
	1.0	0.354	0.991	0.334	-0.082	0.990
	1.5	0.332	0.994	0.314	-0.028	0.993
SBA-MP500	0.5	0.503	0.985	0.483	-0.204	0.981
	1.0	0.446	0.991	0.426	-0.132	0.989
	1.5	0.447	0.993	0.428	-0.118	0.990
SBA-M600	0.5	0.329	0.987	0.310	-0.054	0.985
	1.0	0.349	0.972	0.329	-0.114	0.968
	1.5	0.344	0.967	0.323	-0.141	0.962
SBA-4200	0.5	0.298	0.995	0.278	-0.100	0.993
	1.0	0.294	0.989	0.274	-0.107	0.986
	1.5	0.284	0.998	0.264	-0.069	0.997
SBA-4400	0.5	0.286	0.989	0.265	-0.107	0.987
	1.0	0.306	0.980	0.284	-0.158	0.976
	1.5	0.298	0.987	0.277	-0.133	0.983
SBA-4600	0.5	0.316	0.986	0.294	-0.162	0.983
	1.0	0.296	0.985	0.275	-0.146	0.982
	1.5	0.281	0.990	0.260	-0.105	0.990
SBA-IRA 958	0.5	0.410	0.992	0.389	-0.161	0.991
	1.0	0.408	0.958	0.386	-0.196	0.951
	1.5	0.421	0.985	0.400	-0.150	0.984
SBA-IRA 458	0.5	0.257	0.995	0.238	-0.052	0.996
	1.0	0.250	0.986	0.231	-0.044	0.987
	1.5	0.276	0.984	0.255	-0.048	0.982
WBA-IRA 67	0.5	0.074	0.948	0.066	0.029	0.945
	1.0	0.051	0.917	0.046	0.046	0.913
	1.5	0.042	0.868	0.038	0.047	0.863

Table S11. Adsorption isotherm parameters for the Ln(III)-GLDA complexes adsorption on SAC, SBA, and WBA ion exchangers at the temperature of 293 K.

Model	**Langmuir**

Ion exchanger	REE	$q_{e.exp}$ [mg/g]	q_0 [mg/g]	K_L [L/mg]	R^2	χ^2
SAC-S950	La(III)	120.10	109.16	0.099	0.914	127.973
	Nd(III)	64.96	66.69	0.111	0.977	9.433
	Ho(III)	55.66	59.33	0.054	0.997	1.057
SAC-S957	La(III)	138.66	135.99	0.924	0.995	9.262
	Nd(III)	152.72	153.21	0.176	0.994	12.990
	Ho(III)	151.29	141.55	3.971	0.957	85.678
SAC-SP112	La(III)	155.49	154.40	1.724	0.998	3.927
	Nd(III)	150.23	151.73	0.163	0.992	17.309
	Ho(III)	132.77	129.06	0.542	0.991	12.991
SBA-M500	La(III)	73.18	72.09	0.273	0.991	3.670
	Nd(III)	59.37	61.51	0.236	0.999	0.556
	Ho(III)	86.56	83.09	0.915	0.992	6.080
SBA-MP500	La(III)	73.21	72.62	0.224	0.994	2.341
	Nd(III)	59.28	60.43	0.169	0.997	0.999
	Ho(III)	81.64	79.11	0.926	0.985	10.146
SBA-M600	La(III)	72.08	70.60	0.314	0.995	1.871
	Nd(III)	57.57	58.83	0.266	0.997	1.017
	Ho(III)	82.86	80.15	1.054	0.989	7.732
SBA-4200	La(III)	72.70	72.75	0.396	0.996	1.781
	Nd(III)	64.46	65.47	0.208	0.995	2.150
	Ho(III)	86.58	82.88	1.198	0.992	5.957
SBA-4400	La(III)	67.25	67.47	0.264	0.999	0.357
	Nd(III)	50.44	53.62	0.238	0.997	1.305
	Ho(III)	75.27	73.72	0.728	0.997	1.701
SBA-4600	La(III)	70.84	69.57	0.356	0.993	2.576
	Nd(III)	61.67	62.77	0.268	0.999	0.319
	Ho(III)	86.71	84.19	0.679	0.995	3.639
SBA-IRA 958	La(III)	72.09	70.55	0.279	0.995	1.894
	Nd(III)	61.61	65.55	0.107	0.992	3.106
	Ho(III)	86.15	83.31	0.876	0.991	6.384
SBA-IRA 458	La(III)	78.62	77.19	0.309	0.985	6.611
	Nd(III)	69.49	73.05	0.161	0.995	2.257
	Ho(III)	94.17	90.51	1.189	0.982	15.536
WBA-IRA 67	La(III)	52.83	45.77	0.069	0.805	39.905
	Nd(III)	41.10	34.69	0.125	0.836	19.703
	Ho(III)	61.28	47.49	0.195	0.762	62.090

	Freundlich				**Temkin**			
	K_F [mg/g]	n	R^2	χ^2	A [L/g]	B [J/mol]	R^2	χ^2

SAC-S950	La(III)	32.06	4.50	0.989	15.826	3.30	16.11	0.992	11.745
	Nd(III)	17.66	3.61	0.969	12.771	1.82	12.00	0.991	3.900
	Ho(III)	10.66	3.07	0.967	11.325	0.77	11.23	0.996	1.423
SAC-S957	La(III)	100.07	9.17	0.996	7.631	$5.40x10^4$	8.93	0.997	5.353
	Nd(III)	84.35	8.67	0.999	2.547	110.97	15.44	0.999	2.101
	Ho(III)	110.29	9.92	0.994	11.141	$25.86 x10^4$	8.79	0.996	7.795
SAC-SP112	La(III)	128.75	9.39	0.999	2.672	$12.16 x10^7$	6.86	0.999	2.530
	Nd(III)	82.35	8.59	0.999	2.124	94.18	15.44	0.999	1.834
	Ho(III)	88.59	9.84	0.993	10.229	$20.09 x10^3$	8.55	0.995	6.992
SBA-M500	La(III)	44.45	9.82	0.987	4.932	879.54	6.01	0.990	3.957
	Nd(III)	36.31	9.19	0.968	12.078	373.10	5.46	0.974	9.846
	Ho(III)	54.21	8.96	0.977	16.911	2512.88	6.67	0.982	12.890
SBA-MP500	La(III)	41.06	8.82	0.992	3.288	143.85	7.25	0.994	2.483
	Nd(III)	32.25	8.59	0.985	5.490	77.19	6.20	0.990	3.811
	Ho(III)	52.39	9.46	0.985	9.852	3647.91	6.15	0.990	6.571
SBA-M600	La(III)	43.88	9.45	0.993	2.677	782.40	6.07	0.995	1.983
	Nd(III)	36.37	9.20	0.974	9.281	980.39	4.80	0.978	7.632
	Ho(III)	54.10	9.04	0.979	14.738	6946.14	5.93	0.984	11.280
SBA-4200	La(III)	46.84	9.12	0.982	7.421	1598.96	5.94	0.985	6.056
	Nd(III)	34.23	7.93	0.978	9.254	53.57	7.18	0.985	6.318
	Ho(III)	55.65	9.53	0.978	16.144	5104.39	6.34	0.984	12.004
SBA-4400	La(III)	43.38	9.84	0.992	3.030	2151.80	5.23	0.994	2.342
	Nd(III)	31.25	9.09	0.984	6.939	181.79	5.30	0.987	5.946
	Ho(III)	50.71	9.72	0.985	8.816	$22.77 x10^3$	4.87	0.988	6.953
SBA-4600	La(III)	45.04	9.46	0.991	3.615	2153.78	5.50	0.992	3.028
	Nd(III)	36.76	9.81	0.973	10.704	316.96	5.71	0.979	8.451
	Ho(III)	53.37	8.56	0.969	22.457	1404.73	7.01	0.975	17.868
SBA-IRA 958	La(III)	43.26	9.32	0.992	3.198	639.82	6.13	0.994	2.546
	Nd(III)	30.85	7.38	0.959	16.357	18.52	7.73	0.967	13.314
	Ho(III)	54.39	9.08	0.972	20.090	2698.58	6.63	0.978	15.983
SBA-IRA 458	La(III)	44.08	8.44	0.982	8.227	141.01	7.97	0.984	7.003
	Nd(III)	33.45	6.49	0.960	19.468	13.79	9.48	0.971	14.278
	Ho(III)	58.37	8.72	0.961	33.198	1211.90	8.00	0.967	27.673
WBA-IRA 67	La(III)	12.14	4.11	0.980	4.105	2.78	6.77	0.929	14.619
	Nd(III)	12.56	5.24	0.993	0.860	5.25	4.94	0.971	3.534
	Ho(III)	4.95	17.33	0.982	4.626	8.06	6.68	0.941	15.349

Table S12. Adsorption isotherm parameters for the La(III)-GLDA complexes adsorption on SAC, SBA,

and WBA ion exchangers at the temperature of 313 K and 333 K.

Model				**Langmuir**					
Ion exchanger	T [K]	$q_{e.exp}$ [mg/g]	q_0 [mg/g]	K_L [L/mg]	R^2	χ^2			
SAC-S950	313	125.56	118.73	0.141	0.951	84.075			
	333	135.40	133.09	0.273	0.985	29.837			
SAC-S957	313	146.30	139.84	1.247	0.988	22.421			
	333	151.60	145.55	1.495	0.991	17.894			
SAC-SP112	313	155.84	153.68	2.483	0.998	4.427			
	333	156.22	153.66	2.967	0.998	5.264			
SBA-M500	313	75.49	72.67	0.454	0.983	6.852			
	333	77.36	74.97	0.463	0.989	4.680			
SBA-MP500	313	75.95	73.43	0.370	0.989	4.649			
	333	77.93	77.07	0.359	0.997	1.583			
SBA-M600	313	73.83	71.78	0.498	0.994	2.496			
	333	75.45	73.42	0.591	0.995	2.337			
SBA-4200	313	75.38	74.00	0.632	0.995	2.421			
	333	77.80	73.44	1.095	0.973	12.403			
SBA-4400	313	69.47	68.72	0.416	0.996	1.632			
	333	72.74	71.78	0.392	0.993	2.766			
SBA-4600	313	71.54	69.61	0.556	0.994	2.440			
	333	72.57	70.75	0.621	0.994	2.348			
SBA-IRA 958	313	70.69	69.42	0.329	0.994	2.478			
	333	69.23	68.37	0.321	0.993	2.515			
SBA-IRA 458	313	77.09	75.51	0.356	0.987	5.535			
	333	76.37	74.69	0.371	0.988	5.140			
WBA-IRA 67	313	42.91	53.01	0.006	0.978	3.490			
	333	39.38	52.57	0.005	0.985	2.011			
	Freundlich					**Temkin**			
	T [K]	K_F [mg/g]	n	R^2	χ^2	A [L/g]	B [J/mol]	R^2	χ^2
SAC-S950	313	37.56	4.60	0.964	62.628	3.67	18.05	0.991	15.652
	333	49.96	5.14	0.908	185.179	7.73	19.22	0.967	67.061
SAC-S957	313	104.52	9.76	0.993	12.910	10.77×10^4	8.83	0.995	9.869
	333	107.79	9.31	0.991	17.917	37.45×10^3	10.05	0.993	13.757
SAC-SP112	313	130.93	9.89	0.999	1.417	68.24×10^7	6.40	0.999	1.306
	333	132.03	9.30	0.999	1.381	11.68×10^8	6.29	0.999	1.268
SBA-M500	313	47.19	9.44	0.989	4.434	2331.11	5.74	0.991	3.558
	333	47.92	9.91	0.988	5.243	1413.47	6.19	0.992	3.625
SBA-	313	44.00	9.09	0.996	1.666	278.33	7.14	0.998	0.829

MP500	333	45.15	8.68	0.988	5.412	182.94	7.84	0.992	3.434
SBA-M600	313	47.08	9.18	0.992	3.344	2186.58	5.79	0.994	2.446
	333	48.46	9.99	0.990	4.348	2034.09	6.04	0.993	2.951
SBA-4200	313	49.22	9.11	0.986	6.381	2282.36	6.05	0.990	4.604
	333	50.73	9.91	0.993	3.207	3016.46	6.12	0.996	1.798
SBA-4400	313	45.83	9.15	0.992	2.935	4121.27	5.19	0.994	2.121
	333	45.45	9.51	0.991	3.873	941.69	6.17	0.993	2.793
SBA-4600	313	47.68	9.63	0.992	3.216	8606.35	5.04	0.994	2.517
	333	48.57	9.47	0.990	3.930	7788.84	5.19	0.993	2.933
SBA-IRA 958	313	45.11	9.80	0.988	4.763	2734.13	5.34	0.989	4.184
	333	45.19	9.47	0.987	5.018	4886.24	5.01	0.988	4.498
SBA-IRA 458	313	45.40	9.34	0.983	7.626	337.99	7.14	0.985	6.465
	333	45.91	9.84	0.982	7.783	540.62	6.74	0.985	6.690
WBA-IRA 67	313	2.00	2.01	0.983	2.662	0.07	11.10	0.980	3.157
	333	1.44	1.88	0.989	1.462	0.06	10.63	0.977	3.167

Table S13. Adsorption isotherm parameters for the Nd(III)-GLDA complexes adsorption on SAC, SBA, and WBA ion exchangers at the temperature of 313 K and 333 K.

Model				**Langmuir**		
Ion exchanger	T [K]	$q_{e.exp}$ [mg/g]	q_0 [mg/g]	K_L [L/mg]	R^2	χ^2
SAC-S950	313	66.94	65.83	0.220	0.961	17.427
	333	69.07	68.31	0.359	0.930	33.201
SAC-S957	313	156.55	154.84	0.388	0.990	24.763
	333	160.37	159.39	0.544	0.993	16.186
SAC-SP112	313	151.49	153.34	0.159	0.994	13.314
	333	152.17	154.82	0.163	0.993	15.708
SBA-M500	313	62.07	63.03	0.292	0.999	0.439
	333	64.26	63.92	0.343	0.997	1.155
SBA-MP500	313	61.92	61.34	0.260	0.990	4.051
	333	64.42	62.52	0.325	0.987	5.436
SBA-M600	313	59.33	60.49	0.322	0.994	2.123
	333	60.39	61.27	0.382	0.993	2.538
SBA-4200	313	65.64	65.17	0.332	0.991	3.905
	333	67.29	65.56	0.490	0.981	8.689
SBA-4400	313	51.81	54.72	0.355	0.996	1.799
	333	53.34	55.55	0.529	0.996	1.825
SBA-4600	313	63.24	63.43	0.485	0.997	1.062
	333	65.24	63.24	1.423	0.990	4.502
SBA-IRA	313	59.74	63.33	0.110	0.992	3.186

958	333	58.92		62.99	0.096		0.991		3.412
SBA-IRA 458	313	64.68		67.71	0.179		0.989		4.844
	333	62.76		66.28	0.155		0.974		10.762
WBA-IRA 67	313	37.57		67.96	0.003		0.997		0.319
	333	33.69		57.22	0.003		0.996		0.392
		Freundlich				**Temkin**			
	T [K]	K_F [mg/g]	n	R^2	χ^2	A [L/g]	B [J/mol]	R^2	χ^2
SAC-S950	313	22.91	4.24	0.967	14.751	6.05	10.27	0.981	8.345
	333	28.08	4.79	0.926	35.206	16.52	9.46	0.938	29.330
SAC-S957	313	95.55	9.60	0.998	4.656	485.67	14.29	0.998	3.581
	333	101.52	9.54	0.997	7.133	640.47	14.78	0.998	4.395
SAC-SP112	313	82.12	8.38	0.999	1.244	77.56	15.94	1.000	0.665
	333	81.90	8.10	0.998	3.938	62.66	16.58	0.999	3.082
SBA-M500	313	37.43	10.00	0.971	11.685	392.88	5.65	0.977	9.239
	333	37.79	9.62	0.977	9.661	332.10	5.90	0.983	7.105
SBA-MP500	313	34.28	8.83	0.989	4.421	140.17	6.09	0.993	2.876
	333	35.47	8.81	0.990	4.055	170.62	6.18	0.994	2.510
SBA-M600	313	37.92	9.30	0.968	12.160	1241.67	4.89	0.973	10.138
	333	39.05	9.52	0.965	13.486	1703.18	4.87	0.971	11.220
SBA-4200	313	36.77	8.60	0.984	7.115	140.35	6.62	0.990	4.431
	333	38.88	9.01	0.984	7.280	271.36	6.38	0.990	4.478
SBA-4400	313	34.20	9.02	0.979	9.843	554.87	4.97	0.982	8.562
	333	36.16	9.27	0.978	10.566	951.04	4.94	0.982	8.993
SBA-4600	313	40.23	11.06	0.972	11.610	1575.73	5.13	0.977	9.429
	333	43.70	12.40	0.985	6.720	11.87 x10^3	4.55	0.989	4.693
SBA-IRA 958	313	31.07	7.89	0.962	14.470	29.01	7.04	0.968	12.094
	333	29.84	7.59	0.962	13.959	20.06	7.26	0.969	11.601
SBA-IRA 458	313	35.41	8.19	0.951	21.492	57.90	7.23	0.959	18.066
	333	35.14	8.64	0.937	26.321	74.93	6.77	0.944	23.625
WBA-IRA 67	313	0.78	1.59	0.999	0.077	0.03	14.01	0.984	1.768
	333	0.83	1.67	0.998	0.166	0.03	12.25	0.984	1.371

Table S14. Adsorption isotherm parameters for the Ho(III)-GLDA complexes adsorption on SAC, SBA, and WBA ion exchangers at the temperature of 313 K and 333 K.

Model				**Langmuir**		
Ion exchanger	T [K]	$q_{e.exp}$ [mg/g]	q_0 [mg/g]	K_L [L/mg]	R^2	χ^2
SAC-S950	313	58.09	60.86	0.072	0.995	1.756
	333	60.99	62.33	0.101	0.990	3.947
SAC-S957	313	160.89	149.14	3.668	0.959	89.545

	333	163.40	154.68	4.312	0.981	42.187
SAC-SP112	313	135.82	128.76	0.758	0.982	26.810
	333	137.17	128.90	1.016	0.976	36.117
SBA-M500	313	88.27	84.97	1.018	0.992	6.348
	333	90.31	88.17	1.098	0.988	9.313
SBA-MP500	313	86.15	82.27	0.998	0.989	8.272
	333	87.44	84.02	1.226	0.988	8.865
SBA-M600	313	85.83	81.91	1.113	0.984	11.239
	333	87.22	83.57	1.089	0.983	12.540
SBA-4200	313	90.33	86.09	1.370	0.982	14.124
	333	93.41	88.71	1.450	0.981	15.810
SBA-4400	313	78.68	77.70	0.759	0.997	1.795
	333	80.03	78.27	1.452	0.992	5.495
SBA-4600	313	87.80	85.79	0.817	0.995	3.783
	333	88.88	86.58	1.124	0.994	4.510
SBA-IRA 958	313	84.81	82.70	0.830	0.994	4.376
	333	83.55	81.90	0.823	0.994	4.164
SBA-IRA 458	313	91.84	89.41	1.061	0.984	12.756
	333	89.82	88.04	0.902	0.989	8.437
WBA-IRA 67	313	53.67	43.90	0.013	0.985	3.193
	333	53.01	41.97	0.007	0.980	4.126

		Freundlich				**Temkin**			
	T [K]	K_F [mg/g]	n	R^2	χ^2	A [L/g]	B [J/mol]	R^2	χ^2
SAC-S950	313	12.35	3.17	0.962	14.459	1.01	11.50	0.998	0.897
	333	14.52	3.31	0.971	12.111	1.77	11.05	0.996	1.671
SAC-S957	313	114.27	9.06	0.989	23.109	20.55 x10^3	11.42	0.993	14.885
	333	120.27	9.71	0.984	34.237	45.38 x10^3	11.19	0.990	22.263
SAC-SP112	313	89.84	9.94	0.996	5.927	28.91 x10^3	8.44	0.998	3.449
	333	91.57	9.28	0.997	4.550	49.58 x10^3	8.23	0.998	2.443
SBA-M500	313	55.29	8.50	0.977	17.272	1806.36	7.11	0.984	11.891
	333	57.75	8.60	0.958	33.306	2176.89	7.28	0.966	27.156
SBA-MP500	313	54.04	8.99	0.981	13.428	2737.86	6.59	0.987	9.605
	333	55.87	8.95	0.978	16.557	3049.11	6.76	0.984	11.790
SBA-M600	313	54.59	9.27	0.981	13.539	3728.60	6.43	0.987	9.521
	333	54.73	8.54	0.982	13.813	1946.31	6.98	0.988	9.082
SBA-4200	313	57.14	8.57	0.975	19.576	2607.75	7.09	0.981	15.123
	333	58.64	8.12	0.970	24.926	1892.47	7.60	0.977	19.359
SBA-4400	313	52.37	9.71	0.977	14.661	9367.27	5.51	0.982	11.662

	333	55.38	9.74	0.978	14.495	37.72 x10^3	5.14	0.983	11.179
SBA-4600	313	55.19	8.60	0.965	26.569	1591.48	7.16	0.973	20.379
	333	57.24	8.89	0.966	26.758	2660.86	7.03	0.974	20.117
SBA-IRA 958	313	54.27	9.39	0.970	21.456	3246.82	6.45	0.976	17.068
	333	54.02	9.60	0.970	20.802	3793.89	6.29	0.976	16.497
SBA-IRA 458	313	57.81	9.18	0.956	35.724	1556.53	7.62	0.963	29.928
	333	56.51	9.33	0.958	32.994	1472.31	7.45	0.966	27.036
WBA-IRA 67	313	0.13	1.02	0.985	3.134	0.01	24.09	0.912	18.856
	333	0.10	0.98	0.981	4.050	0.01	23.96	0.897	21.443

Table S15. Thermodynamic parameters for the Nd(III)-GLDA complexes adsorption on SAC, SBA, and WBA ion exchangers.

Ion exchanger	$\Delta H°$ [kJ/mol]	$\Delta S°$ [J/mol K]	$\Delta G°$ [kJ/mol]		
			293 K	313 K	333 K
SAC-S950	7.49	75.70	-14.72	-16.16	-17.75
SAC-S957	12.53	98.86	-16.48	-18.31	-20.45
SAC-SP112	2.34	63.02	-16.12	-17.41	-18.64
SBA-M500	5.60	63.88	-13.11	-14.39	-15.67
SBA-MP500	5.89	64.78	-13.10	-14.37	-15.69
SBA-M600	3.05	54.40	-12.88	-14.00	-15.05
SBA-4200	3.61	59.40	-13.81	-14.95	-16.19
SBA-4400	2.66	50.67	-12.20	-13.18	-14.23
SBA-4600	4.24	60.22	-13.42	-14.57	-15.83
SBA-IRA 958	-2.99	35.49	-13.41	-14.06	-14.83
SBA-IRA 458	-8.85	19.48	-14.62	-14.79	-15.42
WBA-IRA 67	-7.20	13.30	-11.08	-11.40	-11.60

Table S16. Thermodynamic parameters for the Ho(III)-GLDA complexes adsorption on SAC, SBA, and WBA ion exchangers.

Ion exchanger	$\Delta H°$ [kJ/mol]	$\Delta S°$ [J/mol K]	$\Delta G°$ [kJ/mol]		
			293 K	313 K	333 K
SAC-S950	8.45	75.91	-13.82	-15.23	-16.87
SAC-S957	19.32	121.14	-16.04	-18.90	-20.85
SAC-SP112	3.08	58.96	-14.18	-15.41	-16.53
SBA-M500	4.80	66.32	-14.65	-15.92	-17.31
SBA-MP500	6.56	70.34	-14.00	-15.59	-16.79
SBA-M600	4.99	65.40	-14.15	-15.54	-16.76
SBA-4200	9.44	82.19	-14.65	-16.27	-17.94
SBA-4400	4.49	60.70	-13.27	-14.58	-15.69

SBA-4600	2.70	59.26	-14.67	-15.84	-17.04
SBA-IRA 958	-2.93	39.81	-14.59	-15.39	-16.18
SBA-IRA 458	-6.60	31.83	-15.94	-16.55	-17.21
WBA-IRA 67	-7.07	17.84	-12.40	-12.42	-13.14

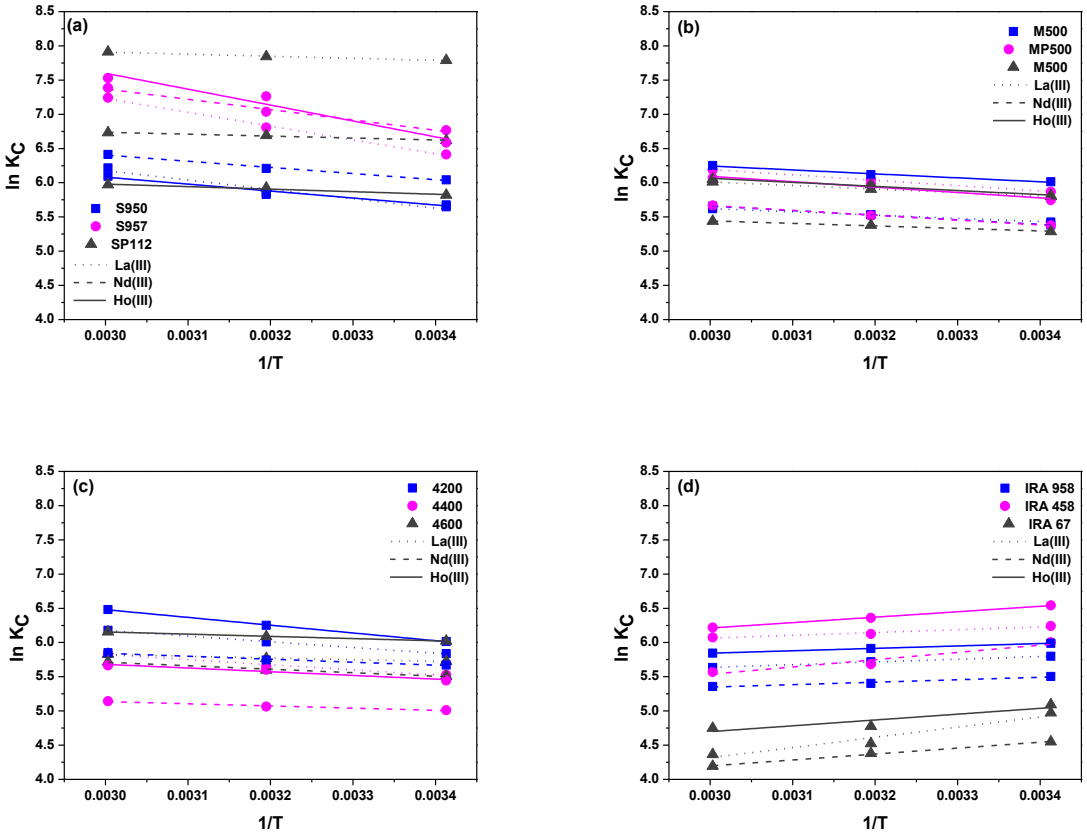

Fig. S8. Plots of lnK_C as a function of reciprocal of temperature (1/T) for the Ln(III)-GLDA complexes adsorption on SAC ion exchangers (a) S950, S957, SP112, on SBA and WBA ion exchangers (b) M500, MP500, M600, (c) 4200, 4400, 4600, (d) IRA 958, IRA 458, IRA 67.

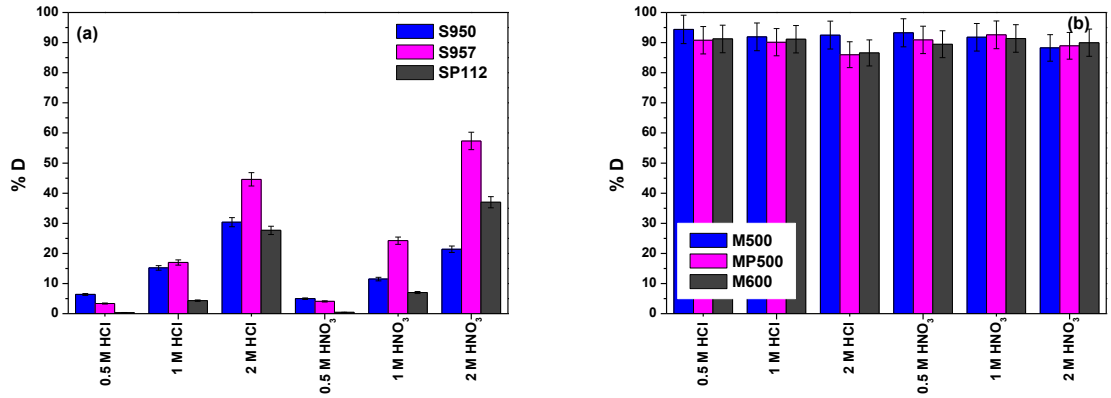

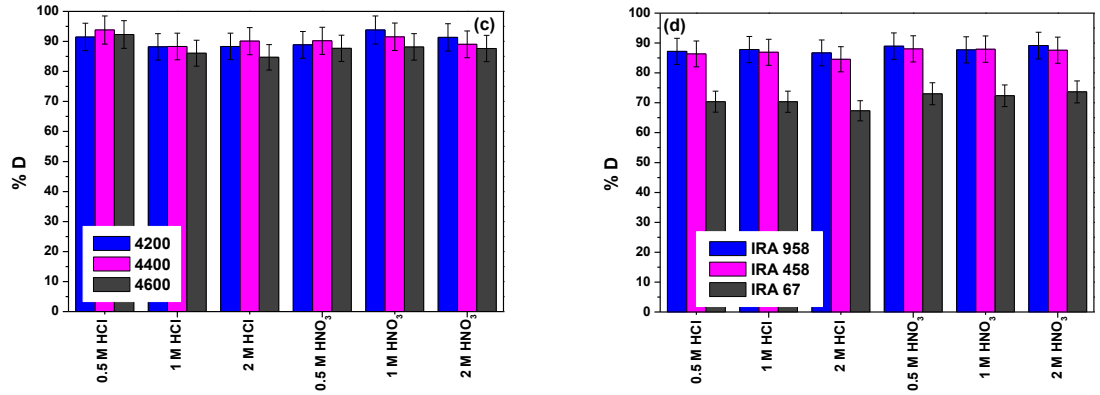

Fig. S9. Effect of the desorbing agent (type and concentration) on the desorption process of Nd(III) from the SAC ion exchangers (a) S950, S957, SP112, the SBA and WBA ion exchangers (b) M500, MP500, M600, (c) 4200, 4400, 4600, and (d) IRA 958, IRA 458, IRA 67.

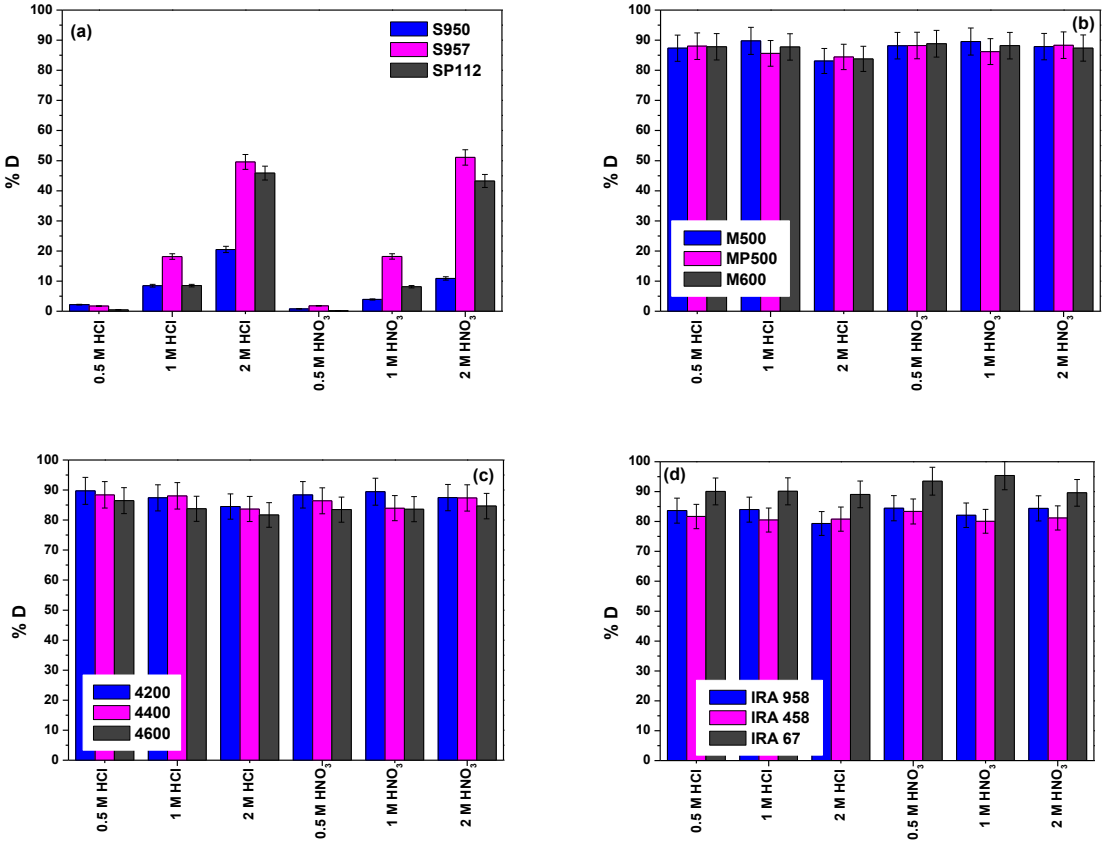

Fig. S10. Effect of the desorbing agent (type and concentration) on the desorption process of Ho(III) from the SAC ion exchangers (a) S950, S957, SP112, the SBA and WBA ion exchangers (b) M500, MP500, M600, (c) 4200, 4400, 4600, and (d) IRA 958, IRA 458, IRA 67.

Table S17. Breakthrough fitting models results for the La(III)-GLDA complexes adsorption.

Model	**Thomas**			**Adams–Bohart**		
Ion exchanger	$k_{Th} \times 10^3$ [mL/mg min]	q_0 [mg/g]	R^2	$k_{AB} \times 10^6$ [L/mg min]	q [mg/L]	R^2
SAC-S950	7.42	225.08	0.963	5.07	78545.23	0.967

SAC-S957	4.52	308.95	0.966	2.32	130779.92	0.866
SAC-SP112	31.12	211.95	0.951	19.69	68067.98	0.974
SBA-M500	52.08	105.21	0.987	26.17	31369.54	0.888
SBA-MP500	47.61	112.16	0.964	13.77	27941.56	0.707
SBA-M600	49.06	95.76	0.928	28.87	30225.15	0.937
SBA-4200	36.58	102.88	0.938	19.30	34455.67	0.945
SBA-4400	40.16	101.63	0.945	18.16	36157.47	0.886
SBA-4600	30.78	100.29	0.970	17.10	33818.91	0.927
SBA-IRA 958	45.47	70.91	0.925	21.28	22539.70	0.764
SBA-IRA 458	33.48	85.90	0.879	20.18	30087.47	0.945
WBA-IRA 67	23.72	9.69	0.755	9.91	7044.66	0.422
	Yoon–Nelson			**Wolborska**		
	k_{YN} [1/min]	τ [min]	R^2	β [1/min]	q [mg/L]	R^2
SAC-S950	0.0011	9851.82	0.963	0.398	78545.23	0.967
SAC-S957	0.0007	15275.70	0.966	0.304	130779.92	0.866
SAC-SP112	0.0045	9243.01	0.951	1.340	68067.98	0.974
SBA-M500	0.0074	4113.00	0.987	0.821	31369.54	0.888
SBA-MP500	0.0067	3299.67	0.964	0.385	27941.56	0.707
SBA-M600	0.0069	3953.88	0.928	0.873	30225.15	0.937
SBA-4200	0.0052	4401.19	0.938	0.665	34455.67	0.945
SBA-4400	0.0057	4743.96	0.945	0.657	36157.47	0.886
SBA-4600	0.0044	4266.00	0.970	0.578	33818.91	0.927
SBA-IRA 958	0.0064	2703.94	0.925	0.480	22539.70	0.764
SBA-IRA 458	0.0047	3796.18	0.879	0.607	30087.47	0.945
WBA-IRA 67	0.0032	438.41	0.755	0.070	7044.66	0.422

← Submissions Being Processed for Author

Page: 1 of 1 (1 total submissions) Results per page 10

Action	Manuscript Number	Title	Authorship	Initial Date Submitted	Status Date	Current Status
Action Links	SUSMAT-D-23-00546	GLDA AND ION EXCHANGERS: UNLOCKING SUSTAINABLE SOLUTIONS FOR RECOVERY OF RARE EARTH ELEMENTS	Other Author	May 30, 2023	Sep 23, 2023	Required Reviews Completed

Page: 1 of 1 (1 total submissions) Results per page 10